



HAL
open science

Transition metal-catalyzed reactions: mechanistic studies and methodology developments

Luca Alessandro Perego

► **To cite this version:**

Luca Alessandro Perego. Transition metal-catalyzed reactions: mechanistic studies and methodology developments. Analytical chemistry. Université Paris sciences et lettres, 2018. English. NNT: 2018PSLEE003 . tel-01872957

HAL Id: tel-01872957

<https://theses.hal.science/tel-01872957>

Submitted on 12 Sep 2018

HAL is a multi-disciplinary open access archive for the deposit and dissemination of scientific research documents, whether they are published or not. The documents may come from teaching and research institutions in France or abroad, or from public or private research centers.

L'archive ouverte pluridisciplinaire **HAL**, est destinée au dépôt et à la diffusion de documents scientifiques de niveau recherche, publiés ou non, émanant des établissements d'enseignement et de recherche français ou étrangers, des laboratoires publics ou privés.

THÈSE DE DOCTORAT

de l'Université de recherche Paris Sciences et Lettres
PSL Research University

Préparée à l'Ecole Normale Supérieure

Transition metal-catalyzed reactions: mechanistic studies and methodology developments

Réactions catalysées par des complexes métalliques :
études mécanistiques et développements méthodologiques

Ecole doctorale n° 388

CHIMIE PHYSIQUE ET CHIMIE ANALYTIQUE DE PARIS CENTRE

Spécialité CHIMIE THEORIQUE, PHYSIQUE, ANALYTIQUE

Soutenue par
Luca Alessandro PEREGO
le 6 février 2018

Dirigée par Mme **Ilaria CIOFINI**
et Mme **Laurence GRIMAUD**

COMPOSITION DU JURY :

M. Alain DE MESMAEKER
Syngenta,
Président du jury

M. Didier BOURISSOU
Université Toulouse III Paul Sabatier,
Rapporteur

M. Olivier Riant
Université Catholique de Louvain,
Rapporteur

Mme Karine COSTUAS
Université de Rennes 1,
Membre du jury

Mme Ilaria CIOFINI
Chimie ParisTech,
Directrice de thèse

Mme Laurence GRIMAUD
Ecole Normale Supérieure,
Directrice de thèse



Remerciements

Je tiens à remercier M. Didier Bourissou et M. Olivier Riant d'avoir accepté d'être rapporteurs de cette thèse ainsi que Mme Karine Costuas et M. Alain De Mesmaeker d'avoir accepté d'examiner et juger ce travail. Je remercie aussi M. Fabio Bellina et M. Laurent El Kaïm d'avoir accepté de participer à ma soutenance de thèse en qualité de membres invités.

Je remercie très chaleureusement mes directrices de thèse, Mme Ilaria Ciofini et Mme Laurence Grimaud, pour leur disponibilité, leurs bons conseils et leur temps consacré à l'encadrement, mais aussi pour leur confiance, qui m'a permis de faire mes propres choix. Au-delà de leurs compétences scientifiques, elles ont fait preuve de grandes qualités humaines et ce fut un réel plaisir de travailler avec elles.

Merci à Mme Anny Jutand et à M. Christian Amatore pour les nombreuses discussions éclairantes, et pour ne pas avoir ignoré un message que je leur ai envoyé il y a quatre ans. Sans cela cette thèse n'aurait pas pu exister.

Un gros merci à mes collègues doctorants et post-doctorants à l'ENS : Indira Fabre, Baptiste Haddou, Hakim Lakmini, Aude Nyadanu, Na Pan and Pierre-Adrien Payard. J'ai beaucoup apprécié leur aide (scientifique et non) et leur amabilité.

Merci à M. Carlo Adamo et à tous les membres de l'équipe de chimie théorique et modélisation de l'ENSCP : Marta Alberto, Marco Campetella, Stefania Di Tommaso, Juan Sanz García, Frédéric Labat, Laura Le Bras, Federica Maschietto, Eleonora Menicacci, Alistar Ottochian, Aurelie Perrier, Chiara Ricca, Alexandra Szemjonov and Liam Wilbraham.

Je souhaite également remercier nos collaborateurs de l'Ecole Nationale Supérieure de Chimie de Montpellier, M. Florian Monnier et M. Marc Taillefer, qui m'ont permis de travailler sur un sujet très intéressant. Je remercie aussi Rémi Blicq, grâce à sa grande disponibilité un véritable travail d'équipe a été possible. Merci à M. Paul Fleurat-Lessard pour son implication dans une collaboration fructueuse.

Merci à Antoine Groué, qui a participé à ce travail durant son stage de M1.

Merci également à M. Bernard Goetz de l'ENS, M. Vincent Jactel de l'Ecole Polytechnique, et à Mme Céline Fosse et Mme Claudine Fleurant de l'ENSCP pour leur disponibilité et leur efficacité dans le traitement des diverses analyses.

Un grand merci aussi à toutes autres personnes qui ne sont pas nommées ici et qui m'ont soutenu pendant ces trois années.

Table of contents

Abbreviations.....	9
General introduction	11
Chapter I – Experimental and Theoretical Methods for Mechanistic Studies	13
1. Experimental techniques.....	15
1.1. Nuclear Magnetic Resonance spectroscopy of heteronuclei	15
1.2. Conductometry for the characterization of ionic organometallic compounds ...	20
2. Theoretical background	23
2.1. Fundamentals of wave mechanics for a molecular system.....	23
2.2. The Born-Oppenheimer approximation.....	24
2.3. The variational principle	25
2.4. Slater determinants and the associated energy.....	26
2.5. The independent particle model and the Hartree-Fock equations.....	28
2.6. The limits of the Hartree-Fock approach, correlation energy	31
2.7. Fundamental ideas of DFT, the Hohenberg-Kohn theorems.....	32
2.8. The Kohn-Sham method.....	34
2.9. Approximating the exchange-correlation functional	36
2.10. Empirical dispersion corrections.....	38
2.11. Implicit solvation – the PCM model	39
2.12. Basis set and effective core potentials	40
3. Selected theoretical tools used in this thesis.....	42
3.1. Calculation of thermodynamic functions	42
3.2. Distortion-interaction analysis	43
3.3. Population analysis.....	44
4. References	46
CHAPTER II – Multiple Roles of Isocyanides in Palladium-Catalyzed Imidoylative Couplings: A Mechanistic Study	49
1. Context of the Study.....	51
1.1. Introduction	51
1.2. Early studies on the insertion of isocyanides in the C-Pd bond.....	52
1.3. Palladium catalyzed imidoylative couplings.....	54
1.4. Earlier mechanistic studies related to palladium-catalyzed imidoylative couplings.....	61
2. Results and discussion	70
2.1. Choice of the model reaction.....	70
2.2. Generation of Pd(0) from Pd(II) precursors	71
2.3. Oxidative addition to isocyanide-ligated palladium(0)	71
2.4. Characterization of the product of oxidative addition	77
2.5. Interaction of complex 1 with triphenylphosphine	83
2.6. Interaction of complex 1 with 1,2-bis-(diphenylphosphino)ethane (dppe)..	85
2.7. C-O bond forming reductive elimination	87
2.8. Theoretical study of the catalytic cycle.....	91
2.9. Theoretical study of the C-O bond forming reductive elimination	95
3. Conclusions	98
4. Computational details.....	101
5. References	102

CHAPTER III – Palladium-Catalyzed Reductive Benzofuran Ring-Opening Indole Ring-Closure *via* β -Phenoxide Elimination107

1. Context of the Study.....	109
1.1. Palladium-catalyzed reactions involving unfunctionalized heteroarenes	109
1.2. Palladium-catalyzed direct arylation and dearomative couplings of benzofurans.....	110
2. Results and discussion.....	116
2.1. First steps.....	116
2.2. Optimization of reaction conditions.....	117
2.3. Scope of the reaction.....	119
2.4. Going beyond the synthesis of indoles.....	122
2.5. Mechanistic studies.....	125
2.6. Proposed catalytic cycle.....	127
3. Conclusions.....	131
4. References.....	132

CHAPTER IV – Copper-Catalyzed Hydroamination of Allenes: Mechanistic Studies and Methodology Development.....135

1. Context of the Study.....	137
1.1. Introduction.....	137
1.2. Thermodynamic aspects of the hydroamination of alkenes and allenes	140
1.3. A survey of the literature on the hydroamination of allenes.....	140
2. Results and discussion.....	165
2.1. Object of the study.....	165
2.2. Nature of the catalytically active species.....	166
2.3. Catalytic cycle and the origin of selectivity.....	174
2.4. From mechanistic insight to methodology development – hydroamination of allenamides.....	182
2.5. Application of the hydroamination to the synthesis of an API – P-3374.....	186
2.6. Mechanistic insight into the hydroamination of allenamides.....	187
2.7. Extension to allenyl ethers.....	193
2.8. Extension to <i>N</i> -allenylazoles.....	196
2.9. Mechanistic insight into the copper-catalyzed hydroamination of azoles...	201
2.10. Extension to <i>N</i> -allenylsulfonamides.....	205
2.11. Mechanistic aspects of the copper-catalyzed hydroamination of <i>N</i> -allenylsulfonamides.....	207
3. Conclusions.....	216
4. Computational details.....	217
5. Bibliography.....	218

General conclusions and perspectives 223

Experimental sections..... 225

1. Experimental section of chapter II.....	227
1.1. General remarks.....	227
1.2. Synthesis and characterization of organometallic complexes.....	227
1.3. Synthesis of reference materials.....	230
1.4. X-Ray data for compound 1	230
References.....	232

2. Experimental section of chapter III.....	233
2.1. General remarks	233
2.2. General procedure A – Pd-catalyzed ring-opening of benzofuran derivatives	233
2.3. Synthesis of starting materials	240
2.4. General procedure B for the alkylation of compounds S3a-d	243
2.5. Synthesis of complex 13	255
References	256
3. Experimental section of chapter IV	257
3.1. General remarks	257
3.2. General procedure for the hydroamination of <i>N</i> -allenylamides	257
3.3. Pictet-Spengler-type cyclization of hydroamination products	265
3.4. Synthesis of substrates for mechanistic studies	266
3.5. General procedure for the isomerization of <i>N</i> -propargylamides, carbamates and ethers to <i>N</i> -allenylamides carbamates, and ethers	268
3.6. General procedure for the preparation of <i>N</i> -propargyl amides and carbamates	274
3.7. Study of the reaction between morpholine and Cu(OTf) ₂ – identification of the organic products	280
3.8. Hydroamination of <i>N</i> -allenylazoles	282
3.9. Synthesis of <i>N</i> -propargyl heteroarenes	285
3.10. Hydroamination of <i>N</i> -allenylsulfonamides	292
3.11. Synthesis of <i>N</i> -allenylsulfonamides	297
3.12. Synthesis of miscellaneous allenes	304
3.13. Synthesis of miscellaneous starting materials	309
References	311
Résumé.....	313

Abbreviations

9-BBN	9-borabicyclo[3.3.1]nonane	IR	infrared
Ac	acetyl	IRC	intrinsic reaction coordinate
AIBN	2,2'-azobis(isobutyronitrile)	LCAO	linear combination of atomic orbitals
API	active pharmaceutical ingredient	LDA	local density approximation
APT	attached proton test	LUMO	lowest unoccupied molecular orbital
Ar	aryl group	MCR	multi-component reaction
BINAP	2,2'-bis(diphenylphosphino)- 1,1'-binaphthyl	Me	methyl
bipy	2,2'-bipyridyl	MS	mass spectrometry
Bn	benzyl	Ms	methanesulfonyl
BOC	<i>tert</i> -butoxycarbonyl	MW	microwave
Bu	butyl	NBO	natural bond orbitals
Bz	benzoyl	NMM	<i>N</i> -methylmorpholine
Cbz	carboxybenzyl	NMR	nuclear magnetic resonance
cod	<i>cis,cis</i> -1,5-cyclooctadiene	NOE	nuclear Overhauser effect
Cp	cyclopentadienyl	NOESY	nuclear Overhauser effect spectroscopy
Cy	cyclohexyl	NPA	natural population analysis
dba	<i>trans,trans</i> -dibenzylidene acetone	PCM	polarizable continuum model
DFT	density functional theory	PES	potential energy surface
DIPEA	<i>N,N</i> -diisopropylethylamine	Ph	phenyl
DMA	<i>N,N</i> -dimethylacetamide	Piv	pivaloyl (trimethylacetyl)
DMF	<i>N,N</i> -dimethylformamide	ppm	parts per million
DMSO	dimethyl sulfoxide	Pr	propyl
dppb	1,4-bis(diphenylphosphino)butane	RMSD	root mean square deviation
dppe	1,2-bis(diphenylphosphino)ethane	STO	Slater-type orbital
dppf	1,1'-bis(diphenylphosphino)ferrocene	TBDMS	<i>tert</i> -butyldimethylsilyl
dppp	1,3-bis(diphenylphosphino)propane	<i>t</i> Bu	<i>tert</i> -butyl
ECP	effective core potential	TEMPO	2,2,6,6-tetramethyl-1- piperidinyloxy radical
EI	electron ionization	Tf	trifluoromethanesulfonyl
ESI	electro-spray ionization	TFA	trifluoroacetic acid
Et	ethyl	THF	tetrahydrofuran
FSOT	fused silica open tubular	TLC	thin layer chromatography
GGA	general gradient approximation	TMEDA	<i>N,N,N',N'</i> - tetramethylethylenediamine
GLC	gas-liquid chromatography	TMP	2,2,6,6-tetramethylpiperidine
GTO	Gaussian-type orbital	TMS	tetramethylsilane or trimethylsilyl
HMBC	heteronuclear multi-bond correlation	TOCSY	totally correlated spectroscopy
HMDS	hexamethyldisilazide	Tol	tolyl
HOMO	highest occupied molecular orbital	Ts	<i>p</i> -toluenesulfonyl
HRMS	high resolution mass spectrometry	UV	ultraviolet
HSQC	heteronuclear single quantum correlation	Xyl	xylyl
<i>i</i> Pr	isopropyl		

General introduction

Developing new synthetically useful reactions is a far-reaching goal of organic chemistry, giving access to novel compounds or to more efficient ways to perform known transformations. Despite the wealth of information that is available on countless organic reactions, many new discoveries are still made by a time- and resource-intensive trial-and-error process.

The aim of this thesis is to explore the potentialities of a different approach, i.e. to carry out at the same time mechanistic studies and methodology development. These two processes have been traditionally kept separated, both in space and time: the mechanism of a transformation is often studied several years after the reaction was first reported and in most cases by a different research group. We have tried to intertwine productively these two activities in the same laboratory.

We have also adopted a complementary approach using both experimental and theoretical tools for mechanistic studies. Theoretical modeling can often answer questions that are extremely difficult to address experimentally and experiments are often necessary to provide key information that is of critical importance to perform meaningful calculations.

After an introduction on the principles of the main methods used in this thesis (both experimental and theoretical), the rest of the material presented here can be subdivided into two main parts that have in common the same *modus operandi*. Part 1, comprising chapters II and III, concerns two palladium-catalyzed transformations, while part 2, which encompasses chapter IV and constitutes the main topic of this thesis, is about the copper-catalyzed hydroamination of allenes.

More in detail, in chapter II we present the mechanistic study of the synthesis of amides from haloarenes, isocyanides and water. This transformation is a prototypical palladium-catalyzed coupling involving the insertion of isocyanides and the conclusions reached may be generalized to other examples of the numerous transformations belonging to this class. We individuated the causes of some problems that may arise in this kind of reactions, and we suggested how some of them could be overcome.

Chapter III presents the study of the palladium-catalyzed ring-opening of benzofurans, a reaction that was discovered a few years ago in our laboratory. After exploring the scope of this original transformation giving access to functionalized indoles, some key intermediates of the catalytic cycle have been identified, giving a sound base for the proposed mechanism.

The theme of Chapter IV stems from a long-standing collaboration with the group of Marc Taillefer and Florian Monnier working in the Ecole Nationale Supérieure de Chimie in Montpellier and find its place in the framework on a broader program on the use of copper and iron catalysis in organic synthesis (ANR project CuFeCCBond). Starting from the conditions developed by our co-workers in Montpellier, the actual active species promoting the copper-

catalyzed hydroamination of allene derivatives has been characterized in conditions close to the synthetic reaction. The mechanism of this transformation has been investigated in detail using theoretical modelling and the information so obtained allowed choosing an optimal substrate class for the reaction: allenamides. Conditions for the regioselective and stereoselective addition of amines to these compounds under very mild conditions were established. Deeper investigation on the mechanism of this transformation revealed the fundamental role of secondary substrate-catalyst interactions, which spurred the extension to other substrate classes (*N*-allenylazoles and suitably substituted *N*-allenylsulfonamides).

CHAPTER I

Experimental and Theoretical Methods for Mechanistic Studies

In this chapter an overview of the less common experimental techniques adopted for the studies presented in this thesis will be given first. A brief account of the theoretical methods used will then follow. For the sake of conciseness, this discussion will not be exhaustive, so we will refer the reader to the pertinent literature for more details.

1. Experimental techniques

We will outline here some aspects of two analytical techniques that have been widely exploited in this thesis, and namely NMR spectroscopy of heteronuclei (^{19}F and ^{31}P in our case) and conductimetry.

1.1. Nuclear Magnetic Resonance spectroscopy of heteronuclei

The discussion of routine ^1H and ^{13}C 1D and 2D NMR experiments, which are part of the toolbox of the practicing organic chemist, is beyond the scope of this introduction. Instead, we will discuss in some detail the peculiarities of the NMR spectroscopy of two heteronuclei, namely ^{19}F and ^{31}P , which have been exploited extensively in the studies presented herein.

1.1.1. ^{19}F Nuclear Magnetic Resonance spectroscopy

^{19}F NMR spectroscopy is an important analytical technique and many parallels can be established with the familiar ^1H NMR spectroscopy. A comprehensive, but not specialized monography on this topic has been written by Dolbier. The following discussion is mainly based on this text.^[1]

Fluorine occurs naturally as a single isotope, ^{19}F . This spin $1/2$ nucleus has almost the ideal properties to be studied by NMR: not only it has 100% natural abundance, but it also has a favorable gyromagnetic ratio, its receptivity being about 83% that of ^1H . It yields sharp lines within a very wide chemical shift range of more than 300 ppm for common organofluorine compounds. On a standard NMR instrument in which ^1H resonates at 300 MHz, ^{19}F is observed at 282.231 MHz.

For its favorable properties, ^{19}F NMR developed historically almost contemporaneously as ^1H , and ^{19}F NMR were easily recorded already on early continuous wave instruments. Hence, extensive compilations of data on chemical shifts and coupling constants exist in the literature. Some caution is needed when comparing older literature, since a popular reference compound in the early history of ^{19}F NMR was external CF_3COOH , while now volatile and inert CFCl_3 is generally adopted as an internal standard (CF_3COOH resonates at -78.5 ppm on the CFCl_3 scale). Occasionally fluorobenzene was used as a reference for ^{19}F NMR chemical shifts (-113.6 with reference to CFCl_3). Signals upfield of the CFCl_3 resonance are assigned negative chemical shift values, but in older literature the sign was often omitted. Most organofluorine compounds give negative chemical shift.

Spin-lattice relaxation for ^{19}F nuclei is fast (it generally takes place on the timescale of seconds), so quantitative spectra with integrals proportional to the concentration are easily

recorded by properly adjusting the relaxation delay. Normally it takes no more than 5 minutes of machine time to get a good-quality quantitative ^{19}F NMR spectrum for a sample of a few milligrams of a compound of molecular weight smaller than 1000 Da. Several analytical applications of ^{19}F NMR have been proposed recently, most importantly for fluorine containing APIs.^[2–4]

^{19}F NMR spectra are often recorded with proton decoupling, as to get one singlet for each fluorine atom present in the molecule, if ^{19}F - ^{19}F coupling or coupling to other NMR-active nuclei is not present. Proton decoupling does not involve significant alteration of the integration due to the NOE enhancement, so quantitation is possible without resorting to special precautions (e.g. inverse gated decoupling).

Chemical shift for ^{19}F are notoriously difficult to predict based only on qualitative considerations, as it is often possible for ^1H . Introducing a commonly used notation, the effective magnetic field B_{eff} felt by each nucleus differ from the imposed external field B_0 as follows:

$$B_{\text{eff}} = B_0(1 - \sigma) \quad (1)$$

in which σ is the dimensionless shielding constant. The shielding constant σ is made up of three contributions:

$$\sigma = \sigma_{\text{dia}} + \sigma_{\text{para}} + \sigma^{\text{i}} \quad (2)$$

The diamagnetic contribution σ_{dia} corresponds to the shielding due to the electron cloud surrounding the nucleus that reacts to the imposed field. In this case, electrons that reside closer to the nucleus give a greater shielding than distant ones. The paramagnetic term σ_{para} originates from the excitation of p electrons by the imposed field, and its sign is opposite to that of σ_{dia} . The last term, σ^{i} , is due to the effect of neighboring groups on the same molecule and it can either increase or decrease the effective field. A fourth term taking into account intermolecular effects, such as those due to interaction with the solvent, can also be included.

In the case of proton spectra, only s-type orbitals are populated. As a consequence, only σ_{dia} is important, whereas σ_{para} is dominant in ^{19}F NMR. This is why the chemical intuition that generally works for ^1H chemical shift prediction is not easily applied to ^{19}F NMR. For instance, the fluorine nucleus of $\text{ClCH}_2\text{CH}_2\text{F}$ is more shielded ($\delta = -220$ ppm) than that of $\text{CH}_3\text{CH}_2\text{F}$ ($\delta = -212$ ppm). Moreover, the effect of anisotropic magnetic fields, such as those due to *ring currents*, are of little importance for fluorine NMR. As a consequence, the chemical shift ranges of vinyl fluorides and fluoroarenes overlap to a large extent.

In order to have a spectroscopic probe which is very sensitive to small changes of its molecular environment, which is of interest for mechanistic studies, it is better to incorporate in the a single carbon-bound fluorine substituent rather than, for instance, CF_2 or CF_3 moieties. Generally speaking, the single fluorine substituent chemical shift range is from about -70 ppm to -238 ppm (this latter value is for fluoromethane), while the corresponding ranges for CF_2 groups is from -80 to -130 ppm and for CF_3 it is smaller, between about -52 and -87 ppm.

Typical chemical shift ranges for some common fluorinated organic moieties are reported in Figure 1.

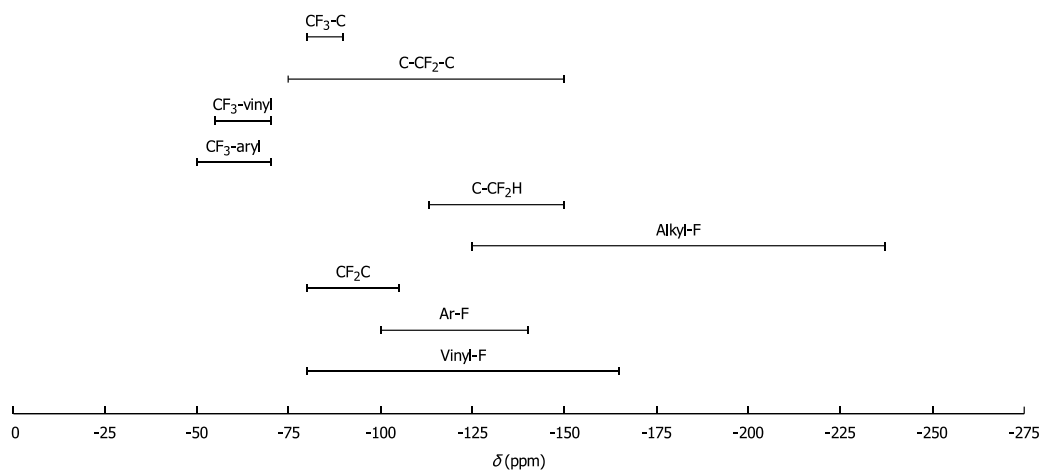


Figure 1 – Chemical shift range for common organofluorine moieties.^[1]

For our case, a single fluorine substituent on a aromatic ring was the most appropriate choice for both the studies reported in Chapter II and Chapter III. For reference we report in Table 1 the chemical shift data for a variety of substituted fluorobenzenes.^[1] The values reported for *para*-substituted fluorobenzenes have a good correlation with Hammett's σ_p values (Figure 2) and vary in the intuitive way, *i.e.* electron-withdrawing groups lead to a deshielding of the fluorine nucleus and electron-donating groups to a shielding. It is worth noting that these derivatives span a range of almost 30 ppm. The chemical shifts of *ortho*-substituted fluorobenzenes exhibit only a rough correlation, while the correlation is almost inexistent for *meta*-substituted derivatives and their chemical shifts vary in a much narrower range of less than 5 ppm. The wide variation of chemical shift upon relatively minor changes of the electronic properties of the aromatic ring, together with the sharpness of ¹⁹F resonances (normally peak width is less than 0.005 ppm at 282 MHz), the ease of the obtention of good quality quantitative spectra, and the inertness of the fluorine substituent in a variety of reaction conditions make the use of a fluorine substituent on an aromatic moiety an ideal spectroscopic probe for mechanistic studies.

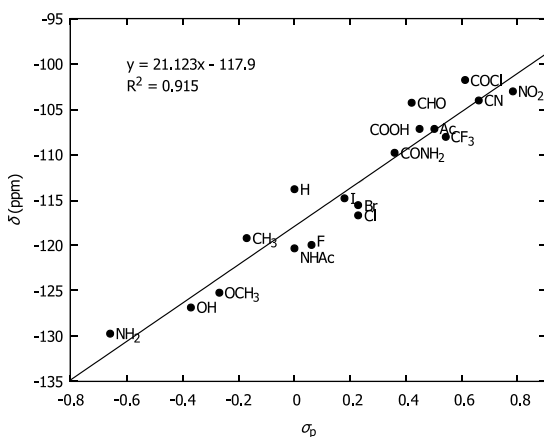
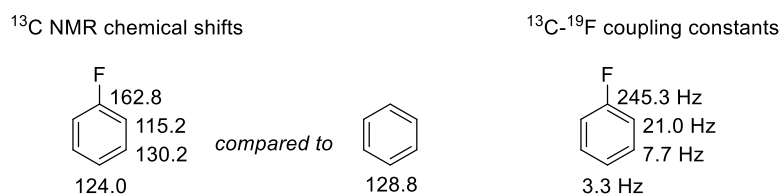


Figure 2 – Hammett correlation for the ¹⁹F NMR chemical shifts of *para*-substituted fluorobenzenes (measured in acetone).^[1]

Table 1 – ^{19}F NMR chemical shifts for monosubstituted fluorobenzenes.^[1]

	<i>ortho</i>		<i>meta</i>		<i>para</i>		σ_{p}
	acetone	DMSO	acetone	DMSO	acetone	DMSO	
COCl	-109.5		-113.6		-101.8		0.61
NO₂	-119.7	-119.0	-110.0	-109.5	-103.0	-102.4	0.78
CN	-108.6	-107.9	-110.9	-110.0	-104.0	-102.8	0.66
CHO	-122.4	-120.7	-112.6	-111.6	-104.3	-103.2	0.42
COCH₃	-110.6	-110.0	-113.1	-112.0	-107.1	-105.9	0.50
COOH	-110.0	-110.1	-113.3	-112.0	-107.2	-106.5	0.45
CF₃	-115.8	-115.4	-111.4	-110.3	-108.0	-106.8	0.54
CONH₂	-113.6	-113.3	-113.4	-112.6	-109.8	-109.2	0.36
H	-113.8	-112.6					0.00
I	-94.4	-106.2	-110.9	-110.3	-114.8	-114.2	0.18
Br	-108.1	-107.7	-110.8	-110.0	-115.6	-114.7	0.23
Cl	-116.3	-115.9	-111.2	-110.3	-116.7	-115.2	0.23
F	-139.7	-138.8	-110.6	-109.5	-120.0	-119.4	0.06
CH₃	-118.4	-117.3	-114.9	-113.7	-119.2	-118.0	-0.17
NHAc	-125.6	-124.6	-112.8	-111.8	-120.3	-119.4	0.00
OCH₃	-136.1	-135.3	-112.6	-111.4	-125.2	-124.0	-0.27
OH	-138.0	-136.3	-113.2	-112.1	-126.8	-125.0	-0.37
NH₂	-136.3	-134.9	-115.6	-113.5	-129.7	-129.4	-0.66

As a final remark, we recall that a fluorine substituent on benzenoid ring has a characteristic effect upon the ^{13}C spectrum, and it couples in a distinctive and highly consistent manner with the *ipso*, *ortho*, *meta*, and *para* carbons, as here exemplified for unsubstituted fluorobenzene (Scheme 1).

**Scheme 1** – ^{13}C NMR chemical shift and ^{13}C - ^{19}F coupling constants for fluorobenzene in CDCl_3 .^[1]

1.1.2. ^{31}P Nuclear Magnetic Resonance spectroscopy

Phosphorous is one of the most often studied heteronuclei in NMR spectroscopy. Among the numerous excellent monographies on this technique, we may advise that recently compiled by Kühl for its accessibility,^[5] and an older one by Pregosin and Kunz especially devoted to phosphines and their metal complexes.^[6]

The only natural occurring isotope of phosphorus is ^{31}P . Performing NMR experiments with ^{31}P poses no difficulties; ^{31}P is a spin $\frac{1}{2}$ nucleus with a positive magnetogyric ratio (10,840). On a 300 MHz instrument (proton frequency), it resonates at 121.44 MHz. ^{31}P nuclei yield sharp

peaks in a wide chemical shift range of more than 1500 ppm, its receptivity is 0.663% that of ^1H , but 37.7 times that of ^{13}C . Proton decoupling is usually applied, as to simplify spectral interpretation. The maximum theoretical NOE enhancement from proton decoupling is 1.23. To get reliable integration in $^{31}\text{P}\{^1\text{H}\}$ NMR spectra, the use of inverse-gated decoupling is advisable. The reference compound for ^{31}P NMR spectra is concentrated phosphoric acid (85% H_3PO_4 in water) and it has been used consistently since the early history of phosphorous NMR, substantial literature data are available and reliable.

The main interest of ^{31}P NMR is its usefulness for the study of phosphorus-containing biomolecules. For the organometallic chemist, its main use is for the characterization of phosphorus-containing ligands and their metal complexes. Whereas ^1H and ^{13}C NMR spectroscopies are mainly concerned with contributions due to σ -bonding or to well-defined π -bonded structural elements, the influence of π -bonding in ^{31}P NMR is larger in magnitude and more frequent. The same considerations about the relatively little importance of the diamagnetic contribution to the shielding constant with respect to the paramagnetic term and the contribution of neighboring groups we exposed above for ^{19}F NMR also apply in the case of ^{31}P . Simple empirical formulas to predict the phosphorous chemical shift based on additive group contributions (like those normally used for ^1H and ^{13}C NMR) are normally not available. Consideration based on electronegativity of substituents, π -bond involvement, bond angles and cone angles allow reasonable prediction in most cases, but comparison with known data or with theoretically predicted chemical shifts is of paramount importance. As oxidation states do not reflect the true electron density on phosphorous, considerations based on oxidation states are usually misleading.

1.1.3. Practicalities of NMR spectroscopy for mechanistic studies

Modern NMR spectrometers normally need deuterated solvents to *lock* the deuterium signal *via* an appropriate channel. The ^2H lock of an NMR spectrometer continuously monitors the frequency of the deuterated solvent used to prepare the sample. If the frequency of the ^2H resonance changes due to an environmental perturbation of the B_0 magnetic field, a feedback mechanism is used to correct B_0 itself, returning the ^2H resonance to its original position. This technique reduces environmental instability from NMR data collected over periods of time spanning minutes or hours. Moreover, some instruments use the ^2H signals of the solvent to perform *shimming* of the magnetic field in an automated fashion.

Some deuterated solvents that may be useful for conducting mechanistic studies or for organometallic reactions, however, are not readily available or command high prices on the market. In the recent years, the technique of *not* using deuterated solvents to perform quick NMR experiments for which field stability is not critical, without resorting to ^2H signal lock, has been popularized as *no-D NMR*.^[7] For example, this technique is especially useful for the quantitative determination of polar organometallic species.^[8] The presence of a large solvent peak is of no concern if it falls in an area of the spectrum in which there are no resonances of interest, *e.g.* in aliphatic solvents if the analytical peaks are vinyl or aryl proton resonances or if they lie at negative chemical shifts, which is sometimes the case for polar organometallic compounds. In

general, solvent suppression techniques are easy to implement on modern spectrometers and offer a simple means to solve cases of near superposition. In our opinion, techniques based on excitation sculpting (DPFGSE, Double Pulse Field Gradient Spin Echo) are reliable and easy to use also for the layman in NMR spectroscopy.^[9]

In general, even if a deuterated solvent was not used, we preferred to have a deuterium signal to perform proper *lock* and *shim*, taking also advantage of automated routine procedures. At this end, we resorted to the use of glass tubes containing a small amount of a deuterated solvent giving an intense signal (DMSO-*d*₆ is most suitable). Such coaxial inserts are commercially available, and they are precision-built to have a regular cylindrical shape. For routine work, a cheap homemade alternative is to fill commercially available melting point capillary tubes with the deuterated solvent and to seal them permanently with a flame.

1.2. Conductometry for the characterization of ionic organometallic compounds

Conductimetry is an electroanalytical techniqueⁱ based on the measurement of the electrical conductivity of a solution to monitor the progress of a chemical reaction or to obtain information related to a chemical system. This technique is very often used in many industrial and environmental applications where monitoring the concentration of ionic compounds in water is required, *e.g.* to check the effectiveness of deionization processes. Due to its simplicity, it is easily adapted to in-line sensors. For what concerns organometallic and coordination chemistry, conductivity measurements are often performed using organic solvents. The use of conductivity data to characterize coordination compounds has been reviewed by Geary in 1977,^[10] and the specific applications to organopalladium chemistry by Jutand in 2003.^[11]

Conductivity or specific conductance (normally represented by the Greek letter κ) is the reciprocal of resistivity, also known as specific electrical resistance (normally noted as ρ). For a conductor having uniform cross section and uniform electric current flow, the resistivity is defined as:

$$\kappa^{-1} = \rho = R \frac{A}{l} \quad (3)$$

where R is the electrical resistance, l is the length of the specimen and A is its cross-sectional area (Figure 3). The SI unit for conductivity is the siemens-meter (S m^{-1}), one siemens is the

ⁱ It is improper to classify conductometry as an electrochemical technique, as chemical change due to electron transfer is the principle on which electrochemical techniques are usually considered to be based on. Conductometry does not involve chemical reactions, so it is best viewed as the measurement of a *physical property* of a solution, like the measurement of the refractive index or of the boiling point. The term *conductimetry* is usually employed for applications involving a titration (*i.e.* *conductimetric titration*, the *conductimetric* determination of the equivalence point of a titration), while *conductometry* normally refers to applications other than titrations.

reciprocal of one ohm ($1 \text{ S} = 1 \text{ } \Omega^{-1}$). Sometimes the siemens is called mho, which is ohm spelled backwards. In practice, $\mu\text{S cm}^{-1}$ or mS cm^{-1} are commonly used to report conductivities of ionic solutions.

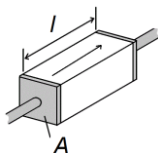


Figure 3 – Idealized setup for the definition of electrical resistivity, a resistive material between two conductive plates through which electrical current is passed.

The electrical conductivity is measured by determining the resistance of the solution between two inert flat or cylindrical electrodes separated by a fixed distance. More complicated cell designs (*e.g.* multi-electrode cells) are also available and useful for specialty applications. An alternating voltage is used to avoid electrolysis (typically with frequencies of a few kHz). In practice, the conductivity cell is calibrated by the use of a solution of known conductivity (most often solutions of KCl in water, for which accurate data are available),^[12] so that A and l need not to be known precisely.

The molar (specific) conductivity (Λ_m) of a solution containing an electrolyte is defined as the ratio between the measured conductivity and the concentration (c) of the electrolyte itself:

$$\Lambda_m = \frac{\kappa}{c} \quad (4)$$

The most usual unit for Λ_m is $\text{S cm}^2 \text{ mol}^{-1}$.

The molar conductivity of strong electrolytes (*i.e.* those which are completely dissociated) at low concentration follow Kohlrausch's law, which is derived from Debye's and Huckel's theory of strong electrolytes:

$$\Lambda_m = \Lambda_m^0 - K\sqrt{c} \quad (5)$$

in which Λ_m^0 is known as the molar limiting conductivity at infinite dilution and K is an empirical constant. The limit conductivity Λ_m^0 has the property that it can be written as the sum of partial molar limiting conductivities of individual ions: $\Lambda_m^0 = \lambda_+^0 + \lambda_-^0$, in which λ_+^0 and λ_-^0 are the partial limiting conductivities of the cation and of the anion. Kohlrausch's law is not valid if ions interact significantly, *i.e.* if they form ion pairs.

At very low concentrations, $\Lambda_m^0 \gg K\sqrt{c}$, so the conductivity is approximately proportional to the concentration of the ionic species:

$$\kappa \approx \Lambda_m^0 c \quad (6)$$

In this approximation, that is usually valid for ionic species in polar organic solvents for concentrations in the mM range, conductivity measurements can be easily used, for example, to monitor the kinetics of reactions that generate or consume ionic species.

2. Theoretical background

We will survey briefly here the fundamentals of the electronic structure methods that have been used in this thesis.

2.1. Fundamentals of wave mechanics for a molecular system

According to the *postulates* of quantum mechanics, each physical system is associated with a separable Hilbert space \mathcal{H} defined on the field of complex number and equipped with the inner product $\langle \phi | \psi \rangle$. Each state accessible to the system is associated with a vector subspace of unitary size in H (a *ray* in \mathcal{H}). For every physical observable, a linear, self-adjoint operator \hat{A} in \mathcal{H} is defined. The possible values of the physical observable are the eigenvalues of this operator (*i.e.* the *spectrum* of \hat{A}). The expectation value of the observable A if the system is in a state represented by Ψ is proportional to $\langle \Psi | \hat{A} \Psi \rangle$. If the eigenvalue α is measured on state $|\Psi\rangle$, the wavefunction Ψ is projected on the eigenspace associated to α (the postulate of *collapse*). The Hilbert space of a system composed of several subsystems is the tensor product of the Hilbert spaces of the components.

The time evolution of the system is given by the Schrödinger equation:ⁱⁱ

$$i \frac{\partial}{\partial t} |\Psi\rangle = \hat{H} |\Psi\rangle \quad (7)$$

in which \hat{H} is the Hamiltonian, *i.e.* the self-adjoint operator associated to the energy of the system, and i is the imaginary unit. For most problems of chemical interest excluding photochemistry and optical spectroscopies, the eigenfunction Ψ_0 of \hat{H} associated to its smallest eigenvalue, known as the *ground-state wavefunction* and the *ground-state energy* respectively, are the only needed. The goal is thus to solve the time-independent Schrödinger equation:

$$\hat{H}\Psi = E\Psi \quad (8)$$

For a molecular system, the non-relativisticⁱⁱⁱ Hamiltonian operator \hat{H} has contributions associated to the electrons and to the nuclei:

ⁱⁱ In the following, we will write all formulas using atomic units, *i.e.* the units in which the reduced Planck constant \hbar , the electron rest mass m_e , the Coulomb force constant $(4\pi\epsilon_0)^{-1}$, and the elementary charge e are numerically equal to 1. In these units, the unit of length is the bohr ($a_0 \approx 5.29 \cdot 10^{-11}$ m) and the unit of energy is the hartree ($E_h \approx 4.36 \cdot 10^{-18}$ J).

ⁱⁱⁱ Relativistic corrections are required when particles approach the speed of light. This is the case for core electrons of heavy nuclei. Solving the relativistic version of the Schrödinger equation poses additional difficulties. A common approximation for molecular systems is to utilize an effective potential for heavy

$$\hat{H} = \hat{T}_N + \hat{V}_{NN} + \hat{T}_e + \hat{V}_{Ne} + \hat{V}_{ee} \quad (9)$$

in which

$$\begin{aligned} \hat{T}_N &= \sum_A^{\text{nuclei}} -\frac{1}{2} \nabla_A^2 & \hat{V}_{NN} &= \sum_{A < B}^{\text{nuclei}} \frac{Z_A Z_B}{r_{AB}} \\ \hat{T}_e &= \sum_i^{\text{electrons}} -\frac{1}{2} \nabla_i^2 & \hat{V}_{Ne} &= -\sum_{i,A} \frac{Z_A}{r_{Ai}} & \hat{V}_{ee} &= \sum_{i < j}^{\text{electrons}} \frac{1}{r_{ij}} \end{aligned}$$

where \hat{T}_N is the kinetic energy operator of the nuclei, \hat{V}_{NN} is the potential energy operator of the nuclei, \hat{T}_e is the kinetic energy operator of the electrons, \hat{V}_{Ne} is the nuclei/electron potential energy operator, \hat{V}_{ee} is the electron/electron potential energy operator, and r is the distance between the particles specified by the subscripts.

Solving the time-independent equation exactly is not possible for multi-electron systems, so approximations are introduced. The rest of this section will be devoted to some of the approximate methods for the solution of the Schrödinger equation, and the next one to some techniques useful for extracting information from the resulting models.

2.2. The Born-Oppenheimer approximation

The total wavefunction associated to a molecular system $\Psi(\mathbf{R}, \mathbf{r})$ depends on the coordinates of all the nuclei (\mathbf{R}) and of all the electrons (\mathbf{r}). Since nuclei are much heavier than electrons (the mass of a proton is 1836 times the mass of an electron), electrons move much faster than nuclei and they respond almost instantaneously to changes in the position of the nuclei. The total molecular wavefunction can thus be factorized into a part that depends only on the nuclear coordinates and a part that depends only on the electronic coordinates:

$$\Psi(\mathbf{R}_1, \mathbf{R}_2, \dots, \mathbf{R}_N, \mathbf{r}_1, \mathbf{r}_2, \dots, \mathbf{r}_n) = \Phi(\mathbf{R}_1, \mathbf{R}_2, \dots, \mathbf{R}_N) \psi(\mathbf{r}_1, \mathbf{r}_2, \dots, \mathbf{r}_n) \quad (10)$$

This simplification implies that the positions of the nuclei can be considered fixed and the Schrödinger equation solved only for the electronic part, leaving the nuclear coordinates as parameters. This approximation, due to Born and Oppenheimer, is normally valid for most of the chemical problems.

Neglecting nuclear kinetic energy \hat{T}_N , the molecular Hamiltonian can thus be rewritten as follows:

$$\hat{H} = \hat{H}_e + \hat{V}_{NN} \quad \hat{H}_e = \hat{T}_e + \hat{V}_{Ne} + \hat{V}_{ee} \quad (11)$$

nuclei that accounts for relativistic effects (*vide infra*). For first- and second-row elements, relativistic contributions are usually negligible.

in which \hat{H}_e is known as the electronic Hamiltonian. The electronic wavefunction ψ is an eigenfunction of this operator:

$$\hat{H}_e |\psi\rangle = E_e |\psi\rangle \quad (12)$$

The total energy of the molecular system is simply given by the sum of the nuclear repulsion energy, which can be calculated with the standard Coulomb-law derived formula for the potential energy of a distribution of point charges, and the electronic energy E_e :

$$E = E_e + \sum_{A<B}^{\text{nuclei}} \frac{Z_A Z_B}{r_{AB}} \quad (13)$$

It is convenient for the following to write the electronic Hamiltonian of a system comprising n electrons as the sum of n one-electron operators \hat{h}_i and a two-electron part:

$$\hat{H} = \sum_{i=1}^n \hat{h}_i + \sum_{\substack{i,j=1,\dots,n \\ i<j}} \frac{1}{r_{ij}} \quad \hat{h}_i = -\frac{1}{2} \nabla_i^2 - \sum_A^{\text{nuclei}} \frac{Z_A}{r_{Ai}} \quad (14)$$

The Born-Oppenheimer approximation is deeply rooted in the chemists' point of view on molecules. Indeed, it allows reasoning in terms of the potential energy surface (PES). The PES is built by calculating the energy of the system (including the electronic energy and the nuclear repulsion energy) while varying the positions of the nuclei. The characterization of the stationary point of the PES is what is usually done to study chemical reactions theoretically: local minima on the PES correspond to stable molecules and saddle points to transition states. Whenever these common terms are used, the Born-Oppenheimer approximation is implicitly assumed.

2.3. The variational principle

Let us suppose that ϕ is function we want to use as an approximation of the ground state wavefunction ψ_0 of a certain system. Function ϕ may be completely arbitrary, we only require that it belongs to the correct function space of ψ_0 and that it is normalizable (*i.e.* $\langle \phi | \phi \rangle < \infty$). Let ϕ' be the normalized counterpart of ϕ :

$$\phi' = \frac{\phi}{\sqrt{\langle \phi | \phi \rangle}} \quad (15)$$

From the fact that the eigenfunctions of \hat{H} constitute a complete basis for \mathcal{H} , it follows directly that the expectation value of \hat{H} over ϕ' is greater or equal to E_0 , the minimum eigenvalue of \hat{H} :

$$\langle \phi' | \hat{H} \phi' \rangle \geq E_0 \quad (16)$$

The variational principle is not an approximation, but it gives a useful criterion to look for an approximation of the ground-state energy of a system. Even if there is no general theorem that guarantees that if a wavefunction is “good” according to the variational principle (*i.e.* that it gives an expectation value of \hat{H} close to E_0), then it is also a good approximation of the exact ground-state wavefunction, it often turns out that the wavefunction optimized according to the variational method gives reasonable results for the calculation of properties other than energies.

2.4. Slater determinants and the associated energy^{iv}

The wavefunction ψ depends on the coordinate of all the electrons: $\psi = \psi(\mathbf{r}_1, \mathbf{r}_2 \dots \mathbf{r}_n)$. It may be tempting to assume that it could be written as the product of n one-electron wavefunctions, called spin-orbitals: $\psi(\mathbf{r}_1, \mathbf{r}_2 \dots \mathbf{r}_n) = \phi_1(\mathbf{r}_1)\phi_2(\mathbf{r}_2)\dots\phi_n(\mathbf{r}_n)$. This approximation, which is called Hartree product, is not viable, because such a wavefunction would not respect the basic requirement of antisymmetry upon exchange of two identical fermions. A satisfactory approach is to use an antisymmetrized product of n one-electron wavefunctions, known as the Slater determinant:

$$\psi(\mathbf{r}_1, \mathbf{r}_2 \dots \mathbf{r}_n) = \frac{1}{\sqrt{n!}} \begin{vmatrix} \phi_1(\mathbf{r}_1) & \phi_2(\mathbf{r}_1) & \dots & \phi_n(\mathbf{r}_1) \\ \phi_1(\mathbf{r}_2) & \phi_2(\mathbf{r}_2) & \dots & \phi_n(\mathbf{r}_2) \\ \dots & \dots & \dots & \dots \\ \phi_1(\mathbf{r}_n) & \phi_2(\mathbf{r}_n) & \dots & \phi_n(\mathbf{r}_n) \end{vmatrix} = \frac{1}{\sqrt{n!}} \sum_P \sigma_P \hat{P} |\phi_1(\mathbf{r}_1)\phi_2(\mathbf{r}_2)\dots\phi_n(\mathbf{r}_n)| \quad (17)$$

in which \hat{P} is the permutation operator acting on the spin-orbitals ϕ_i and σ_P is the parity of the permutations, the sum runs over all the possible permutations P of the indexes. The Slater determinant has the correct symmetry properties upon exchange of particles and it satisfies the Pauli exclusion principle.

We will now calculate the expectation value of the Hamiltonian operator on this wavefunction, in the form reported in equation (14). We will first consider the one-electron operator $\hat{h}(1)$. The integral $\langle \psi | \hat{h}(1) | \psi \rangle$ contains $(n!)^2$ terms, each one of the form

$$\pm \frac{1}{n!} [\phi_a(i)\phi_b(j)\dots\phi_x(x)]^* \hat{h}(1) [\phi_a(i')\phi_b(j')\dots\phi(x')] \quad (18)$$

If the spin orbitals ϕ_i are orthonormal, these integral vanish unless $i=i'$, $j=j'$, ... The remaining terms have thus the form

$$\pm \frac{1}{n!} [\phi_a^*(i)\phi_b^*(j)\dots\phi_w^*(w)] [\phi_a(i)\phi_b(j)\dots\phi_w(w)] \cdot \phi_x^*(1)\hat{h}\phi_x(1) \quad (19)$$

^{iv} This section and the following on the Hartree-Fock theory essentially follow the presentation made by McWeeny^[41] and by Szabo and Ostlund.^[42]

This product can be formed in $(n-1)!$ ways, which is the number of permutations of $(n-1)$ labels, so the expectation value of $\hat{h}(1)$ is $(n-1)!$ times the sum of the expectation values over each spin-orbital:

$$\langle \psi | \hat{h}(1) | \psi \rangle = \frac{(n-1)!}{n!} \sum_i^n \langle \phi_i | \hat{h}(1) | \phi_i \rangle = \frac{1}{n} \sum_i^n \langle \phi_i | \hat{h}(1) | \phi_i \rangle \quad (20)$$

The expectation value of the one-electron part of the Hamiltonian, for the indistinguishability of the electrons, is thus composed of n identical terms, thus:

$$\left\langle \psi \left| \sum_i^n \hat{h}(i) \right| \psi \right\rangle = \sum_i^n \langle \phi_i | \hat{h}(1) | \phi_i \rangle \quad (21)$$

The expectation value of the bielectronic part is slightly more involved, but similar arguments show that

$$\left\langle \psi \left| \sum_{i<j} \frac{1}{r_{ij}} \right| \psi \right\rangle = \sum_{i<j} [\langle \phi_i \phi_j | g | \phi_i \phi_j \rangle - \langle \phi_i \phi_j | g | \phi_j \phi_i \rangle] \quad (22)$$

in which we will use the convention that

$$\langle \phi_i \phi_j | g | \phi_k \phi_l \rangle = \int \phi_i^*(\mathbf{r}_1) \phi_j^*(\mathbf{r}_2) \frac{1}{r_{ij}} \phi_k(\mathbf{r}_1) \phi_l(\mathbf{r}_2) d\mathbf{r}_1 d\mathbf{r}_2 \quad (23)$$

The first integral in equation (22) is known as the *Coulomb integral* and the second one as the *exchange integral*.

In summary, the expectation value of the energy associated to a normalized Slater determinant of orthonormal spin-orbitals is given by the following equation:

$$\langle \psi | \hat{H} | \psi \rangle = \sum_i \langle \phi_i | \hat{h} | \phi_i \rangle + \frac{1}{2} \sum_{i,j} [\langle \phi_i \phi_j | g | \phi_i \phi_j \rangle - \langle \phi_i \phi_j | g | \phi_j \phi_i \rangle] \quad (24)$$

in which the term in the last sum vanishes identically for $i = j$. We will also define two new operators that will be useful in the following. The first one is the *Coulomb operator* \hat{J}_k associated with the spin-orbital ϕ_k , operating on an arbitrary wavefunction of the variable \mathbf{r}_1 :

$$\hat{J}_k \psi(\mathbf{r}_1) = \left[\int d\mathbf{r}_2 \frac{1}{r_{12}} \phi_k^*(\mathbf{r}_2) \phi_k(\mathbf{r}_2) \right] \psi(\mathbf{r}_1) \quad (25)$$

In simple terms, \hat{J}_k simply multiplies its operand by the potential energy due to the charge distribution $|\phi_k|^2$. The second one is a non-local operator known as the *exchange operator* \hat{K}_k

$$\hat{K}_k \psi(\mathbf{r}_1) = \int d\mathbf{r}_2 \frac{1}{r_{12}} \phi_k^*(\mathbf{r}_1) \phi_k(\mathbf{r}_2) \psi(\mathbf{r}_2) \quad (26)$$

which describes a sort of non-local potential deriving from the requirement of antisymmetry of the wavefunction (these terms do not appear in the energy of a Hartree product). Contrarily to

the Coulomb operator, there is no classical interpretation of the exchange operator. The exchange operator gives a negative (stabilizing) contribution to the total energy of the multi-electron system. It is also convenient to define the *total* Coulomb and exchange operators:

$$\hat{J} = \sum_k \hat{J}_k \quad \hat{K} = \sum_k \hat{K}_k \quad (27)$$

Thanks to these definitions, equation (24) can be written in a particularly telling form:

$$\langle \psi | \hat{H} | \psi \rangle = \sum_i^n \left\langle \phi_i \left| \hat{h} + \frac{1}{2} \hat{G} \right| \phi_i \right\rangle \quad \hat{G} = \hat{J} - \hat{K} \quad (28)$$

In this way, the energy associated to a Slater determinant can be seen as the sum of *orbital* (one-electron) energies corrected by a term ($\frac{1}{2} \hat{G}$) that accounts for the mean effect of all the other electrons composing the system. This is why approximating the exact wavefunction with a Slater determinant is equivalent to assuming an *independent particle model* with a *mean-field approximation*.

2.5. The independent particle model and the Hartree-Fock equations

The idea at the basis of the Hartree-Fock theory is to approximate the exact ground-state wavefunction of a polyelectronic system using a Slater determinant constructed starting from spin-orbitals chosen in such a way that they are optimal according to the variational principle.

The expression for the energy of a Slater determinant is thus to be minimized with a proper choice of the spin orbitals ϕ_i with the constraint that the ϕ_i remain orthonormal. The method of Lagrange undetermined multipliers can be used for this constrained stationary value problem. A Lagrange auxiliary function \mathcal{L} is thus constructed in the usual way:

$$\mathcal{L}[\{\phi_k\}] = E[\{\phi_k\}] - \sum_{i,j} \epsilon_{ij} [\langle \phi_i | \phi_j \rangle - \delta_{ij}] \quad (29)$$

in which E is the energy given by equation (24), ϵ_{ij} are the undetermined multipliers and δ_{ij} is the Kronecker symbol. \mathcal{L} must be real and $\langle \phi_i | \phi_j \rangle = \langle \phi_j | \phi_i \rangle^*$, thus ϵ_{ij} are the elements of an Hermitian matrix:

$$\epsilon_{ij} = \epsilon_{ij}^* \quad (30)$$

The functional differential of E can be calculated with usual rules:^v

^v Without entering into mathematical details, the differential of a functional is the part of the difference $F[f + \delta f] - F[f]$ that depends linearly from δf . The functional derivative of $\frac{\delta F}{\delta f(x)}$ is defined such that

$$\begin{aligned}
 \delta E &= \sum_i \left[\langle \delta\phi_i | \hat{h} | \phi_i \rangle + \langle \phi_i | \hat{h} | \delta\phi_i \rangle \right] + \\
 &+ \frac{1}{2} \sum_{i,j} \left[\langle \delta\phi_i \phi_j | g | \phi_i \phi_j \rangle + \langle \phi_i \delta\phi_j | g | \phi_i \phi_j \rangle - \langle \delta\phi_i \phi_j | g | \phi_j \phi_i \rangle - \langle \phi_i \delta\phi_j | g | \phi_j \phi_i \rangle + c.c. \right] = \quad (31) \\
 &= \sum_i \langle \delta\phi_i | \hat{h} | \phi_i \rangle + \sum_{i,j} \left[\langle \delta\phi_i \phi_j | g | \phi_i \phi_j \rangle - \langle \delta\phi_i \phi_j | g | \phi_j \phi_i \rangle \right] + c.c.
 \end{aligned}$$

in which *c.c.* stands for the complex conjugate of the preceding terms and the last equality comes from the fact that the antisymmetrized integrals are invariant under exchange of the indices on both sides of the scalar product, and the summation indices are immaterial. The differential of \mathcal{L} can thus be calculated:

$$\delta \mathcal{L} = \sum_i \langle \delta\phi_i | \hat{h} | \phi_i \rangle + \sum_{i,j} \left[\langle \delta\phi_i \phi_j | g | \phi_i \phi_j \rangle - \langle \delta\phi_i \phi_j | g | \phi_j \phi_i \rangle \right] - \sum_{i,j} \epsilon_{ij} \langle \delta\phi_i | \phi_j \rangle + c.c. = 0 \quad (32)$$

Equation (32) can be rewritten using the Coulomb and exchange operators we defined before:

$$\delta \mathcal{L} = \sum_i \left\{ \langle \delta\phi_i | \hat{h} + \hat{J} - \hat{K} | \phi_i \rangle - \sum_j \epsilon_{ij} \langle \delta\phi_i | \phi_j \rangle \right\} + c.c. = 0 \quad (33)$$

Since the $\delta\phi_i$ can be varied independently, each term in the sum must vanish identically:

$$\left[\hat{h} + \hat{J} - \hat{K} \right] | \phi_i \rangle = \sum_j \epsilon_{ij} | \phi_j \rangle \quad (34)$$

By defining the Fock operator $\hat{F} = \hat{h} + \hat{J} - \hat{K}$, equation (34) takes the form

$$\hat{F} | \phi_i \rangle = \sum_j \epsilon_{ij} | \phi_j \rangle \quad (35)$$

This expression would have the form of an eigenvalue equation if ϵ_{ij} formed a diagonal matrix. As already stated, ϵ_{ij} is a Hermitian matrix, so it can be diagonalized by the application of a unitary transformation, *i.e.* a Hermitian matrix exists such that $\bar{\epsilon} = U^\dagger \epsilon U$ is diagonal and $\det U = e^{i\varphi}$.

$$\delta F = \int \frac{\delta F}{\delta f(x)} \delta f(x) dx.$$

The functional derivative can be calculated by using the usual limit of an incremental ratio:

$$\lim_{\epsilon \rightarrow 0} \frac{F[f(x) + \epsilon\phi] - F[f(x)]}{\epsilon} = \left[\frac{d}{d\epsilon} (F[f(x) + \epsilon\phi(x)]) \right]_{\epsilon=0}$$

in which $\phi(x)$ is an arbitrary function.

It is easy to prove that a Slater determinant is invariant under unitary transformation of the spin orbitals from which it is built. Let A be the matrix such that the Slater determinant ψ is written as $\psi = \frac{1}{\sqrt{n!}} \det A$. If \bar{A} corresponds to A after application of the transformation, for the well-known property of the determinant of the product of two matrices:

$$\bar{\psi} = \frac{1}{\sqrt{n!}} \det \bar{A} = \frac{1}{\sqrt{n!}} \det(UA) = \frac{1}{\sqrt{n!}} \det U \det A = \frac{1}{\sqrt{n!}} e^{i\varphi} \psi \quad (36)$$

Since the phase factor $e^{i\varphi}$ does not influence physical observables, we can state that there is no change in the physical significance of ψ . An important consequence of this observation is that the spin-orbitals that give a given electronic energy are by no means unique and no physical significance can be rigorously given to a particular set of spin orbitals. The Fock operator is also invariant under unitary transformations of the spin orbitals, as \hat{h} does not depend on the spin orbitals and the invariance of \hat{J} and \hat{K} can be verified by explicit calculations.

Equation (35) can thus be rewritten by taking the particular set of spin-orbitals for which ϵ_{ij} is diagonal, thus it reads:

$$\hat{F}\phi_i = \epsilon_i \phi_i \quad \hat{F} = \hat{h} + \hat{J} - \hat{K} \quad (37)$$

Equation (37) is known as the *canonical form of the Hartree-Fock equations* and the corresponding spin-orbitals are the *canonical orbitals*. In summary, we can say that every canonical spin-orbital must be an eigenfunction of the Fock operator to make the total energy of the Slater determinant stationary.

The derivation we presented started from the Slater determinant as an approximate form for the wavefunction and proceeded by looking for the optimal choice of spin-orbitals (according to the variational method) to construct the Slater determinant itself. The exact Hamiltonian of the system was considered for this process. There is an equivalent view of the Hartree-Fock theory that is more focused on the Hamiltonian. The Hartree-Fock Hamiltonian can be considered as the exact eigenfunction of an *approximate Hamiltonian*, which is simply the sum of the Fock operators for all n electrons:

$$\hat{H}_0 = \sum_i^n \hat{F}(i) \quad (38)$$

The variational energy of this fictitious system is *not* the expectation value of this approximate Hamiltonian operator \hat{H}_0 :

$$\langle \psi | \hat{H}_0 | \psi \rangle = \sum_i^n \langle \phi_i | \hat{h} + \hat{J} - \hat{K} | \phi_i \rangle, \quad (39)$$

but as we have already seen in equation (28) the variational energy is given by:

$$E_e = \sum_i^n \left\langle \phi_i \left| \hat{h} + \frac{1}{2} (\hat{J} - \hat{K}) \right| \phi_i \right\rangle \quad (40)$$

in which the factor $1/2$ avoids double counting electron-electron interactions. By treating the difference between the Hartree-Fock approximate Hamiltonian and the exact Hamiltonian with the perturbation theory, the first-order correction to energy is given by the expectation value of the perturbation operator $\hat{V} = \hat{H} - \hat{H}_0$:

$$\langle \psi | \hat{V} | \psi \rangle = -\frac{1}{2} \sum_i^n \langle \phi_i | \hat{J} - \hat{K} | \phi_i \rangle, \quad (41)$$

thus the variational energy coincides with the first-order perturbative energy.

2.6. The limits of the Hartree-Fock approach, correlation energy

Despite its relative simplicity, the Hartree-Fock method can be applied successfully to atomic calculations and it correctly predicts the existence of molecular binding. It usually gives qualitatively correct results for organic molecules. However, from the quantitative point of view, Hartree-Fock energies can have large deviations from experimental results and they are nowhere near the *chemical accuracy* of a few kcal mol⁻¹.

The difference between the exact energy of a multi-electron system and its Hartree-Fock energy must be negative, because of the variational principle. This difference is usually called *correlation energy* (E_{corr}):

$$E_{\text{corr}} = E - E_{\text{HF}} \quad (42)$$

The correlation energy can be understood qualitatively as the error due to the fact that electrons actually “see” each other as individual particles and *not* as an averaged potential.^{vi}

The correlation energy is traditionally decomposed into two contributions: the *dynamic correlation*, due to the instantaneous interaction between electrons, and the *static correlation*, due to the fact that two (or more) Slater determinants of similar energy may exist and the system is not well-described by a single-determinant wavefunction. In the latter case, the Hartree-Fock method may give qualitatively wrong results.

A variety of methods have been developed to include correlation in the multi-electron wavefunction, and they are collectively known as *post-Hartree-Fock* methods. For example the MC-SCF method (multi-configurational self-consistent field) uses a linear combination of Slater determinants instead of one only. Other post Hartree-Fock techniques are the configuration-interaction method (CI) in which the wavefunction is written as a linear combination of the Hartree-Fock wavefunction with higher-energy Slater determinants and the coefficient of the expansion are optimized according to the variational principle. Non-variational methods also

^{vi}It is often said that the Hartree-Fock method include in a primitive way electron correlation because two electrons having the same spin avoid being in the same point in space, due to the exchange term, which in turn is a consequence of the antisymmetric form of the Slater determinant. This phenomenon is often called *Fermi correlation* and it is not related to the correlation energy as it is commonly understood.

exist, such as the Møller-Plesset perturbation theory. The computational time needed to employ these methods generally scales unfavorably with the size of the system, so they are not often used for large systems, such as those considered in this thesis.

2.7. Fundamental ideas of DFT, the Hohenberg-Kohn theorems^{vii}

Density functional theory (DFT) is at present the most popular quantum method for the study of large-size chemical systems. DFT is not a wavefunction-based method, but it relies on a simpler mathematical object: the electron density. This quantity ($\rho(\mathbf{r})$) can be written as the integral of the square modulus of the wavefunction performed over $n-1$ spatial and spin coordinates and also over the residual spin coordinate:^{viii}

$$\rho(\mathbf{r}) = n \int |\psi(\mathbf{x}_1, \mathbf{x}_2, \dots, \mathbf{x}_N)|^2 ds_1 d\mathbf{x}_2 d\mathbf{x}_3 \dots d\mathbf{x}_n \quad (43)$$

Clearly, the integration of $\rho(\mathbf{r})$ all over the space yields the number of electrons (n):

$$n = \int \rho(\mathbf{r}) d\mathbf{r} \quad (44)$$

The use of the electron density as the basic variable instead of the wavefunction is legitimized by the two fundamental theorems of DFT, which bear the names of Hohenberg and Kohn.

The first Hohenberg-Kohn theorem states that *the external potential ($V(\mathbf{r})$) is determined, within a trivial additive constant, by the ground-state electron density $\rho(\mathbf{r})$* . Since $\rho(\mathbf{r})$ also gives the number of electrons, it follows that it determines ground-state wavefunction and all the other electronic properties of the system. Note that this theorem is valid without restrictions on the form of $V(\mathbf{r})$, so not only for the Coulomb potential.

The proof of this theorem is quite simple. We have already seen that n is given by the integral of ρ all over the space. Consider now density $\rho(\mathbf{r})$ of a non-degenerate ground-state. If there were two external potentials V and V' differing by other than a constant, each giving the same ground-state density ρ , there would be two different Hamiltonians \hat{H} and \hat{H}' with the two associated different ground-state wavefunctions ψ and ψ' . If the function ψ' is used as a trial function for the problem associated to \hat{H} , by the variational principle:

$$E_0 < \langle \psi' | \hat{H} | \psi' \rangle = \langle \psi' | \hat{H} | \psi' \rangle + \langle \psi' | \hat{H} - \hat{H}' | \psi' \rangle = E_0' + \int \rho(\mathbf{r}) [V(\mathbf{r}) - V'(\mathbf{r})] d\mathbf{r} \quad (45)$$

^{vii} This section and the following on DFT are based on the book by Parr and Yang.^[43]

^{viii} We change slightly the notation from here onwards: \mathbf{r}_i will indicate only spatial coordinates, \mathbf{x}_i will stand for the complete coordinate, comprising spatial and spin coordinates.

in which E_0 and E_0' are the ground-state energies for \hat{H} and \hat{H}' . Analogously, by using ψ as a trial function for the problem associated to \hat{H}' :

$$E_0' < \langle \psi | \hat{H}' | \psi \rangle = \langle \psi | \hat{H} | \psi \rangle + \langle \psi | \hat{H}' - \hat{H} | \psi \rangle = E_0 - \int \rho(\mathbf{r}) [V(\mathbf{r}) - V'(\mathbf{r})] d\mathbf{r} \quad (46)$$

Adding (45) to (46) would give $E_0 + E_0' < E_0' + E_0$, which proves the thesis.

If \hat{V} is uniquely determined by the density, in principle the problem can be solved without ambiguities knowing ρ only. The expression for the electronic energy can thus be rewritten as a function of the density:

$$E_e = T_e[\rho] + V_{Ne}[\rho] + V_{ee}[\rho] = \int \rho(\mathbf{r}) V(\mathbf{r}) d\mathbf{r} + F_{\text{HK}}[\rho] \quad (47)$$

in which F_{HK} is known as the Hohenberg-Kohn functional. An alternative statement of the first Hohenberg-Kohn theorem is thus the following: *there is an universal functional of the electron density $\rho(\mathbf{r})$ that allows to calculate the electronic energy, which is uniquely determined by the electron density itself for any external potential V .*

By defining the Coulomb functional, corresponding to the classical electron-electron repulsion:

$$J[\rho] = \frac{1}{2} \int d\mathbf{r}_1 d\mathbf{r}_2 \frac{1}{r_{12}} \rho(\mathbf{r}_1) \rho(\mathbf{r}_2) \quad (48)$$

the Hohenberg-Kohn functional can be written as the sum of three contributions:

$$F_{\text{HK}}[\rho] = T[\rho] + J[\rho] + E_{\text{NC}}[\rho] \quad (49)$$

in which E_{NC} is a *non-classical* term, that include most of the *exchange-correlation energy* that will be discussed later. The major issue here is that no exact expression is known for the Hohenberg-Kohn functional, so numerous different approximate functional forms have been proposed in the past and this is still an active field of research, as we will discuss more in detail later.

The second Hohenberg-Kohn theorem provides analogue of the variational theorem for the DFT. It states: *for a trial density $\tilde{\rho}(\mathbf{r})$ such that $\tilde{\rho}(\mathbf{r}) \geq 0$ and $\int \tilde{\rho}(\mathbf{r}) d\mathbf{r} = n$,*

$$E_0 \leq E_e(\tilde{\rho}) \quad (50)$$

in which E_e is the energy functional defined in equation (47). The proof starts with the first theorem, which guarantees that $\tilde{\rho}(\mathbf{r})$ unambiguously defines its potential $\tilde{v}(\mathbf{r})$, Hamiltonian \tilde{H} and ground-state wavefunction $\tilde{\psi}$. The latter can be taken as a trial wavefunction for the variational problem having external potential V , for the variational theorem $\langle \tilde{\psi} | \hat{H} | \tilde{\psi} \rangle \geq E_0$. By writing explicitly the expectation value of \hat{H} over $\tilde{\psi}$:

$$\langle \tilde{\psi} | \hat{H} | \tilde{\psi} \rangle = \int \tilde{\rho}(\mathbf{r}) V(\mathbf{r}) d\mathbf{r} + F_{\text{HK}}[\tilde{\rho}] = E_e[\tilde{\rho}] \geq E_0, \quad (51)$$

which proves the statement.

If the second Hohenberg Kohn-theorem holds, E_e is stationary with respect to the electron density, with the constraint that the integration of $\rho(\mathbf{r})$ gives the number of electrons n , its functional differential is thus zero:

$$\delta \left\{ E_e[\rho] - \mu \left[\int \rho(\mathbf{r}) d\mathbf{r} - n \right] \right\} = 0 \quad (52)$$

which corresponds to the Euler-Lagrange equation

$$\mu = \frac{\delta E_e[\rho]}{\delta \rho(\mathbf{r})} = V(\mathbf{r}) + \frac{\delta F_{\text{HK}}[\rho]}{\delta \rho(\mathbf{r})}, \quad (53)$$

which is alternative way to state the second Hohenberg-Kohn theorem.

2.8. The Kohn-Sham method

The main obstacle found in the application of DFT is that no exact expression is known for the functional F_{HK} .

Concerning the kinetic energy part $T[\rho]$ and the electron-electron interaction, explicit approaches have been attempted. The earliest of these approximations are based on the results obtained for the homogeneous electron gas (Thomas-Fermi model). Within this framework, the kinetic energy has a very simple dependence only on the density itself:

$$T[\rho] = C_F \int \rho^{\frac{5}{3}}(\mathbf{r}) d\mathbf{r} \quad C_F = \frac{3}{10} (3\pi^2)^{\frac{2}{3}} \quad (54)$$

Unfortunately, the simple formulas based on the homogeneous electron gas give reasonable results only for system having only slowly-changing electron densities, which is not the case for atoms and molecules.

In 1965 Kohn and Sham proposed an ingenious approach to overcome the difficulty of obtaining a correct functional form for $T[\rho]$ and thus paving the way for the use of DFT in chemistry. The fundamental idea of the Kohn-Sham method is to compute exactly the kinetic energy by introducing the use of orbitals, leaving a residual correction that can be handled separately.

A fictitious reference system of non-interacting electrons is considered, for which the corresponding kinetic energy can be simply calculated with a sum over the *occupied spin-orbitals*:

$$T_s[\rho] = \sum_i^n \left\langle \phi_i \left| -\frac{1}{2} \nabla^2 \right| \phi_i \right\rangle \quad (55)$$

Equation (55) is exact for a system composed of n noninteracting electrons described by a Slater determinant constructed starting from the ϕ_i . The complete Hamiltonian for this reference system would thus be:

$$\hat{H}_s = \sum_i^n \left(\frac{1}{2} \nabla_i^2 \right) + \sum_i^n V_s(\mathbf{r}_i) \quad (56)$$

in which there are no electron/electron repulsion terms. For this system, a ground-state wavefunction expressed as a Slater determinant ψ exists:

$$\psi(\mathbf{r}_1, \mathbf{r}_2, \dots, \mathbf{r}_n) = \frac{1}{\sqrt{n!}} \sum_P \sigma_P \hat{P} |\phi_1(\mathbf{r}_1) \phi_2(\mathbf{r}_2) \dots \phi_n(\mathbf{r}_n)| \quad (57)$$

in which the ϕ_i are the n lowest-energy eigenfunctions of the one-electron Hamiltonian \hat{h}_i :

$$\hat{h}_i \phi_i = \left[-\frac{1}{2} \nabla^2 + V_s(\mathbf{r}) \right] \phi_i = \epsilon_i \phi_i \quad (58)$$

With this definition of $T_s[\rho]$, equation (47) takes a new form:

$$E_e[\rho] = T_s[\rho] + J[\rho] + E_{xc}[\rho] \quad E_{xc}[\rho] = T[\rho] - T_s[\rho] + V_{ee}[\rho] - J[\rho] \quad (59)$$

E_{xc} is known as the *exchange-correlation functional* and it contains the difference between $T[\rho]$ and $T_s[\rho]$ and the non-classical contribution to electron/electron interactions E_{NC} .

The Kohn-Sham equations can be derived by a technique perfectly analogous to that we have exposed in detail for the Hartree-Fock equations. The method of Lagrange undetermined multipliers is used to impose that $E_e[\rho]$ is stationary with the constraint that the spin-orbitals are orthonormal, so the Lagrange auxiliary functional \mathcal{L} is set up:

$$\mathcal{L}[\{\phi_k\}] = E[\rho] - \sum_{i,j} \epsilon_{ij} \left[\langle \phi_i | \phi_j \rangle - \delta_{ij} \right] \quad (60)$$

Imposing $\delta\mathcal{L} = 0$ leads to equations similar to those of the Hartree-Fock theory:

$$\hat{h}_{\text{eff}} \phi_i = \left[\frac{1}{2} \nabla^2 + V_{\text{eff}} \right] \phi_i = \sum_i^n \epsilon_{ij} \phi_i \quad (61)$$

in which V_{eff} is known as the *Kohn-Sham effective potential*:

$$V_{\text{eff}}(\mathbf{r}) = V(\mathbf{r}) + \int \frac{\rho(\mathbf{r}')}{|\mathbf{r} - \mathbf{r}'|} d\mathbf{r}' + V_{xc}(\mathbf{r}) \quad (62)$$

As shown in the derivation of the Hartree-Fock equation, by a suitable unitary transformation of the ϕ_i (under which the Slater determinant is invariant, except for a phase factor, as we have already shown), ϵ_{ij} becomes a diagonal matrix, and equation (60) can be written in the form of a pseudo-eigenvalue problem:

$$\left[-\frac{1}{2} \nabla^2 + V_{\text{eff}} \right] \phi_i = \epsilon_i \phi_i \quad (63)$$

Just as in Hartree-Fock theory, the total energy is *not* the sum of orbital energies, but it is that given by equation (59), so explicitly:

$$E_e = \sum_i^n \epsilon_i - \frac{1}{2} \int \frac{\rho(\mathbf{r})\rho(\mathbf{r}')}{|\mathbf{r}-\mathbf{r}'|} d\mathbf{r}d\mathbf{r}' + E_{xc}[\rho] - \int V_{xc}(\mathbf{r})d\mathbf{r} \quad (64)$$

As the Kohn-Sham orbitals have an auxiliary nature – they are chosen in such a way that their sum of squares adds up to the total electron density – their associated energies have no obvious physical interpretation.

In summary, the Kohn-Sham equations have a similar form to that of the Hartree-Fock theory, except that the former contain a more general local potential $V_{\text{eff}}(\mathbf{r})$ and the latter contain a non-local operator (the exchange operator) in the one-electron Hamiltonian. The Kohn-Sham theory, indeed, is exact and provided that an exact form of E_{xc} was available, it would reduce the many-electron problem to the solution of one-electron equations naturally including correlation energy.

2.9. Approximating the exchange-correlation functional

The main limit of DFT is the fact that no exact form is known for the exchange-correlation functional E_{xc} . For practical purposes, the exchange-correlation functional is normally split into two contributions: the exchange one and the so-called correlation one:

$$E_{xc}[\rho] = E_x[\rho] + E_c[\rho] \quad E_x[\rho] = \int \rho(\mathbf{r})\epsilon_x[\rho]d\mathbf{r} \quad E_c[\rho] = \int \rho(\mathbf{r})\epsilon_c[\rho]d\mathbf{r} \quad (65)$$

in which ϵ_x and ϵ_c are single-particle contributions to energy and in general they are functionals of ρ , *i.e.* they depend on the whole function $\rho(\mathbf{r})$ and not only on its value at a given point.

In the crudest possible approximation, ϵ_x and ϵ_c may depend only on the value of ρ at the point considered, this is known as the local density approximations (LDA). This is equivalent to assuming that the exchange-correlation energy for a non-uniform system can be obtained by applying uniform gas formulae to an infinitesimal portion of a non-uniform electron distribution, and then integrating over the space. The LDA gives reasonable results for system having slowly-varying electron densities, but its shortcomings become evident for highly inhomogeneous densities in atoms and molecules, especially near the nuclei. LDA functionals are not accurate enough for molecular chemistry applications, however, in the past they were applied with success in many problems in the field of material science.

An improvement to the LDA is the use of models that take into account also the gradient of the density, and this is known as the generalized gradient approximation (GGA). There are several different possible parameterizations of the GGA. Some of these are semi-empirical, *i.e.* they are parametrized on experimental data (*e.g.* atomization energies), while other are derived from first principles only. As several combinations of exchange and correlation functionals are possible, two-part acronyms are often used to indicate these DFT methods. For example, one of the most popular exchange functional is the one developed by Becke^[13] by introducing a correction term to the LDA exchange functional (which in turn has been obtained from Dirac's treatment of the uniform electron gas) and it is commonly indicated with the letter "B". Among

the most popular correlation functionals, there are those proposed by Lee, Yang and Parr (commonly indicated as “LYP”)^[14] and by Perdew and Wang (referred as “PW91”).^[15] So the acronym BLYP indicates the functional having the Becke exchange functional and the LYP correlation functional, while BPW91 is the combination of the Becke exchange with the PW91 correlation.

Given that in the Kohn-Sham procedure Hartree-Fock-like orbitals are used, the exact Hartree-Fock exchange can be calculated and used to improve the DFT energy. The methods based on this idea are known as *hybrid methods*, and in general they perform better than “pure” functionals. For example, the popular B3LYP (Becke - three parameters – Lee Yang Parr) hybrid functional,^[16,17] which has been used for the calculations in Chapter IV of this thesis, uses Becke’s exchange functional and the LYP correlation functional in addition to exact Hartree-Fock exchange combined as follows:

$$E_{xc} = (1-A)E_x^{\text{LDA}} + AE_x^{\text{HF}} + B\Delta E_x^{\text{B}} + (1-C)E_c^{\text{LDA}} + CE_c^{\text{LYP}} \quad (66)$$

in which E_x^{LDA} is the LDA exchange energy, E_x^{HF} is the exact Hartree-Fock exchange, ΔE_x^{B} is Becke’s gradient-based correction to E_x^{LDA} , E_c^{LDA} is the VWN LDA correlation functional,^[18] and E_c^{LYP} is the LYP correlation functional presented above. The optimal A , B and C parameters have been determined by fitting a set of atomization energies, ionization potentials, proton affinities, and total atomic energies. Other functionals have non-empirical parameters, but the weights of the different contributions are established in such a way to respect some physical constraints. An example of this class of functionals is PBE0.^[19]

Hybrid functionals are generally quite successful for ground-state geometry optimization and ground-state properties, but in some case they fail for excited-state properties, Rydberg states and charge-transfer excitations. To overcome these problems, long range-corrected functionals have been proposed. In these cases the electron/electron interaction is split (while keeping continuity) into two contributions, for example using an expression of this kind:

$$\frac{1}{r_{12}} = \frac{1 - [\alpha + \beta \text{erf}(\mu r_{12})]}{r_{12}} + \frac{\alpha + \beta \text{erf}(\mu r_{12})}{r_{12}} \quad (67)$$

The two parts are then treated with different functional forms and the parameters of the splitting function optimized. An example of this approach is the functional CAM-B3LYP, in which the percentage of exact Hartree-Fock exchange varies from 19% (short range) to 65% (at long range).^[20]

An improvement over the GGA approximation can be made by including terms depending on the kinetic energy density in addition to the density and density gradients. These recently developed methods are known as metaGGA. In this class, we can quote the TPSS functional^[21] and the M06 family of functionals.^[22,23] The functionals of the latter class rely on heavy parametrization, for example the M06-L non-hybrid functional has 37 adjustable parameters (of which a few are not really independent, but are adjusted to satisfy the proper physical limits).^[22] This family also includes the hybrid functionals M06, M06-2X and M06-HF,

having increasingly high percentages of exact Hartree-Fock exchange (27%, 54% and 100% respectively).^[23]

Another approach that may drastically improve the accuracy of density functionals is the inclusion of contributions deriving from second-order Møller-Plesset perturbation theory (MP2), a post-Hartree-Fock method. It is worth noting that these *double hybrid* functionals have improved performance, but they have a computational cost that is comparable to MP2 itself. Among the functionals of this class, we may quote B2PLYP,^[24] mPW2PLYP^[25] and PBE0DH.^[26]

2.10. Empirical dispersion corrections^{ix}

One of the shortcomings of DFT is that most functionals cannot provide the correct asymptotic $\frac{1}{r^6}$ dependence of London dispersion forces. This is not generally true at intermediate distances, as the electron densities of the interacting fragments have some overlap and DFT can describe binding.

Qualitatively, it is well-known that London forces arise from *charge fluctuations* on one of the interacting fragments, which induces a dipole on the other fragment. From this viewpoint, it is clear that dispersion forces are a consequence of electronic correlation. More precisely, charge fluctuations can be viewed as electron excitations that cannot be described by standard Kohn-Sham DFT, which is a single-determinant theory.

A common approach to this problem is to evaluate dispersion interactions semi-classically and to add this interaction energy to the DFT energy (a sort of quantum mechanics – molecular mechanics approach). This approach is commonly called DFT-D (*dispersion-corrected DFT*). Several variants have been proposed, but normally the general form for the empirical dispersion energy (to be added to the DFT energy in the same way as nuclei/nuclei repulsion) is as follows:

$$E_{\text{disp}}^{\text{DFT-D}} = - \sum_{\text{AB}} \sum_{n=6,8,10,\dots} s_n \frac{C_n^{\text{AB}}}{r_{\text{AB}}^n} f_{\text{damp}}(r_{\text{AB}}) \quad (68)$$

in which the first sum runs over all the atom pairs, s_n is a damping factor that depends on the choice of the density functional, C_n^{AB} is the n -th order dispersion coefficient for the atom pair AB, r_{AB} is the distance between atom A and atom B and $f_{\text{damp}}(r_{\text{AB}})$ is a damping function. The latter term avoids near-singularities for small r_{AB} and mitigate double-counting effects, as intermediate-range dispersion is already described by DFT methods. Clearly, the additional computational cost due to this kind of empirical corrections is negligible compared to the calculation of DFT energy.

For the calculations presented in Chapter IV of this thesis, Grimme's D3 empirical correction for dispersion^[27] with the Becke-Johnson damping function^[28] has been used in

^{ix} A tutorial review on this topic has been made by Grimme.^[44]

conjunction with the B3LYP hybrid functional. The main features of the D3 model are the use of pair-specific coefficients that also depend on the coordination number (polarizability of atoms is heavily influenced by formal *hybridization*).

It is commonly stated that functionals of the M06 family (metaGGA hybrids) perform better than most other functionals for the description of dispersion interactions, at least on the medium-range scale. Indeed, they are heavily parameterized and the chosen training set includes non-covalent interactions with a large weight.^[22] Consequently, we have used no empirical correction for dispersion for the calculations presented in Chapter IV of this thesis, as the M06-2X functional has been employed.^[23]

2.11. Implicit solvation – the PCM model^x

To take into account in a cost-effective way the effects due to solvation, the polarizable continuum model (PCM) has been employed in the calculations presented in this thesis. The main idea at the basis of this model is that the solvent can be described as a polarizable dielectric medium that surrounds the molecular system of interest. As a consequence, mainly the *electrostatic* contribution to the solvation energy is taken into account. Effects due to specific solute/solvent interaction (*e.g.* hydrogen bonding interactions) are not described by this model.

The fundamental equation of the PCM model is Gauss's law of classical electrostatics:

$$\nabla \times [\epsilon(\mathbf{r})\nabla\Phi(\mathbf{r})] = -4\pi\rho_M(\mathbf{r}) \quad (69)$$

in which Φ is the electrostatic potential, ρ_M is the charge distribution of the solute and $\epsilon(\mathbf{r})$ is the dielectric permittivity. As regards the latter, a molecular cavity of appropriate shape is defined and ϵ is taken as 1 (the permittivity of vacuum) inside the cavity and equal to the dielectric constant of the solvent outside.

The electrostatic problem can be solved in terms of the potential Φ , which can be thought as the sum of the contribution due to the solute Φ_M plus the contribution of a fictitious surface charge distribution located on the surface Γ of the molecular cavity:

$$\Phi(\mathbf{r}) = \Phi_M(\mathbf{r}) + \Phi_\sigma(\mathbf{r}) \quad \Phi_\sigma(\mathbf{r}) = \int_\Gamma \frac{\sigma(\mathbf{s})}{|\mathbf{r} - \mathbf{s}|} d^2s \quad (70)$$

Once $\sigma(\mathbf{s})$ is determined, the electrostatic component to solvation free energy can be calculated:

$$\Delta G_{\text{solv}}^{\text{el}} = \frac{1}{2} \int_\Gamma \sigma(\mathbf{s}) \left[\int_V \frac{\rho_M(\mathbf{r})}{|\mathbf{r} - \mathbf{s}|} d^3r \right] d^2s. \quad (71)$$

The factor $\frac{1}{2}$ in equation (71) accounts for the polarization work necessary to create the charge distribution in the dielectric.

^x This topic has been reviewed by Mennucci and Tomasi^[45,46] and by Barone.^[47]

The molecular cavity is usually defined by taking a sphere for each atom of the solute having the appropriate van der Waals radius scaled by a factor appropriate to take into account the solvent-excluded volume. The surface integrals are performed by the boundary element method: the surface of the cavity is approximated by a finite number of *tesserae* according to a suitable algorithm.

It is worth noting that the solvent model adds term to the molecular Hamiltonian accounting for the polarization charges of the solvent and it adds a further layer of self-consistency to energy calculations.

2.12. Basis set and effective core potentials

In practical molecular calculations, molecular orbitals ϕ_i are written as the linear combination of atom-centered basis functions χ_i , which are reminiscent of the exact eigenfunctions of hydrogen-like atoms:

$$\phi_i(\mathbf{r}) = \sum_j c_{ij} \chi_j. \quad (72)$$

This approach is commonly known by the acronym LCAO (linear combination of atomic orbitals); it would be exact if infinitely many basis functions were used (*i.e.* the basis set would be complete). In practice, the expansion has to be truncated, so a judicious choice of the form of χ_i has to be made to achieve rapid convergence with a few terms.

Slater-type orbitals (STOs), which have the exact exponentially decaying radial part R_n , have the following form in polar coordinates (in atom-centered coordinates):

$$\chi(r, \theta, \varphi) = \frac{(2\zeta)^{\frac{n+\frac{1}{2}}{1}}}{[(2n)!]^{\frac{1}{2}}} r^{n-1} Y_{l,m}(\theta, \varphi) e^{-\zeta r} \quad R_n = r^{n-1} e^{-\zeta r}. \quad (73)$$

They perform well, but in practice the evaluation of bielectronic integrals is very computationally demanding. The well-known alternative is the use of gaussian-type orbitals (GTOs). These functions have the useful property that the product of two GTOs centered on different atoms is a finite sum of GTOs centered on a point along the axis connecting the two centers. This speeds up calculations, since the integrals can be evaluated analytically. In Cartesian, atom-centered coordinates, a gaussian-type function has the form:

$$\chi(r, \theta, \varphi) = N_{i,j,k,\alpha} x^i y^j z^k e^{-\zeta(x+y+z)^2}, \quad (74)$$

in which $N_{i,j,k,\alpha}$ is a normalization factor. In practice, using only one Gaussian function for each Slater-type orbital is an unsatisfactory approximation (GTOs do not have the good asymptotic behavior and they do not reproduce the cusp on the nucleus of STOs), so the exponential function composing the radial part of each STO is approximated by a finite sum of Gaussian functions. If the expansion coefficients are fixed (*i.e.* by fitting the corresponding STO), the resulting function is called *contracted gaussian*.

In this thesis, we have used Pople’s standard split-valence basis sets for light (first, second and third-row) atoms. In these basis sets, typically indicated with the $X\text{-}YZG$ notation, one contracted Gaussian composed of X primitive Gaussian is used for each core orbital and two uncontracted Gaussians, composed of Y and Z primitives each, are associated to each valence orbital. In this case, as each valence orbital is described by two contracted Gaussians, we have a *double zeta* basis set. Similarly constructed $X\text{-}YZW$ G and $X\text{-}YZWV$ G basis sets are denoted as *triple zeta* and *quadruple zeta* basis sets respectively. The addition of basis functions of higher angular momentum (*polarization functions*) – important for atoms having lone pairs in the Lewis model – is indicated by the symbol * and the addition of slowly-decaying *diffuse functions* – useful for the correct description of anions and other species having extended electron clouds – is indicated by the symbol +. For example, the 6-31+G* basis set is a *double zeta*, split valence basis set equipped with polarization and diffuse functions.

It is clear to chemical intuition that core electrons do not intervene directly in bonding and chemical reactivity. It is thus advantageous to replace them by an effective potential and to treat explicitly only the valence electrons. These potentials are known as *effective core potentials* (ECPs). The use of ECPs not only results in reduced computational effort, but it also allows to include relativistic effects indirectly. As we stated before, relativistic effects come into play for heavier atoms principally because of the electrons residing close to the nuclei and the parameters of the ECP can be fitted on atomic relativistic calculations. ECPs must take into account not only electrostatic effects, but also adherence to the Pauli principle (i.e., outlying atomic orbitals must be orthogonal to core orbitals having the same angular momentum).

In this thesis, the Los-Alamos LANL2 pseudopotential with the associated basis sets have been used for palladium and copper.

3. Selected theoretical tools used in this thesis

We will present briefly in this section three *interpretative* theoretical tools we used in this thesis to obtain chemically-relevant information from electronic structure theory calculations, *i.e.* the computation of thermodynamic functions from the results of electronic structure calculations, the distortion-interaction models and charge partition schemes (population analysis).

3.1. Calculation of thermodynamic functions

Electronic structure method calculations yield electronic energy values, which cannot be directly compared to typical experimentally measured data. Standard statistical mechanics is used to compute the thermal contributions to thermodynamic functions with perfect gas formulae in the framework of the harmonic oscillator – rigid rotator model.

We recall that the thermodynamic quantities can be expressed in terms of the canonical partition function Q . More in detail, the Helmholtz free energy A is the natural potential associated to the canonical ensemble and the internal energy U can be expressed easily in terms of the partition function:

$$A = -k_B T \ln Q \quad U = Nk_B T^2 \left(\frac{\partial \ln Q}{\partial T} \right)_V \quad (75)$$

in which T is the temperature as N the number of particles. From equations (75), all the thermodynamic functions are easily calculated. For example, entropy, enthalpy and Gibbs free energy:

$$S = \frac{U - A}{T} \quad H = U + PV = U + Nk_B T \quad G = A + PV = A + Nk_B T \quad (76)$$

The total partition function Q is written in a simple way for a perfect gas of indistinguishable particles as a function of the molecular partition function q : $Q = \frac{1}{N!} q^N$. The molecular partition function, in turn, is obtained by assuming additivity of the contributions to energy due to translation, rotation, vibration and electronic motion: $q = q_{\text{trans}} q_{\text{vib}} q_{\text{rot}} q_{\text{ele}}$. Here follow the expressions for the translational, vibrational and rotational molecular partition functions:

$$q_{\text{trans}} = \left(\frac{2\pi m k_B T}{h^2} \right)^{\frac{3}{2}} V \quad q_{\text{rot}} = \frac{\sqrt{\pi}}{\sigma_r} \left(\frac{T^{\frac{3}{2}}}{\sqrt{\Theta_{r,x} \Theta_{r,y} \Theta_{r,y}}} \right) \quad q_{\text{vib}} = \prod_k \frac{1}{1 - e^{-\Theta_{v,k}/T}} \quad (77)$$

in which the V is the volume, σ_r is the rotational symmetry number (related to the point group of the molecule), $\{\Theta_{r,i}\}$ are the rotational temperatures, $\Theta_{v,k}$ is the vibrational temperature associated to the normal mode k and the last product is understood to run over the normal modes of vibration of the molecule. The rotational temperatures are related to the canonical

moments of inertia (I_i) of the molecule: $\Theta_{r,x} = \frac{h^2}{8\pi^2 I_x k_B}$, and the vibrational temperatures to the frequencies of the normal modes: $\Theta_{v,k} = \frac{h\nu_k}{k_B}$. Since most molecules cannot access excited electronic states at room temperature, the electronic partition function is equal to the degeneracy of the ground state of the molecule (*i.e.* its spin multiplicity).

Gibbs free energy is without doubt the most informative thermodynamic quantity for typical lab conditions (constant temperature and pressure). As a general remark, we must point out that the reliable evaluation of entropic contributions to ΔG is particularly challenging for molecular systems in condensed phases. The standard approach we sketched above is oversimplified. The approximation that there are no intermolecular interaction is clearly not justified in the condensed phase, vibration in real systems are anharmonic and the contribution due to the degrees of freedom of the solvent, that may also be relevant, are not taken into account in any way. The net result of these rather crude approximations is that the entropic cost of molecular association is usually overestimated.

A number of empirical corrections have been proposed to alleviate this problem: scaling the entropic contribution by a fixed factor,^[29–31] approximating the translational entropy of the solute with that of the solvent,^[32,33] using a pressure that would make a perfect gas have the same density of the solvent.^[34] All these corrections are somehow arbitrary and they have not been validated by comparison with extensive experimental data sets, so we preferred not to use any of them in the calculations presented in this thesis. Nonetheless, we are conscious that the computed free energy of reactions implying change of molecularity is generally affected by a substantial error.

3.2. Distortion-interaction analysis

The distortion-interaction analysis (DIA), also known as activation-strain analysis, developed independently by Houk and Bickelhaupt,^[35–37] is a fragment-based approach that allows to separate the contribution to activation barriers due to structural deformations of the reactants and to the interaction of the deformed fragments. It can be performed only at the transition state or at multiple points of the reaction path connecting reagent and products (*e.g.* all along an intrinsic reaction coordinate calculation).

This model is most suited for a bimolecular reactions. The geometries of the reactants are first optimized separately and the sum of their energy is taken as zero. Then, the structure of the transition state is obtained and the activation energy barrier calculated. The geometries of the two reactants are then extracted from the transition state structure and their energies are obtained by single-point calculations. The energy difference between these fragments and that of the corresponding reactants is defined as the distortion energy of each reactant. The difference between the activation barrier and the total distortion energy defines the interaction energy, which is always negative. An illustration of this model is given graphically in Figure 4.

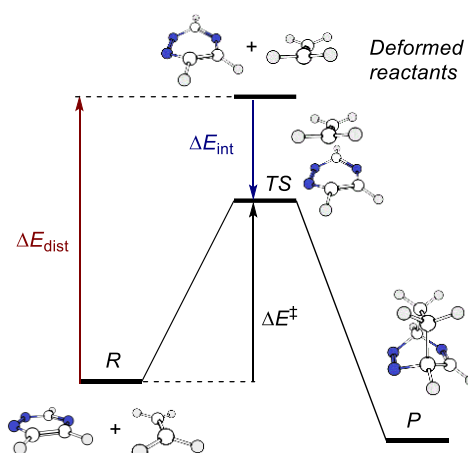


Figure 4 – Illustration of the distortion-interaction analysis for a model reaction (inverse electron-demand Diels-Alder addition of ethylene to 1,2,4-triazine).

DIA often allows establishing a relationship between reactivity, properties of the reactants and characteristics of the reaction mechanism. The interaction energy can often be interpreted by steric and electrostatic considerations and/or by frontier molecular orbital interaction, while the distortion energy is linked to structural features (*i.e.* to the rigidity of the reactants).

3.3. Population analysis^{xi}

It is usual in organic chemistry to rationalize reactivity pattern by reasoning in terms of atomic charges. The concept of *partial atomic charge* is somehow ill defined and it does not correspond naturally to a quantum mechanical observable. Numerous methods have been devised to compute atomic charges, but they necessarily have an arbitrary character.

The simplest method is perhaps the one proposed by Mulliken. If a wavefunction ψ is expressed as a single Slater determinant and each of the spin orbitals is expressed as a linear combination of atomic orbitals ϕ_i , the total number of electrons can be expressed (taking real functions for simplicity) as:

$$n = \sum_i^{\text{electrons}} \int [\phi_i(r_i)]^2 d\mathbf{r}_i = \sum_i^{\text{electrons}} \left(\sum_r c_{ir}^2 + 2 \sum_{r < s} c_{ir} c_{is} S_{rs} \right) \quad (78)$$

in which c_{ij} are the expansion coefficient and S_{rs} is the overlap matrix ($S_{rs} = \langle \phi_r | \phi_s \rangle$). Mulliken proposed that the electrons described by the first term in parenthesis “belong” to the atom on which the spin-orbital is centered and decided that the one associated to the second term in parenthesis are to be shared equally between the two centers r and s , thus the population associated to atom k is given by:

^{xi} For an overview of the most common population analysis, the book by Cramer can be advised.^[48]

$$n_k = \sum_i^{\text{electrons}} \left(\sum_{r \in k} c_{ir}^2 + \sum_{r,s \in k; r \neq s} c_{ir} c_{is} S_{rs} + \sum_{r \in k; s \notin k} c_{ir} c_{is} S_{rs} \right). \quad (79)$$

The Mulliken partial charge is then defined by $q_k = Z_k - n_k$ in which Z_k is the atomic number of atom k .

Mulliken charges have several shortcomings. The rule that “shared” electrons should be divided up equally between the atoms on which the sharing basis functions reside ignore the intuitive concept of electronegativity. The result of Mulliken analysis is very basis-set dependent, the most reasonable results are normally obtained with *small* basis sets. Meaningless results are obtained when basis sets are not balanced (*i.e.* on one atom are centered many more basis function than on another one).

To alleviate some of the problems of Mulliken population analysis, Lödwin^[38] proposed to transform the basis function into an orthonormal set by application of the inverse of the square root of the overlap matrix:

$$\chi_r = \sum_s S_{rs}^{-\frac{1}{2}} \varphi_s \quad (80)$$

The Mulliken procedure is then applied on the χ_i orbitals so obtained. Lödwin charges are less sensitive to the choice of basis set, but they become unstable for very large ones. This difficulty is due to the fact that in a large basis set only a few atomic orbitals are really important, but the Lödwin procedure distorts them all in a similar fashion to achieve orthonormality.

Much of those troubles are resolved by the natural population analysis (NPA) scheme proposed by Weinhold.^[39,40] Without entering into the mathematics involved, natural atomic orbitals (NAOs) are constructed in such a way that they meet the simultaneous requirement of orthonormality and maximum occupancy. They mostly retain one-centre character, and thus they are well-suited for describing the molecular electron density around each atomic centre. They often correspond to the elementary Lewis structure diagram, in the sense that their occupancy for closed-shell molecules is almost always close to 2. The atomic partial charge based on NAOs are not much affected by the choice of a basis set, but even converge to a stable value with increasing basis-set size.

As a general remark, it is better to analyse *trends* in partial atomic charges due to the variation of some parameter, while limited insight can be gained by considering absolute values.

4. References

- [1] W. R. Dolbier, *Guide to Fluorine NMR for Organic Chemists*, John Wiley & Sons, Hoboken, NJ, USA, **2009**.
- [2] W. He, F. Du, Y. Wu, Y. Wang, X. Liu, H. Liu, X. Zhao, *J. Fluor. Chem.* **2006**, *127*, 809–815.
- [3] N. M. Do, M. A. Olivier, J. J. Salisbury, C. B. Wager, *Anal. Chem.* **2011**, *83*, 8766–8771.
- [4] F.-F. Zhang, M.-H. Jiang, L.-L. Sun, F. Zheng, L. Dong, V. Shah, W.-B. Shen, Y. Ding, *Analyst* **2015**, *140*, 280–286.
- [5] O. Kühn, *Phosphorus-31 NMR Spectroscopy - A Concise Introduction for the Synthetic Organic and Organometallic Chemist*, Springer-Verlag, Berlin - Heidelberg, **2008**.
- [6] P. S. Pregosin, R. W. Kunz, *31P NMR and 13C NMR of Transition Metal Phosphine Complexes - NMR Basic Principles and Progress - NMR Grundlagen Und Fortschritte*, Springer-Verlag, Berlin - Heidelberg - New York, **1978**.
- [7] T. R. Hoye, B. M. Eklov, T. D. Ryba, M. Voloshin, L. J. Yao, *Org. Lett.* **2004**, *6*, 953–6.
- [8] T. R. Hoye, B. M. Eklov, M. Voloshin, *Org. Lett.* **2004**, *6*, 2567–2570.
- [9] T. L. Hwang, A. J. Shaka, *J. Magn. Reson. Ser. A* **1995**, *112*, 275–279.
- [10] W. J. Geary, *Coord. Chem. Rev.* **1971**, *7*, 81–122.
- [11] A. Jutand, *Eur. J. Inorg. Chem.* **2003**, *2003*, 2017–2040.
- [12] K. W. Pratt, V. F. Koch, Y. C. Wu, P. A. Berezansky, *Pure Appl. Chem.* **2001**, *73*, 1783–1793.
- [13] A. D. Becke, *Phys. Rev. A* **1988**, *38*, 3098–3100.
- [14] C. Lee, W. Yang, R. G. Parr, *Phys. Rev. B* **1988**, *37*, 785–789.
- [15] J. P. Perdew, in *Electron. Struct. Solids '91* (Eds.: P. Eschrig, H. Ziesche), Akademie Verlag, Berlin (Germany), **1991**, pp. 11–20.
- [16] A. D. Becke, *J. Chem. Phys.* **1993**, *98*, 5648–5652.
- [17] P. J. Stephens, F. J. Devlin, C. F. Chabalowski, M. J. Frisch, *J. Phys. Chem.* **1994**, *98*, 11623–11627.
- [18] S. H. Vosko, L. Wilk, M. Nusair, *Can. J. Phys.* **1980**, *58*, 1200–1211.
- [19] C. Adamo, V. Barone, *J. Chem. Phys.* **1999**, *110*, 6158–6170.
- [20] T. Yanai, D. P. Tew, N. C. Handy, *Chem. Phys. Lett.* **2004**, *393*, 51–57.
- [21] J. Tao, J. P. Perdew, V. N. Staroverov, G. E. Scuseria, *Phys. Rev. Lett.* **2003**, *91*, 146401.
- [22] Y. Zhao, D. G. Truhlar, *J. Chem. Phys.* **2006**, *125*, 194101.
- [23] Y. Zhao, D. G. Truhlar, *Theor. Chem. Acc.* **2008**, *120*, 215–241.
- [24] S. Grimme, *J. Chem. Phys.* **2006**, *124*, 34108.
- [25] T. Schwabe, S. Grimme, *Phys. Chem. Chem. Phys.* **2006**, *8*, 4398.
- [26] E. Brémont, C. Adamo, *J. Chem. Phys.* **2011**, *135*, 24106.
- [27] S. Grimme, J. Antony, S. Ehrlich, H. Krieg, *J. Chem. Phys.* **2010**, *132*, 154104.
- [28] S. Grimme, S. Ehrlich, L. Goerigk, *J. Comput. Chem.* **2011**, *32*, 1456–1465.
- [29] J. Cooper, T. Ziegler, *Inorg. Chem.* **2002**, *41*, 6614–6622.
- [30] S. Tobisch, T. Ziegler, *J. Am. Chem. Soc.* **2004**, *126*, 9059–9071.
- [31] R. Raucoles, T. de Bruin, P. Raybaud, C. Adamo, *Organometallics* **2009**, *28*, 5358–5367.
- [32] M. Mammen, E. I. Shakhnovich, J. M. Deutch, G. M. Whitesides, *J. Org. Chem.* **1998**, *63*, 3821–3830.
- [33] Y. Luo, Y. Luo, J. Qu, Z. Hou, *Organometallics* **2011**, *30*, 2908–2919.
- [34] R. L. Martin, P. J. Hay, L. R. Pratt, *J. Phys. Chem. A* **1998**, *102*, 3565–3573.
- [35] I. Fernández, F. M. Bickelhaupt, *Chem. Soc. Rev.* **2014**, *43*, 4953–4967.
- [36] L. P. Wolters, F. M. Bickelhaupt, *WIREs Comput. Mol. Sci.* **2015**, *5*, 324–343.
- [37] D. H. Ess, K. N. Houk, *J. Am. Chem. Soc.* **2007**, *129*, 10646–10647.
- [38] P. Löwdin, *J. Chem. Phys.* **1950**, *18*, 365–375.
- [39] J. P. Foster, F. Weinhold, *J. Am. Chem. Soc.* **1980**, *102*, 7211–7218.
- [40] A. E. Reed, R. B. Weinstock, F. Weinhold, *J. Chem. Phys.* **1985**, *83*, 735.
- [41] R. McWeeny, *Methods of Molecular Quantum Mechanics*, Academic Press, San Diego (CA), **1992**.
- [42] A. Szabo, N. S. Ostlund, *Modern Quantum Chemistry - Introduction to Electronic Structure Theory*, Dover, Mineola (NY), **1989**.
- [43] R. G. Parr, W. Yang, *Density-Functional Theory of Atoms and Molecules*, Oxford University Press, New York, USA, **1989**.
- [44] S. Grimme, *WIREs Comput. Mol. Sci.* **2011**, *1*, 211–228.
- [45] J. Tomasi, B. Mennucci, R. Cammi, *Chem. Rev.* **2005**, *105*, 2999–3093.
- [46] B. Mennucci, *WIREs Comput. Mol. Sci.* **2012**,

- 2, 386–404.
- [47] M. Cossi, G. Scalmani, N. Rega, V. Barone,
J. Chem. Phys. **2002**, *117*, 43–54.
- [48] C. J. Cramer, *Essentials of Computational*

Chemistry Theories and Models, John Wiley
& Sons, Chichester, UK, **2004**.

CHAPTER II

Multiple Roles of Isocyanides in Palladium-Catalyzed Imidoylative Couplings: A Mechanistic Study

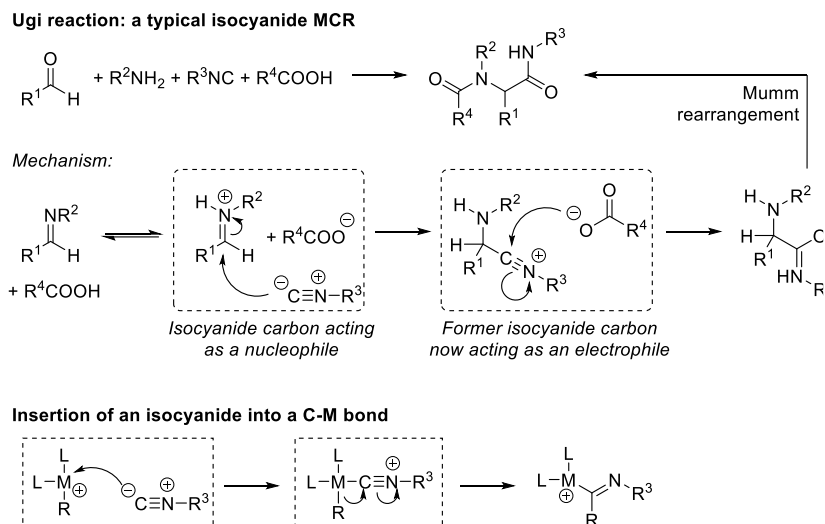
The work exposed in this chapter resulted in a publication:

L. A. Perego,* P. Fleurat-Lessard, L. El Kaïm, I. Ciofini,* L. Grimaud,*
Multiple Roles of Isocyanides in Palladium-Catalyzed Imidoylative Couplings: A Mechanistic Study,
Chem. Eur. J. **2016**, 22(43), 15491-15500.

1. Context of the Study

1.1. Introduction

Isocyanides have become extremely valuable building blocks in present-day organic chemistry. They have a key role in combinatorial chemistry, principally due to their use in the Passerini and Ugi multicomponent reactions (MCRs) and their innumerable variations and extensions.^[1-4] Modern isocyanide-based MCRs encompass an impressive diversity of bond-making processes giving a rapid access to libraries of compounds, among which we can reckon peptidomimetics, aromatic and non-aromatic heterocycles and numerous natural product-like scaffolds.^[1-4]

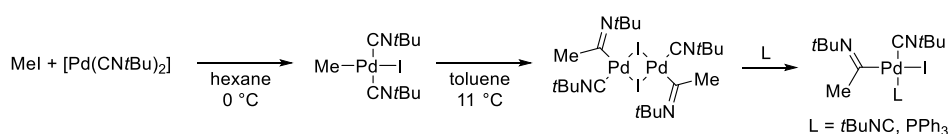


Scheme 1 - Two typical reactions of isocyanides: Ugi MCR and insertion into a carbon metal bonds, showing the same sequential nucleophilic/electrophilic reactivity pattern for the isocyanide carbon.

The distinctive feature of isocyanides, which accounts for their versatility in MCRs, is the presence of a carbon atom that can sequentially act as a nucleophile and as an electrophile, allowing the consecutive participation of an electrophilic and a nucleophilic reactant and thus the formation of two new covalent bonds. In a conceptually related fashion, isocyanides can insert across carbon-metal bonds, in the same way as CO, carbenes and carbenoid species; indeed, isocyanides can be considered as aza-analogues of carbon monoxide, since they are isoelectronic to the latter molecule. This process is formally analogous to that associated to MCRs, as it can be thought to take place by an initial coordination to the metal center, in which the isocyanide is formally acting as a nucleophile, followed by addition of a nucleophilic species (either already coordinated to the metal in an inner-sphere process, or coming from the exterior, in an outer-sphere process).

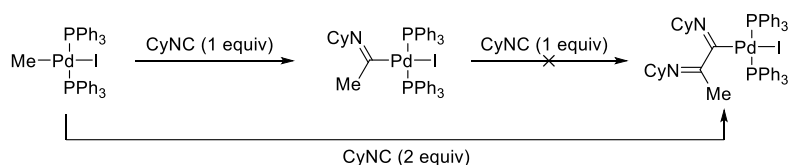
1.2. Early studies on the insertion of isocyanides in the C-Pd bond

The first studies concerning isocyanide insertion into the C-Pd bond were performed on isolated organopalladium complexes long before the development of the related catalytic reactions. This process was described as early as in 1969 by Otsuka^[5] and in 1970 by Yamamoto and Yamazaki.^[6] In his pioneering study, Otsuka reported that on adding MeI to the Pd(0) complex $[\text{Pd}(\text{CN}t\text{Bu})_2]$ at 0 °C oxidative addition took place, leading to the square planar *trans*- $[\text{MePd}(\text{CN}t\text{Bu})_2\text{I}]$. Increasing the temperature to 11 °C resulted in insertion of one of the coordinated *t*BuNC in the CH₃-Pd bond, giving a complex of stoichiometry $[(\text{MeC}=\text{N}t\text{Bu})\text{Pd}(\text{CN}t\text{Bu})\text{I}]$, that is probably a dimer. The latter species was not stable enough to be isolated, but on adding a ligand L (L = *t*BuNC or PPh₃), stable square-planar $[(\text{MeC}=\text{N}t\text{Bu})\text{PdL}(\text{CN}t\text{Bu})\text{I}]$ complexes were obtained (Scheme 2).^[5]

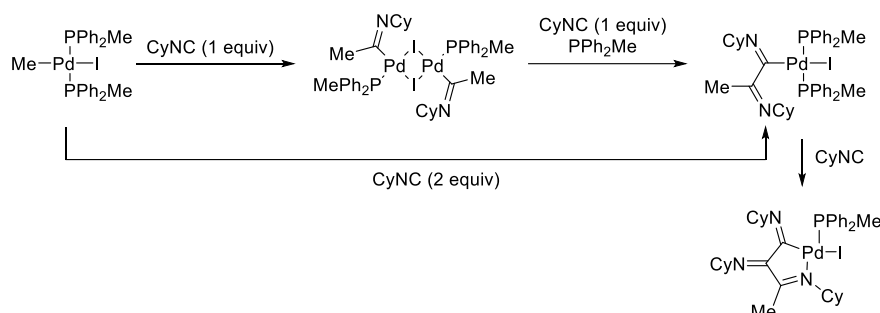


Scheme 2 – First report concerning the insertion of an isocyanide into the C-Pd bond, as reported by Otsuka and coworkers.^[5]

Yamamoto and Yamazaki studied the interaction of *trans*- $[(\text{MePd}(\text{PPh}_2\text{R})_2)\text{I}]$ (R = Ph, Me) with CyNC. In this case, the outcome of the reaction was dependent on the nature of the phosphine ligand. For R = Ph, the reaction with a stoichiometric amount of CyNC resulted in a clean mono-insertion of the isocyanide and the product so obtained was stable towards excess CyNC (Scheme 3). However, treatment of the same starting material with two equivalent of CyNC gave easily a double insertion of isocyanide (Scheme 3). As a consequence, the authors concluded that double insertion was not proceeding in a stepwise fashion. Differently, for R = Me, successive insertion of one, two or three molecules of CyNC could be performed (Scheme 4). It is especially remarkable that the mono-inserted product could be isolated in a dimeric form featuring only a PPh₂Me ligand and that the tris-imino complex resulting from triple insertion of CyNC had a chelate structure featuring a five-membered ring in which the terminal imino nitrogen atom is coordinated to palladium (Scheme 4).^[6]



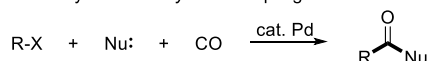
Scheme 3 – Reactions of *trans*- $[(\text{CH}_3)\text{Pd}(\text{PPh}_3)_2\text{I}]$ with CyNC.^[6]



Scheme 4 – Reactions of $\text{trans-}[(\text{CH}_3)\text{Pd}(\text{PPh}_2\text{Me})_2\text{I}]$ with CyNC .^[6]

The development of Pd-catalyzed reactions involving CO incorporation (*i.e.* carbonylative couplings, Scheme 5, a) has been undertaken since the 1980s, approximately as the same time as ordinary Pd-catalyzed cross-couplings.^[7–17] Since isocyanides behave rather like an electron-rich variant of CO, as already stated, and their stoichiometric reactions with organometallic species are known since the late Sixties,^[5,6,18] it may be expected that Pd-couplings involving isocyanide insertion (*i.e.* imidoylative couplings, Scheme 5, b) would have been developed simultaneously as carbonylative couplings. Nonetheless, this field started to flourish almost two decades later, and most of the fundamental studies in this domain have been published after 2000. Two reviews, appeared in 2013, summarize the main recent advances on this topic.^[19,20] A review published in 2014 cover more in general insertion and condensation reactions initiated by complexation of isocyanides with electrophilic centers.^[21] A general overview of metal-mediated and metal catalyzed reaction of isocyanides, covering the literature appeared before 2014, has been given in a very comprehensive survey by Kukushkin and coworkers, who have also carefully indexed previous reviews and reference works.^[22] Metal-mediated C-H activation processes involving isocyanide insertion have been also reviewed recently.^[23]

a) Pd-catalyzed *carbonylative* couplings



b) Pd-catalyzed *imidoylative* couplings



Scheme 5 – Comparison between Pd-catalyzed carbonylative and imidoylative cross couplings.

As observed by Orru and coworkers,^[20] the lateness of the development of imidoylative Pd-catalyzed coupling is rather surprising, considering the significant practical advantages of isocyanides compared to CO. Isocyanides are easily handled liquid or solids – albeit frequently foul-smelling –, while special equipment is needed to deal with CO, which is a notoriously toxic gas. Moreover, isocyanides offer a further diversity point represented by the organic residue bound to nitrogen, thus offering more flexibility in designing new transformations.

A possible explanation for the delayed interest in this chemistry may be the tendency of isocyanides to undergo multiple insertions into the C-Pd bond, which was already underlined in the pioneering work by Yamamoto and Yamazaki presented above (Scheme 4).^[6] Poly-insertion

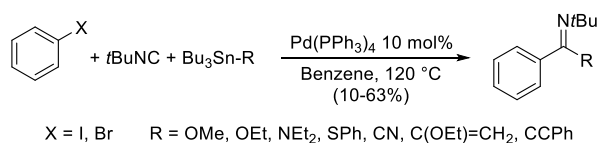
is usually dependent on several factors, such as the nature of the organic residue bound to palladium and on the isocyanide, the ligand and the solvent.^[6,24–26] Usually insertion cannot take place more than three times, as stable chelates are formed, as reported in the example in Scheme 4,^[6,26,27] but polymerization can also occur.^[18,28–32]

Probably due to the reasons exposed above, many of the literature examples of Pd-catalyzed imidoylative couplings involve sterically hindered isocyanides (most used are the commercially available CyNC, *t*BuNC, 1,1,3,3-tetramethylbutyl isocyanide – also known as Walborsky's reagent or *tert*-octyl isocyanide – and 2,6-dimethylphenyl isocyanide), which are intrinsically less prone to parasitic reactions due to poly-insertion, or involve intramolecular five- or six-membered ring-closure with a tethered nucleophile.^[19,20] This last strategy most likely shortens the life-time of any imidoypalladium intermediate and so disfavors multiple additions of the isocyanide.

1.3. Palladium catalyzed imidoylative couplings

A comprehensive survey of the published Pd-catalyzed reactions involving isocyanide insertion is beyond the scope of this introduction and we may refer the interested reader to the several excellent reviews covering this field.^[19–22,33] Nevertheless, some selected examples will be presented and commented here to give a sense of the capabilities of this powerful methodology in organic synthesis and a historic timeline of its development.

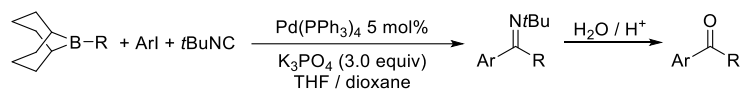
The first palladium-catalyzed imidoylative coupling was described by Kosugi and Migita in 1986.^[34] They reported that Pd(PPh₃)₄ catalyzes the reaction of bromobenzene and iodobenzene with several different organotin reagents (tributyltin alkoxides, amides, thiophenolates, cyanides, enol ethers, and acetylides) in the presence of *t*BuNC to give the corresponding imidoylation products (imidates, amidines, thioimidates, imidoyl cyanides, and imines, respectively) in poor to fair yields (Scheme 6). The reaction failed when the R-SnBu₃ reagent had a less polar R-Sn bond, and notably for R = H, CH₂=CH, Ph, All.



Scheme 6 – Imidoylative couplig of iodobenzene and bromobenzene with organotin nucleophiles.^[34]

It was not until 1992 that Suzuki and Miyaura described an imidoylative version of their eponymous coupling reaction.^[35] They showed that iodoarenes react with *B*-alkyl-9-BBN (BBN = 9-borabicyclo[3.3.1]nonane) derivatives in the presence of *t*BuNC, K₃PO₄ as a base and a catalytic amount Pd(PPh₃)₄ to give *N*-*tert*-butylketimines, which can be hydrolyzed to the corresponding ketones (Scheme 7). Some interesting observations were reported: 1) *B*-alkyl-9-BBN derivatives cannot be replaced by trialkylboranes, which give no ketimine product; 2) when (*E*)-1-iodohexene was employed as an electrophile instead of a iodoarene, the expected α,β -unsaturated ketimine was not obtained, but (*E*)-*N*-*tert*-butyl-2-heptenamide was formed instead; 3) most importantly, the molar ratio between *B*-alkyl-9-BBN and *t*BuNC had a

great influence on the outcome of the reaction. As regards the latter observation, the yield of the model reaction of *B*-octyl-9-BBN with PhI dropped gradually from 97% for a 1:1 ratio to zero for a ratio of 1:1.5. The authors interpreted these results by observing that a strong adduct is formed between the organoboron reagent and *t*BuNC (Scheme 8), which may act as a reservoir that releases only a small amount of free isocyanide in the reaction mixture. No explanation of the reason why excess *t*BuNC inhibits catalyst turnover was proposed.

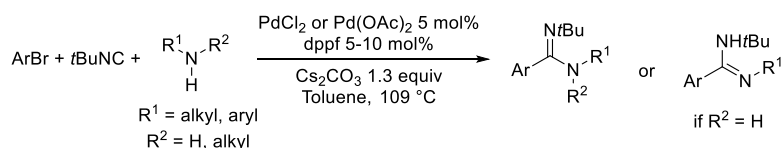


Scheme 7 – Imidoylative Suzuki coupling of *B*-alkyl-9-BBN derivatives.



Scheme 8 – Complex formation between *B*-alkyl-9-BBN derivatives and *t*BuNC.

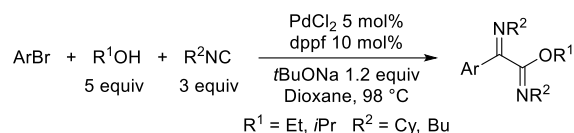
Only in 2000 Whitby and coworkers reexamined the transformation originally described by Kosugi and Migita (Scheme 6),^[34] and they demonstrated that trialkylstannylamines can be replaced by primary or secondary amines in the presence of Cs₂CO₃ and a Pd(II)/dppf precatalyst system (Scheme 9).^[36] Unfortunately, this reaction was limited to *t*BuNC, as yields were severely diminished when CyNC was employed instead. The authors did not propose any explanation for the latter experimental observation.^[36] However, in a subsequent report concerning the extension of this reaction to sodium alkoxides and thiolates as nucleophiles to obtain imidates and thioimidates respectively (Scheme 10),^[37] they observed that the double insertion of the isocyanide was a major side reaction. Slow addition of this reagent was thus suggested, enabling the use of unhindered isocyanides such as BuNC and BnNC. This precaution was unnecessary when electron-poor bromoarenes were employed as substrates. The imidates so obtained could be converted to amidines by a one-pot sequence involving amines in the presence of acid catalysts (Scheme 10), thus providing access to the amidines that could not be obtained by the direct method (Scheme 9). Alkenyl bromides can also be employed as substrates in the same conditions as bromoarenes, giving access to α,β -unsaturated amidines and imidates.^[38] By slightly varying the reaction conditions, the aforementioned double insertion could become the main pathway, thus providing preparatively useful yields of α -aminoimidates (Scheme 11).^[39]



Scheme 9 – Synthesis of amidines by the imidoylative coupling of bromoarenes and amines.

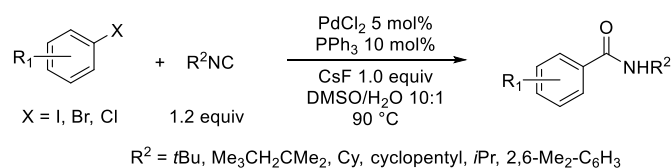


Scheme 10 – Synthesis of imidates and thioimidates by imidoylative coupling of bromoarenes with sodium alkoxydes and thiolates.^[37]



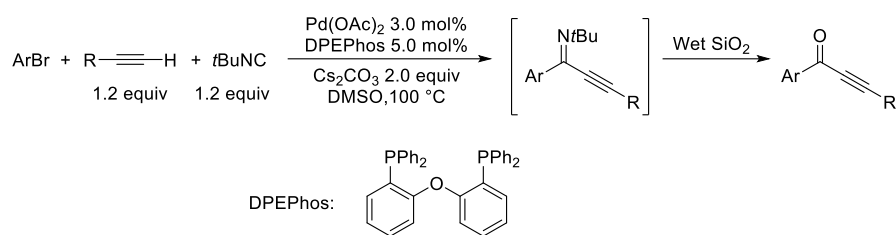
Scheme 11 – Synthesis of α -aminoimidates by double insertion of isocyanides.^[39]

After these early reports by Whitby, comparatively few three-component imidoylative couplings have been reported. In 2011 Jiang described conditions in which water can act as the nucleophile, resulting in an effective strategy for the synthesis of secondary amides from haloarenes (Scheme 12).^[40] Iodo-, bromo- and chlorobenzenes could be employed, albeit the latter generally gave moderate yields; alkenyl and benzyl bromides were also suitable substrates. The reaction appears less general regarding the isocyanide, as only tertiary, secondary and sterically hindered aromatic *N*-substituents were employed in the examples illustrating this methodology.^[40]

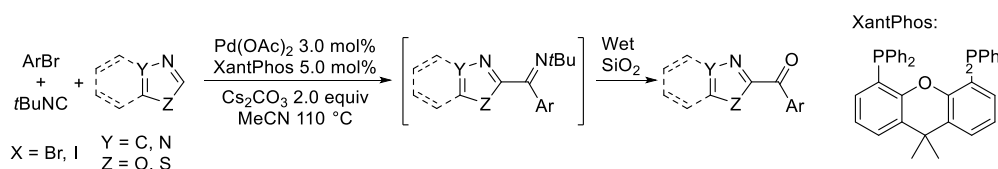


Scheme 12 – Pd-catalyzed amidation of haloarenes described by Jiang.^[40]

In addition to the Suzuki coupling described above (Scheme 7),^[35] few other reactions involving carbon nucleophiles and isocyanide insertion have been reported. An imidoylative version of the Sonogoshira coupling employing the diphosphine DPEPhos has been described (Scheme 13).^[41] α -Acetylenic ketones were obtained after hydrolysis of the *N*-*tert*-butyl ketimines first formed. Similar conditions employing the related ligand XantPhos can be used to effect the direct arylation of azoles (1,3,4-oxadiazoles, oxazoles, benzoxazoles and their sulfur analogues) at the C2 position with the insertion of *t*BuNC (Scheme 14). A parallel can often be established between the reactivity of these azole C2-H moieties and the C-H of terminal alkynes, and indeed they have comparable acidity (*e.g.* $\text{p}K_a = 28.8$ for phenylacetylene^[42] and $\text{p}K_a = 28.0$ for 4-methyloxazole^[43] in DMSO).

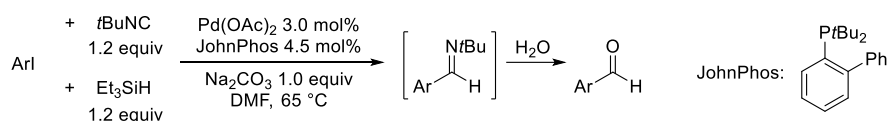


Scheme 13 – Imidoylative variant of the Sonogashira coupling involving *t*BuNC.^[41]



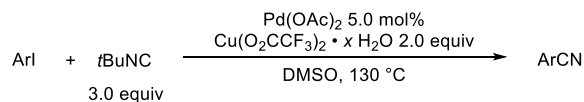
Scheme 14 – Imidoylative direct arylation of azoles.^[44]

The intermediate imidoylpalladium complex can also be trapped by the hydride donor Et_3SiH , thus giving access to aldimines that are not isolated, but immediately hydrolyzed to aldehydes starting from iodoarenes and *t*BuNC (Scheme 15). The monodentate, bulky electron-rich ligand JohnPhos proved to be especially efficient for this reaction, but also bidentate ligands such as 4-bis(diphenylphosphino)butane (dppb) could be employed.^[45]



Scheme 15 – Pd-catalyzed formylation of iodoarenes by insertion of *t*BuNC.^[45]

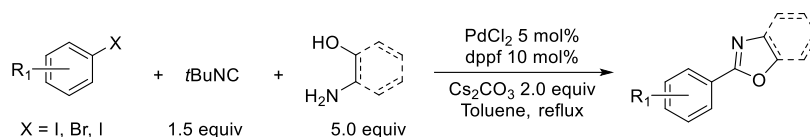
In a related transformation, *t*BuNC can formally act as a cyanide donor, thus converting iodoarenes into nitriles. A more than stoichiometric amount of copper(II) trifluoroacetate is necessary, in addition to $\text{Pd}(\text{OAc})_2$, to accomplish this transformation. The reaction does not proceed by initial formation of a *N-tert*-butyl benzamide that is dealkylated and dehydrated *in situ*, since the authors verified that this putative intermediate does not convert into the nitrile in the reaction conditions. Direct dealkylation of an intermediate imidoyl-palladium(II) complex was thus proposed.^[46]



Scheme 16 – Pd-catalyzed, Cu-mediated cyanation of iodoarenes with *t*BuNC.^[46]

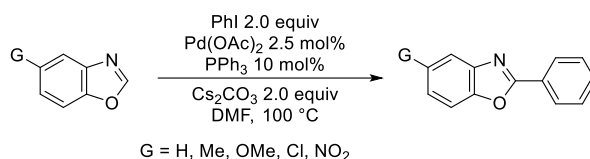
β -Aminoalcohols and *ortho*-aminophenols can also act as nucleophiles in conditions close to those originally described by Whitby (Scheme 10). In this case, however, cyclization takes place spontaneously and oxazolines and benzoxazoles are isolated directly (Scheme 17)^[47] The related reaction of *ortho*-aminothiophenols giving benzothiazoles has been shown to proceed by an entirely different mechanism, since simply heating *ortho*-aminothiophenol with *t*BuNC at 120 °C in the absence of palladium salts gives unsubstituted benzothiazole with concurrent loss

of the *t*Bu group.^[48] The 2-arylbenzothiazole is thus produced by subsequent direct arylation with activation of the C2-H bond, which is most efficient in the presence of Cu(I) salts.^[48]



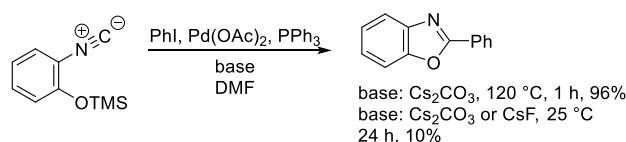
Scheme 17 – Pd-catalyzed synthesis of oxazolines and benzoxazoles from β -aminoalcohols and *ortho*-aminophenols.

Related to this transformation, it is worth mentioning that in 2007 Zhuravlev and coworkers^[49] investigated some mechanistic aspects of the palladium-catalyzed direct arylation of benzoxazoles at C2. A Hammett plot was obtained for the direct arylation of several 5-substituted benzoxazoles (Scheme 18), an excellent correlation was found for σ_{-} , a poorer correlation for σ_{p} and no correlation with σ_{+} , σ and σ_{m} constants^[50]. Electron-withdrawing groups significantly accelerated the reaction and a positive slope was found ($\rho = 2.8$) and measurable deuterium kinetic isotope effect was detected.^[49] The authors interpreted these observations by noticing that the C2-H position of benzoxazole is acidic and its conjugate base exists predominantly as a 2-isocyanophenolate. They thus proposed that the reaction proceeds by a ring-opening pathway, in which the reactive species is the 2-isocyanophenolate itself, as it would be consistent with the Hammett correlation found with σ_{-} .

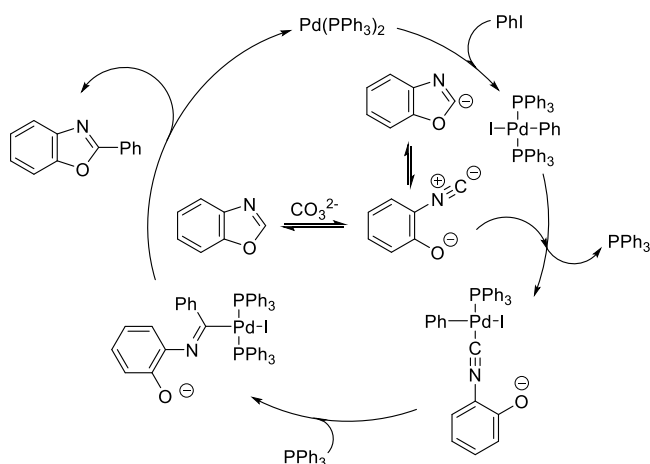


Scheme 18 – Palladium-catalyzed direct arylation reaction of benzoxazoles.^[49]

The validity of this pathway was also verified by subjecting 2-(trimethylsilyloxy)phenyl isocyanide to the direct arylation conditions. At 120 °C the reaction was completed in less than 1 h and it could also be performed at room temperature, albeit in longer times and with CsF as the base (Scheme 19).^[49] The mechanism that would allow to explain the experimental observations is represented in Scheme 20.



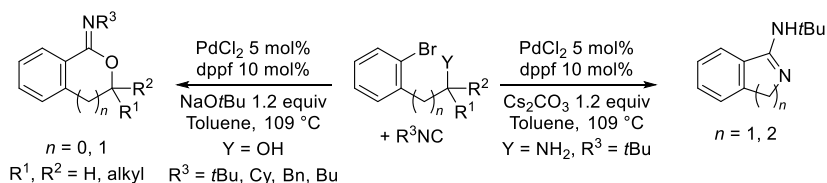
Scheme 19 – Cyclization of 2-(trimethylsilyloxy)phenyl isocyanide with iodobenzene to give 2-phenylbenzoxazoles.^[49]



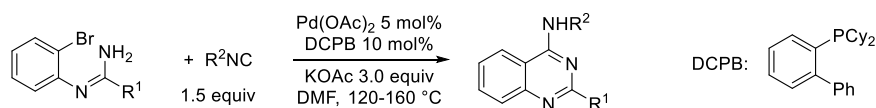
Scheme 20 – Proposed ring-opening mechanism for the direct arylation of benzoxazole with PhI.

As already stated, for brevity we will not review exhaustively all the Pd-catalyzed heterocycle-forming cyclizations that have been developed in the last decade. Broadly speaking, most of these reactions can be classified in three main classes according to the reagent providing the tethered nucleophile that effects the final ring closure: A) use of bifunctional nucleophiles; B) use of haloarenes having tethered nucleophilic moieties; C) use of isocyanides having nucleophilic functions. The synthesis of benzoxazoles and oxazolines presented in Scheme 17 is an example of a reactions in class A.

Concerning strategy B, which is arguably the most common, transformations analogous to those originally reported by Whitby^[36,37] but involving intramolecular ring closure of bromobenzenes suitably substituted with amine or alcohol functions have been described (Scheme 21).^[51] Interestingly, only primary *ortho*-bromobenzylamines and phenethylamines could be employed, secondary amines were not suitable substrates. Moreover, only tertiary isocyanides were tolerated (Scheme 21, right). The reaction employing alcohols was significantly more general, since primary, secondary and tertiary alcohols and isocyanides could be employed (Scheme 21, left).^[51] In another example illustrating reactions of class B, substituted 4-aminoquinazolines can be obtained by imidoylative intramolecular coupling of (*N*)-(2-bromoaryl)amidines (Scheme 22).^[52]

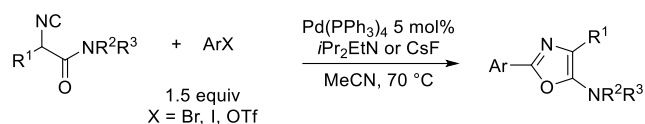


Scheme 21 – Synthesis of cyclic imidates and amidines by isocyanide insertion.^[51]



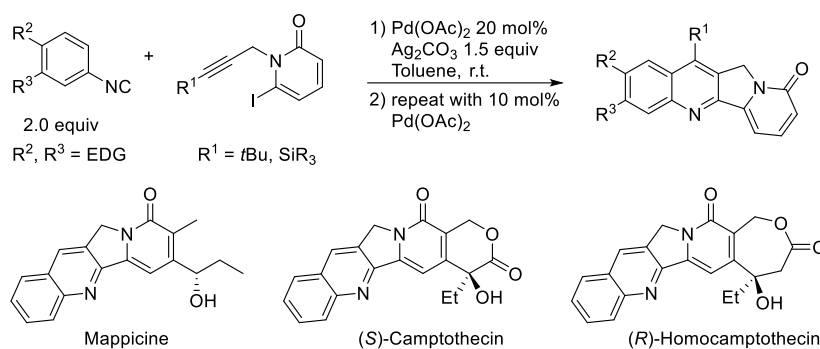
Scheme 22 – Synthesis of 4-aminoquinazolines from (*N*)-(2-bromoaryl)amidines.^[52]

Reactions belonging to class C are scarce, probably due to the fact that suitably substituted isocyanides are not always readily available. In a recent example, substituted 5-aminoxazoles were obtained by the reaction of isocyanoacetamides with aryl halides and triflates, in this case the oxygen atom of the isocyanoacetamide is the nucleophile responsible for ring closure (Scheme 23). Slow addition of the isocyanide was needed to achieve preparatively useful yields.^[53]

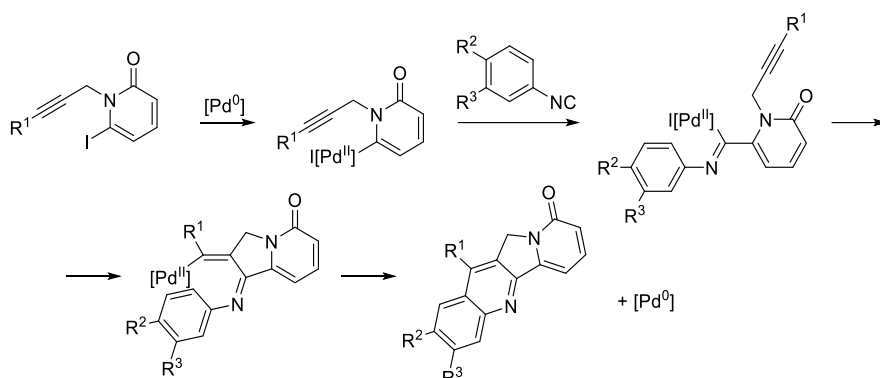


Scheme 23 – Synthesis of 5-aminoxazoles from isocyanoacetamides.^[53]

We will conclude this section about the potential of palladium-catalyzed transformations involving insertion of isocyanides by illustrating two examples highlighting the use of these reactions for the construction of biologically relevant scaffolds in connection with new atom- and step-economical strategies. As early as in 2002 Curran and Du, as a part of their studies on the synthesis of Mappicine, Camptothecin and Homocamptothecin analogues, reported a C-H activation process terminating a double insertion process concerning an aromatic isocyanide and a tethered alkyne (Scheme 24).^[54] More in detail, protected 6-iodo-1-propargyl-2-pyridones reacted with electron-rich aromatic isocyanides in the presence of Pd(OAc)₂ and a more than stoichiometric amount of Ag₂CO₃ to give the tetracyclic skeleton characteristic of this class of natural products. The mechanism proposed for this transformation is outlined in Scheme 25. This method complements one described previously involving a radical cyclization cascade.^[55]

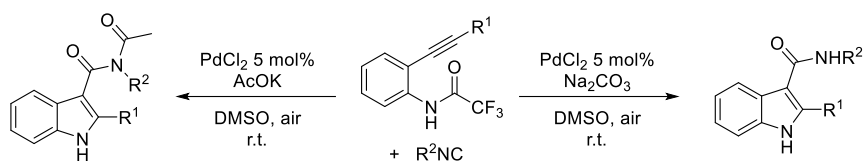


Scheme 24 – Synthesis of natural product analogues by isocyanide insertion and C-H activation.^[54]



Scheme 25 – Proposed mechanism for the Pd-catalyzed synthesis of camptothecin analogues. Ligands are not shown for clarity in this schematic representation.^[54]

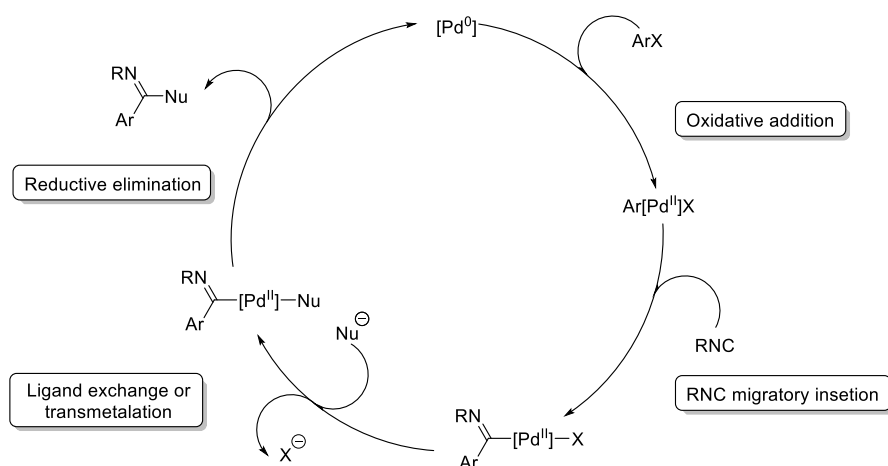
In another interesting example by Zhu and co-workers, indole-3-carboxamides could be prepared by 5-*exo*-dig cyclization of *o*-alkynyl trifluoroacetanilides (Scheme 26). Atmospheric oxygen acts as an oxidant in this process.^[56] A number of oxidative and C-H activation processes involved in isocyanides have been reported in recent years.^[23]



Scheme 26 – Synthesis of indole-3-carboxamides from *o*-alkynyl trifluoroacetanilides and isocyanides.^[56]

1.4. Earlier mechanistic studies related to palladium-catalyzed imidoylative couplings

The commonly proposed mechanism of imidoylative couplings involving halogenoarenes is outlined in Scheme 27. After oxidative addition of ArX to a palladium(0) complex, a σ -arylpalladium(II) intermediate is formed. Migratory insertion of RNC converts the latter into an imidoylpalladium(II) complex, that can undergo ligand exchange with the incoming nucleophile or transmetalation (in the case of organometallic nucleophiles). Finally, reductive elimination generates the coupling product and regenerates palladium(0).



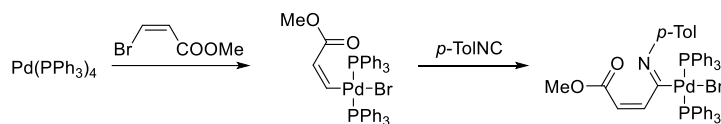
Scheme 27 – General catalytic cycle for Pd-catalyzed imidoylative couplings. Ligands are not shown for clarity and generality.

All the four main steps of this catalytic cycle have been already studied to some extent. Oxidative addition to palladium(0) is central to many Pd-catalyzed transformations other than imidoylative couplings and it has been the subject of much research, and electroanalytical techniques have been very useful in this field.^[57,58] An impressive amount of data exist on the OA reactions involving Pd(0) complexes featuring monodentate phosphine ligands;^[59–71] bidentate phosphines;^[72–75] species generated in situ from Pd₂(dba)₃ and phosphines;^[76–82] anionic complexes^[83,84] formed by phosphine ligated Pd(0) in the presence of common anions such as Cl⁻,^[85,86] AcO⁻,^[87] CF₃COO⁻,^[88] Pd(0) complexes with *N*-heterocyclic carbenes.^[89,90] The main results of these investigations is that the active species is usually the 14-electron complex [Pd(0)L₂], when L is a monodentate phosphine.^[59] This observation has general validity,^[62,63] though very hindered ligands such as P(*o*-Tol)₃ and P(*t*Bu)₃ are an exception, since in that case the active species is mono-ligated [Pd(0)L].^[64–71] To the best of our knowledge, even if oxidative addition to [Pd(CN*t*Bu)₂] has long been known,^[5] no kinetic data exist on the oxidative addition of haloarenes to isocyanide-ligated Pd(0) complexes and no detailed mechanistic studies have been reported.

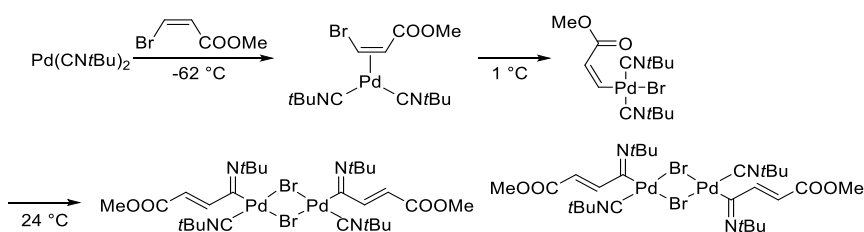
Also the insertion of isocyanides in the C-Pd bond has been the subject of thorough mechanistic studies.^[91–100] More in detail, in 1976 Ataka and Otsuka^[91] studied this process in *trans*-[RPd(CN*t*Bu)₂X] complexes (R = Me, X = I; R = Bn, X = Cl, Br, I). As already reported in the previous section for *trans*-[MePd(CN*t*Bu)₂I] (Scheme 2), these complexes are not stable at room temperature and they undergo insertion of one of the coordinated *t*BuNC molecules in the R-Pd bond.^[5] The reaction gives dimers in the absence of ligands and square-planar monomers in the presence of additional nucleophiles L [L = CN*t*Bu, PPh₃, P(OPh)₃]. The authors observed that the reaction rate was independent from the nature and from the concentration of added L, and that it was first-order with respect to the concentration of the palladium complex itself. Moreover, the reaction was faster in chlorobenzene than in hexane and rates varied according to the nature of X in the order Cl > Br > I. Based on these observations and on the fact that insertion was generally faster with more electrophilic isocyanides (aryl isocyanides > alkyl isocyanides) and that more nucleophilic R groups linked to Pd facilitate the insertion process

(alkyl > vinyl, *vide infra*), the authors concluded that the transition state for isocyanide insertion is polarized in such a way that R behaves as a nucleophile and the coordinated isocyanide as an electrophile.^[91]

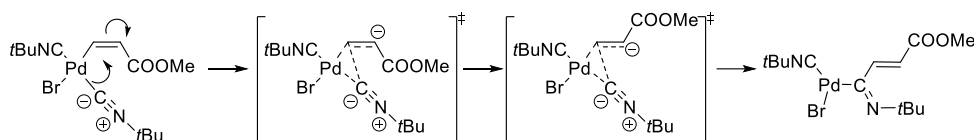
In the same study, the behavior of (*Z*)-(2-methoxycarbonyl)vinyl palladium(II) complexes was also analyzed.^[91] The reaction of Pd(PPh₃)₄ with methyl (*Z*)-2-bromoacrylate resulted in *trans*-[*((Z)*)-2-(MeOOC)CH=CH]Pd(PPh₃)₂Br], which reacted with *p*-TolNC to give an insertion product in which the *Z* geometry of the double bond was retained (Scheme 28). Likewise, *trans*-[*((Z)*)-2-(MeOOC)CH=CH]Pd(dppe)Br], featuring a chelating diphosphine ligand, readily underwent poly-insertion of at least three molecules of *t*BuNC. In a similar set of experiments, methyl (*Z*)-2-bromoacrylate reacted with [Pd(CN*t*Bu)₂] at -62 °C to give a tricoordinate complex in which the double bond was bound to the metal in an η² fashion. On heating to 1 °C, oxidative addition took place, yielding *trans*-[*((Z)*)-2-(MeOOC)CH=CH]Pd(CN*t*Bu)₂Br] with retention of the configuration of the double bond. Further increasing the temperature to 24 °C triggered insertion of *t*BuNC in the C-Pd bond, resulting in a mixture of pseudo-*cis* and pseudo-*trans* dimeric complexes. Surprisingly, the stereochemistry of the double bond was inverted, both products having *E* configuration (Scheme 29).^[91] The authors interpreted this observation in terms of polarization of the double bond during insertion of the isocyanide. If the dipolar structure D in Scheme 30 has a great contribution to the transition state for the latter transformation, the C-C bond would partly lose its double bond character, thus allowing isomerization. Interestingly, this hypothesis is in contrast with the previous conclusions on the polarization of the transition state for the insertion of isocyanide, as this time the coordinated isocyanide is supposed to act as a nucleophile, while the unsaturated organic moiety as an electrophile (in a way akin to conjugate addition to an α,β-unsaturated carbonyl compound).^[91]



Scheme 28 – Insertion of *p*-TolNC in a PPh₃-ligated vinyl-Pd(II) complex.

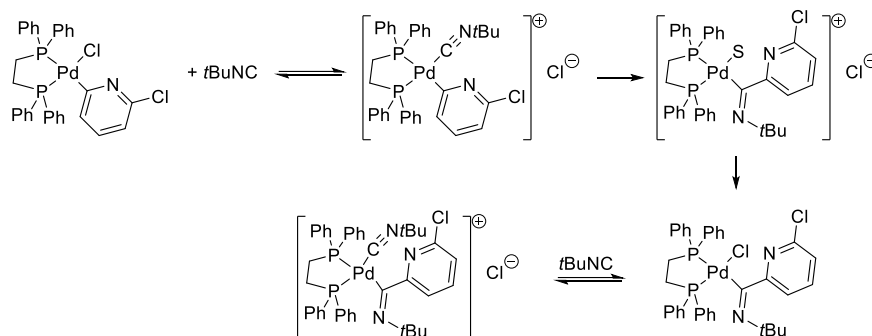


Scheme 29 – Insertion of *t*BuNC in a *t*BuNC-ligated vinyl-Pd(II) complex.



Scheme 30 – Isomerization of the double bond during isocyanide insertion.

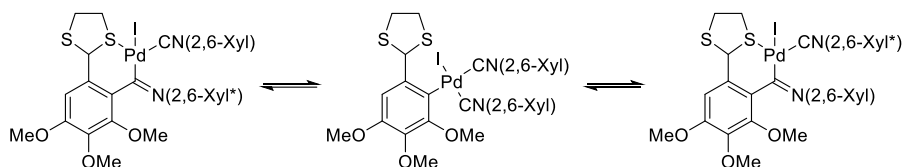
Later on, Uguagliati and Mantovani studied the insertion of *t*BuNC in a dppe-ligated organopalladium complex featuring an electron-poor pyridine organic moiety. The reaction was much slower, given the poor nucleophilicity of this organic residue, and an intermediate cationic complex, deriving from the displacement of Cl⁻ by excess isocyanide, could be observed in equilibrium with the reactant (Scheme 31). The reaction rate was first-order with respect to the concentration of the cationic intermediate, without any dependence on excess isocyanide, again in agreement with a unimolecular insertion process. No successive insertion of further molecules of isocyanide were observed.^[92]



Scheme 31 – Mechanism of the insertion of *t*BuNC in [(6-chloro-2-pyridyl)Pd(dppe)Cl].^[92]

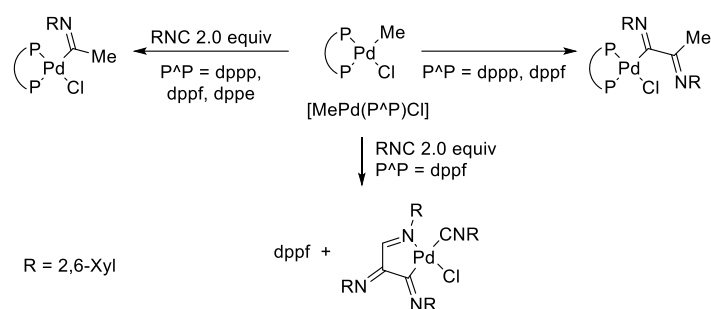
An analogous formation of cationic intermediates by displacement of the halide was also described by van Leeuwen, Vrieze and co-workers for [MePd(N[^]N)Cl] complexes (N[^]N = 1,10-phenanthroline, 2,2'-bipyridine^[94,95]) and by Canovese and Visentin for organopalladium(II) complexes having mixed nitrogen-sulfur and nitrogen-phosphorus ligands.^[97] Some intermediates involved in the insertion of isocyanides in allylpalladium complexes have also been identified.^[98–100]

Insertion of isocyanides can be a reversible process, as elegantly demonstrated by Vicente and co-workers.^[101] An *N*-(2,6-xylyl)imidoyl palladium(II) complex featuring a chelating thioacetal moiety and 2,6-XylNC as a ligand surprisingly had only one apparent resonance in the ¹H NMR spectrum at room temperature corresponding to the four methyl protons of the 2,6-xylyl substituents (Scheme 32). Cooling to –60 °C caused this resonance to split into three singlets with a 1:2:1 intensity ratio. This experimental observation is compatible with the fact that at room temperature the coordinated 2,6-XylNC molecule exchanges with the inserted one at a fast rate on the NMR timescale. Upon lowering the temperature this exchange becomes slow on the NMR timescale and the inserted isocyanide has hindered rotation around the N-C bond, while rotation is free for the 2,6-XylNC molecule bound to palladium.^[101]



Scheme 32 – Experiment showing the reversibility of the insertion of RNC in the C-Pd bond.^[101]

Beyond the early studies by Yamamoto and Yamazaki (Scheme 4),^[6] the multiple insertion of isocyanides in the C-Pd bond has been studied thoroughly by Vilar.^[25] They examined the behavior of *trans*-[MePd(P[^]P)Cl] complexes (P[^]P = dppe, dppp, dppf) with 2,6-XylNC and *t*BuNC. With two equivalents of the former isocyanide in THF, clean mono-insertion was obtained at room temperature only for P[^]P = dppe. In the case of the two other ligands, which have a wider bite-angle, double insertion prevails and in the case of dppf three molecules can insert, giving a cyclometalated compound similar to the one reported by Yamamoto (Scheme 4);^[6] excess 2,6-XylNC even displaced completely dppf, giving an isocyanide-ligated complex. Interestingly, switching the solvent from THF to CH₂Cl₂ decreased the tendency to give polyinsertion. Even if the authors do not comment this point, this experimental observation can be explained by assuming that insertion takes place *via* the cationic intermediate formed by replacement of Cl⁻, as proposed by Uguagliati.^[92] Indeed, in the less ionizing solvent, formation of ionic products – and thus insertion – is less favorable. The reactions described above are summarized in Scheme 33. In the case of *t*BuNC, monoinsertion was obtained again for P[^]P = dppe, while for dppp and dppf complex mixtures were obtained that were not amenable to characterization.^[25]

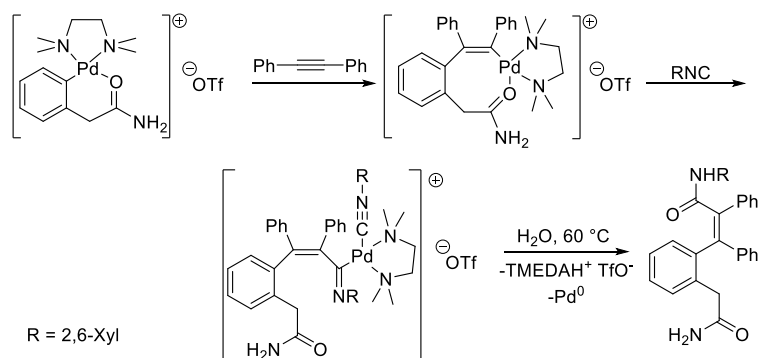


Scheme 33 – Multiple insertions of 2,6-XylNC in *trans*-[MePd(P[^]P)Cl] complexes.^[25]

To the best of our knowledge no studies have been devoted to the following step in the general mechanism reported in Scheme 27, *i.e.* ligand exchange with the nucleophilic partner of the imidoylative coupling. In fact, exchange of neutral or anionic ligands (not involving carbon-metal bonds) on a square planar Pd(II) complex is usually fast, so this step should not hinder catalytic turnover. In the case of organometallic nucleophiles, such as for the Suzuki coupling reported in Scheme 7,^[35] this step consists in a transmetalation. Even if this step is much more complicated than a simple ligand exchange and it should present several subtleties, we have no knowledge of mechanistic studies about this process.

Moreover, as far as we know, no published studies examine the closing step of the catalytic cycle, namely reductive elimination from imidoypalladium(II) complexes. This is rather surprising, given the wealth of information available about reductive elimination from the related acylpalladium complexes,^[102–108] which are intermediates in carbonylative cross-couplings. An impressive variety of structurally diverse imidoypalladium complexes (chiefly cyclometalated) have been described, mainly by Vicente and coworkers, in the last three decades.^[32,101,109–136] Occasionally, organic products have been obtained from these compounds by inducing reductive elimination by heating, treatment with a halide abstracting agent, such as Ag(I) or Tl(I) salts

having poorly coordinating anions, or by treatment with strong acids for complexes having basic ligands. No systematic study has been performed concerning this step. As an example, as shown in Scheme 34, treatment of a cationic TMEDA-coordinated orthopalladated phenylacetamide with diphenylacetylene affords an eight-membered palladacycle. Insertion of 2,6-XylNC breaks the palladacycle by decooordination of the amide tether. Thermolysis of the resulting complex in the presence of traces of moisture affords a complex *ortho*-substituted cinnamamide together with metallic palladium.^[127]



Scheme 34 – Synthesis of a substituted cinnamamide by thermal decomposition of an imidoypalladium complex.^[127]

All the studies presented in the previous paragraphs concern reactions of isolated palladium complexes that may be representative of intermediates formed during a real-life catalytic cycle. Only a theoretical study,^[137] that appeared while our study was in progress, is devoted to a catalytic reaction. More in detail, this study is focused on the amidation reaction described by Jiang (Scheme 12).^[40] Bromobenzene and *t*BuNC were chosen as the model substrates and PPh₃ – the ligand used in the optimized conditions – was replaced by PH₃ for convenience. Intermediates featuring only one PH₃ ligand were postulated all through the mechanism. The main conclusion drawn from these calculations at the DFT level is that a standard mechanism following the general pattern depicted in Scheme 27 may be operative. Oxidative addition was found to be the rate-determining step and the Cs⁺ cation (introduced as a counter-cation of the inorganic base) was suggested to have a major role in facilitating Br⁻-to-OH⁻ exchange on the imidoypalladium(II) intermediate. A pathway in which H₂O instead of OH⁻ enters the coordination sphere of palladium (a “base free” pathway) has been found too high in energy. Water also assists the tautomerization of the intermediately formed *N-tert*-butylbenzimidic acid to *N-tert*-butylbenzamide.^[137] The computed structures for these two processes, together with selected geometric parameters, are represented in Figure 1.

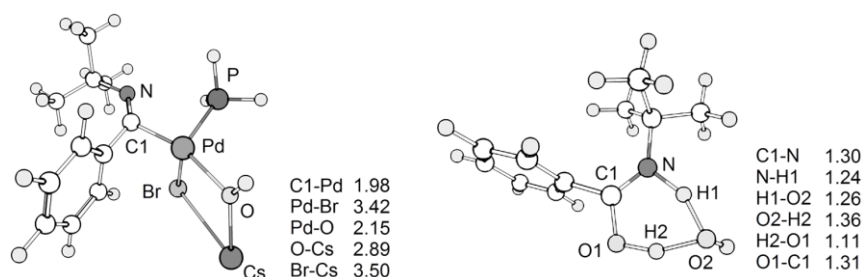
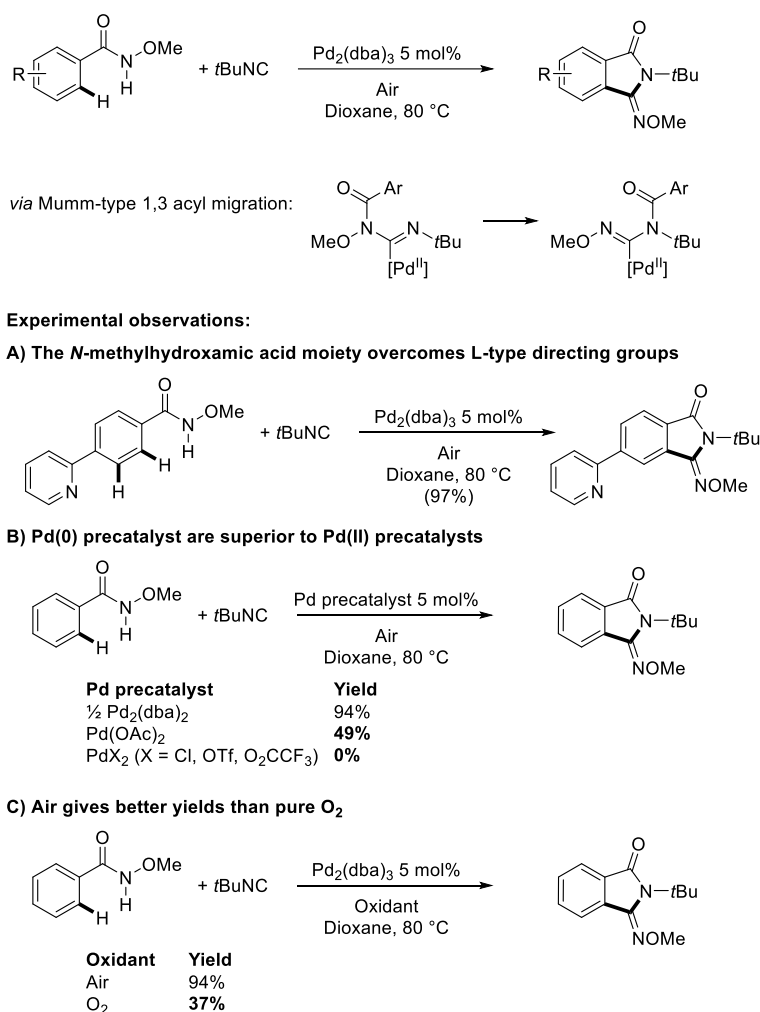


Figure 1 – Computed transition states for Cs⁺-assisted Br⁻-OH⁻ exchange on an imidoypalladium(II) intermediate (left), and for water-assisted tautomerization of *N*-*tert*-butylbenzimidic acid to *N*-*tert*-butylbenzamide (right), as reported by Ren and Wu.^[137]

After our work was published, Stahl reported^[138] a mechanistic study on a palladium-catalyzed oxidative coupling of *O*-methylbenzohydroxamic acids with *t*BuNC terminated by a C-H activation giving access to *N*-(*tert*-butyl)-3-(methoxyimino)isoindolin-1-ones (Scheme 35). This reaction, originally disclosed by Yu,^[139] has several interesting features. First, L-type directing groups such as a tethered 2-pyridyl moiety do not interfere with the selectivity of the C-H activation process (Scheme 35, A). Secondly, the Pd(0) precatalyst Pd₂(dba)₃ is most efficient, while Pd(OAc)₂ gives diminished yields and PdX₂ salts featuring less basic X⁻ anions are completely ineffective (Scheme 35, B). Lastly, using air as an oxidant gives better yields than performing the reaction in an atmosphere of pure O₂ (Scheme 35, C).

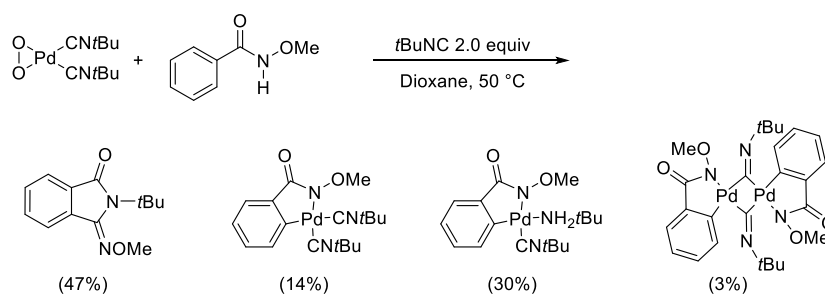
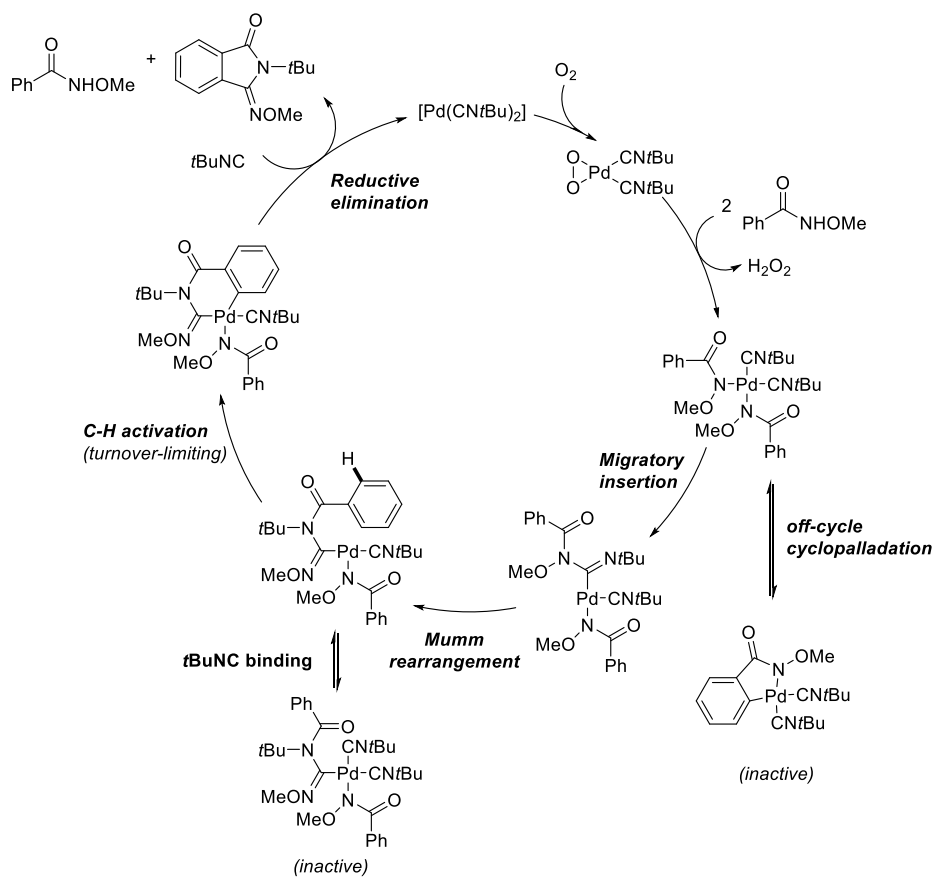
Stahl studied in detail the kinetics of this transformation and found that it is first order in the palladium precatalyst, zeroth order in the hydroxamic acid substrate (except for inhibition at high concentrations), zeroth order in O₂ and order is -1 with respect to *t*BuNC. A significant intermolecular kinetic isotope effect ($k_{\text{H}}/k_{\text{D}} = 6.7 \pm 0.2$) was found, which is indicative of a turnover-limiting C-H bond cleavage process. The superior efficiency of air compared to O₂ (Scheme 35, C) was readily explained by the observation that in the presence of a high partial pressure of O₂ *t*BuNC is quickly oxidized to *t*BuNCO, which is in turn transformed into (*t*BuNH)₂CO (*N,N'*-di-*tert*-butylurea) by traces of moisture. This parasitic reaction, which is expected to be first-order in *t*BuNC, thus consumes the substrate, which is not available for the desired process. The negligible effect of L-type directing groups (Scheme 35, A) was explained by showing that *t*BuNC has a much greater affinity than these neutral L-type ligands, which cannot thus coordinate to palladium under the experimental conditions.

Concerning the influence of the nature of the precatalyst (Scheme 35, B), it was rationalized by observing that the substrate must be coordinated in the deprotonated form (*i.e.* as an anionic X-type ligand) for the reaction to take place, so the ease of this substrate coordination step correlates with the basicity of the anionic ligands coordinated to Pd(II). Pd(0) catalyst precursors are most effective because they afford the very basic Pd(II)-peroxo complex [Pd(CN*t*Bu)₂(O₂)] *in situ* by reaction with O₂, as already shown by Otsuka.^[5]



Scheme 35 – Synthesis of *N*-(*tert*-butyl)-3-(methoxyimino)isoindolin-1-ones by Pd-catalyzed aerobic oxidative coupling of *O*-methylbenzohydroxamic acids with *t*BuNC and mechanistically relevant experimental observations.^[138,139]

Isolated $[\text{Pd}(\text{CN}t\text{Bu})_2(\text{O}_2)]$ reacted with *O*-methylbenzohydroxamic acid in the presence of excess *t*BuNC to give the expected isoindole in 47% yield, together with three cyclopalladated complexes (Scheme 36). The cyclopalladated complexes were deemed not to be intermediates of the catalytic cycle based on kinetic analysis. Excess *t*BuNC inhibits the C-H activation process by forming unreactive coordinatively saturated complexes. The overall catalytic cycle proposed by Stahl is represented in Scheme 37.^[138]

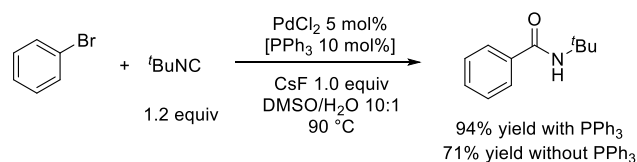
Scheme 36 – Reaction of $[\text{Pd}(\text{CNtBu})_2(\text{O}_2)]$ with *O*-methylbenzohydroxamic acid.^[138]Scheme 37 – Proposed catalytic cycle for the transformation shown in Scheme 35.^[138]

2. Results and discussion

2.1. Choice of the model reaction

Given the scarcity of the studies concerning the mechanism of catalytic imidoylative coupling, contrasting with the wealth of information available on some of the elementary steps of the catalytic cycle, we decided to devote our attention to a prototypical example of intramolecular imidoylative coupling, that would be also representative of other similar transformations. We wanted to keep a broad focus on the catalytic cycle as a whole, while investigating more in depth the less understood steps.

Among the literature examples enumerated in the previous section, the elegantly simple synthesis of secondary amides from aryl halides reported by Jiang^[40] (Scheme 12) looked promising. In this reaction, as we already stated, water is formally acting as nucleophile in the presence of CsF as a base. Through their optimization studies, the authors established that the best results in this transformation were obtained when a mixture of PdCl₂ and PPh₃ in 1:2 molar ratio was used as a precatalyst and a DMSO/H₂O mixture (10:1 volume ratio) as the solvent (Scheme 12). Nevertheless, they also realized that addition of a phosphine ligand is not required for the reaction to proceed. In fact, the analogous “ligandless” experimental protocol using only PdCl₂ gave the expected product in satisfactory yield.^[40] Other examples of phosphine ligand-free imidoylative coupling exist. Among the ones illustrated in the previous section, we may quote Curran’s total synthesis of camptothecin analogues (Scheme 24),^[54] Zhu’s synthesis of indoles-3-carboxamides (Scheme 26)^[56] and the cyanation of aryl halides using *t*BuNC in the presence of Cu(OCOCF₃)₂ (Scheme 16).^[46]



Scheme 38 – Pd-catalyzed amidation of bromobenzene in the presence of PPh₃ and under “ligandless” conditions.^[40]

Isocyanides have very high affinity for both Pd(0) and Pd(II), to the point that isocyanide-functionalized silica gel has been proposed as a scavenger to reduce the palladium contamination of active pharmaceutical ingredients down to sub-ppm levels.^[140] In analogy to what we have shown in a previous study concerning the arylation of imidazole derivatives *via* C-H activation,^[141] we expected that isocyanides play the role of both substrate and ligand in this reaction.

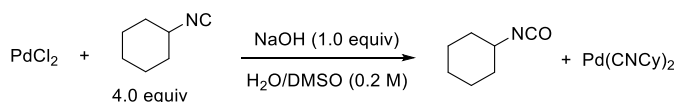
The choice of a phosphine ligand-free system was dictated also by the difficulties previously encountered in the laboratory in the characterization of the products deriving from the interaction of isocyanides with PPh₃-ligated arylpalladium(II) complexes. Despite painstaking efforts, no conclusive results could be obtained from mechanistic studies employing these organometallic compounds as a starting point^[142].

2.2. Generation of Pd(0) from Pd(II) precursors

Palladium(II) salts are almost universally employed as pre-catalysts in imidoylative couplings, but the commonly proposed mechanism involving oxidative additions of organic halides requires a palladium(0) complex as a starting point. A reduction step is thus required.

When PPh₃ or another phosphine is employed as a ligand, it is well known one equivalent is readily oxidized to OPPh₃, along with the generation of Pd(0), already at room temperature in the presence of traces of water and a base.^[61,143] In the absence of phosphorus ligands, the isocyanide itself may act as a reducing agent, being at the same time oxidized to an isocyanate in the presence of water. This reaction requires a base, as formal release of H⁺ takes place. A thorough literature search revealed that this reaction was described by Malatesta in 1955.^[144] He reported that by treating a solution of [Pd^{II}I₂(CNR)₂] (R = Ph, 4-Me-C₆H₄, 4-MeO-C₆H₄) in ethanol with KOH, [Pd⁰(CNR)₂] complexes were obtained, but only if two equivalents of added RNC were present. No reaction took place with a smaller excess.

Since in Malatesta's report no characterization of the organic co-product was reported,ⁱ we performed a simple control experiment to ascertain the nature of the oxidized organic species. A colorless solution of PdCl₂ (0.2 M in DMSO) and CyNC (4.0 equiv) changed to yellow upon treatment with NaOH (dispensed as a 1.0 M solution in water, 1.0 equiv) at room temperature. Gas-chromatographic analysis of the resulting mixture was performed after one minute and CyNCO was identified by comparison with the chromatogram of an authentic sample (Scheme 39). No cyclohexylamine, coming from addition of water to CyNCO and decarboxylation of the resulting carbamic acid, or *N,N'*-dicyclohexylurea (deriving from addition of CyNH₂ itself to CyNCO) were detected after a so short reaction time.



Scheme 39 – Reduction of Pd(II) by CyNC in the presence of a base.

2.3. Oxidative addition to isocyanide-ligated palladium(0)

As noted in the previous section, oxidative addition of an organic iodide to [Pd(CN*t*Bu)₂] was first reported as early as in 1969 (Scheme 2),^[5] but surprisingly the mechanism of this reaction has never been studied. Given that the oxidative addition to isocyanide-ligated palladium(0) is expected to be the first step of the catalytic cycle of an imidoylative coupling reaction performed in the absence of phosphine ligands, we studied its kinetic profile in detail.

ⁱ In principle, the alcohol could also act as a reducing agent in Malatesta's experiment, being oxidized to the corresponding aldehyde. This happens for example when a solution of Pd(II) salts in MeOH is treated with AcOK in the presence of dba (*trans,trans*-dibenzylideneacetone): Pd₂(dba)₃•dba and formaldehyde are produced.^[173]

The synthesis of $[\text{Pd}(\text{CN}t\text{Bu})_2]$ is rather tedious and this material is very air-sensitive.^[145] For convenience, we devised a procedure to generate it *in situ*. When excess *t*BuNC (10 equiv) was added to a purple-violet solution of $\text{Pd}(\text{dba})_2$ (dba = *trans,trans*-dibenzylideneacetone, 20 mM in CDCl_3), the color rapidly turned to orange-yellow. ^1H NMR analysis of the resulting mixture showed only the peaks of uncoordinated dba, with no trace of the characteristic signature peaks of ligated dba.^[146] From this preliminary experiment we concluded that this could have been a good model system to study the oxidative addition reaction.

Electroanalytical techniques, and more specifically amperometry at a rotating disk electrode, are often the method of choice to study oxidative addition reactions to $\text{Pd}(0)$,^[57] but in the case under study several practical problems arose. Cyclic voltammetry experiments evidenced only ill-defined oxidation peaks associated to $[\text{Pd}(\text{CN}t\text{Bu})_2]$.^[142] Moreover, gold – the usual electrode material – is easily oxidized in the presence of isocyanides, thus narrowing the usable potential window. We thus resorted to NMR spectroscopy for kinetic monitoring and we chose 4-fluoriodobenzene as a substrate, to follow the progress of the reaction conveniently also by $^{19}\text{F}\{^1\text{H}\}$ NMR.

When 4-fluoriodobenzene (1.0 equiv) was added to a solution of $\text{Pd}(\text{dba})_2$ (18 mM in benzene-*d*₆) in the presence of *t*BuNC (25 equiv), a comparatively fast reaction ensued. The resonance of the iodoarene in the ^{19}F NMR spectrum ($\delta = -114.5$ ppm) gradually disappeared and a new peak started growing downfield ($\delta = -113.3$ ppm). Similarly, the peaks of the starting material in the ^1H NMR spectrum (multiplets centered around $\delta = 6.81$ and 7.59 ppm) were gradually replaced by more deshielded signals [$\delta = 7.85$ (apparent dd, $J = 8.6, 5.7$ Hz, 2H), 7.00 (apparent t, $J = 8.6$ Hz, 2H)]. This picture is not compatible with the formation of organometallic species in which the Pd atom is linked directly to the aromatic ring, since shielding of the ring protons is expected in this case (*vide infra* for the characterization of the product).

The kinetics of this reaction could be easily studied, as the reciprocal of the concentration of leftover 4-iodofluorobenzene (as determined by ^{19}F NMR by using 1,4-difluorobenzene as an internal standard) fitted a straight line when plotted as a function of time (Figure 2), as expected for an overall second-order kinetic law:

$$-\frac{d[\text{ArI}]}{dt} = k[\text{ArI}][\text{Pd}^0] \quad (\text{i})$$

The second-order kinetic constant could be determined from the slope of the regression line ($k = 0.59 \text{ L mol}^{-1} \text{ min}^{-1}$).

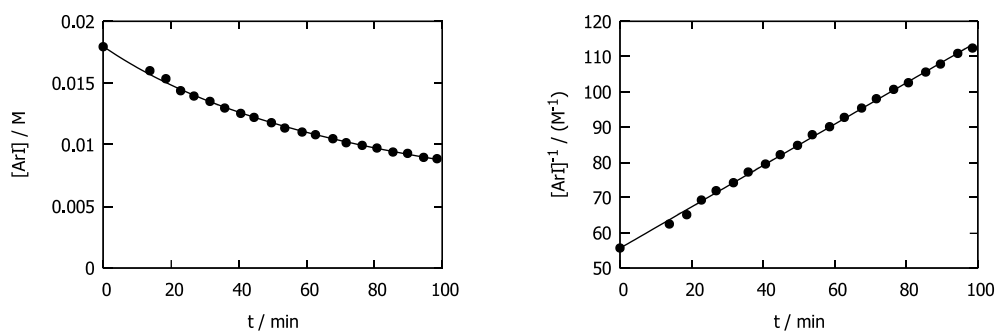


Figure 2 – Left: kinetics of the disappearance of 4-fluoriodobenzene (18 mM in benzene- d_6) in the presence of Pd(dba) $_2$ (1.0 equiv) and t BuNC (25 equiv) at 25 °C, as determined by ^{19}F NMR spectroscopy. Right: same data, reported in a reciprocal plot.

Similar experiments were performed with different excess amounts of t BuNC, showing that the rate constant did not change beyond experimental error varying the concentration of the isocyanide, *i.e.* that the rate law is zeroth order with respect to t BuNC (Figure 3).

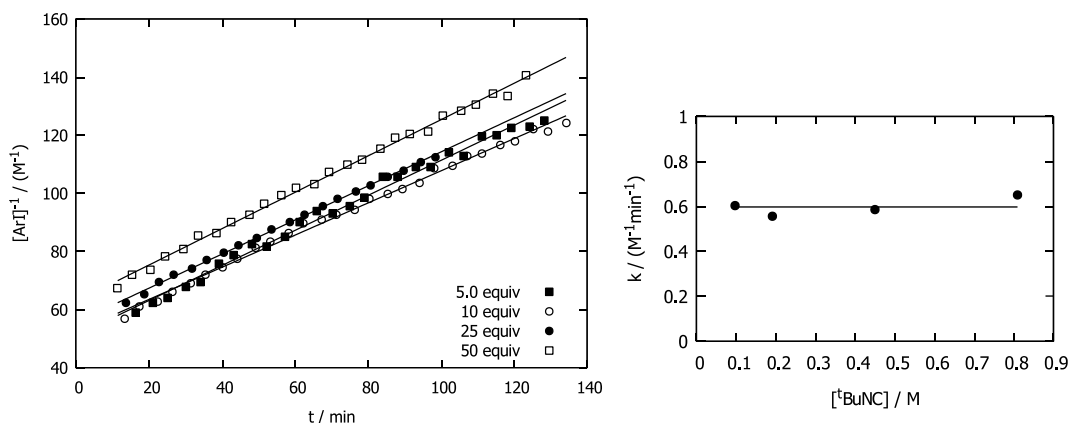


Figure 3 - Determination of the order of reaction with respect to the isocyanide for the reaction of 4-fluoriodobenzene (16–20 mM in benzene) with Pd(dba) $_2$ (1.0 equiv) in the presence of varying amounts of t BuNC at 25 °C. Left: plot of the reciprocal of the concentration of iodoarene as a function of time. Right: dependence of the apparent rate constant on the initial concentration of t BuNC.

In order to confirm the validity of equation (i), the reaction was performed with excess iodoarene and monitored in the same way.ⁱⁱ In this case data treatment is slightly more elaborate. Let C_0 be the initial total concentration of Pd(0), nC_0 the initial concentration of ArI (*i.e.* n equiv of ArI are used with respect to Pd, $n > 1$), and xC_0 the amount of Pd(0) converted to the product (*i.e.* x is the extent of reaction). If (i) holds, by integration with the condition that $x(t=0) = 0$, equation (ii) is easily obtained:

ⁱⁱ It was not convenient to use the flooding method, *i.e.* to use different excess amounts of iodoarene (> 10 equiv), which can be considered constant all through the reaction, because under those conditions the reaction was too fast to allow for reliable kinetic monitoring by NMR.

$$\ln \left[\frac{n-x}{n(1-x)} \right] k C_0 (n-1) t \quad (\text{ii})$$

The reaction of Pd(dba)₂ (19 mM in benzene) in the presence of *t*BuNC (20 equiv) with two different excess amounts of 4-fluoroiodobenzene (2.0 equiv and 10 equiv) was thus performed. By plotting the left member of equation (ii) as a function of *t* straight lines were obtained. The validity of (i) was thus confirmed and the values of the kinetic constant *k* were thus calculated from the slopes. The values found (*k* = 0.55 L mol⁻¹ min⁻¹ and *k* = 0.59 L mol⁻¹ min⁻¹) were in agreement with that determined previously.

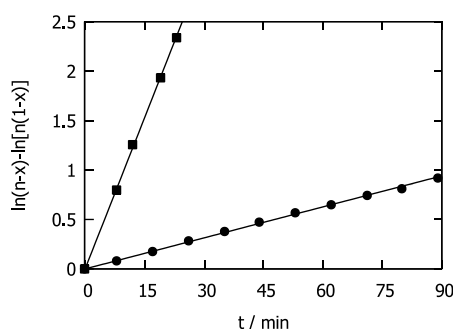


Figure 4 – Kinetics of the reactions of Pd(dba)₂ (19 mM in benzene) with 4-fluoroiodobenzene (● 2.0 equiv, ■ 10 equiv) in the presence of *t*BuNC (20 equiv), as monitored by ¹⁹F NMR spectroscopy at 25 °C. From the slope of the linear fitting according to equation (ii), *k* = 0.55 L mol⁻¹ min⁻¹ for ● and *k* = 0.59 L mol⁻¹ min⁻¹ for ■.

The kinetics we observed are consistent with the complete displacement of dba from the coordination sphere of Pd(0), thus validating *a posteriori* our choice of the model system, and the reactivity of *t*BuNC-ligated Pd(0) complexes towards the iodoarene. The zeroth order in *t*BuNC suggests that the oxidative addition reaction can take place without prior dissociation of one of the coordinated isocyanide molecules. This picture is different from the well-known oxidative addition of haloarenes to the model compound [Pd(PPh₃)₄]. In this case, dissociation of PPh₃ to give a dicoordinate 14-electron complex [Pd(PPh₃)₂] is necessary for the reaction to proceed (see the introduction, §1.4). The observed kinetic behavior, thus, suggests that the major species formed in solution would be [Pd(CN*t*Bu)₂].

Indeed, the nature of RNC-ligated Pd(0) species formed in solution in the presence of excess RNC, which is relevant for the understanding of catalytic reactions, has not been investigated so far. Isolated complexes of empirical formula Pd(CNR)₂ have long been known.^[144,145,147–150] As stated previously (§2.2) in 1955 Malatesta isolated complexes of this kind with aromatic isocyanides, and given their scant solubility in most organic solvents suggested a polymeric structure. Only coordinating solvents such as pyridine and quinoline or excess isocyanides themselves were able to dissolve these compounds, but recrystallization from these solvent was not possible, because some reaction did occur.^{[144]iii} A complex of empirical formula

iii Malatesta could characterise his novel complexes only by elemental analysis and iodometric titration. He had no access to X-ray diffraction facilities at that time, and he asked for help from the scientific

$\text{Pd}(\text{CN}(2,6\text{-Xyl}))_2$ was believed to be a trimer by analogy with the corresponding *triangulo*- $[\text{Pt}(\mu^2\text{-CNR})(\text{CNR})_2]_3$, but molecular weight determination performed with a solution in CHCl_3 (by using an unspecified technique) gave an apparent MW of 502, which is about half of the expected MW of 1106 for the trimer. Moreover, the two distinct isocyanide ligands (bridging and terminal) should give distinct NMR resonances, but even at $-90\text{ }^\circ\text{C}$ no resolved signals were apparent.^[147] The complex $\text{Pd}(\text{CNCy})_3$ was actually shown to be a trimer in the solid state (Figure 5), but there are no data regarding its structure in solution except for cryoscopic molecular weight determinations in benzene, which were not conclusive, since the apparent degree of association increased as the solution aged.^[145] The palladium(0) complex $[\text{Pd}(\text{CNAr})_2]$ formed by the exceedingly sterically hindered isocyanide with $\text{Ar} = 2,6\text{-}(2,6\text{-}i\text{Pr})_2\text{C}_6\text{H}_3)_2\text{C}_6\text{H}_3$, was shown to be monomeric also in the solid state.^[150]

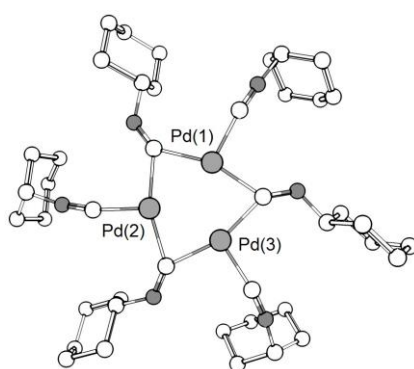


Figure 5 – X-ray structure of *triangulo*- $[\text{Pd}(\mu^2\text{-CyNR})(\text{CNCy})]_3$.^[148]

Under catalytic conditions, excess isocyanide with respect to palladium is always present, so in principle it would be possible that palladium(0) complexes having a coordination number higher than two form. Moreover, it is known since 1950 that for $\text{Ni}(0)$ the 18-electron complexes $[\text{Ni}(\text{CNR})_4]$ are isolable, which are isoelectronic to $\text{Ni}(\text{CO})_4$.^[151,152] To get some insight on this point, which to the best of our knowledge has never been investigated explicitly, we performed DFT calculations to investigate the relative stability of mononuclear $[\text{Pd}(\text{CN}i\text{Bu})_n]$ species ($n = 0 - 4$, Figure 6). Formation of the mono-coordinate complex $[\text{Pd}(\text{CN}i\text{Bu})]$ from a Pd and $i\text{BuNC}$ is highly exothermic and exergonic ($\Delta_f H = -30.2\text{ kcal mol}^{-1}$, $\Delta_f G = -22.9\text{ kcal mol}^{-1}$), as well as the formation of linear, dicoordinate $[\text{Pd}(\text{CN}i\text{Bu})_2]$ ($\Delta_f H = -56.2\text{ kcal mol}^{-1}$, $\Delta_f G = -39.5\text{ kcal mol}^{-1}$). Addition of a third and of a fourth isocyanide ligand is practically athermic, so the free energies of formation of the tricoordinate and tetracoordinate complexes ($\Delta_f G = -31.8\text{ kcal mol}^{-1}$ and $\Delta_f G = -20.3\text{ kcal mol}^{-1}$ respectively) are less negative than for dicoordinate $[\text{Pd}(\text{CN}i\text{Bu})_2]$. Even though an overestimation of the entropic contribution to free energy is highly likely, this result is in agreement with the experimentally observed independence of the rate of oxidative addition on the concentration of added isocyanide, because the most stable

community. In his own words: “*The elucidation of the stereochemistry of these interesting compounds must, however, await an X-ray structure determination, and the author is prepared to supply samples to those interested in such a study*”. To the best of our knowledge, his request has remained unanswered, as no solid state structure of a $\text{Pd}(0)$ complex with a simple aromatic isocyanide has ever been reported.

species, *i.e.* the 14-electron complex $[\text{Pd}(\text{CN}t\text{Bu})_2]$, is also the one expected to react with the iodoarene.

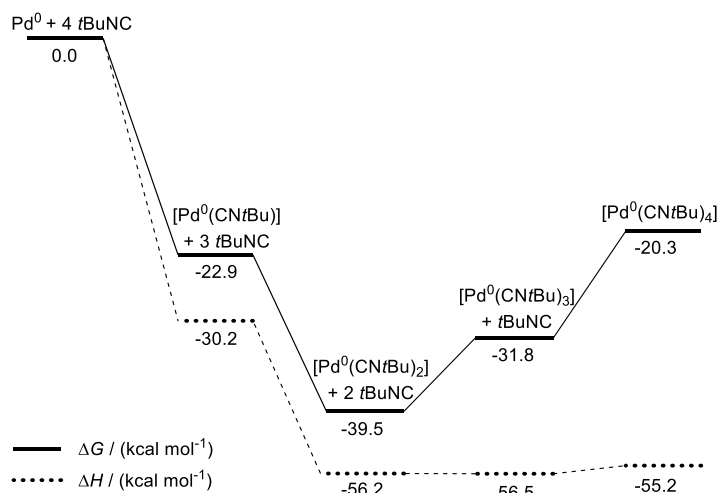


Figure 6 – Relative stabilities of *t*BuNC-ligated mononuclear Pd(0) complexes, as assessed by DFT computations. Computed free energies and enthalpies of formation at 25 °C are reported relative to non-interacting Pd(0) and *t*BuNC.

Concerning the structure of these *t*BuNC-ligated palladium(0) complexes, in every case the ligands keep a linear CNC moiety after coordination. The dicoordinate $[\text{Pd}(\text{CN}t\text{Bu})_2]$ is predicted to be linear with a CPdC angle of almost 180°, while $[\text{Pd}(\text{CN}t\text{Bu})_3]$ is triangular planar and $[\text{Pd}(\text{CN}t\text{Bu})_4]$ has an almost perfect tetrahedral arrangements of the ligands (Figure 7). In every case, the CN bond length is 1.17 Å, while the Pd-C distance lengthens as the coordination number increases (1.98, 2.03, 2.12 and 2.21 Å for $n = 1, 2, 3, 4$, respectively), reflecting the decreasing strength of the carbon-metal bond.

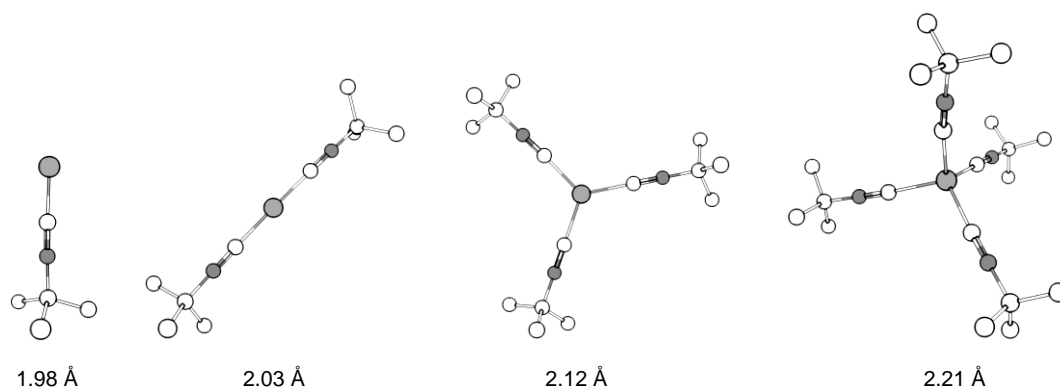


Figure 7 – Structures of complexes $[\text{Pd}(\text{CN}t\text{Bu})_n]$ ($n = 1 - 4$), as resulting from DFT calculations. Hydrogen atoms not shown for clarity. Pd-C bond distances are also reported.

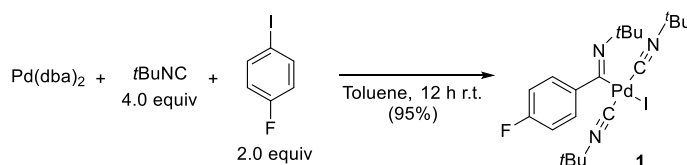
The stability of a trinuclear *triangulo*- $[\text{Pd}(\mu^2\text{-CN}t\text{Bu})(\text{CN}t\text{Bu})_3]$ trimer, analogous to the CyNC-ligated complex that has been characterized in the solid state (Figure 5),^[148] has also been examined computationally. The formation of this species from its monomer is predicted to be only slightly exothermic ($\Delta H = -1.5 \text{ kcal mol}^{-1}$ for the trimerization) and endergonic ($\Delta G = +26.0 \text{ kcal mol}^{-1}$). As a check, similar calculations were performed also for the known CyNC

complex. The structure optimized at the DFT level compares favorably with that obtained by X-ray diffraction, as it could be assessed by comparison of some relevant geometric parameters; e.g. the average Pd-C bond distance is 2.07 Å for κ^1 -CNCy ligands (experiment: 2.01 Å) and 2.16 Å for bridging CNCy (experiment: 2.16 Å). Interestingly, *triangulo*-[Pd(μ^2 -CNCy)(CNCy)]₃ was predicted less unfavorable to form ($\Delta H = -9.7$ kcal mol⁻¹ and $\Delta G = +22.7$ kcal mol⁻¹), thus suggesting that association may be highly dependent on the nature of the isocyanide. Additionally, the structure in the solid state might not be representative of the behavior of the complex in solution.

In summary, kinetic data on the oxidative addition and DFT calculations suggest that most likely [Pd(CNR)₂] is the species present in solution and that higher-coordinated complexes are not formed in the presence of excess RNC. Association of these species to give trimers or other polynuclear species is probably weak or not favorable, and it depends on the nature of RNC.

2.4. Characterization of the product of oxidative addition

We then attempted to characterize the product formed by the reaction of Pd(dba)₂ with 4-iodofluorobenzene in the presence of *t*BuNC. When the experiment was performed on a preparative scale, the air-stable imidoypalladium complex **1** could be isolated in excellent yield as a crystalline golden yellow material after flash chromatography on silica gel (Scheme 40).^{iv}



Scheme 40 – Synthesis of *trans*-[(ArC=N*t*Bu)Pd(CN*t*Bu)₂I] (**1**).

The structure of complex **1** was confirmed spectroscopically and by single-crystal X-ray diffraction analysis (Figure 8).^v In the solid state, the four ligands are in the expected square-planar arrangement around the palladium center. The imidoyl moiety features a *trans* arrangement of the *t*Bu substituent with respect to the aromatic ring, which is not perpendicular to the plane of the complex (the Pd-C1-C2-C7 dihedral angle is 63.4°). The two *t*BuNC ligands are not arranged symmetrically. Even the Pd-C bond distance is the same for both (1.98 Å), one of them is slightly more bent than the other one (\angle Pd-C12-N2: 176.3°, \angle Pd-C17-N3: 171.9°). This asymmetry may be due to packing in the solid state (the unit cell of the complex is depicted in Figure 9), that creates a different environment for the two *t*BuNC ligands.

^{iv} The synthesis of similar complexes has already been described in the literature.^[174]

^v Crystallographic data have been deposited at The Cambridge Crystallographic Data Centre, CCDC 145600 (**1**).

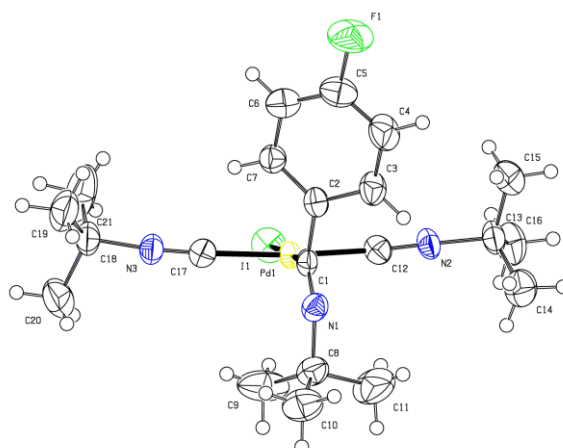


Figure 8 – Ortepe view of **1**. Displacement ellipsoids drawn at the 50% probability level. H atoms are shown as spheres of arbitrary radius.

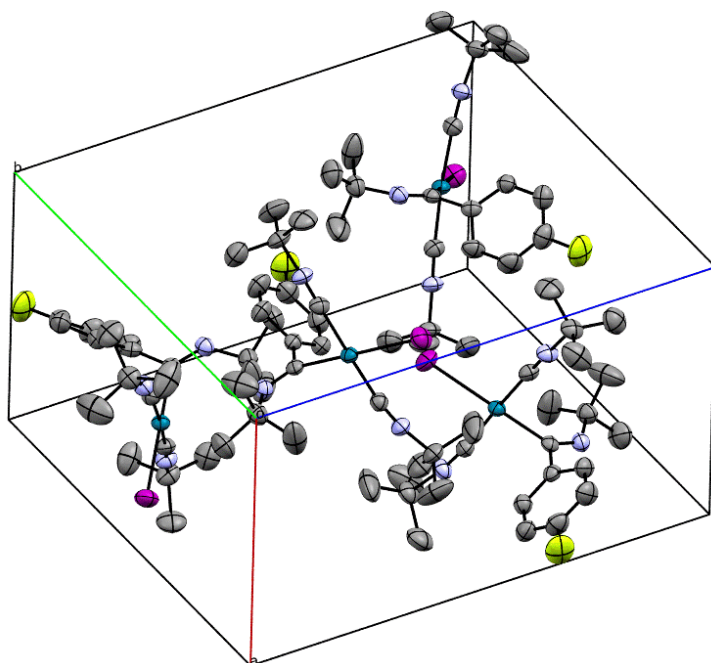


Figure 9 – Unit cell view of compound **1**. Displacement ellipsoids drawn at the 50% probability level.

Comparison of ^1H and ^{19}F NMR spectra proved that the oxidative addition of 4-iodofluorobenzene with $\text{Pd}(\text{dba})_2/\text{tBuNC}$ of which we studied the kinetics apparently gives **1** without any detectable intermediate. This demonstrates that under these conditions (*i.e.* in the presence of excess tBuNC), insertion of the isocyanide is faster than oxidative addition, which indeed also takes place readily at room temperature. A solution of **1** (20 mM in $\text{DMSO-}d_6$) and excess tBuNC (10 equiv) gave a broadened $^{19}\text{F}\{^1\text{H}\}$ NMR peak, and no significant change in the ^1H and ^{19}F NMR spectra occurred within 72 h at room temperature. This suggests that complex **1** is rather stable in the presence of excess of isocyanide and poly-insertion does not occur readily at room temperature.

The line broadening we observed, however, prompted us to investigate further. When more *t*BuNC was added, the peak became sharper and it moved further downfield. This behavior was compatible with an equilibrium taking place with fast kinetics on the NMR timescale, and an NMR titration was performed with different excess amounts of *t*BuNC (Figure 10).

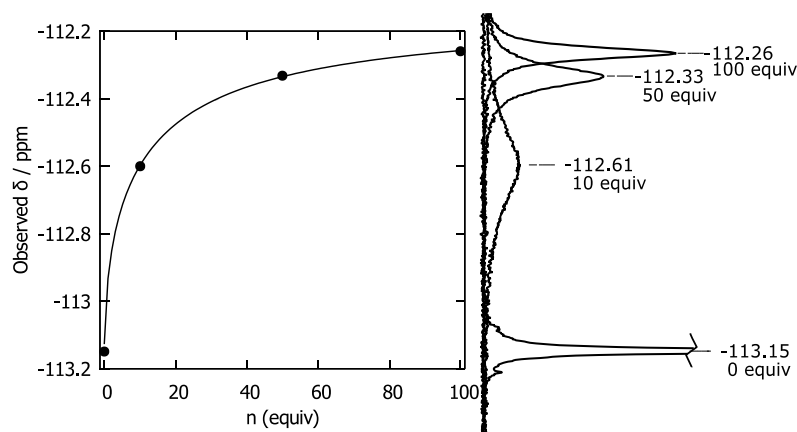


Figure 10 – Left: fitting of the observed ^{19}F NMR chemical shift of **1** (20 mM in $\text{DMSO-}d_6$, at 25 °C) in the presence of n equiv of excess *t*BuNC. The continuous line represents the fitting function, as per equation (iv). Right: sections of the $^{19}\text{F}\{^1\text{H}\}$ NMR spectra from which experimental data are derived.

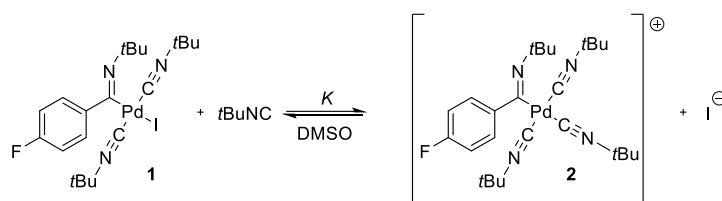
This equilibrium was interpreted as the displacement of coordinated I^- with a third molecule of *t*BuNC, thus resulting in the release of a cationic complex (**2**) loosely associated with the iodide anion (Scheme 41). As a first test of this hypothesis, an equation for the apparent chemical shift as a function of the number of equivalents of added *t*BuNC was derived. More in detail, if the equilibrium depicted in Scheme 41 was operative and fast with respect to the NMR timescale, the apparent ^{19}F NMR chemical shift could be expressed as:

$$\delta_{\text{obs}} = x\delta_2 + (1-x)\delta_1 = \delta_1 + x\Delta\delta \quad (\text{iii})$$

where δ_1 and δ_2 are, respectively, the chemical shift of **1** and **2**, $\Delta\delta$ is $\delta_2 - \delta_1$, and x is the molar fraction of **2**, *i.e.* $x = [\mathbf{2}]/([\mathbf{1}] + [\mathbf{2}])$. The expression of x as a function of the number of equivalents of *t*BuNC added n and the thermodynamic constant K can be obtained from elementary calculations. Substitution into (iii) gives the final expression (iv):

$$\delta_{\text{obs}} = \delta_1 + \Delta\delta \cdot \frac{n+1 - \sqrt{(n-1)^2 + \frac{4n}{K}}}{2\left(1 - \frac{1}{K}\right)} \quad (\text{iv})$$

Equation (v) was fitted to experimental data, using $\delta_1 = -113.15$ (Figure 10), and the procedure gave $\Delta\delta = 1.083$ and $K = 0.0658$ (asymptotic standard errors: 0.45% and 3.8% respectively) in DMSO at 25 °C.



Scheme 41 – I⁻ / tBuNC ligand exchange reaction of complex **1**.

The agreement of our model with the experimental titration data was encouraging, so electrical conductivity measurements were performed to confirm the validity of the hypothesis depicted in Scheme 41. An expression for the conductometric titration curve of a fixed quantity of **1** with increasing amounts of tBuNC was first obtained. Under the hypothesis that at fixed total Pd concentration the conductivity κ is proportional of the molar fraction x of **2**:

$$\kappa = A \cdot x = A \frac{n+1 - \sqrt{(n-1)^2 + \frac{4n}{K}}}{2 \left(1 - \frac{1}{K}\right)} \quad (\text{v})$$

Fitting of the experimental conductometric titration curve with equation (v) gave access to the equilibrium constant K . The value found ($K = 0.0672$, asymptotic standard error 1.2%) was in agreement with that found by NMR titration (Figure 10), thus confirming the validity of our hypothesis.

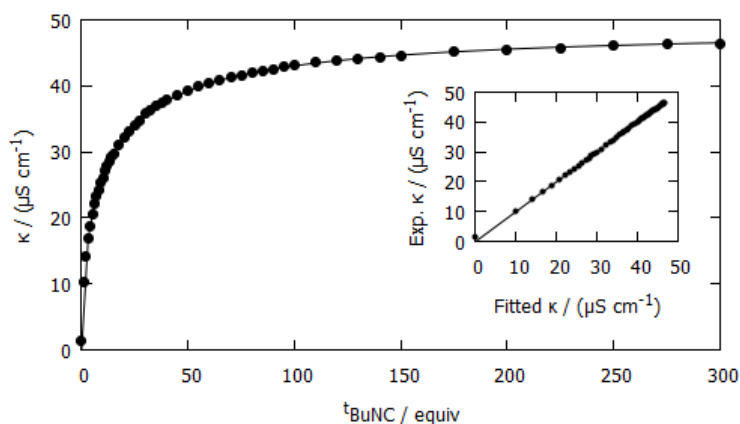


Figure 11 – Conductometric titration of complex **1** (2 mM in DMSO at 25 °C) with increasing amounts of tBuNC. The conductivity κ is plotted as a function of the number of equiv of tBuNC added. The continuous line shows the fitting function, as per equation (v). For clarity, in the inset the same fitting is reported as a linearized plot.

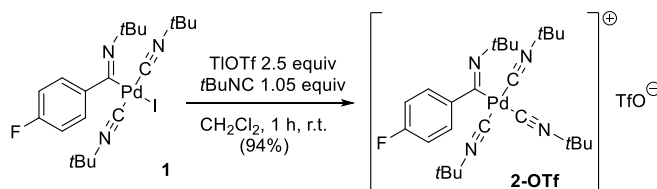
Similar titration experiments were performed in two other different common polar solvents (DMF, MeCN) and a ternary solvent mixture (DMSO/THF/H₂O 5:1:1 by volume), the interest of which will be clarified in the following. The titration curves and fittings according to equation (v) are shown in Figure 12. These data demonstrate that I⁻ exchange with tBuNC and formation of a cationic complexes takes place in all the studied solvents. The values of the equilibrium constants found are reported in Table 1.

Table 1 – Equilibrium constants for the reaction represented in Scheme 41, as determined by conductometric titration at 25 °C in different solvents and solvent mixtures.

Solvent	<i>K</i>	Asymptotic standard error
DMSO	0.0672	1.2%
DMF	0.0118	1.7%
MeCN	0.080	2.4%
DMSO/THF/H ₂ O 5:1:1	0.118	3.7%

The cationic complex **2** was isolated in good yield with TfO⁻ as a counter-anion by treating the parent iodide complex **1** with Tl(OTf) in the presence of *t*BuNC (Scheme 42). Several attempts to perform an analogous transformation with Ag(I) salts under a variety of reaction conditions invariably failed because of extensive precipitation of metallic palladium. This is probably due to the great affinity of Ag(I) for isocyanides.^{vi} We thus speculate that Ag(I) salts extract the coordinated *t*BuNC molecules from **1**, thus yielding coordinatively unsaturated species that are not stable.

Complex **2-OTf** could be characterized by multinuclear NMR and IR spectra. The NMR data were in agreement with those of the species formed by treating **1** with excess *t*BuNC. IR in the solid state showed that the main band corresponding to the isocyanide CN stretching moved from 2190 cm⁻¹ (for neutral **1**) to 2217 cm⁻¹ (for **2-OTf**), consistently with the expected reduction of back-donation for the charged species.



Scheme 42 – Synthesis of complex **2-OTf**.

^{vi} For example, AgI is soluble in organic solvents in the presence of excess *t*BuNC, but TlI does not dissolve under similar conditions.

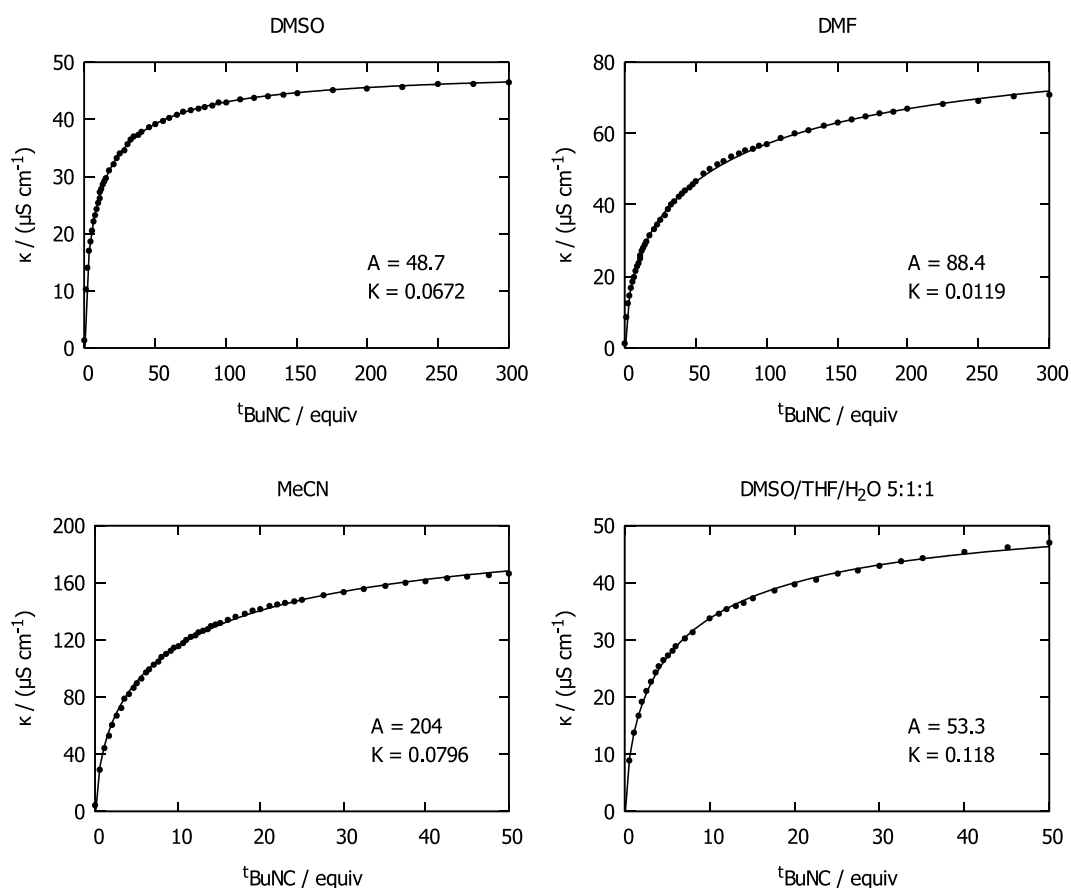


Figure 12 – Conductometric titration curves for complex 1 (2.0 mM in the specified solvents or solvent mixtures) with increasing amounts of $t\text{BuNC}$. The parameters A (in $\mu\text{S cm}^{-1}$) and K (dimensionless) fitted according to equation (v) are reported, as well as fitting curves (solid lines).

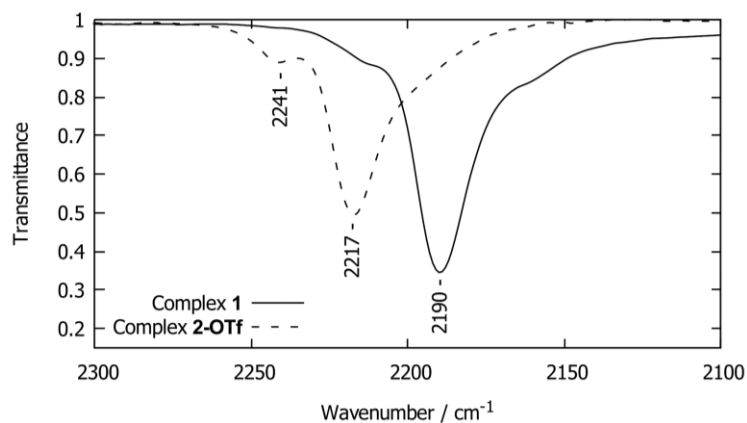


Figure 13 – Section of the IR spectra of complexes 1 and 2-OTf.

The formation of such a cationic complex under conditions relevant for catalytic transformations, when no halide-abstracting agent is introduced, to the best of our knowledge,

has never been pointed out before.^{vii} In the analogous case of phosphine-ligated acylpalladium complexes, the displacement of I⁻ is possible under very high pressure of carbon monoxide. This step has an important role in the double insertion of CO and thus in the associated catalytic reactions, such as the double carbonylation of haloarenes in the presence of amines to give α -ketoamides.^[103,105,106]

2.5. Interaction of complex **1** with triphenylphosphine

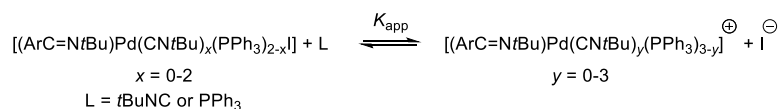
As reported in many examples quoted in the introduction of this chapter, phosphine ligands are often part of the catalytic systems useful to accomplish Pd-catalyzed transformations with insertion of isocyanides.^[19,20,36–38] Unfortunately, previous attempts to study the mechanism of imidoylative couplings involving phosphine-ligated complexes did not lead to conclusive results due to the difficulties encountered in the characterization of the species formed when both an isocyanide and a phosphine are present.^[142] It is thus of interest to study the interaction of the well-characterized complex **1** with common phosphines, as to gain insight into the relative affinities of phosphines and isocyanides for palladium and to gather useful information about the species that might actually be formed under catalytic conditions and either be active in the formation of the wanted product, or be responsible for side reactions, or be unreactive resting states for the catalyst.

First, we studied triphenylphosphine as a model ligand, since it used in the optimized conditions for our model reaction (Scheme 38).^[40] On adding one equivalent of PPh₃ to a solution of **1** (20 mM in DMSO-*d*₆), a very complex mixture was obtained. At least eight different resonances were apparent in the ¹⁹F{¹H} NMR spectrum and seven in the ³¹P{¹H} NMR spectrum. Moreover, some of the signals were broad, thus suggesting the existence of multiple species in equilibrium that exchange on a timescale comparable to that typical of NMR measurements. Addition of more PPh₃ (up to 5 equiv) did not simplify the spectra. Mixtures of analogous complexity were obtained when *t*BuNC was added to a solution of preformed *trans*-[ArPd(PPh₃)₂I] complexes,^[153] as already observed in previous studies performed in our laboratory.^[142]

To probe in a simple way the formation of cationic complexes, the interaction of compound **1** with PPh₃ was also studied by conductivity measurements. A conductometric titration of a fixed amount of **1** in DMSO with PPh₃ (1–5 equiv) was performed. A rigorous treatment of these data is not possible, since the structure of the formed species is not known. We resorted to equation (v) to fit the titration curve. The parameters of the fitting should be interpreted cautiously and only in a semi-quantitative fashion for the reason exposed above. Assuming that only tetra-coordinate complexes are formed (which is reasonable for such *d^B* organometallic species with not to sterically-demanding ligands), the parameter *K* of equation (v)

^{vii} The formation of cationic complexes as intermediates for the insertion of isocyanides in the C-Pd bond in the presence of bidentate ligands was indeed known, as we showed in the introduction (§1.4, Scheme 31).^[92,94,95,97]

fitted to conductometric titration data should be interpreted as an *apparent* thermodynamic constant associated to the equilibria between all the possible neutral imidoypalladium complexes featuring *t*BuNC and/or PPh₃ ligands and their cationic counterparts deriving from displacement of I⁻ either by PPh₃ or *t*BuNC (Scheme 43). As a further complication, several geometric isomers can exist for some of these complexes.



Scheme 43 – Equilibria between neutral and cationic imidoypalladium(II) complexes.

The curve fitted according to equation (v) follows reasonably well the experimental trend, as shown in Figure 14. Parameter *A* is of the same order of magnitude of that found for the same experiment performed with *t*BuNC instead of PPh₃ (Figure 12) and it can be interpreted as the conductivity expected in the limit of full conversion of all the imidoypalladium (II) complexes to cationic species. Assuming as usual that the conductivity is proportional to the concentration of ionic species, we can estimate that about 61% of the total palladium is present in cationic form in the presence of one equivalent of PPh₃ and 82% of it with two equivalents. The measured apparent constant *K*_{app} is about two order of magnitude greater than that associated to the equilibrium depicted in Scheme 41 (*K*_{app} = 2.8), thus we can reasonably conclude that formation of cationic species is more favored in the presence of PPh₃ than with *t*BuNC alone.

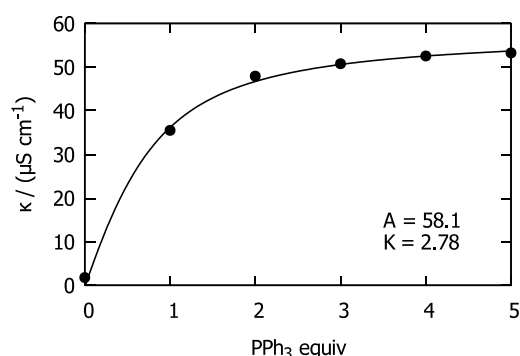


Figure 14 – Conductometric titration of **1** (2.0 mM in DMSO) with PPh₃. Fitting curve according to equation (v), as well as the fitting parameters *A* (in μS cm⁻¹) and *K* (dimensionless) fitted are reported.

The complexity of this system prevented us to characterize more in detail the structure of the species formed. Nevertheless, it should be noted that under the optimized catalytic conditions described by Jiang,^[40] at least one equivalent^{viii} of PPh₃ is present in solution with respect to palladium, together with excess isocyanide. As it was also evidenced by a previous study,^[142] a part of the formed imidoypalladium(II) complexes should feature isocyanide ligands.

^{viii} Two equiv of PPh₃ are employed, but as already stated (§2.2) one equiv can be oxidised to poorly coordinating PPh₃O. At this point, it is not clear whether PPh₃ or the isocyanide is oxidised preferentially by Pd(II) when both are present in solution.

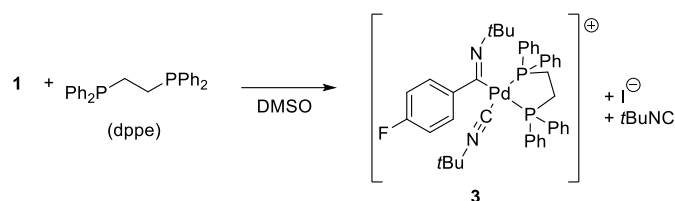
Moreover, as demonstrated by our data, a significant fraction of the species formed in solution is of ionic nature. This observation should be considered when interpreting the results of a recent DFT study^{157]} on the mechanism model transformation we have chosen. In this work, only neutral phosphine-ligated complexes were evaluated, and the formation of isocyanide-ligated species and of cationic complexes overlooked.

In apolar solvents, that are sometimes used for imidoylative couplings, the formation of cationic complexes is not expected to occur. It is interesting, anyway, to get an appreciation of the relative affinities of PPh₃ and isocyanides for the imidoylpalladium(II) moiety also under these conditions. At this end, the interaction of complex **1** with PPh₃ (2.0 equiv) in benzene-*d*₆ was studied by multinuclear NMR spectroscopy. Multiple products were formed, but the picture was not as complex as in DMSO. Approximately only one equiv of PPh₃ was bound to palladium, giving only one apparent broad peak in ³¹P{¹H} NMR ($\delta = 21.1$ ppm), half of the phosphine originally introduced remained free. The ¹⁹F{¹H} NMR spectrum was more complicated, with three major resonances ($\delta = -113.2, -113.3, -113.8$ ppm) accounting for about 90% of the total integration, probably corresponding to the starting material (**1**) and two geometric isomers of the mixed complex [(ArC=N*t*Bu)Pd(PPh₃)(CN*t*Bu)I], and a minor one (approx. 5% of the total integration, $\delta = -115.7$ ppm), that we can tentatively assign to [(ArC=N*t*Bu)Pd(PPh₃)₂I], also in comparison with the chemical shift on analogous complexes formed with diphosphine ligands (*vide infra*).

2.6. Interaction of complex **1** with 1,2-bis-(diphenylphosphino)ethane (dppe)

Bidentate phosphine ligands are often employed in Pd-catalyzed imidoylative couplings.^[36,37,154–157] We selected 1,2-bis-(diphenylphosphino)ethane (dppe) as a representative example. Mixing complex **1** and dppe in a 1:1 molar ratio in DMSO gave quantitatively only one species in which dppe is acting a chelate ligand, as attested by the single resonance observable in the ¹⁹F{¹H} NMR spectrum ($\delta = -114.0$ ppm) and by the two doublets in the ³¹P{¹H} NMR spectrum [$\delta = 42.85$ (d, ²J_{PP} = 41.1 Hz), 38.98 (d, ²J_{PP} = 41.1 Hz) ppm]. Quite surprisingly, dppe did not displace the two *t*BuNC ligands, but instead it expelled one molecule of *t*BuNC and I⁻, resulting in the formation of cationic complex **3** (Scheme 44). This point is demonstrated most clearly by a ¹³C{¹H} spectrum (Figure 15). In the region of the quaternary carbons of the *t*Bu groups, three peaks were evident: a singlet for the substituent of the imidoyl nitrogen ($\delta = 59.5$ ppm), a doublet of doublets for the coordinated isocyanide of **3** [$\delta = 57.7$ ppm (dd, ⁴J_{C-P} = 11.5, 2.0 Hz)], and a 1:1:1 triplet for the quaternary carbon of the *t*Bu group of free *t*BuNC, since for this very symmetric molecule the ¹⁴N,¹³C ¹J-coupling can be observed ($\delta = 54.1$ ppm ¹J_{C-N} = 4.5 Hz).^{ix}

^{ix} The coupling between ¹³C and ¹⁴N (and all the common quadrupolar nuclei other than ²H) is very rarely observed. The reason for this is that ¹⁴N has a substantial quadrupolar coupling constant and then the relaxation among its energy levels is very fast. A ¹³C nucleus that would in principle *J*-couple with it thus sees the ¹⁴N in a single time-averaged state, and as a result it appears as a singlet. However, when the ¹⁴N is in a very symmetric environment, the quadrupolar coupling constant is much smaller and, consequently,

Scheme 44 – Reaction of complex **1** with dppe.

Analogously to what already observed for **2**, the CN stretching frequency in the IR spectrum in DMSO moved from 2195 cm⁻¹ for **1** to 2203 cm⁻¹ for **3**. The specific electrical conductivity of **3** (28 S cm² mol⁻¹ at 25 °C in DMSO) was in the range expected for a 1:1 electrolyte in such a viscous solvent and it was close to the specific conductivities of complex **2** (24 S cm² mol⁻¹ at 25 °C in DMSO, as determined by extrapolation of the titration curve of **1** with *t*BuNC, Figure 11) and for the species formed by interaction of **1** with PPh₃ (28 cm² mol⁻¹ at 25 °C in DMSO, as determined from the titration curve shown in Figure 14).

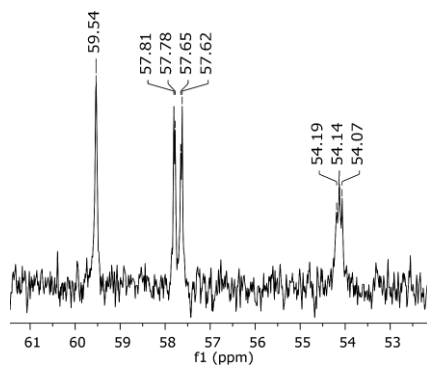


Figure 15 – Section of the ¹³C{¹H} NMR spectrum of complex **1** (62.5 mM in DMSO-*d*₆) in the presence of dppe (1.0 equiv) showing the region of the *tert*-butyl group quaternary carbon. Three peaks are evident: one for the imine nitrogen substituent [$\delta = 59.5$ ppm (s)], one for the coordinated isocyanide of **3** [$\delta = 57.7$ ppm (dd, ⁴*J*_{C-P} = 11.5, 2.0 Hz)] and one for uncoordinated isocyanide [$\delta = 54.1$ ppm (1:1:1 triplet, ¹*J*_{C-N} = 4.5 Hz)]. This picture corresponds to the quantitative formation of species **3**.

Similar experiments were also performed in a less polar solvent, namely acetone-*d*₆. In that case, two complexes were formed. Based on NMR and IR data (see the experimental section for the detailed characterization) and comparison with the same spectra recorded in DMSO solution, we propose that a mixture of [(ArC=N*t*Bu)Pd(dppe)I] and [(ArC=N*t*Bu)Pd(dppe)(CN*t*Bu)]⁺ (**3**) in approximate 70 : 30 ratio is formed. As expected, the ionic product is less favored in this less dissociating solvent than in DMSO. Switching to a completely apolar solvent, *i.e.* benzene-*d*₆, as expected favored the formation of what we tentatively identified as [(ArC=N*t*Bu)Pd(dppe)I], but equilibria were definitely operative, as suggested by the line broadening of most of the associated NMR peaks [³¹P{¹H} NMR:

the relaxation is much slower. In these cases one ¹⁴N, ¹³C *J* coupling becomes observable. Besides simple isocyanides, for instance this coupling is often observed for symmetric quaternary ammonium salts.

$\delta = 37.24$ (d, $^2J_{\text{PP}} = 48.8$ Hz), 22.68 (d, $^2J_{\text{PP}} = 48.8$ Hz) ppm; $^{19}\text{F}\{^1\text{H}\}$ NMR: $\delta = -115.9$ ppm (broad)]. This transformation was not quantitative, and some free dppe (approx. 30%) remained. Other minor unidentified resonances were also detected in the $^{31}\text{P}\{^1\text{H}\}$ spectrum.

The wide bite-angle phosphine 1,1'-bis(diphenylphosphino)ferrocene (dppf) is used in some imidoylative couplings.^[36,37,51] The interaction of this ligand with complex **1** was also studied. In DMSO, it behaves in the same way as dppe, and a complex analogous to **3**, $[(\text{ArC}=\text{N}/\text{Bu})\text{Pd}(\text{dppf})(\text{CN}/\text{Bu})]^+$, could be characterized *in situ* (see the experimental section for spectral data).

The stability of the cationic species **3** towards excess isocyanide was also examined. When a solution of **3** (20 mM in DMSO-*d*₆) was left at room temperature in the presence of ten equivalents of *t*BuNC, several new peaks appeared in the $^{19}\text{F}\{^1\text{H}\}$ spectrum and only 80% of the starting material was left after 72 h. We inferred that compound **3** is less stable than the analogous cationic *t*BuNC-ligated species **2** with respect to excess *t*BuNC.

In summary, we showed that imidoypalladium complexes are often under cationic form in polar solvents, both when excess isocyanide is present (which necessarily happens in catalytic reactions, where the substrate is in excess with respect to the palladium catalyst) as the only ligand and even more with monodentate or bidentate phosphine ligands. The cationic species might also be involved in multiple insertion of isocyanide, as for the analogous case of CO poly-insertion.^[105,106,158] Considering that poly-insertion and polymerization of the isocyanide are parasitic reaction that often plague imidoylative couplings, this observation should be taken into account to design new Pd-catalyzed transformations involving isocyanides.

2.7. C-O bond forming reductive elimination

With complex **1** in hands and after having characterized its behavior in the presence of excess isocyanides, we wanted to confirm that it can be an intermediate of the catalytic synthesis of amides from haloarenes under phosphine ligand-free conditions (Scheme 38).^[40] With this purpose in mind, we studied the reaction of compound **1** with several sources of OH⁻, in order to verify whether *N-tert*-butyl-4-fluorobenzamide (**4**), the final product of the corresponding catalytic reaction, could be generated.

As a first experiment, a solution of complex **1** (20 mM in DMSO-*d*₆) was treated with tetrabutylammonium hydroxide (1.0–2.0 equiv, dispensed as a 1.54 M solution in water). The yellow solution immediately turned dark red-brown and $^{19}\text{F}\{^1\text{H}\}$ NMR analysis showed that a variety of fluorine containing products was generated, among which the amide **4** could not be identified. Exposure of the resulting solution to air lightened its color, so we speculated that some air-sensitive palladium(0) species was generated. Since the desired product **4** was not formed, no further characterization of the products of this reaction was attempted.

When the same experiment was repeated by replacing tetrabutylammonium hydroxide with KOH (dispensed as a 1.0 M solution in water), surprisingly a slow reaction ensued, leading to the expected product **4**. However, conversion stopped before 40% yield and the kinetics of this reaction were highly irreproducible. No simple kinetic law could be fitted to these data. At

that point, we realized that even if the solution obtained by mixing the reactants appeared homogeneous, KOH has very scant solubility in DMSO and precipitation of this reactant in a very finely subdivided form (*e.g.* in a colloidal state) could have taken place. Indeed, a literature search revealed that the solubility of KOH in DMSO is less than 1.0 mM,^[159] while we expected a final concentration of 20 mM, moreover no agitation or stirring whatsoever was applied to the tube. When similar experiments were performed in DMSO / water mixtures (5 : 1 by volume),^x as to ensure that KOH was completely soluble, a mixture of products as complex as that obtained with tetrabutylammonium hydroxide was obtained.

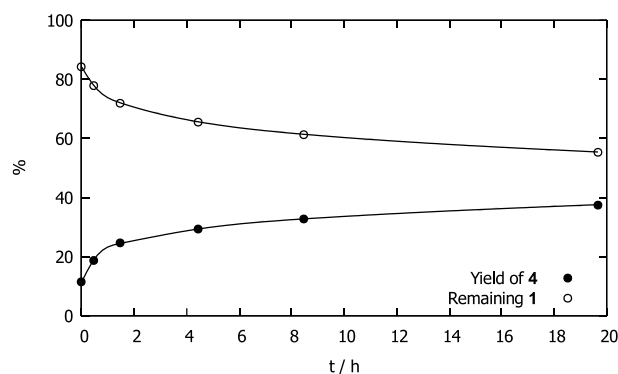


Figure 16 – Kinetics of the reaction of complex **1** (20 mM in DMSO-*d*₆) with KOH (1.0 equiv, dispensed as a 1.0 M solution in water) at 25 °C, as monitored by ¹⁹F NMR spectroscopy.

The experiments described above involving KOH suggested that establishing a low concentration of available OH⁻ was essential to obtain the amide **4**. Considering that CsF is the most efficient base under catalytic conditions (Scheme 38),^[40] but it has scant solubility in DMSO at room temperature, an F⁻ / HF mixture was used in a water / organic solvent mixture instead of a strong base, in order to better mimic the catalytic conditions. A solution of *n*Bu₄NF (8.5 equiv) and HF (1.5 equiv) in THF was added to compound **1** dissolved in aqueous DMSO to give a final concentration of 14 mM in a DMSO / THF / H₂O mixture in a 5 : 1 : 1 ratio by volume.^{xi} In these conditions, a smooth reaction occurred, giving the expected amide **4** as the

^x The solubility of KOH and NaOH in water / DMSO mixtures increases dramatically with the water content.^[159] A 17% water content was enough to maintain the 10 equiv of KOH (dispensed as a 1.0 M aqueous solution) completely dissolved.

^{xi} In the beginning, we meant to use only *n*Bu₄NF as a base in the presence of water, so we resorted to a commercial solution of this reagent (nominally 1.0 M in THF). However, analysis of a freshly opened bottle revealed that a significant amount of free HF was also present. In the ¹⁹F NMR spectrum a doublet was apparent for the HF₂⁻ anion [$\delta = -143.1$ (d, $^1J_{\text{HF}} = 121.7$ Hz) ppm in a 5 : 1 DMSO / THF mixture], which become a singlet when ¹H decoupling was applied, together with a singlet for F⁻ ($\delta = -102.7$ ppm). Quantitative NMR analysis was possible by using a long relaxation delay (20 s) and no ¹H decoupling, as to prevent the NOE effect to alter the intensity of the signal of HF₂⁻. Results were in agreement with a titration in water with standard NaOH and phenolphthalein as an indicator. A very weak resonance at -123.6 was also detected, corresponding to a small trace of SiF₆²⁻ originated by the attack of glass, as also confirmed by the existence of the ²⁹Si satellites, integrating for about 5% of the major peak of SiF₆²⁻

only product, as confirmed by $^{19}\text{F}\{^1\text{H}\}$ and ^1H NMR spectroscopic analysis of the reaction mixture and spiking with an authentic sample. It is worth noting that this reaction proceeded at room temperature, albeit on the timescale of several hours, whereas the catalytic reaction is invariably performed at high temperature (90 °C, Scheme 38).^[40] The kinetics of this transformation could be followed easily by $^{19}\text{F}\{^1\text{H}\}$ NMR spectroscopy, and apparent first-order behavior was observed ($t_{1/2} = 26$ h at 25 °C, Figure 17).

To gain more insight into the possible mechanism of this reaction, the influence of the other species present in the reaction mixture under catalytic conditions on the kinetics of the reaction was evaluated (Table 2). In the presence of excess *t*BuNC (10 equiv), the reaction was severely slowed down, and about half of the complex was under the cationic form **3**, as inferred from its apparent ^{19}F NMR chemical shift (by comparison with the data in Figure 10). On the other hand, addition of $[\text{Pd}(\text{NCPh})_2\text{Cl}_2]$ (5.0 equiv), which can act as an isocyanide scavenger by competition for binding *t*BuNC, accelerated strongly the reaction. Iodide anions, added in the form of *n*Bu₄NI (10 equiv) also slowed the reaction down. Lowering the F^- / HF ratio from 85 : 15 to 50 : 50 also decreased the rate of reaction, thus suggesting that the latter is an increasing function of $[\text{OH}^-]$. As we have shown previously, however, a too high concentration of OH^- , such as that generated by the addition of stoichiometric amounts of strong bases, causes decomposition of the complex and does not result in the formation of significant amounts of the amide (**4**).

($^1J_{\text{SiF}} = 112.8$ Hz).^[175] It is worth-noting that HF was not originated by the degradation of the salt by the Hofmann elimination pathway, as no signals attributable to 1-butene or to tributylamine were detected in the ^1H spectrum, which was also devoid of any other spurious peak except for a trace of water. We assumed, thus, that HF had been introduced during the manufacturing process.

The choice of this ternary mixture, also including water, was made to mimic the catalytic conditions as close as possible (Scheme 38) and to ensure the solubility of all the components. Water was essential for the reaction to take place to give the desired amide **4**; rapid decomposition of complex **1** to other products was observed in its absence.

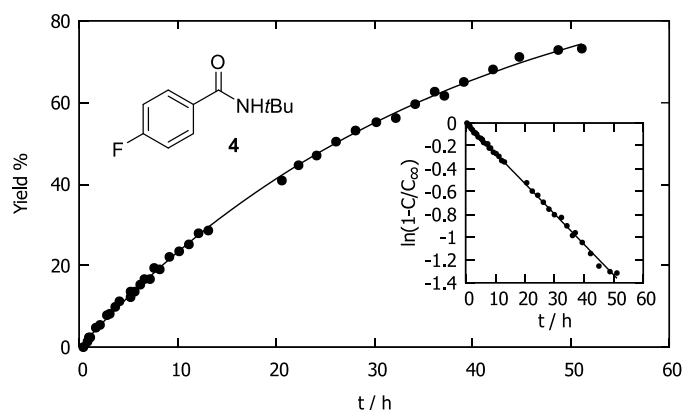
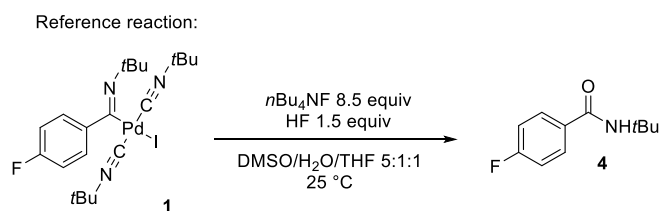


Figure 17 – Kinetics for the appearance of the amide **4** by the reaction of **1** (14 mM in a DMSO / THF / H₂O mixture in 5 : 1 : 1 ratio by volume) in the presence of a F⁻/HF mixture (*n*Bu₄NF 8.5 equiv, HF 1.5 equiv) at 25 °C, as determined by ¹⁹F{¹H} NMR spectroscopy. In the inset, the same data are reported in a semi-logarithmic plot (*C* and *C*_∞ are the concentrations of **4** at any time and at reaction completion respectively), thus evidencing first-order behavior.

Table 2 – Influence of variation of the reaction conditions on the rate of the C-O bond forming reductive elimination of complex **1** in the presence of water and an F⁻ / HF mixture. First order half-reaction times (as determined by ¹⁹F{¹H} NMR kinetic monitoring) are reported for each variation of the experimental conditions with respect to the reference reaction.



Variation	<i>t</i> _{1/2} / h
None	26
+ <i>t</i> BuNC (10 equiv)	~130
+ [Pd(NCPh) ₂ Cl ₂] (5.0 equiv)	< 1
+ <i>n</i> Bu ₄ NI (10 equiv)	~101
<i>n</i> Bu ₄ NF / HF ratio = 1 : 1	44

In summary, we demonstrated that complex **1** can be an intermediate in our model reaction – the synthesis of secondary amides from haloarenes, isocyanides and water –, as it undergoes reductive elimination in alkaline solution containing water even at room temperature. However, high concentrations of OH⁻, such as those generated by stoichiometric amounts of alkali hydroxides or *n*Bu₄NOH, cause degradation of the complex and do not lead to significant amounts of the amide (**4**). Either the use of a buffer (F⁻ / HF in the present case)^{xiii} or of scarcely

^{xiii} It may arise the doubt that F⁻ has a specific role in this reaction other than generating an appropriate concentration of OH⁻, for example, one could envisage a C-F bond forming reaction leading to an imidoil fluoride, which is hydrolyzed in a subsequent step. This scenario is highly unlikely, as bases other than

soluble bases can secure the appropriate concentration of [OH⁻]. Both *t*BuNC and I⁻ inhibit this reaction, which is instead accelerated by [Pd(NCPh)₂Cl₂], which can act as an isocyanide scavenger.

2.8. Theoretical study of the catalytic cycle

To substantiate the deduction drawn from the experimental observation exposed previously and to get insight into the non-isolable intermediates of the catalytic cycle, we investigated the complete mechanism of the model reaction (Scheme 38) by DFT calculations.

We took advantage of experimental data as a guide to explore the potential energy landscape, the overall computed catalytic cycle is reported in Figure 18 (Gibbs free energies) and Figure 19 (enthalpies).

Oxidative addition of ArI (Ar = 4-F-C₆H₄) with [Pd(CN*t*Bu)₂] can take place *via* **TS1** with a comparatively small barrier ($\Delta G^\ddagger = +22.1$ kcal mol⁻¹, $\Delta H^\ddagger = +9.1$ kcal mol⁻¹), it is exothermic and exergonic ($\Delta G = -13.3$ kcal mol⁻¹, $\Delta H = -26.3$ kcal mol⁻¹) and it delivers the square-planar complex *cis*-[ArPd(CN*t*Bu)₂I] (**I1**) as the product. IRC calculations did not lead to a stable pre-complex in which the palladium is coordinated to the iodoarene, *e.g.* in an η^2 fashion. The reaction, thus, is predicted to take place directly by the bimolecular encounter of [Pd(CN*t*Bu)₂] and ArI.

The structure and selected geometric parameters of **TS1** are reported in Figure 20. For what concerns the [Pd(CN*t*Bu)₂] moiety, there is significant deviation from the linear coordination geometry, the C-Pd-C being of 111°, so quite close to the square planar geometry of the product. For what concerns the iodoarene, the C-I bond is not much elongated (2.27 Å, to be compared with 2.11 Å in the isolated ArI). In this respect the TS may be qualified as quite reactant-like. Interestingly, the *t*BuNC ligand situated *trans* to the iodine atom is further away from the metal than that *trans* to the newly forming C-Pd bond (*t*BuNC-Pd bond distances: 2.32 and 2.16 Å, respectively) and coordination has a slightly bent Pd-C-N arrangement (the Pd-C-N angle is 157°, Figure 20).

Isomerization of the *cis* complex **I1** its *trans* isomer **I2** is thermodynamically favorable ($\Delta G = -4.2$ kcal mol⁻¹, $\Delta H = -3.3$ kcal mol⁻¹). Starting from **I2**, insertion of one of the isocyanide ligands into the C-Pd bond can take place through transition state **TS2** and delivers the tricoordinate, T-shape imidoypalladium complex **I3** in which the remaining *t*BuNC ligand is *trans* with respect to the imidoyl moiety. The computed activation barrier for this process ($\Delta G^\ddagger = +19.5$ kcal mol⁻¹, $\Delta H^\ddagger = +17.0$ kcal mol⁻¹) is lower than that of the previous step, compatibly with the fact that intermediate **I2** is not observed experimentally (at least if excess isocyanide is present). In **TS2** the C-C distance corresponding to the new C-C bond is 1.85 Å, that is to be compared with 1.49 Å in **I3**, meaning that the TS is not much product-like in this

fluorides (Cs₂CO₃, K₂CO₃, KOH) can be used to accomplish the transformation with catalytic palladium, albeit with diminished yields.^[40]

respect (Figure 20). This reaction is endothermic and endergonic ($\Delta G = +8.0$ kcal mol⁻¹, $\Delta H = +8.0$ kcal mol⁻¹) but addition of a second molecule of *t*BuNC to **13**, giving the tetracoordinate, square planar *trans*-[(ArC=N*t*Bu)Pd(CN*t*Bu)₂] (**1**, which is an isolable intermediate) is thermodynamically favorable ($\Delta G = -20.3$ kcal mol⁻¹, $\Delta H = -34.3$ kcal mol⁻¹) and it is the driving force of the insertion reaction. The X-ray structure of **1** is in reasonable agreement with the corresponding computationally optimized structure (without the implicit solvation model, Kabsch RMSD:^[160] 0.71 Å, excluding the Ar ring: 0.36 Å), which reassured us about the validity of the theoretical protocol we employed.^{xiii} Several attempts to locate a *pentacoordinate* transition state in which a molecule *t*BuNC associates to **12** before insertion of *t*BuNC in the C-Pd bond takes place, thus delivering directly complex **1**, invariably failed, because one of the *t*BuNC molecules was expelled from the coordination sphere of palladium during the optimization.

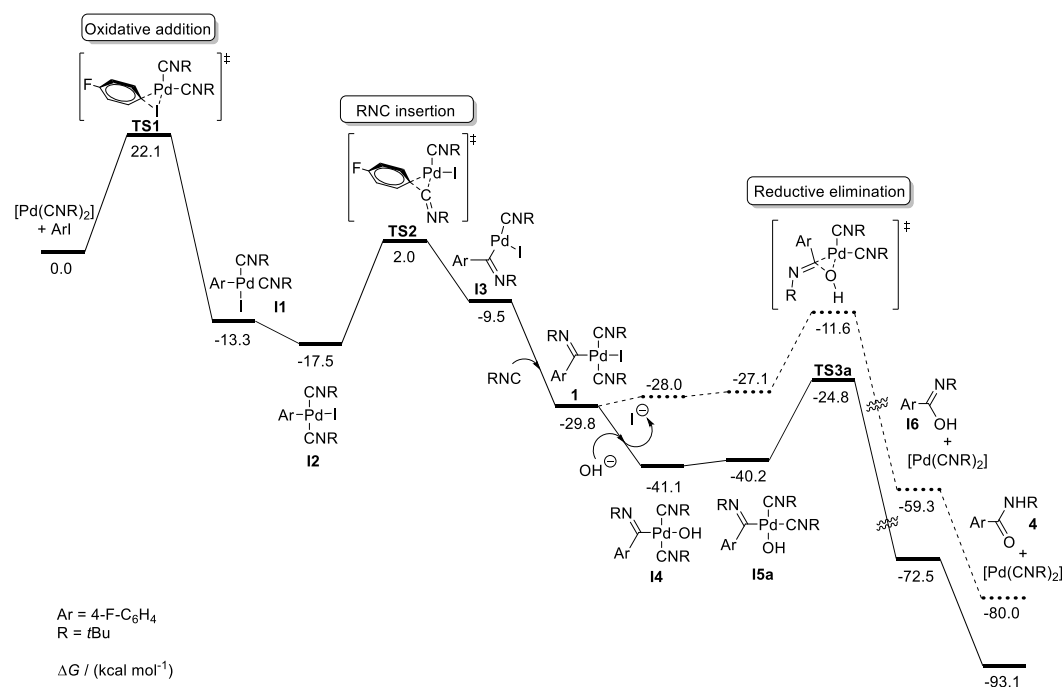


Figure 18 –Reaction path for the amidation of 4-fluoriodobenzene with *t*BuNC. Solid line: computed Gibbs free energies reported for all the species at concentration 0.04 M (1 atm) at 298 K. Dashed lines: Gibbs free energies for all the species at 0.04 M except [OH⁻] = 10⁻¹¹ M.

^{xiii} The torsion angle between the Ar ring and the imidoyl moiety of the theoretically optimized structure of **1** is close to zero, making the ArC=N*t*Bu moiety flat and perpendicular to the plane of the complex. By contrast, in the X-ray structure the Pd-C1-C2-C7 dihedral is 63.4°. This difference may be due to the effects of packing in the solid state (Figure 9), so it appeared reasonable to exclude the Ar ring from the calculation of the RMSD between the computed geometry in the gas phase and the solid-state experimental structure.

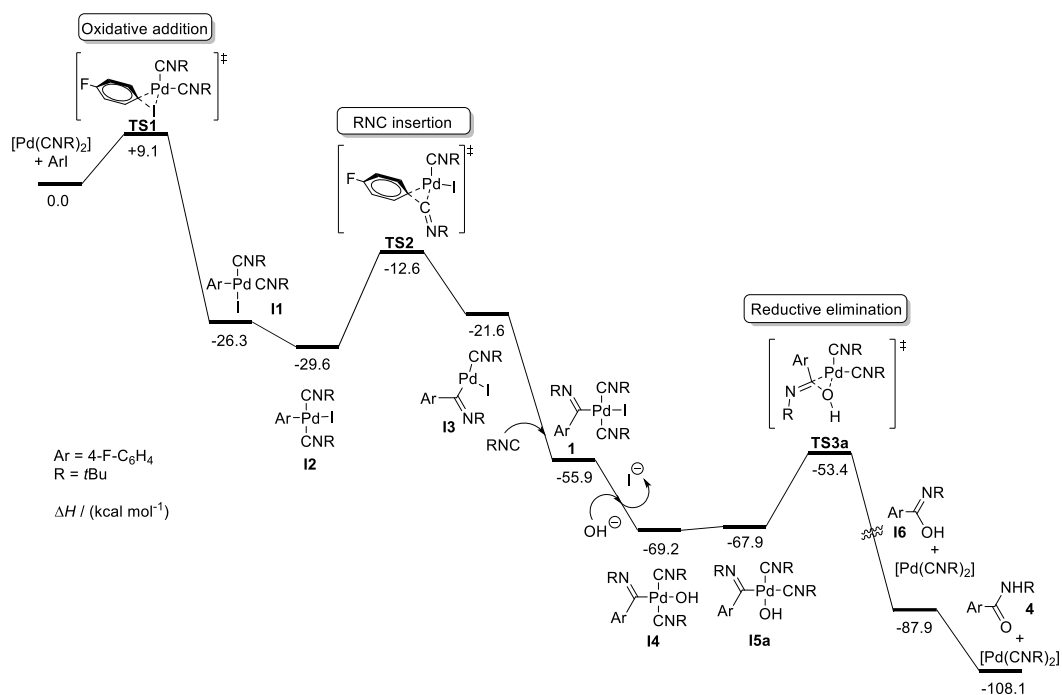


Figure 19 – Reaction path for the amidation of 4-fluoriodobenzene with *t*BuNC. Computed enthalpies reported for all the species at concentration 0.04 M (1 atm) at 298 K.

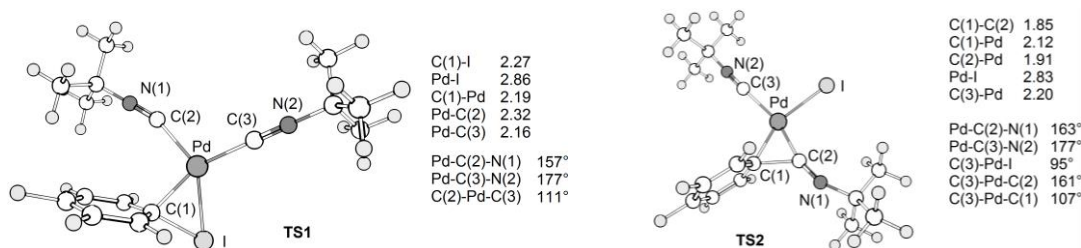


Figure 20 – Structures and selected geometric parameters for **TS1** and **TS2**, as resulting from DFT calculations.

Iodide exchange with OH⁻ is favorable ($\Delta G = -11.3$ kcal mol⁻¹, $\Delta H = -13.3$ kcal mol⁻¹) and delivers *trans*-[(ArC=N*t*Bu)Pd(CN*t*Bu)₂(OH)] (**I4**). Isomerization of **I4** to *cis* isomer **I5a** can take place easily at room temperature ($\Delta G = +0.9$ kcal mol⁻¹, $\Delta H = +1.3$ kcal mol⁻¹). The latter complex is the starting point for C-O bond forming reductive elimination, which takes place through **TS3a** ($\Delta G^\ddagger = +15.5$ kcal mol⁻¹, $\Delta H^\ddagger = +14.5$ kcal mol⁻¹) and produces the amide tautomer (imidic acid) **I6** and regenerates [Pd(CN*t*Bu)₂] in a highly exothermic and exergonic process ($\Delta G = -32.3$ kcal mol⁻¹, $\Delta H = -20.0$ kcal mol⁻¹). IRC calculations starting from **TS3a** did not lead to a complex formed between [Pd(CN*t*Bu)₂] and **I6**, but it linked **TS3a** directly to the two dissociated products. The C-O bond distance in **TS3a** is 1.83 Å, which is to be compared with 1.36 Å of the product (**I6**), meaning that this bond is quite not formed in the TS, *i.e.* that the TS is quite reactant-like, if judged from this parameter (Figure 21). The two *t*BuNC ligands do not deviate much the initial square planar geometry (the C-Pd-C angle is 103°), and differently from **TS1** the two *t*BuNC ligands are coordinating with an almost linear linear Pd-C-N arrangement (the angles are 177° and 171°), even if the *t*BuNC ligand *trans* to the imidoyl moiety

is less strongly bound than the other one (Pd-C bond distance: 2.30 Å, while for the other it is 2.07 Å). Tautomerization of **16** to the amide **4** is again favorable ($\Delta G = -20.6$ kcal mol⁻¹, $\Delta H = -20.2$ kcal mol⁻¹) and it should take place by a solvent-mediated proton transfer, as already pointed out by Wu (Figure 1).^[137]

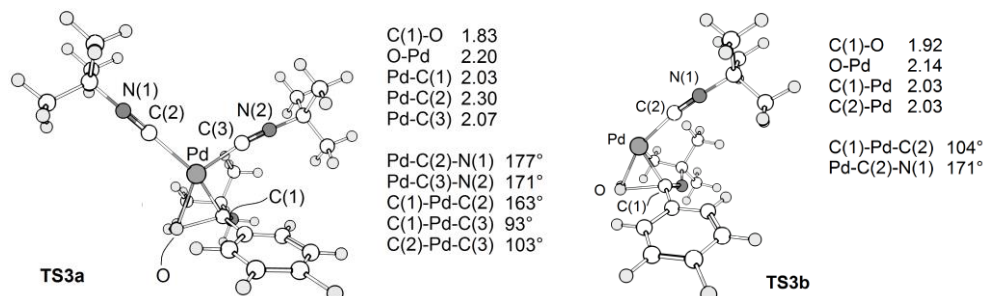


Figure 21 – Structures and selected geometric parameters for **TS3a** and **TS3b**, as resulting from DFT calculations.

At first sight, from the Gibbs free energy profile reported in Figure 18, it may be expected that complexes **14** and **15a** would be observable intermediates when the reaction is performed in the presence of OH⁻. In this respect, it is worth noting that free energies calculated as usual assuming a partial pressure of 1 atm for all the species (*i.e.* at a concentration of about 0.04 M within the ideal gas approximation at 298 K) are not representative of the conditions in which the experiments with a F⁻ / HF mixture are performed, since the concentration of OH⁻ secured by this buffer is much smaller.

To give a very rough estimate of [OH⁻], we may consider that the pK_a of HF in water is approximately 3.2, so the order of magnitude of [OH⁻] in the presence of equal molar quantities of F⁻ and HF in water is 10⁻¹¹ M. Assuming [OH⁻] = 10⁻¹¹ M (even if this calculation is not valid in the mixed water/organic solvent system used in the experiments), the difference in free energy is approximately +13.1 kcal mol⁻¹ at 298 K. Applying this correction where appropriate (dashed lines in Figure 18), **14** is now at a higher free energy than **1**, which is in accordance with the fact that **14** could not be identified spectroscopically under conditions close to the catalytic reaction.

To obtain some information about the byproduct-forming double insertion of isocyanide, the relevant transition states (**TS4** and **TS5**) for the insertion into the C-Pd bond of second molecule of coordinate isocyanide starting either from neutral complex **1** or from cationic [ArPd(CN*t*Bu)₃]⁺ (**2**) to give the bis-inserted complexes [Ar(C=N*t*Bu)₂Pd(CN*t*Bu)I] and [Ar(C=N*t*Bu)₂Pd(CN*t*Bu)₂] respectively have been located by DFT calculations (Figure 22). Comparable activation barriers were found ($\Delta G^\ddagger = 22.0$ kcal mol⁻¹ for both cases and $\Delta H^\ddagger = +21.0$ kcal mol⁻¹ and $\Delta H^\ddagger = +20.4$ kcal mol⁻¹ respectively), and not much higher than those of the other steps of the catalytic cycle, in agreement with the hypothesis that this reaction can be competitive with respect to the steps leading to the desired amide **4**.

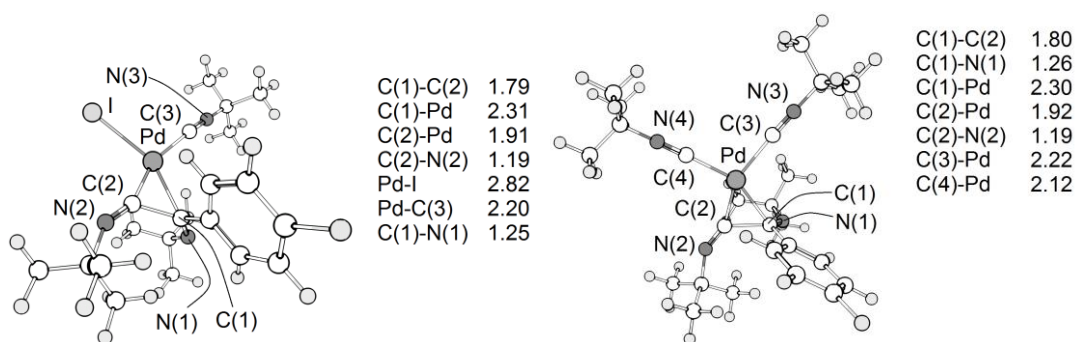


Figure 22 – Structures and selected geometric parameters of the transition states for the double insertion of *t*BuNC, starting from *trans*-[(ArC=N*t*Bu)Pd(CN*t*Bu)₂I] (**1**, left) and from [(ArC=N*t*Bu)Pd(CN*t*Bu)₃]⁺ (**2**, right), as resulting from computations at the DFT level.

2.9. Theoretical study of the C-O bond forming reductive elimination

Considering that reductive elimination is arguably the most critical step of the catalytic cycle, we studied it more in detail. In the pathways we reported in the previous section (Figure 18 and Figure 19), we assumed that reductive elimination takes place starting from a tetracoordinate *cis*-[(ArC=N*t*Bu)Pd(CN*t*Bu)₂(OH)] complex (**I5a**). Actually, multiple complexes featuring a *cis* arrangement of OH⁻ and the imidoyl residue can in principle be formed in solution and take part into this process, by ejection of one of the *t*BuNC ligands or by substitution with another species present in the reaction medium. We have evaluated the stability of several of these complexes and the barrier of the reductive elimination starting from each of them (Figure 23).

More in detail, two tricoordinate, T-shape complexes of this kind may exist: one in which the *t*BuNC ligand *trans* to the imidoyl moiety is removed (**I5b**) or one in which the *t*BuNC ligand *cis* to it is detached (**I5c**). In accordance with the *thermodynamic trans effect*,^[161] the *t*BuNC ligand *trans* to the imidoyl group is easier to remove (**I5b**, $\Delta G = +0.3$ kcal mol⁻¹) than the one *trans* to OH⁻ (**I5c**, $\Delta G = +14.3$ kcal mol⁻¹). For each of this two possible structures, a solvent molecule (DMSO) can occupy the empty coordination site. DMSO is an ambidentate ligand, and it can either coordinate through the oxygen atom (**I5d**, **I5e**) or through the sulfur atom (**I5f**, **I5g**). In general, O-coordination appears to be more favorable than S-coordination (Figure 23).

Concerning the barriers for C-O bond forming reductive elimination, the lowest one is computed starting from the coordinatively unsaturated complex **I5b**, corresponding to the transition state **TS3b**. It was not possible to locate a transition state associated to the high-energy T-shape complex **I5c**, because during optimization ready isomerization to the more stable isomer featuring an empty coordination site *trans* to the imidoyl group took place. All the solvent-coordinated TSs (**TS3d-g**) lie higher in free energy than **TS3b**.

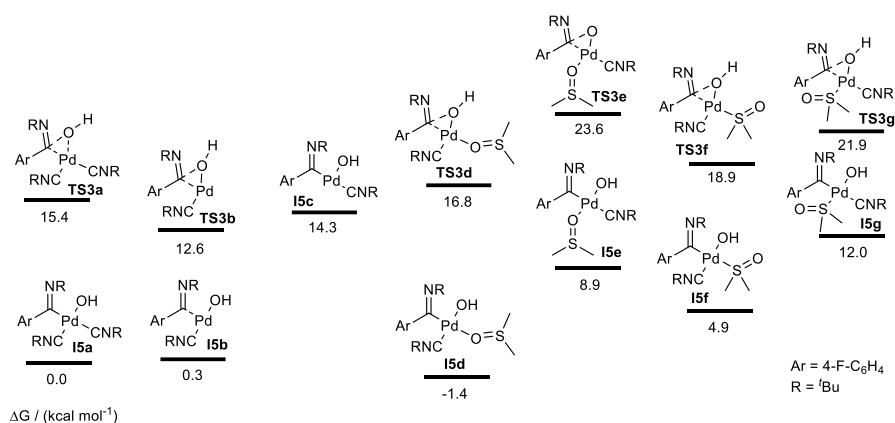


Figure 23 – Relative stabilities (calculated ΔG at 25 °C) of different imidoyl-palladium cis-hydroxo-complexes **I5a-g** and of the respective transition states for reductive elimination **TS3a-b,d-g**. It is not possible to locate a TS corresponding to **I5c**, since isomerization to **I5b** occurs.

It is instructive to compare, for example, the stable intermediates **I5b** and **I5d** with the corresponding TSs (**TS3b** and **TS3d**). Binding a DMSO molecule (through the oxygen atom) to **I5b**, thus affording **I5d**, gives a modest stabilization ($\Delta G = -1.7$ kcal mol⁻¹). By contrast, addition of a DMSO molecule to **TS3b** to give **TS3d** corresponds to a destabilization ($\Delta G = + 4.4$ kcal mol⁻¹). It has been already observed that, quite puzzlingly,^{xiv} C-C bond forming reductive elimination is easier for coordinatively unsaturated species.^[162]

Comparing the geometric parameters of **TS3a** and **TS3b** (Figure 21) is not illuminating about a possible reason for the different stability of tricoordinate and tetracoordinate TSs for reductive elimination, the C-O bond distance for example being shorter for the former than for the latter (1.83 Å and 1.92 Å respectively). A rationale for this behavior, that has been already noted earlier on other systems on the basis of either extended Huckel and DFT calculations,^[163,164] can be given by analyzing the orbital diagram shown in Figure 24. If we consider the interaction of a “metal” fragment (either ML or ML₂, L = ligand) with a X-Y fragment (XY is the product of reductive elimination), the key factor is the different occupation of the molecular orbital corresponding to an interaction of approximate σ symmetry between the two fragments. Whereas for both types of complex the interactions roughly corresponding to π symmetry are bonding, those roughly corresponding to σ -symmetry are repulsive for the two interacting full orbitals in the tetracoordinate system, but bonding for the empty-full interaction in the tricoordinate system. These considerations justify the reduced activation barrier for the reductive elimination proceeding from the coordinatively unsaturated T-shape complex.

^{xiv} It is quite paradoxical, at first sight, that elimination of coordinated ligands takes place more easily from a complex that is somehow already unsaturated.

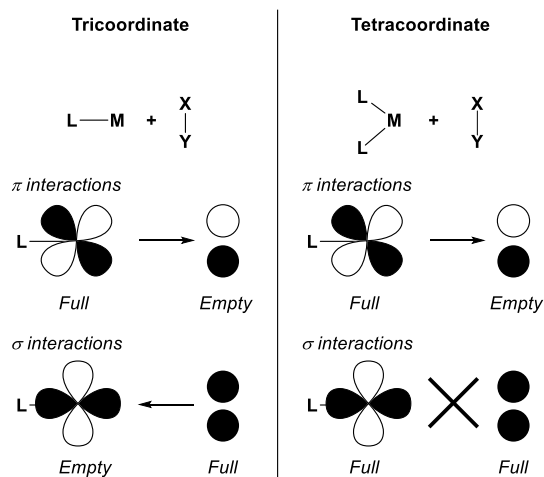


Figure 24 – Main orbital interactions for the reductive elimination from tricoordinate and tetracoordinate d^8 metal complexes.^[162]

In summary, the enhanced reactivity of coordinatively unsaturated species predicted by DFT calculations may contribute to explain the inhibition of reductive elimination exerted by excess *t*BuNC we observed experimentally (§2.7) and the rate acceleration in the presence of $[\text{PdCl}_2(\text{NCPH})_2]$, which can act as a scavenger for *t*BuNC.

3. Conclusions

We performed a detailed mechanistic study on the synthesis of secondary amides by the Pd-catalyzed coupling of haloarenes with isocyanides and water. This is a prototypical imidoylative coupling in which the isocyanide inserts into the C-Pd bond and water acts formally as a nucleophile.

First, studies were performed as to mimic under stoichiometric conditions the reaction that occurs in the absence of any added ligand (such as phosphines), *i.e.* the so-called *ligandless* conditions. It was established that the isocyanide substrate could play the role of a ligand for palladium complexes in all the intermediates of the catalytic cycle and modulate their reactivity in several ways. On the basis of the results shown in the previous sections, we can propose the revised mechanism depicted in Figure 25, featuring isocyanide-ligated complexes in every step of the catalytic cycle. Intermediates and resting states that have been isolated and characterized are highlighted in dashed rectangles.

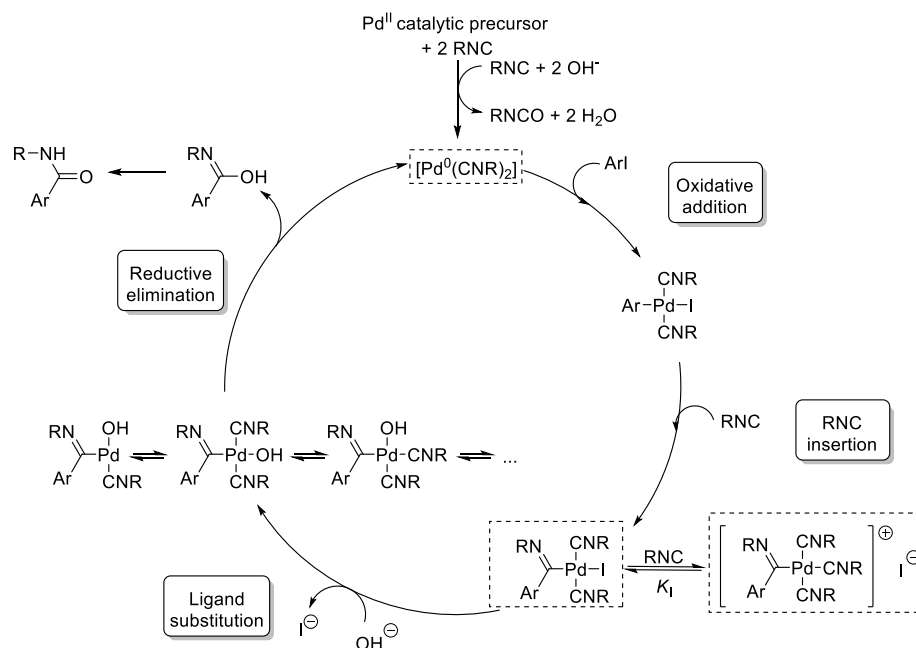


Figure 25 – Revised catalytic cycle for the palladium-catalyzed synthesis of secondary amides from iodoarenes and isocyanides.

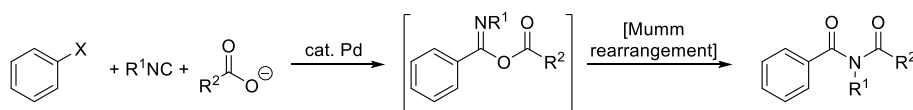
Oxidative addition, the entry point of the catalytic cycle, can take place on isocyanide-ligated palladium(0) complexes. The kinetics of this reaction were studied and remarkably it was observed that excess isocyanide does not inhibit the reaction, as it normally happens with other ligands such as phosphines. The latter, indeed, have the tendency to form unreactive tricoordinate 16-electron complexes instead of the active dicoordinate 14-electron species. Interestingly, isocyanides do not display this behavior. Insertion of the isocyanide in the C-Pd bond is faster than oxidative addition, so it could not be studied in the conditions of our reaction, albeit it has been examined in detail in previous studies on related systems (see §1.4).

In polar solvents, such as DMSO, the medium in which the model reaction is most efficient (Scheme 38),^[40] the intermediate $[(\text{ArC}=\text{N}/\text{Bu})\text{Pd}(\text{CNR})_2\text{I}]$ have the tendency to undergo displacement of the coordinated iodide, thus giving cationic $[(\text{ArC}=\text{N}/\text{Bu})\text{Pd}(\text{CNR})_3]^+$. These latter species are not directly involved in the product forming reductive elimination with OH^- , but they are most likely a resting state responsible for catalyst deactivation and side reactions, such as poly-insertion of isocyanide.

Isolated *trans*- $[(\text{ArC}=\text{N}/\text{Bu})\text{Pd}(\text{CN}/\text{Bu})_2\text{I}]$ undergoes reductive elimination in the presence of water and a F^- / HF buffer at room temperature. This reaction is severely hampered by excess isocyanide, probably because of the formation of the abovementioned cationic species and prevention of the formation of coordinatively unsaturated complexes. The latter are expected to be more reactive towards reductive elimination, as DFT calculation attests.

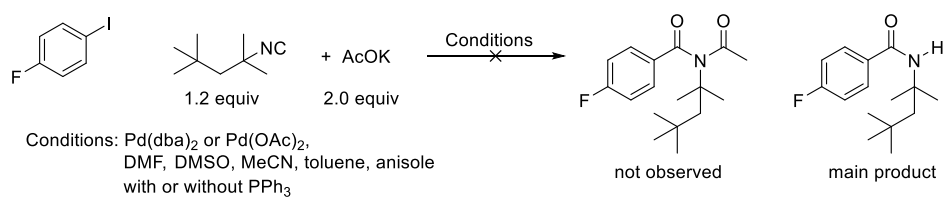
Since several imidoylative couplings are better performing in the presence of monodentate or bidentate phosphines (see §1.3), the interaction of *trans*- $[(\text{ArC}=\text{N}/\text{Bu})\text{Pd}(\text{CN}/\text{Bu})_2\text{I}]$ with two model ligands (PPh_3 and dppe) has been examined. In both cases, cationic complexes deriving from displacement of I^- from the coordination sphere are readily formed in polar and moderately polar solvents. Generally speaking, the formation of these cationic complexes is also not desirable, as they are not intermediate of the catalytic cycle, but they can take part into side-reactions, *i.e.* poly-insertion of isocyanide.

As a development of this study we also hoped to extend the scope of nucleophiles useable in Pd-catalyzed imidoylative couplings. For example, up to date no conditions have been described for the use of carboxylates as nucleophiles.^{xv} In principle, this reaction would lead to *O*-acyl imidates that are known to rearrange readily to imides by a Mumm-type rearrangement (Scheme 45). Unfortunately, despite several efforts we were not able to find conditions to effect this transformation (Scheme 46). The secondary amide was the main product formed in most of the conditions we screened for this transformation, probably due to adventitious water introduced together with the reagents (Scheme 46). The *in situ* use of dehydrating agents compatible with the catalyst may be key to the successful development of this transformation.



Scheme 45 – Hypothetical imidoylative coupling involving carboxylates as nucleophiles and subsequent Mumm-type rearrangement leading to unsymmetrical tertiary imides.

^{xv} A formally similar reaction, involving the addition of aryl radicals generated from aryldiazonium salts to isocyanides and subsequent trapping with carboxylates in the absence of any metal catalyst has been developed in our laboratory.^[176]



Scheme 46 – Attempted imidoylative coupling reactions involving AcO⁻ as a nucleophile.

4. Computational details

All DFT calculations were performed with the Gaussian09 program (Rev. A02).^[165] The structures of all minima and transition states were fully optimized using the M06-2X functional^[166] and the following basis set: LANL2DZ with the associate effective core potential for Pd,^[167,168] 6-31+G(d) for N, O, S, P and C atoms directly bound to Pd, 6-311G* for I and 6-31G for all the others atoms. Bulk solvent effects were accounted for by using an implicit solvation model (IEF-PCM) as implemented in Gaussian.^[169,170] The default spheres radii, static and optical dielectric constants were used. All stationary points were characterized as minima or first-order transition states by analytical frequency calculations. IRC calculations were used to confirm that transition states linked the proper minima. Computed harmonic frequencies were also used to calculate the free energy of all molecules at $T = 298$ K and $P = 1$ atm assuming an ideal gas behavior.

5. References

- [1] A. Dömling, *Chem. Rev.* **2006**, *106*, 17–89.
- [2] J. E. Biggs-Houck, A. Younai, J. T. Shaw, *Curr. Opin. Chem. Biol.* **2010**, *14*, 371–382.
- [3] L. El Kaïm, L. Grimaud, *Tetrahedron* **2009**, *65*, 2153–2171.
- [4] A. V. Gulevich, A. G. Zhdanko, R. V. A. Orru, V. G. Nenajdenko, *Chem. Rev.* **2010**, *110*, 5235–5331.
- [5] S. Otsuka, A. Nakamura, T. Yoshida, *J. Am. Chem. Soc.* **1969**, *91*, 7196–7198.
- [6] Y. Yamamoto, H. Yamazaki, *Bull. Chem. Soc. Jpn.* **1970**, *43*, 2653–2653.
- [7] J.-J. Brunet, R. Chauvin, *Chem. Soc. Rev.* **1995**, *24*, 89.
- [8] M. Beller, B. Cornils, C. D. Frohning, C. W. Kohlpaintner, *J. Mol. Catal. A Chem.* **1995**, *104*, 17–85.
- [9] B. El Ali, H. Alper, *Synlett* **2000**, *2000*, 161–171.
- [10] R. Skoda-Foldes, L. Kollar, *Curr. Org. Chem.* **2002**, *6*, 1097–1119.
- [11] T. Morimoto, K. Kakiuchi, *Angew. Chem. Int. Ed. Engl.* **2004**, *43*, 5580–8.
- [12] A. M. Trzeciak, J. J. Ziółkowski, *Coord. Chem. Rev.* **2005**, *249*, 2308–2322.
- [13] C. F. J. Barnard, *Organometallics* **2008**, *27*, 5402–5422.
- [14] R. Grigg, S. P. Mutton, *Tetrahedron* **2010**, *66*, 5515–5548.
- [15] X.-F. Wu, H. Neumann, M. Beller, *Chem. Soc. Rev.* **2011**, *40*, 4986–5009.
- [16] I. Omae, *Coord. Chem. Rev.* **2011**, *255*, 139–160.
- [17] X.-F. Wu, H. Neumann, M. Beller, *Chem. Rev.* **2013**, *113*, 1–35.
- [18] Y. Yamamoto, H. Yamazaki, *Coord. Chem. Rev.* **1972**, *8*, 225–239.
- [19] S. Lang, *Chem. Soc. Rev.* **2013**, *42*, 4867–4880.
- [20] T. Vlaar, E. Ruijter, B. U. W. Maes, R. V. A. Orru, *Angew. Chem. Int. Ed.* **2013**, *52*, 7084–7097.
- [21] S. Chakrabarty, S. Choudhary, A. Doshi, F.-Q. Q. Liu, R. Mohan, M. P. Ravindra, D. Shah, X. Yang, F. F. Fleming, *Adv. Synth. Catal.* **2014**, *356*, 2135–2196.
- [22] V. P. Boyarskiy, N. A. Bokach, K. V. Luzyanin, V. Y. Kukushkin, *Chem. Rev.* **2015**, *115*, 2698–2779.
- [23] B. Song, B. Xu, *Chem. Soc. Rev.* **2017**, *46*, 1103–1123.
- [24] Y. Yamamoto, H. Yamazaki, *Inorg. Chem.* **1974**, *13*, 438–443.
- [25] G. R. Owen, R. Vilar, A. J. P. White, D. J. Williams, *Organometallics* **2002**, *21*, 4799–4807.
- [26] Y. Yamamoto, T. Tanase, T. Yanai, T. Asano, K. Kobayashi, *J. Organomet. Chem.* **1993**, *456*, 287–291.
- [27] T. Tanase, T. Ohizumi, K. Kobayashi, Y. Yamamoto, *Organometallics* **1996**, *15*, 3404–3411.
- [28] F. Millich, *Chem. Rev.* **1972**, *72*, 101–113.
- [29] Y. Ito, M. Suginome, in *Handbook of Organopalladium Chemistry for Organic Synthesis*, John Wiley & Sons, Inc., New York, USA, **2003**, pp. 2705–2712.
- [30] M. Suginome, Y. Ito, in *Adv. Polym. Sci.*, Springer GmbH, Heidelberg, **2004**, pp. 77–136.
- [31] P. Veya, C. Floriani, A. Chiesi-Villa, C. Rizzoli, *Organometallics* **1993**, *12*, 4899–4907.
- [32] J. Vicente, J.-A. Abad, E. Martínez-Viviente, P. G. Jones, *Organometallics* **2002**, *21*, 4454–4467.
- [33] G. Qiu, Q. Ding, J. Wu, *Chem. Soc. Rev.* **2013**, *42*, 5257–69.
- [34] M. Kosugi, T. Ogata, H. Tamura, H. Sano, T. Migita, *Chem. Lett.* **1986**, *15*, 1197–1200.
- [35] T. Ishiyama, T. Oh-e, N. Miyaura, A. Suzuki, *Tetrahedron Lett.* **1992**, *33*, 4465–4468.
- [36] C. G. C. Saluste, R. R. J. Whitby, M. Furber, *Angew. Chem. Int. Ed. Engl.* **2000**, *39*, 4156–4158.
- [37] C. G. Saluste, R. J. Whitby, M. Furber, *Tetrahedron Lett.* **2001**, *42*, 6191–6194.
- [38] K. K. R. Tetala, R. J. Whitby, M. E. Light, M. B. Hurtshouse, *Tetrahedron Lett.* **2004**, *45*, 6991–6994.
- [39] R. J. Whitby, C. Gustaf Saluste, M. Furber, *Org. Biomol. Chem.* **2004**, *2*, 1974–1976.
- [40] H. Jiang, B. Liu, Y. Li, A. Wang, H. Huang, *Org. Lett.* **2011**, *13*, 1028–1031.
- [41] T. Tang, X.-D. Fei, Z.-Y. Ge, Z. Chen, Y.-M. Zhu, S.-J. Ji, *J. Org. Chem.* **2013**, *78*, 3170–3175.
- [42] W. S. Matthews, J. E. Bares, J. E. Bartmess, F. G. Bordwell, F. J. Cornforth, G. E. Drucker, Z. Margolin, R. J. McCallum, G. J. McCollum, N. R. Vanier, *J. Am. Chem. Soc.* **1975**, *97*, 7006–7014.
- [43] F. G. Bordwell, *Acc. Chem. Res.* **1988**, *21*, 456–463.
- [44] U. K. Sharma, N. Sharma, J. Xu, G. Song, E. V. Van der Eycken, *Chem. Eur. J.* **2015**, *21*, 4908–4912.

- [45] X. Jiang, J.-M. Wang, Y. Zhang, Z. Chen, Y.-M. Zhu, S.-J. Ji, *Org. Lett.* **2014**, *16*, 3492–3495.
- [46] X. Jiang, J.-M. Wang, Y. Zhang, Z. Chen, Y.-M. Zhu, S.-J. Ji, *Tetrahedron* **2015**, *71*, 4883–4887.
- [47] P. J. Boissarie, Z. E. Hamilton, S. Lang, J. A. Murphy, C. J. Suckling, *Org. Lett.* **2011**, *13*, 6256–6259.
- [48] V. N. Bochatay, P. J. Boissarie, J. A. Murphy, C. J. Suckling, S. Lang, *J. Org. Chem.* **2013**, *78*, 1471–1477.
- [49] R. S. Sanchez, F. A. Zhuravlev, *J. Am. Chem. Soc.* **2007**, *129*, 5824–5.
- [50] C. Hansch, A. Leo, R. W. Taft, *Chem. Rev.* **1991**, *91*, 165–195.
- [51] C. G. Saluste, S. Crumpler, M. Furber, R. J. Whitby, *Tetrahedron Lett.* **2004**, *45*, 6995–6996.
- [52] G. Van Baelen, S. Kuijter, L. Rýček, S. Sergejev, E. Janssen, F. J. J. de Kanter, B. U. W. Maes, E. Ruijter, R. V. A. Orru, *Chem. Eur J.* **2011**, *17*, 15039–15044.
- [53] J. Wang, S. Luo, J. Huang, T. Mao, Q. Zhu, *Chem. Eur J.* **2014**, *20*, 11220–11224.
- [54] D. P. Curran, W. Du, *Org. Lett.* **2002**, *4*, 3215–3218.
- [55] H. Josien, S.-B. Ko, D. Bom, D. P. Curran, *Chem. Eur J.* **1998**, *4*, 67–83.
- [56] Z. Hu, D. Liang, J. Zhao, J. Huang, Q. Zhu, *Chem. Commun.* **2012**, *48*, 7371.
- [57] A. Jutand, *Chem. Rev.* **2008**, *108*, 2300–47.
- [58] A. Jutand, *Eur. J. Inorg. Chem.* **2003**, *2003*, 2017–2040.
- [59] J.-F. Fauvarque, F. Pflüger, M. Troupel, *J. Organomet. Chem.* **1981**, *208*, 419–427.
- [60] C. Amatore, F. Pflüger, *Organometallics* **1990**, *9*, 2276–2282.
- [61] C. Amatore, E. Carre, A. Jutand, M. A. M'Barki, *Organometallics* **1995**, *14*, 1818–1826.
- [62] M. R. Netherton, G. C. Fu, *Angew. Chem. Int. Ed.* **2002**, *41*, 3910–3912.
- [63] I. D. Hills, M. R. Netherton, G. C. Fu, *Angew. Chem. Int. Ed.* **2003**, *42*, 5749–5752.
- [64] F. Barrios-Landeros, J. F. Hartwig, *J. Am. Chem. Soc.* **2005**, *127*, 6944–6945.
- [65] F. Barrios-Landeros, B. P. Carrow, J. F. Hartwig, *J. Am. Chem. Soc.* **2009**, *131*, 8141–8154.
- [66] E. Lyngvi, F. Schoenebeck, *Tetrahedron* **2013**, *69*, 5715–5718.
- [67] A. Kurbangalieva, D. Carmichael, K. K. M. Hii, A. Jutand, J. M. Brown, *Chem. Eur. J.* **2014**, *20*, 1116–1125.
- [68] C. L. McMullin, N. Fey, J. N. Harvey, *Dalt. Trans.* **2014**, *43*, 13545.
- [69] S. Borjian, M. C. Baird, *Organometallics* **2014**, *33*, 3936–3940.
- [70] J. F. Hartwig, F. Paul, *J. Am. Chem. Soc.* **1995**, *117*, 5373–5374.
- [71] F. Proutiere, F. Schoenebeck, *Angew. Chem. Int. Ed.* **2011**, *50*, 8192–8195.
- [72] M. Portnoy, D. Milstein, *Organometallics* **1993**, *12*, 1665–1673.
- [73] L. M. Alcazar-Roman, J. F. Hartwig, A. L. Rheingold, L. M. Liable-Sands, I. A. Guzei, *J. Am. Chem. Soc.* **2000**, *122*, 4618–4630.
- [74] L. M. Alcazar-Roman, J. F. Hartwig, *Organometallics* **2002**, *21*, 491–502.
- [75] A. Jutand, K. K. (Mimi) Hii, M. Thornton-Pett, J. M. Brown, *Organometallics* **1999**, *18*, 5367–5374.
- [76] I. J. S. Fairlamb, *Org. Biomol. Chem.* **2008**, *6*, 3645.
- [77] C. Amatore, A. Jutand, *Coord. Chem. Rev.* **1998**, *178–180*, 511–528.
- [78] C. Amatore, A. Jutand, F. Khalil, M. A. M'Barki, L. Mottier, *Organometallics* **1993**, *12*, 3168–3178.
- [79] C. Amatore, G. Broeker, A. Jutand, F. Khalil, *J. Am. Chem. Soc.* **1997**, *119*, 5176–5185.
- [80] C. Amatore, A. Fuxa, A. Jutand, *Chem. Eur. J.* **2000**, *6*, 1474–1482.
- [81] C. Amatore, A. Bucaille, A. Fuxa, A. Jutand, G. Meyer, A. Ndedi Ntepe, *Chem. Eur. J.* **2001**, *7*, 2134–2142.
- [82] C. Amatore, A. Jutand, F. Khalilb, *ARKIVOC* **2006**, *2006*, 38–48.
- [83] C. Amatore, A. Jutand, *J. Organomet. Chem.* **1999**, *576*, 254–278.
- [84] C. Amatore, A. Jutand, *Acc. Chem. Res.* **2000**, *33*, 314–321.
- [85] C. Amatore, M. Azzabi, A. Jutand, *J. Organomet. Chem.* **1989**, *363*, C41–C45.
- [86] C. Amatore, A. Jutand, A. Suarez, *J. Am. Chem. Soc.* **1993**, *115*, 9531–9541.
- [87] C. Amatore, E. Carre, A. Jutand, M. A. M'Barki, G. Meyer, *Organometallics* **1995**, *14*, 5605–5614.
- [88] C. Amatore, A. Jutand, F. Lemaître, J. L. Ricard, S. Kozuch, S. Shaik, *J. Organomet. Chem.* **2004**, *689*, 3728–3734.
- [89] A. Jutand, J. Pytkowicz, S. Roland, P. Mangeney, *Pure Appl. Chem.* **2010**, *82*, 1393–1402.
- [90] J. C. Green, B. J. Herbert, R. Lonsdale, *J. Organomet. Chem.* **2005**, *690*, 6054–6067.
- [91] S. Otsuka, K. Ataka, *J. Chem. Soc., Dalt. Trans.* **1976**, 327–334.
- [92] A. Campagnaro, A. Mantovani, P. Uguagliati, *Inorganica Chim. Acta* **1985**,

- 99, L15–L19.
- [93] R. Bertani, A. Berton, F. Di Bianca, B. Crociani, *J. Organomet. Chem.* **1986**, *303*, 283–299.
- [94] J. G. P. Delis, P. G. Aubel, P. W. N. M. van Leeuwen, K. Vrieze, N. Veldman, A. L. Spek, *J. Chem. Soc., Chem. Commun.* **1995**, 2233–2234.
- [95] J. G. P. Delis, P. G. Aubel, K. Vrieze, P. W. N. M. van Leeuwen, N. Veldman, A. L. Spek, F. J. R. van Neer, *Organometallics* **1997**, *16*, 2948–2957.
- [96] Y. Kayaki, I. Shimizu, A. Yamamoto, *Bull. Chem. Soc. Jpn.* **1997**, *70*, 917–927.
- [97] L. Canovese, F. Visentin, C. Santo, C. Levi, A. Dolmella, *Organometallics* **2007**, *26*, 5590–5601.
- [98] L. Canovese, F. Visentin, C. Santo, C. Levi, *Organometallics* **2009**, *28*, 6762–6770.
- [99] L. Canovese, G. Chessa, F. Visentin, *Inorganica Chim. Acta* **2010**, *363*, 3426–3431.
- [100] L. Canovese, F. Visentin, C. Santo, V. Bertolasi, *Organometallics* **2014**, *33*, 1700–1709.
- [101] J. Vicente, J.-A. Abad, F. S. Hernandez-Mata, B. Rink, P. G. Jones, M. C. Ramirez de Arellano, *Organometallics* **2004**, *23*, 1292–1304.
- [102] J. T. Chen, A. Sen, *J. Am. Chem. Soc.* **1984**, *106*, 1506–1507.
- [103] F. Ozawa, H. Soyama, H. Yanagihara, I. Aoyama, H. Takino, K. Izawa, T. Yamamoto, A. Yamamoto, *J. Am. Chem. Soc.* **1985**, *107*, 3235–3245.
- [104] F. Ozawa, N. Kawasaki, H. Okamoto, T. Yamamoto, A. Yamamoto, *Organometallics* **1987**, *6*, 1640–1651.
- [105] L. Huang, F. Ozawa, A. Yamamoto, *Organometallics* **1990**, *9*, 2603–2611.
- [106] A. Yamamoto, F. Ozawa, K. Osakada, L. Huang, T. Son, N. Kawasaki, M.-K. Doh, *Pure Appl. Chem.* **1991**, *63*, 687–696.
- [107] Y.-S. Lin, A. Yamamoto, *Organometallics* **1998**, *17*, 3466–3478.
- [108] P. W. N. M. van Leeuwen, M. A. Zuideveld, B. H. G. Swennenhuis, Z. Freixa, P. C. J. Kamer, K. Goubitz, J. Fraanje, M. Lutz, A. L. Spek, *J. Am. Chem. Soc.* **2003**, *125*, 5523–5539.
- [109] R. D. O’Sullivan, A. W. Parkins, *J. Chem. Soc. Chem. Commun.* **1984**, 1165.
- [110] J. Dupont, M. Pfeffer, *J. Chem. Soc., Dalt. Trans.* **1990**, 3193–3198.
- [111] J. Vicente, I. Saura-Llamas, J. Turpin, M. C. Ramirez de Arellano, P. G. Jones, *Organometallics* **1999**, *18*, 2683–2693.
- [112] J. Vicente, J.-A. Abad, W. Foertsch, P. G. Jones, A. K. Fischer, *Organometallics* **2001**, *20*, 2704–2715.
- [113] J. Vicente, J.-A. Abad, A. D. Frankland, J. Lopez-Serrano, M. C. Ramirez de Arellano, P. G. Jones, *Organometallics* **2002**, *21*, 272–282.
- [114] J. Vicente, J.-A. Abad, E. Martinez-Viviente, P. G. Jones, *Organometallics* **2003**, *22*, 1967–1978.
- [115] G. R. Owen, R. Vilar, A. J. P. White, D. J. Williams, *Organometallics* **2003**, *22*, 4511–4521.
- [116] J. Vicente, J.-A. Abad, W. Foertsch, M.-J. López-Sáez, P. G. Jones, *Organometallics* **2004**, *23*, 4414–4429.
- [117] J. Vicente, A. Arcas, J. M. Fernández-Hernández, D. Bautista, P. G. Jones, *Organometallics* **2005**, *24*, 2516–2527.
- [118] J. Vicente, M. T. Chicote, A. J. Martinez-Martinez, P. G. Jones, D. Bautista, *Organometallics* **2008**, *27*, 3254–3271.
- [119] J. Vicente, M. T. Chicote, A. J. Martinez-Martinez, D. Bautista, *Organometallics* **2009**, *28*, 5915–5924.
- [120] J. Vicente, I. Saura-Llamas, J.-A. García-López, D. Bautista, *Organometallics* **2009**, *28*, 448–464.
- [121] J. Vicente, M. T. Chicote, A. J. Martinez-Martinez, A. Abellan-Lopez, D. Bautista, *Organometallics* **2010**, *29*, 5693–5707.
- [122] J. Vicente, A. Arcas, F. Julia-Hernandez, D. Bautista, P. G. Jones, *Organometallics* **2010**, *29*, 3066–3076.
- [123] J. Vicente, J. A. Abad, R.-M. Lopez-Nicolas, P. G. Jones, *Organometallics* **2011**, *30*, 4983–4998.
- [124] J. Vicente, P. Gonzalez-Herrero, R. Frutos-Pedreno, M.-T. Chicote, P. G. Jones, D. Bautista, *Organometallics* **2011**, *30*, 1079–1093.
- [125] M.-T. Chicote, I. Vicente-Hernandez, P. G. Jones, J. Vicente, *Organometallics* **2012**, *31*, 6252–6261.
- [126] M.-J. Oliva-Madrid, J.-A. Garcia-Lopez, I. Saura-Llamas, D. Bautista, J. Vicente, *Organometallics* **2012**, *31*, 3647–3660.
- [127] R. Frutos-Pedreño, P. González-Herrero, J. Vicente, P. G. Jones, *Organometallics* **2012**, *31*, 3361–3372.
- [128] J. Vicente, M.-T. Chicote, A. Abellan-Lopez, D. Bautista, *Dalt. Trans.* **2012**, *41*, 752–762.
- [129] A.-J. Martinez-Martinez, J. Vicente, M.-T. Chicote, D. Bautista, *Organometallics* **2012**, *31*, 2697–2708.
- [130] A. Abellan-Lopez, M.-T. Chicote, D. Bautista, J. Vicente, *Organometallics* **2013**, *32*, 7612–7624.

- [131] M.-J. Oliva-Madrid, I. Saura-Llamas, D. Bautista, J. Vicente, *Chem. Commun.* **2013**, 49, 7997–7999.
- [132] R. Frutos-Pedreño, P. González-Herrero, J. Vicente, P. G. Jones, *Organometallics* **2013**, 32, 4664–4676.
- [133] R. Frutos-Pedreño, P. González-Herrero, J. Vicente, P. G. Jones, *Organometallics* **2013**, 32, 1892–1904.
- [134] M.-J. Oliva-Madrid, J.-A. García-Lopez, I. Saura-Llamas, D. Bautista, J. Vicente, *Organometallics* **2014**, 33, 6420–6430.
- [135] M.-J. Fernández-Rodríguez, E. Martínez-Viviente, J. Vicente, P. G. Jones, *Organometallics* **2015**, 34, 3282–3291.
- [136] I. Vicente-Hernández, M.-T. Chicote, J. Vicente, D. Bautista, *Chem. Commun.* **2016**, 52, 594–596.
- [137] Y. Liang, Y. Ren, J. Jia, H.-S. Wu, *J. Mol. Model.* **2016**, 22, 53.
- [138] S. J. Tereniak, S. S. Stahl, *J. Am. Chem. Soc.* **2017**, 139, 14533–14541.
- [139] Y.-J. Liu, H. Xu, W.-J. Kong, M. Shang, H.-X. Dai, J.-Q. Yu, *Nature* **2014**, 515, 389–393.
- [140] J. M. French, J. R. Griffiths, S. T. Diver, *Adv. Synth. Catal.* **2015**, 357, 361–365.
- [141] L. A. Perego, L. Grimaud, F. Bellina, *Adv. Synth. Catal.* **2016**, 358, 597–609.
- [142] E. Martinand-Lurin, PhD Thesis, Université Paris Sud, ED 470, **2015**.
- [143] C. Amatore, A. Jutand, M. A. M'Barki, *Organometallics* **1992**, 11, 3009–3013.
- [144] L. Malatesta, *J. Chem. Soc.* **1955**, 3924–3926.
- [145] E. O. Fischer, H. Werner, *Chem. Ber.* **1962**, 95, 703–708.
- [146] A. R. Kapdi, A. C. Whitwood, D. C. Williamson, J. M. Lynam, M. J. Burns, T. J. Williams, A. J. Reay, J. Holmes, I. J. S. Fairlamb, *J. Am. Chem. Soc.* **2013**, 135, 8388–99.
- [147] A. Christofides, *J. Organomet. Chem.* **1983**, 259, 355–365.
- [148] C. G. Francis, S. I. Khan, P. R. Morton, *Inorg. Chem.* **1984**, 23, 3680–3681.
- [149] Y. Yamamoto, H. Yamazaki, *J. Chem. Soc., Dalton Trans.* **1989**, 2161–2166.
- [150] L. A. Labios, M. D. Millard, A. L. Rheingold, J. S. Figueroa, *J. Am. Chem. Soc.* **2009**, 131, 11318–11319.
- [151] F. Klages, K. Mönkemeyer, *Chem. Ber.* **1950**, 83, 501–508.
- [152] W. Hieber, *Z. Naturforsch.* **1950**, 5b, 129–130.
- [153] P. Fitton, E. A. Rick, *J. Organomet. Chem.* **1971**, 28, 287–291.
- [154] T. Vlaar, E. Ruijter, A. Znabet, E. Janssen, F. J. J. de Kanter, B. U. W. Maes, R. V. A. Orru, *Org. Lett.* **2011**, 13, 6496–6499.
- [155] K. Onitsuka, S. Suzuki, S. Takahashi, *Tetrahedron Lett.* **2002**, 43, 6197–6199.
- [156] S. Kamijo, T. Jin, Y. Yamamoto, *J. Am. Chem. Soc.* **2001**, 123, 9453–9454.
- [157] X.-D. Fei, Z.-Y. Ge, T. Tang, Y.-M. Zhu, S.-J. Ji, *J. Org. Chem.* **2012**, 77, 10321–10328.
- [158] P. Beak, S. T. Kerrick, S. Wu, J. Chu, *J. Am. Chem. Soc.* **1994**, 116, 3231–3239.
- [159] *Technical Bulletin - Reaction Solvent Dimethyl Sulfoxide (DMSO)*, Gaylord Chemical Corporation, **2003**.
- [160] W. Kabsch, *Acta Crystallogr. Sect. A* **1976**, 32, 922–923.
- [161] T. G. Appleton, H. C. Clark, L. E. Manzer, *Coord. Chem. Rev.* **1973**, 10, 335–422.
- [162] M. Pérez-Rodríguez, A. A. C. Braga, M. García-Melchor, M. H. Pérez-Temprano, J. A. Casares, G. Ujaque, A. R. de Lera, R. Álvarez, F. Maseras, P. Espinet, *J. Am. Chem. Soc.* **2009**, 131, 3650–3657.
- [163] K. Tatsumi, R. Hoffmann, A. Yamamoto, J. K. Stille, *Bull. Chem. Soc. Jpn.* **1981**, 54, 1857–1867.
- [164] V. P. Ananikov, D. G. Musaev, K. Morokuma, *Eur. J. Inorg. Chem.* **2007**, 2007, 5390–5399.
- [165] M. J. Frisch, G. W. Trucks, H. B. Schlegel, G. E. Scuseria, M. A. Robb, J. R. Cheeseman, G. Scalmani, V. Barone, B. Mennucci, G. A. Petersson, H. Nakatsuji, M. Caricato, X. Li, H. P. Hratchian, A. F. Izmaylov, J. Bloino, G. Zheng, J. L. Sonnenberg, M. Hada, et al., **2009**.
- [166] Y. Zhao, D. G. Truhlar, *Theor. Chem. Acc.* **2008**, 120, 215–241.
- [167] P. J. Hay, W. R. Wadt, *J. Chem. Phys.* **1985**, 82, 299–310.
- [168] P. J. Hay, W. R. Wadt, *J. Chem. Phys.* **1985**, 82, 270–283.
- [169] J. Tomasi, B. Mennucci, R. Cammi, *Chem. Rev.* **2005**, 105, 2999–3093.
- [170] M. Cossi, G. Scalmani, N. Rega, V. Barone, *J. Chem. Phys.* **2002**, 117, 43–54.
- [171] G. R. Fulmer, A. J. M. Miller, N. H. Sherden, H. E. Gottlieb, A. Nudelman, B. M. Stoltz, J. E. Bercaw, K. I. Goldberg, *Organometallics* **2010**, 29, 2176–2179.
- [172] S. Chiavarelli, E. F. Rogers, G. B. Marino-Bettolo, *Gazz. Chim. Ital.* **1953**, 83, 347–356.
- [173] T. Ukai, H. Kawazura, Y. Ishii, J. J. Bonnet, J. A. Ibers, *J. Organomet. Chem.* **1974**, 65, 253–266.
- [174] M. Morishita, H. Amii, *J. Organomet.*

- Chem.* **2007**, 692, 620–624.
- [175] K. O. Christe, W. W. Wilson, *J. Fluor. Chem.* **1990**, 46, 339–342.
- [176] U. M. V. Basavanag, A. Dos Santos, L. El Kaim, R. Gámez-Montaño, L. Grimaud, *Angew. Chem. Int. Ed.* **2013**, 52, 7194–7197.

CHAPTER III

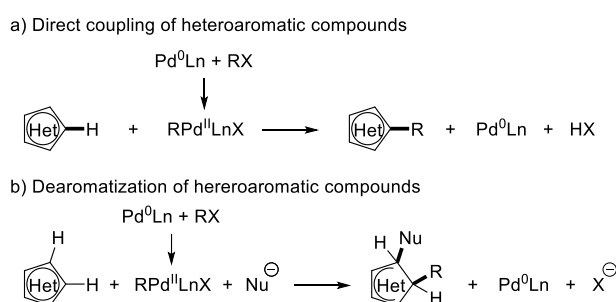
Palladium-Catalyzed Reductive Benzofuran Ring-Opening

Indole Ring-Closure *via* β -Phenoxide Elimination

1. Context of the Study

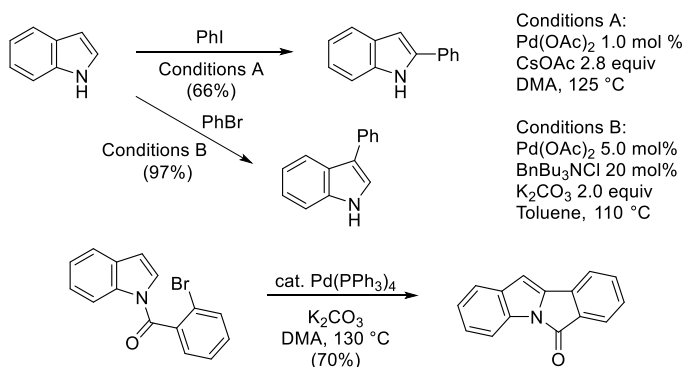
1.1. Palladium-catalyzed reactions involving unfunctionalized heteroarenes

Broadly speaking, unfunctionalized aromatic heterocycles can undergo two main kinds of palladium-catalyzed transformations involving organo-palladium(II) species (Scheme 1): (a) C-H activation and formation of a new C-C bond with preservation of the aromatic character, i.e. direct coupling reactions;^[1-4] (b) dearomatization via Heck-type carbopalladation, that can result in several different outcomes, depending on the reaction conditions and the structure of the substrate.^[5-10]



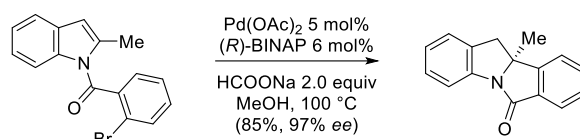
Scheme 1 – Possible reaction of heteroarenes with organopalladium(II) species.

For example, indoles can undergo reactions of type **a** either at the C2^[11] or at the C3 position^[12] depending on the experimental conditions to yield 2- or 3-arylindoles (Scheme 2). Similarly 1-(2-bromobenzoyl)-1*H*-indole cyclizes under similar experimental conditions.^[13]



Scheme 2 – Direct arylation reactions of indoles.^[11-13]

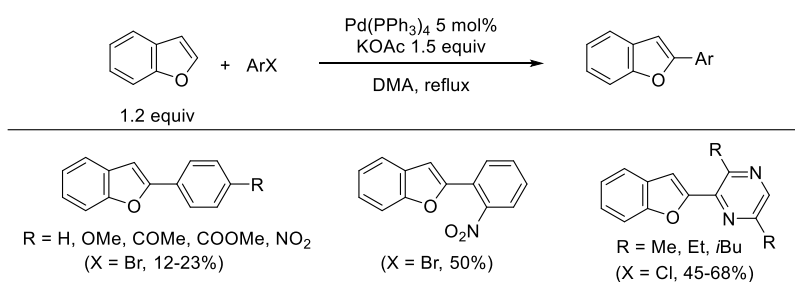
As an example of reaction of type **b**, 1-(2-bromobenzoyl)-2-methyl-1*H*-indole undergoes a palladium-catalyzed dearomative cyclization under the influence of Pd(OAc)₂ and BINAP. In this reductive Heck-type reaction, sodium formate acts as a hydride source and the reaction takes place with excellent enantioselectivity (Scheme 3).^[14]



Scheme 3 – Enantioselective reductive Heck cyclization of 1-(2-bromobenzoyl)-2-methyl-1*H*-indole.^[14]

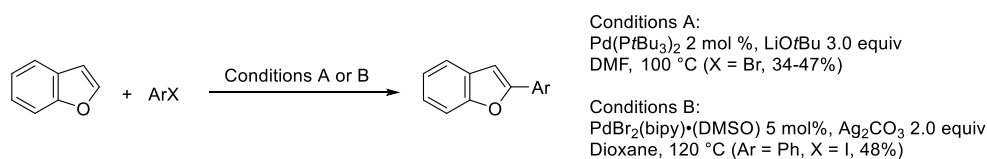
1.2. Palladium-catalyzed direct arylation and dearomative couplings of benzofurans

Despite the great advances in the field of palladium catalyzed reactions involving heterocycles made in the last two decades, benzofurans received comparatively little attention. Some protocols for intermolecular reactions belonging to class **a** have been reported intermittently in the literature.ⁱ As early as in 1990, Ohta and coworkers reported that benzofuran could be arylated with halogenoarenes by using $\text{Pd(PPh}_3)_4$ as a catalyst and potassium acetate as a base. Poor yields were obtained with substituted bromobenzenes,^[15] but yields were fair with electron-poor 2-bromonitrobenzene^[15] and 2-chloropyrazines (Scheme 4).^[16] In every case, the isolated product derived from cleavage of the C2-H bond of benzofuran.



Scheme 4 – First direct arylations of benzofuran reported by Ohta.^[15,16]

Improved yields for the C2 arylation of benzofuran could be obtained by Mori using $\text{Pd(P}^t\text{Bu}_3)_2$ as a catalyst and $t\text{BuOLi}$ as the base,^[17] and by Itami with $\text{PdBr}_2(\text{bipy}) \cdot (\text{DMSO})$ and Ag_2CO_3 (Scheme 5).^[18]

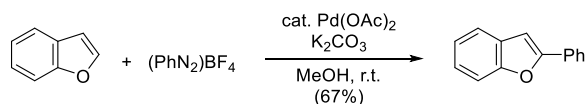


Scheme 5 – Mori's^[17] and Itami's^[18] conditions for the arylation of benzofuran.

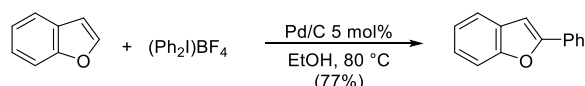
Electrophiles other than haloarenes can also be used. Correia and co-workers demonstrated that benzofuran is arylated at room temperature by the use of aryldiazonium salts and catalytic amounts of Pd(OAc)_2 (Scheme 6).^[19] Glorius employed $(\text{Ph}_2\text{I})\text{BF}_4$ as the arylating agent and Pd/C as a catalyst (Scheme 7).^[20] Complete C2 selectivity was also obtained by Doucet

ⁱ The direct arylation of benzofurans, among other benzofused heterocycles, has been reviewed recently.^[78]

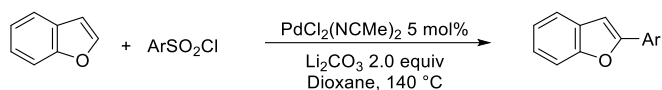
and coworkers in the desulfative coupling involving arenesulfonylchlorides (Scheme 8), which indeed left bromo- substituents unaltered.^[21] The latter observation suggests that this reaction does not proceed by a standard Pd(0)/Pd(II) mechanism, but probably involves Pd(IV) intermediates.



Scheme 6 – Pd- catalyzed arylation of benzofuran with diazonium salts.^[19]



Scheme 7 – Pd/C-catalyzed arylation of benzofuran with (Ph₂I)BF₄.^[20]

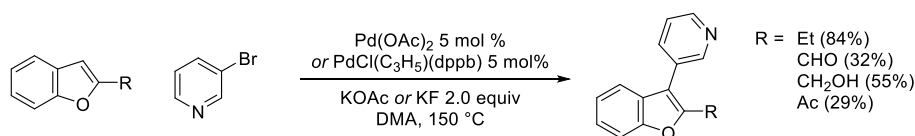


Scheme 8 – Pd-catalyzed desulfative coupling of arylsulfonyl chlorides with benzofuran.^[21]

When the C2 position of benzofuran has a substituent other than hydrogen, normally the C3-H bond can be activated. For example, Fagnou and coworkers employed a Pd(OAc)₂/P(*t*Bu)₂Me·HBF₄/PivOH catalyst system to effect the arylation of 2-chlorobenzofuran at C3 using bromoarenes as coupling partners.^[22] Doucet and coworkers reported that the arylation of 2-functionalized benzofurans with 3-bromopyridines with PdCl(C₃H₅)(dppb) or Pd(OAc)₂ as pre-catalysts proceeded in variable yields according to the nature of the substituent.^[23,24] The bidentate phosphine Sylphos [1,1'-bis-((diphenylphosphino)-2-propyl)ferrocene] was particularly effective for the arylation of 2-ethylbenzofuran, but again when unsubstituted benzofuran was used as a substrate, arylation at C2 prevailed (C2/C3 ratio: 11:6). The conditions described by Fagnou^[25] have been successfully applied by Bertounesque^[26] for the arylation of 2-benzoylfurans and by Kim for the synthesis of analogues of the natural product Diptoindonesin G.^[27]



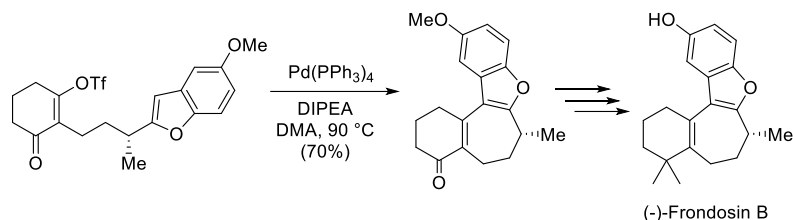
Scheme 9 – Fagnou's arylation of 2-chlorobenzofuran.^[22]



Scheme 10 – Doucet's conditions for the arylation of 2-substituted benzofurans.^[23,24]

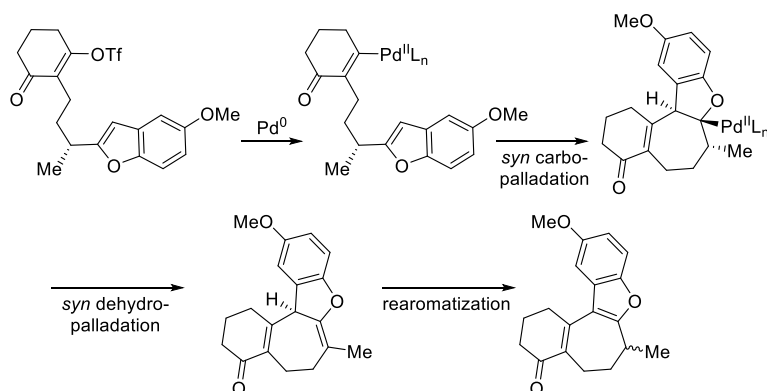
Intramolecular variants of reactions of class **a** are also known. An intramolecular ring closure of a vinyl trifluoromethanesulfonate with a tethered benzofuran was applied by Trauner

in the total synthesis of (-)-Fronodosin B.^[28,29] The required seven-membered ring was obtained by activation of the C3-H bond of benzofuran under the influence of Pd(PPh₃)₄ and *i*PrNEt₂ (Scheme 11). No racemization took place at the benzylic stereocenter.^[28]



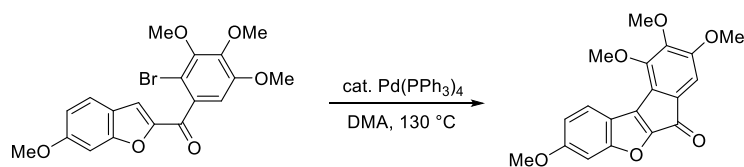
Scheme 11 – Palladium-catalyzed C-H vinylation of a benzofuran as a key step in Trauner's total synthesis of (-)-Fronodosin B.^[28,29]

The authors speculated that if a Heck-type process was operative, as depicted in Scheme 12, an exocyclic bond would be formed first by *syn* dehydropalladation. The aromaticity of the benzofuran ring would be subsequently restored by double bond migration, resulting in loss of optical activity.^[28]

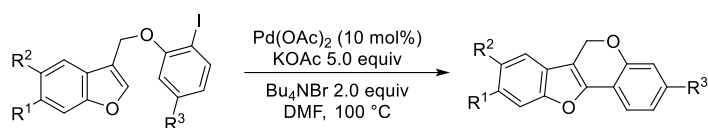


Scheme 12 – Heck-type pathway for the reaction depicted in Scheme 11.^[28]

A related formal 5-*endo-trig* palladium-catalyzed cyclization has been employed in the synthesis of a candidate tubulin polymerization inhibitor (Scheme 13).^[30] A 6-*endo-trig* cyclization of 3-benzofuranylmethyl ethers useful for the preparation of pterocarpene-type compounds takes place under Jeffery conditions (Scheme 14).^[31] Similar cyclization have been quoted also in the patent literature.^[32]

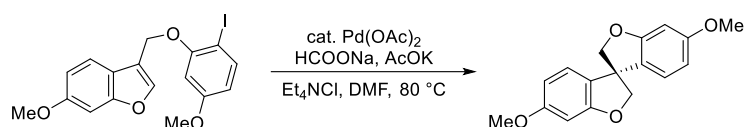


Scheme 13 – Intramolecular direct arylation of a benzofuran derivative *en route* to a candidate tubulin polymerization inhibitor.^[30]



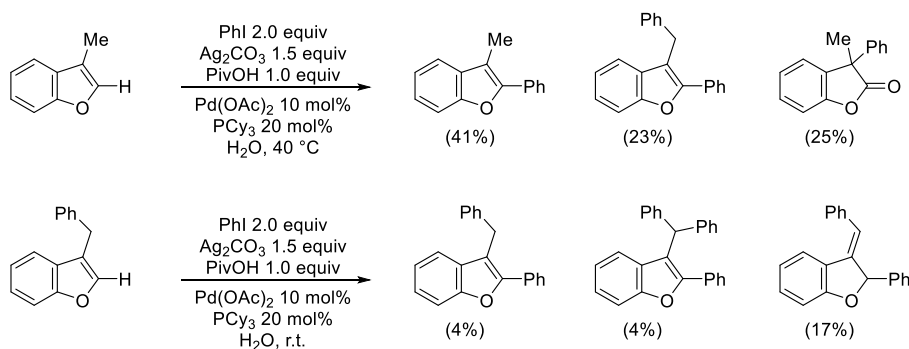
Scheme 14 – Synthesis of pterocarpene-type products by Pd-catalyzed intramolecular direct arylation of benzofuran.^[31]

Interestingly, when the same transformation was performed in the presence of sodium formate as a hydride donor, a spirocyclic product deriving from formal 5-*exo-trig* cyclization could be isolated (Scheme 15), resulting in a class **b** process.^[31]

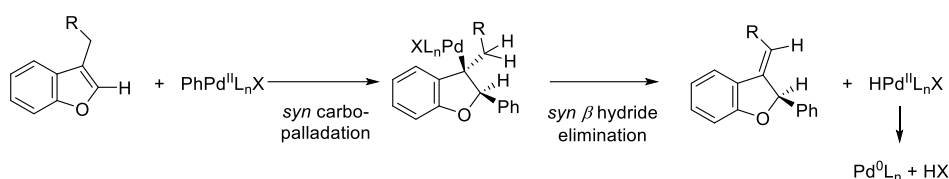


Scheme 15 – Reductive Heck cyclization of one of the substrates of the reaction shown in Scheme 14 in the presence of sodium formate as a hydride donor.^[31]

When 3-alkylbenzofurans were used as substrates for a direct arylation reaction with iodobenzene using Ag_2CO_3 as a base and a $\text{Pd}(\text{OAc})_2/\text{PCy}_3/\text{PivOH}$ catalyst system *on water*, mixture of products in which either the C2-H bond or the C-H bonds at the benzylic position were activated. Dearomatized products were also isolated from the reaction mixtures: in the case of 3-methylbenzofuran as the substrate, 3-methyl-3-phenylbenzofuran-2(3*H*)-one was identified, while 3-benzylfuran yielded 3-benzylidene-2-phenyl-2,3-dihydrobenzofuran (Scheme 16).^[33] The authors did not comment on the possible mechanism of formation of this product. A mechanism involving carbopalladation with the usual *syn* stereochemistry yielding an intermediate having palladium at the C3 position could not undergo *syn* β -hydride elimination restoring the aromaticity of the heterocyclic ring, thus the only possibility would be formation of the exocyclic double bond (Scheme 17).

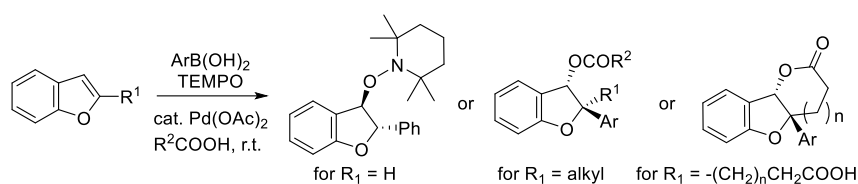


Scheme 16 – Arylation of 3-methylbenzofuran and 3-benzylbenzofuran.^[33]

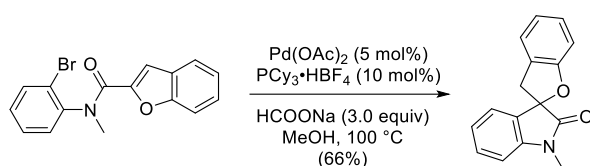


Scheme 17 – Mechanistic hypothesis for the transformation reported in Scheme 16.

Few other examples of reaction of class **b** involving benzofurans have been reported. Studer and coworkers described a family of related palladium-catalyzed oxidative oxyarylations of benzofurans with arylboronic acids using TEMPO as a stoichiometric oxidant (Scheme 18)^[34–37] and very recently Jia and co-workers^[38] reported a single example of reductive cyclization of a benzofuran-2-carboxamide leading to a spiro-oxindole derivative (Scheme 19).

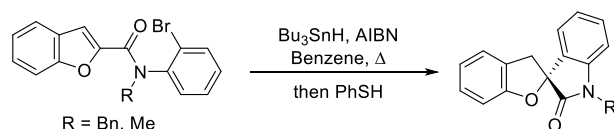


Scheme 18 – Oxidative oxyarylations of benzofurans reported by Studer and coworkers.^[34–37]

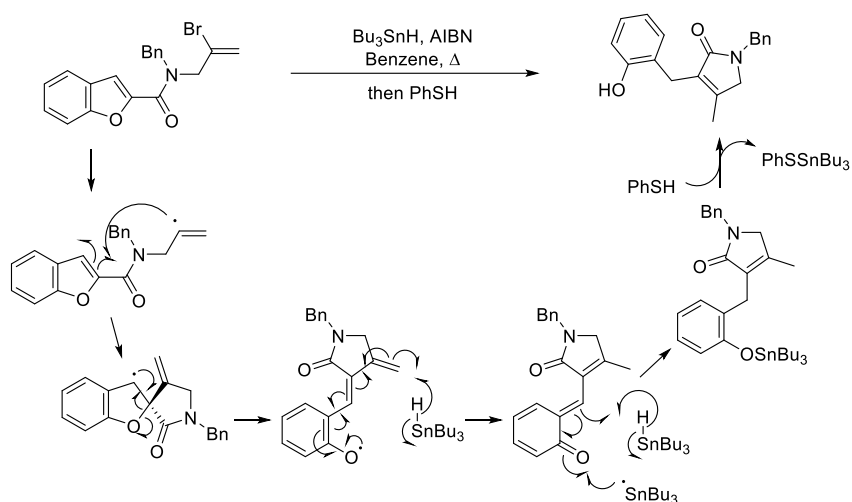


Scheme 19 – Reductive spirocyclization of a benzofuran-2-carboxamide.^[38]

Other dearomatization reactions not involving palladium catalysis are known.^[39–45] For the sake of conciseness, we will report here only one example. Baldwin and Adlington demonstrated that suitably substituted benzofuran-2-carboxamides undergo a radical reductive spirocyclization with Bu_3SnH and AIBN as a radical initiator (Scheme 20).^[40] When the same conditions were applied to a substrate that generates a vinyl radical instead of an aryl radical, ring-opening of the benzofuran ring terminated the reaction, and a phenol derivative was isolated instead of a spiro compound. This reaction, together with its proposed mechanism, is reported in Scheme 21.^[40]



Scheme 20 – Radical cyclization of a benzofuran-2-carboxamide.^[40]



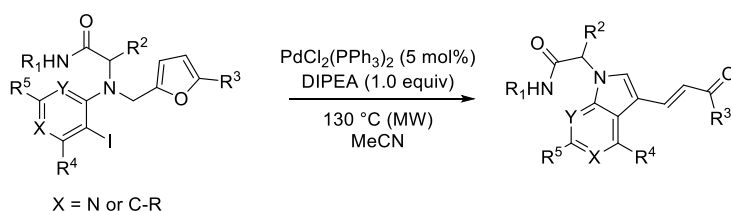
Scheme 21 – Radical cyclization of a *N*-(2-bromoallyl)-benzofuran-2-carboxamide, terminated by the ring-opening of the benzofuran ring, and proposed mechanism.^[40]

Having a Dewar resonance energy (DRE) of 20.3 kcal mol⁻¹, benzofuran is considered less aromatic than indole (DRE = 23.8 kcal mol⁻¹).^[46] It is thus surprising quite few Heck reactions involving benzofurans have been reported so far, considering that this chemistry is well developed for indoles.^[47–53] In this chapter, a palladium-catalyzed reductive intramolecular Heck reaction of benzofurans that is terminated by an unusual β -phenoxide elimination is presented. Suitably substituted benzofuran-tethered 2-iodoanilines give synthetically interesting 2-(3-indolylmethyl)phenols after double bond isomerization.

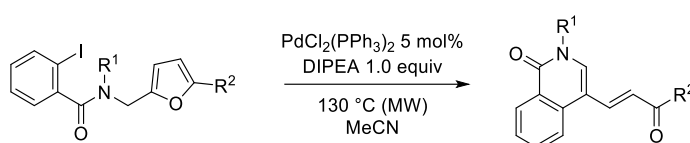
2. Results and discussion

2.1. First steps

A few years ago, the palladium-catalyzed ring-opening of furans giving α,β -unsaturated carbonyl compounds was studied in our laboratory.^[54,55] A series of Ugi-Smiles adducts deriving from furfurylamine underwent fragmentation, and functionalized indoles and 5,7-diazaindoles were obtained in good yields by using $\text{PdCl}_2(\text{PPh}_3)_2$ as a catalyst and DIPEA as a base (Scheme 22). *N*-(2-Furylmethyl)-2-iodobenzamides also reacted under these conditions to give functionalized isoquinolin-1(2*H*)-ones (Scheme 23).^[54,55]

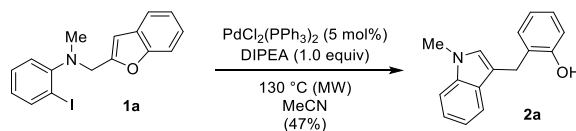


Scheme 22 – Palladium-catalyzed fragmentation of furfurylamine-derived Ugi-Smiles adduct.^[54,55]



Scheme 23 – Palladium-catalyzed fragmentation leading to isoquinolin-1(2*H*)-ones.^[54,55]

At that time, the reactivity of the corresponding benzofuran derivatives was also briefly examined. When the reaction conditions described above were applied to the benzofuran-containing substrate **1a**, indole **2a** was isolated in 47% yield (Scheme 4, b). Simple electron counting attests that this is a reductive process, *i.e.* that reactant **1a** is more oxidized than product **2a**, while the previously described fragmentation of furans (Scheme 22 and Scheme 23) is a redox-neutral transformation.^[55]



Scheme 24 – First attempt of Pd-catalyzed ring-opening of benzofuran.^[54]

No cyclization product deriving from the direct arylation of benzofuran at C3 could be isolated from the reaction mixture. This result was quite surprising, especially in view of Trauner's results in the total synthesis of (–)-Fronodosin B that we have shown in the introduction (Scheme 11).^[28,29]

2.2. Optimization of reaction conditions

Building on this unexpected result, we focused on finding optimal conditions for this transformation (Table 1).

Increasing the amount of DIPEA from 1.0 to 2.0 equiv had a beneficial effect (entry 2). Substituting MeCN with EtCN also increased the yield (entry 3),ⁱⁱ but other solvents (DMF, dioxane, 2-methyl-1-propanol) proved to be equivalent or inferior to MeCN (entries 4-6). Having established EtCN as the best solvent, several different bases were screened. Tertiary (NMM, DIPEA, Et₃N) or secondary amines (*i*Pr₂NH) are suitable (entries 7-9), but the hindered base 2,2,4,4-tetramethylpiperidine (TMP) and CsOAc gave very poor yields of **2a** (entries 10-11).

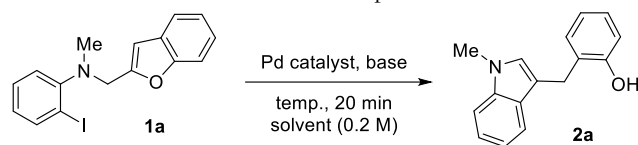
Having confirmed DIPEA as the most efficient amine, some palladium precatalysts different from PdCl₂(PPh₃)₂ were tested. Phosphine ligand-free PdCl₂(NCPH)₂ (entry 12) is completely unsuitable and palladium black was formed quickly on heating. Little conversion took place with this pre-catalyst. A mixture of Pd(dba)₂ and PPh₃ in 1:2 ratio was practically as effective as PdCl₂(PPh₃)₂ (entry 13). Hindered alkyl phosphines (PCy₃ and *t*Bu₃P) gave disappointing results (entries 14 and 15). Analysis of the crude reaction mixture revealed that much starting material was left. Scant conversion was also found for Pd(dba)₂/P(*o*-Tol)₃ (entry 16), and also Pd(dba)₂/P(2-furyl)₃ was inferior to PdCl₂(PPh₃)₂ (entry 17). The combination of electron-rich (4-MeO-C₆H₄)₃P with PdCl₂(NCPH)₂ was as efficient as the initially selected pre-catalyst (entry 18), while (4-Me₂N-C₆H₄)₃P and electron-poor (4-CF₃-C₆H₄)₃P were not effective (entries 19-20).

The palladium(0) complex Pd(PPh₃)₄ was as effective as PdCl₂(PPh₃)₂ (entry 21). Lowering the temperature to 110 °C with Pd(PPh₃)₄ slightly decreased the yield (entry 22), but going down to 80 °C deeply affected the efficiency of the reaction (entry 23). The effect of decreasing the temperature was more severe if PdCl₂(PPh₃)₂ was employed instead of Pd(PPh₃)₄ (entry 24), probably because at the lower metal/ligand ratio if oxidative addition does not take place quickly enough, metallic palladium precipitates more readily. Finally, using conventional heating (oil bath) instead of microwave irradiation resulted in a decreased yield (entry 25).ⁱⁱⁱ

ⁱⁱ Even if it may not be obvious at first sight, MeCN and EtCN have quite different properties as solvents. For example, EtCN has a dielectric constant of 27.7, while the value for acetonitrile is 37.5 (both values measured at 20 °C).^[79]

ⁱⁱⁱ Specific effects due to microwave irradiation are highly unlikely. Given the sensitivity of the reaction even to small temperature variations (Table 1), we speculate that heating rate (most likely faster with our commercial MW setup than for an oil bath) could be the reason for the reduced yields with conventional heating.

Table 1 – Reaction optimization.



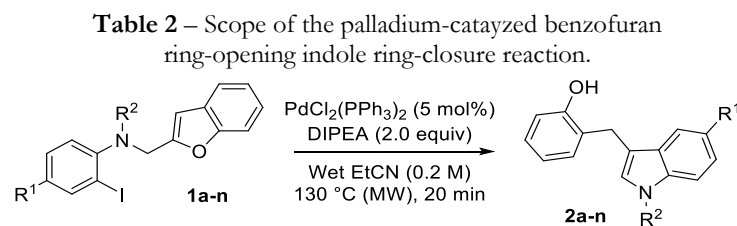
Entry	Catalyst (mol%)	Base (equiv)	Solvent (wet) ^[a]	Temp. (°C)	Recovered 1a (%) ^[b]	Yield of 2a (%) ^[b]
1	PdCl ₂ (PPh ₃) ₂ (5)	DIPEA (1.0)	MeCN	130	-	51 (47) ^[c]
2	PdCl ₂ (PPh ₃) ₂ (5)	DIPEA (2.0)	MeCN	130	-	57
3	PdCl₂(PPh₃)₂ (5)	DIPEA (2.0)	EtCN	130	-	67^[d] (65)^[e]
4	PdCl ₂ (PPh ₃) ₂ (5)	DIPEA (2.0)	DMF	130	-	50
5	PdCl ₂ (PPh ₃) ₂ (5)	DIPEA (2.0)	1,4-dioxane	130	51	27
6	PdCl ₂ (PPh ₃) ₂ (5)	DIPEA (2.0)	2-methyl-1-propanol	130	-	55
7	PdCl ₂ (PPh ₃) ₂ (5)	NMM ^[f] (2.0)	EtCN	130	64	20
8	PdCl ₂ (PPh ₃) ₂ (5)	Et ₃ N (2.0)	EtCN	130	-	62
9	PdCl ₂ (PPh ₃) ₂ (5)	(<i>i</i> Pr) ₂ NH (2.0)	EtCN	130	-	48
10	PdCl ₂ (PPh ₃) ₂ (5)	TMP ^[f] (2.0)	EtCN	130	45	8
11	PdCl ₂ (PPh ₃) ₂ (5)	CsOAc (2.0)	EtCN	130	-	5
12	PdCl ₂ (NPh) ₂ (5)	DIPEA (2.0)	EtCN	130	86	-
13	Pd(dba) ₂ (5) Ph ₃ P (10)	DIPEA (2.0)	EtCN	130	3	62
14	PdCl ₂ (PCy ₃) ₂ (5)	DIPEA (2.0)	EtCN	130	36	25
15	Pd(dba) ₂ (5) (<i>t</i> -Bu) ₃ P•HBF ₄ (10)	DIPEA (2.0)	EtCN	130	56	11
16	Pd(dba) ₂ (5) (<i>o</i> -Tol) ₃ P (10)	DIPEA (2.0)	EtCN	130	78	5
17	Pd(dba) ₂ (5) (2-furyl) ₃ P (10)	DIPEA (2.0)	EtCN	130	7	41
18	PdCl ₂ (NPh) ₂ (5) (4-MeO-C ₆ H ₄) ₃ P (10)	DIPEA (2.0)	EtCN	130	-	68
19	PdCl ₂ (NPh) ₂ (5) (4-Me ₂ N-C ₆ H ₄) ₃ P (10)	DIPEA (2.0)	EtCN	130	66	13
20	PdCl ₂ (NPh) ₂ (5) (4-CF ₃ -C ₆ H ₄) ₃ P (10)	DIPEA (2.0)	EtCN	130	-	16
21	Pd(PPh ₃) ₄ (5)	DIPEA (2.0)	EtCN	130	-	67
22	Pd(PPh ₃) ₄ (5)	DIPEA (2.0)	EtCN	110	-	63
23	Pd(PPh ₃) ₄ (5)	DIPEA (2.0)	EtCN	80	21	35
24	PdCl ₂ (PPh ₃) ₂ (5)	DIPEA (2.0)	EtCN	100	-	31
25	PdCl ₂ (PPh ₃) ₂ (5)	DIPEA (2.0)	EtCN	130 (oil bath)	-	44

[a] All solvents were *not* dried, no precautions were taken to exclude air and moisture. The use of thoroughly dried MeCN or EtCN lead to reproducibility issues and once explosion of the reaction vessel occurred due to deposition of a Pd mirror and excessive MW heating. EtCN and MeCN were thus deliberately moistened with 1% of water. See ref. [56,57] for an explanation of the role of water in the formation of Pd(0) from Pd(II) precursors. [b] Determined by GLC with octadecane as an internal standard, unless otherwise stated. Reactions performed on 0.1 mmol scale. [c] Isolated yield. [d] Average of four determinations, standard deviation: 0.5. [e] *N*-Methylmorpholine. [f] 2,2,6,6-Tetramethylpiperidine.

For practical reasons and simplicity, we adopted PdCl₂(PPh₃)₂ as the pre-catalyst of choice instead of a more expensive substituted phosphine or air-sensitive Pd(PPh₃)₄. The conditions of entry 3 were thus retained for further work.

2.3. Scope of the reaction

The optimized conditions were applied to several different benzofuran-tethered 2-iodoanilines (Table 2).



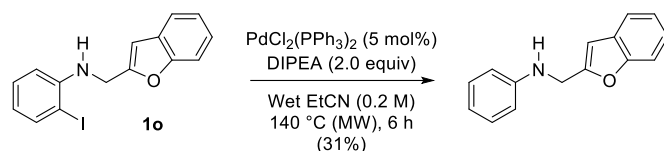
Entry	Substrate	Product	R1	R2	Yield (%) ^[a]
1	1a	2a	H	Me	65
2	1b	2b	F	Me	64
3	1c	2c	H	Bn	71
4	1d	2d	H	<i>n</i> -Octyl	68
5	1e	2e	F	<i>p</i> -Methoxybenzyl	76
6	1f	2f	OMe	(2-Naphthyl)CH ₂ -	54
7	1g	2g	OMe	Bn	58
8	1h	2h	Me	TBDMSO-(CH ₂) ₆ -	55
9	1i	2i	Me	BzO-(CH ₂) ₆ -	62
10	1j	2j	Me	HO-(CH ₂) ₆ -	48
11	1k	2k	Me	TBDMSO-(CH ₂) ₄ -	55
12	1l	2l	NO ₂	Bn	24
13	1m	2m	NH(BOC)	Bn	50
14	1n	2n	H	Ac	<15 ^[b]
15	1o	2o	H	H	trace ^[b,c]

[a] Isolated yields, if not stated otherwise. [b] Determined by NMR analysis of the crude reaction mixture. [c] Reaction time: 6 h, 140 °C (MW). Identified by comparison with literature data.^[58]

Several different alkyl substituents on nitrogen are tolerated (Table 2), but the reaction is not efficient for the *N*-acetyl substrate **1o** and for *N*-unsubstituted **1n**. This transformation is

also compatible with esters (entry 9), unprotected OH (entry 10) and *tert*-butyldimethylsilyl ethers (entries 8 and 11). Both electron-releasing and electron-withdrawing groups can be present on the iodoarene moiety of the substrate without significantly affecting the results. The nitro-substituted substrate **1l** is an exception, since it gave a modest yield. The *N*-acetylated substrate **1n** was not a suitable substrate (entry 14), while *N*-unsubstituted **1o** gave the expected NH indole in modest yield and heating for a prolonged time (6 h) at 140 °C was needed to achieve full conversion of the starting material. (entry 15). Our procedure, thus, give access to indoles decorated with diverse substituents on the carbocyclic ring. The 2-(3-indolylmethyl)phenol structural motif so formed is present in some APIs and it is an useful intermediate for further transformations.^[59–61]

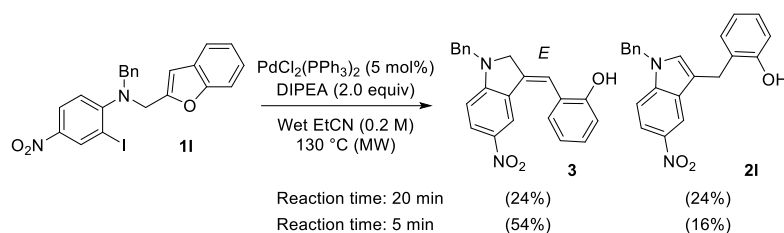
The *N*-unsubstituted substrate **1o** gave only traces of the expected indole **2o**.^[58] Heating to 140 °C for a long time (6 h) was required to obtain full conversion of the starting material. The main reaction that took place was reductive deiodination of **1o**, the corresponding product was isolated in 31% yield (Scheme 25).



Scheme 25 – Reductive deiodination of compound **1o**.

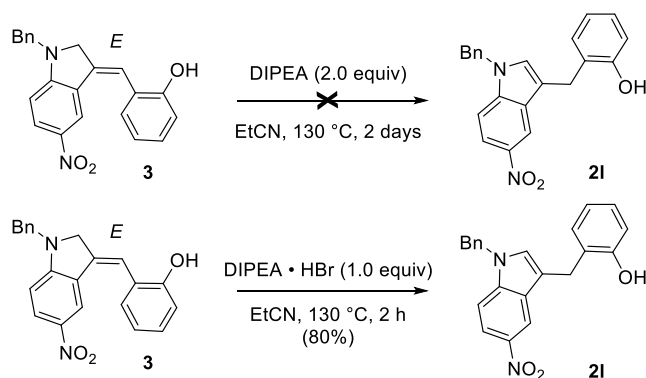
With the aim of finding the reason why **2l** was obtained in a so modest yield, we analyzed more in detail the crude reaction mixture coming from the reaction of **1l**. Besides **2l**, the isomeric product **3** could be isolated by careful separation by flash chromatography (Scheme 26). Shortening the reaction time from 20 minutes to only 5 minutes allowed isolating pure **3** in 54% yield together with a small amount of **2l**. Interestingly, in every case **3** was obtained as a pure stereoisomer, the configuration being established to be *E* by NOE experiments and by measurement of $^3J_{\text{CH}}$ (see the experimental section for detailed NMR analysis). It is worth noting that the *E* isomer is not expected to be the thermodynamically most stable one, as elementary considerations and theoretical calculations^{iv} suggest. No isomerization from **3** to (*Z*)-**3** should thus be possible in the reaction conditions and the formation of **3** should thus be under kinetic control.

^{iv} According to DFT calculations at the B3LYP/6-31+G* level (Gibbs free energies calculated *in vacuo* for the lowest-energy conformer reported), (*Z*)-**3** is 3.5 kcal mol⁻¹ more stable than **3**, and in turn **2l** is 11.2 kcal mol⁻¹ more stable than (*Z*)-**3**.



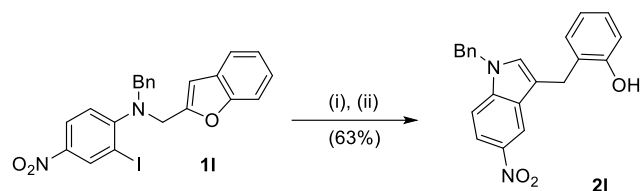
Scheme 26 – Isomeric products arising from the benzofuran ring-opening reaction applied to **11**. Isolated yields are reported.

We hypothesized that **3** is an intermediate that is converted into indole **21** by double bond migration. Taking into account the K₂CO₃-mediated isomerization of related compounds reported by Kim and co-workers,^[62] we first guessed that DIPEA might be an effective catalyst for this base-promoted process at the temperature at which the reaction is performed. A straightforward test demonstrated that this is not the case, but heating in the presence of the ammonium salt DIPEA·HBr effected the conversion of **3** to **21** in 80% yield, as determined by ¹H NMR analysis (Scheme 27). Considering that HI is formally produced during the catalytic reaction, we concluded that most likely the isomerization takes place by acid catalysis in the reaction medium.



Scheme 27 – Conditions for the isomerization of **3** into **21**. NMR yield reported.

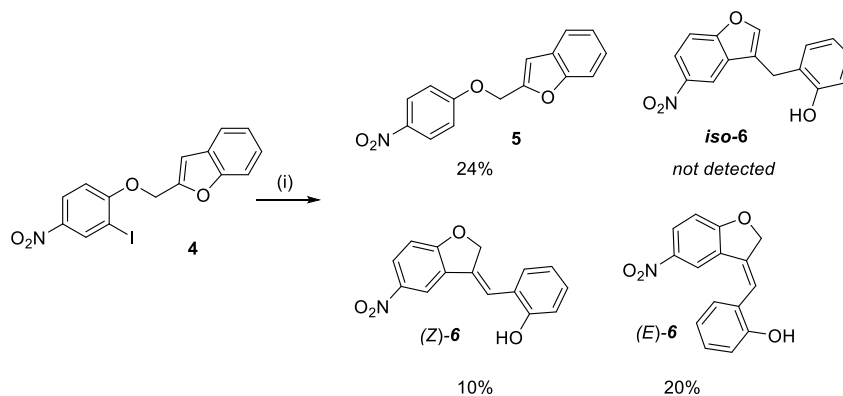
Having this piece of information in hand, we devised an efficient protocol for the synthesis of **21**. After applying our optimized conditions to **11**, DIPEA·HBr (1.0 equiv) was added to the crude reaction mixture and heated again. The required product was thus isolated in 63% yield (Scheme 28), in line with the other related derivatives (Table 2).



Scheme 28 – Improved one-pot protocol for the synthesis of **21**.
 Conditions: (i) PdCl₂(PPh₃)₂ (5 mol%), DIPEA (2.0 equiv), wet EtCN, 130 °C (MW), 20 min;
 (ii) DIPEA · HBr (1.0 equiv), 130 °C, overnight.

2.4. Going beyond the synthesis of indoles

Aiming to verify whether it is essential to have a nitrogen atom in the side chain of the benzofuran, substrate **4** – featuring an ether moiety instead of a tertiary amine was tested under the optimized conditions (Scheme 29). Unfortunately, no product could be isolated in a pure state. However, three main isomeric products could be identified by NMR spectroscopy and mass spectrometry on partially purified samples: the dehalogenated compound **5** and alkenes (*Z*)-**6** and (*E*)-**6**. Remarkably, benzofuran *iso*-**6** could not be isolated in any useful amount. We speculate that cyclization is slowed for conformational reasons in the case of this ether substrate, so reduction forming **5** – which was not observed in any significant amount for substrates **1a-o** – is competitive in this case. Most likely (*E*)-**6**, which is expected to be the less thermodynamically stable stereoisomer^v is formed first, in analogy to what observed for the reaction of substrate **1m**, and then isomerises to (*Z*)-**6** *via* acid catalysis.

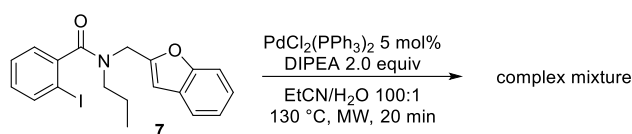


Scheme 29 – Attempted Pd-catalyzed ring-opening reaction of ether substrate **4**. Conditions: (i) PdCl₂(PPh₃)₂ (5 mol%), DIPEA (2.0 equiv), wet EtCN, 130 °C, 1 h; NMR yields reported.

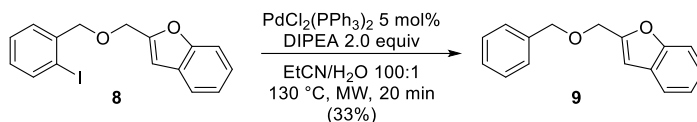
In an attempt to obtain isoquinoline derivatives by ring-opening of benzofuran (compare Scheme 23), amide **7** was prepared and subjected to the reaction conditions we optimized for the synthesis of indoles. Unfortunately, a very complex mixture of unidentifiable products was obtained (Scheme 30). Likewise, when ether **8** was engaged in the same reaction conditions, nothing other than the dehalogenation product **9** could be obtained (Scheme 31).^{vi} Probably ring closure in those cases is slow enough to allow undesired reactions to occur at a competitive rate.

^v According to DFT calculations at the B3LYP/6-31+G* level (Gibbs free energies calculated *in vacuo* for the lowest-energy conformer reported), (*Z*)-**6** is 3.0 kcal mol⁻¹ more stable than (*E*)-**6**, and in turn *iso*-**6** is 5.6 kcal mol⁻¹ more stable than (*Z*)-**6**.

^{vi} The NMR data of compound **9** matched those reported in the literature.^[80]

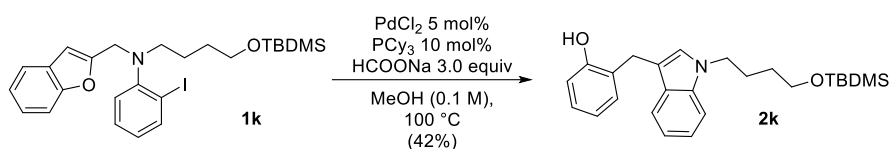


Scheme 30 – Attempted reaction employing a 2-iodobenzamide substrate.



Scheme 31 – Attempted reaction of an ether-type substrate.

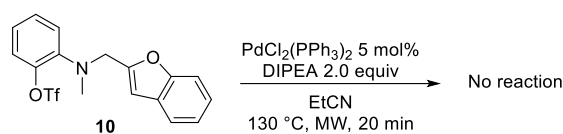
In an attempt to obtain spiro compounds (compare the reactions reported in Scheme 15 and Scheme 19), reductive Heck conditions were tried on compound **1k** (Scheme 32). Unexpectedly, only indole **2k** (*i.e.* the same product obtained with our optimized ring-opening conditions) was obtained and no trace of spiro compound was detected by NMR analysis of the reaction mixture.



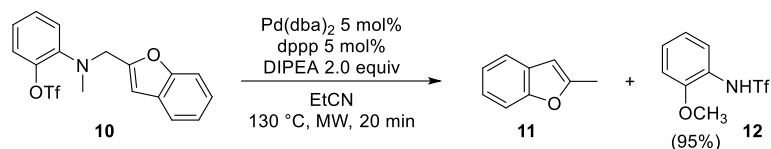
Scheme 32 – Attempted reductive Heck reaction of substrate **1k**.

Aiming at obtaining cyclization instead of fragmentation, like in Trauner's synthesis of (–)-frondosin B (Scheme 11), we speculated that aryl trifluoromethanesulfonates could have a behavior different than halides. In fact, Trauner's cyclization employed a ketone-derived enol trifluoromethanesulfonate.^[28,29] This hypothesis was also justified by the fact that trifluoromethanesulfonates give cationic palladium(II) complexes upon oxidative addition to Pd(0), which have a peculiar reactivity in Heck reactions.^[63] Unfortunately, under our standard optimized conditions, triflate **10** was not reactive and metallic palladium precipitated on heating (Scheme 33). Using a bidentate phosphine (dppp) in an attempt to stabilize Pd(0) and prevent precipitation did not give access to any cyclization product. Curiously, 2-methylbenzofuran (**11**) and *N*-trifluoromethanesulfonyl 2-anisidine were identified as the major products under these conditions (Scheme 34). The identity of these compounds was established beyond doubt by comparison of NMR spectra with published data.^[64,65] We hypothesized that 2-methylbenzofuran (**11**) forms by palladium-mediated hydrogenolysis of the benzylic C-N bond, while 1,4-sulfonyl migration and then intermolecular nucleophilic substitution would be responsible for the transfer of the methyl group from nitrogen to oxygen (Scheme 35).^{vii}

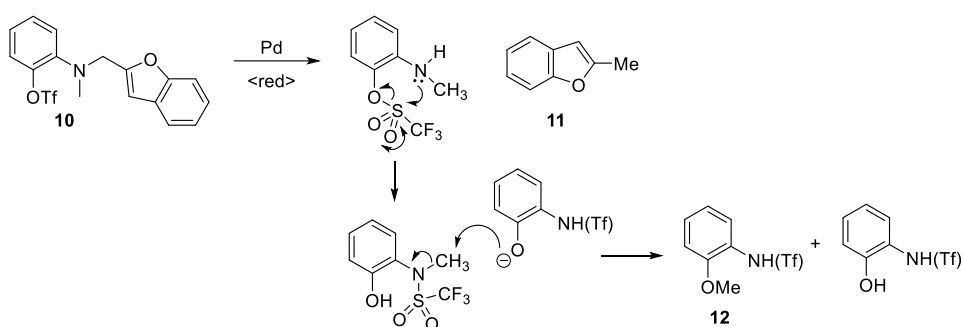
^{vii} A related transformation in which a *N*-phenyltriflamide acts as a leaving group in a nucleophilic substitution reaction has been reported recently.^[81]



Scheme 33 – Attempted reaction of triflate **10**.

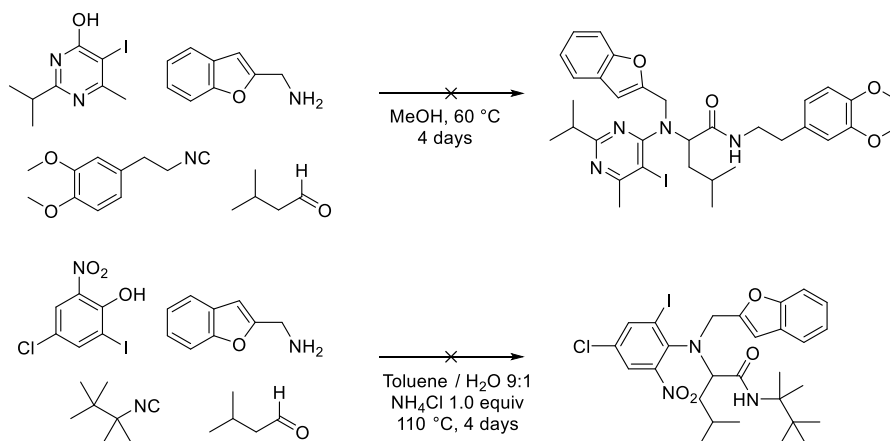


Scheme 34 – Attempted reaction of triflate **10** with dppp as a ligand.



Scheme 35 – Mechanistic hypothesis for the formation of products **11** and **12**.

To rapidly generate a small library of substrates to test our reaction, several Ugi-Smiles reactions employing electron-poor 2-iodophenols and 2-benzofurylmethylamine were attempted (two examples are reported in Scheme 36), following the protocols that were demonstrated to work for furfurylamine as the substrate.^[54,55] For reasons that are not clear to us, these reactions failed in our case and only intractable mixtures of products were obtained.

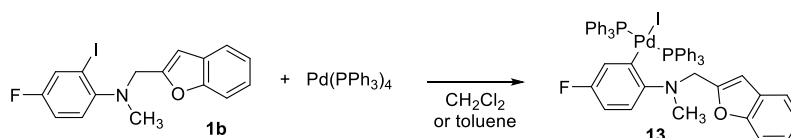


Scheme 36 – Attempted Ugi-Smiles reactions to generate a library of substrates for the benzofuran ring-opening reaction.

2.5. Mechanistic studies

To get insight into the mechanism of the transformation under study, we first considered the oxidative addition of compound **1b** to Pd(PPh₃)₄ as a source of Pd(0). The fluorine-tagged **1b** was chosen to follow easily the reaction by ¹⁹F NMR.

A solution of Pd(PPh₃)₄ (20 mM in CD₂Cl₂)^{viii} was treated with **1b**. After about 1 h at room temperature and heating at 50 °C for a few minutes, the *trans*-[ArPd^{II}(PPh₃)₂I] complex **13** was formed in almost quantitative yield, as attested by multinuclear NMR analysis (Scheme 37). The organometallic nature of this complex was confirmed by the strongly shielded aromatic resonances in the ¹H spectrum due to the ring directly attached to the metal (Figure 1) and by the shielding of the ¹⁹F NMR resonance ($\delta = -123.8$ ppm, to be compared with $\delta = -118.3$ for the starting material). Only one singlet ($\delta = 21.85$ ppm) was present in the ³¹P NMR spectrum, compatibly with the *trans* geometry of the complex. The reaction observed is analogous to that of simple iodoarenes.^[66] The product was not very stable and it decomposed slowly on standing at room temperature (*vide infra*). It was nonetheless possible to isolate it in the solid state – albeit only in 19% yield – by switching to toluene as a solvent and by performing the crystallization at low temperature (–20 °C).



Scheme 37 – Formation of complex **13** from compound **1b**.

Complex **13** was generated *in situ* from Pd(PPh₃)₄ (40 mM in CD₂Cl₂) and **1b** (1.5 equiv). Et₃N·HI was then added (2.5 equiv) as a mild source of HI^{ix} and the resulting mixture was heated at 60 °C for 8 h. After cooling, an abundant precipitate of *trans*-[Pd(PPh₃)₂I₂]·(CD₂Cl₂) under the form of orange-red needles was produced.^x Analysis of the supernatant revealed that 80% of **13** had been converted to other products, the most abundant of which we identified as compound **14** (Scheme 38), which was obtained in approx. 70% yield (based on converted **13**), as assessed by ¹⁹F NMR spectroscopy. Other unidentified products formed in small amounts. No trace of indole **2b** could be identified by NMR analysis (¹H and ¹⁹F) of the *crude* reaction mixture. An attempt to isolate compound **14** by preparative TLC on silica gel was not successful,

^{viii} It was not possible to perform these experiments in propionitrile or acetonitrile because EtCN-*d*₅ is not commercially available and Pd(PPh₃)₄ has scant solubility in CD₃CN.

^{ix} This salt was added to avoid deprotonation of phenolic compounds, which would make the identification of the formed products difficult or impossible. Since HI is formally released in the overall reaction, this is relevant for the catalytic conditions.

^x The complex *trans*-[Pd(PPh₃)₂I₂]·(CD₂Cl₂) was identified by comparison of the lattice parameters of the crystals and of the ³¹P NMR spectrum with literature data^[82,83]

as only indole **2b** was recovered instead.^{xi} We speculate that in the reaction conditions isomerization of **14** to **2b** does not take place easily, while silica gel is able to promote more efficiently this transformation.

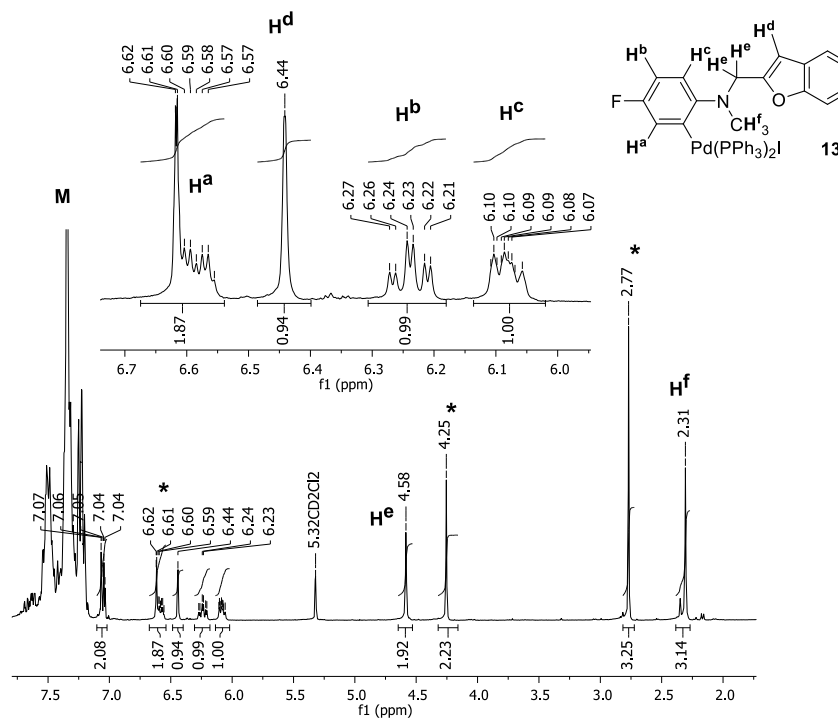
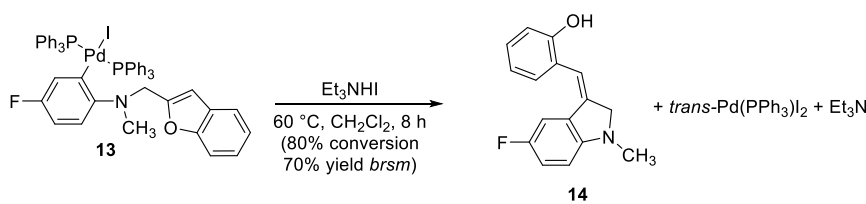


Figure 1 – ^1H NMR spectrum of complex **13**, generated *in situ* by reaction of $\text{Pd}(\text{PPh}_3)_4$ (20 mM in CD_2Cl_2) and compound **1b** (2.0 equiv). The assignment of each characteristic peak of the complex is noted, peaks of excess **1b** are noted with *. The multiplet **M** comprises the resonances of PPh_3 and other aromatic protons of **13** and **1b**.



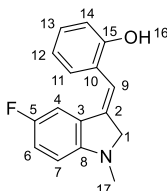
Scheme 38 – Thermal decomposition of complex **13** in the presence of $\text{Et}_3\text{N}\cdot\text{HI}$.

Since it was not possible to isolate **14**, it could only be characterized *in situ* by NMR spectroscopy. The complexity of the mixture prevented us to individuate all the ^{13}C and ^1H resonances of this compound, nonetheless its identity can be stated beyond reasonable doubt for several reasons: 1) its formation is analogous to that of compound **3**, which was indeed stable

^{xi} To ensure that compound **14** was not lost for some reason on the TLC plate, the entire layer of adsorbent was scooped and extracted repeatedly with MeOH. NMR analysis of the extract failed to reveal the characteristic resonances of **14**, indicating that it was entirely consumed.

to chromatography and could be characterized completely (Scheme 26); 2) it is converted to **2b** upon chromatography on silica gel; 3) its characteristic ^1H and ^{13}C NMR resonances could be individuated by 1D spectra and standard 2D techniques (Table 3) and they compare favorably with those of **3**; 4) its ^{19}F NMR chemical shift ($\delta = -128.5$ ppm) is close to that of *N*-methyl-5-fluoroindoline ($\delta = -127.7$ ppm^[67], for comparison for **2b** $\delta = -125.1$ ppm and for **1b** $\delta = -118.3$ ppm).

Table 3 – Characteristic NMR resonances of compound **14**.



Nucleus	^1H δ (ppm)	^{13}C δ (ppm)	Notes
1	4.24 (d, $J = 2.9$ Hz, 2H)	62.4	^{13}C assigned by HSQC and HSQC-TOCSY, HMBC with H ₁₇
3	-	124.1	HMBC with H ₁
8	-	154.3	HMBC with H ₁ and H ₁₇
9	6.45 (t, $J = 2.9$ Hz, 1H)	114.4	^{13}C assigned by HSQC-TOCSY (^1H peak superposed to impurity) HMBC with H ₁
17	2.80 (s, 3H)	35.8	^{13}C assigned by HSQC, HMBC with H ₁

When the same experiment was repeated in the absence of added $\text{Et}_3\text{N}\cdot\text{HI}$, analogous results were obtained as judged by ^{19}F and ^{31}P NMR spectroscopy, but interpretation of the ^1H spectrum was not possible, as peaks were broadened, probably due to protonation and coordination equilibria.

2.6. Proposed catalytic cycle

Based on the data collected, the catalytic cycle illustrated in Figure 2 can be put forward for the transformation under study. Intermediates that have been isolated or characterized spectroscopically are shown in dashed rectangles. The first step is oxidative addition of the iodoarene substrate to Pd(0). The resulting arylpalladium(II) complex effects carbopalladation of the C=C double bond of benzofuran, giving a *spiro* organopalladium intermediate. As it usually happens,^[68,69] this reaction should proceed in a *syn* fashion. *Anti* β -alkoxodepalladation would deliver the indoline having the exocyclic double bond with the observed *E* stereochemistry. This step can be thought as the reverse of the key step of the Wacker-Hoechst process, *i.e.* the addition of an oxygen nucleophile to a Pd(II)-alkene complex.

The latter process would deliver a Pd(II) species, that needs to be reduced back to Pd(0) to allow catalytic turnover. We propose that DIPEA can act as a reducing agent, being in turn oxidized to the corresponding imine or enamine. It has already been demonstrated that DIPEA

can fulfill this role (*vide infra*). Moreover, other amines having α hydrogens can replace DIPEA (Et_3N , $i\text{Pr}_2\text{NH}$, N -methylmorpholine, Table 1, entries 7-9), while 2,2,6,6-tetramethylpiperidine – having no α hydrogens – gives almost no catalytic turnover (TMP, Table 1, entry 10). Finally, isomerization of the exocyclic double bond would re-establish aromaticity and deliver the indole, which is the final product of the reaction.

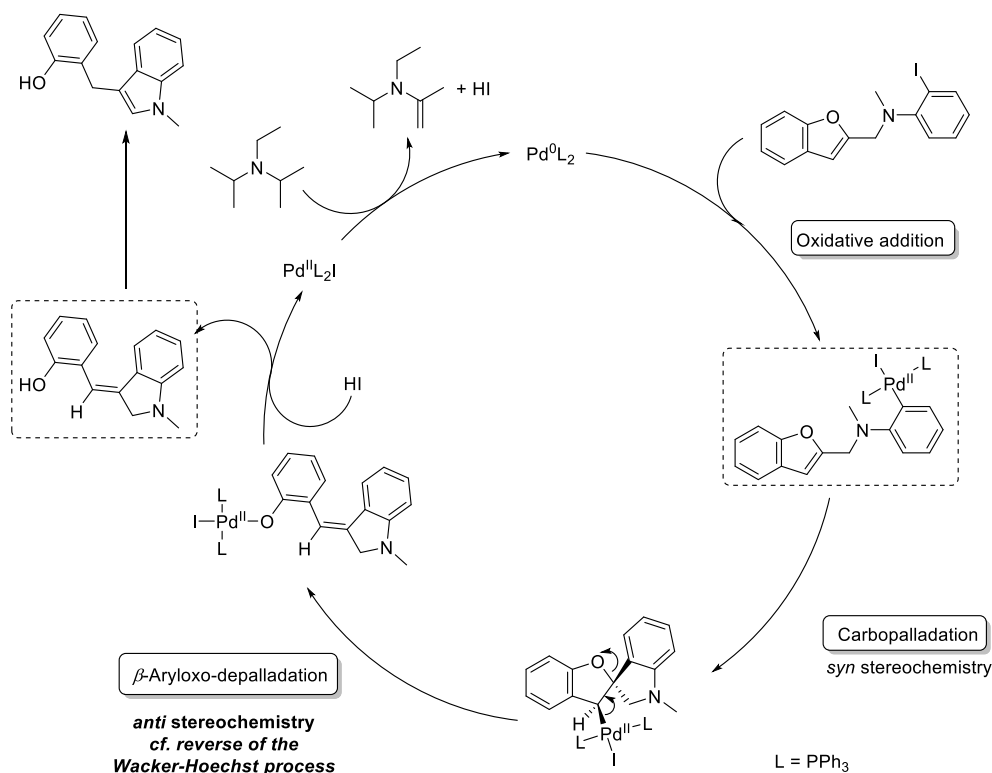
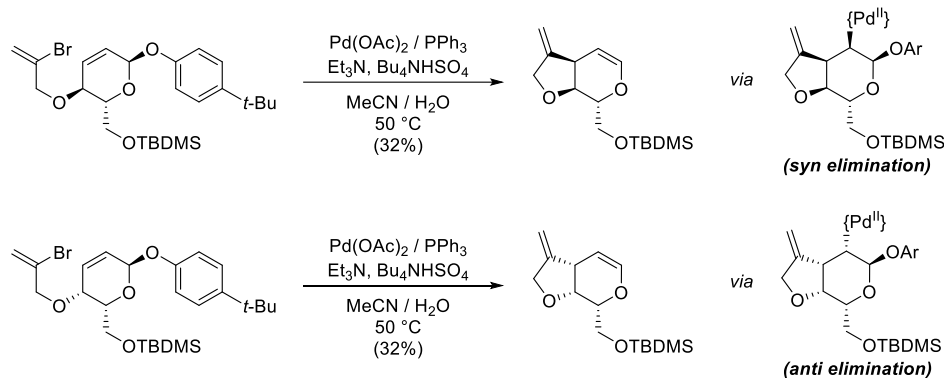


Figure 2 – Proposed catalytic cycle. Intermediates that have been isolated or characterized spectroscopically are shown in dashed rectangles.

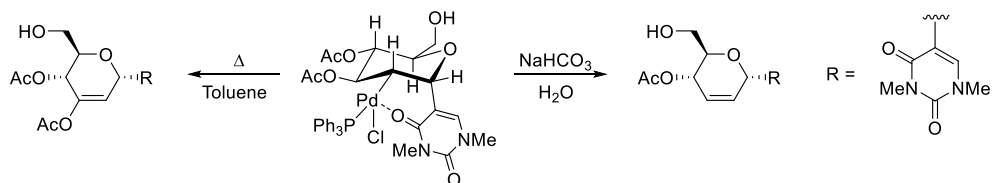
Evidence for each step of the proposed catalytic cycle has been already reported in the literature. The spirocyclic product issuing from carbopalladation has been intercepted by reducing agents, resulting in a reductive Heck coupling (see the introduction, Scheme 19) or by oxidizing agents (Scheme 18). Evidence for the carbopalladation of benzofuran has been also been given in intermolecular reactions (see the introduction, Scheme 16 and Scheme 17).

β -Aryloxo-depalladation proceeding in an *anti* fashion is perhaps more exotic, but it is also known. In an example drawn from carbohydrate chemistry, it has been demonstrated that this reaction can proceed either with *syn* or *trans* stereochemistry (Scheme 39). Some cases of the related *anti* de-acetoxypalladation are known. In the example shown in Scheme 40, a glucopyranosyl palladium (II) derivative featuring an ancillary pyrimidine coordinating moiety can either undergo a *syn* β hydride elimination by refluxing in toluene or an *anti* β -deacetoxypalladation by treatment with aqueous sodium bicarbonate.^[70] A very clever demonstration of the preference for *anti* stereochemistry in the reverse reaction (β -acetoxypalladation) has been given by studying the mixture of products obtained by the

oxidation of 3,3,6,6-tetradeuterocyclohexene with Pd(OAc)₂ and CuCl₂.^{[71]xii} It is worth noting that all the examples of *anti*-demetallation involving oxygen leaving group involve protic conditions, which would be suggestive of a protonation-assisted process.

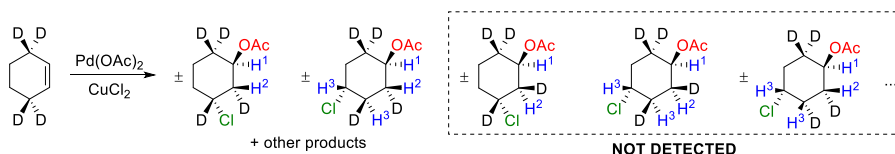


Scheme 39 – Heck-type cyclizations of unsaturated sugar-derived compounds.^[72]

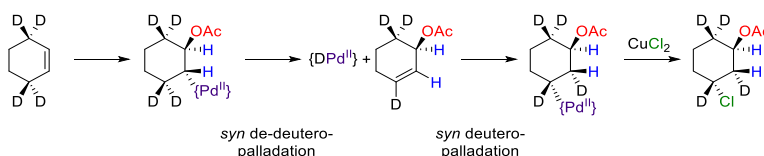


Scheme 40 – Alternative reactions of a glucopyranosyl palladium (II) derivative.^[70]

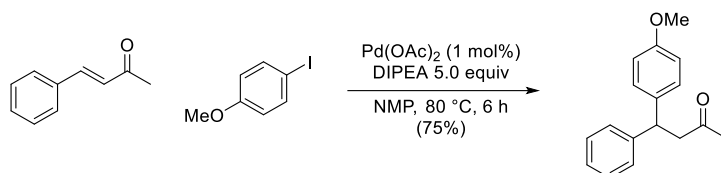
xii When 3,3,6,6-tetradeuterocyclohexene was oxidized with a mixture of Pd(OAc)₂ and CuCl₂, NMR analysis showed that no deuterium was lost and that the H¹ and H² protons in the *trans*-3-chlorocyclohexyl acetate so formed are *trans* to each other, as it happens for the H¹, H², H³ and H⁴ of *trans*-4-chlorocyclohexyl acetate:



This remarkable stereochemical feature can be explained by admitting that the reaction proceeds through an initial acetoxy-palladation of the double bond followed by stepwise migration of Pd along the ring by successive dehydropalladation/hydropalladation (or dedeuteropalladation/deuteropalladation). Since the latter reaction have *syn* stereochemistry, acetoxy-palladation needs to be *anti*. Here is the reaction for the formation of the 1,3 isomers:^[71]



Finally, the behaviour of tertiary amines such as DIPEA as reducing agents in Pd-catalyzed reaction has already been observed. For instance, a reductive Heck arylation in which no other external reducing agent is present has been described.^[73,74] The role of DIPEA as a reducing agent in this transformation has been studied in detail.^[75]



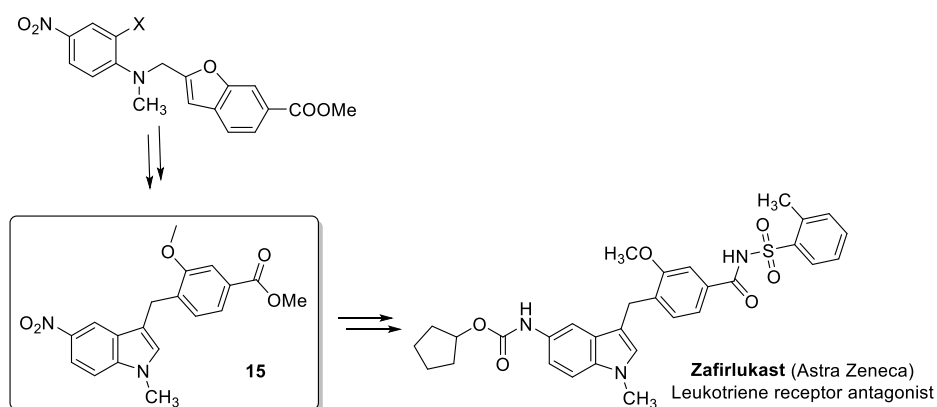
Scheme 41 – Reductive Heck arylation of enones with DIPEA acting as a reducing agent.^[73]

3. Conclusions

The experimental conditions to effect a palladium-catalyzed ring-opening reaction with phenoxide elimination as the key step have been optimized. Suitably substituted benzofuran-tethered 2-iodoanilines give synthetically interesting 2-(3-indolylmethyl)phenols after double bond isomerization. In these transformations, *N,N*-diisopropylethylamine acts as a base and a reducing agent.

Mechanistic studies on pre-formed organopalladium intermediates suggested that the reaction proceeds by intramolecular Heck-type carbopalladation of the heterocyclic ring of benzofuran terminated by an unusual stereospecific *trans*- β -phenoxide elimination giving stereospecifically an exocyclic olefin. Theoretical studies, already started by Raymond Grüber^[76] and Paul Fleurat-Lessard, are being completed to shed more light on the mechanism of this transformation, and in particular on the role of proton donors in the β -aryloxidepalladation step.

In perspective, this methodology could be applied to the synthesis of compound **15**, an intermediate for the preparation of the leukotriene receptor agonist Zafirlukast (Scheme 42).^[59,77]



Scheme 42 – Intermediate for the synthesis of Zafirlukast.^[59,77]

4. References

- [1] R. Rossi, M. Lessi, C. Manzini, G. Marianetti, F. Bellina, *Synthesis* **2016**, *48*, 3821–3862.
- [2] R. Rossi, F. Bellina, M. Lessi, C. Manzini, L. Perego, *Synthesis* **2014**, *46*, 2833–2883.
- [3] R. Rossi, F. Bellina, M. Lessi, C. Manzini, *Adv. Synth. Catal.* **2014**, *356*, 17–117.
- [4] I. Hussain, T. Singh, *Adv. Synth. Catal.* **2014**, *356*, 1661–1696.
- [5] C.-X. Zhuo, W. Zhang, S.-L. You, *Angew. Chem. Int. Ed.* **2012**, *51*, 12662–12686.
- [6] C.-X. Zhuo, W. Zhang, S.-L. You, *Angew. Chem.* **2012**, *124*, 12834–12858.
- [7] L. M. Repka, S. E. Reisman, *J. Org. Chem.* **2013**, *78*, 12314–12320.
- [8] S. P. Roche, J.-J. Youte Tendoung, B. Tréguier, *Tetrahedron* **2015**, *71*, 3549–3591.
- [9] C. Zheng, S.-L. You, *Chem* **2016**, *1*, 830–857.
- [10] R. Kuwano, in *Asymmetric Dearomatization Reactions* (Ed.: S.-L. You), WILEY-VCH, Weinheim, **2016**, pp. 69–102.
- [11] X. Wang, D. V. Gribkov, D. Sames, *J. Org. Chem.* **2007**, *72*, 1476–1479.
- [12] F. Bellina, F. Benelli, R. Rossi, *J. Org. Chem.* **2008**, *73*, 5529–35.
- [13] A. P. Kozikowski, D. Ma, *Tetrahedron Lett.* **1991**, *32*, 3317–3320.
- [14] C. Shen, R.-R. Liu, R.-J. Fan, Y.-L. Li, T.-F. Xu, J.-R. Gao, Y.-X. Jia, *J. Am. Chem. Soc.* **2015**, *137*, 4936–4939.
- [15] A. Ohta, Y. Akita, T. Ohkuwa, M. Chiba, R. Fukunaga, A. Miyafuji, T. Nakata, N. Tani, Y. Aoyagi, Y. Akita, T. Ohkuwa, M. Chiba, R. Fukunaga, A. Miyafuji, T. Nakata, N. Tani, *Heterocycles* **1990**, *31*, 1951.
- [16] Y. Aoyagi, A. Inoue, I. Koizumi, R. Hashimoto, K. Tokunaga, K. Gohma, J. Komatsu, K. Sekine, A. Miyafuji, J. Kunoh, R. Honma, A. Yasu, A. Ohta, *Heterocycles* **1992**, *33*, 257–272.
- [17] S. Tamba, Y. Okubo, S. Tanaka, D. Monguchi, A. Mori, *J. Org. Chem.* **2010**, *75*, 6998–7001.
- [18] S. Yanagisawa, K. Itami, *Tetrahedron* **2011**, *67*, 4425–4430.
- [19] A. F. P. Biajoli, E. T. da Penha, C. R. D. Correia, *RSC Adv.* **2012**, *2*, 11930.
- [20] D.-T. D. Tang, K. D. Collins, J. B. Ernst, F. Glorius, *Angew. Chem. Int. Ed.* **2014**, *53*, 1809–1813.
- [21] L. Loukotova, K. Yuan, H. Doucet, *ChemCatChem* **2014**, *6*, 1303–1309.
- [22] B. Liegault, I. Petrov, S. I. Gorelsky, K. Fagnou, B. Liégault, *J. Org. Chem.* **2010**, *75*, 1047–1060.
- [23] M. Ionita, J. Roger, H. Doucet, *ChemSusChem* **2010**, *3*, 367–376.
- [24] M. Baloch, D. Roy, S. Bensaid, V. Guerchais, H. Doucet, *Eur. J. Inorg. Chem.* **2012**, *2012*, 4454–4462.
- [25] H. Y. Sun, S. I. Gorelsky, D. R. Stuart, L. C. Campeau, K. Fagnou, *J. Org. Chem.* **2010**, *75*, 8180–8189.
- [26] A. Carrër, D. Brinet, J.-C. Florent, P. Rousselle, E. Bertounesque, *J. Org. Chem.* **2012**, *77*, 1316–1327.
- [27] K. Kim, I. Kim, *Org. Lett.* **2010**, *12*, 5314–5317.
- [28] C. C. Hughes, D. Trauner, *Angew. Chem. Int. Ed.* **2002**, *41*, 1569–1572.
- [29] C. C. Hughes, D. Trauner, *Tetrahedron* **2004**, *60*, 9675–9686.
- [30] R. Romagnoli, P. G. Baraldi, M. D. Carrion, C. L. Cara, O. Cruz-Lopez, M. Tolomeo, S. Grimaudo, A. Di Cristina, M. R. Pipitone, J. Balzarini, N. Zonta, A. Brancale, E. Hamel, *Bioorg. Med. Chem.* **2009**, *17*, 6862–6871.
- [31] K. J. Fowler, J. L. Ellis, G. W. Morrow, *Synth. Commun.* **2013**, *43*, 1676–1682.
- [32] N. Matsumoto, H. Shinya, *Arylamine Compound and Use Thereof*, **2014**, WO2014181878 (A1).
- [33] B. S. Cho, Y. K. Chung, *Chem. Commun.* **2015**, *51*, 14543–14546.
- [34] S. Kirchberg, R. Fröhlich, A. Studer, *Angew. Chem. Int. Ed.* **2010**, *49*, 6877–6880.
- [35] S. Kirchberg, R. Fröhlich, A. Studer, *Angew. Chem.* **2010**, *122*, 7029–7032.
- [36] K. Hata, Z. He, C. G. Daniliuc, K. Itami, A. Studer, *Chem. Commun.* **2014**, *50*, 463–465.
- [37] V. Ramella, Z. He, C. G. Daniliuc, A. Studer, *Eur. J. Org. Chem.* **2016**, *2016*, 2268–2273.
- [38] R.-R. Liu, Y. Xu, R.-X. Liang, B. Xiang, H.-J. Xie, J.-R. Gao, Y.-X. Jia, *Org. Biomol. Chem.* **2017**, *15*, 2711–2715.
- [39] D. Qin, R. X. Ren, T. Siu, C. Zheng, S. J. Danishefsky, *Angew. Chem. Int. Ed.* **2001**, *113*, 4709–4713.
- [40] A. S. Kyei, K. Tchabanenko, J. E. Baldwin, R. M. Adlington, *Tetrahedron Lett.* **2004**, *45*, 8931–8934.
- [41] S. France, J. Boonsombat, C. A. Leverett, A. Padwa, *J. Org. Chem.* **2008**, *73*, 8120–8123.
- [42] N. Chopin, H. Gérard, I. Chataigner, S. R. Piettre, *J. Org. Chem.* **2009**, *74*, 1237–1246.
- [43] G. Stork, A. Yamashita, J. Adams, G. R. Schulte, R. Chesworth, Y. Miyazaki, J. J. Farmer, *J. Am. Chem. Soc.* **2009**, *131*, 11402–11406.
- [44] Y.-C. Xiao, C.-Z. Yue, P.-Q. Chen, Y.-C. Chen, *Org. Lett.* **2014**, *16*, 3208–3211.
- [45] D. Janssen-Müller, M. Fleige, D. Schlüns, M. Wollenburg, C. G. Daniliuc, J. Neugebauer, F. Glorius, *ACS Catal.* **2016**, *6*, 5735–5739.
- [46] A. T. Balaban, D. C. Oniciu, A. R. Katritzky, *Chem. Rev.* **2004**, *104*, 2777–2812.

- [47] K.-J. Wu, L.-X. Dai, S.-L. You, *Org. Lett.* **2012**, *14*, 3772–3775.
- [48] L. Zhao, Z. Li, L. Chang, J. Xu, H. Yao, X. Wu, *Org. Lett.* **2012**, *14*, 2066–2069.
- [49] D. A. Petrone, A. Yen, N. Zeidan, M. Lautens, *Org. Lett.* **2015**, *17*, 4838–4841.
- [50] S. Gao, C. Yang, Y. Huang, L. Zhao, X. Wu, H. Yao, A. Lin, *Org. Biomol. Chem.* **2016**, *14*, 840–843.
- [51] K. Douki, H. Ono, T. Taniguchi, J. Shimokawa, M. Kitamura, T. Fukuyama, *J. Am. Chem. Soc.* **2016**, *138*, 14578–14581.
- [52] D. A. Petrone, M. Kondo, N. Zeidan, M. Lautens, *Chem. Eur J.* **2016**, *22*, 5684–5691.
- [53] S. Chen, X.-X. Wu, J. Wang, X.-H. Hao, Y. Xia, Y. Shen, H. Jing, Y.-M. Liang, *Org. Lett.* **2016**, *18*, 4016–4019.
- [54] S. Wagschal, Synthèse D'hétérocycles et Réactions Pallado-Catalysées, PhD Thesis, Ecole Polytechnique, **2010**.
- [55] L. El Kaïm, L. Grimaud, S. Wagschal, *Chem. Commun.* **2011**, *47*, 1887–1889.
- [56] V. V. Grushin, H. Alper, *Organometallics* **1993**, *12*, 1890–1901.
- [57] C. Amatore, L. El Kaïm, L. Grimaud, A. Jutand, A. Meignié, G. Romanov, *Eur. J. Org. Chem.* **2014**, *2014*, 4709–4713.
- [58] G. Di Gregorio, M. Mari, F. Bartocchini, G. Piersanti, *J. Org. Chem.* **2017**, *82*, 8769–8775.
- [59] G. Goverdhan, A. R. Reddy, A. Sampath, K. Srinivas, V. Himabindu, G. M. Reddy, *Org. Process Res. Dev.* **2009**, *13*, 67–72.
- [60] A. Coluccia, S. Passacantilli, V. Famiglini, M. Sabatino, A. Patsilnakos, R. Ragno, C. Mazzoccoli, L. Sisinni, A. Okuno, O. Takikawa, R. Silvestri, G. La Regina, *J. Med. Chem.* **2016**, *59*, 9760–9773.
- [61] L. Han, W. Zhang, X.-X. Shi, S.-L. You, *Adv. Synth. Catal.* **2015**, *357*, 3064–3068.
- [62] H. S. Kim, H. S. Lee, S. H. Kim, J. N. Kim, *Tetrahedron Lett.* **2009**, *50*, 3154–3157.
- [63] A. Jutand, A. Mosleh, *Organometallics* **1995**, *14*, 1810–1817.
- [64] D. Qiu, J. He, X. Yue, J. Shi, Y. Li, *Org. Lett.* **2016**, *18*, 3130–3133.
- [65] *SDBSWeb*: [Http://sdb.sdb.aist.go.jp](http://sdb.sdb.aist.go.jp) (National Institute of Advanced Industrial Science and Technology), **2017**.
- [66] P. Fitton, E. A. Rick, *J. Organomet. Chem.* **1971**, *28*, 287–291.
- [67] A. Zakrzewska, E. Kolehmainen, B. Osmialowski, R. Gawinecki, *J. Fluor. Chem.* **2001**, *111*, 1–10.
- [68] E. Negishi, *Handbook of Organopalladium Chemistry for Organic Synthesis*, John Wiley & Sons, Inc., New York, USA, **2002**.
- [69] M. Oestreich, *The Mizoroki-Heck Reaction*, John Wiley & Sons, **2009**.
- [70] I. Arai, G. D. Daves, *J. Am. Chem. Soc.* **1981**, *103*, 7683–7683.
- [71] P. M. Henry, G. A. Ward, *J. Am. Chem. Soc.* **1971**, *93*, 1494–1497.
- [72] K. Bedjeguel, L. Joseph, V. Bolitt, D. Sinou, *J. Carbohydr. Chem.* **2000**, *19*, 221–232.
- [73] S. Mannathan, S. Raoufmoghaddam, J. N. H. Reek, J. G. de Vries, A. J. Minnaard, *ChemCatChem* **2016**, *8*, 2572–2572.
- [74] S. Mannathan, S. Raoufmoghaddam, J. N. H. Reek, J. G. de Vries, A. J. Minnaard, *ChemCatChem* **2016**, *8*, 2572–2572.
- [75] S. Raoufmoghaddam, S. Mannathan, A. J. Minnaard, J. G. de Vries, J. N. H. Reek, *Chem. Eur J.* **2015**, *21*, 18811–18820.
- [76] R. Grüber, Etude Théorique de Réactions de Heck Intramoléculaires, PhD Thesis, Ecole Normale Supérieure de Lyon, **2014**.
- [77] K. Srinivas, N. Srinivasan, M. R. Krishna, C. R. Reddy, M. Arunagiri, R. Lalitha, K. S. R. Reddy, B. S. Reddy, G. M. Reddy, P. P. Reddy, M. K. Kumar, M. S. Reddy, *Org. Process Res. Dev.* **2004**, *8*, 952–954.
- [78] S. El Kazzouli, J. Koubachi, N. El Brahmi, G. Guillaumet, *RSC Adv.* **2015**, *5*, 15292–15327.
- [79] D. R. Lide, *CRC Handbook of Chemistry and Physics*, CRC Press, **2003**.
- [80] B. Gabriele, R. Mancuso, G. Salerno, *J. Org. Chem.* **2008**, *73*, 7336–7341.
- [81] B. A. Shainyan, Y. S. Danilevich, *Russ. J. Org. Chem.* **2016**, *52*, 1112–1117.
- [82] T. Debaerdemaeker, A. Kutoglu, G. Schmid, L. Weber, *Acta Cryst. B* **1973**, *29*, 1283–1288.
- [83] F. E. Hahn, T. Lügger, M. Beinhoff, Z. *Naturforsch. B* **2004**, *59B*, 196–201.

CHAPTER IV

Copper-Catalyzed Hydroamination of Allenes: Mechanistic Studies and Methodology Development

The material presented in this chapter is the subject of three publications:

Luca A. Perego,* R. Blicck, A. Groué, F. Monnier,* M. Taillefer,* I. Ciofini,* L. Grimaud,*
Cu-Catalyzed Hydroamination of Allenes: from Mechanistic Understanding to Methodology Development
ACS Catal. **2017**, 7, 4253-4264

L. A. Perego, R. Blicck, J. Michel, I. Ciofini,* L. Grimaud,* M. Taillefer,* F. Monnier*
Copper-Catalyzed Hydroamination of N-Allenylazoles: Access to Amino-Substituted N-Vinylazoles
Adv. Synth. Catal. **2017**, 359, accepted – doi: 10.1002/adsc.201700965

R. Blicck, L. A. Perego, I. Ciofini, L. Grimaud, M. Taillefer, F. Monnier
Copper-Catalyzed Hydroamination of N-Allenylsulfonamides
Manuscript in preparation

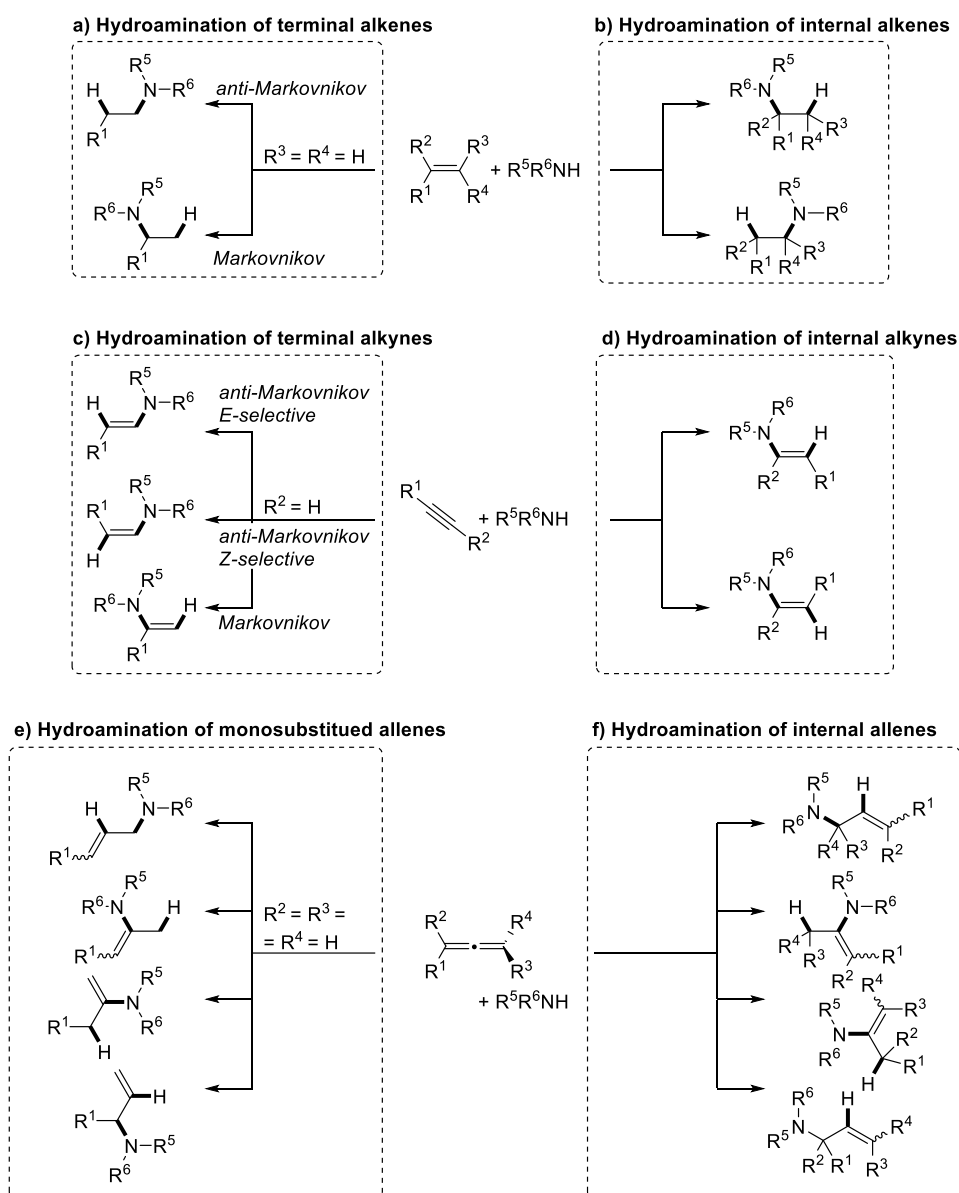
1. Context of the Study

1.1. Introduction

A hydroamination reaction is the addition of a N-H moiety of ammonia or amines across a C-C double or triple bond with concomitant cleavage of the N-H bond. A C-N and a C-H bond are thus formed in the process. Somehow improperly, this term is also often used to designate the addition of related nitrogen-containing compounds to C-C multiple bonds. More in detail, acyl, sulfonyl and phosphonyl groups make the N-H proton 5-20 order of magnitudes more acidic than in the unsubstituted amines and the N atom less nucleophilic. The corresponding amides, sulfonamides, and phosphoramides are useful substrates for the catalytic addition to C-C bonds, and these reactions related to hydroaminations are better called hydroamidations. This terminology is not only more accurate, but it also highlights the differences existing in substrate scope and reactivity. Other N-H bond containing organic compounds, such as hydrazines, carbamates, ureas, amidines, guanidines, azoles, and hydrazoic acid can also participate into hydroamination-related reactions.

Generally speaking, hydroamination of double bonds leads to amines (Scheme 1, a-b), while hydroamination of alkynes generates enamines (Scheme 1, c-d). If the amine employed is primary ($R^1 = H$), tautomerization to the corresponding imine is possible. If the amine substrate is secondary, the enamine tautomer is stable. The hydroamination of both terminal alkenes and alkynes can proceed either in anti-Markovnikov fashion (*i.e.* the nitrogen atom ends up on the terminal carbon atom) or with Markovnikov-type selectivity (*i.e.* the nitrogen atom is attached to the most substituted carbon). The enamines deriving from the hydroamination of triple bonds can also feature *E/Z* isomerism. The mono-hydroamination of terminal allenes can in principle lead to four constitutional isomers, depending on which of the two double bonds is involved in the reaction and on the regiochemistry of the addition (Scheme 1, e-f). Two isomeric allylic amines and two enamines can be generated, and *E/Z* isomers are possible for the products deriving from addition to the terminal double bond.

Compared to traditional methods for the synthesis of amines, enamines, imines and enamides, hydroamination and hydroamidation reactions are advantageous in terms of complete atom economy and employ readily available and inexpensive starting materials. Moreover, stoichiometric amounts of coupling-promoting agents are not needed. However, as we have shown above, several different products can form and chemo- and regioselectivity are major concerns. Fortunately, as it will be clear from the examples reported in the following paragraphs, selectivity issues are readily resolved for intramolecular reactions, and often protocols offering good regio- and stereoselectivity exist for intermolecular reactions. Consequently, hydroamination reactions have the potential to be useful for the practical synthesis of complex molecules.



Scheme 1 – Possible isomers generated by the hydroamination reaction of alkenes, alkynes, and allenes.

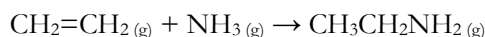
Due to the interest of this transformation, an impressive amount of literature has been produced in this field. Since it is impossible to give here a representative account of the metal-catalyzed hydroamination reactions involving all kinds of unsaturated compounds, we will limit ourselves to a discussion concerning only the hydroamination of allene-type substrates. For the rest, the reader is referred to the numerous existing reviews. A list of selected reviews is given in Table 1, together with a brief description of the main topics covered.

Table 1 – Selected reviews concerning the hydroamination of unsaturated compounds

Authors, Year	Description
Mueller, Beller 1998 ^[1]	A survey on the hydroamination of unactivated alkenes and alkynes catalyzed by alkali metal, zeolites and transition metals.
Brunet, Neibecker 2003 ^[2]	A general review on hydroamination of alkenes, alkynes and allenes.
Pohlki, Doye 2003 ^[3]	A survey of the literature concerning hydroamination of alkynes.
Alonso, Beletskaya, Yus 2004 ^[4]	A review on the addition of hydrogen-heteroatom compounds to alkynes.
Beller, Seayad, Tillack, Jiao 2004 ^[5]	An overview of recent developments on the metal-catalyzed functionalization of alkenes and alkynes, with a focus on regioselectivity. Also covers hydroamination of alkenes and alkynes.
Widenhofer, Han 2006 ^[6]	A succinct survey of gold-catalyzed hydroaminations of unactivated alkenes, alkynes, allenes, and 1,3-dienes.
Severin, Doye 2007 ^[7]	A tutorial review covering the results on the hydroamination of alkynes appeared in 2002-2006.
Mueller, Hultsch, Yus, Foubelo, Tada 2008 ^[8]	Very comprehensive work, updates the 1998 review by Beller and Mueller. ^[1] Reference works and reviews not focused on hydroamination, but that contain substantial information of this reaction are also carefully indexed in tabular form.
Alcaide, Almendros 2011 ^[9]	Review focused on the cyclization of amino-substituted allenes. Recent developments are reported together with early results in the field.
Yadav, Antony, Rao, Subba Reddy 2011 ^[10]	Review covering recent developments in metal-catalyzed hydrofunctionalization chemistry of non-activated alkenes, among which hydroamination.
Patil, Kavthe, Shinde 2012 ^[11]	Comprehensive report on the transition metal-catalyzed addition of C-, N- and O-nucleophiles to unactivated alkenes, alkynes and allenes.
Zeng 2013 ^[12]	Review on recent cascade, domino and tandem reactions involving catalytic heterofunctionalization of C-C multiple bonds.
Reznichenko, Hultsch 2011 ^[3]	A survey part of the collection <i>Topics in Organometallic Chemistry</i> covering the early transition-metal catalyzed hydroamination of unsaturated compounds.
Nishina, Yamamoto 2012 ^[11]	A survey part of the collection <i>Topics in Organometallic Chemistry</i> covering the late transition-metal catalyzed hydroamination of unsaturated compounds. Gives a mechanistic overview and scope of the reactions in a concise form.
Evano, Gaumont, Alayrac, <i>et al.</i> 2014 ^[15]	Report on the state-of-the art on the metal-catalyzed synthesis of heteroatom-substituted alkenes and alkynes. Hydroamination and hydroamidation of alkynes are covered in the section dealing with the synthesis of enamines and enamides.
Huang, Arndt, Goossen, Heydt, Goossen 2015 ^[6]	Very comprehensive and systematic review on the late-transition metal catalyzed hydroamination of alkenes, alkynes and allenes. Other nitrogen nucleophiles (amides, carbamates, sulfonamides, ...) are also considered.
Bernoud, Lepori, Mellah, Schulz, Hannedouche 2015 ^[17]	A perspective article outlining some recent advances in metal-free and late-transition metal-catalyzed hydroaminations of alkenes, including allenes, 1,3-dienes and strained alkenes.
Coman, Parvulescu 2015 ^[18]	A review on hydroaminations and C-N couplings catalyzed by non-precious metals in an application-oriented perspective.
Lepori, Hannedouche 2017	Short review providing an outline of the hydroamination of unactivated alkenes catalyzed by Zn, Cu, Ni, Co, and Fe-based systems.

1.2. Thermodynamic aspects of the hydroamination of alkenes and allenes

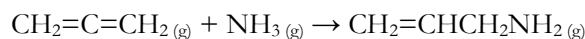
The synthesis of alkylamines by the direct addition of amines to alkenes is an exothermic process. Accurate standard enthalpies of formation are available for the prototypical alkene hydroamination reaction, *i.e.* the addition of ammonia to ethylene resulting in ethylamine.^[19,20] The enthalpy associated to the reaction



at 298 K is $\Delta_r H^\circ = -13.0 \text{ kcal mol}^{-1}$. Taking into account the negative entropy change associated to this process, the Gibbs free energy can be estimated as $\Delta_r G^\circ \approx -4 \text{ kcal mol}^{-1}$ at the same temperature.^[1]

In practice, this thermodynamically favorable reaction does not take place without a catalyst. A viable uncatalyzed pathway is actually difficult to conceive. For example, nucleophilic attack onto electron-rich nonactivated alkenes is not possible due to electrostatic repulsion and thermal concerted [2+2] cycloaddition would be a symmetry-forbidden process.

Allenes are generally considered more reactive compounds than monoalkenes, and indeed the addition of amines to allenes is expected to be more exothermic than the corresponding reaction involving simple alkenes. As a simple example, the enthalpy associated to the addition of ammonia to unsubstituted allene:



at 298 K can be estimated as $\Delta_r H^\circ = -21.0 \text{ kcal mol}^{-1}$.ⁱ As a consequence, by applying in a somehow licentious way the Bell-Evans-Polanyi principle, we may expect that hydroamination of allenes is easier than that of simple alkenes. Judging on the basis of the abundance and variety of catalysts known to be effective for the hydroamination of allenes under conditions that are usually milder than those applicable to simple olefins, we may conclude that indeed this is the case. An account of the richness of the chemistry related to the catalytic hydroamination of allenes will be given in the following section.

1.3. A survey of the literature on the hydroamination of allenes

The protocols for the hydroamination of unsaturated compounds can be subdivided into three main classes: A) non-metal catalyzed processes, such as those corresponding to activation by the use of strong bases, most frequently alkali metal amides, or by protic acids; B) transformations

ⁱ A reliable value for the enthalpy of formation of allylamine is not available, so this quantity was calculated theoretically using the CBS-QB3 composite method. Isodesmic correction obtained using the accurate $\Delta_f H^\circ$ of CH₄, propylene and methylamine available in the ATcT database^[19] was negligible (< 0.1 kcal mol⁻¹). The $\Delta_f H^\circ$ of allene and NH₃ used for the calculation of $\Delta_r H^\circ$ were also taken from the ATcT database.^[19]

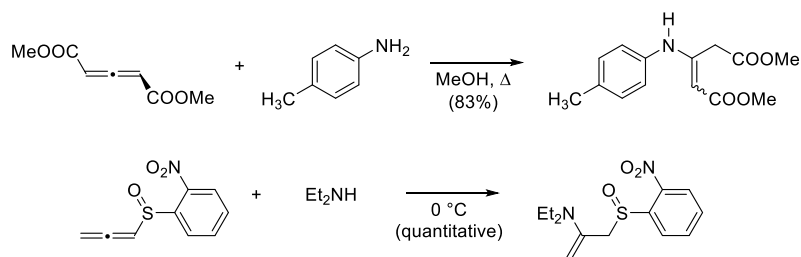
using catalysts based on early transition metals and lanthanides; C) reactions promoted by catalysts based on late transition metals. This distinction is meaningful because the reactions in each class are often characterized by some common mechanistic features and similar substrate scope, functional group tolerance and typical target application.

Selected results reported in the literature concerning hydroamination reactions of allenes and related additions of nitrogen nucleophiles will be presented in the following sections according to this classification. Metal-catalyzed processes will be reported following the order of the periodic table, according to the group to which the metal belongs to. Reactions employing activated nitrogen reagents, such as electrophilic amine derivatives together with hydride donors to effect the *formal* hydroamination of unsaturated compounds are beyond the scope of this survey.

1.3.1. Base-Catalyzed Hydroamination Reactions

Base-catalyzed reactions of class A normally proceed by generation of the deprotonated form of the amine (*i.e.* of the corresponding alkali metal amide), which may be a nucleophile strong enough to effect addition to a double bond, even in the absence of activating electron-withdrawing groups. Functional group tolerance and usefulness of these transformations in the synthesis of fine chemicals are clearly limited.

For completeness, we should remind that allenes substituted with electron-withdrawing groups can add nucleophiles (with or without a base catalyst) as Michael acceptor, with the expected selectivity for double bond conjugated with the electron-withdrawing group itself. As an example, dimethyl penta-2,3-dienoate^[21] and allenyl sulfoxides^[22] undergo Michael additions of amines without a catalyst at or below room temperature (Scheme 2).

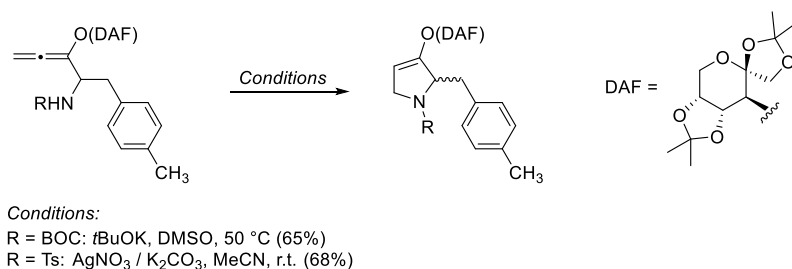


Scheme 2 – Michael addition of amines to activated electron-poor allenes.^[21,22]

Very few examples of base-catalyzed hydroaminations of allenes are known, probably due to the easy polymerization of these substrates under such harsh conditions.ⁱⁱ Basic conditions may occasionally be used to achieve the intramolecular addition of relatively acidic N-H moieties to tethered allene functions. As an example of this transformation, in a chiral-auxiliary based strategy for the synthesis of the antibiotic anisomycin, an alkoxyallene featuring a “diacetone

ⁱⁱ This side-reaction is already important with less reactive alkenes, such as styrenes. Hydroamination of simple alkenes catalyzed by alkali salts of amines are discussed in details in Beller’s and Mueller’s review.^[1]

fructose” substituent at oxygen having a tethered BOC-protected amine moiety cyclizes under the influence of *t*BuOK in DMSO at 50 °C in a 5-endo-trig process (Scheme 3).^[23] These conditions were not suitable when a *p*-toluenesulfonyl protecting group was employed instead of BOC, probably because of the reduced nucleophilicity of the deprotonated sulfonamide compared to the deprotonated carbamate. A strategy based on the use of a late transition metal catalyst (AgNO₃) was efficient in that case (Scheme 3).^[23]

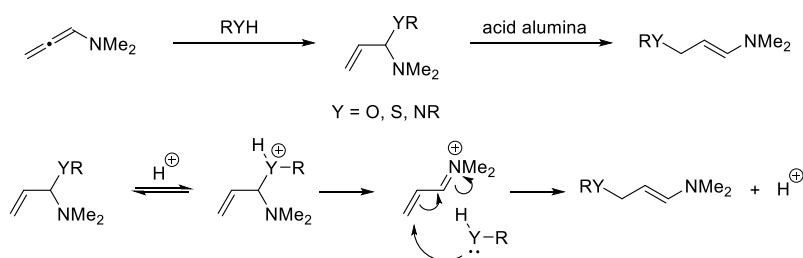


Scheme 3 – Intramolecular base- or AgNO₃-catalyzed intramolecular hydroamination of a chiral allenyl ether *en route* to anisomycin.^[23]

1.3.2. Brønsted acid-catalyzed hydroamination reactions

Acid-catalyzed hydroamination reactions are not common for allenes. Normally very harsh conditions are needed for this reaction, which are not compatible with relatively fragile allene functions.

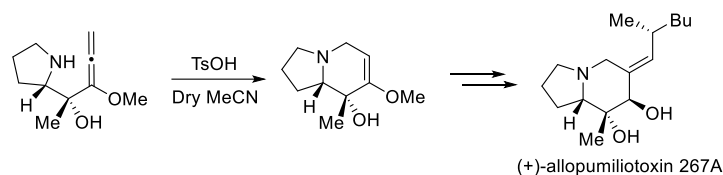
Formal hydroamination of allenylamines can proceed by acid catalysis. As shown by Brandsma and coworkers,^[24] *N,N*-dimethylaminoallene undergoes addition of alcohols, thiols and amines at C1 without any intentionally added catalyst. As the addition of bases (KOH, KO*t*Bu) inhibited the reaction, the authors concluded that this is a Brønsted acid-catalyzed process having an iminium ion intermediate (Scheme 4). The resulting acrolein semiaminal (thio)ethers and aminals undergo a rearrangement induced also by very weak acids (H₂O, NH₄Cl, or acid alumina) to give the corresponding isomeric *E* enamines. This isomerization most likely takes place in an intermolecular fashion by conjugate addition to an iminium intermediate (Scheme 4).



Scheme 4 – Addition of nucleophiles to *N,N*-dimethylaminoallene and acid-catalyzed isomerization.^[24]

A similar intramolecular acid-catalyzed process has been applied by Overman in the total synthesis of allopumiliotoxin 267A. TsOH-catalyzed formal 6-*endo-trig* intramolecular

hydroamination of a proline-derived allenyl ether gave the carbon skeleton of the target alkaloid (Scheme 5).^[25]



Scheme 5 – A key step in Overman's synthesis of (+)-allopumiliotoxin 267A.^[25]

1.3.3. Hydroamination reactions with catalysts based on early transition metals and lanthanides

We will summarize here the main results reported in the literature about the allene hydroamination reactions of class B, i.e. those catalyzed by complexes of the early transition metals (groups 3-5) and of lanthanides. All these catalysts have some common features. Early transition metals are highly electrophilic and *hard* Lewis acids, with little to no possibility to engage in π -backbonding. These catalysts usually operate by activating the amine rather than the allene and the intermediates featuring carbon-metal σ bonds are normally very reactive and short-lived. The high electrophilicity and high sensitivity to hydrolysis of many catalysts based on early transition-metal complexes normally impose the use of strictly anhydrous conditions and limits the tolerance of polar functional groups.

From the mechanistic point of view, two kinds of pathways have been proposed for this family of catalysts: 1) the *lanthanide-like* mechanism, according to which the allene inserts in the metal-amide bond; 2) the [2+2] cycloaddition pathway, in which a four-membered ring intermediate forms by reaction of a carbon-carbon double bond with a metal-imido species.

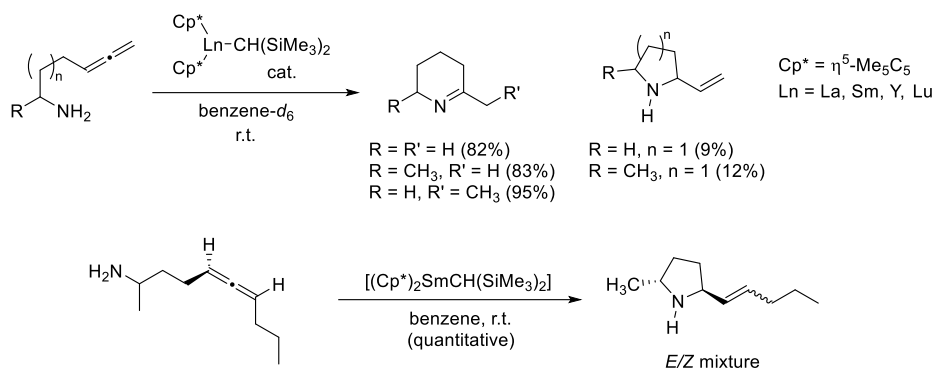
Despite the limited functional group tolerance of catalysts of class B, they often display high reactivity and interesting selectivities in intramolecular reactions, so they have been extensively studied.

1.3.3.1. Hydroamination of allenes with catalysts based on group 3 metals and lanthanides

The scandium-catalyzed intramolecular hydroamination of alkenes has been described,^[26] but no application to allenes has been reported to the best of our knowledge, neither yttrium-based allene hydroamination catalyst are known.

By contrast, lanthanides have been used successfully for the development of allene hydroamination catalysts. In 1998 Marks and coworkers demonstrated that lanthanocenes $[(Cp^*)_2Ln(CH(SiMe_3)_2)]$ ($Cp^* = \eta^5-C_5Me_5$; $Ln = La, Sm, Y, Lu$) catalyze the intramolecular hydroamination of terminal allenes having primary amine pendants.^[27] In the case of γ -aminoallenes, the 6-*exo-dig* pathway prevails, and a 2,3,4,5-tetrahydropyridine derivatives are formed, together with minor amounts of 2-vinylpyrrolines coming from 5-*exo-trig* cyclization (Scheme 6, top). With δ -aminoallenes, only a tetrahydropyridine is produced (Scheme 6, top).

The 2-vinylpyrroline deriving from a 1,3-disubstituted allene was produced as a mixture of *E/Z* double bond isomers, but almost complete selectivity for the product in which the substituents have a mutual *trans* arrangement with respect to the five-membered ring was observed.^[27] The stereoselectivity of this transformation has been exploited in the total synthesis of two naturally occurring compounds.^[28]



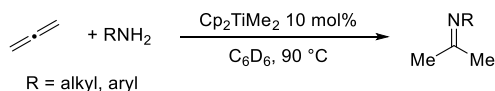
Scheme 6 – Lanthanocene-catalyzed intramolecular hydroamination of 6-amino or 7-amino-1,2-dienes.^[27]

A very detailed theoretical study on the mechanism of this reaction^[29] explained the reasons of the observed stereoselectivity.

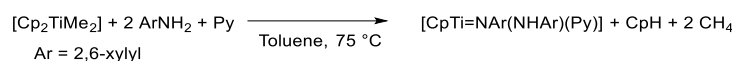
1.3.3.2. Hydroaminations of allenes with catalysts based on group 4 metals

The elements of group 4 have been widely employed to design catalysts for the hydroamination of unsaturated compounds, and a review entirely focused on this topic is available.^[30] As it often happens for early transition metals, the selectivity of intermolecular reactions is usually in favor of the addition to the central carbon of allene. With primary amines, the most successful substrates for these catalytic systems, ketimines are thus produced.

In 2001 Bergman and coworkers reported that $[\text{Cp}_2\text{TiMe}_2]$ is an efficient pre-catalyst for the hydroamination of unsubstituted allenes with primary aliphatic and aromatic amines at 90 °C, giving acetone imines (Scheme 7).^[31] Detailed study of this catalytic system revealed that cyclopentadiene was formed in the reaction medium and that the amide complex $[\text{CpTi}=\text{NAr}(\text{NHAr})]$ ($\text{Ar} = 2,6\text{-xylyl}$) is the active species. The latter complex could be trapped by pyridine and isolated as $[\text{CpTi}=\text{NAr}(\text{NHAr})(\text{Py})]$ (Scheme 8). This complex had enhanced activity and could be used at 45 °C. Terminal and internal allenes were also tolerated, but they reacted only at 90 °C.^[31]

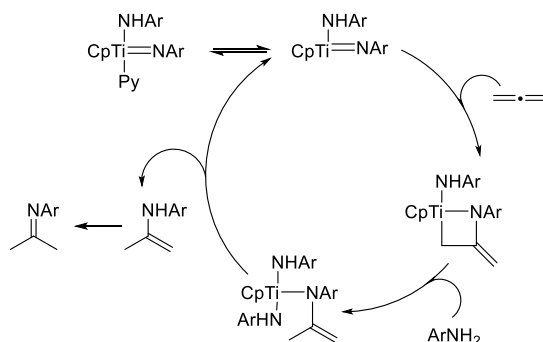


Scheme 7 – Hydroamination of allene catalyzed by Cp_2TiMe_2 .^[31]



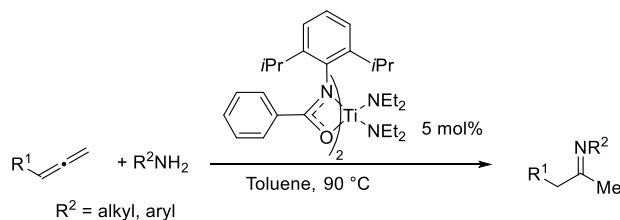
Scheme 8 – Formation of $[\text{CpTi}=\text{NAr}(\text{NHAr})(\text{Py})]$ from catalytic precursors.^[31]

The mechanism of this transformation has been thoroughly studied in a subsequent report.^[32] Briefly, the reaction takes place by formal [2+2] cycloaddition between the Ti=N moiety of the catalyst and formation of an azametallacyclobutane. Protonolysis of the C-Ti and N-Ti bonds by the primary amine substrate delivers the product and regenerates the catalyst. A simplified catalytic cycle is reported in Scheme 9.^[32]



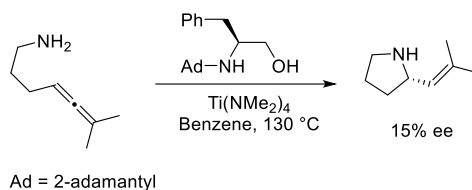
Scheme 9 – Simplified catalytic cycle for the Ti-catalyzed hydroamination of allene.^[31,32]

A titanium diamido complex featuring two deprotonated 2,6-diisopropyl benzamide ligands was also shown to be effective for the intermolecular hydroamination of terminal allenes, albeit it was not effective for 1,1-disubstituted allenes.^[33]



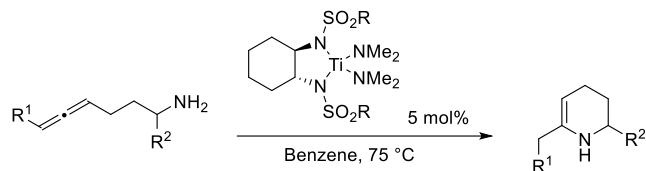
Scheme 10 – Titanium-bisamide complex catalyzing the hydroamination of allenes.^[33]

Intramolecular reactions analogous to those described previously have also attracted much interest. Chiral aminoalcohols featuring bulky *N*-substituents have been evaluated as ligands in conjunction with $[\text{Ti}(\text{NMe}_2)_4]$ as a pre-catalyst for the asymmetric 5-*exo-trig* cyclization of γ -aminoallenes giving 2-vinylpyrrolidines. The best ligand among those examined, however, promoted the reaction only with modest enantioselectivity (Scheme 11).^[34]



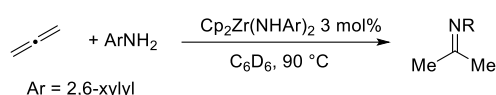
Scheme 11 – Asymmetric intramolecular hydroamination of γ -aminoallenes with a chiral aminoalcohol and $\text{Ti}(\text{NMe}_2)_4$.^[34]

Other systems favors 6-*exo-dig* addition to the allene, thus yielding tetrahydropyridine derivatives. More in detail, titanium complexes featuring bis-sulfonamido ligands are more active than Cp-containing titanium catalysts for this transformation (Scheme 12).^[35,36]



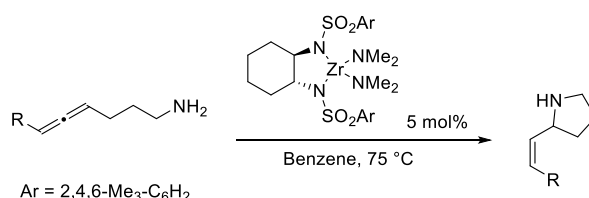
Scheme 12 – Bis-sulfonamide Ti complexes catalyzing the intramolecular hydroamination of γ -aminoallenes.^[35,36]

Zirconium-based catalysts also catalyze the hydroamination of allenes. Similarly to the analogous titanium complexes, $\text{Cp}_2\text{Zr}(\text{NHA}r)_2$ catalyzed the hydroamination of allenes with anilines at moderate temperatures (Scheme 13) giving a Markovnikov addition product.^[37] Thorough theoretical mechanistic studies substantially confirmed the [2+2] cycloaddition pathway we have shown previously for titanium-based catalysts (Scheme 9).^[38,39]



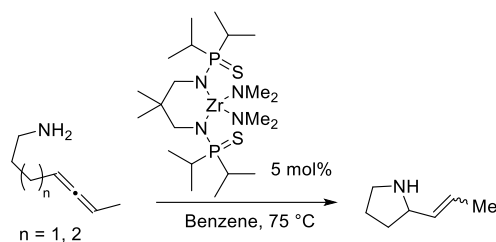
Scheme 13 – Hydroamination of allene catalyzed by $\text{Cp}_2\text{Zr}(\text{NHA}r)_2$.^[37]

Interestingly, zirconium complexes featuring bis-sulfonamide ligands similar to those shown in Scheme 12 favor 5-*exo-trig* cyclization of γ -aminoallenes instead of 6-*exo-dig* ring closure, with a selectivity for the (*Z*)-2-vinylpyrrolidine product (Scheme 14). Trisubstituted allenes are also tolerated, but the temperature needs to be increased from 75 °C (adequate for terminal allenes) to 135 °C.^[36]



Scheme 14 – Bis-sulfonamide Zr complexes catalyzing the intramolecular hydroamination of γ -aminoallenes.^[36]

Other ligands have been reported to be suitable for similar transformations. For example, zirconium complexes featuring bis-thiophosphinamide ligands catalyze the *exo-trig* cyclization of γ - and δ -aminoallenes in good yields, but the products obtained are mixtures of *E/Z* double bond isomers (Scheme 15).^[40]

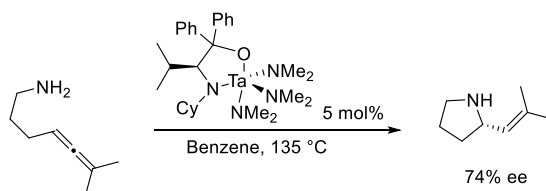


Scheme 15 – Intramolecular hydroamination of γ - and δ -aminoallenes with a Zr catalyst featuring a bis-thiophosphinamide ligand.^[40]

1.3.3.3. Hydroaminations of allenes with catalysts based on group 5 metals

Group 5 metals have not been exploited intensively for the development of allene hydroamination catalysts. To the best of our knowledge, no vanadium- and niobium-based catalysts have ever been disclosed for this transformation.

A single example of a tantalum-catalyzed hydroamination catalyst has been reported. A tantalum amide-alkoxide featuring an valine-derived aminoalcohol catalyzes the 5-*exo-trig* cyclization of 6-methylhepta-4,5-dienylamine with good enantioselectivity (Scheme 16).^[41]



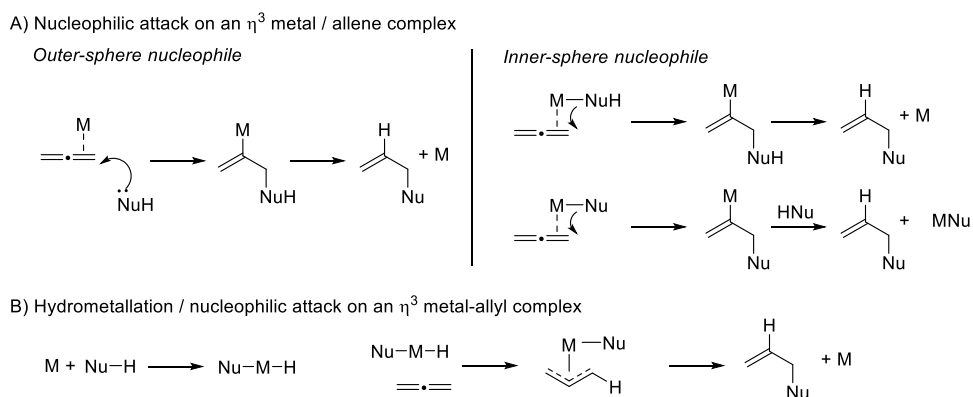
Scheme 16 – Asymmetric 5-*exo-trig* cyclization of 6-methylhepta-4,5-dienylamine catalyzed by a chiral tantalum amide-alkoxide complex.^[41]

1.3.4. Hydroamination of allenes with catalysts based on late transition metals

We will report here the major literature results concerning allene hydroamination reactions of class C, i.e. those catalyzed by complexes of the late transition metals (groups 8-12).

The major common mechanistic feature of these catalysts is that normally they (also) activate the allene, rather than the amine, as it happens for class B hydroamination reactions. This is possible because normally late transition metals, as *soft* Lewis acids, can efficiently engage in π -type interaction with unsaturated compounds. Two main pathways are possible: 1) nucleophilic attack of the nitrogen nucleophile on an allene/metal η^2 complex (Scheme 17, A); 2) nucleophilic attack on η^3 allyl complexes (Scheme 17, B). The rationale for the first mechanism is that metal coordination to the unsaturated system normally lowers the energy of its LUMO, thus making it more electrophilic. In principle, inner-sphere attack of a molecule of the nitrogen nucleophile already coordinated to the metal and outer-sphere attack are both conceivable, but the first possibility is rather unlikely unless the coordinated amine is deprotonated (*i.e.* it is in the amido form). Pathway 2 is normally operative for rhodium- and palladium-based catalysts, which

can form metal-hydrido species by oxidative insertion into N-H bond of the amine and generate η^3 allyl complexes by hydrometallation of the allene.

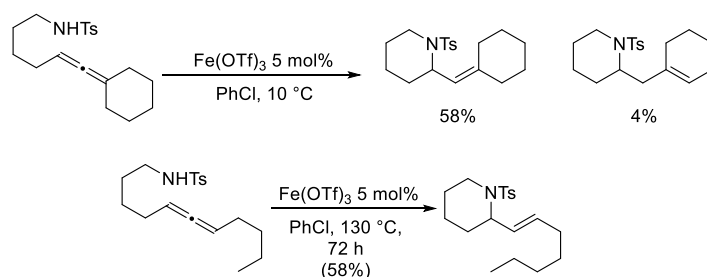


Scheme 17 – General mechanistic pathway for the late-transition metal-catalyzed hydroamination of allenes.

From the practical point of view, late transition metal-based catalysts are normally air-stable (if the metal is not easily oxidizable, such as it happens for zerovalent palladium) and convenient to handle. Strictly anhydrous conditions are normally unnecessary and polar functional groups are tolerated, thus allowing the use of class C hydroamination catalyst for the synthesis of complex molecules.

1.3.4.1. Hydroamination of allenes with catalysts based on group 8 metals

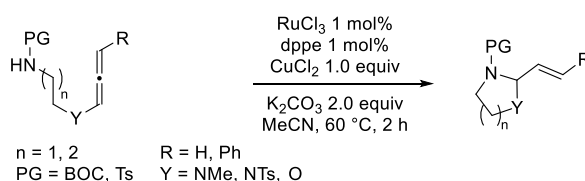
Group 8 has not been prolific in allene hydroamination catalysts. A single example of iron-catalyzed intramolecular hydroamination of aminoallenes is known to us. $\text{Fe}(\text{OTf})_3$ catalyzed the cyclization of tosylated δ -aminoallenes (Scheme 18).^[42] Unfortunately, this reaction is not very general: protecting groups other than sulfonamides (BOC, Bn, Ph) are not tolerated and when it is thermodynamically favorable double bond migration can occur. Disubstituted allenes react very sluggishly, while trisubstituted are the best substrates. No information is available on the mechanism of this transformation.^[42]



Scheme 18 – Fe-catalyzed intramolecular hydroamination of *N*-protected δ -aminoallenes.^[42]

Quite recently Broggin and Poli reported a ruthenium-catalyzed intramolecular hydroamination of heteroatom-substituted allenes bearing tethered *N*-protected amine functions (Scheme 19).^[43] The optimized conditions called for a $\text{RuCl}_3/\text{dppe}$ pre-catalyst system together

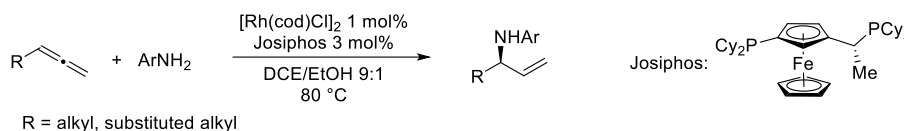
with stoichiometric amounts of CuCl_2 and K_2CO_3 as additives. Heteroatom substitution of the allenyl moiety was essential for reactivity, only allenyl ethers, *N*-allenyl carbamates, *N*-allenylamines and allenamides could undergo this reaction; no conversion was observed for $\text{Y} = \text{CH}_2$. The ruthenium(II) pre-catalyst $[\text{RuCl}_2(p\text{-cymene})]_2$ gave results equivalent to those obtained with RuCl_3 , and dppe was essential for reactivity. The presence of CuCl_2 was essential for the reaction to proceed, but it could be substituted by LiCl with only slightly diminished yields. The authors concluded that the active species is probably a Ru(II) complex and that CuCl_2 serves mainly as a source of Cl^- , which may have the role of keeping the Ru complex under a mononuclear active form rather than forming poorly reactive polynuclear species.^[43]



Scheme 19 – Ru-catalyzed intramolecular hydroamination of heteroatom-substituted allenes.^[43]

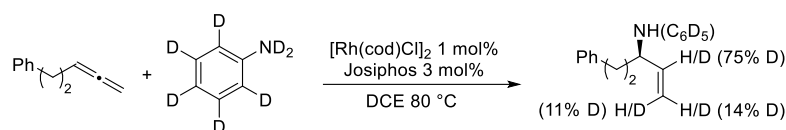
1.3.4.2. Hydroamination of allenes with catalysts based on group 9 metals

Several important examples of allene hydroamination reactions exist for rhodium. In 2013 Breit and coworkers reported that a $[\text{Rh}(\text{cod})\text{Cl}]_2/\text{Josiphos}$ catalyzed the asymmetric addition of anilines to monosubstituted allenes in a Markovnikov fashion to give the branched allylamines in good yields and excellent ee (Scheme 20).^[44] Notably, the same substrate underwent anti-Markovnikov addition to give the corresponding linear *E* allylic amines with a $[\text{Pd}(\eta^3\text{-allyl})\text{Cl}]_2/\text{dppf}$ catalyst system (*vide infra*). The non-asymmetric corresponding reaction is more efficiently accomplished with a $[\text{Rh}(\text{cod})\text{Cl}]_2/\text{DPEPhos}$ system [DPEPhos = bis-(2-diphenylphosphinophenyl) ether].^[44]

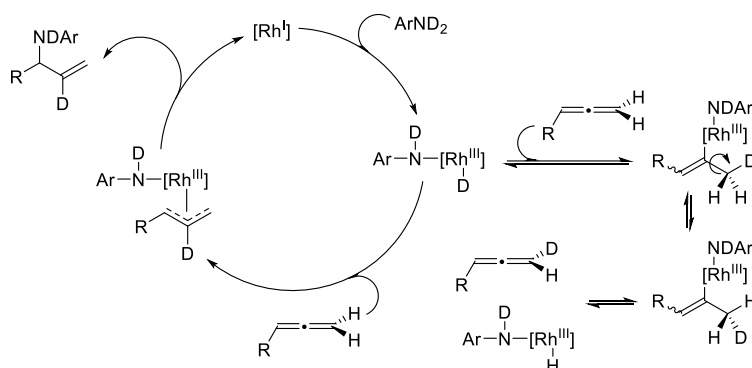


Scheme 20 – Rh(I)-catalyzed intermolecular asymmetric hydroamination of allenes with anilines.^[44]

When perdeuterated aniline was used as a substrate, deuterium incorporation occurred at all the positions of the formed double bond (Scheme 21)^[44] Also based on this evidence, the authors proposed that the reaction takes place by the oxidative addition of aniline to Rh(I) giving a Rh(III) hydride complex, which later effects hydrometallation of the allene to give an allyl-Rh(III) intermediate. Nucleophilic addition of the aniline on this complex delivers the product and regenerates Rh(I).^[44] The proposed catalytic cycle, accounting for the observed H/D scrambling, is outlined in Scheme 22.^[44]

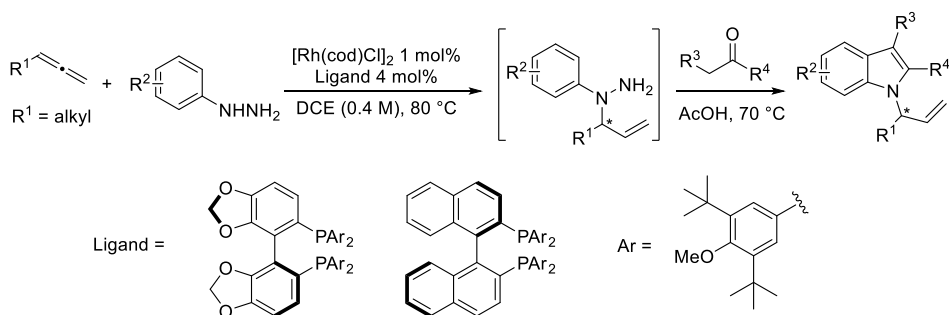


Scheme 21 – Rh(I)-catalyzed intermolecular asymmetric hydroamination of allenes with anilines.^[44]



Scheme 22 – Proposed mechanism for the Rh-catalyzed hydroamination of allenes and pathway for H/D scrambling reaction of the allene substrate.^[44]

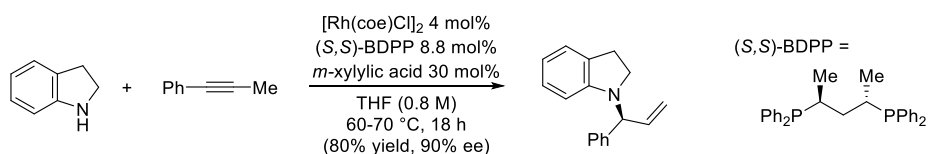
A variety of other (not too basic) nitrogen nucleophiles can be used under similar Rh-catalysis conditions, and with a judicious choice of a chiral ligand good enantioselectivity can be achieved in each case: benzophenone imine,^[45] 2-pyridones,^[46] 4-pyridones,^[47] pyridazinones,^[48] imidazoles and benzimidazoles,^[49] purines,^[50] benzotriazoles (with selectivity for either N1 or N2 according to the ligand),^[51] tetrazoles,^[52] arylhydrazines, with selectivity for the nitrogen atom directly attached to the aromatic ring, giving the possibility to engage the product directly in Fischer indole synthesis.^[53] The latter strategy, that leads to chiral *N*-allylindole derivatives, is illustrated in Scheme 23.^[53]



Scheme 23 – One-pot preparation of chiral *N*-allylindoles by Rh-catalyzed asymmetric hydroamination of arylhydrazines and subsequent Fischer indole synthesis.^[53]

As regards rhodium catalysis, 2-alkynes can also be substrates for the Rh-catalyzed hydroamination with indoline substrates (anilines and secondary aliphatic amines give poor yields). The use of BDPP, a chiral ligand related to 1,4-bis-(diphenylphosphino)propane (dppp), allows obtaining good yields and enantioselectivities (Scheme 24).^[54] Acidic additives, and in this

case *m*-xylylic acid,ⁱⁱⁱ are essential for the reaction to take place. This reaction proceeds by tandem rhodium catalysis: first the 2-alkyne is isomerized to the corresponding terminal allene by a hydrometallation/dehydrometallation pathway involving Rh(III)-H species, then hydroamination occurs, probably by the mechanism outlined in Scheme 22.^[54]

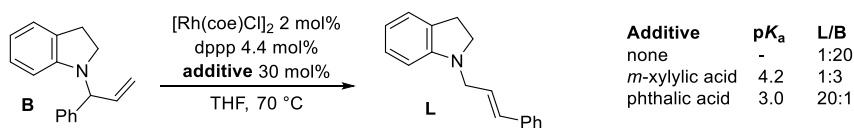


Scheme 24 – Rh-catalyzed asymmetric hydroamination of 2-alkynes leading to branched allylamines.^[54]

Interestingly, when *m*-xylylic acid was replaced by more acidic additives (*i.e.* phthalic acid), the isomeric linear allylic amine was obtained (Scheme 25). The author suggested that this is due to isomerization of the branched allylic amine induced by the rhodium catalyst in conjunction with the carboxylic acid. In a control experiment, the branched amine was put in the conditions of the reaction either with no additive, or with *m*-xylylic acid or with phthalic acid. Isomerization to the linear allylic amine took place only when the latter additive was present (Scheme 26).^[54]



Scheme 25 – Rh-catalyzed hydroamination of 2-alkynes leading to linear allylamines.^[54]

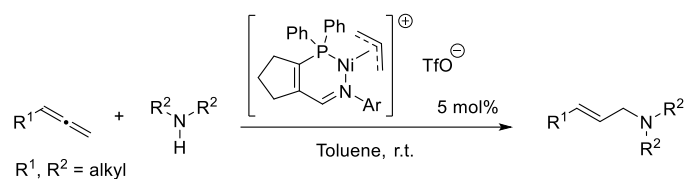


Scheme 26 – Rh- and acid-catalyzed isomerization of allylic amines.^[54]

1.3.4.3. Hydroamination of allenes with catalysts based on group 10 metals

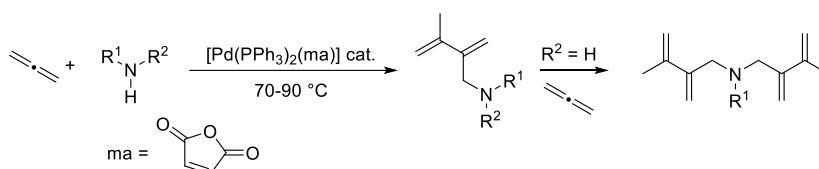
All the elements of group 10 have been used for the hydroamination of allenes. It has been recently reported that cationic [(iminophosphine)Ni(allyl)]⁺ complexes catalyzed the addition of secondary amines to terminal allenes at room temperature.^[55] The linear allylic amine is obtained with prevalent *E* stereochemistry. The reaction worked well with secondary cyclic amines, while primary aliphatic amines, anilines and hydrazines were not reactive. Besides terminal allenes, this catalyst was applicable to 1,1-dimethylallene, albeit longer reaction times were required for this substrate.^[55]

ⁱⁱⁱ The nomenclature *m*-xylylic acid is ambiguous, as three isomeric *m*-xylylic acids can exist. The authors do not clearly state to which one they refer to.



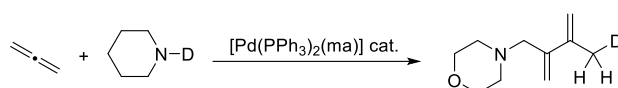
Scheme 27 – Nickel-catalyzed hydroamination of terminal allenes with secondary amines.^[55]

While only one example of nickel-catalyzed hydroamination of allenes is known, the literature about palladium-catalyzed hydroamination is very rich. The palladium-catalyzed reaction of unsubstituted allene with ammonia, primary and secondary amines has been studied as early as in 1973 by Coulson.^[56] With the palladium(0) complex [Pd(PPh₃)₂(ma)] (ma = maleic anhydride) no 1:1 addition product between allene and the amine could be isolated, but dieny and *bis*-dienylamines were produced instead (Scheme 28).

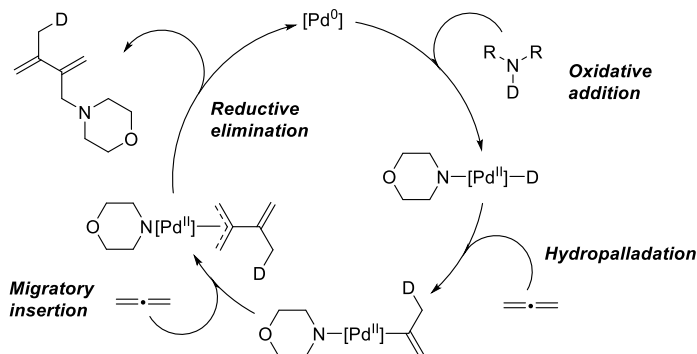


Scheme 28 – Pd-catalyzed formation of dienyamines from allene and amines.^[56]

In a control experiment, allene was reacted with *N*-deuteriomorpholine. Incorporation of deuterium took place almost exclusively at the methyl group of the formed *N*-(3-methyl-2-methylene-3-butenyl)morpholine (Scheme 29).^[56] A mechanism that can explain this observation is reported in Scheme 30. Oxidative addition of *N*-deuterium morpholine gives a Pd(II)-hydride complex, that effects deuteriopalladation of a first molecule of allene. A second molecule of allene inserts in the C-Pd bond of the propenylpalladium complex thus produced, giving a π -allyl complex. Nucleophilic addition of the amine and reductive elimination deliver the product and regenerate the catalyst.

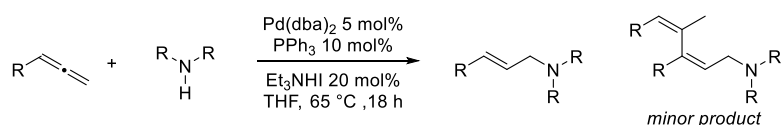


Scheme 29 – Deuterium incorporation experiment.^[56]



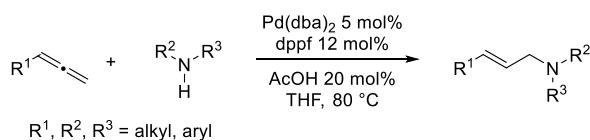
Scheme 30 – Possible mechanism for the reaction of allene with *N*-deuteriomorpholine.

Avoiding the formation of such telomerization product was a key factor in the development of palladium-catalyzed hydroamination reactions. In 1995 Cazes and coworkers reported that in the presence of $\text{Et}_3\text{N}\cdot\text{HI}$ as an acid and $\text{Pd}(\text{dba})_2/\text{PPh}_3$, monosubstituted allenes can successfully undergo hydroamination with secondary amines giving the linear, *E* allylic amines. Primary amines were also reactive, giving bis-allylated tertiary amines. Internal allenes were inert under these conditions. The most favored mechanistic hypothesis called for hydropalladation of the allene by a palladium(II)-hydride complex [in turn formed by oxidative addition of the amine or of the ammonium salt to $\text{Pd}(0)$] and subsequent nucleophilic addition / reductive elimination from the π -allyl complex so formed.^[57]

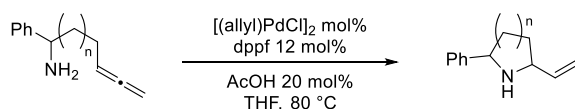


Scheme 31 – Cazes' protocol for the Pd-catalyzed hydroamination of allenes.^[57]

Yields, reaction rates and selectivity of this reaction were improved by the use of a $\text{Pd}(\text{dba})_2/\text{dppf}$ pre-catalyst system and acetic acid as an additive. No measurable amounts of the dienic amine byproduct were observed. Remarkably, aromatic secondary amines were also reactive under those conditions (Scheme 32).^[58] A related protocol based on the use of $[(\text{allyl})\text{PdCl}]_2/\text{dppf}$ is also effective for imidazole derivatives as nucleophiles.^[49] The 5-*exo-trig* or 6-*exo-trig* cyclization of γ - and δ -aminoallenes proceeded smoothly with a similar protocol (Scheme 33).^[59]

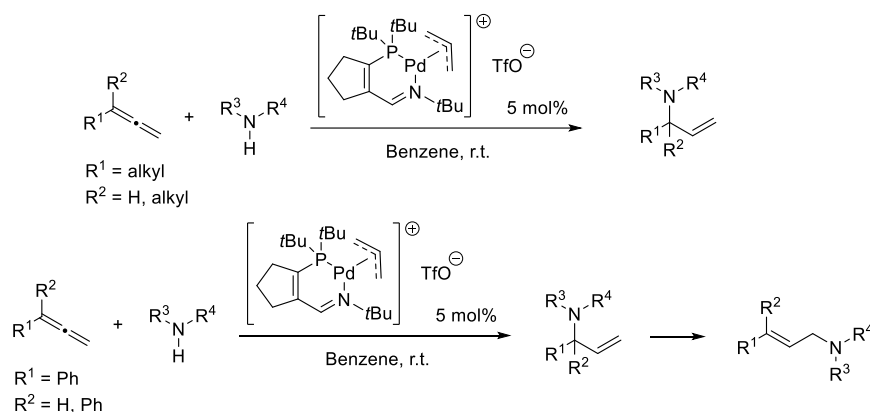


Scheme 32 – Yamamoto's protocol for the Pd-catalyzed hydroamination of allenes.^[57]



Scheme 33 – Synthesis of 2-vinylpyrrolidines and 2-vinylpiperidines by Pd-catalyzed by 5-*exo-trig* or 6-*exo-trig* cyclization of γ - and δ -aminoallenes.^[59]

Cationic allylpalladium complexes having 3-iminophosphine ligands analogous to the nickel-based catalyst reported in Scheme 27 have been shown to be very active in the hydroamination of allenes.^[60,61] More in detail a (3-iminophosphine)allylpalladium triflate serves for the hydroamination of monosubstituted and 1,1-disubstituted allenes with primary and secondary aliphatic amines and with anilines. This catalyst was active at room temperature and it furnished the branched allylic amine as the exclusive product when alkyl-substituted allenes were employed (Scheme 34, top). When phenylallene or 1,1-diphenylallene were used, linear allylic amines were obtained instead (Scheme 34, bottom). *In-operando* analysis of the reaction mixture showed that the branched product was first produced (*i.e.* it is the kinetic product) and then isomerization to the thermodynamically more stable linear amine took place.^[60]



Scheme 34 – Hydroamination of allenes catalyzed by a cationic allylpalladium/3-iminophosphine complex^[60]

To improve the activity of this catalyst, mechanistic studies and systematic variations of the ligand backbone were attempted. The reaction rate was found to have a first-order dependence on the concentration of the amine substrate and zeroth order with respect to the allene. A large kinetic isotope effect was found for the reaction of a *N*-deuterated amine ($k_{\text{H}}/k_{\text{D}} = 5.2$) and the deuterium atom was transferred selectively to the *sp* carbon of the allene.^[62] This observation led the authors to conclude that proton-transfer is involved in the turnover-limiting step of the catalytic cycle. A series of catalyst featuring various *p*-substituted *N*-arylimine moieties were prepared (Figure 1, left). For each of them, a non-monotonic dependence of the reaction rate on Hammett's σ_{p} parameter was found, with a maximum whose position depended on the amine substrate chosen.^[62] The authors interpreted this finding by observing that substituents on the aniline moiety of the ligand affect both the basicity of the imine nitrogen and the affinity for palladium. If this moiety is implicated in an intramolecular deprotonation of the amine, more electron-rich (and more basic) amines accelerate the reaction by facilitating the deprotonation step, but they have also greater affinity for the metal center, making substrate coordination more difficult. The optimal compromise between the two factors, which allows the best reactivity, depends on the basicity and coordination capability of the amine substrates.

The ring-size of the ligand was also varied systematically from 4 to 7 members (Figure 1, right). Interestingly, the ligands featuring a six- or seven-membered ring gave completely ineffective catalysts, while the cyclobutene-derived ligands afforded the most active catalyst. A simple explanation of this behavior, beyond the obvious effect on the cone angle of the ligands, is unknown at present.^[63]

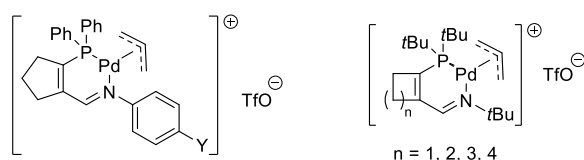
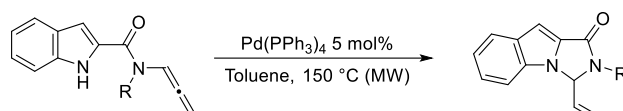
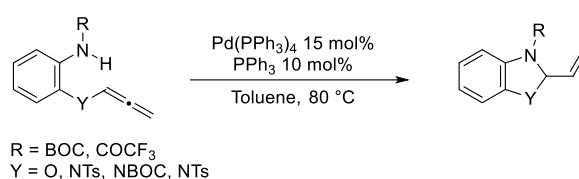


Figure 1 – Structural variants of the 3-iminophosphine allylpalladium catalysts for allene hydroamination.^[62,63]

A variety of applications of the intramolecular palladium-catalyzed hydroamination of allenes have been described for the synthesis of heterocycles. For example, indole-2-carboxamides featuring an allenyl substituent on the amide nitrogen give 5-*exo-trig* cyclization under the influence of a palladium catalyst (Scheme 35)^[64] and so do several different *N*-protected anilines having an ortho heteroatom substituent featuring an allenyl moiety cyclized readily (Scheme 36).^[65]



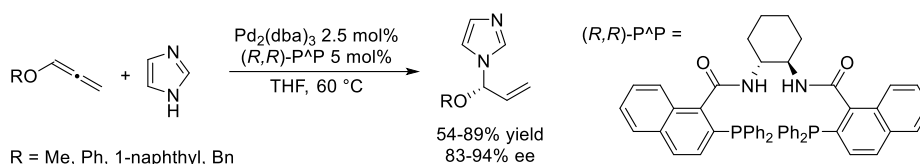
Scheme 35 – Pd-catalyzed intramolecular hydroamination reaction of indole-2-carboxamides.^[64]



Scheme 36 – Pd-catalyzed intramolecular hydroamination of *N*-protected anilines featuring *ortho* allenyl-heteroatom substituents.^[65]

It is worth noting here that 2-alkynes and some other internal alkynes can also be used as substrates for Pd-catalyzed hydroamination reactions delivering allylic amines. These reactions, *i.e.* those catalyzed by Pd(PPh₃)₄/PhCOOH, proceed by isomerization of the alkyne to the corresponding allene and subsequent hydroamination by the formation of a π -allyl intermediate.^[66] Asymmetric variants of the intramolecular reaction represented in Scheme 33, based on the use of chiral diphosphines, have also been reported.^[67–70]

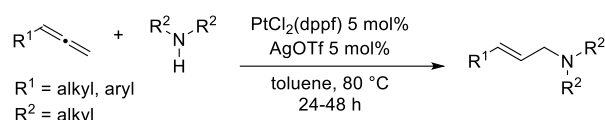
The addition of a number of nitrogen nucleophiles having rather acidic N-H moieties (sulfonamides,^[71–75] pyrimidines,^[76] azoles,^[77] carbamates,^[75] amidophosphates^[75]) have been shown to add to alkoxyallenes in a process catalyzed by Pd(0)/diphosphine complexes. In general, the nitrogen atom add to the most substituted carbon atom, thus generating *O,N*-mixed acetals having a terminal double bond. Stereoselective variants of this transformation have been described by the use of chiral diphosphines.^[72,73,76,77] An example involving imidazole as a nucleophile is shown in Scheme 37.



Scheme 37 – Pd-catalyzed asymmetric addition of imidazole to alkoxyallenes.^[77]

Platinum has also been used to design catalysts for the hydroamination of allenes.^[78] The diphosphine complex [PtCl₂(dppf)] in conjunction with AgOTf as a halide-abstracting agent catalyzes the addition of secondary amines to terminal allenes with complete regioselectivity for the linear allylic amine and *E:Z* ratio from 6.9 : 1 to more than 50 : 1. Bidentate phosphines were

more efficient than their monodentate counterparts and a series of analogous diphosphines with increasing bite angles was tested. The effect was dramatic, and the yield of hydroamination product increased from 0% to 88% as the bite angle was increased from 91° to 108°. No clear correlation of the stereoselectivity was found with this parameter. A control experiment demonstrated that AgOTf alone is not a viable catalyst for this reaction and that it is really a platinum-promoted process.^[78]

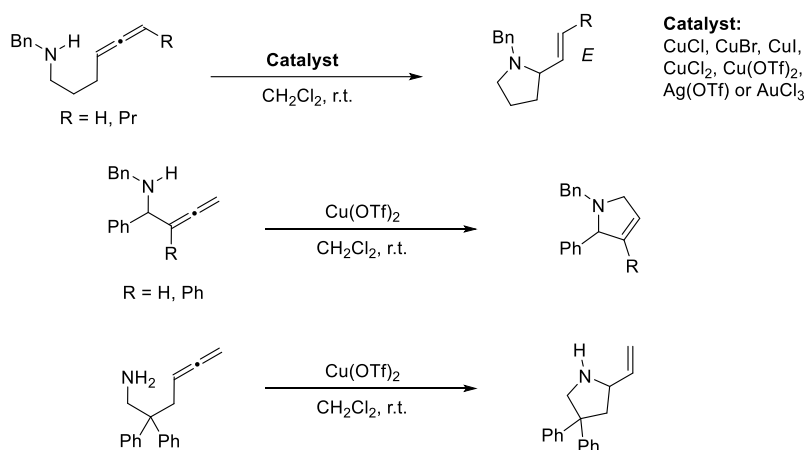


Scheme 38 – Pt-catalyzed hydroamination of allenes with secondary amines.^[78]

1.3.4.4. Hydroamination of allenes with catalysts based on group 11 metals

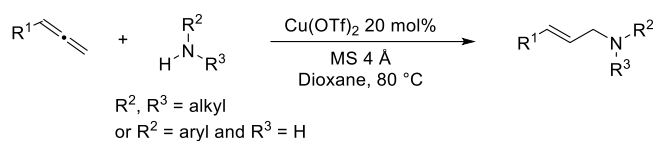
The group of the so-called coinage metals has been prolific of hydroamination catalysts, especially for what concerns silver and gold.

Few reports of copper-catalyzed hydroamination of allenes exist. In 2008 Okamoto and coworkers reported that various copper(I) and copper(II) salts catalyze the room-temperature intramolecular hydroamination of α - and γ -aminoallenes to give 3-pyrrolines or 2-alkenylpyrrolidines in a 5-*exo-trig* fashion (Scheme 38).^[79] AgOTf and AuCl₃ were also suitable catalysts for these transformations, albeit they were less efficient. Amines protected with Ts, BOC or Bz groups were not suitable substrates, but a primary amine cyclized in good yields. In the case of a 1,3-disubstituted allene, the corresponding 2-alkenyl-pyrrolidine was obtained with complete selectivity for the *E* double bond isomer.



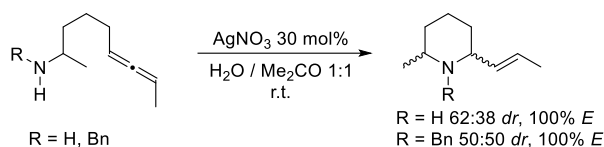
Scheme 39 – Cu-catalyzed intramolecular hydroamination of aminoallenes.^[79]

Very recently, Monnier and Taillefer reported the first intermolecular hydroamination reaction of allenes. Alkyl and aryl monosubstituted allenes underwent smooth addition of secondary amines or primary anilines with selectivity for the unbranched *E* allylic amine by the use of Cu(OTf)₂ as a catalyst at 80 °C. In the case of anilines, selective mono-addition took place with the formation of secondary allylic amines.^[80]



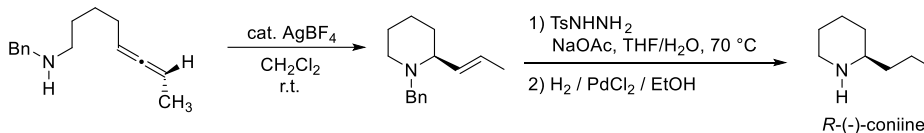
Scheme 40 – Cu-catalyzed intermolecular hydroamination of allenes.^[80]

Silver(I) salts have been used to promote the intermolecular hydroamination of amino-substituted allenes for a long time. As a part of a total synthesis of (\pm)-pinidine reported in 1985,^[81] it was shown that 6,7-nonadien-2-amine and its *N*-benzylated derivative cyclize to the corresponding piperidine in a 6-*exo-trig* process catalyzed by AgNO_3 at room temperature. Poor *cis/trans* diastereoselectivity was observed with respect to the two substituents of the piperidine ring, but the double bond was formed exclusively in the *E* configuration (Scheme 41).



Scheme 41 – Ag-catalyzed cyclization of 6,7-nonadien-2-amine *en route* to (\pm)-pinidine.^[81]

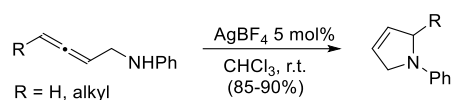
A similar reaction was applied to the total synthesis of *R*-(-)-coniine, the toxic principle of poison hemlock. Optically active *N*-benzyl-5,6-octadien-1-amine cyclized upon treatment with AgBF_4 at room temperature in a 6-*exo-trig* process. Interestingly, the axial chirality of the substrate was transferred to the cyclized product, which was obtained prevalently as the *R* enantiomer. Diimide reduction and debenzoylation delivered optically active *R*-(-)-coniine (Scheme 42).^[82]



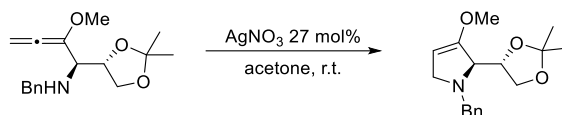
Scheme 42 – Key steps of a total synthesis of *R*-(-)-coniine.^[82]

5-*Endo-trig* cyclizations of α -aminoallenes, that are disfavored according to Baldwin's rules,^{iv} can also be accomplished thanks to silver catalysis (Scheme 43), as reported already in 1979.^[83] These cyclizations, giving access to 3-pyrrolines, have found applications in the total synthesis of natural products (cf. Scheme 3). As another example, *en route* to the total synthesis of (-)-detoxinine, AgNO_3 has been used as a catalyst to promote the 5-*endo-trig* cyclization of an allenyl ether featuring a tethered secondary amine, thus giving a 3-pyrroline ether (Scheme 44).^[84]

^{iv} To the best of our knowledge, no information is available on the mechanism of these Ag-catalyzed cyclizations. Usually Baldwin's rules do not hold for the cyclizations involving cations, so it would be tempting to hypothesize a mechanism featuring an allyl cation intermediate formed by activation of the allene by Ag^+ .

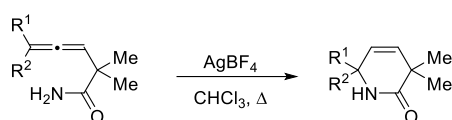


Scheme 43 – AgBF₄-catalyzed 5-*endo-trig* cyclization of α -aminoallenes.^[83]



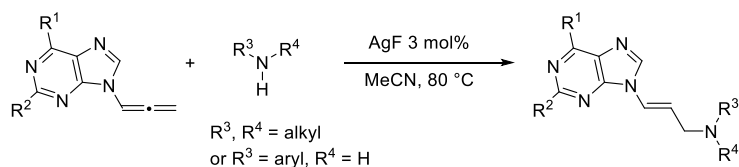
Scheme 44 – A step in the total synthesis of (-)-detoxinine.^[84]

6-*Endo-trig* cyclization is also known: β -allenylamides undergo AgBF₄-catalyzed ring closure to give 3,6-dihydro-1*H*-pyridones in refluxing chloroform (Scheme 45).^[85]



Scheme 45 – AgBF₄ 6-*endo-trig* cyclization of β -allenylamides.^[85]

Despite such a great variety of examples of intramolecular cyclization, intermolecular examples remain scarce. In a recent report,^[86] acyclic nucleoside analogues have been constructed by the AgF-catalyzed hydroamination of 9-allenyl-9*H*-purines with secondary aliphatic amines or primary anilines. Linear *E* allylic amines were obtained with high selectivity (Scheme 46).

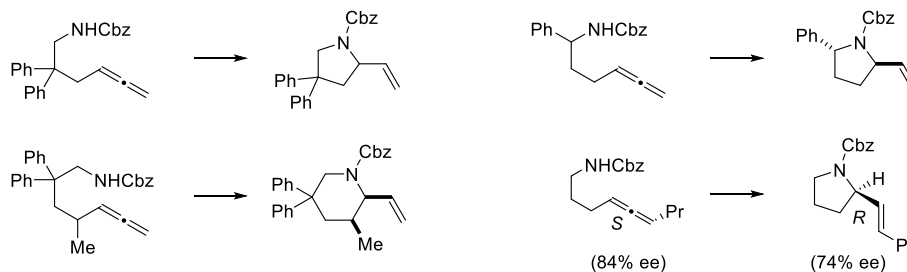


Scheme 46 – AgF-catalyzed hydroamination of 9-allenyl-9*H*-purines.^[86]

Without doubt, gold has been the subject of the most striking development in hydroamination chemistry in recent years. The literature on gold-catalyzed hydroamination up to 2006 has been reviewed by Widenhofer.^[6]

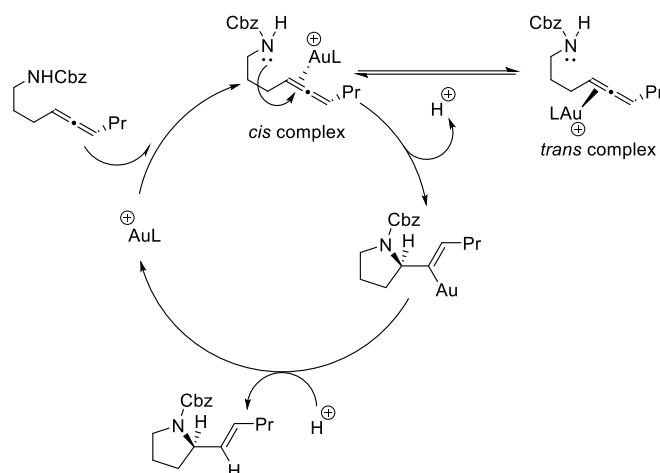
The intramolecular cyclization of aminoallenes and their protected derivatives has been investigated first. The 5-*exo-trig* cyclization of Cbz-protected γ -aminoallenes and the 6-*exo-trig* cyclization of δ -aminoallenes can be accomplished by treatment with a catalytic amount of [Au(P*t*Bu₂(2-biphenyl))Cl] and Ag(OTf) (1:1 mixture) in dioxane at room temperature (Scheme 46).^[87] When an enantiomerically enriched 1,3-disubstituted allene substrate was used, axial-to-central chirality transfer took place. The stereoselectivity of this process was compatible with an outer-sphere nucleophilic attack of the carbamate nitrogen to the gold-coordinated allene. Stereospecific protonolysis of an intermediate vinylgold(I) species with retention of configuration would release the product. The observation that only the *E* alkene is produced is compatible with the involvement of a gold-allene complex in which the Au lies in the same half-space as the substituent at the terminal allene carbon (“*cis*” complex), which is expected to be

less stable than the *trans* one (Scheme 47).^[87] An enantioselective version of this transformation has been developed by the use of chiral phosphines.^[88] Some 7-*exo-trig* cyclization could be achieved by the use of NHC-supported gold catalysts.^[89]



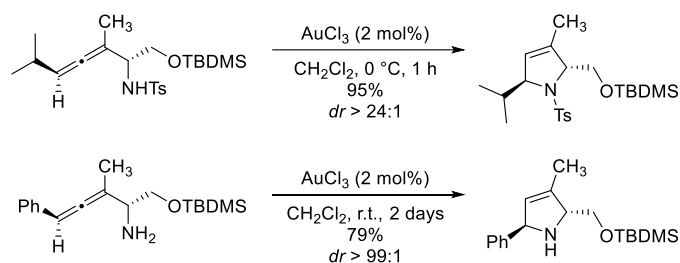
Scheme 47 – Cyclization of allenylcarbamates.

For all the reactions: cat. [Au(P*t*Bu₂(2-biphenyl))Cl], Ag(OTf), dioxane, 25 °C, 5-45 min.^[87]



Scheme 48 – Proposed catalytic cycle for the intramolecular cyclization of Cbz-protected aminoallenes, highlighting the origin of the axial-to-central chirality transfer^[87]

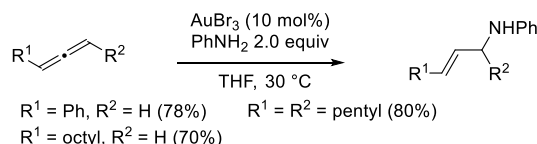
The 5-*endo-trig* cyclization of α -aminoallenes is also possible with AuCl₃ as a catalyst. Two examples are reported in Scheme 49. In each case the *trans* diastereomer prevails.^[90]



Scheme 49 – AuCl₃-catalyzed 5-*endo-trig* cyclization of α -aminoallenes.^[90]

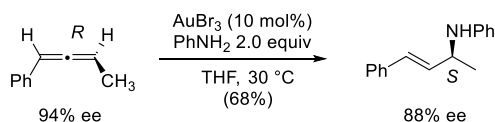
The first successful intermolecular gold-catalyzed hydroamination of allenes was reported in 2006.^[91] Aromatic and aliphatic allenes, either terminal or 1,3-disubstituted, underwent smooth addition of anilines in THF at 30 °C with AuBr₃ as a catalyst and no added ligand

(Scheme 50). Linear allylic amines were obtained with complete selectivity for the *E* double bond isomer. 1,1-Disubstituted allenes reacted only sluggishly with this catalyst system. A 1:1 mixture of [Au(P*t*Bu₂(2-biphenyl))Cl] and Ag(OTf) catalyzes the hydroamination of allenes (also 1,1-disubstituted) with primary and secondary aryl amines, with a greater scope than AuBr₃.^[92]



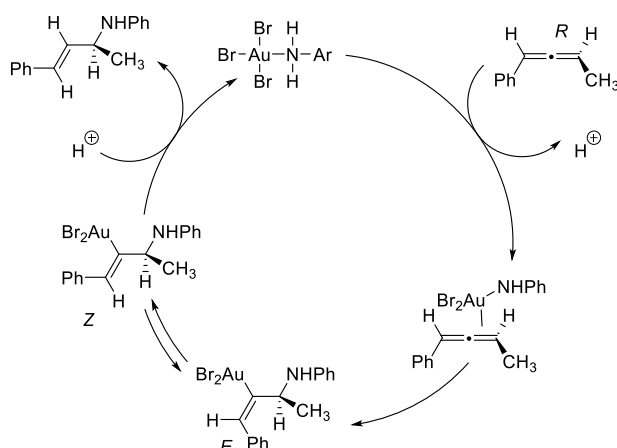
Scheme 50 – Intermolecular AuBr₃-catalyzed hydroamination of allenes with anilines.^[91]

When optically active 1,3-disubstituted allenes were used with AuBr₃ as a catalyst, axial-to-central chirality transfer occurred. More in detail, (*R*)-phenyl-1,2-butadiene (94% ee) gave prevalently (*E*, *S*)-*N*-(4-phenyl-3-buten-2-yl)aniline (88% ee, Scheme 51).^[91] The authors explained the stereochemical outcome of this reaction by admitting that a gold-amine complex^v coordinates on the less hindered face of the allene. Deprotonation of the coordinated amine then gives a gold-amide complex, which takes part into migratory insertion generating an (*E*)-alkenylgold species. Protonolysis of this intermediate with retention of configuration would lead to a *Z* alkene, which is not observed in practice. The authors thus admitted that isomerization of the (*E*)-alkenylgold intermediate to its *Z* isomer takes place before the protodeauration step, which delivers the product and regenerates the catalyst (Scheme 52).^[91] As already pointed out by Widenhoefer,^[6] outer-sphere addition of the amine *anti* with respect to the coordinated gold catalyst would lead to the (*Z*)-alkenylgold intermediate, that gives the observed product without the need of any isomerization step.



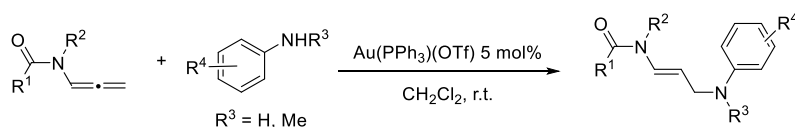
Scheme 51 – AuBr₃-catalyzed stereospecific hydroamination of (*R*)-phenyl-1,2-butadiene.^[91]

^v It is possible, indeed, that when Au(III) pre-catalysts are used, reduction to Au(I) by one of the substrates occurs. The authors did not investigate this point and wrote the mechanism with Au(III) species.



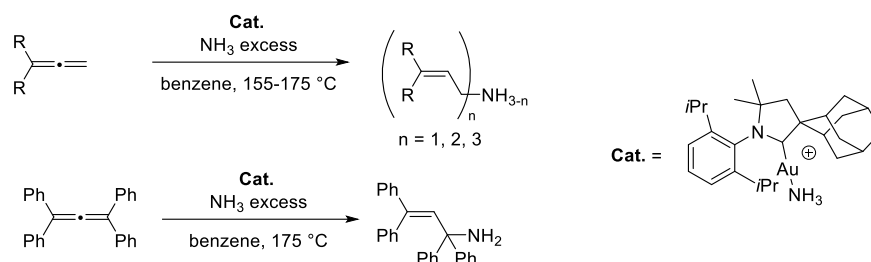
Scheme 52 – Proposed mechanism for the AuBr₃-catalyzed hydroamination of allenes with anilines.^[91]

With AuBr₃, aliphatic amines were not reactive, but morpholine could be reacted with a variety of monosubstituted and 1,1-disubstituted allenes by using a 1:1 mixture of [Au(PPh₃(*o*-Tol))Cl] and Ag(OTf).^[93] With a [Au(PPh₃(IPr))Cl]/Ag(OTf) [IPr = 1,3-bis(2,6-diisopropylphenyl)imidazol-2-ylidene] catalyst system the scope could be extended to carbamates and substituted allenes, even tetramethylallene reacted under those conditions.^[94] [Au(PPh₃)(OTf)] is an effective catalyst for the hydroamination of allenamides with primary and secondary anilines to give synthetically useful (*E*)-enamides (Scheme 53).^[95] By the use of a chiral bidentate phosphine, the asymmetric hydroamination of 1,3-disubstituted allenes with carbamates can be accomplished.^[96] An asymmetric hydroazidation using TMSN₃ as an HN₃ source has also been described.^[97]



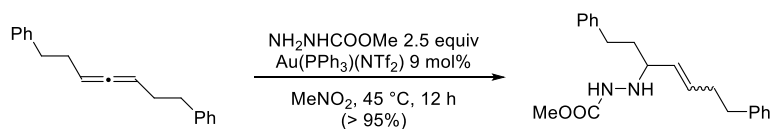
Scheme 53 – Au-catalyzed hydroamination of allenamides with anilines.^[95]

Bertrand and coworkers showed that ammonia can be used as a hydroamination partner with a cationic cyclic carbene–gold(I) catalyst (Scheme 54).^[98] Allenes varying from unsubstituted propadiene to tetraphenylallene were tolerated, albeit the reaction took place at high temperatures (155–175 °C). Mixtures of primary, secondary and tertiary linear allylamines were obtained, but generally secondary and tertiary products prevailed with monosubstituted and 1,1-disubstituted allenes. With tetraphenylallene, only mono-addition was observed (Scheme 54).^[98]



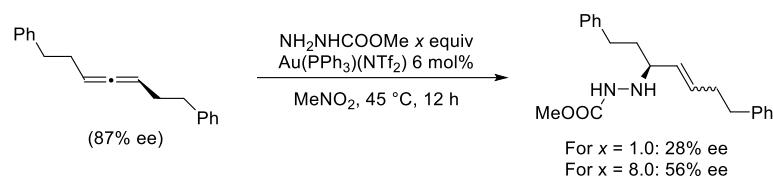
Scheme 54 – Addition of ammonia to allenes catalyzed by an Au(I)-NHC complex.^[98]

After describing an asymmetric cyclization of allene-tethered hydroxylamine and hydrazide-type nucleophiles,^[99] Toste and coworkers showed that hydrazides add smoothly to 1,3-disubstituted allenes in an intermolecular fashion with $[\text{Au}(\text{PPh}_3)(\text{NTf}_2)]$ as a catalyst (Scheme 55) and they studied in detail the mechanism of this transformation.^[100] The resting state of the catalyst under actual reaction conditions was characterized by NMR studies. The main species identified was a $[(\text{Ph}_3\text{P})\text{Au}(\text{allene})]$ complex in which the gold center rapidly exchanges between the two faces of the allene (since the allene is chiral, two diastereotopic π -allene gold complexes can be formed). Kinetic analysis showed that the transformation is of zeroth order in methyl carbazate and first-order in the allene substrate. The order in gold was also determined, as to verify if dinuclear species, possibly formed in small amounts in equilibrium with the mononuclear pre-catalyst, could be involved in the mechanism. A simple first order with respect to the catalyst was found, so the authors ruled out the activity of dinuclear gold(I) species.^[100]



Scheme 55 – Au(I)-Catalyzed addition of methyl carbazate to 1,7-diphenyl-2,4-heptadiene.^[100]

The influence of substituents on the phosphine ligands was also investigated. A series of $[\text{Au}(\text{PAr}_3)(\text{NTf}_2)]$ complexes with $\text{Ar} = p\text{-Y-C}_6\text{H}_4\text{-}$ were used as catalysts for the model reaction (Scheme 55) and a Hammett plot was constructed. A positive slope ($\rho = +0.21$) was found, meaning that the reaction is faster with electron-poor phosphines. When enantio-enriched 1,7-diphenyl-2,4-heptadiene (87% ee) was engaged in the model reaction, axial-to-central chirality transfer took place with an efficiency that was dependent on the concentration of methyl carbazate (Scheme 56). For example, with a 1:1 ratio between the allene and methyl carbazate, the product was obtained with 28% ee, while with 8.0 equiv of the hydrazide, the ee of the product increased to 56%. The authors explained this fact by observing that the allene racemizes in the presence of the gold(I) catalyst and without the added nucleophile. This racemization process occurs at a rate comparable to the trapping of the intermediate by the hydrazide nucleophile, a process which is expected to have first-order kinetics with respect to the nucleophile itself, thus explaining the influence of its concentration on the stereospecificity of the reaction. Crossover experiments demonstrated that the reaction is not reversible under the chosen conditions.^[100]



Scheme 56 – Au(I)-Catalyzed addition of methyl carbazate to enantio-enriched 1,7-diphenyl-2,4-heptadiene.^[100]

Summing-up all these experimental observations and also on the basis of DFT studies,^{vi} the authors proposed a two-step, no intermediate mechanism for this reaction.^[100] More in detail, the starting $[\text{Au}(\text{allene})(\text{PPh}_3)]^+$ complex isomerizes to an activated form, which is not planar and which retains the chirality (**TS1**). This transition state is *not* associated with the carbazate nucleophile and it can evolve either towards a planar, stable Au-bound allyl cation, with loss of chirality, which is responsible for racemization of the allene, or give addition of methyl carbazate with a second transition state (**TS2**), which lies lower in energy than the first. Stereospecific protodemetalation of the alkenylgold (**B**) species so formed finally delivers the product. The computed reaction pathway is shown in Figure 2.^[100]

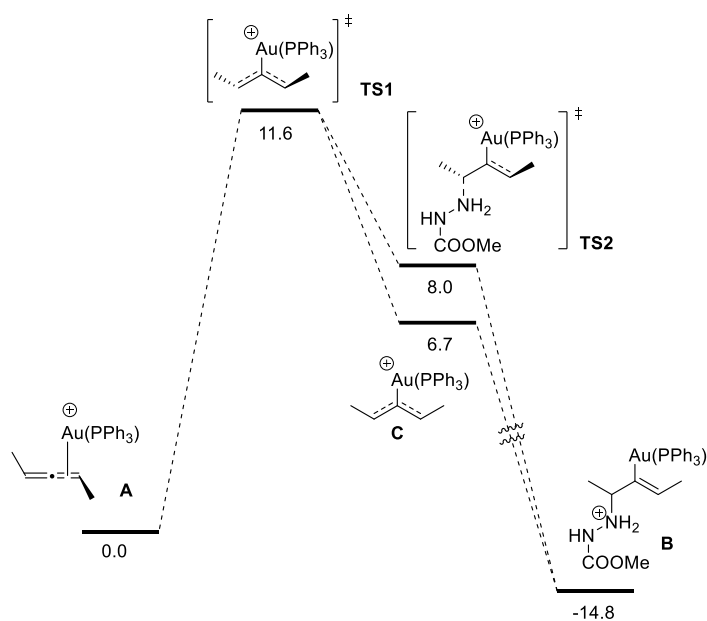


Figure 2 – Gibbs free energy profile for the hydroamination of (*S*)-2,3-pentadiene, as resulting from calculations at the DFT level. Computed Gibbs free energies at 298 K are reported in kcal mol⁻¹.^[100]

^{vi} Computations were performed with the M06 functional, but the authors neither reported additional computational details nor they provided the geometries of the species studied by computational modelling.^[100]

In summary, gold catalysis have proven to be probably the most versatile platform for the development of allene hydroamination methodology, with palladium coming as a close second. The lighter coinage metals (Cu and Ag) have probably much potential yet to be unveiled.

1.3.4.5. Hydroamination of allenes with catalysts based on group 12 metals

Zinc complexes have been used for the intramolecular hydroamination of simple aminoalkenes,^[101–104] but we have no knowledge of applications to allenes.

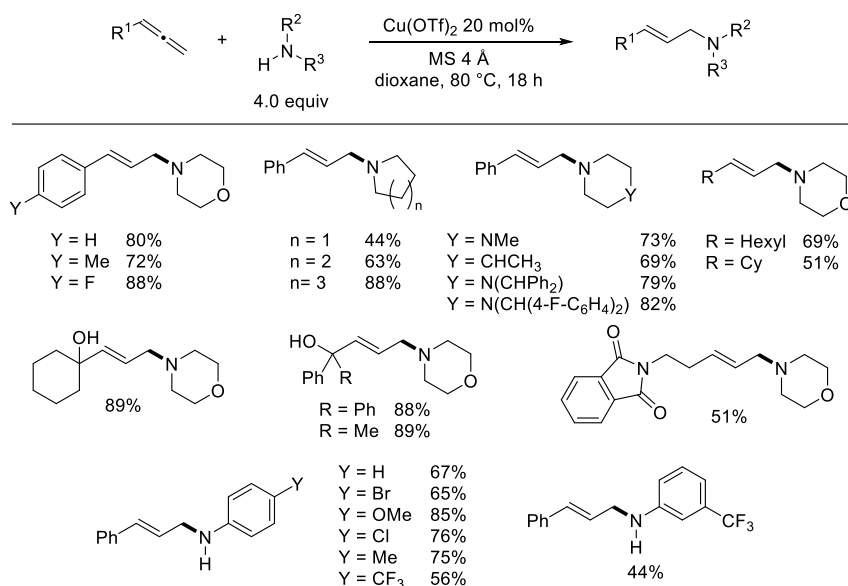
Stoichiometric amounts of mercury(II) salts have been used in the aminomercuration of allenes with anilines^[105] and in the intramolecular aminomercuration of aminoallenes.^[106] The reaction cannot be made catalytic, since the alkenylmercury(II) intermediates so formed are very stable.

2. Results and discussion

2.1. Object of the study, nature of the catalytically active species

Given the relatively few successful protocols for the copper-catalyzed hydroamination of unsaturated compounds and the attractiveness of this metal in terms of price and toxicity, we focused on the conditions recently developed by our collaborators – Florian Monnier and Marc Taillefer – for the hydroamination of terminal allenes (Scheme 40).^[80] This project is situated in the framework of a broader collaborative program concerning the use of copper and iron catalysis in organic synthesis (ANR project CuFeCCBond).

This reaction has several strengths. $\text{Cu}(\text{OTf})_2$, a very simple and commercially available copper(II) salt, is used as a pre-catalyst, and the addition of ligands is not necessary. Both primary anilines and secondary aliphatic amines are viable substrates, which is not the case for most of the catalysts presented in the previous section. Unprotected alcohols were also tolerated, which is not the case for protocols based on very oxophilic early transition metals. The linear product deriving from addition of the amine to the terminal carbon of the allene was obtained with good selectivity for the *E* stereoisomer. Unfortunately, low turnover numbers were achieved, and a comparatively high catalyst loading (20 mol%) had to be employed to ensure good yields. Open-chain amines gave only partly satisfactory results, cyclic secondary amines were the most successful substrates, but they had to be employed in excess (4.0 equiv) for best results. Sterically hindered amines, such as 2-methylpiperidine, gave poor yields. The reaction temperature could not be lowered below 80 °C, otherwise yields were severely diminished.^[80] The successful examples reported by Taillefer and Monnier are summarized in Scheme 57.



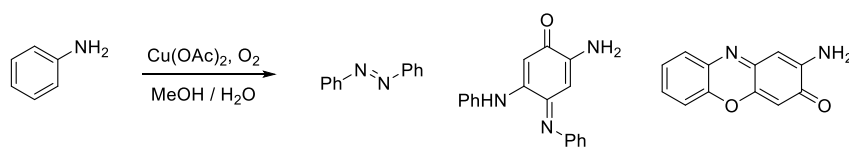
Scheme 57 – Scope of the Cu-catalyzed allene hydroamination reaction reported by Monnier and Taillefer.^[80]

With the aim to better understand this transformation and to gain insight useful to improve its efficiency by a rational approach, and possibly to overcome some of the above-described limitations, we undertook a comprehensive mechanistic study, using a combined experimental and theoretical approach.

To start with, we selected morpholine and phenylallene as model substrates.

First, we investigated the nature of the copper species actually present in the reaction mixture under catalytically relevant condition. $\text{Cu}(\text{OTf})_2$ has poor solubility in dioxane, the reaction solvent. At the usual ratio employed (5 mL of solvent per mmol of copper) most of it remained undissolved, even at the reaction temperature (80 °C). When excess morpholine (20 equiv) was added at room temperature, this white solid acquired a deep blue color, similar to that of $\text{Cu}(\text{II})/\text{ammonia}$ complexes. Nevertheless, it remained mostly undissolved and the supernatant solution had only a slight blue hue. When the mixture was heated at 80 °C under argon for 10 minutes or after stirring at room temperature for 18 h, the salt dissolved and a pale yellow, perfectly homogeneous solution was obtained. No line broadening due to paramagnetic species was observed in the NMR spectrum of the mixture. Exposure of the solution to air restored the deep blue color.

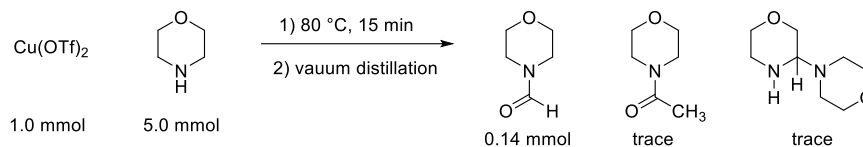
From these simple observations, we inferred that $\text{Cu}(\text{OTf})_2$ is reduced to $\text{Cu}(\text{I})$ species in the reaction environment, as it is often the case for Cu -catalyzed reaction in which amines (or alcohols) are involved.^[107] The reducing agent effecting this transformation must be the amine itself. Indeed, there are several reports in the literature describing the oxidation of amines to imines and amidines by $\text{Cu}(\text{II})$ salts.^[108,109] These products cannot form from amines having no α hydrogen atoms, but anilines – which are viable substrates for the transformation under study – can be oxidized to a complex mixture of azo compounds and quinoid condensation products, analogous to that obtained by the oxidation of aniline with $\text{Cu}(\text{OAc})_2$ in the presence of molecular oxygen (Scheme 58).^[110] An electron-transfer mechanism can be envisaged, as the interaction of aromatic amines with $\text{Cu}(\text{II})$ salts such as $\text{Cu}(\text{ClO}_4)_2$ is indeed a known way to generate the amine radical cations.^[111]



Scheme 58 – Main products obtained by oxidation of aniline with $\text{Cu}(\text{OAc})_2$ and O_2 .^[110]

To shed more light on what happens with morpholine – our model substrate – a suspension of $\text{Cu}(\text{OTf})_2$ (1.0 mmol) in morpholine (5.0 mmol) was heated at 80 °C for 15 minutes. The color changed gradually from deep blue to brownish. The resulting paste was subjected to distillation at reduced pressure (approximately 0.1 mbar). *N*-formylmorpholine (0.14 mmol, purity > 92%) was isolated from the distillate. Small amounts of *N*-acetylmorpholine (about 4% of *N*-formylmorpholine, as assessed by ^1H NMR) and 3,4'-

bimorpholine (about 2% of *N*-formylmorpholine, as assessed by ^1H NMR) were also identified by GLC-MS and by observation of some signature NMR peaks (Scheme 59).^{vii}



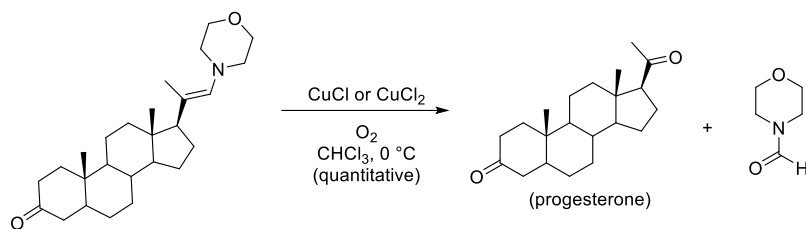
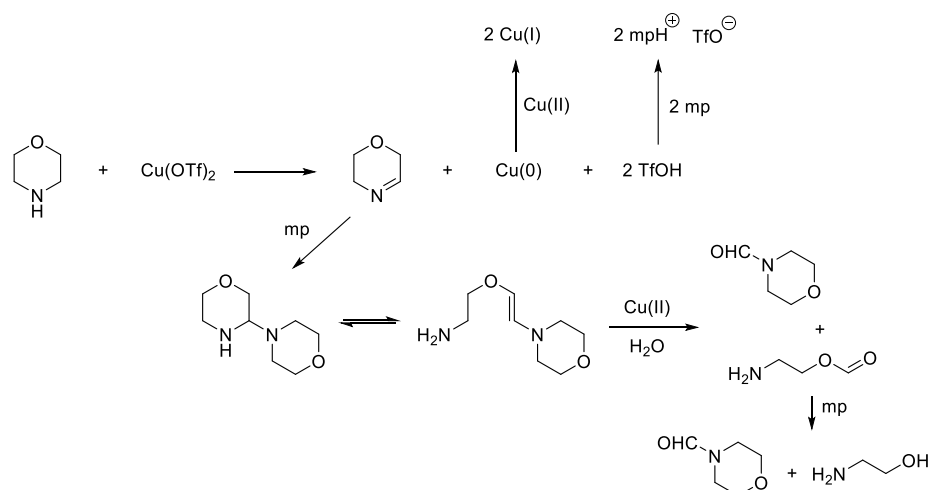
Scheme 59 – Reaction of morpholine with $\text{Cu}(\text{OTf})_2$.

When the same experiment was performed in dioxane as a solvent and the crude reaction mixture was analyzed directly by ^1H NMR (no distillation was performed), the signature resonances of *N*-formylmorpholine were observed, excluding that the formation of this compound was an artefact due to the purification procedure.

We have not fully investigated the mechanism of formation of those oxidation products. It is however known that the $\text{C}=\text{C}$ double bond of aldehyde-derived enamines is cleaved by copper salts in the presence of O_2 to give the corresponding formamide and carbonyl compound, even under mild conditions (an example is given in Scheme 60).^[112–115] A possible mechanism for the formation of *N*-formylmorpholine is thus proposed in Scheme 61, also based on literature reports about the oxidation of amines to imines in the presence of copper salts and on the experimental observation of 3,4'-bimorpholine.^[107–109] Briefly, $\text{Cu}(\text{II})$ oxidizes morpholine to the corresponding cyclic imine, which can undergo either addition of another morpholine molecule, resulting in the formation of 3,4'-bimorpholine or an imine. The latter species may be cleaved to *N*-formylmorpholine and 2-aminoethylformate, which in turn might also undergo aminolysis with another molecule of morpholine, generating *N*-formylmorpholine and 2-aminoethanol. If $\text{Cu}(\text{I})$ is generated in an overall two-electron reduction, comproportionation of $\text{Cu}(\text{II})$ with $\text{Cu}(\text{I})$ may take place. Indeed, the reaction of $\text{Cu}(\text{OTf})_2$ with $\text{Cu}(\text{I})$ is a useful method for the preparation of $\text{Cu}(\text{OTf})$.^[116–118]

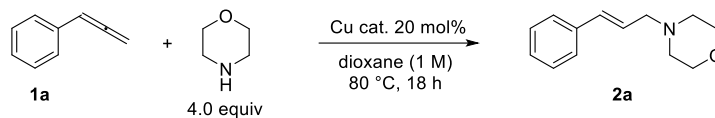
It is well known that $\text{Cu}(\text{I})$ salts having poorly coordinating anions, which for brevity we will call *cationic* $\text{Cu}(\text{I})$ salts, have good affinity for unsaturated compounds, such as olefins and arenes.^[116,117,119–124] Complexes of chelating diolefins with $\text{Cu}(\text{OTf})$ have been isolated and $\text{Cu}(\text{OTf})$ is often commercialized as a stable adduct with benzene or toluene. Several studies have been reported on the formation of complexes between allenes and late-transition metals,^[125] such as Rh ,^[126] Pt ,^[127] and Ag .^[128,129] but very little is known about $\text{Cu}(\text{I})$ /allene complexes. To the best of our knowledge, there is only one report describing the synthesis of complexes composed of CuCl and the cyclic allenes 1,2,6-cyclononatriene, 1,2,6-cyclodecatriene and 1,2,6,7-cyclodecatetraene.^[128] They were characterized only by elemental analysis and IR spectroscopy.

^{vii} Characterization data of these products are reported in the experimental section.

Scheme 60 – Cleavage of an enamine mediated by Cu salts.^[112]Scheme 61 – Proposed pathway for the formation of *N*-formylmorpholine from Cu(OTf)_2 and morpholine.

To corroborate the hypothesis that Cu(I) species are the actual catalyst of the hydroamination reaction, we attempted to replace Cu(OTf)_2 by several Cu(I) sources. The addition of molecular sieves, as suggested in the original protocol by Monnier and Taillefer, does not improve yields if rigorously dried dioxane is employed, thus for simplicity it was omitted.^{viii} It turned out that only Cu(I) salts having poorly coordinating anions (TfO^- , PF_6^-) efficiently promoted the reaction: $\text{Cu(NCMe)}_4(\text{OTf})$ was practically as effective as Cu(OTf)_2 (entry 4), while $\text{Cu(OTf)}\cdot\text{C}_6\text{H}_6$ (entry 3) and $\text{Cu(NCMe)}_4\text{PF}_6$ (entry 5) gave somehow reduced yields. CuSO_4 was completely ineffective (entry 6) and probably it was not reduced under the conditions of the reaction, as it turned blue upon adding morpholine and neither had it dissolved, nor it changed color on heating. CuBr (entry 7) and $\text{CuBr}\cdot\text{LiBr}$ (entry 8, this mixture is well soluble in dioxane, differently from CuBr alone) gave only very poor yields. Interestingly, if Cu(OTf)_2 was reduced by heating at $80\text{ }^\circ\text{C}$ in the presence of morpholine, cooled and *then* the allene was added, a low yield (8%) of the hydroamination product was obtained even at room temperature.

^{viii} Given the well-known difficulty to keep dioxane dry and the dangers associated to distillation from sodium, which is the most satisfactory method for drying this solvent,^[173] the use of the original protocol employing molecular sieves is advisable for synthetic purposes.

Table 2 – Screening of Cu pre-catalysts for the hydroamination of phenylallene.

Entry	Cat.	Unconverted 1a (%) ^a	Yield (%) ^a
1	Cu(OTf) ₂	-	80
2	Cu(OTf) ₂	35	8 ^b
3	Cu(OTf) · benzene	-	59
4	Cu(NCMe) ₄ (OTf)	-	78
5	Cu(NCMe) ₄ PF ₆	-	52
6	CuSO ₄	-	0
7	CuBr	15	11
8	CuBr · LiBr	-	14

^a Determined by ¹H-NMR with 1,3,5-trimethoxybenzene as an internal standard.

^b Reaction performed at room temperature after pre-activation of the catalyst for 5 min at 80 °C in the absence of allene.

Since no quantitative data were available, we investigated this issue by NMR spectroscopy. The addition of Cu(NCMe)₄PF₆ to a solution of phenylallene (**1a**) in DMSO-*d*₆ caused an upfield shift of the allene proton resonances, as expected for a complexation equilibrium which is fast on the timescale of NMR. To get some thermodynamic information from such kind of experiments, a fixed quantity of Cu(NCMe)₄PF₆ was titrated with increasing amounts of three selected allenes: phenylallene (**1a**), *N*-allenyl-2-pyrrolidinone (**1b**) and cyclonona-1,2-diene (**1c**) and the chemical shift of allene proton resonances was recorded after each addition.^{ix}

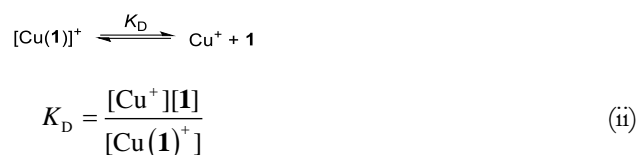
The form of the titration curve can be obtained by simple calculations. Under the hypothesis (which will be verified later) that only a 1:1 Cu/allene complex is formed and that exchange is fast on the NMR timescale, the observed chemical shift would be given by the following equation:

$$\delta_{\text{obs}} = \frac{x\delta_{\text{B}} + (n-x)\delta_{\text{F}}}{n} = \delta_{\text{F}} + \frac{x}{n} \cdot \Delta\delta \quad (1)$$

in which δ_{B} and δ_{F} are respectively the chemical shift of Cu-bound and free allene (**1**), $\Delta\delta = \delta_{\text{B}} - \delta_{\text{F}}$, n is the number of equivalents of allene with respect to copper, and x is the molar fraction of Cu(I) coordinated to the allene.

^{ix} Very small variations of chemical shifts are involved in these experiments, thus the use of an inert internal standard (in our case tetramethylsilane) as a reference was absolutely necessary to get reliable data.

Let K_D be the dissociation constant of the Cu/allene complex, i.e. the thermodynamic constant associated to the following equilibrium:



For convenience, the solvent, whose concentration is approximately constant and does not intervene in the calculations, has not been written explicitly. The molar fraction x can be expressed as a function of K_D and of the number of equivalents of allene (n , with respect to copper) and of the fixed concentration of copper (C_0) through elementary calculations:

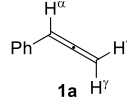
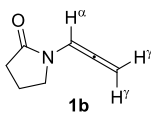
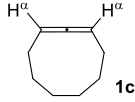
$$x = \frac{1}{2} \left(1 + n + \frac{K_D}{C_0} \right) - \sqrt{\frac{1}{4} \left(1 + n + \frac{K_D}{C_0} \right)^2 - n} \quad (\text{iii})$$

Substituting the expression for x in equation (i) gives:

$$\delta_{\text{obs}} = \delta_F + \frac{\Delta\delta}{n} \cdot \left[\frac{1}{2} \left(1 + n + \frac{K_D}{C_0} \right) - \sqrt{\frac{1}{4} \left(1 + n + \frac{K_D}{C_0} \right)^2 - n} \right] \quad (\text{iv})$$

The parameters δ_F , $\Delta\delta$ and K_D of equation (iv) were fitted to experimental data by a standard non-linear regression procedure at fixed and known C_0 . Good agreement was found between the experimental titration curves and the model, confirming the validity of the assumption that a 1:1 complex is formed between the allene and Cu(I). The data for allenes **1a-c** are reported in Figure 3 and the relevant fitted parameters are summarized in Table 3. For monosubstituted allenes **1a** and **1b**, K_D could be determined by using the chemical shifts of either allene protons. No significant difference was found between the values obtained, the average of the two results is thus reported.

Table 3 – $^1\text{H-NMR}$ data for the formation of complexes between allenes and $\text{Cu}(\text{NCMe})_4\text{PF}_6$ in $\text{DMSO-}d_6$ at 25 °C.

Entry	Allene	δ_F (H^α) ^a	$\Delta\delta$ (H^α) ^{a,b}	δ_F (H^γ) ^a	$\Delta\delta$ (H^γ) ^{a,b}	K_D ^b (mM)
1		6.359	-0.047 ± 0.002	5.280	-0.397 ± 0.017	37 ± 4
2		7.020	-0.156 ± 0.003	5.558	-0.806 ± 0.013	0.65 ± 0.13
3		5.293	-0.398 ± 0.008	-	-	4.9 ± 0.6

^a Chemical shifts are given in ppm with reference to internal TMS.

^b Asymptotic standard errors of the fitting procedure are given as uncertainties.

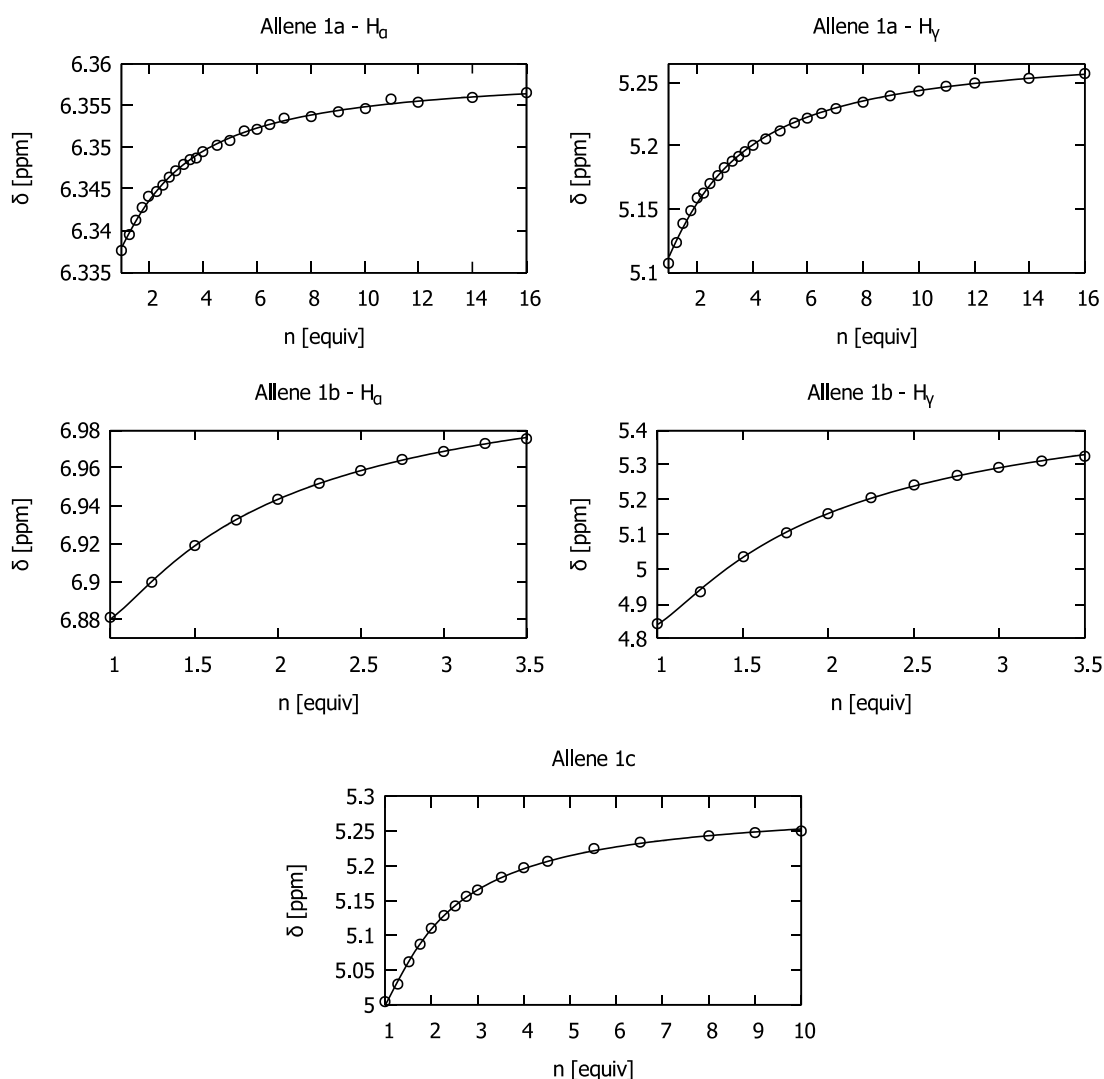
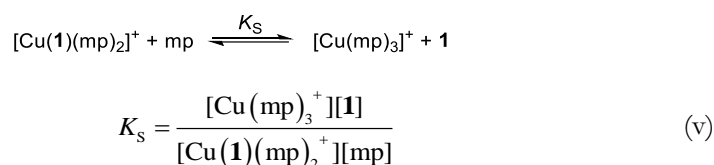


Figure 3 – ^1H NMR titration of $\text{Cu}(\text{NCMe})_4\text{PF}_6$ with allenes **1a**, **1b** and **1c** (total concentration of copper equal to 100 mM, 50 mM and 50 mM respectively in $\text{DMSO}-d_6$ at 25 °C). The chemical shift of allene protons are reported as a function of the number of equivalents of the allene itself with respect to Cu. The solid lines are the curves fitted according to equation (iv). The fitting parameters δ_{f} , $\Delta\delta$ and K_{D} are reported in Table 3.

We must point out that, as it is usual for alkene-metal complexes, coordination causes an upfield chemical shift (all the $\Delta\delta$ are negative). This observation can be interpreted in the framework of the Dewar-Chatt-Duncanson model: the metal-allene bond has an important π -backbonding character, *i.e.* electron density is donated by the metal center into a π^* antibonding orbital of the unsaturated compound. The magnitude of this effect is enough to compensate the opposite influence of σ bonding, which corresponds to a metal-to-ligand transfer of electron density and would cause a downfield chemical shift.^[116,117]

The values presented in Table 3 suggest that cationic copper(I) complexes have comparatively good affinity for allenes. However, under the conditions of the hydroamination reaction, an excess of the amine substrate is present, which can also serve as a ligand and displace the allene itself from the metal center. In order to obtain a semi-quantitative estimate of this phenomenon, a solution of allenes **1a-b** and Cu(NCMe)₄PF₆ was titrated with morpholine and the chemical shift of the allene proton resonances monitored, analogously to what described in the previous paragraphs.

Developing a rigorous model to obtain an equation for the titration curve in this case is more difficult, because several morpholine- and allene-ligated complexes are possible, also with different coordination numbers. Assuming that the largely major species present in solutions are [Cu(mp)₃]⁺ and [Cu(**1**)(mp)₂]⁺ (mp = morpholine), the following ligand displacement equilibrium has been considered:



The molar fraction x of Cu(I) bound to the allene can be calculated as a function of K_s :

$$x = \frac{(3-m)K_s - (n+1) + \sqrt{[(m-3)K_s + n+1]^2 + 4n(K_s-1)}}{2(K_s-1)} \quad (\text{vi})$$

in which m and n are the number of equivalents of morpholine and of **1** (with respect to Cu⁺) respectively.

By substitution of x in equation (i), an expression for the observed chemical shift is obtained:

$$\delta_{\text{obs}} = \delta_{\text{F}} + \frac{\Delta\delta}{n} \cdot \left[\frac{(3-m)K_s - (n+1) + \sqrt{[(m-3)K_s + n+1]^2 + 4n(K_s-1)}}{2(K_s-1)} \right] \quad (\text{vii})$$

Equation (vii) with $n = 2$ (2.0 equiv of allene were introduced with respect to Cu⁺) has been fitted to experimental data using the chemical shifts of H_γ. Our model is meaningful only for $m > 3$, so points with less than 3 equiv of morpholine have been excluded from the fitting. Experimental data and fitted curves are reported in Figure 4.

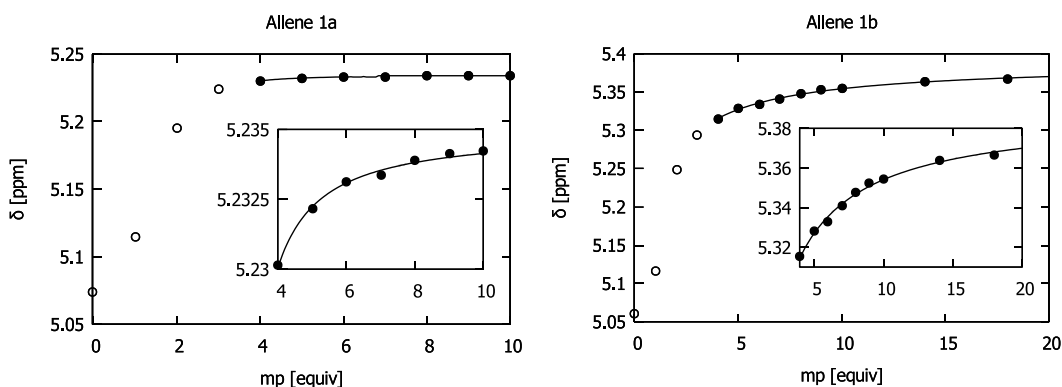


Figure 4 – ^1H NMR titration of $\text{Cu}(\text{NCMe})_4\text{PF}_6$ in the presence allenes **1a** (left) and **1b** (right) (total concentration of copper equal to 100 mM and 50 mM respectively in $\text{DMSO}-d_6$ at 25°C , 2.0 equiv of allene with respect to Cu) with varying amounts of morpholine. The chemical shift of allene H_γ protons is reported as a function of the number of equivalents of morpholine added (m , with respect to Cu). The solid lines are the fitted curves according to equation (vii) with $n = 2$. Only the experimental points drawn in black and shown also in the inset ($m > 4$) have been employed for the fitting procedure. Fitted parameters (fitting standard error as uncertainties): for **1a** $\Delta\delta = (-0.1138 \pm 0.037)$ ppm, $K_S = 18.9 \pm 7.1$; for **1b** $\Delta\delta = (-0.250 \pm 0.010)$ ppm, $K_S = 0.634 \pm 0.052$.

To get a better qualitative appreciation of the difference between **1a** and **1b**, the molar fraction x of Cu^+ coordinated to allene, given by $(\delta_{\text{obs}} - \delta_{\text{F}})/(\Delta\delta)$, has been plotted as a function of the quantity of morpholine (Figure 5). From this graph, it is clear that in the presence of excess morpholine, as under catalytically relevant conditions, in the case of **1a** only a very small fraction of Cu^+ is bound to the allene, while the percentage is much more important for **1b**.

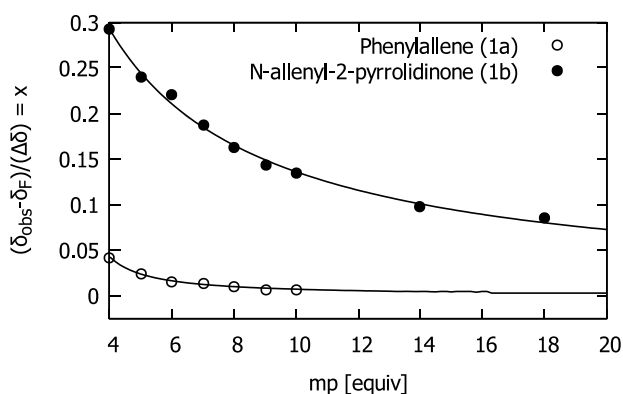
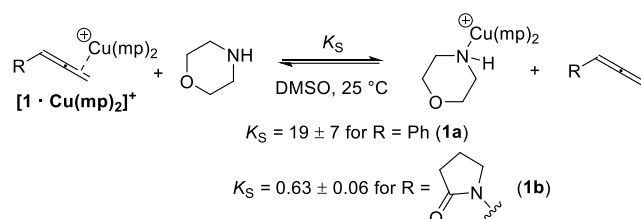


Figure 5 – Fraction of Cu^+ bound to allene as a function of the number of equivalents of added morpholine, derived from the data reported in Figure 4. The solid lines are the theoretical curves obtained with the parameters fitted as shown in Figure 4.

The values found for the thermodynamic constant K_S ($K_S = 19$ for **1a** and $K_S = 0.63$ for **1b**) are such that under the conditions relevant for the catalytic reaction (excess amine and allene with respect to copper) the two substrates compete for binding $\text{Cu}(\text{I})$ (Scheme 62). The ratio of the ligand substitution constants $K_S(\mathbf{1a})/K_S(\mathbf{1b}) = 30$ of the two allenes considered here is of the same order of magnitude of the ratio of the dissociation constants reported in Table 3:

$K_D(\mathbf{1a})/K_D(\mathbf{1b}) = 57$. This observation may be justified considering that both constants mirror the affinity of the allenes for Cu(I).

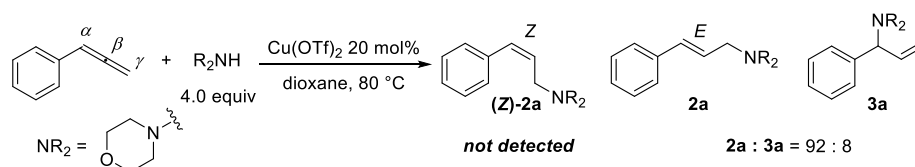


Scheme 62 – Displacement of coordinated allene from cationic Cu(I) by morpholine. Asymptotic standard errors of the fitting procedure are given as uncertainties.

In summary, we have disclosed that under the conditions described by our coworkers for the hydroamination of allenes, the Cu(II) pre-catalyst $\text{Cu}(\text{OTf})_2$ is reduced to Cu(I). The two substrates (allene and amine) compete for coordination at the metal center and semi-quantitative thermodynamic parameters regarding this interaction have been obtained.

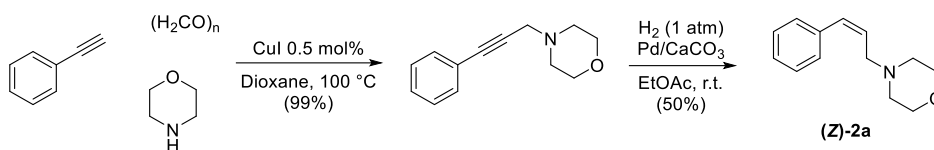
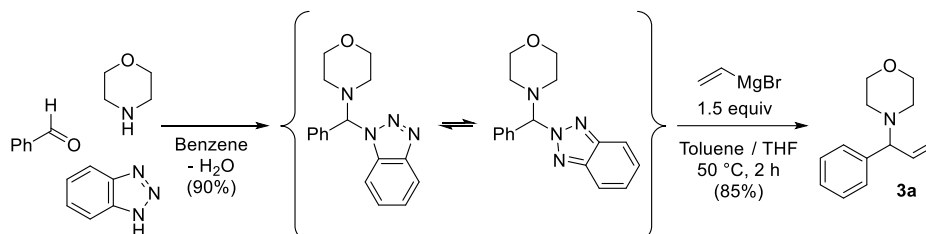
2.2. Catalytic cycle and the origin of selectivity

The reaction under study is both *regio*- and *stereoselective*: addition of the amine takes place mainly at the terminal carbon atom with complete selectivity for the *E* isomer. The geometric isomer (**Z**)-**2a** is not formed in any amount detectable by NMR and the **2a**/**3a** isomer ratio is 92:8 (Scheme 63). This isomer ratio is slightly diminished if a smaller excess of amine is used. For example, it decreases to 82:18 for 2.0 equiv of morpholine.

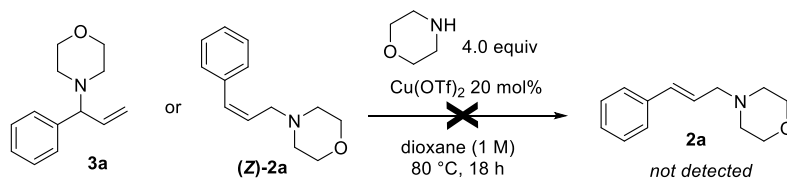


Scheme 63 – Regio- and stereoselectivities of the $\text{Cu}(\text{OTf})_2$ -catalyzed addition of morpholine to phenylallene.

To demonstrate that the reaction is under kinetic control (and then truly selective) and that the apparent selectivity is not simply due to equilibration of **3a** and (**Z**)-**2a** to the most thermodynamically stable isomer **2a**, compounds (**Z**)-**2a** and **3a** were synthesized by an independent route. Briefly, the *cis* alkene (**Z**)-**2a** was obtained by careful hydrogenation of the corresponding propargylic amine, which was in turn prepared by the A3 reaction of phenylacetylene, morpholine and paraformaldehyde (Scheme 64). The branched allylamine **3a** was prepared by reaction of vinylmagnesium bromide with the mixed amination of benzaldehyde with morpholine and benzotriazole, which formally acts as a source of the iminium ion, as shown by Katritzky (Scheme 65).^[130]

Scheme 64 – Synthesis of compound **(Z)-2a**.Scheme 65 – Synthesis of compound **3a**.

When compounds **(Z)-2a** and **3a** were heated under the conditions of the catalytic reaction, no conversion to **2a** took place, as verified by ^1H NMR analysis (Scheme 66). This is different from what demonstrated for some rhodium- and palladium-based hydroamination catalysts, for which similar isomerizations have been shown to proceed, most likely by the intermediacy of η^3 -allylmetal species (see Scheme 26 and Scheme 34).^[54,60]

Scheme 66 – Attempted isomerization of **(Z)-2a** and **3a**.

With these experiments it was established beyond doubt that the reaction is actually under kinetic control, regioselective and stereoselective. Having also in hand reliable experimental information on the nature of the catalytically active species and on its interaction with the substrates, DFT calculations could be performed. In the following, all the enthalpies and free energies (ΔH and ΔG) reported will refer to data computed at 298 K and 1 atm on the basis of the usual approximations (harmonic oscillator-rigid rotator, perfect gas formulae).

On the basis of the data we collected, it was not possible to establish the coordination number of the Cu(I)/morpholine complexes formed in solution. Several reports exist in the literature related to this point, but no definitive conclusion could be made. For instance, the reaction of diethylamine with CuCl can give 1:1 or 2:1 complexes, in dependence of the experimental conditions.^[131] An electrochemical study^x demonstrated that the maximum

^x Iwamoto and co-workers employed a clever and simple method for the determination of the maximum achievable coordination number of metal/amine complexes based on polarography. They considered the following equilibrium of complex formation, with the associated overall thermodynamic constant β_m :

achievable coordination number in solution for cationic Cu(I)/amine complexes deriving from the interaction of $\text{Cu}(\text{NCMe})_4(\text{ClO}_4)$ with excess ligands (which is indeed very close to our experimental conditions) can vary between 2 and 4, depending on the nature of the amine (*e.g.*, it is 2 for piperidine, 3 for butylamine and quinoline, and 4 for pyridine and isoquinoline).^[132] However, complexes of apparent stoichiometry $\text{Cu}(\text{piperidine})_{3.3}(\text{ClO}_4)$ could be isolated, which would suggest that in the solid state coordination numbers higher than 2 are achievable for this amine.^[132]

To shed more light on this point, we evaluated the relative stabilities of cationic Cu(I) complexes with morpholine as a ligand by the means of DFT modeling. Results are summarized in Figure 6. According to the profile of the Gibbs free energy, $\text{Cu}(\text{mp})_3$ and $\text{Cu}(\text{mp})_4$ are the most favored ones, the latter being 4.9 kcal mol⁻¹ more stable. Anyway, for homogeneity and in order to make meaningful comparisons, geometries featuring two coordinated morpholine molecules were assumed for all the catalytic intermediates in the following calculations.

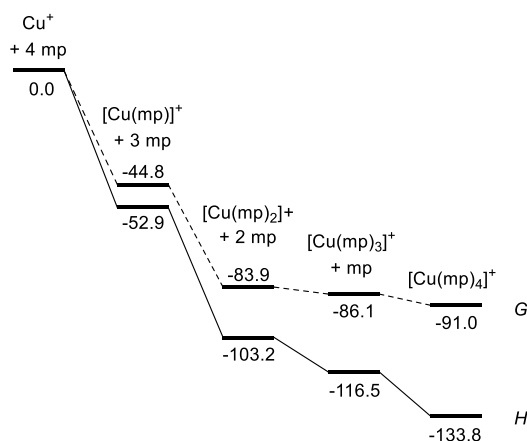


Figure 6 – Relative stabilities of $\text{Cu}(\text{mp})_n$ complexes, as assessed by DFT modeling. The relative Gibbs free energies (*G*, dashed line) and enthalpies at 298 K (*H*, solid line) are reported in kcal mol⁻¹.

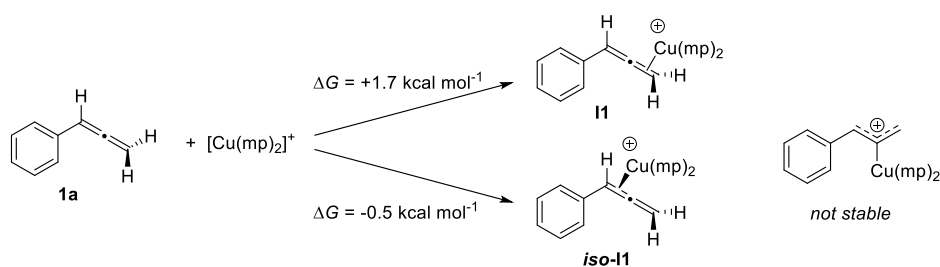


In the presence of a large excess ligand L, all the metal centers M can be considered to be under the form of ML_n complexes, so $[\text{ML}_m]$ can be approximated with the analytical concentration of metal (C_M) and [L] with the analytical concentration of the ligand (C_L): $[\text{M}] \approx C_M$ and $[\text{L}] \approx C_L$. From the Nernst equation, the half-wave potential for the reversible reduction of M depends on [M] as follows:

$$E_{1/2}^{(C)} = E_{1/2}^0 - \frac{RT}{nF} \ln[\text{M}] = E_{1/2}^0 - \frac{RT}{nF} \ln C_M + \frac{RT}{nF} \ln \beta_m + \frac{RT}{nF} m \ln C_L$$

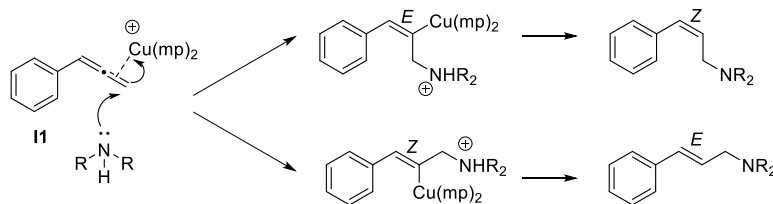
By plotting $E_{1/2}^{(C)}$ as a function of $\ln C_L$ (at fixed C_M), a straight line is obtained; *m* can be calculated from the slope of the regression line and β_m from the intercept.

The complexation of the $[\text{Cu}(\text{mp})_2]^+$ fragment with phenylallene (**1a**) is predicted by DFT calculations to involve only a small variation of Gibbs free energy (Scheme 67) and can either take place at the terminal β,γ double bond (to give complex **I1**, $\Delta G = +1.7 \text{ kcal mol}^{-1}$) or at the α,β double bond (resulting in complex *iso-I1*, $\Delta G = -0.5 \text{ kcal mol}^{-1}$). No stable cationic copper-allyl cation complex could be found. This hypothetical species can actually be thought as an intermediate for the isomerization of **I1** to *iso-I1*, but it is not a minimum of the potential energy surface, but a transition state.



Scheme 67 – Formation of complexes between **1a** and $\text{Cu}(\text{mp})_2^+$.

We hypothesized that the hydroamination reaction could proceed by direct nucleophilic attack of the secondary amine on a copper-allene complex. An alkenyl-copper intermediate would thus be generated, which could give the final product after protodemercuration. Alkenyl-copper organometallic species are normally stereochemically stable and undergo stereospecific protodemercuration in the presence of proton sources with retention of the configuration of the double bond. This happens, for example, for the well-studied stereodefined alkenyl-copper reagents deriving from the carbocupration of alkynes, for which numerous examples of stereospecific protodemercuration are known.^[133–135] With this pathway, the stereoselectivity of the nucleophilic attack would determine directly the *E/Z* selectivity of the overall hydroamination process. The two steps are shown in Scheme 68.



Scheme 68 – Nucleophilic attack of a secondary amine on **I1** and subsequent stereospecific protodemercuration with retention of the configuration of the double bond.

Two idealized stereochemical approaches are conceivable for the nucleophilic attack of morpholine on the $[\text{Cu}(\text{mp})_2]^+$ /allene complex **I1**. With respect to the plane in which the $\text{C}=\text{CH}_2$ moiety lies, the approach can take place either (1) from the opposite side as Cu (*i.e.* in an *anti-periplanar* fashion); (2) from the same side as Cu (*i.e.* in a *syn-periplanar* approach). In both cases the Ph ring can either lie in the same half-space as Cu, resulting in the *Z* alkenylcopper intermediate, or in the opposite half space, corresponding to the formation of an *E* organocopper product. Note that the *E* vinylcopper intermediate yields the *Z* allylamine after

protodecupration with retention of configuration, while the *Z* organocopper species gives the *E* allylamine.

All the possible transition states corresponding to the stereochemical approaches described above are depicted schematically in Figure 7. For **TS1a-b,d** the computed geometries and free energies of formation (ΔG , with respect to free $[\text{Cu}(\text{mp})_2]^+$, mp, and **1a**) are also reported. The hypothetical **TS1c**, corresponding to *syn-periplanar attack* with the Ph ring lying in the same half-space as copper is too sterically crowded and any attempt of geometry optimization invariably led to **TS1a**. In Figure 7 transition state **TS1e** that corresponds to the attack of morpholine to $\text{C}\alpha$ and to the generation of the branched product **3a** is also shown. Clearly, in this case nucleophilic attack must take place not on **I1**, but on *iso-I1*, since the metal center is coordinated to the allene through the α,β double bond. Only attack from the opposite side of copper is conceivable, due to steric hindrance.

As stated above, after stereoconservative protodemetalation, **TS1a** leads to **2a**, **TS1b** and **TS1d** yield (*Z*)-**2a**, and **TS1d** provides **3a**. The computed free energies are in qualitative agreement with the fact that **2a** is the major product, while minor amounts of **3a** are observed and no detectable amounts of (*Z*)-**2a** are produced, since $\Delta G(\text{TS1a}) < \Delta G(\text{TS1e}) < \Delta G(\text{TS1b}) < \Delta G(\text{TS1d})$ with values of 17.0, 18.7, 20.8 and 27.9 kcal mol⁻¹ respectively (Figure 7). Indeed, the free energy difference between **TS1a** and **TS1e** corresponds to a Boltzmann ratio (94:6 at 80 °C) which is of the same order of magnitude of the observed **2a:3a** ratio (92:8).

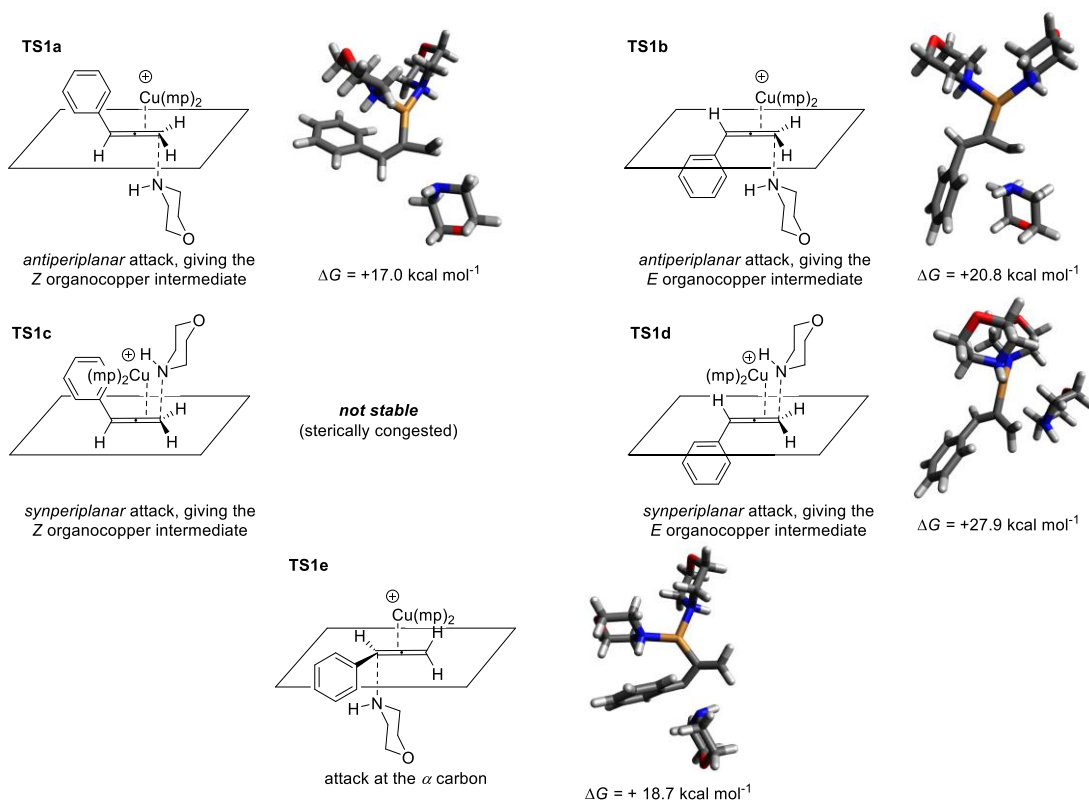


Figure 7 – Modes of nucleophilic attack on the Cu(I)/allene complexes. Reported figures are computed Gibbs free energies at 298 K (ΔG) relative to non-interacting $[\text{Cu}(\text{mp})_2]^+$, mp and **1a**.

In order to get more qualitative insight into the reasons of the observed selectivity, distortion-interaction (DI) analysis of the relevant transition states was performed.^[136,137] The results are summarized in Table 4. The ΔG between the transition states **TS1a-e** and the parent complex $[(\mathbf{1a})\text{Cu}(\text{mp})_2]$ (**I1**) has been dissected into the contributions due to solvation ($\Delta E_{\text{solvation}}$), thermal correction to Gibbs free energy ($\Delta E_{\text{thermal}}$), distortion of morpholine ($\Delta E_{\text{dist}}(\text{mp})$) and of the Cu-allene fragment ($\Delta E_{\text{dist}}(\mathbf{I1})$) – the sum of which gives the total distortion contribution ($\Delta E_{\text{dist}} = \Delta E_{\text{dist}}(\text{mp}) + \Delta E_{\text{dist}}(\mathbf{I1})$) – and interaction between the two fragments (ΔE_{int}).

Table 4 – Distortion-interaction analysis for **TS1a-b** and **TS1d-e**. All reported data are in kcal mol⁻¹.^a

	TS1a	TS1b	TS1d	TS1e
$G(\mathbf{TS})-G(\mathbf{I1})$	15.3	19.1	26.2	17.0
$\Delta E_{\text{solvation}}$	3.4	3.5	2.9	3.5
$\Delta E_{\text{thermal}}$	11.8	12.1	14.3	13.9
$\Delta E_{\text{dist}}(\text{mp})$	0.2	0.3	0.6	0.5
$\Delta E_{\text{dist}}(\mathbf{I1})$	12.4	20.7	24.6	17.7
$\Delta E_{\text{dist}}(\text{total})$	12.6	21.0	25.2	18.2
ΔE_{int}	-12.5	-17.5	-16.2	-18.6

^a The DI analysis has been performed according to the following formulae:

$$G(\mathbf{TS}) - G(\mathbf{I1}) = \Delta E_{\text{solvation}} + \Delta E_{\text{thermal}} + \Delta E_{\text{dist}}(\text{mp}) + \Delta E_{\text{dist}}(\mathbf{I1}) + \Delta E_{\text{int}}; \Delta E_{\text{dist}}(\text{total}) = \Delta E_{\text{dist}}(\text{mp}) + \Delta E_{\text{dist}}(\mathbf{I1}).$$

Inspection of Table 4 reveals that the contributions of solvation and thermal correction to Gibbs free energy are quite homogeneous within the series. As expected, the distortion energy of morpholine is practically negligible. For **TS1a**, which corresponds to the major product observed experimentally, distortion energy of the allene moiety is significantly lower than for the other TSs, and it is almost compensated by the interaction energy between the two fragments. Analogous considerations hold for **TS1e**, which is associated to the formation of the branched minor product **3a**, but here the absolute values of both interaction and distortion energies are higher than **TS1a**. Distortion energy for **TS1b** and **TS1d** are significantly more important than for the other TSs, and they are not compensated by the interaction energy, which is similar to that of **TS1e**. We may conclude that the observed selectivity for the linear, *E* product is largely distortion-controlled.

The complete catalytic cycle for the pathway going through the **TS1a** was analyzed at the same level of theory and the computed free energy profile is reported in Figure 8. Complexation of phenylallene (**1a**) with $[\text{Cu}(\text{mp})_2]^+$, giving the intermediate complex **I1**, is slightly endergonic ($\Delta G = +1.7$ kcal mol⁻¹), as the association with an extra molecule of morpholine in intermediate **I2** ($\Delta G = +3.2$ kcal mol⁻¹). Addition of morpholine on the Cu-activated allene takes place as described previously *via* **TS1a** ($\Delta G^\ddagger = +12.1$ kcal mol⁻¹) in an *anti-periplanar* fashion giving the *Z* alkenylcopper intermediate **I3** ($\Delta G = +6.7$ kcal mol⁻¹) featuring a protonated nitrogen atom. Proton transfer to a morpholine molecule ($\Delta G = +5.9$ kcal mol⁻¹) allows the latter to engage in almost barrierless stereo-conservative protodemetalation *via* **TS2**. This step is exergonic ($\Delta G = -29.8$ kcal mol⁻¹) and delivers the *E* product **2a** in the conformation **I5**. This highly favorable

step makes the whole transformation exergonic and it is the driving force of the process. Isomerization to the more stable conformer **16** ($\Delta G = -1.8$ kcal mol⁻¹) finally takes place.

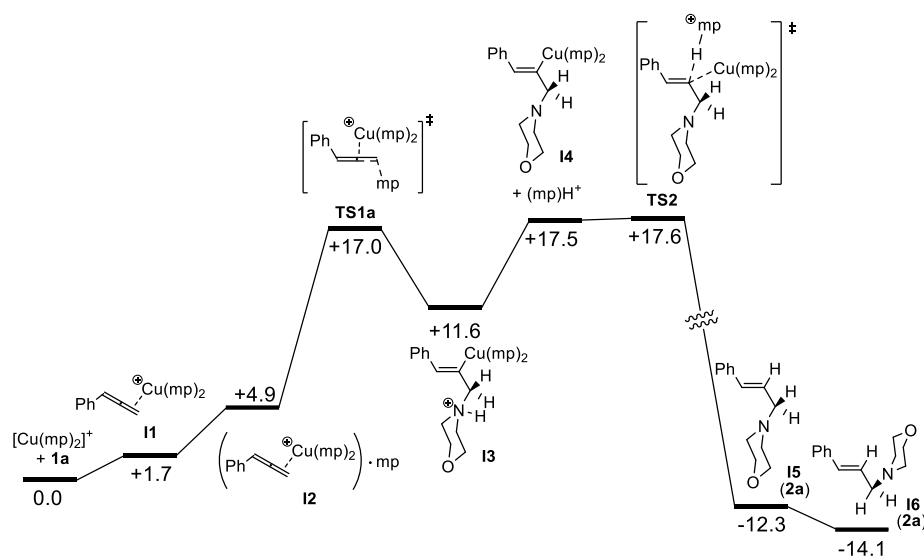
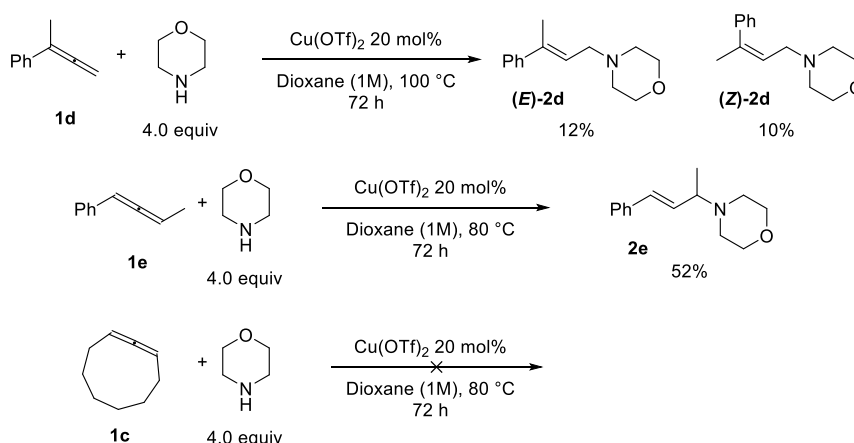


Figure 8 – Computed reaction path for the hydroamination of phenylallene (**1a**) with morpholine. Reported figures are computed Gibbs free energies in kcal mol⁻¹ at 298 K.

Simple inspection of the structure of **TS1a** suggests that introduction of a substituent at the allene α position should severely interfere with the reactivity, because of unfavorable steric hindrance with incoming nucleophile, in a way akin to allylic 1,3-strain. On the other hand, introduction of a substituent on the γ carbon should not affect reactivity much, since the substituent would lie in a comparatively unencumbered region of the transition state. To test this hypothesis, the reactivity of allenes **1d** and **1e**, featuring a methyl group at the α or at the γ carbon respectively, was examined experimentally. In accordance with the expected trend, the α,α -disubstituted allene **1d** gave an isomeric mixture of hydroamination products in 22% overall yield only under forcing conditions (reaction temperature: 100 °C), while the α,γ -disubstituted allene **1e** gave the expected product (**2e**) in 52% yield using the standard protocol.^[80] By contrast, cyclic allene **1c** did not give the expected hydroamination product and no starting material was left at the end of the specified reaction time. We may attribute this behavior to the easy polymerization of this substrate due to ring strain (Scheme 69).^{xi}

^{xi} The stereochemistry of product (**E**)-**2d** and (**Z**)-**2d** was determined by comparison with spectroscopic data available in the literature,^[93] which in turn established unambiguously the assignments by NOE experiments. Also **2e** is a known compound.^[93]



Scheme 69 – Hydroamination of disubstituted allenes **1c**, **1d** and **1e**. Yields were determined by ^1H NMR spectroscopy of the crude reaction mixture with 1,3,5-trimethoxybenzene as an internal standard.

We examined the geometry of the relevant transition state **TS1a** and compared them to Cu-allene parent complex **I1**. A significant structural reorganization of the coordinated allene takes place before the formation of the new C-N bond. This view is reinforced by the distortion-interaction analysis shown previously and inspection of the geometric parameters of **TS1a** (Figure 2) shows that the $\text{C}_\gamma\text{-N}$ distance is long (2.14 Å) and C_β is essentially already a sp^2 center ($\angle\text{C}_\alpha\text{C}_\beta\text{C}_\gamma = 138.8^\circ$, $\angle\text{CuC}_\beta\text{C}_\gamma\text{N} = 174.5^\circ$, $\angle\text{CuC}_\beta\text{C}_\alpha\text{H} = 170.0^\circ$). In this way, positive charge is built at the γ allenic carbon passing from the **I1** to **TS1a**, as natural population analysis^[138,139] evidences (Figure 9).

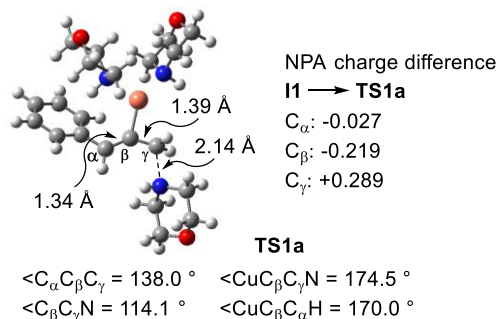


Figure 9 – Selected geometric parameters for **TS1a**.
 NPA charge difference between **TS1a** and **I1** is also shown (in units of $|e^-|$).

In summary, after confirming that the reaction under study is catalyzed by Cu(I) species formed by reduction of the Cu(II) pre-catalyst and that the reaction is under kinetic control, based on DFT calculations we proposed a mechanistic model that accounts for the observed regio- and stereoselectivity and that allows to interpret the relative reactivity of disubstituted allenes. At this point, we tried to take advantage of this information to develop synthetically useful extension of this hydroamination reaction.

2.3. From mechanistic insight to methodology development – hydroamination of allenamides

To extend the applicability of the reaction under study in milder conditions, we speculated that substitution at the α -carbon with a heteroatom having lone pairs could help to stabilize the transition state, effectively delocalizing the positive charge developed at C $_{\gamma}$. With this aim in mind, nitrogen substitution was the most obvious choice. Since *N*-allenylamines are unstable compounds and very prone to polymerization,^[140] moreover they are known to add amines *via* the corresponding iminium ion formed even by traces of protic acids (see the introduction, Scheme 4),^[24] we devoted our attention to allenamides, which are often an optimum compromise between reactivity and stability.^[141] Moreover, allenamides are readily available,^[141] since they can be obtained by base-catalyzed isomerization of the corresponding *N*-propargylamides.^{xii}

We tested the reaction of *N*-allenyl-2-pyrrolidinone (**1b**) with morpholine under the previously reported conditions^[80] and we found, in agreement with our expectations, that the transformation can indeed proceed at room temperature for this substrate (after pre-reduction of Cu(OTf)₂ with morpholine for 10 min at 80 °C in the absence of **1b**, Table 5, entry 1). Reducing the excess of morpholine from 4.0 equiv to 2.0 equiv did not affect the yield (entry 2), but lowering to 1.2 equiv (entry 3) had a detrimental effect on the yields with this catalyst. A screening performed using the Cu(I) pre-catalyst Cu(NCMe)₄(OTf) (entries 4-9), which is a moderately air-stable compound^{xiii} having good solubility in all the solvents tested, revealed that the reaction is most efficient in solvents of medium to low polarity (e.g. THF and benzene). In CHCl₃ the reaction had poor regioselectivity, and approximately 20% of the branched isomer **3b** (Figure 10) was detected by NMR analysis of the crude reaction mixture.^{xiv} Compound **3b** slowly decomposed in solution, most likely by formation of the corresponding iminium ion. Finally, we found that air-stable and commercially available Cu(NCMe)₄PF₆ promotes the reaction in almost quantitative yield at room temperature with a comparatively low catalyst loading of 5 mol% in the presence of only 1.2 equiv of secondary amine, provided that THF is

^{xii} The preparation of all the allenamides and other allenic derivatives employed in this study is described in detail in the experimental section.

^{xiii} In general, Cu(NCMe)₄X complexes (with X⁻ a poorly coordinating anion, such as TfO⁻, BF₄⁻, PF₆⁻, Tf₂N⁻) are not oxidized to Cu(II) by atmospheric oxygen, unless in the presence of water. The most hygroscopic ones (X = TfO⁻, Tf₂N⁻) become quickly bluish upon exposure to moist atmosphere, while Cu(NCMe)₄PF₆ is only slightly hygroscopic and it can be stored for prolonged times in ordinary screw-capped vials without alteration. All these complexes are easily obtained by adding the parent acid to a suspension of air-stable Cu₂O in MeCN (no precautions to exclude air are necessary). They crystallize as white solids after adding Et₂O and cooling to -18 °C.

^{xiv} Compound **3b** was characterized *in situ* by its characteristic NMR resonances. ¹H NMR (300 MHz, CDCl₃): δ = 5.61 (ddd, *J* = 17.3, 10.2, 7.7 Hz, 1H), 5.18 (d, *J* = 17.3 Hz, 1H), 5.09 (d, *J* = 10.3 Hz, 1H), 4.63 (d, *J* = 7.7 Hz, 1H) ppm.

used as a solvent (entry 13). Reducing further the catalyst loading to 2.5 mol% resulted in incomplete conversion after 18 h at room temperature and only 25% yield (entry 14), and no reaction was observed in the absence of any copper salt (entry 15). These very mild conditions complement a known method for the hydroamination of allenamides with primary anilines under gold catalysis (Scheme 53).^[142]

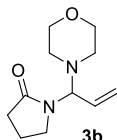
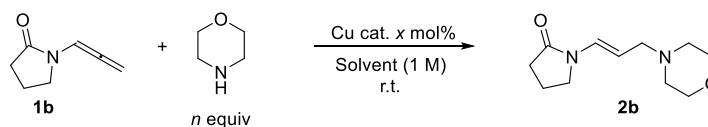


Figure 10 – Structure of byproduct **3b**.

Table 5 – Optimization of the reaction conditions for the Cu-catalyzed hydroamination of allenamides.



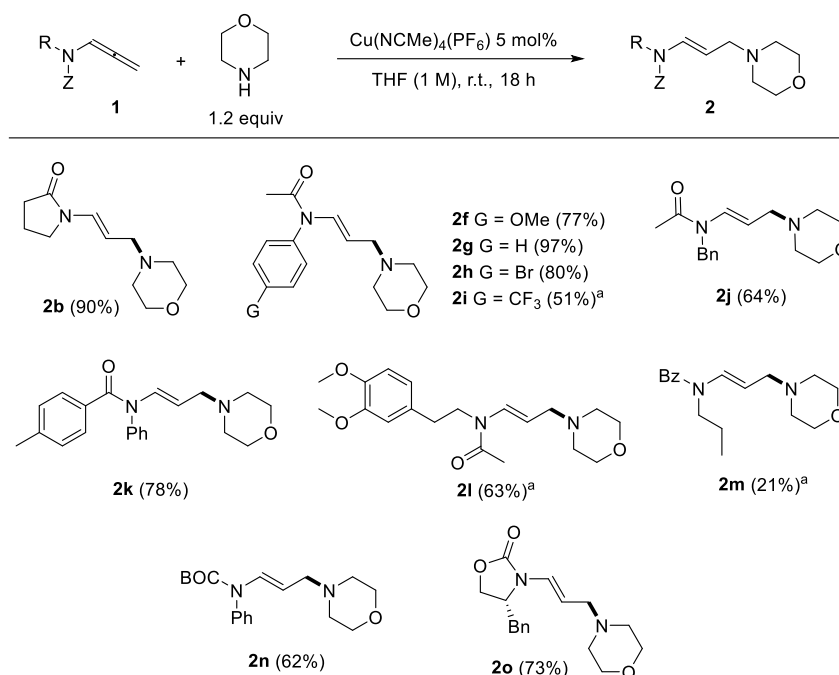
Entry	Catalyst (mol%)	Solvent	mp (equiv)	Time (h)	Yield (%) ^a
1	Cu(OTf) ₂ (20)	dioxane	4.0	1.5	83 ^b
2	Cu(OTf) ₂ (20)	dioxane	2.0	1.5	82 ^b
3	Cu(OTf) ₂ (20)	dioxane	1.2	4	50 ^b
4	Cu(NCMe) ₄ (OTf) (20)	dioxane	1.2	4	54
5	Cu(NCMe) ₄ (OTf) (20)	CHCl ₃	1.2	2	49 ^c
6	Cu(NCMe) ₄ (OTf) (20)	benzene	1.2	2	58
7	Cu(NCMe) ₄ (OTf) (20)	MeCN	1.2	5	45
8	Cu(NCMe) ₄ (OTf) (20)	MeOH	1.2	5	25
9	Cu(NCMe) ₄ (OTf) (20)	THF	1.2	1	53
10	Cu(NCMe) ₄ PF ₆ (20)	dioxane	1.2	0.25	60
11	Cu(NCMe) ₄ PF ₆ (10)	dioxane	1.2	1.5	60
12	Cu(NCMe) ₄ PF ₆ (5)	dioxane	1.2	4	66
13	Cu(NCMe)₄PF₆ (5)	THF	1.2	5	96 (90)^d
14	Cu(NCMe) ₄ PF ₆ (2.5)	THF	1.2	18	25
15	None	THF	1.2	18	0

^a Determined by ¹H-NMR with 1,3,5-trimethoxybenzene as an internal standard, unless otherwise stated.

^b Reaction performed at room temperature after pre-activation of the catalyst for 10 min at 80 °C in the absence of **1b**. ^c Approximately 20% of the branched product **3b** formed, which decomposed slowly in the reaction mixture. ^d Isolated yield.

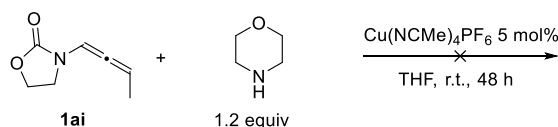
With this efficient catalyst system in hand, we explored the scope of the reaction by varying the allene partner (Scheme 70). A variety of allenamides, featuring aromatic or aliphatic substituents are viable substrates for this reaction. If *N*-aryl-*N*-allenyl amides are employed, both electron-releasing and electron-withdrawing groups are tolerated (compounds **2f-i**), but the reaction is slightly less efficient for electron-poor **1i** as the substrate. For reasons difficult to

rationalize, the reaction was less efficient for *N*-allenyl-*N*-propylbenzamide (**1m**). In addition to allenamides, *N*-allenylcarbamates react smoothly under the optimized conditions (compounds **2n-o**). Importantly, Evans oxazolidinone derivative **2o** was obtained in good yield. Given that as for all other examples the *E* double bond isomer was obtained with complete selectivity, **2o** could be an interesting substrate for diastereoselective reactions involving the stereodefined enecarbamate moiety.^[143]



Scheme 70 – Cu-catalyzed hydroamination of various allenamides and *N*-allenylcarbamates with morpholine.

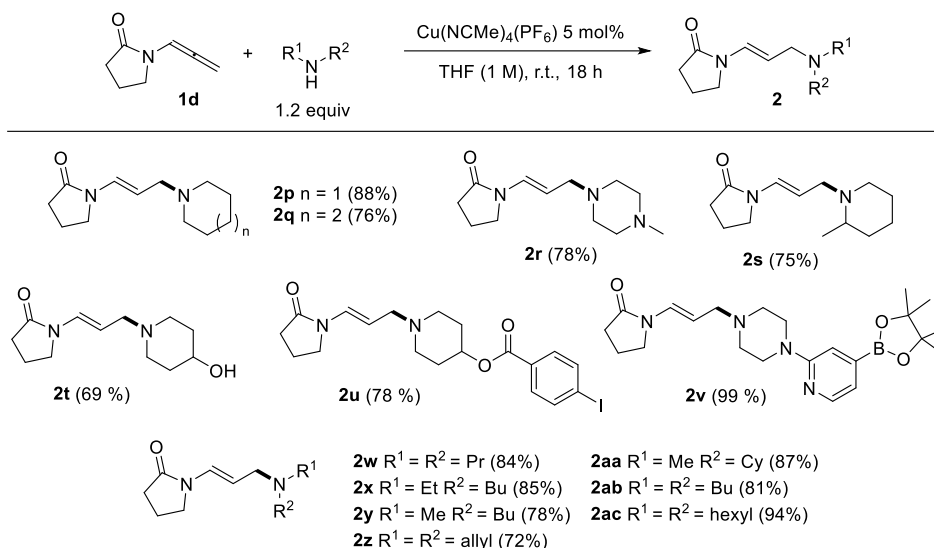
An attempt to use a disubstituted *N*-allenylcarbamate as a substrate had no success. NMR analysis did not allow to identify any trace of the hydroamination product and the starting material decomposed in 48 h at room temperature (Scheme 74).



Scheme 71 – Attempted Cu-catalyzed hydroamination of 13-(buta-1,2-dien-1-yl)oxazolidin-2-one (**1ai**).

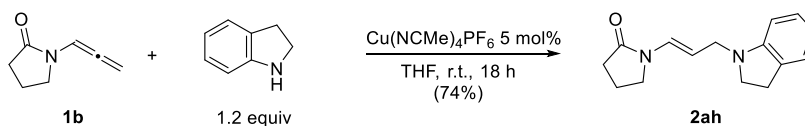
The scope with respect to the amine was also investigated by Remi Blicq in our collaborators' laboratory (Scheme 72). A variety of secondary amines are suitable substrates, including open-chain aliphatic amines and sterically hindered ones (**2s**, **2aa**) that are not very reactive under the conditions they described previously for the hydroamination of simple allenes.^[80] These mild reaction conditions also tolerate several functional groups, such as bromo (**2h**) and iodo (**2u**) substituents, unprotected OH groups (**2t**) and boronic esters (**2v**), which can be employed in subsequent transformations. Importantly, a pharmaceutically relevant pyridine ring does not hamper reactivity (**2v**). Unfortunately, primary aliphatic and aromatic amines were

not suitable substrates for the transformation under study. No conversion was observed at room temperature and heating caused only decomposition of the allene. This is rather surprising, as primary anilines are viable substrates for the hydroamination of simple allenes originally described by our collaborators (Scheme 40).^[80]



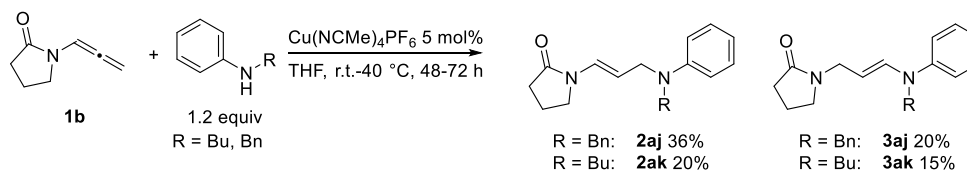
Scheme 72 – Cu-catalyzed hydroamination of *N*-allenyl-2-pyrrolidinone with different amines.

Secondary aromatic/aliphatic amines, however, in some cases display good reactivity. Indoline can be added to *N*-allenyl-2-pyrrolidinone in the usual conditions, giving the expected product in 74% yield (Scheme 73).



Scheme 73 – Cu-catalyzed hydroamination of allenamide **1b** with indoline.

Unfortunately, this reaction could not be generalized to open-chain *N*-alkylanilines. *N*-butylaniline and *N*-benzylaniline were not very reactive at room temperature, upon heating to 40 °C they gave mixtures of the expected product and of the isomeric enamine deriving from double bond migration. Given those disappointing results, this transformation has not been investigated further.



Scheme 74 – Cu-catalyzed hydroamination of allenamide **1b** with *N*-butyl- and *N*-benzylaniline.

2.4. Application of the hydroamination to the synthesis of an API – P-3374

Enamides, which are produced by the hydroamination of allenamides we described in the previous section, are useful synthetic intermediates. Electrophilic additions to the double bond, nucleophilic additions to the amide, radical and metal-mediated reactions, cycloadditions and various heterocycle-forming reactions have been described.^[143] Perhaps the simplest reaction involving enamides is protonation of the double bond, which generates a very reactive *N*-acylated iminium ions.^[144] These species can be trapped by a suitable nucleophile, such as tethered electron-rich aromatic moieties. If cyclization gives a six-membered ring, this is a variant of the well-known Pictet-Spengler reaction.

In this respect, the 1-aminoethyl-(1,2,3,4)-tetrahydroisoquinoline and 1-aminoethyl-(1,2,3,4)-tetrahydro-9*H*- β -carboline skeletons should be accessible by Pictet-Spengler type cyclization of suitable allenamide hydroamination products. These structural motifs occur in a variety of biologically active molecules, such as the marine alkaloids Tarennine^[145,146] and Keramamine C^[147,148] and some experimental APIs^[149,150] (Figure 11). As a proof of concept, we prepared *O*- and *N*-protected P-3374 (**6**), a drug candidate that has been investigated as a vasodilator useful for the treatment of some vascular ailments.^[149]

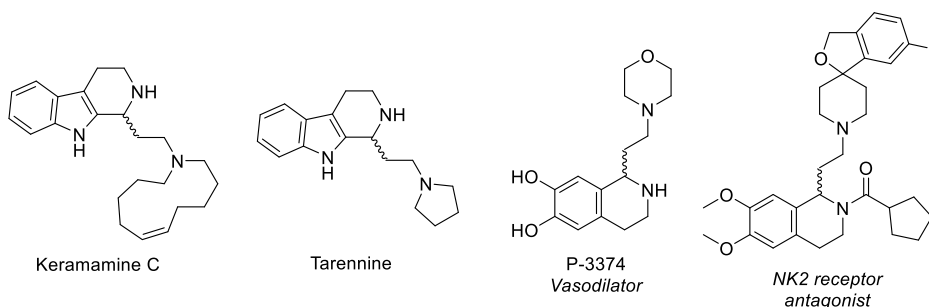
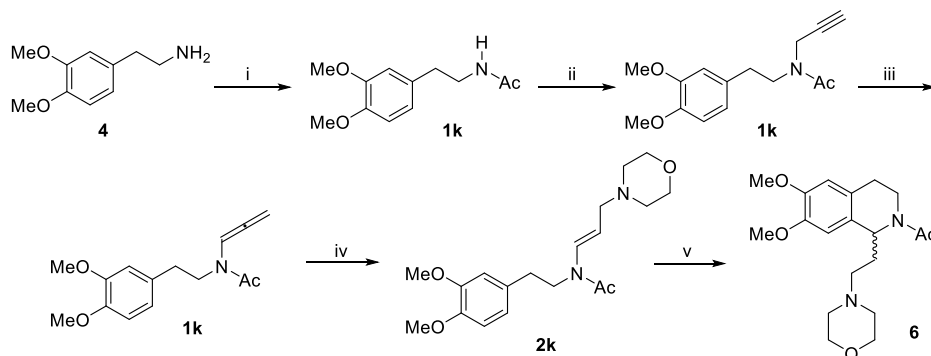


Figure 11 – Natural products and experimental APIs containing the 1-aminoethyl-(1,2,3,4)-tetrahydroisoquinoline and 1-aminoethyl-(1,2,3,4)-tetrahydro-9*H*- β -carboline skeleton.^[145,146,149,150]

Briefly, commercially available homoveratrylamine (**4**) was acetylated with Ac₂O. Normally secondary amides can be *N*-propargylated by deprotonation with NaH and reaction with propargyl bromide. This protocol worked for the preparation of all the starting materials for the synthesis of allenamides **2b**, **2f-k**, **2n-o** (see the experimental section of this chapter), but it invariably failed when it was applied to substrate **4** for reasons that are not clear to us; despite various attempts of solvent optimization (THF, dioxane, 1,2-dimethoxyethane, DMF were tried), no useful amounts of **5** were obtained. However, deprotonation with BuLi at –18 °C followed by treatment with propargyl bromide gave the *N*-propargylamide **5** in 76% yield, which was readily isomerized to allenamide **1k** by treatment with *t*BuOK in THF (72% yield).^[141,151–156] The latter protocol is indeed quite convenient and general for the preparation of allenamides.^{xv}

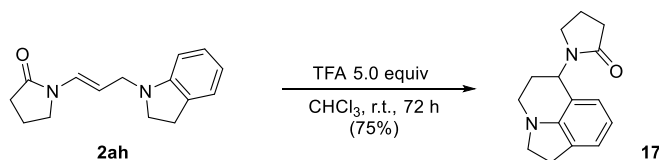
^{xv} It has been shown by DFT calculations that often allenamides are more thermodynamically stable than the isomeric *N*-propargylamides and ynamides, so this reaction corresponds to equilibration *via* deprotonation/protonation.^[174]

Hydroamination with morpholine under our optimized conditions proceeded in a satisfactory 63% yield. The synthesis was concluded by TFA-mediated Pictet-Spengler cyclization that yielded *O*- and *N*-protected P-3374 (**6**) in 90% yield. Compound **6** was thus obtained in overall 31% yield over five steps.



Scheme 75 – Synthesis of *O*- and *N*-protected P-3374. Conditions: i) Ac_2O , Δ (98%); ii) 1- BuLi, THF, $-18\text{ }^\circ\text{C}$, 2- propargyl bromide 1.5 equiv, $-18\text{ }^\circ\text{C}$ to r.t., overnight (76%); iii) *t*BuOK 20 mol%, THF, r.t., 1 min (73%); iv) morpholine 1.2 equiv, $\text{Cu}(\text{NCMe})_4\text{PF}_6$ 5 mol%, THF, r.t., 72 h (63%); v) TFA 5.0 equiv, CH_2Cl_2 , r.t., 5 h (90%).

The indoline-derived hydroamination product **2ah** underwent a TFA-promoted Pictet-Spengler-type cyclization similar to that used for the construction of the carbon skeleton of P-3374 giving an interesting derivative of 1,2,5,6-tetrahydro-4*H*-pyrroloquinoline in 75% yield (Scheme 76).



Scheme 76 – TFA-promoted cyclization of compound **2ah**.

2.5. Mechanistic insight into the hydroamination of allenamides

After having established an efficient protocol for the hydroamination of allenamides under mild conditions, we turned our attention to the detailed mechanism of this transformation, with the aim to make comparisons with the hydroamination of phenylallene we studied previously.

We have already shown (Table 3 and Scheme 62) that *N*-allenyl-2-pyrrolidinone (**1b**), as a representative allenamide, has greater affinity for cationic copper(I) than phenylallene (**1a**) and cyclonona-1,2-diene (**1c**). Under the hypothesis that the mechanism of the hydroamination of these substrates is similar to that we have proposed for phenylallene (**1a**), the transition states corresponding to the *anti-periplanar* attack of the amine nucleophile to the allene/copper complex have been located at the DFT level of theory (Figure 12). The carbonyl oxygen of the enamide moiety plays an important role in the energetics of these transition states. Transition state **TS3b**, in which the amide oxygen coordinates copper (O-Cu distance: 2.22 Å) while the nucleophilic

attack of morpholine takes place, is 3.9 kcal mol⁻¹ more stable than its conformer **TS3a**, for which this interaction is not possible. This oxygen atom can also engage in a hydrogen-bond with the incoming amine (O-H distance: 1.95 Å), provided that the attack of morpholine is such that the product is the *E* vinylcopper intermediate (**TS3c**). This transition state is predicted to be almost as stable as **TS3a**, but significantly less than **TS3b**, and it would lead to the *Z* enamide, which is not observed experimentally. **TS3d**, which in the end also gives the *Z* enamide after *syn-periplanar* attack is decidedly more endergonic than all the others are.

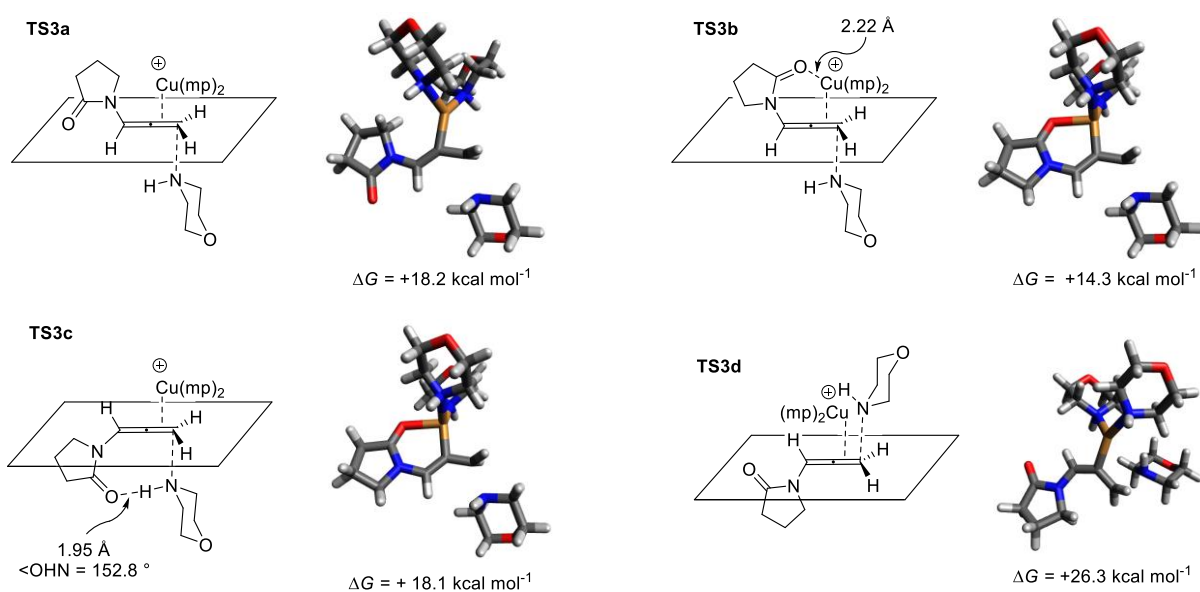


Figure 12 – Transition states for the nucleophilic attack of mp on Cu-coordinated allenamide **1b**. Reported figures are computed Gibbs free energies at 298 K with respect to non-interacting [Cu(mp)₂]⁺, mp and **1b**.

The overwhelming stability of **TS3b** with respect to all the other transition states accounts for the complete *E* stereoselectivity of the transformation. This transition state, indeed, leads to a *Z* alkenylcopper intermediate, which after stereospecific hydrolysis gives the *E* enamide. The whole reaction pathway passing through **TS3b** has been studied computationally (Figure 13). The picture is similar to that reported for the hydroamination of phenylallene (**1a**, Figure 8), but the energetics are different because of the different electronic properties of the allenamide and the ability to coordinate Cu(I) through the amide oxygen. Complexation of the [Cu(mp)₂]⁺ moiety with **1b** is exergonic ($\Delta G = -6.6$ kcal mol⁻¹) and gives intermediate **I7**, which can associate with a further molecule of morpholine, yielding **I8** ($\Delta G = +1.1$ kcal mol⁻¹). Addition of mp to the double bond takes place *via* **TS3b** ($\Delta G^\ddagger = +19.8$ kcal mol⁻¹) and gives the *N*-protonated alkenylcopper intermediate **I9** ($\Delta G = +16.5$ kcal mol⁻¹). Deprotonation of **I9** by an external mp molecule leading to **I10** is favorable ($\Delta G = -3.0$ kcal mol⁻¹). The morpholinium ion carries out the exergonic ($\Delta G = -27.3$ kcal mol⁻¹), essentially barrierless ($\Delta G^\ddagger = +0.6$ kcal mol⁻¹), stereoconservative protodecupration *via* **TS4**, which results in **I11**. Dissociation from copper and

conversion of the intermediate **I12** so formed to a more stable rotamer **I13** deliver the final product **2b** and regenerates the catalyst.

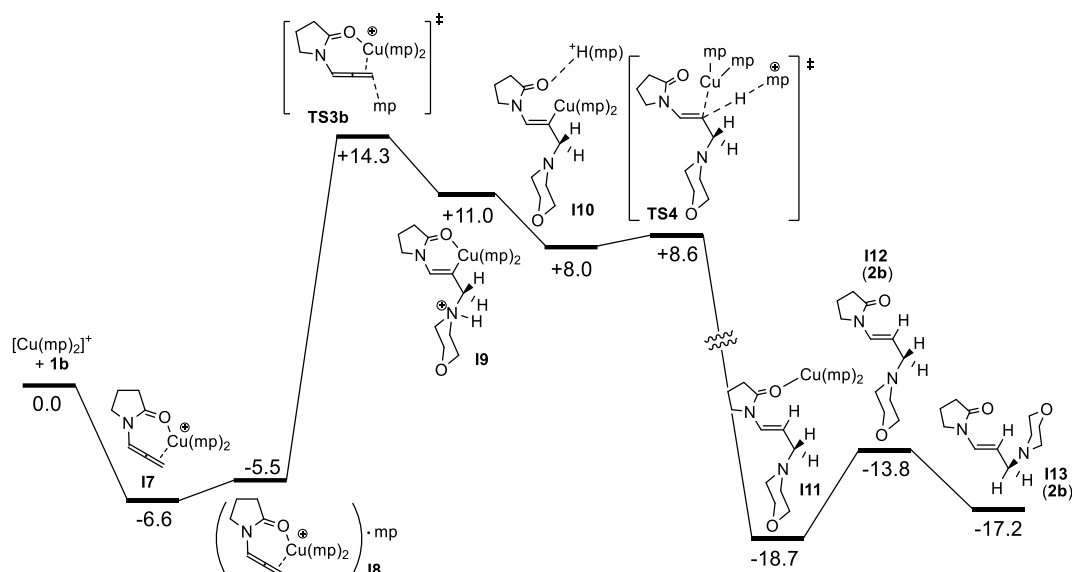


Figure 13 – Reaction pathway for the Cu-catalyzed hydroamination of *N*-allenyl-2-pyrrolidinone (**1b**) with morpholine. Reported numbers are computed relative Gibbs free energies in kcal mol⁻¹ at 298 K.

The main geometrical features of **TS3b** are very similar to that of **TS1a** (Figure 14), the main differences being that the forming C-N bond is shorter (2.00 Å, *i.e.* the transition state is more product-like) and that less positive charge is accumulated on the γ allenic carbon (NBO charge difference for **I7** \rightarrow **TS3b** is +0.267, *i.e.* about 10% less than for **I1** \rightarrow **TS1a**). It is worth noting that the forming C-N bond lies approximately in the same plane as the $C_\alpha=C_\beta$ moiety, so that overlap between the π system encompassing C_α and C_β and the σ orbital associated with the forming bond is poor, compatibly with the relatively modest charge stabilization observed.

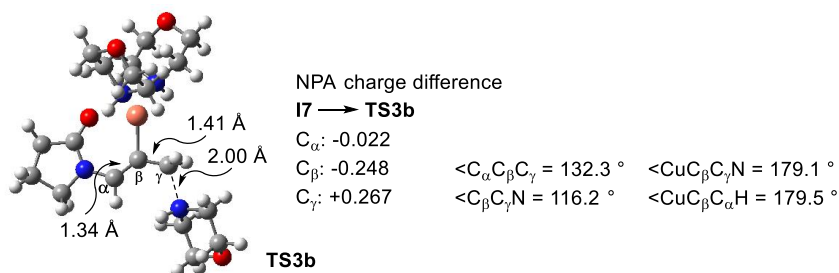


Figure 14 – Tridimensional structure, selected geometric parameters and charge analysis for **TS3b**. Charges are reported in units of |e⁻|.

In order to complement the theoretical predictions, the kinetics of the reactions were studied experimentally (Figure 15).^{xvi} The disappearance of the ¹H-NMR resonance of H $_\alpha$ of the

^{xvi} Even if for synthetic purposes the reaction is most efficiently carried out in THF as a solvent, NMR spectra are better resolved if dioxane is used instead, therefore this solvent has been selected for NMR

starting material **1b** and the appearance of the signal for H $_{\beta}$ of the product **2b** could be easily monitored. The kinetics fitted first-order rate laws when mp was used in excess and apparent first-order rate constants k_{app} could then be obtained (Figure 15A). The reaction is first order with respect to the allenamide substrate **1b** and first order with respect to the catalyst (Figure 15c), so at a fixed excess of mp:

$$\frac{d[\mathbf{2b}]}{dt} = k_{\text{app}} [\mathbf{1b}] \quad k_{\text{app}} = k'[\text{Cu}^+]$$

The formation of dimeric or higher-order polymetallic species is thus not to be expected. The dependence of pseudo-first order rate constants k_{app} on the concentration of mp is more complex (Figure 15B). At low concentrations (< 0.75 M), k_{app} increases with the concentration of mp, until it reaches a maximum around [mp] = 0.75 M. At higher concentrations, k_{app} decreases slightly with [mp]. This bell-shaped curve can be interpreted qualitatively by considering that the reaction should be first-order with respect to mp, assuming an outer-sphere attack of the nucleophile in agreement with DFT calculations. However, mp displaces the allene from the catalyst, thus inhibiting the reaction. The fact that the curve in Figure 15B is not a simple hyperbolic rise to a maximum, as expected if morpholine behaved as a typical competitive inhibitor, suggests that mp intervenes also in a different way in the equilibria involving the catalyst. For instance, the decrease of the observed rate at high [mp] is consistent with the formation of higher-coordinated copper species. Although the analytical derivation of rate equations under the usual assumptions of Michaelis-Menten enzyme kinetics is feasible, several higher-order equilibria are plausible; for instance mp can form homoleptic Cu(mp) $_n$ species, but also [(**1b**) Cu(mp) $_n$] heteroleptic complexes. All the schemes involving higher-coordinate species give a qualitatively similar picture in which the rate decreases at high [mp], thus quantitative modelling of the curve presented in Figure 15B has not been possible.

With the aim to confirm our initial assumption about the polarity of the transition state for the hydroamination reaction, *i.e.* that positive charge is built up and stabilized by the allenamide nitrogen atom, we performed a Hammett study on *para*-substituted *N*-allenylacetanilides **1f-i**. When these compounds were reacted with excess mp (10 equiv), pseudo-first order kinetics were observed (Figure 16) and the apparent rate constants showed excellent correlation with Hammett's σ_p parameters (Figure 17).^[157] In agreement with our hypothesis, electron-rich substrates react faster than electron-poor ones, giving a negative ρ parameter ($\rho = -0.336$, Figure 17).

kinetic studies. For consistency, all theoretical calculations have been carried out by simulating dioxane with the PCM solvation model.

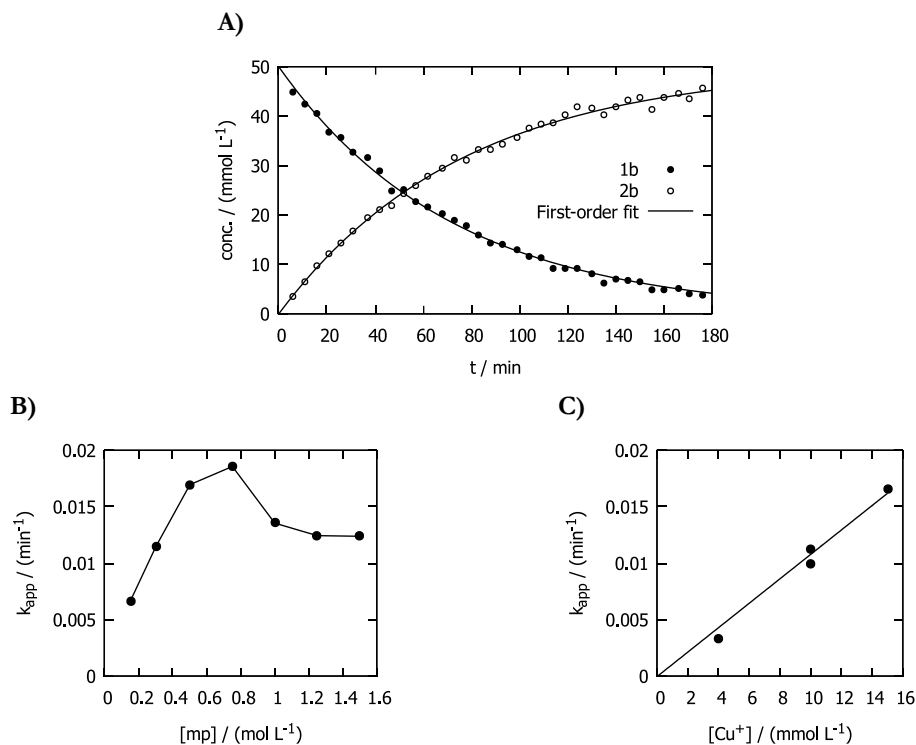


Figure 15 – Kinetics of the reaction between *N*-allenyl-2-pyrrolidinone (**1b**, 50 mM in dioxane) at 25 °C catalyzed by $\text{Cu}(\text{NCMe})_4\text{PF}_6$, as followed by ¹H-NMR spectroscopy, under different conditions: A) With mp (20 equiv) and 20 mol% catalyst loading. The concentration of starting material **1b** and product **2b** are reported, together with first-order rate equation fitting. B) With varying amounts of mp and 20 mol% catalyst loading. The dependence of the apparent first-order rate constant on [mp] is shown. C) With mp (12.5 equiv) and varying amounts of catalyst. The apparent first-order rate constant is reported as a function of the concentration of the catalyst itself.

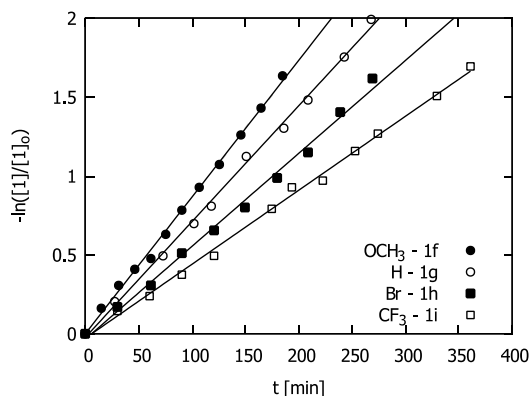


Figure 16 – Kinetic data for the hydroamination of allenamides **1f-i** (0.50 M in THF) with morpholine (10 equiv) catalyzed by $\text{Cu}(\text{NCMe})_4\text{PF}_6$ (20 mol%) at 20 °C, as followed by ¹H NMR spectroscopy. The slopes of the linear regression lines in this semilogarithmic plot give the apparent first-order kinetic constants.

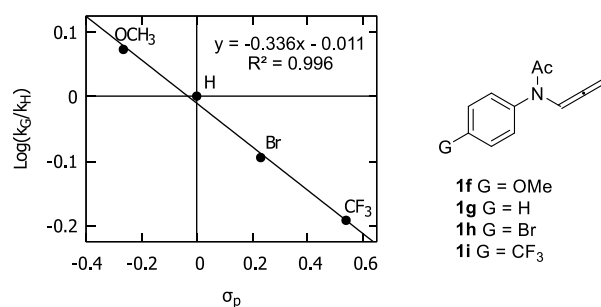


Figure 17 – Hammett plot for the hydroamination of *para*-substituted *N*-allenylacetanilides **1f-i** (conditions: mp 10 equiv, Cu(NCMe)₄PF₆ 20 mol%, THF, 20 °C, initial concentration of **1**: 0.5 M).

The structures of the transition states **TSSf-i** for the hydroamination of allenamides **1f-i** have been optimized at the DFT level,^{xvii} taking into account the same conformation of the lowest-energy transition state for the hydroamination of **2b**, i.e. **TS3b**. The relative transition state enthalpies (with respect to **1f-i** and [Cu(mp)₂]) have been computed and plotted against Hammett's σ_p parameters. The computed figures were in qualitative agreement with the experimentally observed reactivity trend and approximately fitted a straight line (Figure 18).

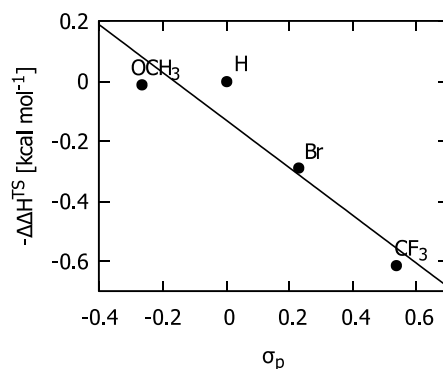


Figure 18 – Hammett plot for the hydroamination of allenamides **1f-i**, according to DFT modeling. The opposite of calculated activation enthalpies with respect to free **1f-i** and [Cu(mp)₂] are reported as a function of Hammett's σ_p parameters, after subtracting the value for the unsubstituted substrate **1g** ($\Delta\Delta H^{TS}$).

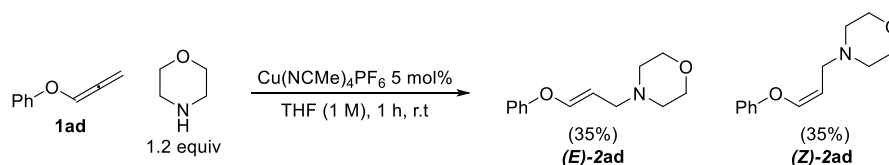
^{xvii} For consistence with the experiments, THF instead of dioxane was simulated by the PCM model, differently from all the previous calculations presented in this chapter.

2.6. Extension to allenyl ethers

To the best of our knowledge, no general protocol has been reported in the literature for the hydroamination of alkoxyallenes having selectivity for addition of nitrogen to the terminal allene carbon, thus delivering 3-alkoxyallylamines.^{xviii} Several palladium-based catalysts are effective for the addition to the internal double bond of allenylethers, giving O,N mixed acetals having a terminal double bond (see for example Scheme 37).^[71–77]

A copper-catalyzed hydroamination of allenyl ethers would have not only a synthetic interest, but it would also give mechanistic information about the mechanism of copper-catalyzed hydroamination in general. Indeed, allenyl ethers are electron-rich allenes featuring no additional coordination points for the metal and would allow to differentiate the effects due to chelation we have verified for allenamides from purely electronic effects due to substitution of the allene with a heteroatom.

With this idea in mind, we have tested phenoxyallene (**1ad**) as a representative allenylether. This compound, indeed, proved to be even more reactive than allenamides. Its reaction with morpholine under the conditions we optimized for allenamides was complete in less than 1 h at room temperature (Scheme 77). Unexpectedly, the reaction was not stereoselective, and the *E* and *Z* vinyl ether products [(*E*)-**2ad** and (*Z*)-**2ad**] formed in 1:1 ratio (Scheme 77).



Scheme 77 – Hydroamination of phenoxyallene (**1ad**) with morpholine. Yields were determined by ¹H NMR analysis of the crude reaction mixture.

To understand this unexpected result, we resorted again to DFT calculations. Inspection of the structures of the computed transition states **TS5a-b** for the formation of the two possible stereoisomeric vinyl-copper intermediates, which are practically isoenergetic ($\Delta\Delta G = 0.6$ kcal mol⁻¹), reveals the existence of two key-hydrogen bonds between mp and the allene oxygen (Figure 19). If the copper center is in the same half space of the OPh group with respect to the plane containing the C=CH₂ moiety (**TS5a**) a hydrogen bond can be established between one of the morpholine molecules coordinated to the metal center. In the other case, *i.e.* when the OPh group lies at the opposite side of copper with respect to the same plane (**TS5b**), a hydrogen bond interaction exist between the incoming morpholine molecule and the oxygen atom.

^{xviii} A single example of palladium-catalyzed addition of a sulfonamide to methoxyallene having this regioselectivity has been reported.^[71]

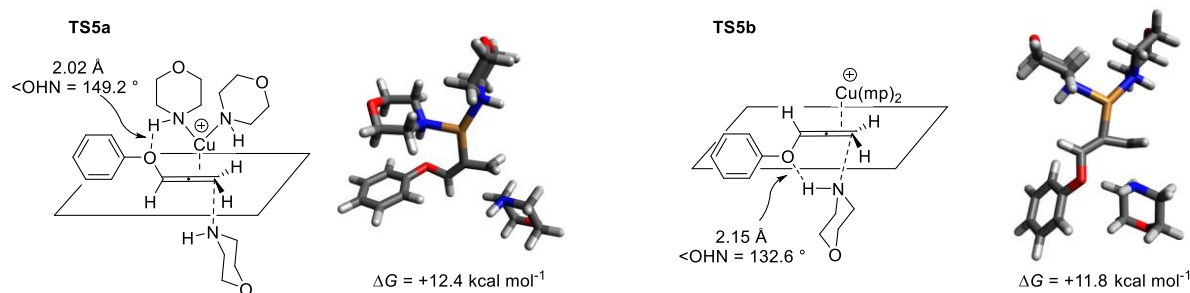


Figure 19 – Computed transition states for the attack of mp on Cu-coordinated allenamide **1ad**.

The ether function can act as a better electron density donor than the allenamide. NBO charge analysis shows that the accumulation of positive charge on the γ carbon passing from the intermediate π complex [(**1ad**)Cu(mp)₂] (**I14** for **5a** and **I15** for **5b**) to **TS5a-b** is less than for **I1** \rightarrow **TS1a** (–13% and –29% for **TS5a** and **TS5b**, respectively) and also less than for **I7** \rightarrow **TS3b** (–6% and –22% for **TS5a** and **TS5b**, respectively). Selected geometric parameters for **TS5a-b** are given in Figure 20. The variation of NPA charges with respect to the parent complexes [(**1ad**)Cu(mp)₂] (**I14** and **I15**) are also reported.

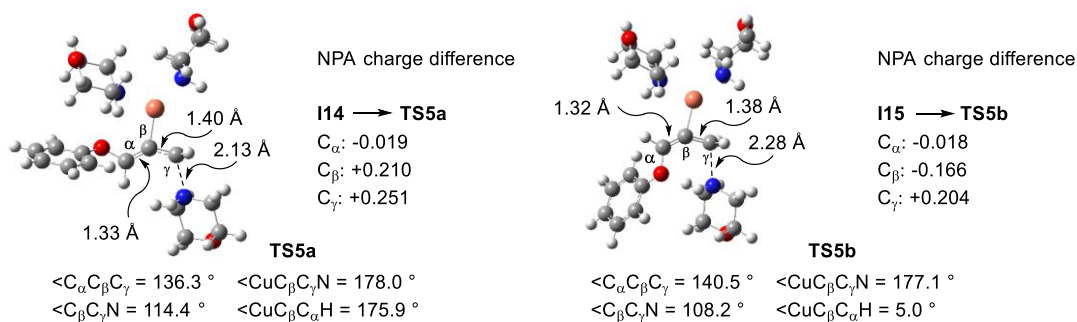
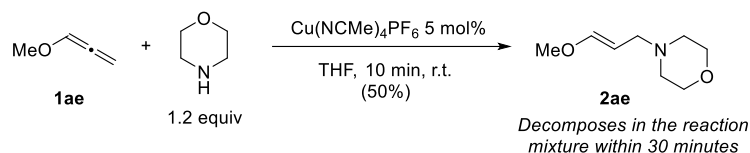


Figure 20 – Selected geometric and parameters for **TS5a-b**. NPA charge difference between **TS5a-b** and their parent allene-catalyst complexes (**I14** and **I15** respectively) are also shown (in units of $|e^{-}|$).

As it is apparent from this latter example, a subtle interplay of sterics, electronic effects and secondary interactions – either with the catalyst or with the incoming nucleophile – tunes the reactivity or governs the selectivity of the Cu-catalyzed hydroamination of heteroatom-substituted allenes.

The reaction we observed for phenoxyallene (**1ad**) was not easily extended to other alkoxyallenes. When methoxyallene (**1ae**) was subjected to the standard reaction conditions we have established, *in situ* NMR analysis demonstrated that after about 10 minutes at room temperature the expected hydroamination product was formed with complete apparent

selectivity for the *E* isomer **2ae** (Scheme 78).^{xix} However, when the reaction mixture was left 20 minutes more at room temperature, the reaction mixture gradually darkened, a resinous precipitate was formed and the characteristic resonances of **2ae** disappeared from the NMR spectrum.



Scheme 78 – Attempted hydroamination of methoxyallene (**1ae**). NMR yield reported.

Benzyloxyallene (**1af**, Figure 21) behaved slightly differently. Its copper-catalyzed reaction with morpholine was slower than that of compound **1ae** under the same experimental conditions. After approximately 10 minutes, 90% of the starting material was still unreacted, but after 2 h complete conversion was achieved. After aqueous work-up, benzyl alcohol was the only identifiable product.

1-(1-(Benzyloxy)allenyl)cyclohexan-1-ol (**1ag**, Figure 21), readily obtained by lithiation of benzyloxyallene with BuLi and addition of the lithium derivative so formed to cyclohexanone, was unreactive towards copper-catalyzed hydroamination under our standard conditions. No conversion was achieved after several days at room temperature, and heating to 50 °C caused only decomposition of the starting material without formation of the hydroamination product, as assessed by ¹H NMR spectroscopy.

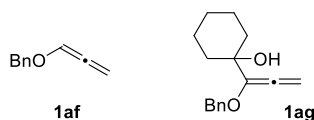


Figure 21 – Unsuitable substrates for the Cu-catalyzed hydroamination reaction.

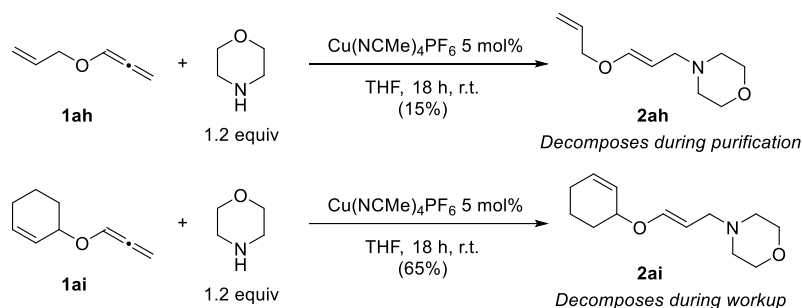
Allyl allenyl ethers were then investigated as substrates. The introduction of an allyl group was attempted for two reasons: 1) it might be able to promote the reaction by offering a second coordination point for the metal catalyst, *i.e.* the double bond can serve as a π ligand for cationic copper(I) (*vide infra*); 2) a hydroamination/[3,3]-sigmatropic rearrangement (Claisen rearrangement) sequence giving access to α -allyl- β -aminoaldehydes was conceivable (Scheme 79).



Scheme 79 – Hypothetical hydroamination / Claisen rearrangement sequence.

^{xix} Compound **2ae** was characterized *in situ* by observation of its characteristic NMR resonances. ¹H NMR (300 MHz, THF): δ = 6.18 (d, J = 13.7 Hz, 1H), 4.62 (dt, J = 13.7, 7.3 Hz, 1H), 3.11 (d, J = 7.3 Hz, 2H) ppm.

Unsubstituted allyloxyallene (**1ah**, Scheme 80) gave the expected *E* hydroamination product in low (about 15%) NMR yield,^{xx} and no pure material could be obtained by chromatographic separation, since even by using carefully neutralized silica gel decomposition of this sensitive compound took place. Cyclohexen-2-yloxyallene (**1ai**, Scheme 80) also underwent hydroamination yielding the linear *E* vinyl ether. NMR analysis showed that **2ai** formed in approximately 65% yield, but the product could not withstand aqueous workup, even under slightly alkaline conditions (NaHCO₃ solution).^{xxi}



Scheme 80 – Hydroamination of two allyloxyallenes. Yields determined by ¹H NMR analysis of the crude reaction mixture are reported.

Given the experimental difficulties encountered and the poor stability of the products, we did not investigate further the hydroamination of allenyl ethers.

2.7. Extension to *N*-allenylazoles

As we elucidated in the previous paragraphs, allenamides are very successful substrate for the copper-catalyzed hydroamination reaction also because the oxygen atom of the amide function can act as an *innate* metal directing group, thus enhancing affinity of the substrate for the metal center and promoting reactivity.

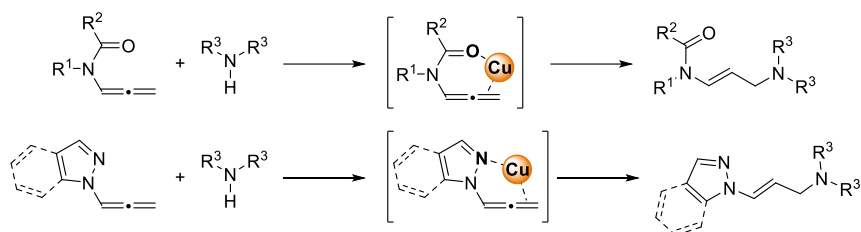
With this idea in mind, we tried to figure out what other class of readily available allene derivatives could also have a *built-in* metal coordinating functional group which would be able to assure enhanced reactivity. A literature search revealed that *N*-allenyl-1,2-azoles are readily available substances, as most of them can be obtained by base-catalyzed isomerization of the corresponding *N*-propargylazoles.^{xxii} These compounds were promising substrates, as the

^{xx} Compound **2ah** was characterized in the crude reaction mixture by observation of its characteristic NMR resonances. ¹H NMR (300 MHz, CDCl₃): δ = 6.36 (d, *J* = 12.6 Hz, 1H), 5.92 (ddd, *J* = 17.3, 10.7, 5.4 Hz, 1H), 5.31 (dq, *J* = 17.3, 1.5 Hz, 1H), 5.22 (dq, *J* = 10.5, 1.5 Hz, 1H), 4.84 (dt, *J* = 12.6, 7.3 Hz, 1H), 4.22 (dt, *J* = 5.4, 1.5 Hz, 2H), 2.88 (d, *J* = 7.3 Hz, 2H) ppm.

^{xxi} Compound **2ai** was identified *in situ* by observation of its NMR signature resonances. ¹H NMR (300 MHz, THF): δ = 5.90 (d, *J* = 14.0 Hz, 1H), 4.34 (dt, *J* = 14.0, 7.2 Hz, 1H), 2.83 (d, *J* = 7.2 Hz, 2H) ppm.

^{xxii} To the best of our knowledge, no systematic study on these isomerizations has ever been performed. However, the syntheses of numerous *N*-allenylazoles have appeared from time to time in the literature.

pyridine-like nitrogen atom could easily serve as an additional coordination point for the catalyst (Scheme 81).

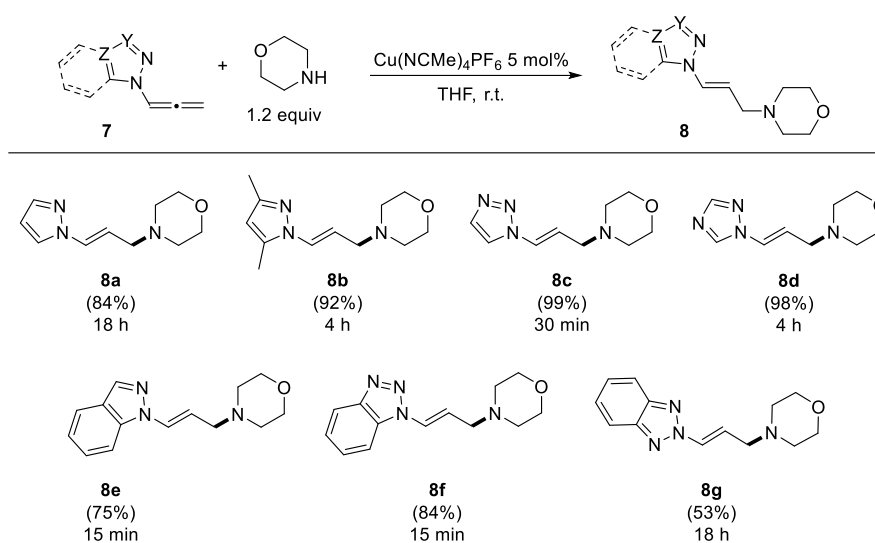


Scheme 81 – Allenamides and *N*-allenyl-1,2-azoles as substrates having *innate directing groups* for the copper-catalyzed hydroamination reaction.

When the experimental conditions we optimized for the hydroamination of allenamides were applied to 1-allenyl-1*H*-benzotriazole (**7f**), we were pleased to find out that the expected hydroamination product (**8f**) was obtained in 84% yield in less than 15 minutes of reaction time at room temperature. As for allenamides, complete selectivity for the *E* linear addition product was observed. Several other *N*-allenyl-1,2-azoles and their benzofused congeners underwent addition of morpholine in excellent yields under these smooth conditions (Scheme 82): *N*-allenylpyrazoles (**8a-b**), 1,2,3-triazole (**8c**), 1,2,4-triazole (**8d**), 1*H*-indazole (**8e**), and 2*H*-benzotriazole (**8f**). The reaction times required to obtain complete conversion of the starting material (as judged by ¹H NMR spectroscopy) varied between a few minutes (**8e** and **8f**) to several hours (**8a,b,d**), but all the reaction could be performed at room temperature.

In collaboration with Remi Blicq, PhD candidate working in the Ecole Nationale Supérieure de Chimie de Montpellier under the supervision of Florian Monnier, the scope of this reaction with respect to the amine coupling partner was also investigated (Table 6). A variety of secondary amines are suitable substrates, including open-chain aliphatic amines and sterically hindered 2-methylpiperidine (**8r**) and *N*-methylcyclohexylamine (**8j**, **8m**, **8p**, **8aa**). Diallylamine can also be employed (**8z**). As for the hydroamination of allenamides described previously, no reaction took place when primary amines were used as substrates.

The ease of this isomerization process, as well as the most suitable base to accomplish it and the stability of the product are highly dependent on the nature of the azole itself. The syntheses of all the *N*-allenylazoles employed in the experiments here described are reported in detail in the experimental section of present chapter.



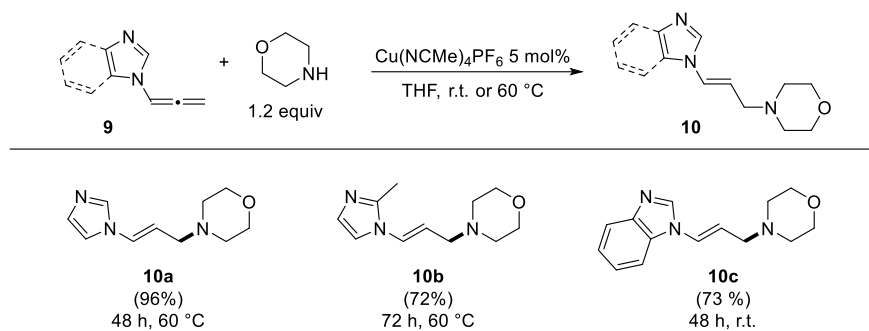
Scheme 82 – Copper-catalyzed hydroamination of *N*-allenyl-1,2-azoles and their benzofused congeners. For each compound, the reaction time is given.

Table 6 – Cu-catalyzed hydroamination of *N*-allenylazoles with various amines.

Structure		R ¹	R ²	Reaction time (h)	Yield (%)
	8h	–(CH ₂) ₅ –		18	76
	8i	Pr	Pr	18	73
	8j	Cy	Me	18	66
	8k	–(CH ₂) ₅ –		4	93
	8l	Pr	Pr	4	95
	8m	Cy	Me	4	91
	8n	–(CH ₂) ₅ –		4	84
	8o	Pr	Pr	4	80
	8p	Cy	Me	4	77
	8q	–(CH ₂) ₅ –		4	80
	8r	–(CHCH ₃)(CH ₂) ₄ –		4	73
	8s	–(CH ₂) ₂ (NCH ₃)(CH ₂) ₂ –		4	86
	8t	–(CH ₂) ₆ –		4	75
	8u	Pr	Pr	4	74
	8v	Hexyl	Hexyl	4	68
	8w	Bu	Et	4	79
	8x	Bu	Me	4	71
	8y	Bu	Bu	4	68
	8z	Allyl	Allyl	4	73
	8aa	Cy	Me	4	78

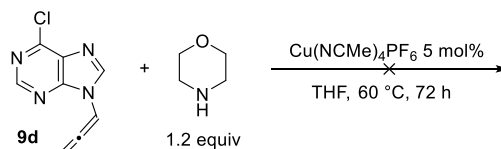
In a second set of experiments, we decided to extend the methodology to *N*-allenyl-(1,3)-azoles and their benzo-fused analogues (Scheme 83), unable to provide anchimeric assistance (Scheme 81). Within this class of substrates, the reactivity is strikingly variable. When *N*-allenylbenzimidazole **9c** was reacted with morpholine under the standard conditions we established, it took an extended reaction time (72 h) at room temperature to obtain the desired

product **10c** in 73% yield. On the other hand, *N*-allenylimidazoles **9a** and **9b** are significantly less reactive. Almost no reaction took place at room temperature and heating the reaction mixture at 60 °C for 48-72 h was needed to obtain the corresponding products **10b** and **10c**. Irrespective of reaction rate, yields were good to excellent (Scheme 83).



Scheme 83 – Copper-catalyzed hydroamination of *N*-allenyl-1,2-azoles and their benzofused congeners. For each compound, the reaction time and temperature are given.

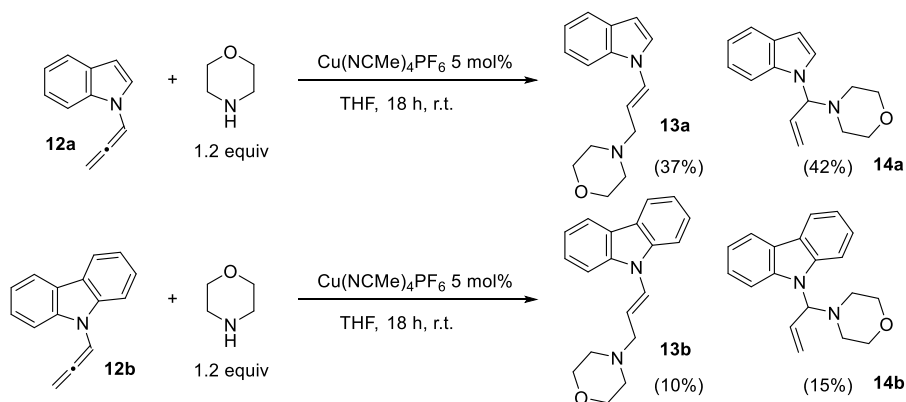
Several other *N*-allenylheterocycles were tested under the optimized conditions. 6-Chloro-9-allenyl-9*H*-purine (**9d**, Scheme 84) did not react even on heating at 60 °C for a prolonged time. This contrasts with the efficient AgF-catalyzed hydroamination of 9-allenyl-9*H*-purines described by Guo as a pathway for the synthesis of non-cyclic nucleoside analogs (Scheme 46). We cannot exclude that this lack of reactivity may be due to the very poor solubility of compound **9d** in THF and in most other common moderately polar organic solvents.



Scheme 84 – Attempted hydroamination of 9-allenyl-6-chloro-9*H*-purine (**9d**).

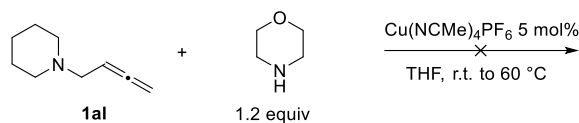
N-Allenylimidole (**12a**) and *N*-allenylcarbazole (**12b**) were also tested as substrates (Scheme 85). Both compounds are rather unstable and polymerize readily at room temperature, and they were obtained by *t*BuOK-catalyzed isomerization of the corresponding *N*-propargyl heteroarenes. Moreover, if extremely short reaction times (< 5 minutes at room temperature) were not used, attempted isomerization of *N*-propargylcarbazole proceeded further towards the isomeric ynamide (*N*-(1-propynylcarbazole). Surprisingly, for both **12a** and **12b** the copper-catalyzed hydroamination took place without the regioselectivity that has been observed for all the substrates we examined before, and a mixture of linear (**13**) and branched products (**14**) was obtained. In both cases, the branched product (**14a** and **14b**) was not stable in the reaction

mixture and it decomposed on standing, presumably by formation of iminium ions.^{xxiii} At present, the reasons of this lack of selectivity are not clear to us.



Scheme 85 – Cu-catalyzed hydroamination reaction of *N*-allenylindole and *N*-allenylcarbazole. Reported yields were determined by ^1H NMR spectroscopy of the crude reaction mixture.

Playing on the concept of assistance by neighboring coordinating groups, we thought that readily available^[158] α -dialkylaminoallenes could be good substrates for the hydroamination reaction. Unfortunately this is not the case, as 1-(buta-2,3-dien-1-yl)piperidine (**1a1**) did not react with morpholine under our standard conditions at room temperature and heating to 40-60 °C only resulted in decomposition of the allene (Scheme 86).



Scheme 86 – Attempted Cu-catalyzed hydroamination of 1-(buta-2,3-dien-1-yl)piperidine (**1a1**).

As a concluding remark, we must point out that the alkenylheterocycles obtained by the hydroamination reaction we described may be amenable to further transformations. Most importantly, benzotriazole derivatives are an access point to the great variety of synthetic methods developed by Katritzky and coworkers. For example, 1-alkenyl-1*H*-benzotriazoles can be readily lithiated at the α carbon and reacted with several kinds of electrophiles,^[159] or employed for the synthesis of original heterocyclic scaffold by formation of doubly lithiated derivatives and addition to bifunctional electrophiles.^[160]

^{xxiii} It was not possible to isolate these hydroamination products, they were only characterized *in situ* by observation of their characteristic ^1H NMR peaks. **13a** - ^1H NMR (300 MHz, THF): δ = 5.65 (dt, J = 14.0, 7.0 Hz, 1H), 2.94 (dd, J = 7.0, 1.3 Hz, 2H) ppm. **14a** - ^1H NMR (300 MHz, THF): δ = 5.99 (ddd, J = 17.1, 10.2, 7.0 Hz, 1H), 5.24 (dt, J = 17.1, 1.4 Hz, 1H), 5.11 (dt, J = 10.2, 1.4 Hz, 1H), 5.05 (d, J = 7.0 Hz, 1H) ppm. **13b** - ^1H NMR (300 MHz, THF): δ = 5.60 (dt, J = 14.1, 6.9 Hz, 1H), 2.67 (dd, J = 6.9, 1.3 Hz, 2H) ppm. **14b** - ^1H NMR (300 MHz, THF): δ = 5.82 (ddd, J = 16.9, 10.1, 8.1 Hz, 1H), 4.91 (d, J = 16.9 Hz, 1H), 4.74 (d, J = 8.1 Hz, 1H), 4.65 (d, J = 10.1 Hz, 1H) ppm.

2.8. Mechanistic insight into the copper-catalyzed hydroamination of azoles

From the results presented in the previous section, it is clear that a striking variability in reactivity exists within the class of *N*-allenylazoles, even if all the substrates could under the appropriate conditions. More in detail, 1-allenylazoles featuring a second nitrogen atom at position 2 are more reactive than imidazoles and benzimidazole is more reactive than imidazole (Figure 22).

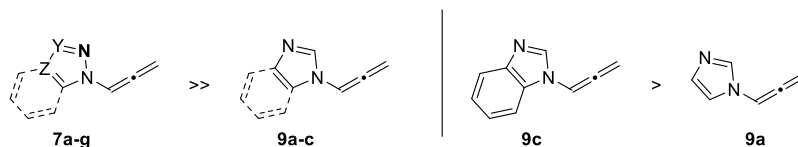


Figure 22 – Reactivity trends in the *N*-allenylazole series towards Cu-catalyzed hydroamination.

In order to explain these trends and confirm our initial working hypothesis on the role of the second N atom as an additional coordination site for the catalyst, we resorted to DFT studies. Four model substrates were chosen (Figure 23): *N*-allenyl-1*H*-pyrazole (**7a**), *N*-allenyl-1*H*-imidazole (**9a**), *N*-allenyl-1*H*-indazole (**7e**), *N*-allenyl-1*H*-benzimidazole (**9c**). Compounds **7a** and **7e** are representative of 1,2-azoles, **9a** and **9c** of 1,3-azoles; **7e** and **9c** are benzo-fused, while **7a** and **9a** are not.

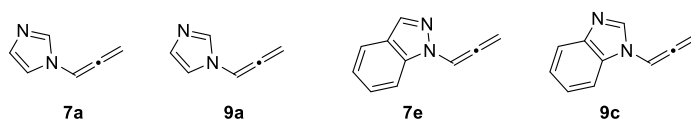


Figure 23 – Model substrates chosen for DFT studies.

Consistently with what we have demonstrated in our previous study concerning the hydroamination of allenamides, we assumed that the reaction takes place by a rate-limiting anti-periplanar attack (with respect to copper) of the amine on the cationic allene/Cu(I) complex. This process leads to the *Z* alkenylcopper intermediate which in turn gives the *trans* alkene after stereospecific proto-demetalation with retention of configuration. With reference to the heterocyclic moiety, two conformers of the relevant transition state are possible, featuring a *proximal* or a *distal* relationship between Cu and the YZ moiety of the heteroaromatic ring (Figure 24). If Y = N, *i.e.* if the substrate is an 1,2-azole, complexation to the copper center is possible only in the *proximal* configuration, and it can stabilize the transition state, similarly to what happens for the oxygen atom of the amide in the case of allenamides (cf. Scheme 81).

The transition states of the type illustrated in Figure 24 have been located by DFT calculations for all four model compounds (**9a**, **7a**, **9c**, **7e**), so that the relative barrier of the rate-limiting step of the catalytic cycle could be evaluated (Figure 25). From the numbers reported in Figure 25 it is clear that for the 1,2-azoles **7a** and **7e** the *proximal* conformation lies lower in free energy than the *distal* one, while for benzimidazole **9c** this is not the case. By considering the lowest-lying conformation for each compound, 1,3-azoles are correctly predicted to react at a lower rate, and imidazole **9a** is ought to be less reactive than benzimidazole **9c**, in agreement with the experiments.

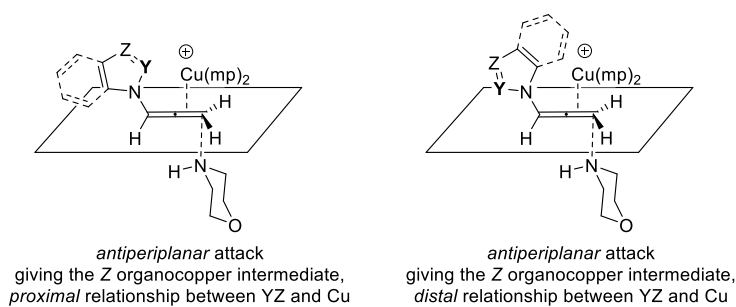


Figure 24 – Schematic representation of two possible conformers of the transition state for the hydroamination of *N*-allenylazoles *via* anti-periplanar attack of the amine on the cationic allene/Cu(I) complex.

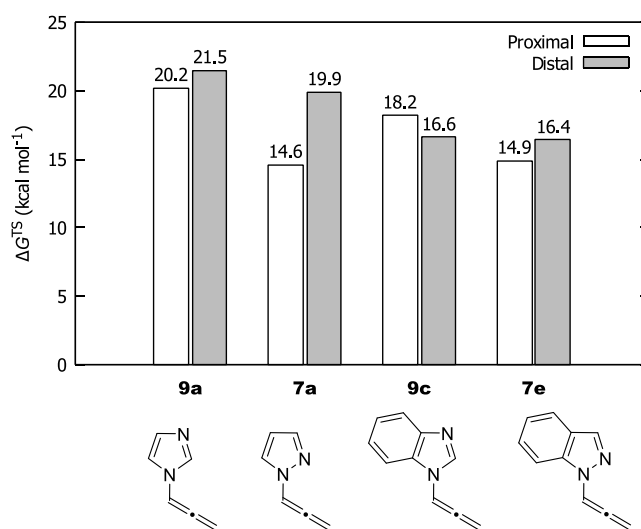


Figure 25 – Energetics of the transition states for the hydroamination of model substrates with morpholine. Gibbs free energies calculated at the DFT level are reported in kcal mol⁻¹ for both proximal and distal conformers (Figure 24), with reference to the uncoordinated allene, morpholine and the complex [Cu(mp)₂]⁺, which have been set to zero.

Inspection of the structures of the transition states confirms the expected coordination of copper by the pyridine-like nitrogen of pyrazole **7a** and indazole **7e**, while this interaction is clearly not possible for imidazole **9a** and benzimidazole **9c**. This interaction not only helps to “bring together” the reactant and the catalyst, increasing the affinity of the allene for copper, but it also has an influence on the structure of the transition state, which was not obvious based on qualitative considerations. The data reported in Table 7 evidence that the C-N interatomic distances associated to the forming bond between morpholine and the terminal carbon atom of the allene. This values can be thought qualitatively as a reaction coordinate: the closer they are to the C-N bond length in the product (1.54 Å in every case), the more appropriate is to consider the transition state product-like (or “late”). From the data in Table 7 it is clear that the *proximal* conformers of the transition state for the hydroamination of 1,2-azoles **7a** and **7e**, in which the secondary interaction with the pyridine-like nitrogen is established, have an enhanced *product-like* character, as the forming C-N bond (2.05–2.06 Å) is shorter than for all the other transition

states considered here (2.19–2.21 Å). These values can be compared also with the corresponding C–N distances of the transition states for the hydroamination of phenylallene (**1a**, 2.14 Å, see Figure 9) and *N*-allenyl-2-pyrrolidinone (**1b**, 2.00 Å, see Figure 14). The Cu–C_β–C_γ angles mirror the trend of C–N bond distances, as they are 109° for the transition states featuring chelation and 92–94° for the others. The tridimensional structures of the transition state for the hydroamination of **7a** and **9a** are reported, with selected bond distances, in Figure 26.

Table 7 – Length of the forming C–N bonds and Cu–C_β–C_γ angles in the transition states for the hydroamination of the model *N*-allenylazoles, as assessed by DFT calculations.

Entry	Substrate	<i>d</i> (C–N) (Å)		∠(Cu–C _β –C _γ) (°)	
		Proximal TS	Distal TS	Proximal TS	Distal TS
1	9a	2.20	2.20	93	92
2	7a	2.05	2.21	109	92
2	9c	2.20	2.20	92	93
4	7e	2.06	2.18	109	94

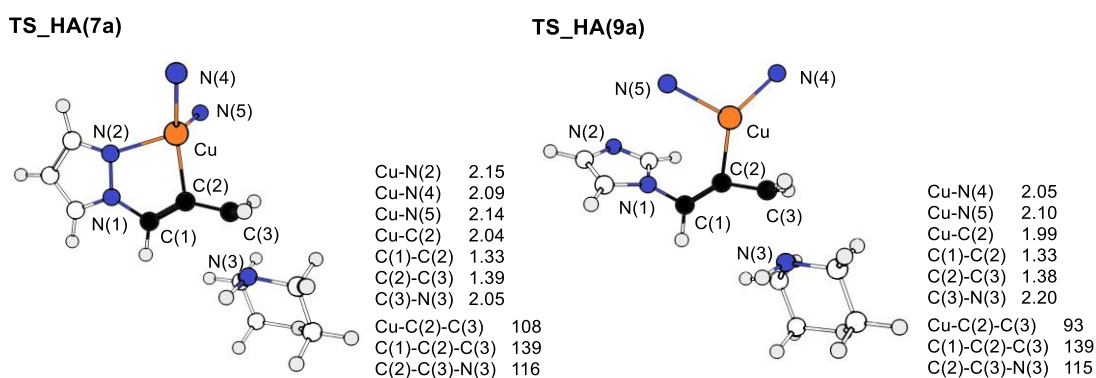


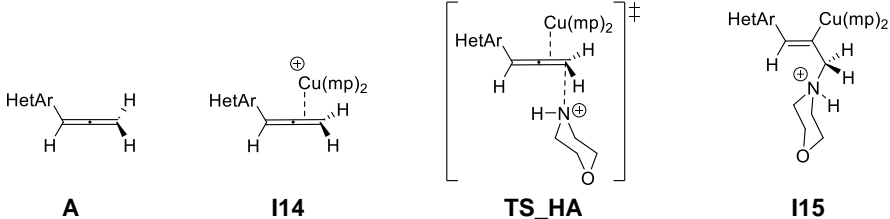
Figure 26 – Transition states for the hydroamination of **7a** and **9a** (the proximal conformation is shown for both substrates), as obtained by DFT modelling. Selected bond lengths are reported in Å and angles in degrees. The morpholine ligands have not been drawn for clarity, only the nitrogen atom is shown.

The pathway for the hydroamination of the four model substrates has been examined at the DFT level. The relative enthalpies and free energies of the intermediates and the transition state (either for the *proximal* and for the *distal* conformation) have been calculated and are reported in Table 8. As already observed for phenylallene (**1a**) and *N*-allenyl-2-pyrrolidinone, formation of the alkenylcopper intermediate **I15** is endergonic and the driving force of the transformation is the exergonic protodemetalation step (not examined here). It is worth noting that the energetics of the reactions involving the four substrates in the two conformations are similar, except for the stabilization due to chelation observed in the case of 1,2-azoles (**7a** and **7e**).

Energetics of the transition state alone may not be the only reason for the enhanced reactivity of benzimidazole **9c** compared to imidazole **9a**. A possible further contribution to this disparity is that the pyridine-like nitrogen of benzimidazole is less available for coordination than the one of imidazole (in agreement with the observation that the latter is a weaker base, the pK_a

of the conjugate acid is 7.1 for imidazole and 5.6 for benzimidazole), so unproductive *N*-coordination is less favorable for the benzannulated heterocycle. Computed thermodynamic parameters for the isomerization of the Cu/allene complexes support this view, since π -to-*N* isomerization is less favorable for **9c** than for **9a** (Figure 27).

Table 8 – Energetics of the hydroamination of the four model heterocycles, for anti-periplanar attack of the nucleophile in the two possible (*proximal* and *distal*) conformers, as assessed by DFT modeling. All data are in kcal mol⁻¹; the enthalpies and free energies of the uncomplexed allene (in the most stable conformer), uncoordinated morpholine and Cu(mp)₂ complexes have been set to zero for reference.



A	Conf.	ΔG	ΔH						
9a	prox.	1.5	1.0	5.0	-9.9	20.2	-5.5	12.7	-14.1
9a	dist.	0.0	0.0	4.3	-9.6	21.5	-4.8	13.0	-13.5
7a	prox.	0.0	0.6	-3.8	-17.0	14.6	-10.1	9.9	-15.7
7a	dist.	0.0	0.0	5.0	-9.6	19.9	-5.5	10.5	-14.8
9c	prox.	0.7	0.7	2.8	-11.4	18.2	-7.2	9.0	-16.5
9c	dist.	0.0	0.0	1.9	-12.6	16.6	-8.9	9.8	-16.8
7e	prox.	0.2	0.9	-4.0	-16.6	14.9	-9.7	9.8	-15.4
7e	dist.	0.0	0.0	1.7	-12.7	16.4	-9.2	9.1	-17.2

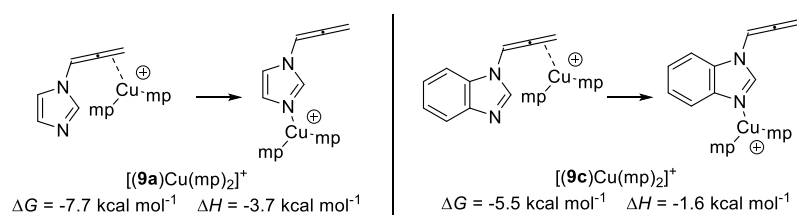


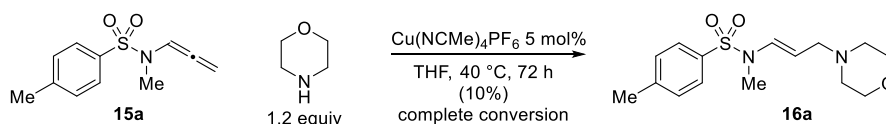
Figure 27 – Competition between *N*- and π -coordination for **9a** and **9c**. Thermodynamic parameters computed at the DFT level are reported.

In summary, we have demonstrated that the reaction conditions we have developed for the hydroamination of allenamides are also suitable for *N*-allenylazoles as substrates. 1,2-Azoles are much more reactive than 1,3-azoles, because the pyridine-like nitrogen can act as an additional coordination point for the former class of heterocycles but not for the latter. DFT calculations allowed interpreting some of the subtleties of the mechanism of this transformation.

2.9. Extension to *N*-allenylsulfonamides

In our quest for other allene derivatives suitable as substrates for the hydroamination reaction we developed, we thought about *N*-allenylsulfonamides as promising candidates. These derivatives are as easily accessible as allenamides, since they are also easily obtained by base-catalyzed isomerization of the corresponding *N*-propargyl derivatives. Given the structural and electronical similarity to allenamides, we expected a comparable reactivity.

Rather disappointingly, when *N*-allenyl-*N*-methyl-*p*-toluenesulfonamide (**15a**) was used as a substrate in our standard experimental conditions, almost no conversion took place at room temperature (Scheme 87). Heating at 40 °C for 72 h was enough to achieve complete conversion of the starting material, but most of the allene derivative decomposed and the expected product was obtained in less than 10% yield (as assessed by ¹H NMR spectroscopy of the crude reaction mixture, Scheme 87).^{xxiv}



Scheme 87 – Hydroamination of *N*-allenyl-*N*-methyl-*p*-toluenesulfonamide (**15a**). NMR yield reported.

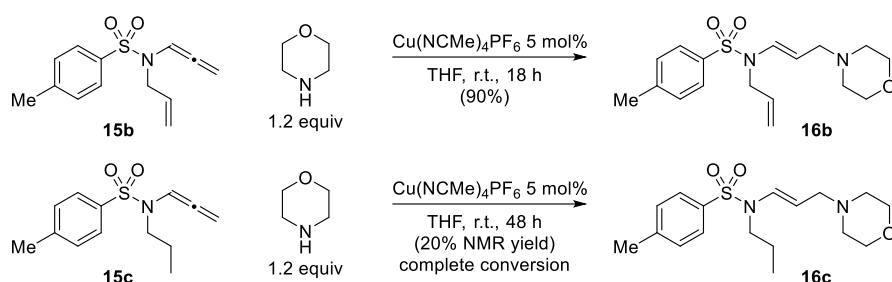
Keeping in mind the striking reaction-promoting effect of ancillary coordinating moieties we observed for 1,2-azoles, we tried to figure out what kind of substrates would have a structural element able to act as an *innate* directing group, in the same way as the pyridine-like nitrogen of the aforementioned heterocycles or the C=O moiety of allenamides. Taking into account the good affinity of cationic copper(I) for carbon-carbon unsaturations, we reasoned that introducing a strategically placed double bond could have been enough to promote reactivity.

When *N*-allenyl-*N*-allyl-*p*-toluenesulfonamide (**15b**) was tested as a substrate, we were pleased to find out that the desired addition product of morpholine could be obtained in 90% yield at room temperature with Cu(NCMe)₄PF₆ as a catalyst (Scheme 88). To exclude that this substantial enhancement of reactivity was due to a conformational effect due to the allyl chain, the reactivity of the analogous *N*-propyl derivative **15c** was also assessed, and the required product indeed formed, but in only 20% NMR yield with complete conversion of the starting material (Scheme 88).^{xxv} This observation, thus, confirmed our initial guess.^{xxvi}

^{xxiv} Compound **16a** was identified by observation of its characteristic ¹H NMR resonances. ¹H NMR (300 MHz, THF): δ = 6.50 (d, *J* = 14.1 Hz, 1H), 4.38 (dt, *J* = 14.1, 7.0 Hz, 1H) ppm.

^{xxv} Compound **16c** was not isolated, but it was identified in the crude reaction mixture by observation of some of its characteristic NMR resonances. ¹H NMR (300 MHz, CDCl₃): δ = 6.77 (d, *J* = 14.2 Hz, 1H), 4.80 (dt, *J* = 14.2, 7.2 Hz, 1H) ppm.

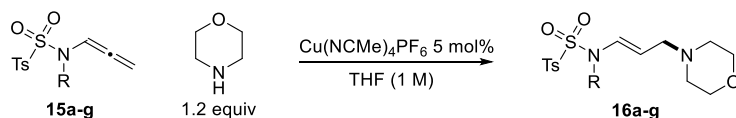
^{xxvi} Bäckvall and coworkers have already observed a similar influence of pendant allyl groups in a copper-catalyzed reaction.^[175] *N*-allylsulfonamides could be coupled with bromoallenes by the use of a CuTC/DMEDA catalyst system (CuTC = copper(I) 2-thiophenecarboxylate, DMEDA =



Scheme 88 – Hydroamination of *N*-allenyl-*N*-allenyl-*p*-toluenesulfonamide (**15b**) and *N*-allenyl-*N*-propyl-*p*-toluenesulfonamide (**15c**).

The influence of the *N*-substituent of the sulfonamide on this reaction was then examined by varying systematically the nature of R in derivatives of general structure $\text{TsNR}(\text{CH}=\text{C}=\text{CH}_2)$, results (including those shown previously) are summarized in Table 9. Passing from R = allyl to R = *trans*-cinnamyl (**15d**) the reaction became less efficient, but the expected hydroamination product was still obtained in a satisfactory yield. The yield was further reduced for R = *trans*-crotyl (**15e**). For R = Bn (**15f**), the hydroamination product was obtained in a fair yield as an 83:17 *E/Z* mixture. Good reactivity and complete selectivity for the *E* alkene was observed for R = Ph (**15g**).

Table 9 – Influence of the *N*-substituent on the reactivity of $\text{TsNR}(\text{CH}=\text{C}=\text{CH}_2)$ towards Cu-catalyzed hydroamination with morpholine.



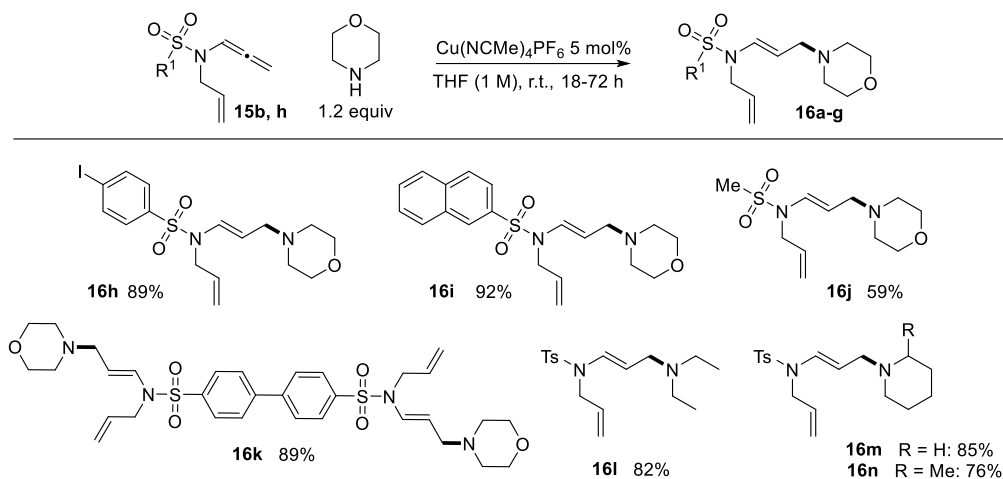
Entry	R	Reactant	Product	Reaction time (h)	Temp. (°C)	<i>E/Z</i> ratio	Yield (%)
1	Me	15a	15a	72	40	>99:1	10 ^a
2	Allyl	15b	15b	18	r.t.	>99:1	90
3	Pr	15c	15c	48	r.t.	>99:1	20 ^a
4	(<i>E</i>)-PhCH=CHCH ₂ -	15d	15d	48	r.t.	>99:1	56
5	(<i>E</i>)-MeCH=CHCH ₂ -	15e	15e	48	r.t.	>99:1	29
6	Bn	15f	15f	72	r.t.	83:17	39
7	Ph	15g	15g	18	r.t.	>99:1	70

^a Yield determined by NMR. Isolated yields if not otherwise stated.

The scope of this transformation with respect to different *N*-allenyl-*N*-allenylsulfonamides was then briefly investigated. (Scheme 89, **16h-k**). Various aromatic

N,N'-dimethylethylenediamine) giving *N*-allenyl-*N*-allylsulfonamides, but the reaction failed when saturated *N*-substituents were employed instead. In analogy with our findings (*vide infra*), the reaction also worked for *N*-arylsulfonamides, albeit in less satisfactory yields, and with *N*-(*tert*-butoxycarbonylmethyl)-*p*-toluenesulfonamide.^[175]

sulfonamide moieties are tolerated, also including an iodo substituent. The same variety of secondary cyclic and open chain secondary amines that are suitable for the hydroamination of allenamides are viable substrates for this transformation involving sulfonamides (Scheme 89, **16l-n**).



Scheme 89 – Scope of the Cu-catalyzed hydroamination of *N*-allenyl-*N*-allylsulfonamides.

2.10. Mechanistic aspects of the copper-catalyzed hydroamination of *N*-allenylsulfonamides

To shed more light on the peculiar behavior of *N*-allenylsulfonamides as substrates for the copper-catalyzed hydroamination, DFT calculations were performed on *N*-allenyl-*N*-allyl-*p*-toluenesulfonamide (**15b**) as a model substrate. This problem is much more complex than those analyzed in the previous sections because this system has much more conformational flexibility and three points of interaction with copper: the double bond of the allyl group and the sulfonamide oxygen atoms. Moreover, the oxygen and nitrogen atoms of the sulfonamide moiety can also engage in hydrogen bonding with the N-H protons of the morpholine molecules acting as a ligand for copper, as the oxygen atoms of allenyl ethers (Figure 19).

In agreement with the mechanism we proposed for other substrates, six conformers of the transition state corresponding to the formation of the *Z* isomer of the alkenylcopper intermediates have been located, their schematic drawings and 3D structures are reported in Figure 28, together with computed free energies of formation (with reference to uninteracting $[\text{Cu}(\text{mp})_2]^+$, mp, and **15b**). In **TS6a** and **TS6b** the double bond of the allyl chain is involved in η^2 coordination with the metal center. In **TS6c** and **TS6d** one of the oxygen atoms of the sulfonamide moiety interacts with the metal, in a similar fashion to what we have previously shown for allenamides. **TS6e** and **TS6f** feature no secondary interaction with the metal center, but one of the oxygens atoms or the nitrogen atom of the sulfonamide are involved in hydrogen-bonding interactions with one of the mp ligands.

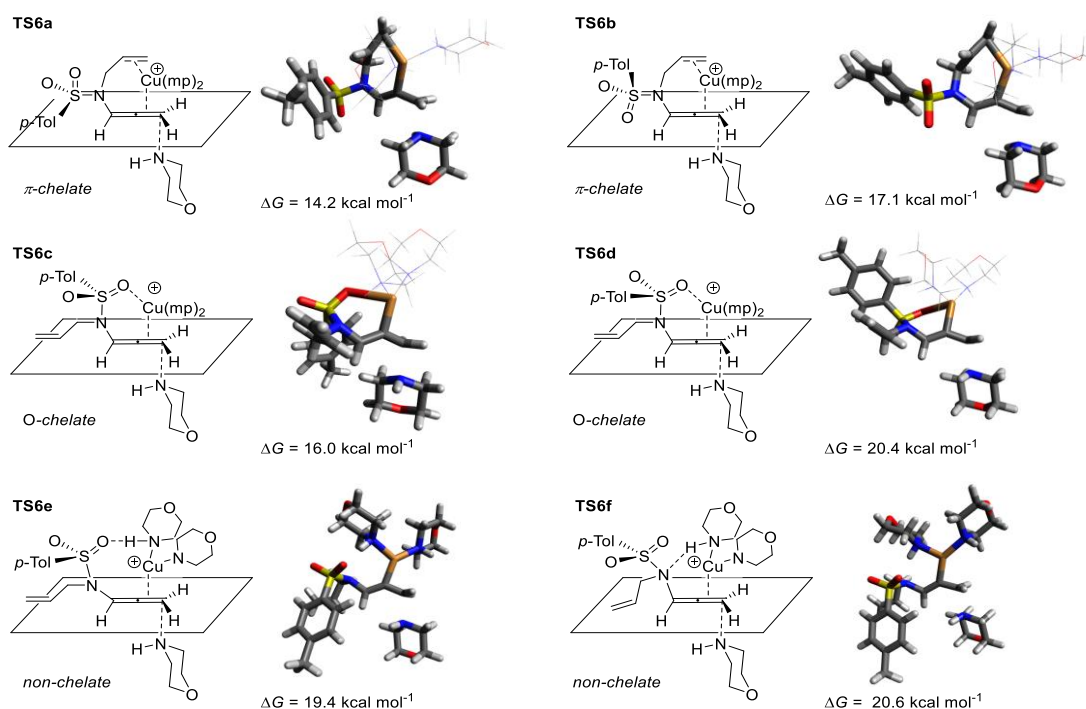


Figure 28 – Possible transition states for the Cu-catalyzed hydroamination of *N*-allenyl-*N*-allyl-*p*-toluenesulfonamide (**15b**). Computed Gibbs free energies at 298 K (ΔG) relative to non-interacting $[\text{Cu}(\text{mp})_2]^+$, mp and **15b**. For clarity, in some of the structures mp ligands are shown as thin wireframe.

Even if at first sight allenylsulfonamides may seem very close to allenamides, they have two structural features that have a deep influence on the geometry of the transition states: 1) while for allenamides the nitrogen atom has an almost perfectly planar trigonal geometry, the nitrogen atom of **15b** can be easily pyramidalized to accommodate for other structural constraints (for example, in **TS6c** the sum of the $\angle\text{CNC}$, $\angle\text{CNS}$ and $\angle\text{SNC}$ angles is 344°); 2) the sulfur atom has a distorted tetrahedral geometry, while the carbon atom of amides is trigonal planar.

It is worthwhile to look closer to the structures of the transition states. In Figure 29 we report the structures of the four transition states featuring secondary interactions of the substrate (**15b**) directly with the copper center, *i.e.* **TS6a-d**. In general, the two transition states in which π coordination by the allyl side chain is involved have a pseudo-tetrahedral arrangement of the four ligands (*i.e.* the allyl double bond, the allenyl moiety and two morpholine molecules) around copper. In **TS6a**, the conformer lowest in free energy, C(4)-C(5) bond distances are equal (2.20 Å). The C-N distance associated to the forming C-N bond is 2.20 Å, so it is close to that we found for phenylallene (2.14 Å, Figure 9) and for *N*-allenylheteroarenes, if there is no coordination by the pyridine-like nitrogen in 1,2-azoles (2.18–2.21 Å, Table 7). The Cu-C(2)-C(3) angle is 95° , so again similar to that found for non-chelating *N*-allenylheteroarenes (Table 7). **TS6b** is very similar to **TS6a**, the only major qualitative difference is that the sulfonamide moiety is in a different arrangement because of rotation around the S-N(2) bond. A potential energy surface scan performed by systematically varying the C(1)-N(2)-S-O(1) dihedral angle failed to identify other conformers.

Transition state in which one of the sulfonamide oxygen interacts with copper (**TS6c-d**) are quite different in structure from **TS6a-b**. Most importantly, this interaction is weaker than for *N*-allenylpyrrolidinone (**2b**) the Cu-O bond distances being 2.50 and 2.72 Å for **TSa-b**, to be compared with 2.22 Å in **TS3b** (Figure 12). The longer C-O distance in **TSd** than in **TSc** mirrors the fact that the former is 4.4 kcal mol⁻¹ higher in free energy than the latter. Differently from **TS6a-b**, the geometry of coordination around the metal center is not pseudo-tetrahedral, but approximately triangular pyramidal with the additional oxygen ligand places as the vertex of pyramid. Interestingly, with respect to the forming C-N bond, **TS6c-d** look more product-like, as the C(3)-N(1) bond distances (2.12 and 2.14 Å) are shorter than for **TS6a-b**. The Cu-C(2)-C(3) angles also reinforce this view, since they are closer to the 120° expected for the *sp*² center of the product.

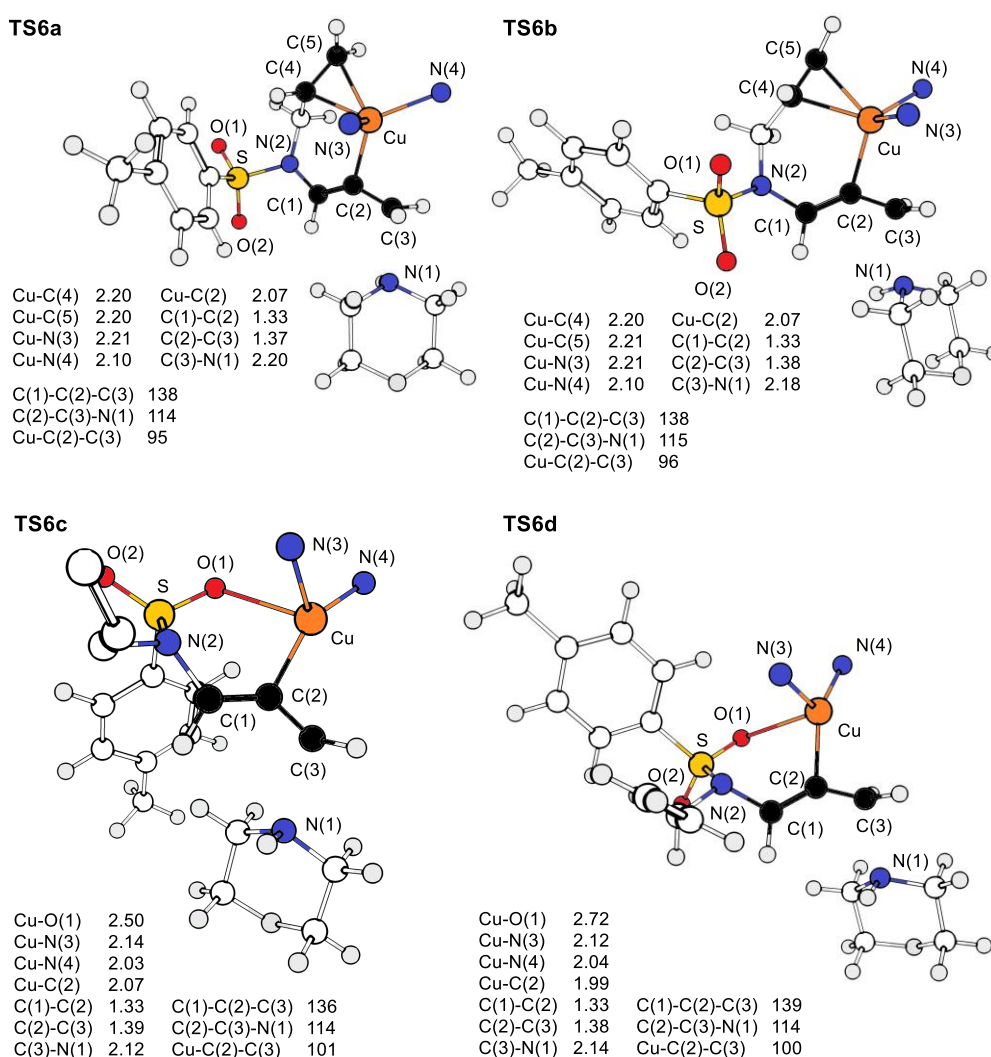


Figure 29 – Tridimensional structures and selected geometric parameters for **TS6a-d**, as resulting from DFT calculations. Bond lengths are reported in Å and angles in degrees. The morpholine ligands have not been drawn for clarity, only the nitrogen atom is shown. For **TS6c**, the hydrogen atoms of the allyl side chain have also been omitted for clarity.

exergonic protodecupration of the vinylcopper intermediate **I18** would be the driving force of the whole process.

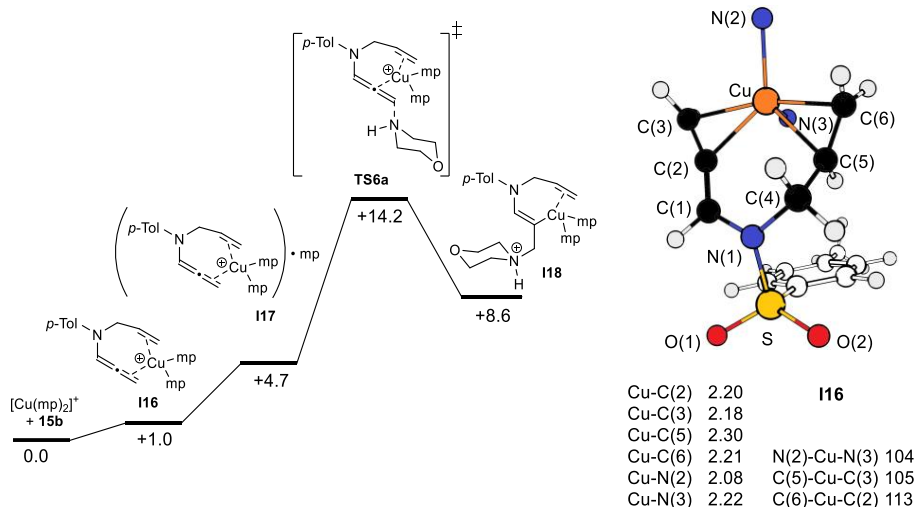


Figure 31 – Free energy profile for the addition of morpholine to sulfonamide **15b**. Computed relative Gibbs free energies are reported in kcal mol⁻¹. The structure and selected bond distances (in Å) and angles (in degrees) of intermediate **I16** are also shown (mp ligands not drawn for clarity).

A similar analysis was performed also for substrate **15g**, having a *N*-phenyl substituent instead of the *N*-allyl moiety, and substrate **15a**, having a *N*-methyl group. The schematic drawings, structures and free energies of formation of the corresponding transition states are reported in Figure 32 and Figure 33.

Briefly, similarly to what happens for **15b**, in the lowest-energy transition states for the hydroamination of **15g** (Figure 32, **TS7a-b**) there is an interaction between the metal center and the *ortho* and *meta* carbon atoms of the phenyl ring. The other transition states, either featuring an interaction between copper and one of the sulfonamide oxygens (Figure 32, **TS7c-d**) or a hydrogen bond between one of the mp ligands and the sulfonamide nitrogen atom (Figure 32, **TS7e**) are at least 4.7 kcal mol⁻¹ higher in free energy.

For what concerns compound **15a**, which cannot establish an interaction with the metal centre through π electrons, the oxygen-coordinated transition states (Figure 33, **TS8a-b,e**) are predicted to be lower in free energy than the others (Figure 33, **TS8a-b,e**), and in general all of them lie higher in energy compared to the transition states associated to **15b** and **15g**, in agreement with the observed scant reactivity of compound **15a** (the lowest-energy TS for the hydroamination of **15a** – **TS8c** – has a computed free energy of formation of 17.2 kcal mol⁻¹ with respect to the uninteracting reactants, while this value is 14.2 kcal mol⁻¹ for **TS6a** – associated to substrate **15b** – and 14.1 kcal mol⁻¹ for **TS7a** – associated to compound **15g**).

The tridimensional structures and selected geometric parameters of **TS7a-e** and **TS8a-e** are reported in Figure 34 and Figure 35. Of special note, the C-Cu distances involved in the interaction between the catalyst and the Ph ring of the substrated in **TS7a** are 2.62 Å (with the *ortho* carbon) and 2.85 Å (with the *ipso* carbon), to be compared with 2.20 Å for the double-bond carbons in **TS6a**.

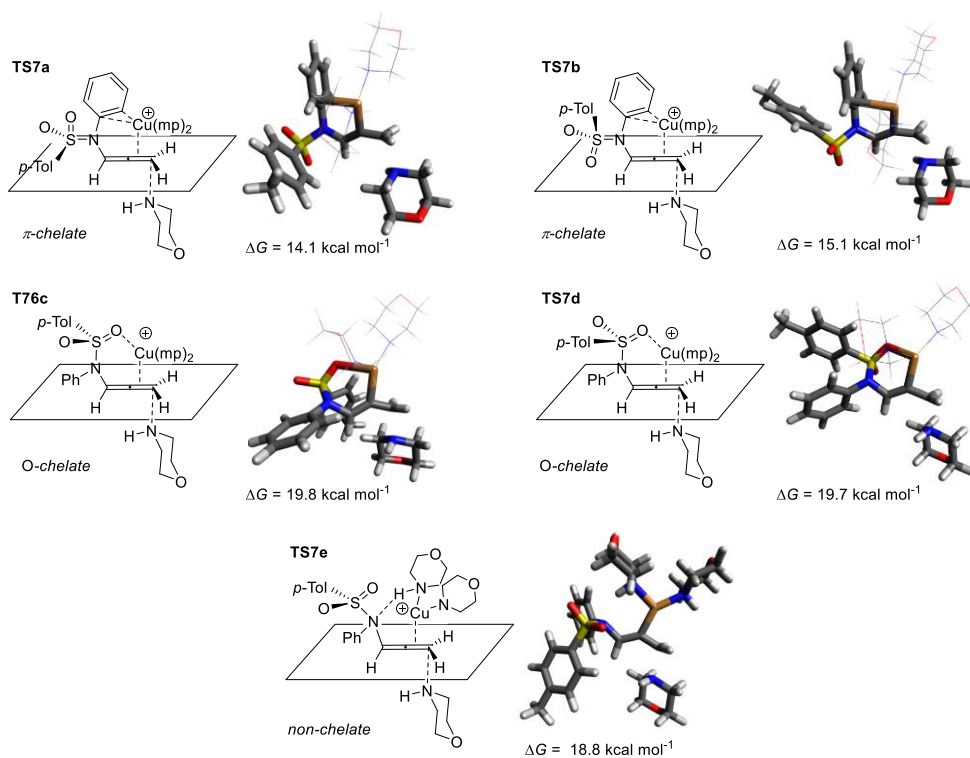


Figure 32 – Possible transition states for the Cu-catalyzed hydroamination of *N*-allenyl-*N*-phenyl-*p*-toluenesulfonamide (**15g**). Computed Gibbs free energies at 298 K (ΔG) relative to non-interacting $[\text{Cu}(\text{mp})_2]^+$, mp and **15g**. For clarity, in some of the structures mp ligands are shown as thin wireframe

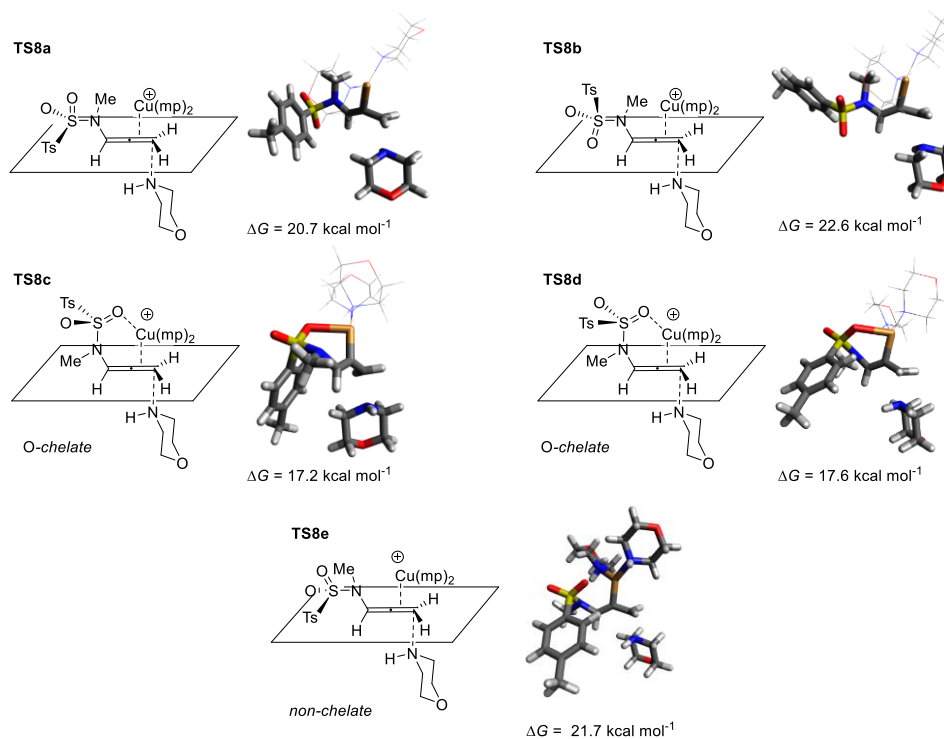


Figure 33 – Possible transition states for the Cu-catalyzed hydroamination of *N*-allenyl-*N*-methyl-*p*-toluenesulfonamide (**15a**). Computed Gibbs free energies at 298 K (ΔG) relative to non-interacting $[\text{Cu}(\text{mp})_2]^+$, mp and **15a**. For clarity, in some of the structures mp ligands are shown as thin wireframe

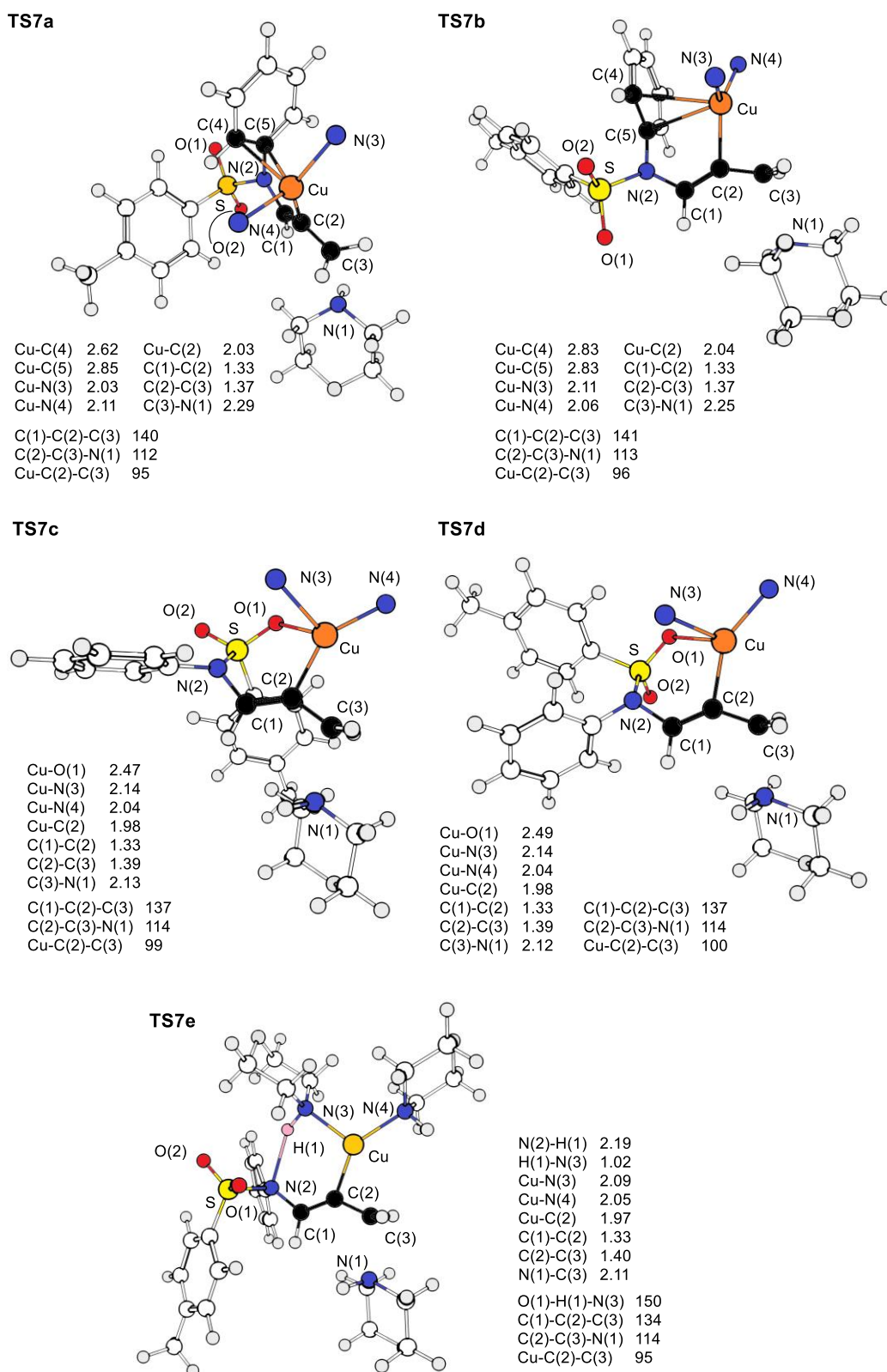


Figure 34 – Tridimensional structures and selected geometric parameters for **T76a-e**, as resulting from DFT calculations. Bond lengths are reported in Å and angles in degrees. The morpholine ligands have not been drawn for clarity, only the nitrogen atom is shown.

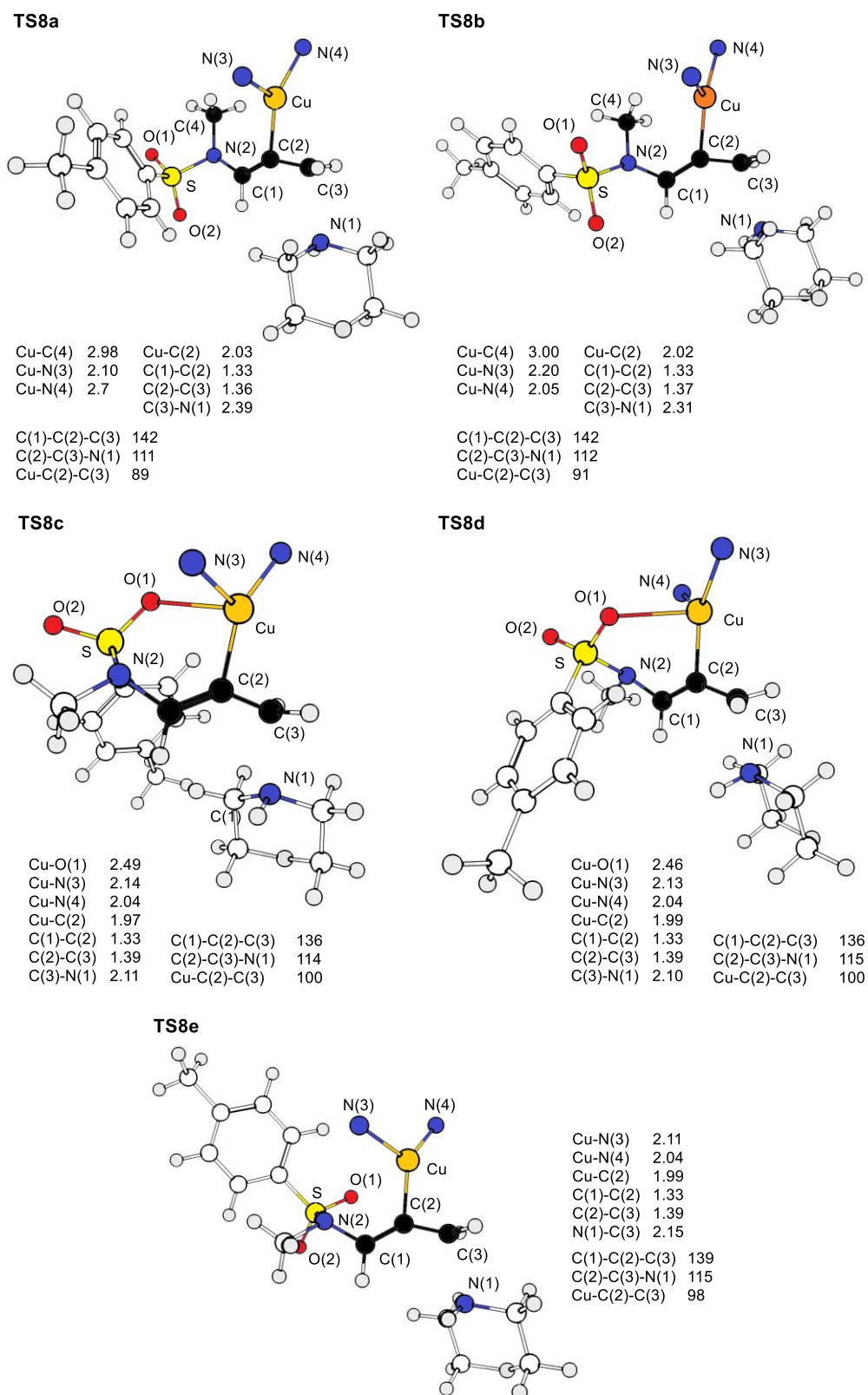


Figure 34 – Tridimensional structures and selected geometric parameters for **T86a-e**, as resulting from DFT calculations. Bond lengths are reported in Å and angles in degrees. The morpholine ligands have not been drawn for clarity, only the nitrogen atom is shown.

In summary, we have demonstrated that the conditions we developed for the copper-catalyzed hydroamination of allenamides can also be applied to *N*-allenylsulfonamides, but they are efficient only provided that an *N*-allyl or *N*-phenyl substituent is present. DFT calculations on the reaction involving *N*-allenyl-*N*-allyl-*p*-toluenesulfonamide (**15b**) confirmed that η^2 coordination of the allyl pendant to the metal center may take place and promote reactivity. Similar conclusions hold for *N*-allenyl-*N*-phenyl-*p*-toluenesulfonamide (**15g**), in which a secondary interaction involving the *ipso* and *ortho* carbons of the phenyl ring is established. Secondary interactions of this kind are not possible in the case of *N*-allenyl-*N*-methyl-*p*-toluenesulfonamide (**15a**).

3. Conclusions

We have performed a mechanistic study on the Cu-catalyzed hydroamination of terminal allenes giving *E* tertiary allylamines.^[80] After adducing evidence that the actual catalytic species is cationic Cu(I) generated *in situ* by reduction of a Cu(II) precursor and having studied the interaction of those species with representative allenes, we used DFT modeling to explain the regio- and stereoselectivity of the reaction.

We proposed that the addition takes place by intermolecular nucleophilic attack of the secondary amine on a Cu(I)/allene complex. The most energetically accessible pathway leads to a *Z* vinylcopper intermediate, which is converted to the *E* alkene by stereospecific protodecupration. As we verified beforehand, the reaction is under kinetic control, *i.e.* even if the *E* linear amine is the most thermodynamically stable product, the other possible isomers (the branched amine and the *E* isomer) do not interconvert in the conditions in which the reaction is performed.

Insight into the mechanism of reaction spurred the extension of the reaction to allenamides, which are reactive under exceptionally mild conditions and with low catalyst loading, challenging the supremacy of precious metal-based protocols for this transformation. The generality and functional group tolerance of this transformation has been explored and its potential for the synthesis of a biologically active molecule has been demonstrated.

Additional mechanistic analysis revealed the important role of the amide oxygen atom as a coordination site for the catalyst and the inhibitory effect of high concentration of the amine substrate. Building on this concept of reaction-enhancing secondary interaction, the scope of the reaction has been extended to other substrates having additional *built-in* coordinating moieties: *N*-allenyl-1,2-azoles and *N*-allenyl-*N*-allylsulfonamides. For the first class of molecules, the pyridine like nitrogen can coordinate to copper, while for the latter family of compounds η^2 coordination involving the double bond of the allyl chain takes place. DFT calculations have been performed in each case to corroborate the proposed mechanism.

In perspective, this efficient activation of allenes could be extended to the addition of nucleophiles other than amines and, more in general, copper-based catalyst may have the potential to replace gold as the preeminent catalytic platform for the activation of unsaturated compounds.

4. Computational details

All DFT calculations were performed with the Gaussian09 program (Rev. E.01).^[161] The structures of all minima and transition states were fully optimized using the B3LYP functional^[162] with Grimme's D3 empirical correction for dispersion^[163] comprising the modified Becke-Johnson damping function^[164] (B3LYP-D3BJ). The following basis set was used for geometry optimizations: 6-31+G* for N, O, F and allene C; 6-31G* for H and C (excluding allene carbons); LANL2TZ(f) with the associated effective core potential (ECP) for Cu, and LANL2DZ(d,p) with the associated effective core potential for Br.^[165–169] Single-point calculations were performed to obtain more accurate electronic energies with a larger basis set: 6-311+G(2d,2p) for C, H, N, O, F; LANL08+(f) with the associated ECP for Cu; LANL08(d) with the associated ECP for Br.^[165–170]

To simulate experimental conditions, bulk solvent effects were accounted for by using an implicit solvation model (IEF-PCM) as implemented in Gaussian.^[171,172] The default spheres radii, static and optical dielectric constants for 1,4-dioxane (studies concerning the phenylallene **1a**, *N*-allenyl-2-pyrrolidinone **1b**) or THF (studies concerning allenamides **1f-1g**, *N*-allenylazoles, and *N*-allenylsulfonamides) were used. All stationary points were characterized as minima or first-order transition states by analytical frequency calculations. IRC calculations were used to confirm that transition states linked the proper minima. Computed harmonic frequencies were used to calculate the thermal contribution to Gibbs free energy with the usual approximations. Temperature and pressure were fixed at 298 K and 1 atm, respectively.

5. Bibliography

- [1] T. E. Mueller, M. Beller, T. E. Müller, M. Beller, *Chem. Rev.* **1998**, *98*, 675–703.
- [2] J.-J. Brunet, D. Neibecker, in *Catal. Hydrofunctionalization* (Eds.: A. Togni, H. Grützmaier), WILEY-VCH Verlag, Weinheim, **2001**, pp. 91–142.
- [3] F. Pohlki, S. Doye, *Chem. Soc. Rev.* **2003**, *32*, 104–114.
- [4] F. Alonso, I. P. Beletskaya, M. Yus, *Chem. Rev.* **2004**, *104*, 3079–3160.
- [5] M. Beller, J. Seayad, A. Tillack, H. Jiao, *Angew. Chem. Int. Ed.* **2004**, *43*, 3368–3398.
- [6] R. A. Widenhofer, X. Han, *Eur. J. Org. Chem.* **2006**, *2006*, 4555–4563.
- [7] R. Severin, S. Doye, *Chem. Soc. Rev.* **2007**, *36*, 1407.
- [8] T. E. Müller, K. C. Hultsch, M. Yus, F. Foubelo, M. Tada, *Chem. Rev.* **2008**, *108*, 3795–3892.
- [9] B. Alcaide, P. Almendros, *Adv. Synth. Catal.* **2011**, *353*, 2561–2576.
- [10] J. S. Yadav, A. Antony, T. S. Rao, B. V. Subba Reddy, *J. Organomet. Chem.* **2011**, *696*, 16–36.
- [11] N. T. Patil, R. D. Kavthe, V. S. Shinde, *Tetrahedron* **2012**, *68*, 8079–8146.
- [12] X. Zeng, *Chem. Rev.* **2013**, *113*, 6864–6900.
- [13] A. L. Reznichenko, K. C. Hultsch, in *Hydrofunctionalization - Top. Organomet. Chem.* **43** (Eds.: V.P. Ananikov, M. Tanaka), Springer-Verlag, Berlin, Heidelberg, **2012**, pp. 51–114.
- [14] N. Nishina, Y. Yamamoto, in *Hydrofunctionalization - Top. Organomet. Chem.* **43** (Eds.: V.P. Ananikov, M. Tanaka), Springer-Verlag, Berlin, Heidelberg, **2013**, pp. 115–143.
- [15] G. Evano, A.-C. Gaumont, C. Alayrac, I. E. Wrona, J. R. Giguere, O. Delacroix, A. Bayle, K. Jouvin, C. Theunissen, J. Gatignol, A. C. Silvanus, *Tetrahedron* **2014**, *70*, 1529–1616.
- [16] L. Huang, M. Arndt, K. Gooßen, H. Heydt, L. J. Gooßen, *Chem. Rev.* **2015**, *115*, 2596–2697.
- [17] E. Bernoud, C. Lepori, M. Mellah, E. Schulz, J. Hannedouche, *Catal. Sci. Technol.* **2015**, *5*, 2017–2037.
- [18] S. M. Coman, V. I. Parvulescu, *Org. Process Res. Dev.* **2015**, *19*, 1327–1355.
- [19] B. Ruscic, *J. Phys. Chem. A* **2015**, *119*, 7810–7837.
- [20] J. B. Pedley, R. D. Naylor, S. P. Kirby, *Thermochemical Data of Organic Compounds*, Chapman And Hall, London, UK, **1986**.
- [21] N. S. Nixon, F. Scheinmann, J. L. Suschitzky, *Tetrahedron Lett.* **1983**, *24*, 597–600.
- [22] H.-J. Altenbach, H. Soicke, *Liebigs Ann. der Chemie* **1982**, *1982*, 1096–1104.
- [23] S. Kaden, M. Brockmann, H.-U. Reissig, *Helv. Chim. Acta* **2005**, *88*, 1826–1838.
- [24] W. Klop, P. A. A. Klusener, L. Brandsma, *Recl. des Trav. Chim. des Pays-Bas* **1984**, *103*, 27–29.
- [25] S. W. Goldstein, L. E. Overman, M. H. Rabinowitz, *J. Org. Chem.* **1992**, *57*, 1179–1190.
- [26] F. Lauterwasser, P. G. Hayes, S. Bräse, W. E. Piers, L. L. Schafer, *Organometallics* **2004**, *23*, 2234–2237.
- [27] V. M. Arredondo, F. E. McDonald, T. J. Marks, *J. Am. Chem. Soc.* **1998**, *120*, 4871–4872.
- [28] V. M. Arredondo, S. Tian, F. E. McDonald, T. J. Marks, *J. Am. Chem. Soc.* **1999**, *121*, 3633–3639.
- [29] S. Tobisch, *Dalt. Trans.* **2011**, *40*, 249–261.
- [30] I. Bytschkov, S. Doye, *Eur. J. Org. Chem.* **2003**, *2003*, 935–946.
- [31] J. S. Johnson, R. G. Bergman, *J. Am. Chem. Soc.* **2001**, *123*, 2923–2924.
- [32] B. F. Straub, R. G. Bergman, *Angew. Chem. Int. Ed. Engl.* **2001**, *40*, 4632–4635.
- [33] R. O. Ayinla, L. L. Schafer, *Inorganica Chim. Acta* **2006**, *359*, 3097–3102.
- [34] J. M. Hoover, J. R. Petersen, J. H. Pikul, A. R. Johnson, *Organometallics* **2004**, *23*, 4614–4620.
- [35] L. Ackermann, R. G. Bergman, *Org. Lett.* **2002**, *4*, 1475–1478.
- [36] L. Ackermann, R. G. Bergman, R. N. Loy, *J. Am. Chem. Soc.* **2003**, *125*, 11956–11963.
- [37] P. J. Walsh, A. M. Baranger, R. G. Bergman, *J. Am. Chem. Soc.* **1992**, *114*, 1708–1719.
- [38] S. Tobisch, *Chem. Eur. J.* **2007**, *13*, 4884–4894.
- [39] S. Tobisch, *Chem. Eur. J.* **2008**, *14*, 8590–8602.
- [40] H. Kim, T. Livinghouse, D. Seomoon, p h Lee, *Bull. Korean Chem. Soc.* **2007**, *28*, 1127–1134.
- [41] M. C. Hansen, C. A. Heusser, T. C. Narayan, K. E. Fong, N. Hara, A. W. Kohn, A. R. Venning, A. L. Rheingold, A. R. Johnson, *Organometallics* **2011**, *30*, 4616–4623.
- [42] M. S. Jung, W. S. Kim, Y. H. Shin, H. J. Jin, Y. S. Kim, E. J. Kang, *Org. Lett.* **2012**, *14*, 6262–6265.
- [43] G. Broggini, G. Poli, E. M. Beccalli, F. Brusa, S. Gazzola, J. Oble, *Adv. Synth. Catal.* **2015**, *357*, 677–682.
- [44] M. L. Cooke, K. Xu, B. Breit, *Angew. Chem. Int. Ed.* **2012**, *51*, 10876–10879.
- [45] K. Xu, Y.-H. Wang, V. Khakyzadeh, B. Breit, *Chem. Sci.* **2016**, *7*, 3313–3316.
- [46] C. Li, M. Kähny, B. Breit, *Angew. Chem. Int. Ed.* **2014**, *53*, 13780–13784.
- [47] J. P. Schmidt, C. Li, B. Breit, *Chem. Eur. J.* **2017**, *23*, 6531–6534.
- [48] S. Parveen, C. Li, A. Hassan, B. Breit, *Org. Lett.* **2017**, *19*, 2326–2329.
- [49] K. Xu, N. Thieme, B. Breit, *Angew. Chem. Int.*

- Ed.* **2014**, *53*, 2162–2165.
- [50] N. Thieme, B. Breit, *Angew. Chem. Int. Ed.* **2017**, *56*, 1520–1524.
- [51] K. Xu, N. Thieme, B. Breit, *Angew. Chem. Int. Ed.* **2014**, *53*, 7268–7271.
- [52] K. Xu, W. Raimondi, T. Bury, B. Breit, *Chem. Commun.* **2015**, *51*, 10861–10863.
- [53] K. Xu, T. Gilles, B. Breit, *Nat. Commun.* **2015**, *6*, 7616.
- [54] Q.-A. Chen, Z. Chen, V. M. Dong, *J. Am. Chem. Soc.* **2015**, *137*, 8392–8395.
- [55] H. Tafazolian, J. A. R. Schmidt, *Chem. Eur. J.* **2017**, *23*, 1507–1511.
- [56] D. R. Coulson, *J. Org. Chem.* **1973**, *38*, 1483–1490.
- [57] L. Besson, J. Goré, B. Cazes, *Tetrahedron Lett.* **1995**, *36*, 3857–3860.
- [58] M. Al-masum, M. Meguro, Y. Yamamoto, *Tetrahedron Lett.* **1997**, *38*, 6071–6074.
- [59] M. Meguro, Y. Yamamoto, *Tetrahedron Lett.* **1998**, *39*, 5421–5424.
- [60] J. F. Beck, D. C. Samblanet, J. A. R. Schmidt, *RSC Adv.* **2013**, *3*, 20708.
- [61] J. F. Beck, J. A. R. Schmidt, *RSC Adv.* **2012**, *2*, 128–131.
- [62] H. Tafazolian, D. C. Samblanet, J. A. R. Schmidt, *Organometallics* **2015**, *34*, 1809–1817.
- [63] N. C. Zingales, A. R. Shaffer, J. A. R. Schmidt, *Organometallics* **2013**, *32*, 578–586.
- [64] E. M. Beccalli, A. Bernasconi, E. Borsini, G. Brogginini, M. Rigamonti, G. Zecchi, *J. Org. Chem.* **2010**, *75*, 6923–6932.
- [65] S. Gazzola, E. M. Beccalli, A. Bernasconi, T. Borelli, G. Brogginini, A. Mazza, *Eur. J. Org. Chem.* **2016**, *2016*, 4534–4544.
- [66] I. Kadota, A. Shibuya, L. M. Lutete, Y. Yamamoto, *J. Org. Chem.* **1999**, *64*, 4570–4571.
- [67] L. M. Lutete, I. Kadota, Y. Yamamoto, *J. Am. Chem. Soc.* **2004**, *126*, 1622–1623.
- [68] N. T. Patil, L. M. Lutete, H. Wu, N. K. Pahadi, I. D. Gridnev, Y. Yamamoto, *J. Org. Chem.* **2006**, *71*, 4270–4279.
- [69] N. T. Patil, H. Wu, Y. Yamamoto, *J. Org. Chem.* **2007**, *72*, 6577–6579.
- [70] M. Narsireddy, Y. Yamamoto, *J. Org. Chem.* **2008**, *73*, 9698–9709.
- [71] K. C. M. F. Tjen, S. S. Kinderman, H. Hiemstra, F. P. J. T. Rutjes, H. E. Schoemaker, *Chem. Commun.* **2000**, 699–700.
- [72] H. Kim, W. Lim, D. Im, D. Kim, Y. H. Rhee, *Angew. Chem. Int. Ed.* **2012**, *51*, 12055–12058.
- [73] W. Lim, Y. H. Rhee, *Tetrahedron* **2015**, *71*, 5939–5945.
- [74] T. J. Donohoe, N. M. Kershaw, A. J. Orr, K. M. P. Wheelhouse (nee Gosby), L. P. Fishlock, A. R. Lacy, M. Bingham, P. A. Procopiou, *Tetrahedron* **2008**, *64*, 809–820.
- [75] S. S. Kinderman, R. de Gelder, J. H. van Maarseveen, H. E. Schoemaker, H. Hiemstra, F. P. J. T. Rutjes, *J. Am. Chem. Soc.* **2004**, *126*, 4100–4101.
- [76] S. Kang, S. H. Jang, J. Lee, D. Kim, M. Kim, W. Jeong, Y. H. Rhee, *Org. Lett.* **2017**, *19*, 4684–4687.
- [77] I. Bernar, B. Fiser, D. Blanco-Ania, E. Gómez-Bengoa, F. P. J. T. Rutjes, *Org. Lett.* **2017**, *19*, 4211–4214.
- [78] K. L. Toups, R. a Widenhoefer, *Chem. Commun.* **2010**, *46*, 1712–1714.
- [79] A. Tsuhako, D. Oikawa, K. Sakai, S. Okamoto, *Tetrahedron Lett.* **2008**, *49*, 6529–6532.
- [80] R. Blicck, J. Bahri, M. Taillefer, F. Monnier, *Org. Lett.* **2016**, *18*, 1482–1485.
- [81] S. Arseniyadis, J. Sartoretti, *Tetrahedron Lett.* **1985**, *26*, 729–732.
- [82] D. Lathbury, T. Gallagher, *J. Chem. Soc., Chem. Commun.* **1986**, 114–115.
- [83] A. Claesson, C. Sahlberg, K. Luthman, K. Lempert, J. Moller, K. Folkers, N. Yanaihara, C. Yanaihara, *Acta Chem. Scand.* **1979**, *33b*, 309–310.
- [84] O. Flögel, M. G. Okala Amombo, H.-U. Reißig, G. Zahn, I. Brüdgam, H. Hartl, *Chem. Eur. J.* **2003**, *9*, 1405–1415.
- [85] J. Grimaldi, A. Cormons, *Tetrahedron Lett.* **1986**, *27*, 5089–5090.
- [86] T. Wei, M.-S. Xie, G.-R. Qu, H.-Y. Niu, H.-M. Guo, *Org. Lett.* **2014**, *16*, 900–903.
- [87] Z. Zhang, C. Liu, R. E. Kinder, X. Han, H. Qian, R. A. Widenhoefer, *J. Am. Chem. Soc.* **2006**, *128*, 9066–9073.
- [88] Z. Zhang, C. F. Bender, R. A. Widenhoefer, *J. Am. Chem. Soc.* **2007**, *129*, 14148–14149.
- [89] D. Pflästerer, P. Dolbundalchok, S. Rafique, M. Rudolph, F. Rominger, A. S. K. Hashmi, *Adv. Synth. Catal.* **2013**, *355*, 1383–1393.
- [90] N. Morita, N. Krause, *Org. Lett.* **2004**, *6*, 4121–4123.
- [91] N. Nishina, Y. Yamamoto, *Angew. Chem. Int. Ed.* **2006**, *45*, 3314–3317.
- [92] A. Duncan, R. Widenhoefer, *Synlett* **2010**, *2010*, 419–422.
- [93] N. Nishina, Y. Yamamoto, *Synlett* **2007**, *2007*, 1767–1770.
- [94] R. E. Kinder, Z. Zhang, R. A. Widenhoefer, *Org. Lett.* **2008**, *10*, 3157–3159.
- [95] A. W. Hill, M. R. J. Elsegood, M. C. Kimber, *J. Org. Chem.* **2010**, *75*, 5406–9.
- [96] K. L. Butler, M. Tragni, R. A. Widenhoefer, *Angew. Chem. Int. Ed.* **2012**, *51*, 5175–5178.
- [97] D. A. Khrakovsky, C. Tao, M. W. Johnson, R. T. Thornbury, S. L. Shevick, F. D. Toste, *Angew. Chem. Int. Ed.* **2016**, *55*, 6079–6083.
- [98] V. Lavallo, G. D. Frey, B. Donnadieu, M. Soleilhavoup, G. Bertrand, *Angew. Chem. Int. Ed.* **2008**, *47*, 5224–5228.

- [99] R. L. LaLonde, Z. J. Wang, M. Mba, A. D. Lackner, F. D. Toste, *Angew. Chem. Int. Ed.* **2010**, *49*, 598–601.
- [100] Z. J. Wang, D. Benitez, E. Tkatchouk, W. A. Goddard III, F. D. Toste, *J. Am. Chem. Soc.* **2010**, *132*, 13064–13071.
- [101] A. Zulys, M. Dochnahl, D. Hollmann, K. Löhnwitz, J.-S. Herrmann, P. W. Roesky, S. Blechert, *Angew. Chem. Int. Ed.* **2005**, *44*, 7794–7798.
- [102] N. Meyer, K. Löhnwitz, A. Zulys, P. W. Roesky, M. Dochnahl, S. Blechert, *Organometallics* **2006**, *25*, 3730–3734.
- [103] M. Dochnahl, K. Löhnwitz, A. Lühl, J.-W. Pissarek, M. Biyikal, P. W. Roesky, S. Blechert, *Organometallics* **2010**, *29*, 2637–2645.
- [104] C. Duncan, A. V. Biradar, T. Asefa, *ACS Catal.* **2011**, *1*, 736–750.
- [105] H. Hodjat-Kachani, J. J. Perie, A. Lattes, *Chem. Lett.* **1976**, *5*, 405–408.
- [106] S. Arseniyadis, J. Gore, *Tetrahedron Lett.* **1983**, *24*, 3997–4000.
- [107] G. Franc, A. Jutand, *Dalt. Trans.* **2010**, *39*, 7873–7875.
- [108] R. D. Patil, S. Adimurthy, *Adv. Synth. Catal.* **2011**, *353*, 1695–1700.
- [109] R. D. Patil, S. Adimurthy, *RSC Adv.* **2012**, *2*, 5119–5122.
- [110] G. Engelsma, E. Havinga, *Tetrahedron* **1958**, *2*, 289–295.
- [111] S. Sumalekshmy, K. R. Gopidas, *Chem. Phys. Lett.* **2005**, *413*, 294–299.
- [112] V. Van Rheenen, *J. Chem. Soc. D Chem. Commun.* **1969**, 314–315.
- [113] É. Balogh-Hergovich, G. Speier, *React. Kinet. Catal. Lett.* **1975**, *3*, 139–141.
- [114] K. Kaneda, T. Itoh, N. Kii, K. Jitsukawa, S. Teranishi, *J. Mol. Catal.* **1982**, *15*, 349–365.
- [115] W. Zhou, W. Fan, Q. Jiang, Y.-F. Liang, N. Jiao, *Org. Lett.* **2015**, *17*, 2542–2545.
- [116] R. G. Salomon, J. K. Kochi, *J. Am. Chem. Soc.* **1973**, *95*, 1889–1897.
- [117] R. G. Salomon, J. K. Kochi, *J. Chem. Soc., Chem. Commun.* **1972**, 559–560.
- [118] C. L. Jenkins, J. K. Kochi, *J. Am. Chem. Soc.* **1972**, *94*, 843–855.
- [119] B. W. Cook, R. G. J. Miller, P. F. Todd, *J. Organomet. Chem.* **1969**, *19*, 421–430.
- [120] R. G. Salomon, J. K. Kochi, *J. Organomet. Chem.* **1974**, *64*, 135–143.
- [121] D. L. Reger, M. D. Dukes, *J. Organomet. Chem.* **1976**, *113*, 173–185.
- [122] M. Munakata, S. Kitagawa, S. Kosome, A. Asahara, *Inorg. Chem.* **1986**, *25*, 2622–2627.
- [123] H. Masuda, N. Yamamoto, T. Taga, K. Machida, S. Kitagawa, M. Munakata, *J. Organomet. Chem.* **1987**, *322*, 121–129.
- [124] T. H. Baum, C. E. Larson, G. May, *J. Organomet. Chem.* **1992**, *425*, 189–200.
- [125] B. L. Shaw, A. J. Stringer, *Inorganica Chim. Acta Rev.* **1973**, *7*, 1–10.
- [126] K. Vrieze, H. C. Volger, A. P. Praat, *J. Organomet. Chem.* **1970**, *21*, 467–475.
- [127] P. Salvadori, G. Uccello-Barretta, R. Lazzaroni, A. M. Caporusso, *J. Chem. Soc., Chem. Commun.* **1990**, 1121–1123.
- [128] G. Nagendrappa, G. C. Joshi, D. Devaprabhakara, *J. Organomet. Chem.* **1971**, *27*, 421–426.
- [129] A. Mannschreck, W. Munninger, T. Burgemeister, J. Gore, B. Cazes, *Tetrahedron* **1986**, *42*, 399–408.
- [130] A. R. Katritzky, K. Yannakopoulou, P. Lue, D. Rasala, L. Urogdi, *J. Chem. Soc. Perkin Trans. 1* **1989**, *2*, 225–233.
- [131] J. R. Clifton, J. T. Yoke, *Inorg. Chem.* **1966**, *5*, 1630–1632.
- [132] K.-L. H. Chen, R. T. Iwamoto, *Inorganica Chim. Acta* **1971**, *5*, 97–102.
- [133] J. F. Normant, A. Alexakis, *Synthesis* **1981**, *1981*, 841–870.
- [134] K. Nilsson, C. Ullenius, N. Krause, *J. Am. Chem. Soc.* **1996**, *118*, 4194–4195.
- [135] A. Basheer, I. Marek, *Beilstein J. Org. Chem.* **2010**, *6*, DOI 10.3762/bjoc.6.77.
- [136] D. H. Ess, K. N. Houk, *J. Am. Chem. Soc.* **2007**, *129*, 10646–10647.
- [137] W.-J. van Zeist, F. M. Bickelhaupt, *Org. Biomol. Chem.* **2010**, *8*, 3118.
- [138] J. P. Foster, F. Weinhold, *J. Am. Chem. Soc.* **1980**, *102*, 7211–7218.
- [139] A. E. Reed, R. B. Weinstock, F. Weinhold, *J. Chem. Phys.* **1985**, *83*, 735.
- [140] L. Brandsma, *Synthesis of Acetylenes, Allenes and Cumulenes: Methods and Techniques (Best Synthetic Methods)*, Elsevier Ltd., Oxford, **2003**.
- [141] T. Lu, Z. Lu, Z.-X. Ma, Y. Zhang, R. P. Hsung, *Chem. Rev.* **2013**, *113*, 4862–4904.
- [142] M. C. Kimber, *Org. Lett.* **2010**, *12*, 1128–1131.
- [143] D. R. Carbery, *Org. Biomol. Chem.* **2008**, *6*, 3455.
- [144] B. E. Maryanoff, H.-C. Zhang, J. H. Cohen, I. J. Turchi, C. A. Maryanoff, *Chem. Rev.* **2004**, *104*, 1431–1628.
- [145] J. R. Boissier, G. Combes, A. H. Effler, K. Klinga, E. Schlittler, *Experientia* **1971**, *27*, 677.
- [146] G. W. Gribble, F. L. Switzer, R. M. Soll, *J. Org. Chem.* **1988**, *53*, 3164–3170.
- [147] M. Tsuda, N. Kawasaki, J. Kobayashi, *Tetrahedron Lett.* **1994**, *35*, 4387–4388.
- [148] A. Pouilhès, M. Duval-Lungulescu, S. Lambel, S. Léonce, Y. Langlois, *Tetrahedron Lett.* **2001**, *42*, 8297–8299.
- [149] J. L. Hughes, J. K. Seyler, *Tetrahydroisoquinoline Compounds*, **1976**, US 3994891 A.
- [150] J. Kehler, A. Poulsen, B. Bjørnholm, F. Kroll, N. M. Bang, *3,4-Dihydro-1H-Isoquinolin-2-Yl-*

- Derivatives*, **2003**, WO2003051869 A1.
- [151] L.-L. Wei, H. Xiong, C. J. Douglas, R. P. Hsung, *Tetrahedron Lett.* **1999**, *40*, 6903–6907.
- [152] L.-L. Wei, J. A. Mulder, H. Xiong, C. A. Zificsak, C. J. Douglas, R. P. Hsung, *Tetrahedron* **2001**, *57*, 459–466.
- [153] M. R. Tracey, T. Grebe, J. A. Mulder, R. P. Hsung, *Org. Synth.* **2005**, *81*, 147–157.
- [154] S. Pascual, P. de Mendoza, A. A. C. Braga, F. Maseras, A. M. Echavarren, *Tetrahedron* **2008**, *64*, 6021–6029.
- [155] T. W. Bousfield, M. C. Kimber, *Tetrahedron Lett.* **2015**, *56*, 350–352.
- [156] Y. Li, J. Chen, R. Qiu, X. Wang, J. Long, L. Zhu, C.-T. Au, X. Xu, *Tetrahedron Lett.* **2015**, *56*, 5504–5507.
- [157] C. Hansch, A. Leo, R. W. Taft, *Chem. Rev.* **1991**, *91*, 165–195.
- [158] F. Barbot, B. Dauphin, P. Miginiac, *Synthesis* **1985**, *1985*, 768–770.
- [159] A. R. Katritzky, J. Li, N. Malhotra, *Liebigs Ann. der Chemie* **1992**, *1992*, 843–853.
- [160] A. R. Katritzky, S. Bobrov, K. Kirichenko, Y. Ji, P. J. Steel, *J. Org. Chem.* **2003**, *68*, 5713–5719.
- [161] M. J. Frisch, G. W. Trucks, H. B. Schlegel, G. E. Scuseria, M. A. Robb, J. R. Cheeseman, G. Scalmani, V. Barone, B. Mennucci, G. A. Petersson, H. Nakatsuji, M. Caricato, X. Li, H. P. Hratchian, A. F. Izmaylov, J. Bloino, G. Zheng, J. L. Sonnenberg, M. Hada, et al., **2009**.
- [162] P. J. Stephens, F. J. Devlin, C. F. Chabalowski, M. J. Frisch, *J. Phys. Chem.* **1994**, *98*, 11623–11627.
- [163] S. Grimme, J. Antony, S. Ehrlich, H. Krieg, *J. Chem. Phys.* **2010**, *132*, 154104.
- [164] S. Grimme, S. Ehrlich, L. Goerigk, *J. Comput. Chem.* **2011**, *32*, 1456–1465.
- [165] P. J. Hay, W. R. Wadt, *J. Chem. Phys.* **1985**, *82*, 270–283.
- [166] W. R. Wadt, P. J. Hay, *J. Chem. Phys.* **1985**, *82*, 284–298.
- [167] P. J. Hay, W. R. Wadt, *J. Chem. Phys.* **1985**, *82*, 299–310.
- [168] A. W. Ehlers, M. Böhme, S. Dapprich, A. Gobbi, A. Höllwarth, V. Jonas, K. F. Köhler, R. Stegmann, A. Veldkamp, G. Frenking, *Chem. Phys. Lett.* **1993**, *208*, 111–114.
- [169] L. E. Roy, P. J. Hay, R. L. Martin, *J. Chem. Theory Comput.* **2008**, *4*, 1029–1031.
- [170] C. E. Check, T. O. Faust, J. M. Bailey, B. J. Wright, T. M. Gilbert, L. S. Sunderlin, *J. Phys. Chem. A* **2001**, *105*, 8111–8116.
- [171] J. Tomasi, B. Mennucci, R. Cammi, *Chem. Rev.* **2005**, *105*, 2999–3093.
- [172] M. Cossi, G. Scalmani, N. Rega, V. Barone, *J. Chem. Phys.* **2002**, *117*, 43–54.
- [173] D. R. Burfield, K.-H. Lee, R. H. Smithers, *J. Org. Chem.* **1977**, *42*, 3060–3065.
- [174] A. Navarro-Vázquez, *Beilstein J. Org. Chem.* **2015**, *11*, 1441–1446.
- [175] A. K. Å. Persson, E. V. Johnston, J.-E. Bäckvall, *Org. Lett.* **2009**, *11*, 3814–3817.

General conclusions and perspectives

This thesis aimed at combining synthetic methodology development with mechanistic studies for the understanding and improvement of transition metal-catalyzed transformations. At this end, both experimental and theoretical techniques were employed.

Three main examples were reported. The first one concerned the palladium-catalyzed synthesis of secondary amides from aryl halides, isocyanides and water. We have established that the isocyanide can play the role of a ligand for Pd complexes in all the steps of the catalytic cycle and that it modulates their reactivity in several ways. RNC-ligated species $[(ArC=NR)Pd(CNR)_2I]$ – formed after insertion of RNC into the C-Pd bond – undergo C-O bond forming reductive elimination at room temperature in the presence of H₂O and a F⁻/HF buffer. RNC hinders this step, most likely by formation of inactive cationic species and preventing the formation of more active coordinatively unsaturated complexes. Expulsion of I-giving cationic complexes also takes place in the presence of added phosphine ligands in polar solvents. These cationic species are not directly involved in the catalytic cycle (*i.e.* they are a resting state for the catalyst) and they can probably take part into side reactions due to poly-insertion of RNC. Even if we did not directly engage in the development of new related palladium-catalyzed coupling with insertion of isocyanides, we expect that these findings could help other workers in this task.

The second topic is the palladium-catalyzed ring-opening of benzofurans giving access to 2-(3-indolylmethyl)phenols starting from benzofuran-tethered 2-iodoanilines. Characterization of key reaction intermediates indicates that this transformation is a reductive Heck reaction proceeding by carbopalladation of the heterocyclic ring of benzofuran and terminated by formal β-elimination of phenoxide. In this process, *N,N*-diisopropylethylamine and related amine bases act as a base and a reducing agent. Theoretical investigation, already started by Raymond Grüber and Paul Fleurat-Lessard, are being completed to shed more light on the detailed mechanism of this reaction.

The third topic is the copper-catalyzed hydroamination of terminal allenes to give *E* tertiary allylamines originally developed by Florian Monnier, Marc Taillefer and co-workers. After establishing that the actual catalytic species is cationic Cu(I) generated *in situ* by reduction of a Cu(II) precursor, we used DFT modeling to explain the regio- and stereoselectivity of the reaction. Insight into the mechanism of reaction spurred the extension of the reaction to allenamides, which are reactive under exceptionally mild conditions and with low catalyst loadings. Theoretical characterization of the detailed mechanism of the reaction involving these compounds highlighted the importance of secondary substrate-catalyst interactions, in this case involving the C=O moiety of the amide itself. Building on this concept of *innate* directing group, the reaction was extended on other substrates: *N*-allenyl-1,2-azoles and *N*-allenylsulfonamides having suitably placed unsaturated moieties. In the first case, the pyridine-like nitrogen of the heterocycle can coordinate to the copper center, while for the latter class of compounds the additional unsaturated residue (that can be an *N*-allyl or an *N*-aryl moiety) interacts with the metal center. Extensions of this protocol to other classes of substrates (both allenes and

nucleophiles) are conceivable. More in general, this reaction demonstrates that in some cases copper catalysis can be efficiently used instead of gold and other precious metals in the activation of unsaturated compounds.

We are confident that studying the mechanism of a reaction at an early stage of its development and not only as an *a posteriori* exercise for specialists in the field is a rewarding approach to organic methodology. A rational strategy to study catalysis, integrating traditional experiment-based understanding of the reaction mechanism and modern theoretical modeling can complement and even be superior to large-scale combinatorial high-throughput screening programs. This approach not only requires communication and collaboration between synthetic chemists, specialists of mechanistic studies and theoretical chemists, but also a shift of paradigm in the way of thinking about chemical problems going beyond the limits of each of those sub-disciplines of chemistry.

Experimental sections

1. Experimental section of chapter II

1.1. General remarks

Unless otherwise stated, commercially available materials were used as received. Precoated silica gel aluminium foils (Fluka Analytical, with fluorescence indicator) were used for TLC analyses. Spots were revealed by observation under UV light (254 nm), exposition to I₂ vapors or charring at 200-400 °C (for Pd-containing compounds). GLC analyses were performed on a Varian 3900 instrument with H₂ as a carrier gas and a Varian VF-1ms FSOT column (15 m x 0.25 mm i.d.). ¹H and ¹³C NMR chemical shift were referenced to TMS as an internal standard using the solvent residual peak.^[1] ¹⁹F and ³¹P were referenced to external CFCl₃ and 85% H₃PO₄ respectively. Conductivity measurement were performed using a two-pole cell (composed of two square platinized platinum plates of apparent surface 0.25 cm² separated by a distance of 0.5 cm) with a Radiometer Analytical CDM 210 apparatus.

1.2. Synthesis and characterization of organometallic complexes

Synthesis of *trans*-[(4-F-C₆H₄C=N^tBu)Pd(CN^tBu)₂] (1)

A 25-mL round-bottom flask with a gas inlet tube and equipped with a magnetic stirrer was charged with Pd(dba)₂ (460 mg, 0.80 mmol) and conditioned under an atmosphere of Ar. Degassed toluene (8 mL) and *tert*-butyl isocyanide (360 μL, 3.2 mmol) were added sequentially by syringe. The initially formed violet-black suspension changed to an orange yellow solution and the starting material dissolved completely in a few minutes. 4-Fluoriodobenzene (185 μL, 1.6 mmol) was added and the mixture was left overnight at room temperature.

Workup can be done without special precautions to exclude air. Chromatographic grade silica gel (approx. 2 g) was added to the crude reaction mixture and volatile components were removed by evaporation under reduced pressure, while keeping the temperature at or below 25 °C. The free-flowing powder thus obtained was then dry-loaded onto a flash-chromatography column (diameter: 25 mm, silica gel) and eluted with petroleum ether/EtOAc (gradient from 75:25 to 50:50 ratio). The fractions containing the product were pooled and a few drops of *tert*-butyl isocyanide were added. Evaporation at reduced pressure (at room temperature or below) gave the title compound in the form of a yellow-orange solid; yield: 441 mg (95%). X-Ray quality crystals were obtained by slow evaporation of a concentrated solution in EtOAc/heptane (1:1).

¹H NMR (300 MHz, CDCl₃): δ = 7.84 (dd, *J* = 8.6, 5.7 Hz, 2H), 7.00 (t, *J* = 8.6 Hz, 2H), 1.56 (s, 9H), 1.39 (s, 18H) ppm.

¹³C NMR (75.5 MHz, CDCl₃): δ = 166.5, 163.0 (d, ¹*J*_{CF} = 248.3 Hz), 141.6, 130.8 (d, ³*J*_{CF} = 8.2 Hz), 114.8 (d, ²*J*_{CF} = 21.5 Hz), 58.1, 57.4, 31.4, 29.9 ppm. The isocyanide carbons bound to Pd gave no apparent peak.

¹⁹F {¹H} NMR (282 MHz, CDCl₃): δ = -113.6 ppm.

IR (ATR): ν = 3054w, 3035w, 2983m, 2929w, 2865w, 2190s, 1645m, 1494m, 1215s, 1190s, 1090m, 886s, 869m, 839s, 794s cm⁻¹.

ESI-MS (positive ion mode, MeCN): *m/z* (%) = 583.3 (7), 580.3 (96), 578.4 (100), 577.4 (80), 576.4 (48) [M+H]; 526.4 (15), 524.4 (36), 522.3 (38), 521.3 (29), 520.4 (14) [M+H-C₄H₈]; 454.4 (22), 452.4 (44), 450.5 (54), 449.5 (44), 448.5 (18) [M-I]; 371.2 (15), 369.2 (39), 367.4 (40), 366.2 (26), 365.0 (19) [M-I-BuNC], 178.3 (18) [4-F-C₆H₄C=N^tBu]

Synthesis of [(4-F-C₆H₄C=N^tBu)Pd(CN^tBu)₃OTf] (2-OTf)

To a solution of **1** (115 mg, 0.20 mmol) and ^tBuNC (24 μL, 0.21 mmol) in dry CH₂Cl₂ (20 mL) was added finely powdered Tl(OTf) (176 mg, 0.50 mmol) and the resulting suspension was stirred for 30 min at room temperature. The mixture was filtered through a short plug of diatomaceous earth and the solid was washed with more CH₂Cl₂ (3 x 5 mL). The combined filtrates were evaporated at reduced pressure, keeping the temperature below room temperature. The title compound was thus obtained in the form of a pale yellow solid; yield: 128 mg (94%). The compound is fairly stable in the solid state, but it decomposes in a few hours when dissolved in common organic solvents.

¹H NMR (300 MHz, DMSO-*d*₆): δ = 7.69 (dd, *J* = 8.7, 5.7 Hz, 2H), 7.25 (t, *J* = 8.8 Hz, 2H), 1.53 (s, 9H), 1.48 (s, 9H), 1.39 (s, 18H) ppm.

¹⁹F NMR (282 MHz, DMSO-*d*₆): δ = -77.8 (s, 3F), -112.6 (br s, 1F) ppm.

¹³C NMR (75.5 MHz, CD₂Cl₂): δ = 163.8 (d, ¹*J*_{CF} = 249.4 Hz), 140.6, 131.3 (d, ³*J*_{CF} = 8.2 Hz), 121.5 (q, ¹*J*_{CF} = 321.3 Hz), 115.5 (d, ²*J*_{CF} = 21.6 Hz), 60.2, 59.5, 58.1, 31.7, 30.2, 29.8 ppm. Carbons directly bound to Pd gave no visible signal.

IR (ATR): ν = 3070w, 2983w, 2943w, 2241w, 2217s, 1617m, 1593m, 1375m, 1265s, 1148s, 1030s, 893m, 849m cm⁻¹.

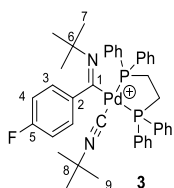
ESI-MS (positive ion mode, MeOH): *m/z* (%) = 454.3 (35), 452.3 (72), 450.4 (80), 449.5 (68), 448.5 (30) [M-OTf-^tBuNC]; 371.2 (46), 369.2 (95), 367.3 (100), 366.3 (98), 365.2 (41) [M-OTf-2^tBuNC]; 315.3 (33), 313.3 (72), 311.3 (71), 310.3 (54), 309.3 (28) [M-OTf-2^tBuNC-C₄H₈].

ESI-MS (negative ion mode, MeOH): *m/z* (%) = 149.3 (100) [OTf].

Characterization of [(4-F-C₆H₄C=N^tBu)Pd(CN^tBu)(dppe)]⁺ (3**)**

The title compound was generated by the reaction of **1** with an equimolar amount of 1,2-bis(diphenylphosphino)ethane (dppe) in DMSO and characterized *in situ* by NMR and IR spectroscopy.

A solution of **1** (14.4 mg, 0.025 mmol) and dppe (10.0 mg, 0.025 mmol) in DMSO-*d*₆ was analyzed directly by multinuclear NMR and IR spectroscopy. Complex **3** formed quantitatively, together with a molecule of uncoordinated ^tBuNC.



¹H NMR (300 MHz, DMSO-*d*₆): δ = 7.77 – 7.24 (m, 22H, dppe aromatics, H₃), 7.11 (t, *J* = 8.6 Hz, 2H, H₄), 1.37 (s, 18H, imidoyl ^tBu and free ^tBuNC), 0.99 (s, 9H, coordinated ^tBuNC) ppm. The CH₂CH₂ moiety of dppe gave no clearly identifiable peaks, probably because they were extremely broad and partly hidden by ^tBu signals.

¹³C NMR (75 MHz, DMSO-*d*₆): δ = 173.3 (d, ²*J*_{CP} = 79.5 Hz, C₁), 161.9 (d, ¹*J*_{CF} = 245.8 Hz, C₅), 152.8 (broad, free Me₃CNC), 142.5 (C₂, detected by HMBC correlation with H₄, not visible in the ordinary ¹³C spectrum), 142.3-141.7 (multiple signals, dppe aromatic CP), 134.1 (d, *J* = 12.8 Hz, dppe aromatic), 132.8-131.5 (multiple overlapping signals, dppe aromatics), 130.5 (d, ³*J*_{CF} = 8.3 Hz, C₃), 129.9-129.5 (m, dppe aromatics), 128.9-128.5 (m, dppe aromatics), 114.5 (d, ²*J*_{CF} = 21.4 Hz, C₄), 59.5 (C₆), 57.7 (dd, ⁴*J*_{CP} = 11.5, 2.0 Hz, C₈), 54.1 (1:1:1 triplet, ¹*J*_{CN} = 4.5 Hz, free

Me₃CNC), 30.6 (C₇), 30.1 (free (CH₃)₃CNC), 28.9 (C₉), 22.2-21.6 (m, dppe CH₂CH₂) ppm. No signal was evident for the isocyanide carbon bound to Pd.

¹⁹F{¹H} NMR (282 MHz, DMSO-*d*₆): δ = -114.0 ppm.

³¹P{¹H} NMR (121 MHz, DMSO-*d*₆) δ = 42.85 (d, ²J_{PP} = 41.1 Hz), 38.98 (d, ²J_{PP} = 41.1 Hz) ppm.

IR (DMSO, ATR): ν = 2203 (coordinated *t*BuNC), 2132 (free *t*BuNC) cm⁻¹.

Specific electrical conductivity (DMSO, 25 °C, 2.0 mM): κ = 28 S cm² mol⁻¹.

When the same experiment was repeated using acetone instead of DMSO, the ¹H and ¹⁹F NMR of **1** disappeared on adding dppe and the ³¹P spectrum showed just a trace of uncoordinated dppe. Two complexes were thus formed in approximate 70:30 ratio. A complete characterization was not attempted because of the complexity of the spectra. However, based the diagnostic peaks reported in Table 3 and comparison with known data we propose that the two complex are [(ArC=N*t*Bu)Pd(dppe)(CN*t*Bu)]⁺ (**3**, major) and [(ArC=N*t*Bu)Pd(dppe)I] (minor, broad NMR peaks).

Table 3 – Spectral data of the complexes formed by interaction of **1** with dppe (1.0 equiv) in acetone and comparison with **1** (in acetone) and **3** (in DMSO), R = *t*Bu.

	Major (70%), acetone	Minor (30%), acetone	3 , DMSO	1 , acetone
Structure	[(ArCNR)Pd(dppe)(CNR)] ⁺ (proposed)	[(ArCNR)Pd(dppe)I] (proposed)	[(ArCNR)Pd(dppe)(CNR)] ⁺	[(ArCNR)Pd(CNR) ₂ I]
¹H	7.77 (dd, <i>J</i> = 8.5, 5.8 Hz) 7.08 (t, <i>J</i> = 8.5 Hz)	7.98 (dd, <i>J</i> = 8.6, 5.9 Hz) ^a 6.90 (t, <i>J</i> = 8.6 Hz)	approx 7.50 ^b 7.11 (t, <i>J</i> = 8.6 Hz)	7.90 (dd, <i>J</i> = 8.8, 5.6 Hz) 7.13 (t, <i>J</i> = 8.8 Hz)
¹⁹F{¹H}	-115.2	-116.5, very broad	-114.0	-115.5
³¹P{¹H}	41.81 (d, <i>J</i> = 42.6 Hz) 37.73 (d, <i>J</i> = 42.6 Hz)	approx. 44.5, broad 28.0, very broad	42.85 (d, <i>J</i> = 41.1 Hz) 38.98 (d, <i>J</i> = 42.6 Hz)	-
IR	2202	n.d.	2203	2195

^a Identified by comparison of ¹H and ¹H{¹⁹F} spectra.

^b Detected by HSQC, overlaps with dppe signals.

Characterization of [(4-F-C₆H₄C=N*t*Bu)Pd(CN*t*Bu)(dppf)]⁺

The title compound was generated by the reaction of **1** with an equimolar amount of 1,1'-bis(diphenylphosphino)ferrocene (dppf) in DMSO and characterized *in situ* by NMR spectroscopy.

A solution of **1** (14.4 mg, 0.025 mmol) and dppf (13.9 mg, 0.025 mmol) in DMSO-*d*₆ was analyzed directly by NMR and IR spectroscopy. The title complex formed quantitatively, together with a molecule of uncoordinated *t*BuNC.

¹H NMR (300 MHz, DMSO-*d*₆): δ = 7.89 – 7.65 (m, 8H, Ph *ortho* protons), 7.61 – 7.02 (m, 14H, Ph *meta* and *para* protons and imidoyl moiety *ortho* protons), 6.88 (br s, 2H, imidoyl moiety *meta* protons), 4.97 (br s, 1H, ferrocene), 4.86 (br s, 1H, ferrocene), 4.69 (br s, 1H, ferrocene), 4.49 (br s, 1H, ferrocene), 4.39 (br s, 2H, ferrocene), 3.64 – 3.56 (m, 1H, ferrocene), 3.51 – 3.41 (m, 1H, ferrocene), 1.43 (s, 9H, imidoyl *t*Bu), 1.38 (s, 9H, free *t*BuNC), 0.98 (s, 9H, coordinated *t*BuNC) ppm.

¹⁹F{¹H} NMR (282 MHz, DMSO-*d*₆): δ = -112.8 ppm.

$^{31}\text{P}\{^1\text{H}\}$ NMR (121 MHz, DMSO- d_6) δ = 23.83 (d, $^2J_{\text{PP}}$ = 54.8 Hz), 11.12 (d, $^2J_{\text{PP}}$ = 54.8 Hz) ppm.

1.3. Synthesis of reference materials

Synthesis of *N*-*tert*-butyl-4-fluorobenzamide (4)

The title compound was synthesized as an authentic reference material by the Ritter reaction.^[2]

To a solution of 4-fluorobenzonitrile (605 mg, 5.0 mmol) in *tert*-butanol (0.50 mL), a previously prepared mixture of concentrated H_2SO_4 (0.50 mL) and glacial AcOH (0.75 mL) was added dropwise with vigorous stirring and cooling, at such a rate that almost no gaseous isobutene was produced. The reaction mixture was left overnight at room temperature, then poured into 10 mL of water. The precipitated solid was collected by filtration at the pump, washed liberally with water until the washings were neutral to litmus paper, then with a little cold diethyl ether and dried *in vacuo*. The title compound was thus obtained in the form of a white solid; yield: 788 mg (81%); m.p. 127-129 °C (lit.^[3] 126-128 °C).

^1H NMR (300 MHz, CDCl_3): δ = 7.72 (dd, J = 8.8, 5.3 Hz, 2H), 7.07 (t, J = 8.6 Hz, 2H), 5.89 (br s, 1H), 1.46 (s, 9H) ppm.

^{19}F NMR (282 MHz, CDCl_3): δ = -109.1 ppm.

Spectral data are in agreement with the literature.^[3]

1.4. X-Ray data for compound 1

Table 4 – Experimental details

Crystal data	
Chemical formula	$\text{C}_{21}\text{H}_{31}\text{F}_1\text{N}_3\text{Pd}$
Crystal system, space group	Orthorhombic, $P2_12_12_1$
Temperature (K)	200
a, b, c (Å)	9.7746(3), 15.2612(4), 17.0015(4)
V (Å ³)	2536.15(6)
Z	4
Radiation type, μ (mm ⁻¹)	Cu $K\alpha$, 15.59
Crystal size (mm)	0.25 × 0.11 × 0.09
Data collection	
Diffractometer	Bruker Kappa Apex2
Absorption correction	Multi-scan <i>SADABS</i>
$T_{\text{min}}, T_{\text{max}}$	0.14, 0.25
No. of measured, independent and observed [$I > 2.0\sigma(I)$] reflections	22723, 4557, 4528
R_{int}	0.040
$\theta_{\text{max}}, \theta_{\text{min}}$	68.3°, 3.9°
Refinement	
$R[F^2 > 2\sigma(F^2)], wR(F^2), S$	0.027, 0.068, 1.00
No. of reflections	4540
No. of parameters, restraints	245, 0
H-atom treatment	Only H-atom displacement parameters refined
$\Delta\rho_{\text{max}}, \Delta\rho_{\text{min}}$ (e Å ⁻³)	1.02, -0.74
Absolute structure	Flack (1983), 1937 Friedel-pairs

Absolute structure parameter ($\sin \theta/\lambda$) _{max} (Å ⁻¹)	-0.012(6) 0.603
---	--------------------

Table 5 – Selected geometric parameters (Å, °)

Pd1—I1	2.7204 (4)	C8—C10	1.533 (7)
Pd1—C1	2.044 (4)	C8—C11	1.503 (8)
Pd1—C12	1.980 (4)	C8—N1	1.487 (6)
Pd1—C17	1.984 (4)	C12—N2	1.149 (5)
C1—C2	1.491 (5)	C13—C14	1.523 (8)
C1—N1	1.252 (5)	C13—C15	1.509 (7)
C2—C3	1.404 (6)	C13—C16	1.502 (7)
C2—C7	1.372 (6)	C13—N2	1.468 (5)
C3—C4	1.388 (7)	C17—N3	1.147 (6)
C4—C5	1.365 (8)	C18—C19	1.531 (8)
C5—C6	1.348 (7)	C18—C20	1.505 (8)
C5—F1	1.380 (5)	C18—C21	1.518 (9)
C6—C7	1.391 (6)	C18—N3	1.455 (5)
C8—C9	1.471 (8)		
I1—Pd1—C1	179.49 (10)	C10—C8—C11	108.4 (5)
I1—Pd1—C12	93.84 (11)	C9—C8—N1	113.8 (4)
C1—Pd1—C12	85.66 (15)	C10—C8—N1	104.6 (4)
I1—Pd1—C17	88.09 (11)	C11—C8—N1	105.9 (5)
C1—Pd1—C17	92.42 (15)	Pd1—C12—N2	176.2 (4)
C12—Pd1—C17	174.84 (17)	C14—C13—C15	110.7 (5)
Pd1—C1—C2	110.0 (3)	C14—C13—C16	110.1 (5)
Pd1—C1—N1	131.2 (3)	C15—C13—C16	114.3 (5)
C2—C1—N1	118.6 (4)	C14—C13—N2	107.0 (4)
C1—C2—C3	118.0 (4)	C15—C13—N2	106.7 (4)
C1—C2—C7	123.5 (4)	C16—C13—N2	107.6 (4)
C3—C2—C7	118.5 (4)	Pd1—C17—N3	172.0 (3)
C2—C3—C4	120.3 (4)	C19—C18—C20	109.6 (5)
C3—C4—C5	118.0 (4)	C19—C18—C21	108.4 (6)
C4—C5—C6	124.0 (5)	C20—C18—C21	115.6 (7)
C4—C5—F1	117.6 (5)	C19—C18—N3	108.3 (4)
C6—C5—F1	118.4 (5)	C20—C18—N3	107.6 (4)
C5—C6—C7	117.6 (4)	C21—C18—N3	107.1 (4)
C6—C7—C2	121.6 (4)	C8—N1—C1	127.9 (4)
C9—C8—C10	108.0 (5)	C13—N2—C12	178.2 (4)
C9—C8—C11	115.5 (7)	C18—N3—C17	170.9 (4)

References

- [1] G. R. Fulmer, A. J. M. Miller, N. H. Sherden, H. E. Gottlieb, A. Nudelman, B. M. Stoltz, J. E. Bercaw, K. I. Goldberg, *Organometallics* **2010**, *29*, 2176–2179.
- [2] S. Chiavarelli, E. F. Rogers, G. B. Marino-Bettolo, *Gazz. Chim. Ital.* **1953**, *83*, 347–356.
- [3] H. Jiang, B. Liu, Y. Li, A. Wang, H. Huang, *Org. Lett.* **2011**, *13*, 1028–1031.

2. Experimental section of chapter III

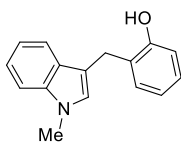
2.1. General remarks

Unless otherwise stated, commercially available materials were used as received from suppliers. THF was distilled from sodium and benzophenone under argon before use. All the air-free manipulations have been performed by standard Schlenk techniques. Precoated F254 silica gel plates on aluminum foil (Fluka analytical or Macherey-Nagel) were used for TLC analyses and visualized under UV light or with alkaline potassium permanganate solution, that readily stains phenols. GLC analyses were performed on a Varian 3900 instrument with H₂ as a carrier gas using a Varian VF-1ms column (15 m x 0.25 mm i.d.). NMR chemical shifts were referenced to the residual solvent peak.^[1]

2.2. General procedure A – Pd-catalyzed ring-opening of benzofuran derivatives

A microwave tube of suitable volume (capable of withstanding pressure up to 20 bar) equipped with a magnetic stirring bar was charged with the appropriate substrate dissolved in EtCN (5.0 mL per mmol of substrate) and water (50 μ L per mmol of substrate), then *N,N*-diisopropylethylamine (DIPEA, Hünig's base, 2.0 equiv) and PdCl₂(PPh₃)₂ (0.05 equiv) were introduced. No special precautions were adopted to exclude air. The tube was hermetically sealed and heated at 130 °C in a microwave apparatus.

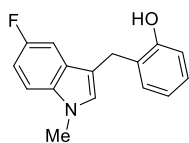
After stirring for 20 minutes at the prescribed temperature, the tube was cooled to room temperature and the mixture was diluted with CH₂Cl₂ (10 mL per mmol of substrate) and water (10 mL per mmol of substrate). Phases were separated and the aqueous layer was extracted with more CH₂Cl₂ (3 x 5 mL). The combined organic extracts were dried over MgSO₄ and evaporated at reduced pressure. The residue was dissolved in a small amount of CH₂Cl₂, dry-loaded on a flash chromatography column, and eluted with the appropriate solvent mixture, as detailed for each compound.



2-((1-Methyl-1*H*-indol-3-yl)methyl)phenol (2a)

The reaction of **1a** (179 mg, 0.493 mmol) according to general procedure **A** (flash chromatography eluent: toluene) gave the title compound in the form of a pale yellow oil (76.5 mg, 65%).

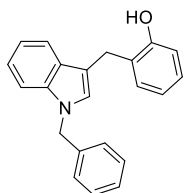
¹H NMR (300 MHz, CDCl₃): δ = 7.53 (d, *J* = 7.9 Hz, 1H), 7.33-7.04 (m, 5H), 6.89 (td, *J* = 7.4, 1.3 Hz, 1H), 6.81 (dd, *J* = 8.0, 1.3 Hz, 1H), 6.78 (br s, 1H), 4.99 (br s, 1H), 4.10 (s, 2H), 3.71 (s, 3H) ppm. ¹³C NMR (75 MHz, CDCl₃): δ = 154.5, 137.6, 130.7, 128.0, 127.7, 127.2, 126.6, 122.2, 121.0, 119.4, 119.3, 116.2, 111.8, 109.5, 32.8, 27.1 ppm. HRMS (EI) *m/z*: [M]⁺ Calcd for C₁₆H₁₅NO 237.1154; Found 237.1151. Spectral data are in agreement with the literature.^[2]



2-((5-Fluoro-1-methyl-1H-indol-3-yl)methyl)phenol (2b)

The reaction of **1b** (182 mg, 0.477 mmol) according to general procedure **A** (flash chromatography eluent: toluene) gave the title compound in the form of a pale brown oil (78.6 mg, 64%).

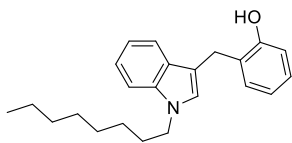
¹H NMR (300 MHz, CDCl₃) δ = 7.22-7.09 (m, 4H), 7.00-6.76 (m, 4H), 4.96 (br s, 1H), 4.03 (s, 2H), 3.69 (s, 3H) ppm. ¹³C NMR (75 MHz, CDCl₃): δ = 157.8 (d, ¹J_{CF} = 234.5 Hz), 154.3, 134.2, 130.6, 128.8, 128.0, 127.9 (d, ³J_{CF} = 11.2 Hz), 126.4, 121.1, 116.1, 112.1 (d, ⁴J_{CF} = 4.9 Hz), 110.5 (d, ²J_{CF} = 26.5 Hz), 110.1 (d, ³J_{CF} = 9.7 Hz), 104.3 (d, ²J_{CF} = 23.4 Hz), 33.1, 26.8 ppm. ¹⁹F{¹H} NMR (282 MHz, CDCl₃): δ = -125.07 ppm. HRMS (EI) m/z: [M]⁺ Calcd for C₁₆H₁₄FNO 255.1059; Found 255.1062.



2-((1-Benzyl-1H-indol-3-yl)methyl)phenol (2c)

The reaction of **1c** (177 mg, 0.403 mmol) according to general procedure **A** (flash chromatography eluent: petroleum ether/EtOAc 90:10) gave the title compound in the form of a pale brown solid (89.2 mg, 71%).

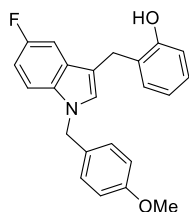
¹H NMR (300 MHz, CDCl₃): δ = 7.53 (d, *J* = 7.8 Hz, 1H), 7.33-7.00 (m, 10H), 6.91-6.84 (m, 2H), 6.79 (dd, *J* = 8.0, 1.2 Hz, 1H), 5.23 (s, 2H), 5.01 (s, 1H), 4.11 (s, 2H) ppm. ¹³C NMR (75 MHz, CDCl₃): δ = 154.5, 137.6, 137.3, 130.7, 128.9, 128.0 (2C, two resolved peaks 128.01 and 127.96), 127.7, 126.8, 126.7, 126.5, 122.4, 120.9, 119.5, 116.1, 112.6, 110.0, 50.1, 27.1 ppm. HRMS (EI) m/z: [M]⁺ Calcd for C₂₂H₁₉NO 313.1467; Found 313.1467.



2-((1-Octyl-1H-indol-3-yl)methyl)phenol (2d)

The reaction of **1d** (157 mg, 0.340 mmol) according to general procedure **A** (flash chromatography eluent: petroleum ether/EtOAc 95:5) gave the title compound in the form of a pale yellow oil (77.3 mg, 68%).

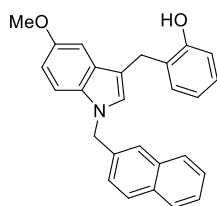
¹H NMR (300 MHz, CDCl₃): δ = 7.50 (d, *J* = 7.9 Hz, 1H), 7.28 (d, *J* = 8.2 Hz, 1H), 7.24-7.00 (m, 4H), 6.91-6.75 (m, 3H), 5.05 (br s, 1H), 4.08 (s, 2H), 3.98 (t, *J* = 7.2 Hz, 2H), 1.75 (quint, *J* = 7.2 Hz, 2H), 1.35-1.15 (m, 10H), 0.84 (t, *J* = 7.1, 3H) ppm. ¹³C NMR (75 MHz, CDCl₃): δ = 154.6, 136.9, 130.6, 127.9, 127.8, 126.6, 126.2, 122.0, 120.9, 119.4, 119.1, 116.1, 111.6, 109.7, 46.4, 31.9, 30.4, 29.3, 29.3, 27.2, 27.1, 22.7, 14.2 ppm. HRMS (EI) m/z: [M]⁺ Calcd for C₂₃H₂₉NO 335.2249; Found 335.2243.



2-((5-Fluoro-1-(4-methoxybenzyl)-1*H*-indol-3-yl)methyl)phenol (**2e**)

The reaction of **1e** (145 mg, 0.297 mmol) according to general procedure **A** (flash chromatography eluent: petroleum ether/EtOAc 90:10) gave the title compound in the form of a pale brown oil (81.3 mg, 76%).

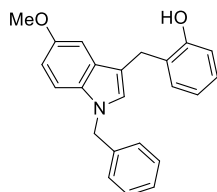
^1H NMR (300 MHz, CDCl_3): δ = 7.22-7.06 (m, 4H), 7.02-6.94 (m, 2H), 6.93-6.73 (m, 6H), 5.10 (br s, 2H), 5.07 (br s, 1H), 4.02 (s, 2H), 3.72 (s, 3H) ppm. ^{13}C NMR (75 MHz, CDCl_3): δ = 159.2, 157.8 (d, $^1J_{\text{CF}}$ = 234.8 Hz), 154.3, 133.7, 130.6, 129.3, 128.4 (d, $^3J_{\text{CF}}$ = 9.7 Hz), 128.2, 127.9, 126.4, 121.0, 116.0, 114.3, 112.7 (d, $^4J_{\text{CF}}$ = 4.8 Hz), 110.7 (d, $^3J_{\text{CF}}$ = 9.6 Hz), 110.6 (d, $^2J_{\text{CF}}$ = 26.5 Hz), 104.4 (d, $^2J_{\text{CF}}$ = 23.4 Hz), 55.4, 49.9, 26.7 ppm. $^{19}\text{F}\{^1\text{H}\}$ NMR (282 MHz, CDCl_3): δ = -124.68 ppm. HRMS (EI) m/z : $[\text{M}]^+$ Calcd for $\text{C}_{23}\text{H}_{20}\text{FNO}_2$ 361.1478; Found 361.1488.



2-((5-Methoxy-1-(2-naphthylmethyl)-1*H*-indol-3-yl)methyl)phenol (**2f**)

The reaction of **1f** (187 mg, 0.360 mmol) according to general procedure **A** (flash chromatography eluent: petroleum ether/EtOAc 80:20) gave the title compound in the form of a pale brown solid (77.0 mg, 54%).

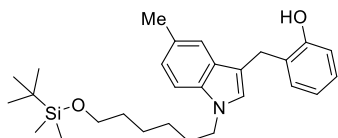
^1H NMR (300 MHz, CDCl_3): δ = 7.86-7.65 (m, 3H), 7.53-7.37 (m, 3H), 7.29-7.07 (m, 4H), 7.00-6.74 (m, 5H), 5.32 (s, 2H), 5.10 (s, 1H), 4.08 (s, 2H), 3.76 (s, 3H) ppm. ^{13}C NMR (75 MHz, CDCl_3): δ = 154.5, 154.1, 135.1, 133.4, 132.9, 132.6, 130.6, 128.8, 128.4, 128.0, 127.8, 127.4, 126.5, 126.1, 125.5, 124.8, 120.9, 116.1, 112.5, 112.1, 110.9, 101.3, 56.0, 50.6, 27.1 ppm. HRMS (EI) m/z : $[\text{M}]^+$ Calcd for $\text{C}_{27}\text{H}_{23}\text{NO}_2$ 393.1729; Found 393.1744.



2-((1-Benzyl-5-methoxy-1*H*-indol-3-yl)methyl)phenol (**2g**)

The reaction of **1g** (227 mg, 0.484 mmol) according to general procedure **A** (flash chromatography eluent: petroleum ether/EtOAc 80:20) gave the title compound in the form of a pale brown solid (96.6 mg, 58%).

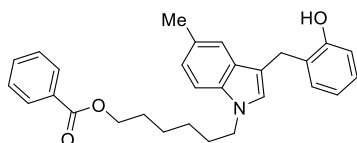
^1H NMR (300 MHz, CDCl_3): δ = 7.30-7.17 (m, 4H), 7.15-6.99 (m, 4H), 6.95 (d, J =2.5, 1H), 6.91-6.75 (m, 4H), 5.16 (s, 2H), 5.14 (s, 1H), 4.06 (s, 2H), 3.75 (s, 3H) ppm. ^{13}C NMR (75 MHz, CDCl_3): δ = 154.5, 154.1, 137.7, 132.5, 130.6, 128.9, 128.4, 127.9, 127.7, 127.3, 126.7, 126.5, 120.9, 116.1, 112.5, 112.0, 110.8, 101.3, 55.9, 50.3, 27.1 ppm. HRMS (EI) m/z : $[\text{M}]^+$ Calcd for $\text{C}_{23}\text{H}_{21}\text{NO}_2$ 343.1572; Found 343.1560.



2-((1-(6-((*tert*-Butyldimethylsilyl)oxy)hexyl)-5-methyl-1*H*-indol-3-yl)methyl)phenol (2h)

The reaction of **1h** (289 mg, 0.50 mmol) according to general procedure **A** (flash chromatography eluent: petroleum ether/EtOAc 95:5) gave the title compound in the form of a pale yellow oil (124 mg, 55%).

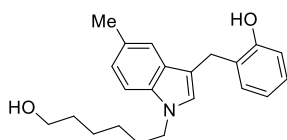
^1H NMR (300 MHz, CDCl_3): δ = 7.35-7.30 (m, 1H), 7.28-7.10 (m, 3H), 7.04 (dd, J = 8.4, 1.6 Hz, 1H), 6.89 (td, J = 7.4, 1.2 Hz, 1H), 6.85-6.76 (m, 2H), 5.22 (s, 1H), 4.08 (s, 2H), 3.99 (t, J = 7.1 Hz, 2H), 3.57 (t, J = 6.4 Hz, 2H), 2.43 (s, 3H), 1.78 (quint, J = 7.2 Hz, 2H), 1.54-1.40 (m, 2H), 1.40-1.16 (m, 4H), 0.89 (s, 9H), 0.04 (s, 6H) ppm. ^{13}C NMR (75 MHz, CDCl_3): δ = 154.7, 135.3, 130.6, 128.4, 128.0, 127.9, 126.7, 126.3, 123.6, 120.8, 119.0, 116.1, 111.0, 109.4, 63.2, 46.4, 32.8, 30.3, 27.1, 26.9, 26.1, 25.6, 21.6, 18.5, -5.1 ppm. HRMS (EI) m/z : $[\text{M}]^+$ Calcd for $\text{C}_{28}\text{H}_{41}\text{NO}_2\text{Si}$ 451.2907; Found 451.2918.



6-(3-(2-Hydroxybenzyl)-5-methyl-1*H*-indol-1-yl)hexyl benzoate (2i)

The reaction of **1i** (290 mg, 0.511 mmol) according to general procedure **A** (flash chromatography eluent: petroleum ether/EtOAc 90:10) gave the title compound in the form of a pale yellow oil (141 mg, 62%).

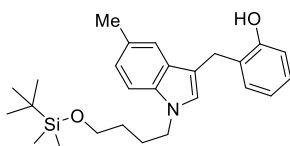
^1H NMR (300 MHz, CDCl_3): δ = 7.99 (d, J = 7.0 Hz, 2H), 7.53-7.44 (m, 1H), 7.41-7.33 (m, 2H), 7.30 (br s, 1H), 7.21-7.11 (m, 2H), 7.07 (td, J = 7.7, 1.7 Hz, 1H), 6.98 (dd, J = 8.4, 1.6 Hz, 1H), 6.86-6.75 (m, 2H), 6.72 (s, 1H), 5.60 (br s, 1H), 4.22 (t, J = 6.7 Hz, 2H), 4.03 (s, 2H), 3.93 (t, J = 7.0 Hz, 2H), 2.38 (s, 3H), 1.76-1.60 (m, 4H), 1.44-1.17 (m, 4H) ppm. ^{13}C NMR (75 MHz, CDCl_3): δ = 166.9, 154.6, 135.1, 133.0, 130.6, 130.4, 129.6, 128.4, 128.3, 128.1, 127.7, 126.8, 126.4, 123.5, 120.6, 119.0, 115.9, 111.4, 109.2, 65.0, 46.2, 30.1, 28.6, 26.9, 26.6, 25.7, 21.6 ppm. HRMS (EI) m/z : $[\text{M}]^+$ Calcd for $\text{C}_{29}\text{H}_{31}\text{NO}_3$ 441.2304; Found 441.2307.



2-((1-(6-Hydroxyhexyl)-5-methyl-1*H*-indol-3-yl)methyl)phenol (2j)

The reaction of **1j** (228 mg, 0.491 mmol) according to general procedure **A** (flash chromatography eluent: petroleum ether/EtOAc 70:30) gave the title compound in the form of a pale yellow oil (79.1 mg, 48%).

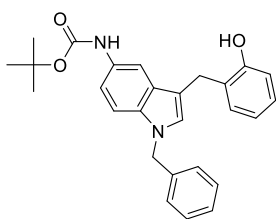
^1H NMR (300 MHz, CDCl_3): δ = 7.31 (br s, 1H), 7.23-7.13 (m, 2H), 7.10 (td, J = 7.7, 1.6 Hz, 1H), 7.00 (dd, J = 8.4, 1.6 Hz, 1H), 6.84 (td, J = 7.4, 1.3, 1H), 6.77 (dd, J = 8.0, 1.2 Hz, 1H), 6.74 (br s, 1H), 5.75 (s, 1H), 4.04 (s, 2H), 3.95 (t, J = 6.9 Hz, 2H), 3.52 (t, J = 6.5 Hz, 2H), 2.40 (s, 3H), 1.72 (quint, J = 7.0 Hz, 2H), 1.51-1.39 (m, 2H), 1.34-1.14 (m, 4H) ppm. ^{13}C NMR (75 MHz, CDCl_3): δ = 154.6, 135.1, 130.6, 128.3, 128.0, 127.7, 126.9, 126.4, 123.5, 120.6, 119.0, 116.0, 111.3, 109.3, 62.7, 46.2, 32.5, 30.1, 26.9, 26.7, 25.3, 21.6 ppm. HRMS (EI) m/z : $[\text{M}]^+$ Calcd for $\text{C}_{22}\text{H}_{27}\text{NO}_2$ 337.2042; Found 337.2042.



2-((1-(6-((*tert*-Butyldimethylsilyl)oxy)butyl)-5-methyl-1*H*-indol-3-yl)methyl)phenol (**2k**)

The reaction of **1k** (200 mg, 0.364 mmol) according to general procedure **A** (flash chromatography eluent: petroleum ether/EtOAc 95:5) gave the title compound in the form of a pale yellow oil (84.9 mg, 55%).

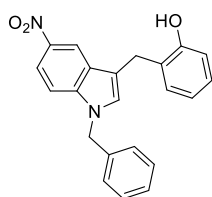
^1H NMR (300 MHz, CDCl_3): δ = 7.32 (s, 1H), 7.26-7.19 (m, 2H), 7.16 (td, J = 7.6 Hz, 1.4, 1H), 7.05 (dd, J = 8.4, 1.4 Hz, 1H), 6.91 (td, J = 7.6, 1.4 Hz, 1H), 6.86-6.80 (m, 2H), 5.08 (s, 1H), 4.09 (s, 2H), 4.05 (t, J = 7.4 Hz, 2H), 3.59 (t, J = 6.2 Hz, 2H), 2.43 (s, 3H), 1.92-1.78 (m, 2H), 1.58-1.43 (m, 2H), 0.88 (s, 9H), 0.03 (s, 6H) ppm. ^{13}C NMR (75 MHz, CDCl_3): δ = 154.7, 135.3, 130.6, 128.5, 128.0, 127.9, 126.6, 126.3, 123.7, 120.9, 119.0, 116.2, 110.9, 109.4, 62.7, 46.4, 30.2, 27.2, 27.0, 26.1, 21.6, 18.5, -5.2 ppm. HRMS (EI) m/z : $[\text{M}]^+$ Calcd for $\text{C}_{26}\text{H}_{37}\text{NO}_2\text{Si}$ 423.2594; Found 423.2580.



tert-Butyl (1-benzyl-3-(2-hydroxybenzyl)-1*H*-indol-5-yl)carbamate (**2l**)

The reaction of **1l** (58.9 mg, 0.106 mmol) according to general procedure **A** (flash chromatography eluent: petroleum ether/EtOAc 90:10) gave the title compound in the form of a pale yellow oil (22.7 mg, 50%).

^1H NMR (300 MHz, CDCl_3): δ = 7.53 (br s, 1H), 7.35-6.97 (m, 9H), 6.96-6.74 (m, 3H), 6.44 (br s, 1H), 5.26 (br s, 1H), 5.18 (s, 2H), 4.05 (s, 2H), 1.49 (s, 9H) ppm. ^{13}C NMR (75 MHz, CDCl_3): δ = 154.4, 153.7, 137.6, 134.2, 130.7, 130.6, 128.9, 128.2, 127.8, 127.7, 127.5, 126.7, 126.6, 120.8, 116.1 (2C, two unresolved peaks), 112.6, 110.2, 80.2, 50.2, 28.6, 26.7 ppm. HRMS (EI) m/z : $[\text{M} - \text{C}_4\text{H}_8]^+$ Calcd for $\text{C}_{27}\text{H}_{28}\text{N}_2\text{O}_3$ 372.1474; Found 372.1460.

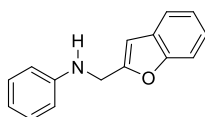


2-((1-Benzyl-5-nitro-1*H*-indol-3-yl)methyl)phenol (**2m**)

The reaction of **1m** (116 mg, 0.240 mmol) according to general procedure **A** (flash chromatography eluent: petroleum ether/EtOAc 80:20) gave the title compound in the form of a yellow solid (20.8 mg, 24%).

¹H NMR (300 MHz, CDCl₃): δ = 8.58 (d, J = 2.2 Hz, 1H), 8.02 (dd, J = 9.1, 2.2 Hz, 1H), 7.37-6.98 (m, 9H), 6.87 (td, J = 7.5, 1.2 Hz, 1H), 6.79 (dd, J = 8.0, 1.2 Hz, 1H), 5.26 (s, 2H), 5.08 (br s, 1H), 4.11 (s, 2H) ppm. ¹³C NMR (75 MHz, CDCl₃): δ = 153.7, 141.5, 139.8, 136.4, 130.7, 129.7, 129.1, 128.2, 128.1, 127.5, 126.8, 126.2, 121.2, 117.8, 117.1, 116.9, 115.8, 109.8, 50.6, 25.8 ppm. HRMS (EI) m/z : [M]⁺ Calcd for C₂₂H₁₈N₂O₃ 358.1317; Found 358.1330.

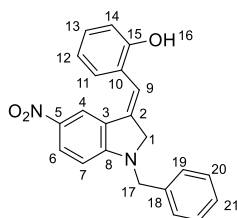
The isomeric compound **3** was also isolated as an orange solid, that eluted just after **2m** (20.8 mg, 24%).



N-(2-Benzofurylmethyl)aniline

When general procedure **A** was applied to **1o** (140 mg, 0.4 mmol) by heating at 140 °C for 6 h, only traces of indole **2b** were observed by NMR analysis of the crude reaction mixture and comparison with literature data.^[3] The title compound was isolated instead in the form of a pale yellow oil (27.9 mg, 31%) by column chromatography on silica gel (eluent: petroleum ether/toluene 50:50).

¹H NMR (300 MHz, CDCl₃): δ = 7.47 (d, J = 7.1 Hz, 1H), 7.42 (d, J = 7.9 Hz, 1H), 7.26-7.12 (m, 4H), 6.76-6.64 (m, 3H), 6.57 (s, 1H), 4.44 (s, 2H), 4.13 (br s, 1H) ppm. ¹³C NMR (75 MHz, CDCl₃): δ = 155.8, 155.0, 147.5, 129.4, 128.5, 124.0, 122.9, 120.9, 118.3, 113.3, 111.2, 103.8, 42.0 ppm. Spectral data are in agreement with the literature.^[2]



(*E*)-2-((1-Benzyl-5-nitroindolin-3-ylidene)methyl)phenol (**3**)

When general procedure **A** was applied to **1m** (115 mg, 0.237 mmol) by heating at 130 °C for a shorter reaction time (5 minutes), the title compound was isolated from the reaction mixture by flash chromatography (eluent: petroleum ether/EtOAc 80:20) in the form of a vermillion solid (45.4 mg, 53%).

The assignment of all ^1H and ^{13}C NMR resonances has been done with the aid of COSY, APT, HSQC, HSQC-TOCSY and HMBC experiments, while the determination of the geometry of the double bond was performed by observing NOE contacts between the ring protons of the phenolic moiety and H_4 , and by the measurement of the 3J between H_9 and C_1 [$^3J(\text{C}_1\text{-H}_9) = 4.8 \text{ Hz}$]. The relevant NOESY map and the section of the HMBC showing the $^3J(\text{C}_1\text{-H}_9)$ are reported in Figure S1 and Figure S2.

^1H NMR (300 MHz, CDCl_3): $\delta = 8.02$ (dd, $J = 9.0, 2.3 \text{ Hz}$, 1H, H_6), 7.75 (d, $J = 2.3 \text{ Hz}$, 1H, H_4), 7.42-7.20 (m, 7H, $\text{H}_{11}, \text{H}_{12}, \text{H}_{13}, \text{H}_{19}, \text{H}_{20}$), 7.03-6.93 (m, 2H, $\text{H}_{14}, \text{H}_{21}$), 6.49-6.40 (m, 2H, H_7, H_9 ; careful analysis of the COSY and HMBC maps shows that the signal for H_9 is a triplet with $J = 3.0 \text{ Hz}$ that overlaps with the doublet of H_7), 5.06 (br s, 1H, H_{16}), 4.51 (s, 2H, H_{17}), 4.49 (d, $J = 3.0 \text{ Hz}$, 2H, H_1) ppm. ^{13}C NMR (75 MHz, CDCl_3): $\delta = 159.4$ (C_8), 152.7 (C_{15}), 138.3 (C_5), 136.6 (C_{18}), 135.9 (C_2), 130.1 (C_{11}), 129.3 (C_{13}), 129.2 (C_{20}), 128.6 (C_6), 128.2 (C_{12}), 127.6 (C_{19}), 124.9 (C_3), 122.5 (C_{10}), 121.2 (C_{21}), 120.9 (C_4), 116.1 (C_{14}), 115.9 (C_7), 104.9 (C_9), 58.7 (C_1), 50.4 (C_{17}) ppm. ^{15}N NMR (30.4 MHz, CDCl_3): $\delta = 276.1, 87.6$ ppm (both resonances were detected by HMBC for enhanced sensitivity). HRMS (EI) m/z : $[\text{M}]^+$ Calcd for $\text{C}_{22}\text{H}_{18}\text{N}_2\text{O}_3$ 358.1317; Found 358.1319.

A minor amount of **2m** was also isolated (13.5 mg, 16%).

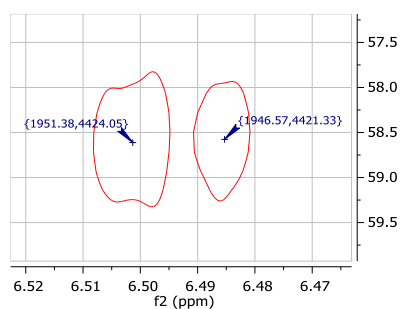


Figure S1 – Section of the HMBC map for compound **3** showing $^3J(\text{C}_1\text{-H}_9) = 4.8 \text{ Hz}$ (corresponding to a *cis* stereochemistry). Chemical shifts in Hz are reported in blue. It is not possible to measure $^3J(\text{C}_3\text{-H}_9)$ by this technique because H_7 and H_9 have very close chemical shifts and both couple with H_3 , thus signals overlap.

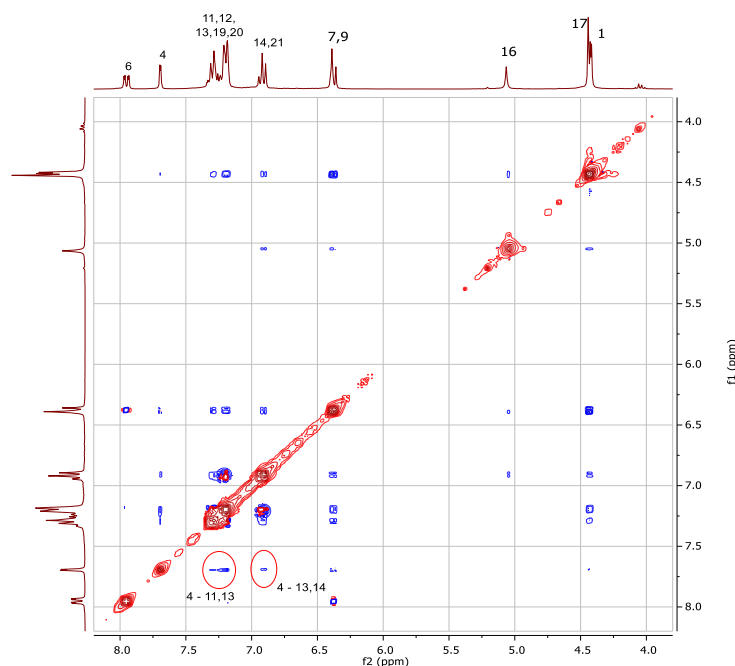
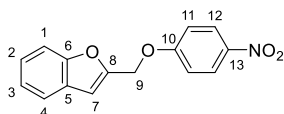
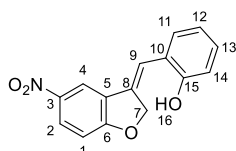


Figure S2 – NOESY map for compound **3**. Signals corresponding to NOE contacts between H_4 and the protons of the phenolic moiety are evidenced in red circles.



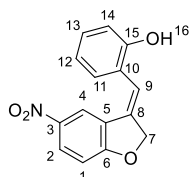
2-((4-Nitrophenoxy)methyl)benzofuran

^1H NMR (300 MHz, CDCl_3): δ = 8.20 (d, J = 9.2 Hz, 2H, H_{12}), 7.60-7.54 (m, 1H, H_4), 7.52-7.46 (m, 1H, H_1), 7.36-7.18 (m, 2H, H_2 and H_3), 7.07 (d, J = 9.2 Hz, 2H, H_{11}), 6.83 (br s, 1H, H_7), 5.24 (s, 2H, H_9) ppm. ^{13}C NMR (75 MHz, CDCl_3): δ = 163.2 (C_{10}), 155.4 (C_6), 151.3 (C_8), 142.1 (C_{13}), 127.8 (C_5), 126.0 (C_{12}), 125.2 (C_2 or C_3), 123.2 (C_3 or C_2), 121.5 (C_4), 115.0 (C_{11}), 111.6 (C_1), 107.2 (C_7), 63.5 (C_9) ppm. HRMS (EI) m/z : $[\text{M}]^+$ Calcd for $\text{C}_{15}\text{H}_{11}\text{NO}_4$ 269.0688; Found 269.0681.



(Z)-2-((5-Nitrobenzofuran-3(2H)-ylidene)methyl)phenol

^1H NMR (300 MHz, CDCl_3): δ 8.41 (d, J = 2.4 Hz, 1H, H_4), 8.15 (dd, J = 8.9, 2.4 Hz, 1H, H_2), 7.32 (t, J = 3.2, 3.2 Hz, 1H, H_9), 7.23-7.15 (m, 1H, H_{13}), 7.09-6.97 (m, 2H, H_{11} and H_{12}), 6.93 (d, J = 8.9 Hz, 1H, H_1), 6.87 (dd, J = 8.0, 1.2 Hz, 1H, H_{14}), 5.53 (d, J = 3.2 Hz, 2H, H_7) ppm. ^{13}C NMR (75 MHz, CDCl_3): δ = 167.3 (C_6), 153.7 (C_{15}), 142.6 (C_3), 133.5 (C_8), 129.4 (C_{13}), 129.0 (C_{10}), 128.1 (C_{11}), 126.7 (C_2), 123.4 (C_5), 121.1 (C_{12}), 116.7 (C_4), 116.1 (C_{14}), 114.5 (C_9), 110.4 (C_1), 76.9 (C_7) ppm. HRMS (EI) m/z : $[\text{M}]^+$ Calcd for $\text{C}_{15}\text{H}_{11}\text{NO}_4$ 269.0688; Found 269.0688.

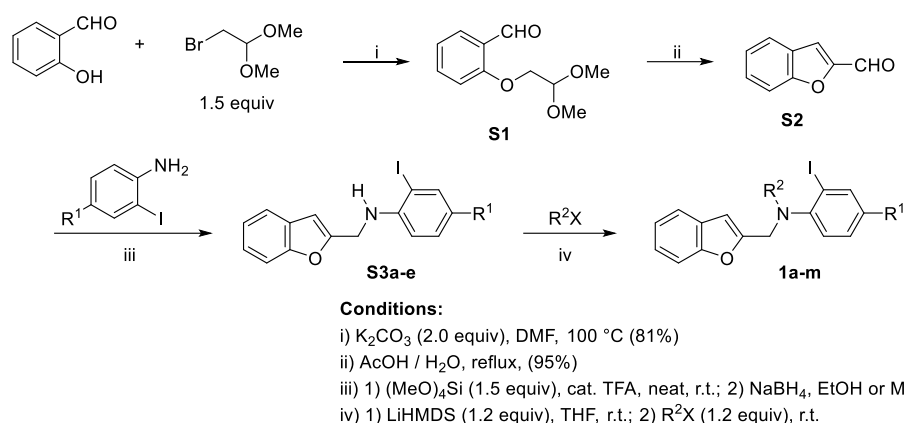


(E)-2-((5-Nitrobenzofuran-3(2H)-ylidene)methyl)phenol

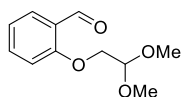
^1H NMR (300 MHz, CDCl_3): δ 8.02 (dd, J = 9.0, 2.4 Hz, 1H, H_2), 7.88 (d, J = 2.4 Hz, 1H, H_4), 7.29-7.18 (m, 2H, H_{11} and H_{13}), 6.99-6.87 (m, 2H, H_{12} and H_{14}), 6.80 (d, J = 9.0 Hz, 1H, H_1), 6.51 (t, J = 2.9 Hz, 1H, H_9), 5.35 (d, J = 2.8 Hz, 2H, H_7) ppm. ^{13}C NMR (75 MHz, CDCl_3): δ = 169.7 (C_6), 152.9 (C_{15}), 142.0 (C_3), 136.0 (C_8), 130.3 (C_{13}), 129.3 (C_{11}), 127.5 (C_2), 125.4 (C_{10}), 122.0 (C_5), 121.1 (C_{12}), 120.4 (C_4), 116.2 (C_{14}), 116.20, 110.6 (C_1), 77.8 (C_7) ppm. HRMS (EI) m/z : $[\text{M}]^+$ Calcd for $\text{C}_{15}\text{H}_{11}\text{NO}_4$ 269.0688; Found 269.0682.

2.3. Synthesis of starting materials

Most substrates for the benzofuran ring-opening reaction were obtained according to the synthetic sequence shown in Scheme S1. The conditions of reaction were adapted for some of the target molecules, as described in detail in the following.



Scheme S1 – Synthesis of substrates for the benzofuran ring-opening reaction.

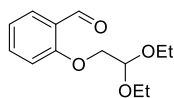


2-(2,2-Dimethoxyethoxy)benzaldehyde (S1)^[4]

A 250 mL round-bottomed flask equipped with a powerful magnetic stirrer was charged with salicylaldehyde (10.7 mL, 0.10 mol), bromoacetaldehyde dimethyl acetal (12.4 mL, 0.105 mol, 1.05 equiv), anhydrous K_2CO_3 (27.6 g, 0.20 mol, 2.0 equiv) and dry DMF (50 mL). The resulting suspension was stirred overnight at 100 °C.

After cooling, the reaction mixture was diluted with EtOAc (200 mL) and filtered through a pad of diatomaceous earth. The clear filtrate was concentrated *in vacuo* and DMF removed by prolonged heating at 70 °C at 5 mbar. The oily residue was purified by short-path distillation in a Kugelrohr apparatus (0.1 mbar) to give the title compound in the form of a pale yellow oil (17.1 g, 81%).

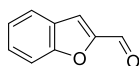
^1H NMR (300 MHz, CDCl_3): δ = 10.5 (s, 1H), 7.84 (dd, J = 7.5, 1.8 Hz, 1H), 7.54 (ddd, J = 8.4, 7.5, 1.8 Hz, 1H), 7.05 (t, J = 7.5 Hz, 1H), 6.98 (d, J = 8.4 Hz, 1H), 4.76 (t, J = 5.2 Hz, 1H), 4.12 (d, J = 5.2 Hz, 2H), 3.48 (s, 6H) ppm. ^{13}C NMR (75 MHz, CDCl_3): δ = 189.7, 161.0, 136.0, 128.5, 125.3, 121.4, 112.9, 102.4, 68.6, 54.7 ppm.



2-(2,2-Diethoxyethoxy)benzaldehyde^[4]

The title compound was obtained by the same procedure described for compound **S1** by substituting bromoacetaldehyde diethyl acetal (15.8 mL, 0.105 mol, 1.05 equiv) to the corresponding dimethyl acetal. Pale yellow oil (19.0 g, 82%).

^1H NMR (300 MHz, CDCl_3): δ = 10.5 (s, 1H), 7.84 (dd, J = 7.5, 1.8 Hz, 1H), 7.54 (ddd, J = 8.4, 7.5, 1.8 Hz, 1H), 7.04 (t, J = 7.5 Hz, 1H), 6.99 (d, J = 8.4 Hz, 1H), 4.89 (t, J = 5.2 Hz, 1H), 4.12 (d, J = 5.2 Hz, 2H), 3.86-3.74 (m, 2H), 3.72-3.59 (m, 2H), 1.25 (t, J = 7.0 Hz, 6H) ppm. Spectral data are in agreement with the literature.^[4]

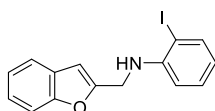


Benzofuran-2-carbaldehyde (S2)^[4]

A solution of 2-(2,2-dimethoxyethoxy)benzaldehyde (**S1**, 7.77 g, 37.0 mmol) in acetic acid (15 mL) and water (2 mL) was refluxed for 48 h. Most of the acetic acid was evaporated under reduced pressure and the residue was dissolved in Et₂O (100 mL) and extracted with saturated NaHCO₃ aqueous solution (3 x 20 mL). The organic phase was dried over Na₂SO₄ and concentrated *in vacuo*. Short-path distillation under reduced pressure (7 mbar) with the aid of a Kugelrohr apparatus gave the title compound in the form of a pale yellow oil (5.12 g, 95%).

The analogous diethyl acetal gave the same yield of benzofuran-2-carbaldehyde with the same protocol.

¹H NMR (300 MHz, CDCl₃): δ = 9.87 (s, 1H), 7.75 (ddd, *J* = 8.0, 1.3, 0.8 Hz, 1H), 7.63-7.55 (m, 3H), 7.52 (ddd, *J* = 8.4, 7.1, 1.3 Hz, 1H) ppm. Spectral data are in agreement those of an authentic sample.

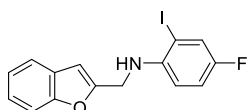


N-(Benzofuran-2-ylmethyl)-2-iodoaniline (S3a)^[5]

A mixture of benzofuran-2-carboxaldehyde (606 μ L, 5.0 mmol), 2-iodoaniline (1.10 g, 5.0 mmol) and tetramethoxysilane (1.12 mL, 7.5 mmol, 1.5 equiv) together with a catalytic amount of trifluoroacetic acid (approx. 20 μ L) was stirred for 30 minutes at room temperature, after which GLC analysis showed complete conversion of the starting materials.

Ethanol (15 mL) was then added and NaBH₄ (567 mg, 15 mmol, 3.0 equiv) was introduced in portions while keeping the mixture cooled with a water bath. After standing overnight, NaOH solution (1 M in H₂O, 30 mL) was added and most of the solvent was evaporated under reduced pressure. The resulting solution was extracted with EtOAc (3 x 20 mL). The combined organic extracts were dried over Na₂SO₄ and concentrated under reduced pressure. The residue was purified by flash chromatography on silica gel (eluent: petroleum ether/CH₂Cl₂ 95:5) to afford the title compound as a colourless oil that solidified slowly on standing (1.49 g, 85%).

¹H NMR (300 MHz, CDCl₃): δ = 7.62 (dd, *J* = 7.8, 1.5 Hz, 1H), 7.47-7.41 (m, 1H), 7.42-7.36 (m, 1H), 7.23-7.09 (m, 3H), 6.60 (dd, *J* = 8.2, 1.4 Hz, 1H), 6.54 (d, *J* = 1.1 Hz, 1H), 6.42 (td, *J* = 7.6, 1.5 Hz, 1H), 4.63 (br t, *J* = 6.1 Hz, 1H), 4.48 (dd, *J* = 6.1, 1.1 Hz, 2H) ppm. ¹³C NMR (75 MHz, CDCl₃): δ = 155.12, 155.07, 146.6, 139.3, 129.6, 128.4, 124.1, 122.9, 121.0, 119.6, 111.3, 111.2, 103.9, 85.7, 42.2 ppm.

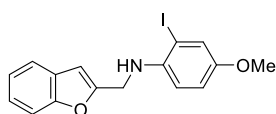


N-(Benzofuran-2-ylmethyl)-4-fluoro-2-iodoaniline (S3b)

A solution of benzofuran-2-carboxaldehyde (891 μ L, 7.35 mmol, 1.12 equiv), 4-fluoro-2-iodoaniline (1.56 g, 7.0 mmol) in CH₂Cl₂ (14 mL) was stirred overnight with 3 Å molecular sieves (700 mg). The solution was then filtered through a short plug of basic alumina and evaporated to give a thick brownish syrup.

Methanol (21 mL) was then added and NaBH₄ (747 mg, 21 mmol, 3.0 equiv) was introduced in portions while keeping the mixture cooled with a water bath. After standing overnight, NaOH solution (1 M in H₂O, 30 mL) was added and most of the methanol was evaporate under reduced pressure. The resulting solution was extracted with Et₂O (3 x 20 mL). The combined organic extracts were dried over Na₂SO₄ and concentrated under reduced pressure. The residue was purified by flash chromatography on silica gel (eluent: petroleum ether/toluene 50:50) to afford the title compound as a pale yellow oil that solidified slowly on standing (2.00 g, 83%).

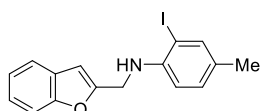
¹H NMR (300 MHz, CDCl₃): δ = 7.52-7.47 (m, 1H), 7.47-7.40 (m, 2H), 7.29-7.15 (m, 2H), 6.93 (ddd, *J* = 9.0, 7.9, 2.9 Hz, 1H), 6.60-6.54 (m, 2H), 4.56-4.45 (m, 3H) ppm. ¹³C NMR (75 MHz, CDCl₃): δ = 155.2 (d, ¹*J*_{CF} = 240.6 Hz), 155.1, 155.0, 143.5 (d, ⁴*J*_{CF} = 2.1 Hz), 128.4, 125.8 (d, ²*J*_{CF} = 24.7 Hz), 124.2, 123.0, 121.0, 116.1 (d, ²*J*_{CF} = 22.0 Hz), 111.3, 111.1 (d, ³*J*_{CF} = 7.5 Hz), 104.0, 84.3 (d, ³*J*_{CF} = 8.5 Hz), 42.8 ppm. ¹⁹F{¹H} NMR (282 MHz, CDCl₃): δ = -126.02 ppm.



N-(Benzofuran-2-ylmethyl)-4-fluoro-2-iodoaniline (S3c)

The procedure described for the synthesis of compound **S3a** was applied to 2-iodo-4-methoxyaniline (900 mg, 3.61 mmol) instead of 2-iodoaniline. The title compound was obtained by purification of the crude material by flash chromatography (eluent: petroleum ether/EtOAc 98:2) in the form of a pale yellow solid (1.07 g, 78%).

¹H NMR (300 MHz, CDCl₃): δ = 7.56-7.42 (m, 2H), 7.30 (d, *J* = 2.8 Hz, 1H), 7.30-7.17 (m, 2H), 6.83 (dd, *J* = 8.9, 2.8 Hz, 1H), 6.63 (d, *J* = 8.9 Hz, 1H), 6.60 (q, *J* = 1.0 Hz, 1H), 4.50 (d, *J* = 4.2 Hz, 2H), 4.37 (br s, 1H), 3.73 (s, 3H) ppm. ¹³C NMR (75 MHz, CDCl₃): δ = 155.5, 155.0, 152.6, 141.3, 128.5, 124.7, 124.1, 122.9, 120.9, 115.6, 112.0, 111.3, 103.9, 85.9, 56.1, 43.1 ppm.



N-(Benzofuran-2-ylmethyl)-4-fluoro-2-iodoaniline (S3d)

The procedure described for the synthesis of compound **S3a** was applied to 2-iodo-4-methylaniline (3.07 g, 13.2 mmol) instead of 2-iodoaniline. The title compound was obtained by purification of the crude material by flash chromatography (eluent: petroleum ether/toluene 95:5) in the form of a colourless oil (3.16 g, 66%).

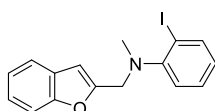
¹H NMR (300 MHz, CDCl₃): δ = 7.47-7.35 (m, 3H), 7.22-7.07 (m, 2H), 6.91 (dd, *J*=8.3, 1.9 Hz, 1H), 6.54-6.45 (m, 2H), 4.51-4.38 (m, 3H), 2.11 (s, 3H) ppm. ¹³C NMR (75 MHz, CDCl₃): δ = 155.4, 155.0, 144.5, 139.5, 130.1, 129.1, 128.5, 124.0, 122.9, 120.9, 111.2 (2C), 103.8, 85.8, 42.5, 20.0 ppm.

2.4. General procedure B for the alkylation of compounds S3a-d

To a solution of the appropriate *N*-(benzofuran-2-ylmethyl)-2-iodoaniline (**S3a-d**) in dry THF (concentration: 0.5 M), LiHMDS (dispensed as a 1.0 M solution in THF, 1.2 equiv) was added

at room temperature, rapidly followed by the appropriate electrophile (1.2 equiv). The mixture was left at room temperature under Ar atmosphere.

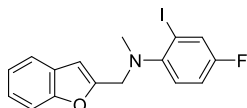
After TLC showed complete consumption of the starting material, the reaction was quenched by addition of a small amount of water and volatiles were evaporated under reduced pressure. The residue was dissolved in CH₂Cl₂ (10 mL per mmol of starting material) and water (10 mL per mmol of starting material). Phases were separated and the aqueous layer was extracted with more CH₂Cl₂ (3 x 5 mL per mmol). The combined organic extracts were dried over MgSO₄ and the residue of evaporation was purified by flash chromatography on silica gel, as detailed below for each compound.



N-(Benzofuran-2-ylmethyl)-2-iodo-N-methylaniline (1a)

The reaction of compound **S1a** (1.23 g, 3.5 mmol) with CH₃I (261 μL, 4.2 mmol, 1.2 equiv) according to general procedure **B** (flash chromatography eluent: petroleum ether/toluene 90:10) gave the title compound in the form of a pale yellow oil (1.04 g, 82%).

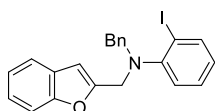
¹H NMR (300 MHz, CDCl₃): δ = 7.90 (dd, *J* = 7.9, 1.5 Hz, 1H), 7.54-7.49 (m, 1H), 7.47-7.42 (m, 1H), 7.34-7.15 (m, 3H), 7.08 (dd, *J* = 8.0, 1.6 Hz, 1H), 6.85-6.78 (m, 1H), 6.61 (br s, 1H), 4.31 (br s, 2H), 2.82 (s, 3H) ppm. ¹³C NMR (75 MHz, CDCl₃): δ = 155.3, 154.9, 153.3, 140.3, 129.1, 128.6, 125.9, 123.9, 122.7, 122.6, 120.9, 111.3, 105.3, 98.3, 54.1, 41.8 ppm. HRMS (EI) *m/z*: [M]⁺ Calcd for C₁₆H₁₄INO 363.0120; Found 363.0122.



N-(Benzofuran-2-ylmethyl)-4-fluoro-2-iodo-N-methylaniline (1b)

The reaction of compound **S1b** (918 mg, 2.5 mmol) with CH₃I (186 μL, 3.0 mmol, 1.2 equiv) according to general procedure **B** (flash chromatography eluent: petroleum ether/toluene 90:10) gave the title compound in the form of a pale brown oil (584 mg, 61%).

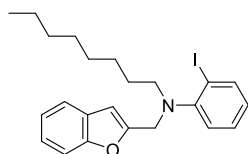
¹H NMR (300 MHz, CDCl₃): δ = 7.60 (dt, *J* = 7.9, 1.6 Hz, 1H), 7.54-7.49 (m, 1H), 7.46-7.41 (m, 1H), 7.30-7.17 (m, 2H), 7.01 (apparent dd, *J* = 6.5, 1.6 Hz, 2H), 6.58 (br s, 1H), 4.24 (s, 2H), 2.78 (s, 3H) ppm. ¹³C NMR (75 MHz, CDCl₃): δ = 159.9 (d, ¹*J*_{CF} = 248.0 Hz), 155.0, 154.9, 149.5 (d, ⁴*J*_{CF} = 3.0 Hz), 128.5, 126.7 (d, ²*J*_{CF} = 24.3 Hz), 124.0, 122.9 (d, ³*J*_{CF} = 8.4 Hz), 122.8, 120.9, 115.8 (d, ²*J*_{CF} = 21.8 Hz), 111.3, 105.4, 98.4 (d, ³*J*_{CF} = 8.2 Hz), 54.2, 42.2 ppm. ¹⁹F NMR (282 MHz, CDCl₃): δ = -117.42 ppm. HRMS (EI) *m/z*: [M]⁺ Calcd for C₁₆H₁₃FINO 381.0026; Found 381.0040.



N-(Benzofuran-2-ylmethyl)-N-benzyl-2-iodoaniline (1c)

The reaction of compound **S1a** (210 mg, 0.60 mmol) with benzyl bromide (86 μ L, 0.72 mmol, 1.2 equiv) according to general procedure **B** (flash chromatography eluent: petroleum ether/toluene 90:10) gave the title compound in the form of a pale yellow oil (206 mg, 78%).

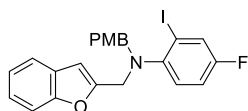
^1H NMR (300 MHz, CDCl_3): δ = 7.87 (dd, J = 7.9, 1.5 Hz, 1H), 7.51-7.36 (m, 4H), 7.34-7.12 (m, 6H), 6.91 (dd, J = 8.0, 1.5 Hz, 1H), 6.77 (td, J = 7.5, 1.5 Hz, 1H), 6.42 (br s, 1H), 4.26 (br s, 4H). ^{13}C NMR (75 MHz, CDCl_3) δ = 155.1, 154.9, 151.5, 140.1, 137.9, 129.1, 128.8, 128.5, 128.4, 127.4, 126.3, 124.8, 123.8, 122.7, 120.9, 111.2, 105.6, 99.7, 57.4, 50.0 ppm. HRMS (EI) m/z : $[\text{M}]^+$ Calcd for $\text{C}_{22}\text{H}_{18}\text{INO}$ 439.0433; Found 439.0449.



N-(Benzofuran-2-ylmethyl)-2-iodo-N-octylaniline (1d)

The reaction of compound **S1a** (210 mg, 0.60 mmol) with 1-bromooctane (124 μ L, 0.72 mmol, 1.2 equiv) according to general procedure **B** (flash chromatography eluent: petroleum ether/toluene 85:15) gave the title compound in the form of a colourless oil (207 mg, 75%).

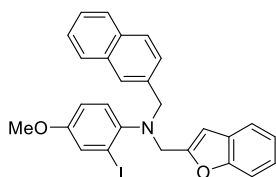
^1H NMR (300 MHz, CDCl_3): δ = 7.90 (dd, J = 7.9, 1.5 Hz, 1H), 7.53-7.47 (m, 1H), 7.45-7.40 (m, 1H), 7.29-7.16 (m, 3H), 7.00 (dd, J = 8.0, 1.6 Hz, 1H), 6.82 (td, J = 7.6, 1.6 Hz, 1H), 6.50 (br s, 1H), 4.30 (s, 2H), 3.10 (t, J = 7.2 Hz, 2H), 1.58-1.17 (m, 12H), 0.87 (d, J = 7.1 Hz, 3H) ppm. ^{13}C NMR (75 MHz, CDCl_3): δ = 155.6, 154.9, 151.6, 140.1, 128.7, 128.6, 126.2, 124.7, 123.7, 122.6, 120.8, 111.2, 105.2, 100.8, 52.9, 52.1, 32.0, 29.5, 29.4, 27.4, 27.2, 22.8, 14.3 ppm. HRMS (EI) m/z : $[\text{M}]^+$ Calcd for $\text{C}_{23}\text{H}_{28}\text{INO}$ 461.1216; Found 461.1224.



N-(Benzofuran-2-ylmethyl)-4-fluoro-2-iodo-N-(4-methoxybenzyl)aniline (1e)

The reaction of compound **S1b** (220 mg, 0.60 mmol) with 4-methoxybenzyl chloride (98 μ L, 0.72 mmol, 1.2 equiv) according to general procedure **B** (flash chromatography eluent: petroleum ether/toluene gradient from 85:15 to 80:20) gave the title compound in the form of a pale yellow oil (185 mg, 63%).

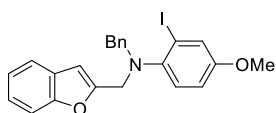
^1H NMR (300 MHz, CDCl_3): δ = 7.59 (dd, J = 7.9, 2.8 Hz, 1H), 7.52-7.46 (m, 1H), 7.42 (d, J = 8.2 Hz, 1H), 7.37-7.32 (m, 2H), 7.28-7.16 (m, 2H), 6.98-6.79 (m, 4H), 6.44 (s, 1H), 4.21 (s, 2H), 4.16 (s, 2H), 3.80 (s, 3H) ppm. ^{13}C NMR (75 MHz, CDCl_3): δ = 159.2 (d, $^1J_{\text{CF}}$ = 248.4 Hz), 159.0, 154.9, 154.9, 147.6 (d, $^4J_{\text{CF}}$ = 3.0 Hz), 130.3, 129.6, 128.4, 126.5 (d, $^2J_{\text{CF}}$ = 24.2 Hz), 125.2 (d, $^3J_{\text{CF}}$ = 8.5 Hz), 123.9, 122.8, 120.9, 115.5 (d, $^2J_{\text{CF}}$ = 21.9 Hz), 113.8, 111.2, 105.7, 99.9 (d, $^3J_{\text{CF}}$ = 8.3 Hz), 57.1, 55.4, 50.0 ppm. ^{19}F $\{^1\text{H}\}$ NMR (282 MHz, CDCl_3): δ = -116.88 ppm. HRMS (EI) m/z : $[\text{M}]^+$ Calcd for $\text{C}_{23}\text{H}_{19}\text{FINO}_2$ 487.0445; Found 487.0445.



N-(Benzofuran-2-ylmethyl)-2-iodo-4-methoxy-N-(2-naphthylmethyl)aniline (1f)

The reaction of compound **S1c** (228 mg, 0.60 mmol) with 2-bromomethylnaphthalene (158 mg, 0.72 mmol, 1.2 equiv) according to general procedure **B** (flash chromatography eluent: petroleum ether/toluene 70:30) gave the title compound in the form of a pale yellow oil (219 mg, 70%).

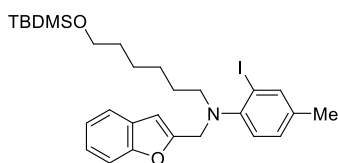
^1H NMR (300 MHz, CDCl_3): δ = 7.90-7.77 (m, 4H), 7.68 (dd, J = 8.5, 1.7 Hz, 1H), 7.55-7.40 (m, 4H), 7.31-7.15 (m, 3H), 6.89 (d, J = 8.8 Hz, 1H), 6.74 (dd, J = 8.8, 2.9 Hz, 1H), 6.48 (s, 1H), 4.39 (s, 2H), 4.25 (s, 2H), 3.74 (s, 3H) ppm. ^{13}C NMR (75 MHz, CDCl_3): δ = 157.0, 155.3, 154.9, 144.4, 135.7, 133.4, 133.0, 129.2, 128.1, 128.0, 127.8 (2C), 127.4, 126.0, 125.7, 125.0, 124.6, 123.8, 122.7, 120.9, 114.7, 111.2, 105.6, 100.8, 58.1, 55.7, 50.7 ppm. HRMS (EI) m/z : $[\text{M}]^+$ Calcd for $\text{C}_{27}\text{H}_{22}\text{INO}_2$ 519.0695 Found 519.0695.



N-(Benzofuran-2-ylmethyl)-N-benzyl-2-iodo-4-methoxyaniline (1g)

The reaction of compound **S1c** (228 mg, 0.60 mmol) with benzyl bromide (86 mg, 0.72 mmol, 1.2 equiv) according to general procedure **B** (flash chromatography eluent: petroleum ether/toluene 70:30) gave the title compound in the form of a pale yellow oil (254 mg, 90%).

^1H NMR (300 MHz, CDCl_3): δ = 7.51-7.37 (m, 5H), 7.35-7.13 (m, 5H), 6.82 (d, J = 8.8 Hz, 1H), 6.72 (dd, J = 8.8, 2.8 Hz, 1H), 6.43 (d, J = 0.9 Hz, 1H), 4.19 (s, 2H), 4.18 (s, 2H), 3.72 (s, 3H) ppm. ^{13}C NMR (75 MHz, CDCl_3): δ = 157.0, 155.3, 154.9, 144.4, 138.0, 129.2, 128.5, 128.4, 127.3, 124.9, 124.5, 123.8, 122.7, 120.9, 114.6, 111.2, 105.5, 100.8, 58.0, 55.7, 50.4 ppm. HRMS (EI) m/z : $[\text{M}]^+$ Calcd for $\text{C}_{23}\text{H}_{23}\text{INO}_2$ 469.0539; Found 469.0558.

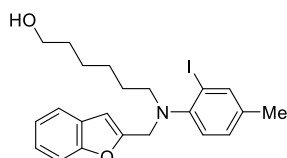


N-(Benzofuran-2-ylmethyl)-N-(6-((tert-butyl dimethylsilyl)oxy)hexyl)-2-iodo-4-methylaniline (1h)

The reaction of compound **S1d** (1.12 g, 3.08 mmol) with 1-bromo-6-((tert-butyl dimethylsilyloxy)hexane (1.09 g, 3.70 mmol, 1.2 equiv) according to general procedure **B** (flash chromatography eluent: petroleum ether/EtOAc 99:1) gave the title compound contaminated with the parent alkyl bromide. The latter impurity was removed by evaporation *in vacuo* with the aid of a Kugelrohr apparatus (0.1 mbar, 200 °C). The title compound was thus obtained in the form of a pale yellow oil (1.25 g, 70%).

^1H NMR (300 MHz, CDCl_3): δ = 7.74-7.71 (m, 1H), 7.53-7.47 (m, 1H), 7.43 (d, J = 7.8 Hz, 1H), 7.26-7.13 (m, 2H), 7.04 (dd, J = 8.1, 1.3 Hz, 1H), 6.88 (d, J = 8.1 Hz, 1H), 6.50 (s, 1H), 4.25 (s,

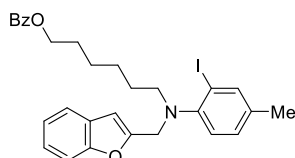
2H), 3.57 (t, $J = 6.6$ Hz, 2H), 3.07 (t, $J = 7.1$ Hz, 2H), 2.27 (s, 3H), 1.58-1.22 (m, 8H), 0.89 (s, 9H), 0.04 (s, 6H) ppm. ^{13}C NMR (75 MHz, CDCl_3): $\delta = 155.8, 154.9, 148.9, 140.3, 136.1, 129.5, 128.6, 124.2, 123.7, 122.6, 120.8, 111.2, 105.2, 101.0, 63.4, 53.0, 52.3, 33.0, 27.4, 27.1, 26.2, 25.7, 20.4, 18.5, -5.1$ ppm. HRMS (EI) m/z : $[\text{M}]^+$ Calcd for $\text{C}_{28}\text{H}_{40}\text{INO}_2\text{Si}$ 577.1873; Found 577.1889.



6-((Benzofuran-2-ylmethyl)(2-iodo-4-methylphenyl)amino)hexan-1-ol (**1j**)

Compound **1h** (693 mg, 1.2 mmol) was deprotected by treatment with a solution of Bu_4NF (TBAF, 1.0 M in THF, 3.6 mL, 3.6 mmol, 3.0 equiv). After standing overnight, the solution was diluted with toluene (50 mL) and extracted successively with water (5 x 30 mL). The organic phase was dried over Na_2SO_4 and concentrated *in vacuo*. The residue was purified by flash chromatography on silica gel (eluent: petroleum ether/EtOAc 80:20) to give the title compound in the form of a pale yellow oil (555 mg, 99%).

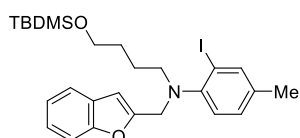
^1H NMR (300 MHz, CDCl_3): $\delta = 7.73\text{-}7.71$ (m, 1H), 7.52-7.47 (m, 1H), 7.45-7.40 (m, 1H), 7.27-7.15 (m, 2H), 7.06-7.01 (m, 1H), 6.88 (d, $J = 8.1$ Hz, 1H), 6.49 (s, 1H), 4.24 (br s, 2H), 3.60 (t, $J = 7.0$ Hz, 2H), 3.07 (t, $J = 6.9$ Hz, 2H), 2.27 (s, 3H), 1.63-1.22 (m, 8H) ppm. ^{13}C NMR (75 MHz, CDCl_3): $\delta = 155.7, 154.9, 148.8, 140.3, 136.2, 129.6, 128.6, 124.3, 123.7, 122.6, 120.8, 111.2, 105.2, 101.0, 63.1, 52.8, 52.4, 32.9, 27.4, 27.0, 25.6, 20.4$ ppm. HRMS (EI) m/z : $[\text{M}]^+$ Calcd for $\text{C}_{22}\text{H}_{26}\text{INO}_2$ 463.1008; Found 463.1021.



6-((Benzofuran-2-ylmethyl)(2-iodo-4-methylphenyl)amino)hexyl benzoate (**1i**)

Compound **1j** (315 mg, 0.679 mmol) was esterified by treatment with benzoyl chloride (100 μL , 0.86 mmol, 1.27 equiv) in dry pyridine (2 mL). Extractive workup (EtOAc/water) and evaporation of volatiles gave the title compound without the need of further purification (310 mg, 81%).

^1H NMR (300 MHz, CDCl_3): $\delta = 8.03$ (d, $J = 7.0$ Hz, 2H), 7.71 (d, $J = 2.0$ Hz, 1H), 7.60-7.38 (m, 5H), 7.26-7.14 (m, 2H), 7.04 (dd, $J = 8.1, 2.0$ Hz, 1H), 6.87 (d, $J = 8.1$ Hz, 1H), 6.48 (s, 1H), 4.28 (t, $J = 6.6$ Hz, 2H), 4.24 (s, 2H), 3.08 (t, $J = 6.7$ Hz, 2H), 2.26 (s, 3H), 1.82-1.67 (m, 2H), 1.55-1.35 (m, 6H) ppm. ^{13}C NMR (75 MHz, CDCl_3): $\delta = 166.8, 155.7, 154.9, 148.7, 140.3, 136.2, 132.9, 130.6, 129.7, 129.6, 128.6, 128.4, 124.3, 123.7, 122.6, 120.9, 111.2, 105.2, 101.0, 65.2, 52.8, 52.4, 28.9, 27.3, 26.9, 25.9, 20.4$ ppm. HRMS (EI) m/z : $[\text{M}]^+$ Calcd for $\text{C}_{29}\text{H}_{30}\text{INO}_3$ 567.1270; Found 567.1254.

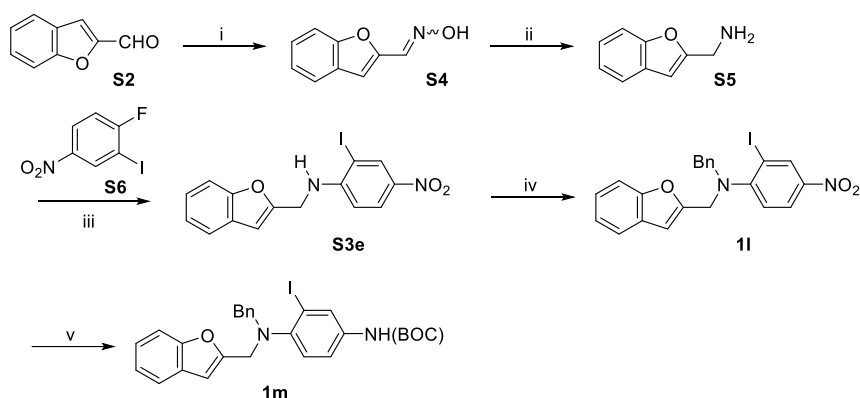


***N*-(Benzofuran-2-ylmethyl)-*N*-(6-((*tert*-butyldimethylsilyl)oxy)butyl)-2-iodo-4-methylaniline (**1k**)**

The reaction of compound **S3d** (363 mg, 1.0 mmol) with *tert*-butyldimethylsilyl trifluoromethanesulfonate (TBDMSOTf, 344 μ L, 1.5 mmol) as an electrophile according to general procedure **B** did not give the expected *N*-TBDMS protected amine, but the title compound, which originates from ring cleavage of THF. Purification by flash chromatography (eluent: petroleum ether/EtOAc 97.5:2.5) thus gave the title compound in the form of a pale yellow oil (523 mg, 93%).

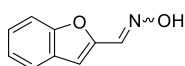
^1H NMR (300 MHz, CDCl_3): δ = 7.72 (br d, J = 2.0 Hz, 1H), 7.55-7.46 (m, 1H), 7.46-7.40 (m, 1H), 7.29-7.14 (m, 2H), 7.04 (ddd, J = 8.1, 2.0, 0.8 Hz, 1H), 6.88 (d, J = 8.1 Hz, 1H), 6.50 (br s, 1H), 4.25 (s, 2H), 3.56 (t, J = 6.0 Hz, 2H), 3.09 (t, J = 6.7 Hz, 2H), 2.26 (s, 3H), 1.63-1.43 (m, 4H), 0.86 (s, 9H), 0.01 (s, 6H) ppm. ^{13}C NMR (75 MHz, CDCl_3): δ = 155.7, 154.9, 148.8, 140.3, 136.2, 129.6, 128.6, 124.3, 123.7, 122.6, 120.8, 111.2, 105.2, 101.0, 63.0, 52.8, 52.3, 30.5, 26.1, 23.8, 20.4, 18.5, -5.1 ppm. HRMS (EI) m/z : $[\text{M}]^+$ Calcd for $\text{C}_{26}\text{H}_{36}\text{INO}_2\text{Si}$ 549.1560.; Found 549.1579.

Substrates **1l** and **1m** were obtained with a different synthetic strategy, which is represented in Scheme S2.

**Conditions:**

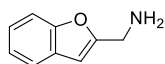
- i) $\text{NH}_2\text{OH}\cdot\text{HCl}$ (1.1 equiv), NaOAc (1.0 equiv), EtOH/ H_2O (87%)
- ii) Zn dust, conc. NH_3/EtOH 2:1, 2 h, r.t. (93%)
- iii) DIPEA (2.0 equiv), EtCN, 140 $^\circ\text{C}$, 8 h (73%)
- iv) BnBr (2.0 equiv), Bu_4NHSO_4 (0.05 equiv), NaOH, toluene / H_2O , r.t. (60%)
- v) 1) $\text{Na}_2\text{S}_2\text{O}_4$ (4.0 equiv), conc. NH_3 / EtOH / THF;
2) $(\text{BOC})_2\text{O}$ (1.2 equiv), EtOH / CH_2Cl_2 (41% over two steps).

Scheme S2 – Preparation of substrates **1l** and **1m**.

**(*syn*, *anti*)-2-Benzofurancarboxaldehyde oxime (**S4**)**

To a solution of 2-benzofurancarboxaldehyde (**S2**, 2.92 g, 20 mmol) in EtOH (5 mL), a solution of hydroxylamine hydrochloride (1.5 g, 22 mmol, 1.1 equiv) in water (3 mL) and a solution of NaOAc (1.64 g, 20 mmol) in water (5 mL) were added sequentially. The resulting mixture was heated briefly to boiling, and then cooled in an ice bath. The precipitate so formed was filtered and dried *in vacuo*. The title compound was thus obtained in the form of a white solid (2.81 g, 87%) as a 1:1 mixture of geometric isomers.

^1H NMR (300 MHz, CDCl_3): δ = 9.28 (br s, 0.5H), 8.48 (br s, 0.5H), 8.18 (s, 0.5H), 7.80-7.51 (m, 2.5H), 7.49-7.24 (m, 1.5H), 7.00 (s, 0.5H) ppm. Spectral data are in agreement with the literature.^[6]



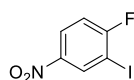
2-Benzofurylmethylamine (S5)

The reduction of oxime **S4** with Zn dust under the customary acidic (AcOH) conditions did not provide the required amine **S5** in any useful yield. An alternative protocol,^[7] which employs concentrated aqueous ammonia as a co-solvent, gave excellent results.

To a solution of 2-benzofurancarboxaldehyde oxime (**S4**, 1.93 g, 12 mmol) in EtOH (6 mL), concentrated aqueous ammonia (approx. 30% in water, 12 mL) was added. Zinc dust (3.14 g, 48 mmol, 4 equiv) was introduced in portions while stirring vigorously, as to moderate the exothermic reaction that ensues after an induction period of a few minutes.

After stirring for 2 h at room temperature, the reaction mixture was filtered through a short plug of diatomaceous earth to remove excess zinc and the filtrate was diluted with Et_2O (50 mL). The resulting mixture was treated with solid KOH to “salt out” the aqueous phase. Phases were separated and the organic layer was extracted with a small amount of ether. The combined organic extracts were dried over solid KOH and the solvent was evaporated. The residue was distilled with the aid of a Kugelrohr apparatus under reduced pressure (7 mbar) to afford the title compound as a colourless liquid (1.65 g, 93%). This amine readily forms a carbonate when in contact with air, so it should be stored in a tightly stoppered vessel.

^1H NMR (300 MHz, CDCl_3): δ = 7.55-7.49 (m, 1H), 7.47-7.41 (m, 1H), 7.29-7.16 (m, 2H), 6.52 (s, 1H), 3.98 (s, 2H), 1.51 (br s, 2H) ppm. ^{13}C NMR (75 MHz, CDCl_3): δ = 159.6, 155.0, 128.7, 123.9, 122.8, 120.8, 111.1, 102.0, 40.0 ppm. Spectral data are in agreement with the literature.^[8]

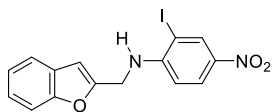


1-Fluoro-2-iodo-4-nitrobenzene (S6)

In a 250 mL-flask equipped with a powerful stirrer, commercially available 2-fluoro-5-nitroaniline (4.68 g, 30 mmol) was dissolved in a warm mixture of concentrated sulfuric acid (14 mL) and water (18 mL). A precipitate of the amine salt formed on cooling to 0 °C and the mixture became difficult to stir. A solution of NaNO_2 (2.17 g, 31.5 mmol, 1.05 equiv) in water (5 mL) was added dropwise, while maintaining the temperature under 5 °C. The amine salt dissolved completely as long as the diazonium salt was formed. The solution so obtained was poured in portions into a solution of KI (10 g, 60 mmol, 2.0 equiv) in water (30 mL). When the addition was complete, the resulting mixture was heated briefly to boiling and then cooled again in an ice bath.

The brown precipitate so formed was filtered and recrystallized from EtOH to give the title compound in the form of a brown solid (5.23 g, 65%).

^1H NMR (300 MHz, CDCl_3): δ = 8.66 (dd, J = 5.2, 2.7 Hz, 1H), 8.25 (ddd, J = 9.0, 4.3, 2.7 Hz, 1H), 7.20 (dd, J = 9.0, 6.9 Hz, 1H) ppm. ^{13}C NMR (75 MHz, CDCl_3): δ = 165.6 (d, $^1J_{\text{CF}}$ = 256.2 Hz), 144.8, 135.4 (d, $^3J_{\text{CF}}$ = 3.8 Hz), 126.0 (d, $^3J_{\text{CF}}$ = 9.2 Hz), 116.1 (d, $^2J_{\text{CF}}$ = 26.4 Hz), 81.5 (d, $^2J_{\text{CF}}$ = 28.6 Hz) ppm. $^{19}\text{F}\{^1\text{H}\}$ NMR (282 MHz, CDCl_3): δ = -83.10 ppm. Spectral data are in agreement with the literature.^[9]

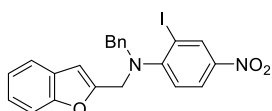


N-(Benzofuran-2-ylmethyl)-2-iodo-4-nitroaniline (S3e)

A solution of amine **S5** (441 mg, 3.0 mmol), 1-fluoro-2-iodo-4-nitrobenzene (**S6**, 801 mg, 3.0 mmol), DIPEA (1.04 mL, 6.0 mmol, 2.0 equiv) in EtCN (3 mL) was heated in a pressure-resistant sealed tube at 140 °C for 8 h.

The crude reaction mixture was diluted with EtOAc (30 mL) and extracted with water (3 x 5 mL). The organic phase was dried over MgSO₄, concentrated in vacuo and the residue purified by recrystallization from EtOH to give the title compound as a yellow powder (864 mg, 73%).

¹H NMR (300 MHz, CDCl₃): δ = 8.62 (d, *J* = 2.5 Hz, 1H), 8.14 (dd, *J* = 9.1, 2.5 Hz, 1H), 7.54 (d, *J* = 7.2 Hz, 1H), 7.47 (d, *J* = 8.0 Hz, 1H), 7.35-7.20 (m, 2H), 6.72-6.60 (m, 2H), 5.47 (br t, *J* = 6.0 Hz, 1H), 4.65 (d, *J* = 6.0 Hz, 2H) ppm. ¹³C NMR (75 MHz, CDCl₃): δ = 155.2, 152.9, 151.4, 139.1, 135.5, 128.0, 126.1, 124.7, 123.3, 121.2, 111.4, 108.6, 104.8, 82.8, 42.0 ppm.

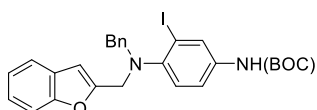


N-(Benzofuran-2-ylmethyl)-N-benzyl-2-iodo-4-nitroaniline (1l)

General procedure **B** for the alkylation of *N*-(benzofuran-2-ylmethyl)anilines failed for substrate **S3e**. A different protocol, employing aqueous NaOH as the base in the presence of a phase-transfer catalyst, proved instead successful.

A solution of compound **S3e** (394 mg, 1.0 mmol), benzyl bromide (238 μL, 2.0 mmol), and Bu₄NHSO₄ (17 mg, 0.05 mmol, 0.05 mmol) in toluene (3 mL) was stirred vigorously with a solution of NaOH in water (50% by weight, 2 mL). After 3 h at room temperature, TLC showed complete conversion. The reaction mixture was diluted with toluene (30 mL) and extracted with water (5 x 10 mL). The organic phase was dried over MgSO₄ and concentrated *in vacuo*. Purification by flash chromatography (eluent: petroleum ether/EtOAc, gradient from 99:1 to 97.5:2.5) gave the title compound in the form of a yellow oil (291 mg, 60%).

¹H NMR (300 MHz, CDCl₃): δ = 8.68 (d, *J* = 2.6 Hz, 1H), 7.99 (dd, *J* = 8.9, 2.6 Hz, 1H), 7.43 (dd, *J* = 7.4, 1.7 Hz, 1H), 7.35-7.09 (m, 8H), 6.88 (d, *J* = 8.9 Hz, 1H), 6.38 (s, 1H), 4.37 (s, 2H), 4.30 (s, 2H) ppm. ¹³C NMR (75 MHz, CDCl₃): δ = 158.0, 155.0, 153.8, 143.8, 136.7, 136.0, 128.8, 128.7, 128.1, 127.8, 124.4, 124.2, 123.5, 123.0, 121.1, 111.3, 106.1, 95.9, 56.6, 49.9 ppm. HRMS (EI) *m/z*: [M – I]⁺ Calcd for C₂₂H₁₇IN₂O₃ 357.1239; Found 357.1231.



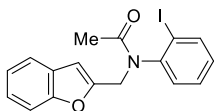
N-(Benzofuran-2-ylmethyl)-2-iodo-N-(tert-butoxycarbonyl)-4-nitroaniline (1m)

Compound **S3e** (148 mg, 0.308 mmol) was dissolved in a mixture of EtOH (3 mL), THF (2 mL), and concentrated aqueous ammonia (30% by weight, 1 mL). Powdered Na₂S₂O₄ (213 mg, 1.22 mmol, 4.0 equiv) was added portionwise. Instant decoloration was observed. After stirring for

20 minutes at room temperature, volatiles were evaporated and the residue partitioned between CH_2Cl_2 (10 mL) and water (5 mL). The aqueous phase was extracted with more CH_2Cl_2 (3 x 3 mL) and the combined organic phases were dried over Na_2SO_4 and concentrated in vacuo.

The residue was dissolved in a mixture of CH_2Cl_2 (1.5 mL) and EtOH (1.5 mL), and di-*tert*-butyl dicarbonate ($(\text{BOC})_2\text{O}$, 78 mg, 0.36 mmol, 1.2 equiv) was added. The solution was left overnight at room temperature, then concentrated under reduced pressure and separated by flash chromatography on silica gel (eluent: petroleum ether/EtOAc 96:4) to give the title compound as a pale brown oil (69.9 mg, 41% over two steps).

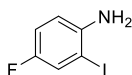
^1H NMR (300 MHz, CDCl_3): δ = 7.94 (br d, J = 2.5 Hz, 1H), 7.50-7.37 (m, 4H), 7.33-7.10 (m, 6H), 6.81 (d, J = 8.6 Hz, 1H), 6.43 (s, 1H), 6.32 (br s, 1H), 4.21 (s, 4H), 1.48 (s, 9H) ppm. ^{13}C NMR (75 MHz, CDCl_3): δ = 155.2, 154.9, 152.6, 146.5, 137.9, 135.9, 129.5, 129.1, 128.4, 127.3, 124.6, 123.8, 122.7, 120.9, 118.9, 111.2, 105.6, 100.2, 81.0, 79.5, 57.7, 50.3, 28.4 ppm. HRMS (EI) m/z : $[\text{M}]^+$ Calcd for $\text{C}_{27}\text{H}_{27}\text{IN}_2\text{O}_3$ 554.1066; Found 554.1046.



***N*-(Benzofuran-2-ylmethyl)-2'-iodoacetanilide (1n)**

Compound **S1a** (175 mg, 0.50 mmol) was acetylated by treatment with acetyl chloride (37.3 μL , 0.53 mmol, 1.05 equiv) in dry pyridine (1 mL). Dilution with Et_2O and extraction with 1 M aqueous HCl yielded the pure product **1n** as a sticky brownish mass (182 mg, 93%).

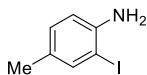
^1H NMR (300 MHz, CDCl_3): δ = 7.94 (dd, J = 7.9, 1.5 Hz, 1H), 7.52-7.39 (m, 2H), 7.34-7.13 (m, 3H), 7.09-6.97 (m, 2H), 6.54 (s, 1H), 5.67 (d, J = 15.3 Hz, 1H), 4.23 (d, J = 15.3 Hz, 1H), 1.84 (s, 3H) ppm. ^{13}C NMR (75 MHz, CDCl_3): δ = 170.3, 155.1, 153.2, 144.4, 140.3, 130.5, 130.2, 129.7, 128.4, 124.3, 122.8, 121.1, 111.4, 106.3, 100.3, 44.6, 22.9 ppm.



4-Fluoro-1-iodoaniline

To a mixture of 4-fluoroaniline (960 μL , 10 mmol) in CH_2Cl_2 (5 mL) and NaHCO_3 (1.68 g, 20 mmol, 2.0 equiv) in water (10 mL), I_2 (2.67 g, 10.5 mmol, 1.05 mmol) was added in portions. After stirring overnight at room temperature, a small amount of $\text{Na}_2\text{S}_2\text{O}_3 \cdot 5 \text{H}_2\text{O}$ was added, phases were separated and the aqueous layer was extracted with more CH_2Cl_2 (3 x 5 mL). The combined organic extracts were dried over Na_2SO_4 and concentrated under reduced pressure. The residue was purified by short-path distillation in vacuum (0.1 mbar) to give the title product in the form of an orange oil (1.91 g, 80%).

^1H NMR (300 MHz, CDCl_3): δ = 7.37 (dd, J = 7.9, 2.9 Hz, 1H), 6.89 (ddd, J = 8.8, 8.0, 2.8 Hz, 1H), 6.68 (dd, J = 8.8, 4.9 Hz, 1H), 3.90 (br s, 2H) ppm. ^{13}C NMR (75 MHz, CDCl_3): δ = 155.3 (d, $^1J_{\text{CF}}$ = 240.7 Hz), 143.4 (d, $^4J_{\text{CF}}$ = 2.4 Hz), 125.1 (d, $^2J_{\text{CF}}$ = 24.5 Hz), 116.3 (d, $^2J_{\text{CF}}$ = 22.3 Hz), 114.8 (d, $^3J_{\text{CF}}$ = 7.5 Hz), 82.9 (d, $^3J_{\text{CF}}$ = 8.7 Hz) ppm. $^{19}\text{F}\{^1\text{H}\}$ NMR (282 MHz, CDCl_3): δ = -125.34 ppm. Spectral data are in agreement with the literature.^[10]



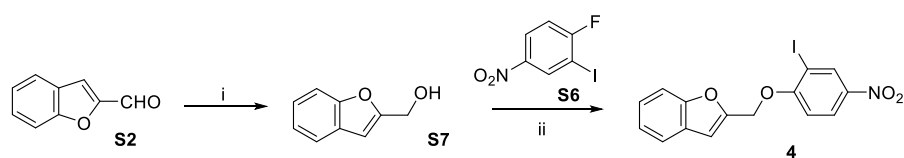
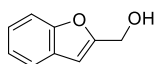
2-Iodo-4-toluidine^[11]

To a solution of *p*-toluidine hydrochloride (7.18 g, 50 mmol), KI (8.72 g, 52.5 mmol, 1.05 equiv), concentrated H₂SO₄ (2.9 mL, 52.5 mmol, 1.05 equiv) in water (10 mL) and MeOH (100 mL), H₂O₂ (30% solution in water, 10.2 mL, 100 mmol, 2.0 equiv) was added dropwise. The resulting mixture was stirred overnight at room temperature and then Na₂S₂O₃ · 5 H₂O was added until no colour change was apparent with further addition.

The mixture was extracted with Et₂O (3 x 15 mL) and the organic extracts were concentrated under reduced pressure. The residue was distilled *in vacuo* (0.1 mbar) with the aid of a Kugelrohr apparatus and the resulting semi-solid distillate was recrystallized from its own melt at 0 °C to give the title compound in the form of an off-white solid (5.08 g, 43%). Purity, as assayed by GC analysis, was better than 97%.

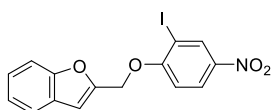
¹H NMR (300 MHz, CDCl₃): δ = 7.47 (d, *J* = 1.9 Hz, 1H), 6.95 (dd, *J* = 8.1, 1.9 Hz, 1H), 6.66 (d, *J* = 8.1 Hz, 1H), 3.93 (br s, 2H), 2.21 (s, 3H) ppm. Spectral data are in agreement with those of an authentic sample.

Compound **4** was obtained by nucleophilic aromatic substitution employing compound **S6** and 2-benzofurylmethanol (**S7**), as represented in Scheme S3

**Conditions:**i) NaBH₄ / EtOH, r.t.ii) NaH (1.1 equiv), DME, then **S6** (1.0 equiv), r.t.**Scheme S3** – Preparation of compound **4**.**2-Benzofurylmethanol (S7)**

The reduction of benzofuran-2-carbaldehyde (**S2**, 606 μL, 5.0 mmol) with NaBH₄ (189 mg, 5.0 mmol) in EtOH (5 mL) at room temperature gave, after Kugelrohr distillation (pressure: 7 mbar) the title compound in the form of a colourless liquid (690 mg, 93%).

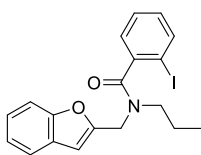
¹H NMR (300 MHz, CDCl₃): δ = 7.57-7.50 (m, 1H), 7.50-7.44 (m, 1H), 7.35-7.19 (m, 2H), 6.61 (br s, 1H), 4.72 (s, 2H), 3.04 (br s, 1H) ppm. ¹³C NMR (75 MHz, CDCl₃): δ = 156.5, 155.1, 128.2, 124.4, 122.8, 121.2, 111.3, 104.1, 58.0 ppm. Spectral data are in agreement with the literature.^[12]

**2-((2-Iodo-4-nitrophenoxy)methyl)benzofuran (4)**

To a solution of 2-benzofurylmethanol (**S7**, 148 mg, 1.0 mmol) in dry 1,2-dimethoxyethane (1 mL), NaH (60% dispersion in mineral oil, 56.0 mg, 1.1 mmol, 1.1 equiv) was added portionwise with stirring. When H₂ evolution ceased, 1-fluoro-2-iodo-4-nitrobenzene (**S6**, 267 mg, 1.0 mmol, 1.0 equiv) was introduced in portions to control the exothermic reaction. After standing

overnight at room temperature, a small amount of water was introduced carefully and the resulting mixture was extracted with EtOAc. The organic layer was evaporated and the residue was recrystallized from boiling EtOH to afford the title compound in the form of a yellow solid (311 mg, 79%).

^1H NMR (300 MHz, CDCl_3): δ = 8.69 (d, J = 2.7 Hz, 1H), 8.25 (dd, J = 9.1, 2.7 Hz, 1H), 7.64-7.55 (m, 1H), 7.51 (dd, J = 8.1, 1.1 Hz, 1H), 7.38-7.22 (m, 2H), 7.06 (d, J = 9.1 Hz, 1H), 6.89 (br s, 1H), 5.35 (s, 2H) ppm. ^{13}C NMR (75 MHz, CDCl_3): δ = 161.9, 155.4, 150.9, 142.5, 135.5, 127.8, 125.7, 125.2, 123.3, 121.6, 111.6, 111.2, 107.3, 86.0, 64.8 ppm. HRMS (EI) m/z : $[\text{M}]^+$ Calcd for $\text{C}_{15}\text{H}_{10}\text{INO}_4$ 394.9655; Found 394.9671.



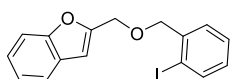
***N*-(Benzofuran-2-ylmethyl)-2-iodo-*N*-propylbenzamide (7)**

Benzofuran-2-carbaldehyde (**S2**, 606 μL , 5.0 mmol) and 1-propanamine (493 μL , 6.0 mmol, 1.2 equiv) were mixed neat. An exothermic reaction took place. The resulting oil was diluted with MeOH (10 mL) and NaBH_4 (757 mg, 20 mmol, 4.0 equiv) was added portionwise. After standing for 1 h at room temperature, most MeOH was evaporated and the residue partitioned between an aqueous solution of NaOH (approx. 1 M) and Et_2O . The organic extract was dried over KOH pellets, concentrated *in vacuo* and the residue was distilled with the aid of a Kugelrohr apparatus under reduced pressure (7 mbar) to yield *N*-(benzofuran-2-ylmethyl)-1-propanamine in the form of a colorless oil (725 mg, 77%).

^1H NMR (300 MHz, CDCl_3): δ = 7.59-7.43 (m, 2H), 7.34-7.19 (m, 2H), 6.58 (br s, 1H), 4.80 (br s, 1H), 3.96 (br s, 2H), 2.66 (d, J = 7.3 Hz, 2H), 1.57 (q, J = 7.3 Hz, 2H), 0.95 (t, J = 7.3 Hz, 3H) ppm.

This material was reacted with 2-iodobenzoylchloride in the usual way ($\text{CH}_2\text{Cl}_2/\text{Et}_3\text{N}$) to yield compound **10** in quantitative yield.

NMR spectra are complicated by the existence of two rotamers in approximately 1:1 ratio. ^1H NMR (300 MHz, CDCl_3): δ = 7.92-7.83 (m, 1H), 7.63-7.36 (m, 4H), 7.34-7.21 (m, 2H), 7.16-7.04 (m, 1H), 6.85 (br s, 0.5H), 6.52 (br s, 0.5H), 5.15 (d, J = 15.2, 0.5H), 4.71 (d, J = 15.4, 0.5H), 4.54-4.37 (m, 1H), 4.05-3.88 (m, 0.5H), 3.32-2.99 (m, 1.5H), 1.80 (q, J = 7.4 Hz, 1H), 1.70-1.50 (m, 1H), 1.03 (t, J = 7.4 Hz, 1H), 0.77 (t, J = 7.4 Hz, 1H) ppm. ^{13}C NMR (75 MHz, CDCl_3): δ = 170.9, 170.8, 155.1, 154.9, 153.4, 152.8, 142.3, 142.3, 139.4, 139.3, 130.4, 130.3, 128.5, 128.5, 128.3, 128.0, 127.8, 127.5, 124.6, 124.2, 123.1, 122.9, 121.1, 121.1, 111.3, 111.3, 106.0, 105.2, 92.9, 92.7, 50.3, 46.8, 46.3, 41.1, 21.5, 20.3, 11.8, 11.3 ppm.

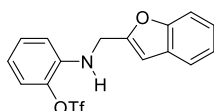


2-(((2-Iodobenzyl)oxy)methyl)benzofuran (8)

To a solution of 2-iodobenzyl alcohol (468 mg, 2.0 mmol) in CH_2Cl_2 (5 mL), PBr_3 (142 μL , 1.5 mmol) was added carefully at 0 $^\circ\text{C}$. After stirring for 1 h, a few drops of water were cautiously added, followed by NaOH solution (50% in water, 3 mL), Bu_4NHSO_4 (34 mg, 0.1 mmol, 0.05 equiv), and 2-benzofurylmethanol (**S7**, 296 mg, 2.0 mmol, 1.0 equiv). The biphasic mixture was stirred vigorously overnight.

The reaction mixture was diluted with CH₂Cl₂ (25 ml) and extracted with water (5 x 10 mL). The organic phase was dried over Na₂SO₄ and concentrated. The residue was purified by flash chromatography on silica gel (eluent: petroleum ether/toluene 80:20) to afford the title compound in the form of a colorless oil (293 mg, 40%).

¹H NMR (300 MHz, CDCl₃): δ = 7.83 (dd, *J* = 7.9, 1.2 Hz, 1H), 7.59-7.54 (m, 1H), 7.52-7.47 (m, 2H), 7.40-7.20 (m, 3H), 6.99 (td, *J* = 7.6, 1.8 Hz, 1H), 6.76 (br s, 1H), 4.74 (s, 2H), 4.63 (s, 2H) ppm. ¹³C NMR (75 MHz, CDCl₃): δ = 155.4, 154.2, 140.2, 139.4, 129.5, 129.1, 128.4, 128.2, 124.6, 122.9, 121.3, 111.5, 106.1, 98.1, 76.3, 65.3 ppm.

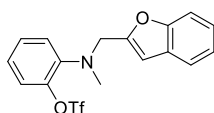


2-((2-Benzofurylmethyl)amino)phenyl trifluoromethanesulfonate (S7)

2-Aminophenyl trifluoromethanesulfonate was prepared in 50% yield over two steps according to a literature procedure: 2-nitrophenol was reacted with Tf₂O and then reduced with iron powder according to Béchamp's method.^[13]

Reductive amination of compound **S7** (500 mg, 2 mmol) with benzofuran-2-carbaldehyde (**S2**) as described for compound **S3a** gave the title product in the form of a pale yellow solid (392 mg, 45%).

¹H NMR (300 MHz, CDCl₃): δ = 7.56-7.48 (m, 1H), 7.40-7.22 (m, 3H), 7.18 (dd, *J* = 8.0, 1.6 Hz, 2H), 6.96-6.83 (m, 2H), 6.60 (br s, 1H), 6.11 (br s, 1H), 5.11 (s, 2H) ppm. ¹³C NMR (75 MHz, CDCl₃): δ = 155.3, 153.3, 150.5, 131.4, 131.0, 127.8, 125.1, 123.4, 123.2, 121.4, 121.3, 120.2 (q, ¹*J*_{CF} = 323.8 Hz), 117.4, 111.5, 107.5, 49.5 ppm. ¹⁹F{¹H} NMR (282 MHz, CDCl₃): δ = -74.27 ppm.

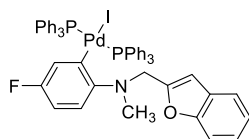


2-((2-Benzofurylmethyl)(methyl)amino)phenyl trifluoromethanesulfonate (10)

Reaction of compound **S7** (320 mg, 0.862 mmol) with MeI (107 μL, 1.72 mmol, 2.0 equiv) according to general procedure **B** (flash chromatography eluent: petroleum ether/toluene 50:50) gave the title compound in the form of a colorless oil (160 mg, 48%).

¹H NMR (300 MHz, CDCl₃): δ = 7.54-7.39 (m, 2H), 7.36-7.15 (m, 3H), 7.09 (dd, *J* = 7.8, 1.7 Hz, 1H), 6.95 (dd, *J* = 8.4, 1.3 Hz), 6.81 (td, *J* = 7.7, 1.3 Hz, 1H), 6.51 (br s, 1H), 5.15 (br s, 1H), 4.89 (br s, 1H), 3.88 (s, 3H) ppm. ¹³C NMR (75 MHz, CDCl₃): δ = 156.2, 155.3, 151.4, 132.3, 131.2, 128.0, 124.8, 123.0, 121.3, 121.0, 112.0, 111.5, 107.0, 55.9, 48.7 ppm. Signals due to quaternary carbons belonging to the ring having the OTf moiety are not visible, probably because of broadening due to the existence of multiple conformations. ¹⁹F{¹H} NMR (282 MHz, CDCl₃): δ = -75.42 ppm.

2.5. Synthesis of complex 13



trans-[ArPd(PPh₃)₂I] (**13**)

A mixture of Pd(PPh₃)₄ (116 mg, 0.10 mmol) and iodoarene **1b** (42 mg, 0.11 mmol, 1.1 equiv) in toluene (1 mL) was stirred for 3 h at room temperature under argon. Pentane (4 mL) was then added and the resulting solution was left overnight at -20 °C. The precipitate was filtered and washed with a small amount of pentane and dried under high vacuum. The title compound was so obtained in the form of pale yellow crystals (18.8 mg, 19%). This material is quite unstable in the solid state and more so in solution, so no ¹³C NMR spectrum could be obtained.

¹H NMR (300 MHz, CD₂Cl₂): δ = 7.58-7.17 (m, 34H), 6.63-6.54 (m, 1H), 6.44 (s, 1H), 6.30-6.18 (m, 1H), 6.14-6.03 (m, 1H), 4.58 (s, 2H), 2.30 (s, 3H) ppm. ³¹P NMR (121 MHz, CD₂Cl₂): δ = 21.86 ppm. ¹⁹F NMR (282 MHz, CD₂Cl₂): δ = -123.83 ppm.

References

- [1] G. R. Fulmer, A. J. M. Miller, N. H. Sherden, H. E. Gottlieb, A. Nudelman, B. M. Stoltz, J. E. Bercaw, K. I. Goldberg, *Organometallics* **2010**, *29*, 2176–2179.
- [2] L. Han, W. Zhang, X.-X. Shi, S.-L. You, *Adv. Synth. Catal.* **2015**, *357*, 3064–3068.
- [3] G. Di Gregorio, M. Mari, F. Bartoccini, G. Piersanti, *J. Org. Chem.* **2017**, *82*, 8769–8775.
- [4] Y. Boukharsa, B. Meddah, R. Y. Tiendrebeogo, A. Ibrahimi, J. Taoufik, Y. Cherrah, A. Benomar, M. E. A. Faouzi, M. Ansar, *Med. Chem. Res.* **2016**, *25*, 494–500.
- [5] B. E. Love, J. Ren, *J. Org. Chem.* **1993**, *58*, 5556–5557.
- [6] J. K. Augustine, R. Kumar, A. Bombrun, A. B. Mandal, *Tetrahedron Lett.* **2011**, *52*, 1074–1077.
- [7] J. C. Jochims, *Monatsh. Chem.* **1963**, *94*, 677–680.
- [8] O. Russo, S. Messaoudi, A. Hamze, N. Olivi, J.-F. Peyrat, J.-D. Brion, S. Sicsic, I. Berque-Bestel, M. Alami, *Tetrahedron* **2007**, *63*, 10671–10683.
- [9] R. D. Chambers, C. J. Skinner, M. J. Atherton, J. S. Moilliet, *J. Chem. Soc. Perkin Trans. 1* **1996**, *14*, 1659.
- [10] M. Layek, U. Lakshmi, D. Kalita, D. K. Barange, A. Islam, K. Mukkanti, M. Pal, *Beilstein J. Org. Chem.* **2009**, *5*, DOI 10.3762/bjoc.5.46.
- [11] J. Iskra, S. Stavber, M. Zupan, *Synthesis* **2004**, *2004*, 1869–1873.
- [12] B. Gabriele, R. Mancuso, G. Salerno, *J. Org. Chem.* **2008**, *73*, 7336–7341.
- [13] P. Tolstoy, S. X. Y. Lee, C. Sparr, S. V. Ley, *Org. Lett.* **2012**, *14*, 4810–4813.

3. Experimental section of chapter IV

3.1. General remarks

Unless otherwise stated, commercially available materials were used as received from suppliers. THF and dioxane were distilled from sodium and benzophenone under argon before use. All the air-free manipulations have been performed by standard Schlenk techniques. Pre-coated F254 silica gel plates on aluminum foil (Fluka analytical) were used for TLC analyses and visualized under UV light, with Dragendorff's reagent for tertiary amines or with alkaline potassium permanganate solution, as appropriate. GLC analyses were performed on a Varian 3900 instrument with H₂ as a carrier gas using a Varian VF-1ms column (15 m x 0.25 mm i.d.). NMR chemical shift were referenced to TMS as an internal standard or to the residual solvent peak.^[1]

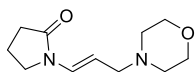
3.2. General procedure for the hydroamination of *N*-allenylamides

An NMR tube (5 mm diameter) or a Schlenk flask of appropriate size was charged with Cu(NCMe)₄PF₆ (0.05 equiv) and closed with a rubber septum. After evacuation and back-filling with Ar repeatedly for three times, dry THF (1 mL per mmol of substrate), the required secondary amine (1.2 equiv) and the *N*-allenylamide (1.0 equiv) were sequentially added. The vessel was shaken until a completely homogeneous solution resulted and the mixture was left overnight at room temperature (or for a longer time if specified otherwise). Complete conversion was checked by no-D ¹H NMR,^[2] taking into consideration the disappearance of the characteristic allene resonances.

The tube was opened to the air and the content poured into 10 volumes of EtOAc and partitioned with 3 volumes of saturated NaCl aqueous solution. The aqueous phase was back-extracted with EtOAc (3 x 3 volumes) and the combined organic phases were exsiccated over Na₂SO₄. Volatiles were evaporated under reduced pressure and the residue was purified by flash chromatography on NaHCO₃-treated silica gel (as detailed below) to afford the required hydroamination product.

Preparation of NaHCO₃-treated silica gel

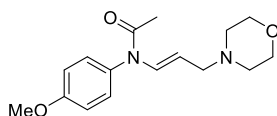
Ordinary flash-chromatography grade silica gel was slurried with about twice its volume of an aqueous NaHCO₃ solution (approx. 50 g/L), washed with water on a Buchner funnel, then with acetone and dried in high vacuum overnight at 140 °C. Alternatively, the packed silica gel column was first treated with three volumes of trimethylamine solution (10 vol% in the selected eluent) and then thoroughly rinsed with three volumes of fresh eluent. Some grades of commercial silica gel caused decomposition of acid-sensitive products if neutralization treatment was omitted (see also ref. ^[3], note 8).



(*E*)-1-(3-Morpholinoprop-1-en-1-yl)pyrrolidin-2-one (2b)

The reaction of *N*-allenylpyrrolidin-2-one (**1b**, 246 mg, 2.0 mmol) with morpholine (210 μ L, 2.4 mmol) according to the general procedure (flash chromatography eluent: EtOAc) gave the title compound in the form of a pale brown oil that solidified on standing (378 mg, 90%).

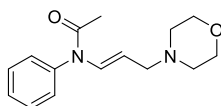
^1H NMR (400 MHz, CDCl_3): δ = 7.00 (d, J = 14.4 Hz, 1H), 4.95 (dt, J = 14.4, 7.2 Hz, 1H), 3.73-3.67 (m, 4H), 3.51 (t, J = 7.2 Hz, 2H), 3.01 (d, J = 7.2 Hz, 2H), 2.51-2.39 (m, 6H), 2.13-2.05 (m, 2H) ppm. ^{13}C NMR (75 MHz, CDCl_3): δ = 173.3, 127.0, 107.3, 67.1, 59.2, 53.6, 45.3, 31.3, 17.6 ppm. IR (ATR): ν = 3037, 2858, 2789, 1694, 1660, 1411, 1300, 1253, 1107, 957 cm^{-1} . HRMS (EI) m/z : $[\text{M}]^+$ Calcd for $\text{C}_{11}\text{H}_{18}\text{N}_2\text{O}_2$ 210.1368; Found 210.1365.



(E)-N-(4-Methoxyphenyl)-N-(3-morpholinoprop-1-en-1-yl)acetamide (2f)

The reaction of *N*-(4-methoxyphenyl)-*N*-allenylacetamide (**1f**, 50.8 mg, 0.25 mmol) with morpholine (26.2 μ L, 0.3 mmol) according to the general procedure (flash chromatography eluent: EtOAc) gave the title compound in the form of a pale brown oil (56.2 mg, 77%).

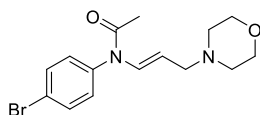
^1H NMR (300 MHz, CDCl_3): δ = 7.56 (d, J = 14.0 Hz, 1H), 7.10-6.97 (m, 2H), 6.96-6.85 (m, 2H), 4.42 (dt, J = 14.0, 7.2 Hz, 1H), 3.79 (s, 3H), 3.67-3.52 (m, 4H), 2.91 (d, J = 7.2 Hz, 2H), 2.32-2.21 (m, 4H), 1.81 (s, 3H) ppm. ^{13}C NMR (75 MHz, CDCl_3): δ = 169.1, 159.6, 132.3, 131.6, 129.7, 115.3, 109.0, 66.9, 58.9, 55.5, 53.4, 23.2 ppm. IR (ATR): ν = 2957, 2917, 2850, 2808, 1675, 1654, 1510, 1300, 1245, 1114, 1032 cm^{-1} . HRMS (EI) m/z : $[\text{M}]^+$ Calcd for $\text{C}_{16}\text{H}_{22}\text{N}_2\text{O}_3$ 290.1630; Found 290.1629.



(E)-N-(3-Morpholinoprop-1-en-1-yl)-N-phenylacetamide (2g)

The reaction of *N*-phenyl-*N*-allenylacetamide (**1g**, 79.1 mg, 0.50 mmol) with morpholine (52.5 μ L, 0.60 mmol) according to the general procedure (no chromatographic purification needed) gave the title compound in the form of a pale brown solid (127 mg, 97%).

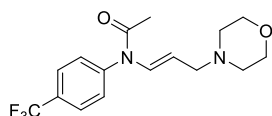
^1H NMR (300 MHz, CDCl_3): δ = 7.61 (d, J = 14.3 Hz, 1H), 7.53-7.35 (m, 3H), 7.16 (d, J = 8.0 Hz, 2H), 4.43 (dt, J = 14.3, 7.1 Hz, 1H), 3.65 (t, J = 4.7 Hz, 4H), 2.95 (d, J = 7.1 Hz, 2H), 2.37 (br t, J = 4.7 Hz, 4H), 1.84 (s, 3H) ppm. ^{13}C NMR (75 MHz, CDCl_3): δ = 168.6, 139.7, 131.4, 130.1, 128.7 (3C), 109.2, 66.9, 59.0, 53.4, 23.2 ppm. IR (ATR): ν = 3057, 3055, 3010, 2958, 2926, 2860, 2808, 1675, 1656, 1299, 1109, 702 cm^{-1} . HRMS (EI) m/z : $[\text{M}]^+$ Calcd for $\text{C}_{15}\text{H}_{20}\text{N}_2\text{O}_2$ 260.1525; Found 260.1522.



(E)-N-(4-Bromophenyl)-N-(3-morpholinoprop-1-en-1-yl)acetamide (2h)

The reaction of *N*-(4-bromophenyl)-*N*-allenylacetamide (**1h**, 126 mg, 0.50 mmol) with morpholine (52.5 μ L, 0.60 mmol) according to the general procedure (flash chromatography eluent: EtOAc) gave the title compound in the form of a pale brown oil (136 mg, 80%).

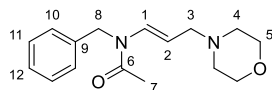
^1H NMR (300 MHz, CDCl_3): δ = 7.62-7.46 (m, 3H), 7.01 (d, J = 8.0 Hz, 2H), 4.38 (dt, J = 14.4, 7.3 Hz, 1H), 3.66-3.55 (m, 4H), 2.90 (d, J = 7.3 Hz, 2H), 2.39-2.25 (m, 4H), 1.81 (s, 3H) ppm. ^{13}C NMR (75 MHz, CDCl_3): δ = 168.2, 138.7, 133.5, 131.2, 130.5, 122.8, 109.5, 66.9, 58.8, 53.4, 23.2 ppm. IR (ATR): ν = 2958, 2917, 2851, 2809, 1678, 1656, 1301, 1114, 731 cm^{-1} . HRMS (EI) m/z : $[\text{M}]^+$ Calcd for $\text{C}_{15}\text{H}_{19}\text{BrN}_2\text{O}_2$ 338.0630; Found 338.0621.



(*E*)-*N*-(3-Morpholinoprop-1-en-1-yl)-*N*-(4-trifluoromethylphenyl)acetamide (**2i**)

The reaction of *N*-(4-trifluoromethylphenyl)-*N*-allenylacetamide (**1i**, 102 mg, 0.50 mmol) with morpholine (52.5 μ L, 0.60 mmol) according to the general procedure (reaction time: 42 h, flash chromatography eluent: EtOAc) gave the title compound in the form of a pale brown oil (76.1 mg, 51%).

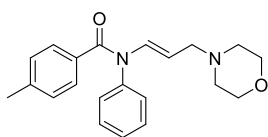
^1H NMR (300 MHz, CDCl_3): δ = 7.76 (d, J = 8.2 Hz, 2H), 7.57 (d, J = 14.2 Hz, 1H), 7.31 (d, J = 8.2 Hz, 2H), 4.40 (dt, J = 14.2, 7.2 Hz, 1H), 3.68-3.63 (m, 4H), 2.95 (d, J = 7.2 Hz, 2H), 2.43-2.30 (m, 4H), 1.88 (br s, 3H) ppm. ^{13}C NMR (75 MHz, CDCl_3): δ = 168.1, 143.0, 131.3, 131.2 (q, $^2J_{\text{CF}}$ = 32.3 Hz), 129.6, 127.5 (q, $^3J_{\text{CF}}$ = 3.7 Hz), 123.7 (q, $^1J_{\text{CF}}$ = 272.3 Hz), 110.0, 67.0, 59.0, 53.5, 23.3 ppm. ^{19}F { ^1H } NMR (282 MHz, CDCl_3): δ = -62.73 ppm. IR (ATR): ν = 2922, 2857, 1682, 1656, 1614, 1322, 1300, 1164, 1113, 1065 cm^{-1} . HRMS (EI) m/z : $[\text{M}]^+$ Calcd for $\text{C}_{16}\text{H}_{19}\text{F}_3\text{N}_2\text{O}_2$ 328.1399; Found 328.1406.



(*E*)-*N*-Benzyl-*N*-(3-morpholinoprop-1-en-1-yl)acetamide (**2j**)

The reaction of *N*-benzyl-*N*-allenylacetamide (**1j**, 39.7, 0.212 mmol) with morpholine (22.3 μ L, 0.25 mmol) according to the general procedure (flash chromatography eluent: EtOAc/acetone 87:13) gave the title compound in the form of a pale brown viscous oil (37.3 mg, 64%).

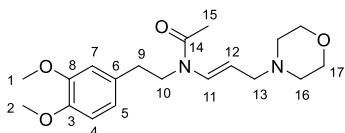
Two rotamers in 60:40 ratio are evident in NMR spectra. Assignment has been done with the aid of COSY and HSQC experiments. ^1H NMR (300 MHz, CDCl_3): δ = 7.49 (d, J = 14.6 Hz, 0.4H, minor H_1), 7.38-7.08 (m, 5H, H_{10-12}), 6.69 (d, J = 13.9 Hz, 0.6H, major H_1), 5.03-4.90 (m, 1H, both H_2), 4.89 (s, 1.2H, major H_8), 4.77 (s, 0.8H, minor H_8), 3.63 (t, J = 4.6 Hz, 4H, both H_5), 2.96 (d, J = 7.1 Hz, 0.8H, minor H_3), 2.91 (d, J = 7.0 Hz, 1.2H, major H_3), 2.32 (s, 1.8H, major H_7), 2.32-2.24 (m, 4H, both H_4), 2.17 (s, 1.2H, minor H_7) ppm. ^{13}C NMR (75 MHz, CDCl_3): δ = 169.8 (minor C_6), 169.4 (major C_6), 136.8 (major C_9), 135.8 (minor C_9), 130.5 (major C_1), 129.1 (minor C_1), 129.0 (minor C_{11}), 128.6 (major C_{11}), 127.5 (minor C_{12}), 127.1 (major C_{12}), 127.0 (major C_{10}), 125.6 (minor C_{10}), 108.8 (major C_2), 107.8 (minor C_2), 66.9 (both C_5), 59.4 (major C_3), 59.3 (minor C_3), 53.4 (both C_4), 49.7 (minor C_8), 46.2 (major C_8), 22.4 (minor C_7), 22.3 (major C_7) ppm. IR (ATR): ν = 2922, 2853, 2803, 1646, 1115, 729 cm^{-1} . HRMS (EI) m/z : $[\text{M}]^+$ Calcd for $\text{C}_{16}\text{H}_{22}\text{N}_2\text{O}_2$ 274.1681; Found 274.1689.



(E)-N-(3-Morpholinoprop-1-en-1-yl)-N-phenyl-p-toluamide (2k)

The reaction of *N*-phenyl-*N*-allenyl-*p*-toluamide (**1k**, 74.8 mg, 0.30 mmol) with morpholine (37.8 μ L, 0.36 mmol) according to the general procedure (flash chromatography eluent: CH₂Cl₂/EtOAc gradient from 70:30 to 50:50) gave the title compound in the form of a brown oil (77.8 mg, 78%).

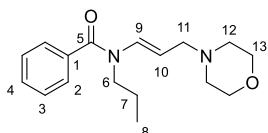
¹H NMR (300 MHz, CDCl₃): δ = 7.56 (d, *J* = 14.3 Hz, 1H), 7.32-7.24 (m, 2H), 7.24-7.17 (m, 3H), 7.10-7.06 (m, 2H), 6.96 (d, *J* = 8.0 Hz, 2H), 4.75 (dt, *J* = 14.3, 7.2 Hz, 1H), 3.66 (t, *J* = 4.7 Hz, 4H), 3.00 (d, *J* = 7.2 Hz, 2H), 2.44-2.35 (m, 4H), 2.23 (s, 3H) ppm. ¹³C NMR (75 MHz, CDCl₃): δ = 168.8, 140.3, 140.1, 132.8, 132.4, 129.5, 129.0, 128.8, 128.5, 127.8, 110.4, 66.9, 59.0, 53.4, 21.4 ppm. IR (ATR): ν = 2956, 2923, 2854, 2808, 1647, 1320, 1115 cm⁻¹. HRMS (EI) *m/z*: [M]⁺ Calcd for C₂₁H₂₄N₂O₂ 336.1838; Found 336.1844.



(E)-N-(3,4-Dimethoxyphenethyl)-N-(3-morpholinoprop-1-en-1-yl)acetamide (2l)

The reaction of *N*-(3,4-dimethoxyphenethyl)-*N*-allenylacetamide (**1l**, 162 mg, 0.50 mmol) with morpholine (52.5 μ L, 0.60 mmol, 1.2 equiv) according to the general procedure (reaction time: 72 h, flash chromatography eluent: acetone/EtOAc 15:85) gave the title compound in the form of a brown oil (110 mg, 63%).

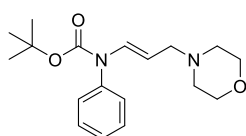
Two rotamers in approximate 65:35 ratio are apparent in the NMR spectra. ¹H NMR (300 MHz, CDCl₃): δ = 7.40 (d, *J* = 14.7 Hz, 0.35H, minor rotamer H₁₁), 6.83-6.59 (m, 3.65H, H₄, H₅, H₇, major rotamer H₁₁), 5.02-5.19 (m, 1H, H₁₂), 3.89-3.76 (m, 8H, H₁, H₂, H₁₀), 3.72 (t, *J* = 4.7 Hz, H₁₇), 3.08 (d, *J* = 7.3 Hz, 0.7H, minor rotamer H₁₃), 3.02 (d, *J* = 7.0 Hz, 1.3H, major rotamer H₁₃), 2.86-2.71 (m, 2H, H₉), 2.51-2.38 (m, 4H, H₁₆), 2.21 (s, 1.95H, major rotamer H₁₅), 1.91 (s, 1.05H, minor rotamer H₁₅) ppm. **Major rotamer** - ¹³C NMR (75 MHz, CDCl₃): δ = 169.0 (C₁₄), 149.1 (C₈), 147.8 (C₃), 131.5 (C₆), 130.9 (C₁₁), 120.8 (C₅), 112.2 (C₄ or C₇), 111.4 (C₇ or C₄), 106.7 (C₁₂), 67.1 (multiplet, C₁₇), 59.7 (C₁₃), 56.1 (C₁ and C₂), 53.6 (C₁₆), 44.6 (C₁₀), 32.7 (C₉), 22.3 (C₁₅) ppm. **Minor rotamer** - ¹³C NMR (75 MHz, CDCl₃): δ = 169.4 (C₁₄), 149.3 (C₈), 148.2 (C₃), 130.7 (C₆), 128.6 (C₁₁), 121.0 (C₅), 112.2 (C₄ or C₇), 111.6 (C₇ or C₄), 106.3 (C₁₂), 67.1 (multiplet, C₁₇), 59.7 (C₁₃), 56.1 (C₁ and C₂), 53.6 (C₁₆), 47.5 (C₁₀), 33.2 (C₉), 22.1 (C₁₅) ppm. IR (ATR): ν = 2956, 2933, 2853, 1673, 1644, 1515, 1261, 1236, 1116, 1028, 730 cm⁻¹. HRMS (EI) *m/z*: [M]⁺ Calcd for C₁₉H₂₈N₂O₄ 348.2049; Found 348.2041.



(E)-N-(3-Morpholinoprop-1-en-1-yl)-N-propylbenzamide (2m)

The reaction of *N*-propyl-*N*-allenyl-benzamide (**1m**, 201.3 mg, 1.0 mmol) with morpholine (105 μ L, 1.2 mmol) according to the general procedure (reaction time: 72 h, flash chromatography eluent: EtOAc) gave the title compound in the form of a brown oil (61.6 mg, 21%).

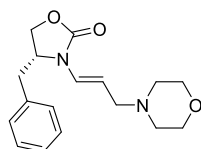
NMR spectra are broadened because of conformational equilibria. ^1H NMR (300 MHz, CDCl_3): δ = 7.56-7.36 (m, 5H, H_{1-4}), 6.56 (v br s, 1H, H_9), 5.06 (dt, J = 14.0, 6.9 Hz, 1H, H_{10}), 3.76-3.64 (m, 6H, H_6 and H_{13}), 2.89 (br s, 2H, H_{11}), 2.53-2.25 (m, 4H), 1.78-1.56 (m, 2H, H_7), 1.05-0.77 (br s, 3H, H_8) ppm. ^{13}C NMR (75 MHz, CDCl_3): δ = 170.4 (C_5), 135.7 (C_1), 132.3 (very broad, detected by HSQC, C_9), 130.3 (C_4), 128.5 (C_3), 127.9 (very broad, C_2), 106.0 (broad, confirmed by HSQC, C_{10}), 67.0 (C_{13}), 59.4 (C_{11}), 53.4 (C_{12}), 45.3 (broad, C_6), 20.27 (broad, C_7), 11.4 (C_8). IR (ATR): ν = 2960, 2854, 2803, 1637, 1330, 1116, 1101 cm^{-1} . HRMS (EI) m/z : $[\text{M}]^+$ Calcd for $\text{C}_{17}\text{H}_{24}\text{N}_2\text{O}_2$ 288.1838; Found 288.1836.



***tert*-Butyl (*E*)-*N*-(3-morpholinoprop-1-en-1-yl)-*N*-phenylcarbamate (**2n**)**

The reaction of *N*-phenyl-*N*-allenyl *tert*-butyl carbamate (**1n**, 116 mg, 0.50 mmol) with morpholine (52.5 μ L, 0.60 mmol) according to the general procedure (flash chromatography eluent: $\text{CH}_2\text{Cl}_2/\text{EtOAc}$ 70:30) gave the title compound in the form of a pale yellow oil (98.6 mg, 62%).

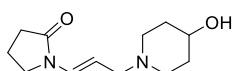
^1H NMR (300 MHz, CDCl_3): δ = 7.42-7.34 (m, 2H), 7.33-7.18 (m, 2H), 7.14-7.08 (m, 2H), 4.40 (dt, J = 16.6, 7.3 Hz, 1H), 3.70-3.62 (m, 4H), 2.92 (d, J = 7.3 Hz, 2H), 2.42-2.32 (m, 4H), 1.40 (s, 9H) ppm. ^{13}C NMR (75 MHz, CDCl_3): δ = 152.7, 138.9, 132.8, 129.4, 128.6, 127.7, 106.3, 81.6, 67.0, 59.2, 53.4, 28.2 ppm. IR (ATR): ν = 2973, 2930, 2825, 2809, 1709, 1661, 1596, 1494, 1316, 1157, 1116 cm^{-1} . HRMS (EI) m/z : $[\text{M}]^+$ Calcd for $\text{C}_{18}\text{H}_{26}\text{N}_2\text{O}_3$ 318.1943; Found 318.1947.



(*R,E*)-4-Benzyl-3-(3-morpholinoprop-1-en-1-yl)oxazolidin-2-one (2o**)**

The reaction of (*R*)-4-benzyl-3-allenyloxazolidin-2-one (**1o**, 108 mg, 0.50 mmol) with morpholine (52.5 μ L, 0.60 mmol) according to the general procedure (reaction time: 18 h, flash chromatography eluent: acetone) gave the title compound in the form of a pale yellow oil (110 mg, 73%).

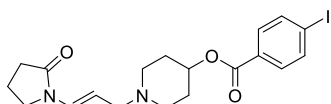
^1H NMR (300 MHz, CDCl_3): δ = 7.36-7.20 (m, 3H), 7.19-7.12 (m, 2H), 6.73 (d, J = 14.6 Hz, 1H), 5.11 (dt, J = 14.6, 7.2 Hz, 1H), 4.33-4.11 (m, 3H), 3.71 (t, J = 4.7 Hz, 4H), 3.22 (dd, J = 13.9, 3.2 Hz, 1H), 3.06 (ABX multiplet, $\Delta\delta_{\text{AB}}$ = 0.05 ppm, J_{AB} = 13.2 Hz, J_{AX} = 7.0 Hz, J_{BX} = 7.0 Hz, 2H), 2.74 (dd, J = 13.9, 8.7 Hz, 1H), 2.54-2.38 (m, 4H) ppm. ^{13}C NMR (75 MHz, CDCl_3): δ = 155.0, 135.0, 129.3, 128.9, 127.3, 126.1, 106.7, 66.9, 66.4, 59.1, 54.8, 53.4, 36.0 ppm. IR (ATR): ν = 2955, 2922, 2853, 1748, 1669, 1416, 1114, 1003, 743, 701 cm^{-1} . HRMS (EI) m/z : $[\text{M}]^+$ Calcd for $\text{C}_{17}\text{H}_{22}\text{N}_2\text{O}_3$ 302.1630; Found 302.1626.



(E)-1-(3-(4-Hydroxypiperidin-1-yl)prop-1-en-1-yl)pyrrolidin-2-one (2t)

The reaction of *N*-allenylpyrrolidin-2-one (**1b**, 61.5 mg, 0.50 mmol) with 4-hydroxypiperidine (60.7 mg, 0.60 mmol) according to the general procedure (flash chromatography eluent: acetone) gave the title compound in the form of a pale yellow solid (77.4 mg, 69%).

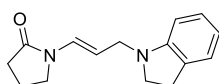
¹H NMR (300 MHz, CDCl₃): δ = 6.97 (d, *J* = 14.4 Hz, 1H), 4.98 (dt, *J* = 14.4, 7.2 Hz, 1H), 3.67 (tt, *J* = 8.8, 4.2 Hz, 1H), 3.50 (t, *J* = 7.2 Hz, 2H), 2.99 (d, *J* = 7.2 Hz, 2H), 2.83-2.71 (m, 2H), 2.46 (t, *J* = 8.1 Hz, 2H), 2.18-2.01 (m, 4H), 1.94-1.82 (m, 2H), 1.64-1.49 (m, 2H). ppm. ¹³C NMR (75 MHz, CDCl₃): δ = 173.3, 126.6, 108.2, 67.9, 58.6, 51.0, 45.3, 34.5, 31.3, 17.5 ppm. IR (ATR): ν = 3378, 2902, 1682, 1656, 1412, 1298, 1060, 954 cm⁻¹. HRMS (EI) *m/z*: [M]⁺ Calcd for C₁₂H₂₀N₂O 224.1525; Found 224.1529.



(E)-1-(3-(2-Oxopyrrolidin-1-yl)allyl)piperidin-4-yl 4-iodobenzoate (2u)

The reaction of *N*-allenylpyrrolidin-2-one (**1b**, 61.5 mg, 0.50 mmol) with piperidin-4-yl 4-iodobenzoate (**S8**, 199 mg, 0.60 mmol) according to the general procedure (flash chromatography eluent: acetone) gave the title compound in the form of a white powder (178 mg, 78%).

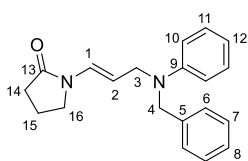
¹H NMR (300 MHz, CDCl₃): δ = 7.83-7.77 (m, 2H), 7.77-7.71 (m, 2H), 7.02 (d, *J* = 14.3 Hz, 1H), 5.11-4.94 (m, 2H), 3.53 (t, *J* = 7.3 Hz, 2H), 3.05 (d, *J* = 7.2 Hz, 2H), 2.80-2.59 (m, 2H), 2.49 (t, *J* = 8.1 Hz, 2H), 2.44-2.28 (m, 2H), 2.20-1.96 (m, 4H), 1.93-1.75 (m, 2H) ppm. ¹³C NMR (75 MHz, CDCl₃): δ = 173.3, 165.5, 137.8, 131.1, 130.2, 126.8, 107.9, 100.7, 71.0, 58.8, 50.7, 45.3, 31.3, 31.0, 17.6 ppm. IR (ATR): ν = 2967, 2901, 2586, 1682, 1599, 1489, 1130, 1071 cm⁻¹. HRMS (EI) *m/z*: [M]⁺ Calcd for C₁₉H₂₈IN₂O₃ 454.0753; Found 454.0742.



(E)-1-(3-(Indolin-1-yl)prop-1-en-1-yl)pyrrolidin-2-one (2ah)

The reaction of *N*-allenylpyrrolidin-2-one (**1b**, 61.5 mg, 0.50 mmol) with indoline (67 μ L, 0.60 mmol) according to the general procedure (flash chromatography eluent: petroleum ether/EtOAc 50:50) gave the title compound in the form of a pale yellow oil (90.2 mg, 74%).

¹H NMR (300 MHz, CDCl₃): δ = 7.19 - 6.99 (m, 3H), 6.65 (t, *J* = 7.3, 1H), 6.53 (d, *J* = 7.8 Hz, 1H), 5.02 (dt, *J* = 14.1, 6.9 Hz, 1H), 3.76 (d, *J* = 6.9 Hz, 2H), 3.49 (t, *J* = 7.9 Hz, 2H), 3.31 (t, *J* = 7.8 Hz, 2H), 2.93 (t, *J* = 7.8 Hz, 2H), 2.48 (t, *J* = 7.9 Hz, 2H), 2.09 (quint, *J* = 7.9 Hz, 2H) ppm. ¹³C NMR (75 MHz, CDCl₃): δ = 173.3, 151.9, 130.5, 127.3, 126.4, 124.6, 117.8, 107.4, 106.9, 52.8, 49.2, 45.3, 31.3, 28.5, 17.5 ppm. HRMS (EI) *m/z*: [M]⁺ Calcd for C₁₅H₁₉N₂O 242.1419; Found 242.1419.

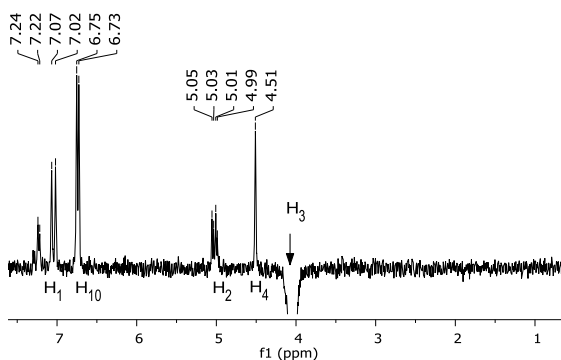


(E)-1-(3-(Benzyl(phenyl)amino)prop-1-en-1-yl)pyrrolidin-2-one (2aj)

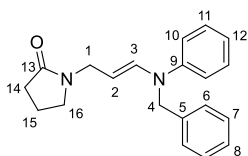
The reaction of *N*-allenylpyrrolidin-2-one (**1b**, 61.5 mg, 0.50 mmol) with *N*-benzylaniline (110 mg, 0.60 mmol) according to the general procedure (reaction time: 72 h, flash chromatography eluent: toluene/EtOAc gradient from 95:5 to 90:10) gave the title compound in the form of a pale yellow oil (54.7 mg, 36%).

^1H NMR (300 MHz, CDCl_3): δ = 7.35-7.14 (m, 7H, H_6 , H_7 , H_8 , and H_{11}), 7.04 (d, J = 14.3 Hz, 1H, H_1), 6.81-6.63 (m, 3H, H_{10} and H_{12}), 5.00 (dt, J = 14.3, 6.4 Hz, 1H, H_2), 4.51 (s, 2H, H_4), 4.03 (d, J = 6.4 Hz, 2H, H_3), 3.45 (t, J = 7.7 Hz, 2H, H_{16}), 2.47 (t, J = 7.7 Hz, 2H, H_{14}), 2.07 (quint, J = 7.7 Hz, 2H, H_{15}) ppm. ^{13}C NMR (75 MHz, CDCl_3): δ = 173.3 (C_{13}), 148.9 (C_9), 139.0 (C_5), 129.4 (C_{11}), 128.7 (C_7), 127.0 (C_1 or C_8), 126.8 (C_6), 126.1 (C_8 or C_1), 116.8 (C_{12}), 112.7 (C_{10}), 107.0 (C_2), 53.7 (C_4), 50.6 (C_3), 45.4 (C_{16}), 31.4 (C_{14}), 17.6 (C_{15}) ppm.

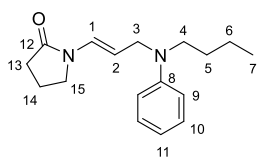
This compound was distinguished unambiguously from its isomer by a selective NOE experiment. Irradiation of H_3 caused measurable through-space polarization transfer to H_1 , H_2 , H_4 and H_{10} . The NOE contact with H_{10} (and not with H_{16}) confirms the proposed structure.



In later fractions, also the isomeric (*E*)-1-(3-(benzyl(phenyl)amino)allyl)pyrrolidin-2-one (**3aj**) could be isolated as a pale yellow oil (30.5 mg, 20%). Rotation around the C_3 -N is partially hindered, two rotamers are evident in approx. 87:13 ratio. Spectral data of the major isomer only are given.



^1H NMR (300 MHz, CDCl_3): δ = 7.40-7.14 (m, 5H, H_5 , H_6 and H_7), 7.02-6.91 (m, 3H, H_3 and H_{11}), 6.77-6.64 (m, 1H, H_{12}), 6.56 (d, J = 8.4 Hz, 2H, H_{10}), 5.03 (dt, J = 14.4, 7.2 Hz, 1H, H_2), 4.29 (s, 2H, H_4), 3.45 (t, J = 7.2 Hz, 2H, H_{16}), 3.27 (dd, J = 7.2, 1.3 Hz, 2H, H_1), 2.45 (t, J = 8.1 Hz, 2H, H_{14}), 2.16-1.97 (m, 2H, H_{15}) ppm. ^{13}C NMR (75 MHz, CDCl_3): δ = 173.0 (C_{13}), 146.7 (C_9), 139.6 (C_5), 129.7 (C_3), 129.3 (C_{11}), 128.7 (C_7), 127.6 (C_6), 127.3 (C_8), 124.1 (C_{12}), 113.1 (C_{10}), 112.1 (C_2), 48.6 (C_4), 45.4 (C_{16} or C_1), 35.8 (C_1 or C_{16}), 31.4 (C_{14}), 17.6 (C_{15}) ppm.

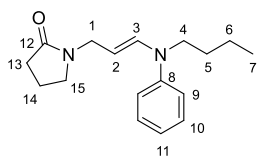


(*E*)-1-(3-(Butyl(phenyl)amino)prop-1-en-1-yl)pyrrolidin-2-one (**2ak**)

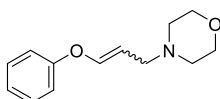
The reaction of *N*-allenylpyrrolidin-2-one (**1b**, 61.5 mg, 0.50 mmol) with *N*-butylaniline (96 μ L, 0.60 mmol) according to the general procedure (temperature: 40 $^{\circ}$ C, reaction time: 48 h, flash chromatography eluent: toluene/EtOAc gradient from 90:10 to 80:20) gave the title compound in the form of a pale yellow oil (27.1 mg, 20%).

^1H NMR (300 MHz, CDCl_3): δ = 7.21 (dd, J = 8.8, 7.2 Hz, 2H, H_{10}), 7.06 (d, J = 14.5 Hz, 1H, H_1), 6.75-6.62 (m, 3H, H_9 and H_{11}), 4.98 (dt, J = 14.4, 6.3 Hz, 1H, H_2), 3.94 (d, J = 6.3 Hz, 2H, H_3), 3.48 (t, J = 7.5 Hz, 2H, H_{15}), 3.35-3.16 (m, 2H, H_4), 2.49 (t, J = 8.1 Hz, 2H, H_{13}), 2.08 (tt, J = 8.1, 7.5 Hz, 2H, H_{13}), 1.65-1.49 (m, 2H, H_5), 1.44-1.24 (m, 2H, H_6), 0.95 (t, J = 7.3 Hz, 3H, H_7) ppm. ^{13}C NMR (75 MHz, CDCl_3): δ = 173.3 (C_{12}), 148.4 (C_8), 129.4 (C_{10}), 125.6 (C_1), 116.0 (C_{11}), 112.3 (C_9), 107.7 (C_2), 50.6 (C_4 or C_3), 50.1 (C_3 or C_4), 45.4 (C_{15}), 31.4 (C_{13}), 29.5 (C_5), 20.5 (C_6), 17.5 (C_{14}), 14.2 (C_7) ppm.

In later fractions, also the isomeric (*E*)-1-(3-(butyl(phenyl)amino)allyl)pyrrolidin-2-one (**3ak**) could be isolated as a pale yellow oil (21.1 mg, 15%). Rotation around the C_3 -N is partially hindered, two rotamers are evident in approx. 75:25 ratio. Spectral data of both isomers are given (as assigned by COSY and HSQC experiments).



^1H NMR (300 MHz, CDCl_3): δ = 7.24-7.09 (m, 1H, minor rotamer H_3 , minor rotamer H_{10} , 0.75H), 7.07-6.88 (m, 2H, major rotamer H_3 , major rotamer H_{10} and H_{11} , 3H), 6.71 (t, J = 7.4 Hz, 0.25H, minor rotamer H_{11}), 6.63 (d, J = 7.7 Hz, 0.5H, minor rotamer H_9), 6.54 (d, J = 8.4 Hz, 1.5H, major rotamer H_9), 5.05 (dt, J = 14.7, 7.8 Hz, 1H, H_2), 3.81 (d, J = 7.8 Hz, 0.5H, minor rotamer H_1), 3.54-3.44 (m, 2H, H_{15}), 3.28 (d, J = 7.2 Hz, 1.5H, major rotamer H_1), 3.09 (t, J = 7.0 Hz, 2H, H_4), 2.53-2.43 (m, 2H, H_{13}), 2.18-2.00 (m, 2H, H_{14}), 1.67-1.53 (m, 2H, H_5), 1.50-1.35 (m, 2H, H_6), 0.95 (t, J = 7.3 Hz, 3H, H_7). ^{13}C NMR (75 MHz, CDCl_3): δ = 173.3 (minor rotamer C_{12}), 173.0 (major rotamer C_{12}), 148.0 (minor rotamer C_8), 147.1 (major rotamer C_8), 129.4 (minor rotamer C_{10}), 129.24 (major rotamer C_{10}), 129.15 (major rotamer C_{11}), 126.1 (minor rotamer C_3), 124.1 (major rotamer C_3), 117.8 (minor rotamer C_{11}), 113.2 (minor rotamer C_9), 113.0 (major rotamer C_9), 112.2 (major rotamer C_2), 108.7 (minor rotamer C_2), 45.4 (major rotamer C_{15}), 45.3 (minor rotamer C_{15}), 44.2 (minor rotamer C_1), 44.0 (C_4), 35.8 (major rotamer C_1), 31.8 (C_{13}), 31.4 (major rotamer C_5), 31.3 (minor rotamer C_5), 20.4 (C_6), 17.6 (C_{14}), 14.0 (C_7) ppm.



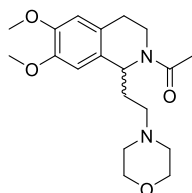
(*E*)- and (*Z*)-4-(3-phenoxyallyl)morpholine (**2ad**)

The reaction of phenoxyallene (66.6 mg, 0.50 mmol) with morpholine (52.5 μ L, 0.60 mmol, 1.2 equiv) according to the general procedure gave the title compound (50:50 *E/Z* mixture) in 70% yield, as determined by ^1H NMR of the crude reaction mixture. Careful separation by flash chromatography (EtOAc + Et₃N 0.1%) allowed to obtain some pure fractions of the *E* isomer (elutes first), and the *Z* isomer, contaminated by unidentified impurities.

(*E*)-4-(3-phenoxyallyl)morpholine - ^1H NMR (300 MHz, CDCl₃) δ = 7.35-7.27 (m, 2H), 7.10-6.93 (m, 3H), 6.57 (dt, J = 12.2, 1.2 Hz, 1H), 5.37 (dt, J = 12.2, 7.6 Hz, 1H), 3.72 (t, J = 4.7 Hz, 4H), 2.98 (dd, J = 7.6, 1.2 Hz, 2H), 2.55-2.41 (m, 4H). ^{13}C NMR (75 MHz, CDCl₃): δ = 157.0, 145.3, 129.8, 123.2, 116.9, 108.1, 67.1, 56.5, 53.5 ppm. HRMS (EI) m/z : [M]⁺ Calcd for C₁₃H₁₇NO₂ 219.1259; Found 219.1268.

(*Z*)-4-(3-phenoxyallyl)morpholine - ^1H NMR (300 MHz, CDCl₃) δ = 7.35-7.27 (m, 2H), 7.10-6.93 (m, 3H), 6.54 (dt, J = 6.2, 1.4 Hz, 1H), 4.91 (dt, J = 6.2, 7.2 Hz 1H), 3.72 (t, J = 4.7 Hz, 4H), 3.22 (dd, J = 7.2, 1.4 Hz, 2H), 2.55-2.41 (m, 4H). ^{13}C NMR (75 MHz, CDCl₃): δ = 157.3, 143.3, 129.8, 123.0, 116.5, 107.7, 67.2, 53.5, 52.4 ppm.

3.3. Pictet-Spengler-type cyclization of hydroamination products

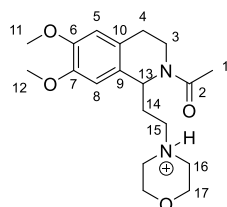


***N*-Acetyl-4-(2-(6,7-dimethoxy-1,2,3,4-tetrahydroisoquinolin-1-yl)ethyl)morpholine (6)**

To a solution of (*E*)-*N*-(3,4-dimethoxyphenethyl)-*N*-(3-morpholinoprop-1-en-1-yl)acetamide (**21**, 251 mg, 0.73 mmol) in dry CH₂Cl₂ (13 mL), trifluoroacetic acid (273 μ L, 3.6 mmol, 5.0 equiv) was added slowly. The mixture was let to react for 24 hours at room temperature, then it was poured into an aqueous solution of NaOH (1 M, 10 mL). Phases was separated and the aqueous layer was extracted with CH₂Cl₂ (3 x 5 mL). The combined organic phases were dried over Na₂SO₄ and volatiles were removed by evaporation under reduced pressure. The title compound was thus obtained in the form of an amber oil (226 mg, 90%).

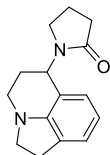
IR(ATR): ν = 2951, 2936, 2835, 1621, 1515, 1442, 1254, 1220, 1113, 866 cm⁻¹. HRMS (EI) m/z : [M]⁺ Calcd for C₁₉H₂₈N₂O₄ 348.2049; Found 348.2041.

Spectra in pure CDCl₃ were difficult to interpret due to multiple conformational equilibria. The product was characterized by NMR in a CDCl₃ / TFA mixture, so the spectral data of the protonated form are given below.



^1H NMR (300 MHz, CDCl₃ / TFA): δ = 9.10 (s, 1H, N-H), 6.71 (s, 1H, H₅), 6.60 (s, 1H, H₈), 5.47 (t, J = 7.3 Hz, 1H, H₁₃), 4.20-4.13 (m, 2H, H₁₇), 3.97-3.76 (m, 3H, H₃ and H₁₇), 3.88 (s, 3H, H₁₁ or H₁₂), 3.85 (s, 3H, H₁₂ or H₁₁), 3.71-3.58 (m, 3H, H₃ and H₁₆), 3.39-3.24 (m, 2H, H₁₅), 3.24-3.07 (m, 2H, H_{16'}), 2.98-2.89 (m, 2H, H₄), 2.37-2.23 (m, 2H, H₁₄), 2.34 (s, 3H, H₁) ppm. ^{13}C NMR (75 MHz, CDCl₃ / TFA): δ = 175.0 (C₂), 148.7 (C₆ or C₇), 147.8 (C₇ or C₆), 126.2 (C₉), 126.1

(C₁₀), 112.2 (C₅), 110.7 (C₈), 64.2 (C₁₇), 56.5 (C₁₁ or C₁₂), 56.2 (C₁₂ or C₁₁), 55.5 (C₁₅), 52.8 (two signals, C₁₆), 52.0 (C₁₃), 42.4 (C₃), 30.5 (C₁₄), 27.7 (C₄), 20.3 (C₁) ppm.



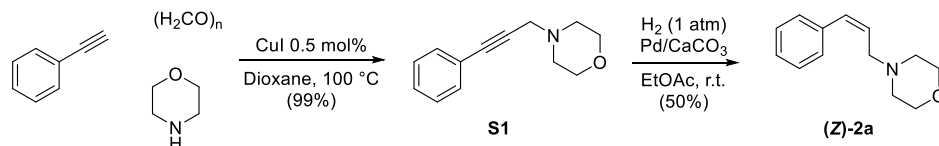
1-(1,2,5,6-tetrahydro-4H-pyrrolo[3,2,1-ij]quinolin-6-yl)pyrrolidin-2-one (17)

To a solution of (*E*)-1-(3-(indolin-1-yl)prop-1-en-1-yl)pyrrolidin-2-one (**2ah**, 24.2 mg, 0.1 mmol) in CHCl₃ (2 mL), trifluoroacetic acid (38 μ L, 0.5 mmol, 5.0 equiv) was added. The solution was left at room temperature, then diluted with CH₂Cl₂ (20 mL), extracted with a solution of NaHCO₃ (5% in water) and dried over Na₂SO₄. The solvent was evaporated at reduced pressure and the residue was purified by preparative TLC (eluent: EtOAc) to give the title compound in the form of a pale brown solid (18.1 mg, 75%).

¹H NMR (300 MHz, CDCl₃): δ = 6.99 (d, *J* = 7.4 Hz, 1H), 6.74 (d, *J* = 7.4 Hz, 1H), 6.65 (t, *J* = 7.4, 7.4 Hz, 1H), 5.46 (d, *J* = 7.7 Hz, 1H), 3.45-3.34 (m, 1H), 3.32-3.06 (m, 4H), 3.06-2.90 (m, 3H), 2.51-2.42 (m, 2H), 2.23-2.11 (m, 2H), 2.06-1.92 (m, 2H) ppm. ¹³C NMR (75 MHz, CDCl₃): δ = 175.6, 151.2, 129.6, 125.2, 123.5, 119.1, 117.3, 55.2, 46.9, 46.1^[4], 43.4, 31.6, 29.2, 27.7, 18.4 ppm. Spectral data are in agreement with the literature.^[4]

3.4. Synthesis of substrates for mechanistic studies

Synthesis of (*Z*)-4-(3-phenylallyl)morpholine ((*Z*)-2a)



4-(3-Phenylprop-2-ynyl)morpholine (S1)

The title compound was prepared by the A³ reaction following a procedure described in the literature.^[5]

To a suspension of CuI (9.5 mg, 0.05 mmol, 0.005 equiv) and paraformaldehyde (330 mg, 11 mmol, 1.1 equiv) in dry dioxane (5 mL) contained in a sealable tube, freshly vacuum-distilled phenylacetylene (1.10 mL, 10 mmol) and morpholine (1.29 mL, 15 mmol, 1.5 equiv) were added under argon atmosphere. The tube was sealed and the mixture was stirred overnight at 100 °C. After cooling, dioxane was evaporated *in vacuo* and the residue was redissolved in toluene (20 mL). The resulting solution was extracted with dilute aqueous ammonia (2 x 10 mL) to remove copper salts, then with water (2 x 10 mL) and brine (10 mL). The organic phase was dried over Na₂SO₄. Concentration under reduced pressure gave the title compound in the form of a brownish liquid (1.94 g, 97%) contaminated with a small amount of morpholine, but pure enough to be used for the subsequent step without any further treatment.

¹H NMR (300 MHz, CDCl₃): δ = 7.46-7.40 (m, 2H), 7.33-7.27 (m, 3H), 3.81-3.74 (m, 4H), 3.51 (s, 2H), 2.68-2.62 (m, 4H) ppm. ¹³C NMR (75 MHz, CDCl₃): δ = 131.8, 128.4, 128.3, 123.1, 85.7,

84.2, 67.1, 52.6, 48.2 ppm. IR (ATR): $\nu = 2970, 2901, 2813, 1489, 1130, 1071, 1005, 861 \text{ cm}^{-1}$. Spectral data are in agreement with the literature.^[6]

(*Z*)-4-(3-Phenylallyl)morpholine ((*Z*)-2a)

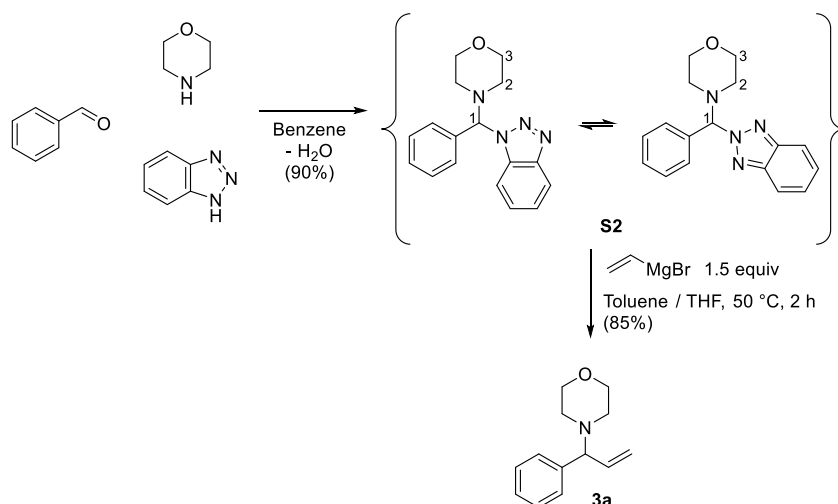
Hydrogenation of **S1** with Lindlar-type catalysts from several different sources invariably failed. Compound (*Z*)-**2a** was obtained by careful reduction of **S1** using palladium on calcium carbonate as a catalyst.

In an apparatus arranged for atmospheric pressure hydrogenation equipped with a gas-volumetric burette, a solution of 4-(3-phenylprop-2-ynyl)morpholine (**S1**, 402 mg, 2.0 mmol) in EtOAc (5 mL) and 5% Pd/CaCO₃ (40 mg) were introduced under argon. After stirring for 15 min (this time is necessary to reduce the activity of the catalyst by absorption of the substrate), the apparatus was flushed with H₂ and the reaction mixture was stirred vigorously until about 70% of the theoretical volume of gas was consumed (approx. 34 mL). Higher conversions invariably led to over-reduction to the saturated amine, which proved difficult to separate by flash chromatography.

The apparatus was flushed with argon and the catalyst was removed by filtration through diatomaceous earth. The residue was composed of the required alkene and unaltered starting material. Careful separation by flash chromatography on silica gel (eluent: petroleum ether / EtOAc 60:40) gave the title compound in the form of a pale yellow liquid (202 mg, 50%, *Z/E* ratio 97:3). The fractions contaminated by the starting material (which elutes first) were discarded.

¹H NMR (300 MHz, CDCl₃): $\delta = 7.41\text{-}7.16$ (m, 5H), 6.58 (dt, $J = 11.8, 2.0$ Hz, 1H), 5.76 (dt, $J = 11.8, 6.5$ Hz, 1H), 3.75-3.66 (m, 4H), 3.26 (dd, $J = 6.5, 2.0$ Hz, 2H), 2.52-3.39 (m, 4H) ppm. ¹³C NMR (75 MHz, CDCl₃): $\delta = 137.1, 131.8, 129.1, 129.0, 128.2, 127.0, 67.1, 56.7, 53.8$ ppm. IR (ATR): $\nu = 2967, 2901, 2856, 1490, 1452, 1130, 1071, 1006, 862 \text{ cm}^{-1}$. Spectral data are in agreement with the literature.^[7]

Synthesis of 4-(1-phenylallyl)morpholine (**3a**)



4-((1*H*(2*H*)-Benzotriazol-1(2)-yl)(phenyl)methyl)morpholine (**S2**)

The title compound was prepared according to a procedure described by Katritzky and coworkers.^[8] It behaves as a mixture of rapidly equilibrating isomers in solution.^[9,10]

A solution of freshly distilled benzaldehyde (511 μ L, 5.0 mmol), morpholine (437 μ L, 5.0 mmol), and benzotriazole (596 mg, 5.0 mmol) in dry benzene (6 mL) was vigorously refluxed under argon in a Dean-Stark apparatus. After 1 h, ¹H NMR analysis of a sample withdrawn from the reaction mixture showed complete conversion of benzaldehyde.

The solvent was evaporated under reduced pressure and the residue was triturated with a 1:1 mixture of diethyl ether and pentane (12 mL) to give the title compound as a white powder (1.32 g, 90%).

Two isomers are present in an approximate 75:25 ratio. ¹H NMR (300 MHz, CDCl₃): δ = 8.12-8.05 (m, 0.75H), 7.96-7.87 (m, 0.75H), 7.46-7.30 (m, 7.5H), 6.76 (s, 0.25H, minor isomer H₁), 6.69 (s, 0.75H, major isomer H₁), 3.84-3.64 (m, 4H), 2.98-2.45 (m, 4 H) ppm. ¹³C NMR (75 MHz, CDCl₃): δ = 146.3, 144.0, 135.4, 135.0, 133.1, 129.0, 128.9, 128.8, 128.6, 127.8, 127.7, 127.4, 126.6, 124.1, 120.2, 118.5, 111.6, 88.8 (minor isomer C₁), 83.1 (major isomer C₁), 67.1 (minor isomer C₃), 66.9 (major isomer C₃), 50.2 (major isomer C₂), 49.2 (minor isomer C₂) ppm. In total there are 17 aromatic carbon resonances (which have not been assigned), as expected taking into account the symmetry of the two isomers. IR (ATR): ν = 2963, 2819, 1610, 1586, 1493, 1450, 1272, 1112, 1012, 873 cm⁻¹.

4-(1-Phenylallyl)morpholine (**3a**)

The title compound was prepared using a procedure reported by Katritzky and coworkers.^[11]

To a solution of aминал **S2** (294 mg, 1.0 mmol) in dry toluene (5 mL), vinylmagnesium bromide (1.0 M in THF, 1.5 mL, 1.5 mmol) was added under argon atmosphere. The resulting mixture was stirred at 50 °C for 2 h.

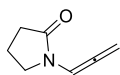
The reaction mixture was then quenched by the careful addition of saturated aqueous NH₄Cl solution (10 mL) and extracted with EtOAc (3 x 5 mL). The combined organic extracts were extracted with NaOH solution (1 M, 2 x 10 mL), dried over Na₂SO₄ and concentrated under reduced pressure. The residue was applied to a flash chromatography column (silica gel) and eluted with petroleum ether until apolar impurities ceased to come out. The title product was then recovered by elution with EtOAc in the form of a pale yellow oil (173 mg, 85%).

¹H NMR (300 MHz, CDCl₃): δ = 7.31-7.13 (m, 5H), 5.83 (ddd, *J* = 17.2, 10.0, 8.8 Hz, 1H), 5.16 (dd, *J* = 17.2, 1.5 Hz, 1H), 5.03 (dd, *J* = 10.0, 1.5 Hz, 1H), 3.62 (t, *J* = 4.7 Hz, 4H), 3.55 (d, *J* = 8.8 Hz, 1H), 2.50-2.35 (m, 2H), 2.33-2.21 (m, 2H) ppm. ¹³C NMR (75 MHz, CDCl₃): δ = 141.7, 139.9, 128.7, 128.1, 127.4, 116.8, 75.7, 67.3, 52.1 ppm. IR (ATR): ν = 3063, 3028, 2956, 2852, 2804, 1639, 1602, 1450, 1276, 1116, 918 cm⁻¹. Spectral data are in agreement with the literature.^[11]

3.5. General procedure for the isomerization of *N*-propargylamides, carbamates and ethers to *N*-allenylamides carbamates, and ethers^[3]

To a 0.2 M solution of the appropriate *N*-propargyl amine in rigorously dried THF under Ar atmosphere were added 0.2 molar equivalents of *t*-BuOK, dispensed as a 1.0 M solution in THF. When GLC or TLC analysis showed complete conversion of the starting material (generally less than one minute is enough), the reaction mixture was treated with 0.2 volumes of a saturated aqueous NH₄Cl solution. The resulting mixture was extracted with EtOAc, exsiccated over

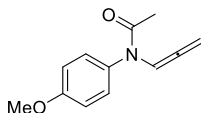
Na₂SO₄ or K₂CO₃ and volatiles were evaporated under reduced pressure. The residue was purified by flash chromatography on NaHCO₃-treated silica gel or vacuum-distilled with the aid of a Kugelrohr apparatus to afford the required allenamide.



N-Allenyl-2-pyrrolidinone (1b)

The reaction of *N*-propargyl-2-pyrrolidinone (**S3b**, 4.76 g, 38.7 mmol) according to the general procedure (reaction time: 5 min, purification by Kugelrohr distillation at 0.1 mbar) gave the title compound in the form of a pale yellow oil (3.30 g, 69%).

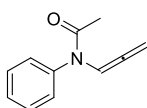
¹H NMR (300 MHz, CDCl₃): δ = 7.04 (t, *J* = 6.4 Hz, 1H), 5.33 (d, *J* = 6.4 Hz, 2H), 3.37 (t, *J* = 7.3 Hz, 2H), 2.42 (t, *J* = 8.1 Hz, 2H), 2.16-1.96 (m, 2H) ppm. ¹³C NMR (75 MHz, CDCl₃): δ = 207.7, 173.0, 95.9, 86.6, 45.8, 31.2, 17.5 ppm. IR (ATR): ν = 2975, 1678, 1455, 1401, 1286, 1255 cm⁻¹. Spectral data are in agreement with the literature.^[12]



N-(4-Methoxyphenyl)-N-allenylacetamide (1f)

The reaction of *N*-(4-methoxyphenyl)-*N*-propargylacetamide (**S3f**, 223 mg, 1.1 mmol) according to the general procedure (reaction time: 10 min, flash chromatography eluent: toluene/EtOAc 85:15) gave the title compound in the form of a pale brown viscous oil (102 mg, 46%).

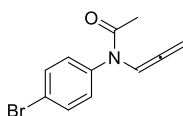
¹H NMR (300 MHz, CDCl₃): δ = 7.67 (t, *J* = 6.4 Hz, 1H), 7.12-7.04 (m, 2H), 6.94-6.86 (m, 2H), 4.99 (d, *J* = 6.4 Hz, 2H), 3.82 (s, 3H), 1.88 (s, 3H) ppm. ¹³C NMR (75 MHz, CDCl₃): δ = 202.8, 169.0, 159.4, 133.0, 129.5, 114.6, 101.3, 86.4, 55.5, 23.0 ppm. IR (ATR): ν = 3051, 2957, 2918, 2849, 1662, 1509, 1243, 1030 cm⁻¹. Spectral data are in agreement with the literature.^[13]



N-Phenyl-N-allenylacetamide (1g)

The reaction of *N*-phenyl-*N*-propargylacetamide (**S3g**, 208 mg, 1.3 mmol) according to the general procedure (reaction time: 10 min, no chromatographic purification needed) gave the title compound in the form of a pale brown solid (184 mg, 88%).

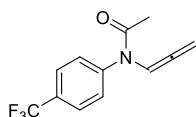
¹H NMR (300 MHz, CDCl₃): δ = 7.68 (t, *J* = 6.4 Hz, 1H), 7.48-7.30 (m, 3H), 7.24-7.09 (m, 2H), 4.93 (d, *J* = 6.4 Hz, 2H), 1.89 (s, 3H) ppm. ¹³C NMR (75 MHz, CDCl₃): δ = 202.7, 168.7, 140.2, 129.5, 128.6, 128.5, 101.0, 86.5, 23.1 ppm. IR (ATR): ν = 2981, 2925, 1654, 1595, 1494, 1372, 1277 cm⁻¹. Spectral data are in agreement with the literature.^[14]



***N*-(4-Bromophenyl)-*N*-allenylacetamide (**1h**)**

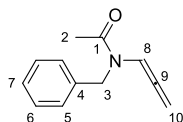
The reaction of *N*-(4-bromophenyl)-*N*-propargylacetamide (**S3h**, 252 mg, 1.0 mmol) according to the general procedure (reaction time: 10 min, flash chromatography eluent: toluene/EtOAc 85:15) gave the title compound in the form of an orange solid (167 mg, 66%).

¹H NMR (300 MHz, CDCl₃): δ = 7.64 (br s, 1H), 7.61-7.48 (m, 2H), 7.09-6.99 (m, 2H), 5.02 (d, *J* = 6.4 Hz, 2H), 1.89 (s, 3H) ppm. ¹³C NMR (75 MHz, CDCl₃): δ = 202.4, 168.2, 139.2, 132.8, 130.3, 122.5, 100.9, 86.9, 23.0 ppm. IR (ATR): ν = 3052, 2974, 1963, 1657, 1487, 1291 cm⁻¹. HRMS (EI) *m/z*: [M]⁺ Calcd for C₁₁H₁₀BrNO 250.9946; Found 250.9954.

***N*-(4-Trifluoromethylphenyl)-*N*-allenylacetamide (**1i**)**

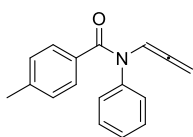
The reaction of *N*-(4-trifluoromethylphenyl)-*N*-propargylacetamide (**S3i**, 482 mg, 2.0 mmol) according to the general procedure (reaction time: 5 min, flash chromatography eluent: toluene/EtOAc 90:10) gave the title compound in the form of a yellow solid (167 mg, 29%).

¹H NMR (300 MHz, CDCl₃): δ = 7.70 (d, *J* = 8.2 Hz, 2H), 7.61 (br s, 1H), 7.32 (d, *J* = 8.2 Hz, 2H), 5.03 (d, *J* = 6.4 Hz, 2H), 1.94 (s, 3H) ppm. ¹³C NMR (75 MHz, CDCl₃): δ = 202.4, 168.0, 143.3, 130.7 (q, ²*J* = 33.5 Hz), 129.1, 126.8 (q, ³*J* = 3.8 Hz), 123.8 (q, ¹*J*_{CF} = 272.5 Hz), 100.9, 87.1, 23.1 ppm. ¹⁹F{¹H} NMR (282 MHz, CDCl₃): δ = -62.62 ppm. IR (ATR): ν = 3055, 2990, 1964, 1663, 1612, 1519, 1306, 1166, 1106, 1066 cm⁻¹.

***N*-Benzyl-*N*-allenylacetamide (**1j**)**

The reaction of *N*-benzyl-*N*-propargylacetamide (**S3j**, 178 mg, 0.95 mmol) according to the general procedure (reaction time: 15 min, flash chromatography eluent: toluene/ethyl acetate 95:5) gave the title compound in the form of a pale yellow oil (55.0 mg, 31%).

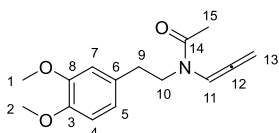
NMR analysis shows the presence of two rotamers in almost equal amounts (52:48 ratio), assignment has been done on the basis of integration and a COSY experiment. ¹H NMR (300 MHz, CDCl₃): δ = 7.60 (t, *J* = 6.4 Hz, 0.48H, minor rotamer H₈), 7.32-7.60 (m, 5H, H₅₋₇), 6.64 (t, *J* = 6.2 Hz, 0.52 H, major rotamer H₈), 5.24 (d, *J* = 6.2 Hz, 1.04H, major rotamer H₁₀), 5.20 (d, *J* = 6.4 Hz, 0.96H, minor rotamer H₁₀), 4.65 (s, 1.04H, major rotamer H₃), 4.68 (s, 1H, minor rotamer H₃), 2.19 (s, 1.56H, major rotamer H₂), 2.06 (s, 1.44H, minor rotamer H₂) ppm. ¹³C NMR (75 MHz, CDCl₃): δ = 202.3 (C₉), 201.5 (C₉), 169.4 (C₁), 168.7 (C₁), 137.7 (C₄), 136.9 (C₄), 128.9 (C₆ or C₅), 128.4 (C₆ or C₅), 128.0 (C₆ or C₅), 127.5 (C₇), 127.2 (C₇), 126.1 (C₆ or C₅), 101.0 (C₈), 99.5 (C₈), 87.7 (C₁₀), 87.2 (C₁₀), 50.0 (C₃), 47.2 (C₃), 22.3 (C₂), 22.0 (C₂) ppm. IR (ATR): ν = 3032, 2975, 2921, 1559, 1665, 1452, 1396, 1222, 975, 730, 695 cm⁻¹. Spectral data are in agreement with literature.^[15]



***N*-Phenyl-*N*-allenyl-*p*-toluamide (1k)**

The reaction of *N*-phenyl-*N*-propargyl-*p*-toluamide (**S3k**, 249 mg, 1.0 mmol) according to the general procedure (reaction time: 15 min, flash chromatography eluent: toluene/EtOAc 97:3) gave the title compound in the form of a brown solid (127 mg, 51%).

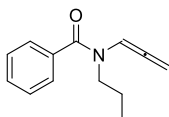
^1H NMR (300 MHz, CDCl_3): δ = 7.64 (t, J = 6.4 Hz, 1H), 7.30-7.16 (m, 5H), 7.08 (d, J = 7.8 Hz, 2H), 6.97 (d, J = 7.8 Hz, 2H), 5.06 (d, J = 6.4 Hz, 2H), 2.25 (s, 3H) ppm. ^{13}C NMR (75 MHz, CDCl_3): δ = 202.9, 168.6, 140.7, 140.5, 132.3, 129.2, 128.9, 128.6 (4C), 127.5, 102.3, 86.8, 21.5 ppm. IR (ATR): ν = 3065, 2975, 2927, 1961, 1635, 1493, 1369, 1332, 1280, 717 cm^{-1} . HRMS (EI) m/z : $[\text{M}]^+$ Calcd for $\text{C}_{17}\text{H}_{15}\text{NO}$ 249.1154; Found 249.1564.



***N*-(3,4-Dimethoxyphenethyl)-*N*-allenylacetamide (1l)**

The reaction of *N*-(3,4-Dimethoxyphenethyl)-*N*-propargylacetamide (**S3l**, 1.30 g, 5.0 mmol) according to the general procedure (reaction time: 10 seconds, flash chromatography eluent: EtOAc/petroleum ether 70:30) gave the title compound in the form of a brown oil (1.20 g, 92%).

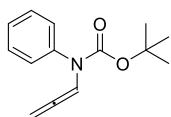
Two rotamers in 50:50 ratio are apparent in the NMR spectra, data of both isomers are given. ^1H NMR (300 MHz, CDCl_3): δ = 7.55 (t, J = 6.5 Hz, 0.5H, H_{11}), 6.82-6.63 (m, 3.5H, H_4 , H_5 , H_7 and H_{11}), 5.44 (d, J = 6.5 Hz, 1H, H_{13}), 5.40 (d, J = 6.3 Hz, 1H, H_{13}), 3.87-3.83 (m, 6H, H_1 and H_2), 3.71-3.56 (m, 2H, H_{10}), 2.83-2.71 (m, 2H, H_9), 2.18 (s, 1.5H, H_{15}), 1.89 (s, 1.5 H, H_{15}) ppm. ^{13}C NMR (75 MHz, CDCl_3): δ = 202.3 (C_{12}), 201.0 (C_{12}), 168.7 (C_{14}), 168.1 (C_{14}), 149.1 (C_8), 148.8 (C_8), 147.9 (C_3), 147.6 (C_3), 131.6 (C_6), 130.9 (C_6), 120.9 (C_5), 120.7 (C_5), 112.2 (C_4 or C_7), 112.1 (C_4 or C_7), 111.5 (C_4 or C_7), 111.2 (C_4 or C_7), 101.0 (C_{11}), 97.9 (C_{11}), 86.8 (C_{13}), 86.5 (C_{13}), 55.9 (multiplet, C_1 and C_2), 48.5 (C_{10}), 45.7 (C_{10}), 33.8 (C_9), 33.1 (C_9), 21.8 (C_{15}), 21.6 (C_{15}) ppm. IR (ATR): ν = 3056, 2931, 2835, 1641, 1516, 1453, 1263, 1237, 1143, 1028 cm^{-1} .



***N*-Allenyl-*N*-propylbenzamide (1m)**

The reaction of *N*-propargyl-*N*-propyl-*p*-toluamide (**S3m**, 283 mg, 1.4 mmol) according to the general procedure (reaction time: 1 min, no chromatographic purification needed) gave the title compound in the form of a brown oil (278 mg, 98%).

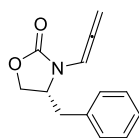
Spectra are broadened because of conformational equilibria take place at rates comparable to the NMR timescale. ^1H NMR (300 MHz, CDCl_3): δ = 7.80-7.32 (m, 5H), 6.65 (br s, 1H), 5.34 (br d, J = 6.2 Hz, 2H), 3.82-3.17 (m, 2H), 1.95-1.44 (m, 2H), 1.16-0.59 (m, 2H) ppm. ^{13}C NMR (75 MHz, CDCl_3): δ = 200.1, 169.3, 135.4, 130.2, 128.6, 128.0, 102.6, 86.6, 46.0, 20.7, 11.3 ppm.



N-Phenyl-N-allenyl *tert*-butyl carbamate (1n)

The reaction of *N*-phenyl-*N*-propargyl *tert*-butylcarbamate (**S3n**, 249 mg, 1.08 mmol) according to the general procedure (reaction time: 15 min, flash chromatography eluent: toluene) gave the title compound in the form of a pale yellow oil (169 mg, 68%).

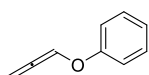
¹H NMR (300 MHz, CDCl₃): δ = 7.38-7.29 (m, 2H), 7.29-7.20 (m, 2H), 7.20-7.13 (m, 2H), 5.00 (d, J = 6.4 Hz, 2H), 1.43 (s, 9H) ppm. ¹³C NMR (75 MHz, CDCl₃): δ = 201.6, 152.5, 139.4, 128.6, 128.2, 127.2, 102.2, 86.5, 81.6, 28.3 ppm. IR (ATR): ν = 2924, 2852, 1703, 1597, 1151 cm⁻¹. Spectral data are in agreement with the literature.^[14]



(*R*)-4-Benzyl-3-allenyloxazolidin-2-one (1o)

The reaction of (*R*)-4-Benzyl-3-propargyloxazolidin-2-one (**S3o**, 186 mg, 0.87 mmol) according to the general procedure (no chromatographic separation needed) gave the title compound in the form of a pale brown oil (186 mg, 99%).

¹H NMR (300 MHz, CDCl₃): δ = 7.26-7.02 (m, 5H), 6.81 (t, J = 6.5 Hz, 1H), 5.44 (ABX multiplet, $\Delta\delta$ = 0.06 ppm, J_{AB} = 10.0 Hz, J_{AX} = 6.5 Hz, J_{BX} = 6.5 Hz, 2H), 4.18-3.95 (m, 3H), 3.16 (dd, J = 13.9, 3.1 Hz, 1H), 2.64 (dd, J = 13.7, 8.9 Hz, 1H) ppm. ¹³C NMR (75 MHz, CDCl₃): δ = 201.8, 155.1, 135.5, 129.4, 129.0, 127.4, 96.1, 88.0, 66.8, 55.8, 37.3 ppm. IR (ATR): ν = 3062, 3031, 1961, 1760, 1496, 1455, 1067 cm⁻¹. Spectral data are in agreement with the literature.^[16]

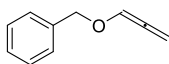


Phenoxyallene (1ad)

The reaction of phenyl propargyl ether (**S3ad**, 1.0 mL, 7.8 mmol) according to the general procedure (reaction time: 15 min) gave a mixture of the title compound with unaltered starting material (85:15 ratio, as assessed by GLC and ¹H NMR analyses).

For the purification, the ability of the alkyne to form poorly soluble copper acetylides was employed as follows. Cu₂O (358 mg, 2.5 mmol) was suspended in MeCN (2 mL) and dissolved by addition of the required amount of concentrated hydrochloric acid (approx. 0.45 mL), triethylamine (1.40 mL, 10 mmol) was then added. The crude mixture obtained as described previously was dissolved in EtOH (7 mL) and added to the copper-containing solution. A yellow precipitate of cuprous acetylide formed quickly. After standing for 30 min, the suspension was filtered through diatomaceous earth. The filtrate was dried over KOH pellets and solvents were removed *in vacuo*. Kugelrohr distillation of the residue (10 mbar) afforded the title compound in the form of a colorless liquid (589 mg, 57%).

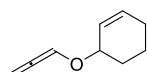
¹H NMR (300 MHz, CDCl₃): δ = 7.39-7.25 (m, 2H), 7.07-6.98 (m, 3H), 6.82 (t, J = 5.9 Hz, 1H), 5.42 (d, J = 5.9 Hz, 2H) ppm. ¹³C NMR (75 MHz, CDCl₃): δ = 202.9, 157.3, 129.6, 122.9, 118.0, 116.9, 89.7 ppm. Spectral data are in agreement with the literature.^[17]



Benzyl propargyl ether (1af)

The reaction of benzyl propargyl ether (**S3af**, 2.92 g, 20 mmol) according to the general procedure (reaction time: 18 h, purification by Kugelrohr distillation in oil pump vacuum) gave the title product in the form of a colorless liquid (2.70 g, 92%).

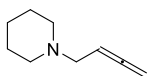
^1H NMR (300 MHz, CDCl_3): δ = 7.45-7.28 (m, 5H), 6.85 (t, J = 5.9 Hz, 1H), 5.49 (d, J = 5.9 Hz, 2H), 4.63 (s, 2H) ppm. ^{13}C NMR (75 MHz, CDCl_3): δ = 201.4, 137.4, 128.5, 128.0, 127.9, 121.7, 91.3, 70.8 ppm. Spectral data are in agreement with the literature.^[18]



Cyclohexen-3-yl propargyl ether (1ai)

The reaction of cyclohex-3-enyl propargyl ether (**S3ai**, 272 mg, 2.0 mmol) according to the general procedure (no chromatographic separation needed) gave the title compound in the form of a pale brown liquid (189 mg, 69%).

^1H NMR (300 MHz, CDCl_3): δ = 6.65 (t, J = 6.0 Hz, 1H), 5.91 (dtd, J = 10.1, 3.6, 1.3 Hz, 1H), 5.85-5.72 (m, 1H), 5.40 (d, J = 6.0 Hz, 2H), 4.31-4.16 (m, 1H), 2.15-1.47 (m, 6H) ppm. ^{13}C NMR (75 MHz, CDCl_3): δ = 201.7, 131.9, 126.8, 120.1, 90.0, 71.8, 28.4, 25.2, 19.1 ppm.



1-(Buta-2,3-dien-1-yl)piperidine (1al)

The title compound was prepared by reduction of 1-(4-methoxybut-2-yn-1-yl)piperidine with AlH_2Cl , generated in situ by a 1:1 mixture of AlCl_3 and LiAlH_4 .^[19]

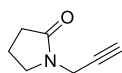
A round-bottomed flask (25 mL capacity) equipped with a magnetic stirrer, a septum, a reflux condenser and an argon inlet tube was charged with anhydrous AlCl_3 (800 mg, 6.0 mmol, 2.0 equiv) and conditioned under argon atmosphere. After cooling with an ice-water bath, dry Et_2O (2 mL) was added cautiously. A perfectly homogeneous solution formed. In another flask, a slurry of LiAlH_4 (228 mg, 6.0 mmol, 2.0 equiv) in dry Et_2O (3 mL) was prepared under argon. The latter suspension was cautiously added to the AlCl_3 solution. A white precipitate (LiCl) formed and the mixture was stirred for 1 h at room temperature, then 1-(4-methoxybut-2-yn-1-yl)piperidine (502 mg, 3.0 mmol) in dry Et_2O (0.5 mL) was added slowly while cooling with an ice bath. After stirring overnight at room temperature, the mixture was refluxed briefly, cooled to room temperature and quenched by addition of EtOAc followed by a solution of Seignette's salt (sodium potassium tartrate). The mixture was extracted with Et_2O , the organic phases were dried over Na_2SO_4 and concentrated *in vacuo*. The residue was distilled under reduced pressure (25 mbar) by the use of a Kugelrohr apparatus to yield the title allene as a colorless liquid (245 mg, 66%).

^1H NMR (300 MHz, CDCl_3): δ = 5.16 (quint, J = 7.3 Hz, 1H), 4.67 (dt, J = 6.6, 2.5 Hz, 2H), 2.99 (dt, J = 7.3, 2.5 Hz, 2H), 2.41 (br t, J = 5.4 Hz, 4H), 1.65-1.52 (m, 4H), 1.46-1.35 (m, 2H) ppm. ^{13}C NMR (75 MHz, CDCl_3): δ = 209.5, 87.0, 74.6, 58.3, 54.2, 26.1, 24.4 ppm. Spectral data were in agreement with the literature.^[19]

3.6. General procedure for the preparation of *N*-propargyl amides and carbamates^[3]

A flask of suitable size equipped with a magnetic stirrer and an gas inlet tube was conditioned under Ar and NaH (60% dispersion in mineral oil, 1.25 equiv) was added. The mineral oil was removed by thorough washing and decantation with petroleum ether (three to five times). Anhydrous THF (5 mL per mmol of substrate) was then added and the appropriate secondary amide or carbamate (1.0 equiv) was introduced slowly, keeping the exothermic reaction and H₂ evolution under control. Then propargyl bromide (80% solution in toluene, approx. 9.2 M, 1.20 equiv) was added and the mixture was stirred overnight at room temperature.

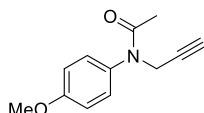
Saturated NH₄Cl solution (0.5 mL per mmol of substrate) was then added carefully and volatiles were evaporated under reduced pressure. Extraction with EtOAc (10 mL per mmol of substrate subdivided into three portions), exsiccation over Na₂SO₄ and evaporation of the solvent gave the required *N*-propargyl compounds, that were purified by flash chromatography on silica gel or by distillation as detailed below for each product.



***N*-Propargyl-2-pyrrolidinone (S3b)**

The reaction of 2-pyrrolidinone (4.56 mL, 60 mmol) according to the general procedure (purification by Kugelrohr distillation at 0.1 mbar) gave the title product in the form of a pale yellow oil (4.89 g, 67%), containing about 10% of the isomeric allene, as assessed by GLC and ¹H NMR analyses.

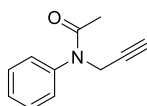
¹H NMR (300 MHz, CDCl₃): δ = 4.10 (d, *J* = 2.5 Hz, 2H), 3.49 (t, *J* = 7.0 Hz, 2H), 2.39 (t, *J* = 8.0 Hz, 2H), 2.21 (t, *J* = 2.5 Hz, 1H), 2.11-2.00 (m, 2H) ppm. ¹³C NMR (75 MHz, CDCl₃): δ = 174.7, 72.2, 46.4, 32.0, 30.8, 17.7 ppm. IR (ATR): ν = 3236, 2953, 2116, 1668, 1421, 1263 cm⁻¹.



***N*-Propargyl-4-methoxyacetanilide (S3f)**

The reaction of 4-methoxyacetanilide (661 mg, 4.0 mmol) according to the general procedure (flash chromatography eluent: toluene/EtOAc 80:20) gave the title product in the form of a pale brown oil (756 mg, 93%).

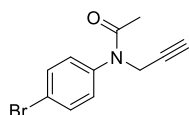
¹H NMR (300 MHz, CDCl₃): δ = 7.23-7.16 (m, 2H), 6.96-6.89 (m, 2H), 4.44 (d, *J* = 2.5 Hz, 2H), 3.83 (s, 3H), 2.19 (t, *J* = 2.5 Hz, 1H), 1.85 (s, 3H) ppm. ¹³C NMR (75 MHz, CDCl₃): δ = 170.6, 159.5, 135.1, 129.3, 114.9, 79.4, 72.1, 55.6, 38.4, 22.5 ppm. IR (ATR): ν = 3290, 2960, 2918, 2849, 2117, 1655, 1509, 1247, 1224, 1024 cm⁻¹. Spectral data are in agreement with the literature.^[20]



***N*-Propargylacetanilide (S3g)**

The reaction of acetanilide (2.03 g, 15 mmol) according to the general procedure (flash chromatography eluent: toluene/EtOAc 90:10) gave the title product in the form of a pale brown solid (2.13 g, 82%).

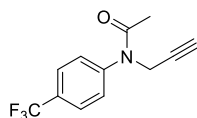
^1H NMR (300 MHz, CDCl_3): δ = 7.62-7.27 (m, 3H), 7.27-7.13 (m, 2H), 4.40 (d, J = 2.5 Hz, 2H), 2.13 (t, J = 2.5 Hz, 1H), 1.80 (s, 3H) ppm. ^{13}C NMR (75 MHz, CDCl_3): δ = 170.2, 142.3, 129.8, 128.5, 128.2, 79.2, 72.1, 38.3, 22.5 ppm. IR (ATR): ν = 3226, 2967, 2912, 2122, 1650, 1593, 1492, 1404, 1273 cm^{-1} . Spectral data are in agreement with the literature.^[21]



N-Propargyl-4-bromoacetanilide (S3h)

The reaction of 4-bromoacetanilide (1.07 g, 5.0 mmol) according to the general procedure (flash chromatography eluent: petroleum ether/EtOAc 80:20) gave the title product in the form of a pale brown solid (980 mg, 78%).

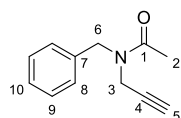
^1H NMR (300 MHz, CDCl_3): δ = 7.60-7.55 (m, 2H), 7.20-7.15 (m, 2H), 4.45 (d, J = 2.5 Hz, 2H), 2.21 (t, J = 2.5 Hz, 1H), 1.87 (s, 3H) ppm. ^{13}C NMR (75 MHz, CDCl_3): δ = 169.8, 141.2, 133.1, 129.9, 122.5, 78.9, 72.5, 38.2, 22.5 ppm. IR (ATR): ν = 3293, 3054, 3034, 2969, 2112, 1660, 1486, 1274, 1010 cm^{-1} .



N-Propargyl-4-trifluoromethylacetanilide (S3i)

The reaction of 4-trifluoromethylacetanilide (762 mg, 3.7 mmol) according to the general procedure (flash chromatography eluent: toluene/EtOAc 80:20) gave the title product in the form of an amber oil (586 mg, 55%).

^1H NMR (300 MHz, CDCl_3): δ = 7.72 (d, J = 8.2 Hz, 2H), 7.44 (d, J = 8.2 Hz, 2H), 4.49 (d, J = 2.5 Hz, 2H), 2.23 (t, J = 2.5 Hz, 1H), 1.91 (br s, 3H) ppm. ^{13}C NMR (75 MHz, CDCl_3): δ = 169.6, 145.4, 130.6 (br q, $^2J_{\text{CF}}$ = 29.6 Hz), 128.6, 127.0 (q, $^3J_{\text{CF}}$ = 3.8 Hz), 123.8 (q, $^1J_{\text{CF}}$ = 272.3 Hz), 78.7, 72.7, 38.3, 22.6 ppm. $^{19}\text{F}\{^1\text{H}\}$ NMR (282 MHz, CDCl_3): δ = -62.65 ppm. IR (ATR): ν = 3309, 2917, 2849, 2120, 1668, 1613, 1519, 1322, 1122, 1066 cm^{-1} .

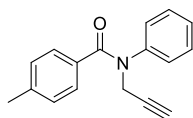


N-Benzyl-N-propargylacetamide (S3j)

The reaction of *N*-benzylacetamide (448 mg, 3.0 mmol) according to the general procedure (flash chromatography eluent: toluene/EtOAc 85:15) gave the title compound in the form of a pale yellow oil (538 mg, 71%).

NMR analysis at room temperature shows two rotamers in 55:45 ratio. ^1H NMR (300 MHz, CDCl_3): δ = 7.46-7.15 (m, 5H, H₇₋₁₀), 4.70 (s, 1.1H, major H₆), 4.69 (s, 0.9H, minor H₆), 4.23 (d,

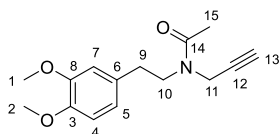
$J = 2.3$ Hz, 1.1 H, major H₃), 3.92 (d, $J = 2.3$ Hz, 0.9H, minor H₃), 2.30 (t, $J = 2.3$ Hz, 0.4H, minor H₅), 2.26 (s, 1.35H, minor H₂), 2.22 (t, $J = 2.3$ Hz, 0.4H, major H₅), 2.19 (s, 1.65H, major H₂) ppm. ¹³C NMR (75 MHz, CDCl₃): $\delta = 170.6$ (C₁), 137.0 (minor C₇), 136.2 (major C₇), 129.1 (major C₉), 128.8 (minor C₉), 128.5 (minor C₈), 128.0 (major C₁₀), 127.7 (minor C₁₀), 126.8 (major C₈), 79.0 (major C₄), 78.3 (minor C₄), 72.8 (minor C₅), 72.0 (major C₅), 51.1 (major C₆), 48.2 (minor C₆), 37.2 (minor C₃), 34.1 (major C₃), 21.8 (C₂) ppm. IR (ATR): $\nu = 3288, 3233, 2923, 2117, 1644, 1415, 1239, 697$ cm⁻¹. Spectral data are in agreement with the literature.^[22]



***N*-Phenyl-*N*-propargyl-*p*-toluamide (S3k)**

The reaction of *N*-phenyl-*p*-toluamide (634 mg, 3.0 mmol) according to the general procedure (flash chromatography eluent: toluene/EtOAc 95:5) gave the title compound in the form of a pale brown oil (556 mg, 74%).

¹H NMR (300 MHz, CDCl₃): $\delta = 7.32$ -7.20 (m, 5H), 7.16 (d, $J = 7.8$ Hz, 2H), 6.98 (d, $J = 7.8$ Hz, 2H), 4.69 (d, $J = 2.4$ Hz, 2H), 2.29-2.24 (m, 4H) ppm. ¹³C NMR (75 MHz, CDCl₃): $\delta = 170.3, 143.3, 140.4, 132.3, 129.3, 129.2, 128.5, 128.5, 127.8, 127.2, 79.3, 72.2, 40.0, 21.5$ ppm. IR (ATR): $\nu = 3292, 3240, 2955, 2920, 2851, 2119, 1642, 1594, 1372, 749, 698$ cm⁻¹.



***N*-(3,4-Dimethoxyphenethyl)-*N*-propargylacetamide (S3l)**

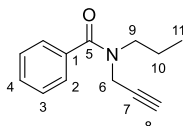
The reported general procedure failed for the synthesis of this compound (deprotonation of the starting material could not be achieved with NaH), so an alternate protocol employing BuLi as the base was employed.

A Schlenk flask equipped with a magnetic stirrer and a gas inlet was conditioned under Ar and *N*-(3,4-dimethoxyphenethyl)acetamide (1.12 g, 5.0 mmol) was introduced together with a spatula-tip of triphenylmethane as an indicator. The solids were dissolved in anhydrous THF (15 mL). The flask was cooled in a NaCl-ice bath (approx. -20 °C), then BuLi (1.6 M in hexanes, approx. 3.10 mL, 5.0 mmol) was slowly dropped in, until the reaction mixture turned red, when all the amide had been deprotonated by BuLi (triphenylmethyl anion is red in solution). The mixture was heated to room temperature, then propargyl bromide (1.09 mL, 10 mmol, 2.0 equiv) was added. The resulting black solution was stirred overnight at room temperature.

Saturated NH₄Cl solution (2.5 mL) was added carefully. Most of the THF was evaporated under reduced pressure, the residue was extracted with EtOAc (50 mL subdivided into three portions), the combined organic phases were exsiccated over Na₂SO₄, then volatiles were evaporated under reduced pressure. The residue was purified by flash chromatography on silica gel (eluent: EtOAc / hexanes 70:30). The title compound was thus obtained in the form of a pale brown oil (1.02 g, 76%).

Two rotamers in approximate ratio 60:40 are apparent in the NMR spectra. ¹H NMR (300 MHz, CDCl₃): $\delta = 6.82$ -6.72 (m, 3H, H₄, H₅ and H₇), 4.20 (d, $J = 2.5$ Hz, 1.2H, major rotamer H₁₁), 3.88-3.82 (m, 6.8H, H₁, H₂ and minor rotamer H₁₁), 3.62 (t, $J = 7.3$ Hz, 2H, H₁₀), 2.88-2.72 (m,

2H, H₉), 2.28 (t, $J = 2.5$ Hz, 0.4H, minor rotamer H₁₃), 2.23 (t, $J = 2.5$ Hz, 0.6H, major rotamer H₁₃), 2.15 (s, 1.8H, major rotamer H₁₅), 1.89 (s, 1.2H, minor rotamer H₁₅) ppm. **Major rotamer** - ¹³C NMR (75 MHz, CDCl₃): $\delta = 170.3$ (C₁₄), 149.2 (C₈), 148.0 (C₃), 130.7 (C₆), 120.9 (C₅), 112.1 (C₄ or C₇), 111.6 (C₇ or C₄), 79.4 (C₁₂), 71.9 (C₁₃), 56.0 (multiplet, C₁ and C₂), 50.0 (C₁₀), 34.5 (C₉), 33.7 (C₁₁), 21.2 (C₁₅) ppm. **Minor rotamer** - ¹³C NMR (75 MHz, CDCl₃): $\delta = 170.4$ (C₁₄), 149.0 (C₈), 147.7 (C₃), 131.7 (C₆), 120.8 (C₅), 112.1 (C₄ or C₇), 111.4 (C₇ or C₄), 78.6 (C₁₂), 72.7 (C₁₃), 56.0 (multiplet, C₁ and C₂), 48.4 (C₁₀), 39.1 (C₁₁), 34.5 (C₉), 21.9 (C₁₅) ppm. IR (ATR): $\nu = 3240, 3247, 2936, 2836, 2116, 1639, 1515, 1260, 1235, 1026$ cm⁻¹.



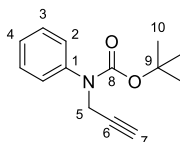
N-propargyl-N-propylbenzamide (S3m)

As for compound **2l**, the alternate protocol using BuLi was employed for the synthesis of this compound.

A solution of *N*-propylbenzamide (816 mg, 5.0 mmol) and a spatula-tip of triphenylmethane in dry THF (15 mL) was prepared in a Schlenk flask under Ar. After cooling to 0 °C, BuLi (1.6 M solution in hexanes, approx. 3.1 mL, 5.0 mmol, 1.0 equiv) was dropped in until a permanent red color appeared. Propargyl bromide (80% in toluene, 0.78 mL, 7.5 mmol, 1.5 equiv) was then added by syringe and the cold bath removed. The mixture was stirred overnight at room temperature.

Saturated aqueous NH₄Cl solution (2 mL) was then added and, after evaporation of THF under reduced pressure, the solution was extracted with EtOAc (3 x 15 mL). The combined organic extracts were dried over MgSO₄ and concentrated *in vacuo*. The residue was purified by flash chromatography (eluent: petroleum ether / EtOAc 90:10) to afford the title product as a pale yellow liquid (615 mg, 62%).

NMR peaks are broadened or doubled due to conformational equilibria in solution. ¹H NMR (300 MHz, CDCl₃): $\delta = 7.50$ -7.32 (m, 5H, H₂, H₃ and H₄), 4.62-3.83 (m, 2H, H₆), 3.70-3.16 (m, 2H, H₉), 2.28 (br s, 1H, H₈), 1.85-1.52 (m, 2H, H₁₀), 1.11-0.67 (m, 3H, H₁₁) ppm. ¹³C NMR (75 MHz, CDCl₃): $\delta = 171.7$ (C₇), 169.6 (C₇), 136.2 (C₁), 129.8 (C₄), 128.6 (C₃), 126.9 (C₂), 79.1 (C₇), 72.7 (C₈), 72.1 (C₈), 50.3 (C₉), 47.0 (C₉), 39.6 (C₆), 33.9 (C₆), 21.3 (C₁₀), 20.6 (C₁₀), 11.2 (C₁₃) ppm. IR (ATR): $\nu = 3233, 2964, 2934, 2116, 1630, 1416, 1254, 1097$ cm⁻¹.

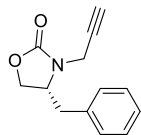


tert-Butyl N-phenyl-N-propargylcarbamate (S3n)

The reaction of *tert*-butyl *N*-phenylcarbamate (580 mg, 3.0 mmol) according to the general procedure (flash chromatography eluent: toluene) gave the title compound in the form of a pale yellow oil (489 mg, 71%).

¹H NMR (300 MHz, CDCl₃): $\delta = 7.39$ -7.30 (m, 4H, H₂₋₃), 7.26-7.17 (m, 1H, H₄), 4.37 (d, $J = 2.4$ Hz, 2H, H₅), 2.24 (t, $J = 2.4$ Hz, 1H, H₇), 1.46 (s, 9H, H₁₀) ppm. ¹³C NMR (75 MHz, CDCl₃): $\delta = 154.2$ (C₈), 142.3 (C₁), 128.9 (C₃), 126.5 (C₂), 126.4 (C₄), 81.2 (major rotamer C₉), 80.2 (minor

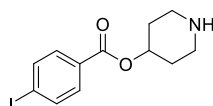
rotamer C₉), 71.8 (C₆), 39.9 (C₅), 28.4 (C₁₀) ppm. IR (ATR): $\nu = 3294, 3258, 2978, 2931, 2120, 1697, 1367, 1144, 1046, 1019, 696 \text{ cm}^{-1}$.



(R)-4-Benzyl-3-propargyloxazolidin-2-one (S3o)

The reaction of (R)-4-benzylloxazolidin-2-one (phenylalanine-derived Evans oxazolidinone, 532 mg, 3.0 mmol) according to the general procedure (flash chromatography eluent: petroleum ether / EtOAc 70:30) gave the title compound in the form of a pale yellow oil (562 mg, 87%).

¹H NMR (300 MHz, CDCl₃): $\delta = 7.45\text{--}7.26$ (m, 3H), 7.25–7.16 (m, 2H), 4.46 (dd, $J = 17.8, 2.5$ Hz, 1H), 4.31–4.17 (m, 2H), 4.12–4.09 (m, 1H), 3.86 (dd, $J = 17.8, 2.5$ Hz, 1H), 3.33–3.21 (m, 1H), 2.72 (dd, $J = 13.7, 6.8$ Hz, 1H), 2.36 (t, $J = 2.5$ Hz, 1H) ppm. ¹³C NMR (75 MHz, CDCl₃): $\delta = 157.8, 135.4, 129.2, 129.1, 127.4, 77.0, 73.5, 67.3, 55.8, 38.4, 32.6$ ppm. IR (ATR): $\nu = 3285, 2918, 2115, 1740, 1431, 1244, 1088, 1027 \text{ cm}^{-1}$. Spectral data are in agreement with the literature.^[23]



Piperidin-4-yl 4-iodobenzoate (S8)

This substrate for the synthesis of **2u** was prepared from 4-piperidinol using standard BOC chemistry.

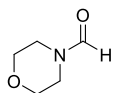
Piperidin-4-ol (506 mg, 5.0 mmol) and di-*tert*-butyl dicarbonate (BOC anhydride, 1.09 g, 5.0 mmol) were dissolved in a mixture of ethanol (10 mL) and water (10 mL) and left overnight at room temperature. Removal of the solvents under high vacuum gave crude *N*-(*tert*-butoxycarbonyl)-4-piperidinol (**S6**) that was used for the subsequent step without further treatment. ¹H NMR (300 MHz, CDCl₃): $\delta = 3.93\text{--}3.77$ (m, 3H), 3.02 (ddd, $J = 13.4, 9.8, 3.4$ Hz, 2H), 1.63 (br s, 1H), 1.96–1.79 (m, 2H), 1.55–1.32 (m, 11H) ppm. IR (ATR): $\nu = 3460, 2935, 2876, 1666, 1427, 1364, 1235, 1165, 1073 \text{ cm}^{-1}$. Spectral data are in agreement with the literature.^[24]

To a solution of crude *N*-(*tert*-butoxycarbonyl)-4-piperidinol (**S6**, 604 mg, 3.0 mmol) and triethylamine (836 μ L, 6.0 mmol, 2.0 equiv) in CH₂Cl₂ (10 mL) and a drop of pyridine, 4-iodobenzoyl chloride (799 mg, 3.0 mmol) was added portionwise. After stirring for 1 h at room temperature, the mixture was poured into 10 mL of water and phases were separated. The aqueous layer was extracted with more CH₂Cl₂ (2 x 5 mL) and the combined organic extracts were exsiccated over Na₂SO₄ and concentrated under reduced pressure. Purification of the residue by flash chromatography on silica gel (eluent: toluene/EtOAc 95:5) gave *N*-(*tert*-butoxycarbonyl)-piperidin-4-yl 4-iodobenzoate (**S7**) as a white solid (788 mg, 59%). ¹H NMR (300 MHz, CDCl₃): $\delta = 7.84\text{--}7.78$ (m, 2H), 7.77–7.71 (m, 2H), 5.17 (tt, $J = 7.8, 3.8$ Hz, 1H), 3.85–3.68 (m, 2H), 3.33 (ddd, $J = 13.6, 8.3, 3.7$ Hz, 2H), 2.03–1.87 (m, 2H), 1.85–1.66 (m, 2H), 1.47 (s, 9H) ppm. ¹³C NMR (75 MHz, CDCl₃): $\delta = 165.4, 154.9, 137.9, 131.1, 130.0, 100.9, 79.9, 70.7, 30.8, 28.6$ ppm. IR (ATR): $\nu = 2926, 2868, 1712, 1678, 1584, 1428, 1274, 1165, 1116 \text{ cm}^{-1}$.

A solution of *N*-(*tert*-butoxycarbonyl)-piperidin-4-yl 4-iodobenzoate (**S7**, 705 mg, 1.58 mmol) in CH₂Cl₂ (2 mL) and trifluoroacetic acid (2 mL) was left overnight at room temperature. Treatment with saturated NaHCO₃ solution and extraction with CH₂Cl₂ gave the title compound in the form of a pale pink solid (522 mg, 90%). ¹H NMR (300 MHz, CDCl₃): δ = 7.82-7.77 (m, 2H), 7.77-7.72 (m, 2H), 5.10 (tt, *J* = 8.6, 4.0 Hz, 1H), 3.12 (dt, *J* = 12.9, 7.7 Hz, 2H), 2.89-2.71 (m, 2H), 2.09-1.93 (m, 2H), 1.77-1.61 (m, 2H), 1.55 (br s, 1H) ppm. ¹³C NMR (75 MHz, CDCl₃): δ = 165.5, 137.8, 131.2, 130.3, 100.7, 71.8, 44.2, 32.4 ppm. IR (ATR): ν = 3290, 2945, 2928, 2857, 1707, 1584, 1271, 1117, 1104 cm⁻¹.

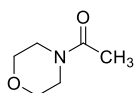
3.7. Study of the reaction between morpholine and Cu(OTf)₂ – identification of the organic products

A suspension of Cu(OTf)₂ (362 mg, 1.0 mmol) in morpholine (431 μL, 5.0 mmol) was heated at 80 °C for 15 minutes. The colour changed gradually from deep blue to brownish. The resulting paste was subjected to distillation at reduced pressure with the aid of a Kugelrohr apparatus (0.1 mbar, air bath temperature: 200 °C). A part of the distillate condensed only in liquid nitrogen, GLC analysis showed that it was composed unchanged morpholine. Another fraction of the distillate condensed in a bulb kept at room temperature, it was found to be practically pure *N*-formylmorpholine, as confirmed by GLC-MS analysis and comparison of ¹H and ¹³C NMR spectra with published data.^[25,26] Small amounts of *N*-acetylmorpholine (about 4% of *N*-formylmorpholine, as assessed by ¹H NMR) and 3,4'-bimorpholine (about 2% of *N*-formylmorpholine, as assessed by ¹H NMR) were also identified by GLC-MS and by observation of some signature NMR peaks.



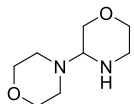
N-Formylmorpholine

¹H NMR (300 MHz, CDCl₃): δ = 8.05 (s, 1H), 3.71-3.62 (m, 4H), 3.59-3.53 (m, 2H), 3.41-3.36 (m, 2H) ppm. ¹³C NMR (75 MHz, CDCl₃) δ = 161.0, 67.4, 66.6, 45.9, 40.7 ppm. EI-MS (EI, 70 eV): *m/z* (%) = 115 (100, M⁺), 100 (75), 86 (57), 57 (72), 56 (95), 42 (79). CI-MS (reagent gas NH₃): *m/z* = 133 ([M+NH₄]⁺), 116 ([M+H]⁺). Spectral data are in agreement with the literature.^[25,26]



N-Acetylmorpholine

Signature peaks - ¹H NMR (300 MHz, CDCl₃): δ = 2.08 (s, 3H) ppm. ¹³C NMR (75 MHz, CDCl₃) δ = 21.1 ppm (detected by HSQC). EI-MS (EI, 70 eV): *m/z* (%) = 129 (20, M⁺), 114 (25), 86 (58), 57 (100), 56 (78), 43 (65). CI-MS (reagent gas NH₃): *m/z* = 147 ([M+NH₄]⁺), 130 ([M+H]⁺). The EI-MS spectrum is in agreement with that of an authentic sample.



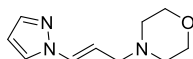
3,4'-Bimorpholine

Signature peaks - ¹H NMR (300 MHz, CDCl₃): δ = 4.33-4.21 (m, 1H), 3.85-3.80 (m, 2H, detected by COSY correlation with the signal at 4.33-4.21 ppm), 3.60-3.66 (m, 4H, detected by COSY correlation with the signal at 2.93-2.83 ppm), 2.93-2.83 (m, 4H) ppm. ¹³C NMR (75 MHz, CDCl₃) δ = 67.2 (HSQC correlation with the signal at 3.85-3.80 ppm), 49.9 (HSQC correlation with the signal at 4.33-4.21 ppm), 46.2 (HSQC correlation with the signal at 2.93-2.83). EI-MS (EI, 70 eV): *m/z* (%) = 172 (55, M⁺), 114 (28), 86 (62), 56 (100), 55 (22) CI-MS (reagent gas NH₃): *m/z* = 173 ([M+H]⁺).

A further unidentified peak appeared in the gas chromatogram (accounting for about 1% of the total integrated area of the GC-FID chromatogram). EI-MS (EI, 70 eV): m/z (%) = 116 (20, M⁺), 86 (27), 56 (100), 55 (53), 41 (25). CI-MS (reagent gas NH₃): m/z = 134 ([M+NH₄]⁺), 117 ([M+H]⁺).

3.8. Hydroamination of *N*-allenylazoles

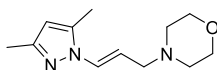
The general procedure described for the hydroamination of allenamides was applied without change to *N*-allenylazoles. The description of the products here follows.



(*E*)-4-(3-(1*H*-Pyrazol-1-yl)allyl)morpholine (**8a**)

The reaction of 1-allenyl-1*H*-pyrazole (**7a**, 53.1 mg, 0.50 mmol) with morpholine (52.5 μ L, 0.60 mmol) according to general procedure (flash chromatography eluent: ethyl acetate/acetone 50:50) gave the title compound in the form of a pale yellow oil (85.2 mg, 88%).

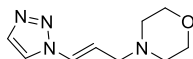
^1H NMR (300 MHz, CDCl_3): δ = 7.60-7.56 (m, 2H), 7.01 (dt, J = 14.2, 1.4 Hz, 1H), 6.33 (t, J = 2.2 Hz, 1H), 6.06 (dt, J = 14.2, 7.2 Hz, 1H), 3.75-3.70 (m, 4H), 3.12 (dd, J = 7.2, 1.4 Hz, 2H), 2.54-2.47 (m, 4H) ppm. ^{13}C NMR (75 MHz, CDCl_3): δ = 140.9, 130.1, 127.4, 112.9, 107.2, 67.1, 58.3, 53.6 ppm. HRMS (EI) m/z : $[\text{M}]^+$ Calcd for $\text{C}_{10}\text{H}_{15}\text{N}_3\text{O}$ 193.1215; Found 193.1218.



(*E*)-4-(3-(3,5-Dimethyl-1*H*-pyrazol-1-yl)allyl)morpholine (**8b**)

The reaction of 3,5-dimethyl-1-allenyl-1*H*-pyrazole (**7b**, 67.0 mg, 0.50 mmol) with morpholine (52.5 μ L, 0.60 mmol) according to the general procedure (chromatographic purification not required) gave the title compound in the form of a pale brown oil (102 mg, 92%).

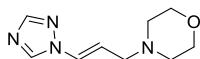
^1H NMR (300 MHz, CDCl_3): δ = 6.78 (dt, J = 13.9, 1.3 Hz, 1H), 6.15 (dt, J = 13.9, 7.2 Hz, 1H), 5.83 (s, 1H), 3.72-3.67 (m, 4H), 3.09 (dd, J = 7.2, 1.3 Hz, 2H), 2.53-2.46 (m, 4H), 2.25 (s, 3H), 2.22 (s, 3H) ppm. ^{13}C NMR (75 MHz, CDCl_3): δ = 149.9, 139.0, 126.4, 112.5, 106.8, 67.1, 58.7, 53.5, 13.7, 11.2 ppm. HRMS (EI) m/z : $[\text{M}]^+$ Calcd for $\text{C}_{12}\text{H}_{19}\text{N}_3\text{O}$ 221.1528; Found 221.1532.



(*E*)-4-(3-(1*H*-1,2,3-Triazol-1-yl)allyl)morpholine (**8c**)

The reaction of 1-allenyl-1,2,3-1*H*-triazole (**7c**, 56.0 mg, 0.52 mmol) with morpholine (54.6 μ L, 0.62 mmol) according to the general procedure (chromatographic purification not needed) gave the title compound in the form of a white solid (100 mg, 99%).

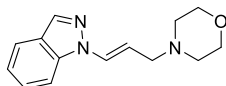
^1H NMR (300 MHz, CDCl_3): δ = 7.75 (d, J = 1.2 Hz, 1H), 7.70 (d, J = 1.2 Hz, 1H), 7.32 (dt, J = 14.2, 1.5 Hz, 1H), 6.25 (dt, J = 14.2, 6.8 Hz, 1H), 3.74-3.68 (m, 4H), 3.16 (dd, J = 6.8, 1.5 Hz, 2H), 2.54-2.47 (m, 4H) ppm. ^{13}C NMR (75 MHz, CDCl_3): δ = 134.1, 126.6, 120.9, 118.8, 67.0, 57.9, 53.7 ppm. HRMS (EI) m/z : $[\text{M}]^+$ Calcd for $\text{C}_9\text{H}_{14}\text{N}_3\text{O}$ 194.1168; Found 194.1171.



(*E*)-4-(3-(1*H*-1,2,4-Triazol-1-yl)allyl)morpholine (**8d**)

The reaction of 1-allenyl-1*H*-1,2,4-triazole (**7d**, 107 mg, 1.0 mmol) with morpholine (105 μ L, 1.2 mmol) according to the general procedure (reaction time: 30 min, no chromatographic purification needed) gave the title compound in the form of a pale brown solid (191 mg, 98%).

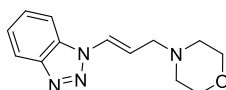
^1H NMR (300 MHz, CDCl_3): δ = 8.19 (s, 1H), 7.96 (s, 1H), 7.03 (d, J = 14.0 Hz, 1H), 6.33 (dt, J = 14.0, 6.9 Hz, 1H), 3.87-3.50 (m, 4H), 3.13 (d, J = 6.9 Hz, 2H), 2.69-2.29 (m, 4H) ppm. ^{13}C NMR (75 MHz, CDCl_3): δ = 152.4, 141.8, 125.7, 118.2, 67.0, 57.8, 53.7 ppm. HRMS (EI) m/z : $[\text{M}]^+$ Calcd for $\text{C}_9\text{H}_{14}\text{N}_3\text{O}$ 194.1168; Found 194.1162.



(*E*)-4-(3-(1*H*-Indazol-1-yl)allyl)morpholine (8e**)**

The reaction of 1-allenyl-1*H*-indazole (**7e**, 55.0 mg, 0.35 mmol) with morpholine (36.8 μ L, 0.42 mmol) according to the general procedure (flash chromatography eluent: ethyl acetate/toluene 50:50) gave the title compound in the form of a greenish solid (64.1 mg, 75%). This compound – as the parent allene – is rather unstable even on NaHCO_3 -treated silica gel and should be purified by chromatography rather quickly. Some impurities – that are evident in the aliphatic zone of the ^1H NMR spectrum – form by decomposition during flash chromatography.

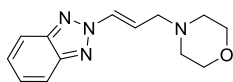
^1H NMR (300 MHz, CDCl_3): δ = 8.09 (s, 1H), 7.74 (d, J = 8.1 Hz, 1H), 7.57 (d, J = 8.4 Hz, 1H), 7.47-7.42 (m, 1H), 7.28 (d, J = 14.2 Hz, 1H), 7.24-7.17 (m, 1H), 6.29 (dt, J = 14.2, 7.2 Hz, 1H), 3.77-3.73 (m, 4H), 3.22 (d, J = 7.2 Hz, 2H), 2.62-2.50 (m, 4H) ppm. ^{13}C NMR (75 MHz, CDCl_3): δ = 138.5, 135.7, 127.4, 127.4, 124.9, 121.9, 121.5, 111.6, 109.5, 67.1, 58.9, 53.7 ppm. HRMS (EI) m/z : $[\text{M}]^+$ Calcd for $\text{C}_{14}\text{H}_{17}\text{N}_3\text{O}$ 243.1372; Found 243.1377.



(*E*)-4-(3-(1*H*-Benzotriazol-1-yl)allyl)morpholine (8f**)**

The reaction of 1-allenyl-1*H*-benzotriazole (**7f**, 78.6 mg, 0.50 mmol) with morpholine (52.5 μ L, 0.60 mmol) according to the general procedure (flash chromatography eluent: gradient ethyl acetate/acetone 100:0 to 90:10) gave the title compound in the form of a white solid (103 mg, 84%).

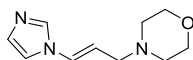
^1H NMR (300 MHz, CDCl_3): δ = 8.07 (d, J = 7.0 Hz, 1H), 7.67 (d, J = 8.4 Hz, 1H), 7.57-7.47 (m, 2H), 7.43-7.38 (m, 1H), 6.51 (dt, J = 14.2, 7.1 Hz, 1H), 3.76-3.72 (m, 4H), 3.26 (dd, J = 7.1, 1.0 Hz, 2H), 2.59-2.53 (m, 4H) ppm. ^{13}C NMR (75 MHz, CDCl_3): δ = 146.4, 131.4, 128.4, 125.9, 124.6, 120.5, 117.7, 110.2, 67.0, 58.6, 53.7 ppm. HRMS (EI) m/z : $[\text{M}]^+$ Calcd for $\text{C}_{13}\text{H}_{16}\text{N}_4\text{O}$ 244.1324; Found 244.1328.



(*E*)-4-(3-(2*H*-Benzotriazol-2-yl)allyl)morpholine (8g**)**

The reaction of 2-allenyl-2*H*-benzotriazole (**7g**, 10.0 mg, 0.064 mmol) with morpholine (6.7 μ L, 0.076 mmol) according to the general procedure (flash chromatography eluent: ethyl acetate) gave the title compound in the form of a white solid (8.2 mg, 53%).

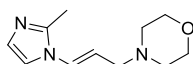
¹H NMR (300 MHz, CDCl₃): δ = 7.89-7.81 (m, 2H), 7.53 (dt, *J* = 14.1, 1.5 Hz, 1H), 7.43-7.35 (m, 2H), 6.94 (dt, *J* = 14.1, 6.9 Hz, 1H), 3.77-3.72 (m, 4H), 3.27 (dd, *J* = 6.9, 1.5 Hz, 2H), 2.59-2.53 (m, 4H) ppm. ¹³C NMR (75 MHz, CDCl₃): δ = 144.8, 130.6, 127.4, 122.1, 118.3, 67.1, 57.8, 53.7 ppm. HRMS (EI) *m/z*: [M]⁺ Calcd for C₁₃H₁₆N₄O 244.1324; Found 244.1314.



(E)-4-(3-(1*H*-Imidazol-1-yl)allyl)morpholine (10a)

The reaction of 1-allenyl-1*H*-imidazole (**9a**, 57.7 mg, 0.54 mmol) with morpholine (56.7 μL, 0.65 mmol) according to the general procedure (chromatographic purification was not necessary) gave the title compound in the form of an off-white solid (101 mg, 96%).

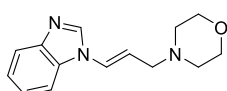
¹H NMR (300 MHz, CDCl₃): δ = 7.61 (br s, 1H), 7.13 (br s, 1H), 7.07 (br s, 1H), 6.83 (dt, *J* = 14.2, 1.4 Hz, 1H), 5.83 (dt, *J* = 14.2, 7.0 Hz, 1H), 3.74-3.69 (m, 4H), 3.08 (dd, *J* = 7.0, 1.4 Hz, 2H), 2.51-2.45 (m, 4H) ppm. ¹³C NMR (75 MHz, CDCl₃): δ = 136.2, 130.5, 126.2, 116.3, 115.0, 67.0, 58.3, 53.7 ppm. HRMS (EI) *m/z*: [M]⁺ Calcd for C₁₀H₁₅N₃O 193.1215; Found 193.1218.



(E)-4-(3-(2-Methyl-1*H*-imidazol-1-yl)allyl)morpholine (10b)

The reaction of 1-allenyl-2-methyl-1*H*-imidazole (**9b**, 60.1 mg, 0.50 mmol) with morpholine (52.5 μL, 0.60 mmol) according to the general procedure (flash chromatography eluent: acetone) gave the title compound in the form of a white solid (74.1 mg, 72%).

¹H NMR (300 MHz, CDCl₃): δ = 7.06 (d, *J* = 1.5 Hz, 1H), 6.88 (d, *J* = 1.5 Hz, 1H), 6.74 (d, *J* = 14.1 Hz, 1H), 5.71 (dt, *J* = 14.1, 7.1 Hz, 1H), 3.73-3.66 (m, 4H), 3.07 (d, *J* = 7.1 Hz, 2H), 2.50-2.42 (m, 4H), 2.38 (s, 3H) ppm. ¹³C NMR (75 MHz, CDCl₃): δ = 144.4, 128.4, 125.6, 115.8, 115.2, 66.9, 58.4, 53.6, 13.4 ppm. HRMS (EI) *m/z*: [M]⁺ Calcd for C₁₁H₁₇N₃O 207.1372; Found 207.1376.



(E)-4-(3-(1*H*-Benzimidazol-1-yl)allyl)morpholine (10c)

The reaction of 1-allenyl-1*H*-benzimidazole (**9c**, 78.1 mg, 0.50 mmol) with morpholine (52.5 μL, 0.60 mmol) according to the general procedure (flash chromatography eluent: ethyl acetate/acetone gradient from 80:20 to 70:30) gave the title compound in the form of a pale brown oil (89.4 mg, 73%).

¹H NMR (300 MHz, CDCl₃): δ = 8.09 (s, 1H), 7.86-7.78 (m, 1H), 7.58-7.50 (m, 1H), 7.41-7.28 (m, 2H), 7.05 (dt, *J* = 14.2, 1.3 Hz, 1H), 6.09 (dt, *J* = 14.2, 7.0 Hz, 1H), 3.80-3.72 (m, 4H), 3.21 (dd, *J* = 7.0, 1.3 Hz, 2H), 2.59-2.50 (m, 4H) ppm. ¹³C NMR (75 MHz, CDCl₃): δ = 144.1, 141.0, 132.7, 124.9, 124.0, 123.2, 120.9, 116.2, 110.4, 67.1, 58.8, 53.7 ppm. HRMS (EI) *m/z*: [M]⁺ Calcd for C₁₄H₁₇N₃O 243.1372; Found 243.1361.

3.9. Synthesis of *N*-propargyl heteroarenes

Generally speaking, *N*-allenylheterocycles **7a-g** and **9a-c** were obtained by base-catalyzed isomerization^[27–31] of the corresponding *N*-propargylheterocycles, which in turn were prepared by propargylation of the unsubstituted heteroarenes. Sometimes these intermediates were not isolated pure, since isomerization easily took place under the alkaline conditions employed for their synthesis and the crude mixture was then employed in the subsequent step. The general procedures **P** and **I** reported below apply in most cases, but they had to be adapted for some substrates, as detailed in the following.

All the compounds described in this section have been reported in the literature, except for allene **8c**.

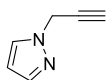
General procedure P – *N*-Propargylation of nitrogen heterocycles under PTC conditions

A solution of the appropriate nitrogen heterocycle in toluene (0.66 M) was stirred with NaOH (7.5 equiv) dissolved in an equal weight of water, together with Bu₄NHSO₄ (0.05 equiv) and propargyl bromide (80% solution in toluene, approx. 9.2 M, 1.5 equiv) at room temperature.

When TLC showed complete consumption of the starting material, an equal volume of toluene was added and phases were separated. The organic layer was washed with water (half volume, five times). The crude product obtained after drying over Na₂SO₄ and concentration under reduced pressure was purified by the method specified for each product.

General procedure I – Isomerization of *N*-propargyl heterocycles to *N*-allenyl heterocycles

To a 0.2 M solution of the appropriate *N*-propargyl heterocycle in rigorously dried THF under Ar atmosphere, ^tBuOK (dispensed as a 1.0 M solution in THF, 0.2 equiv) was added. When GC or TLC analysis showed complete conversion of the starting material or a stationary equilibrium mixture, the solution was treated with 0.2 volumes of a saturated aqueous NH₄Cl solution. The resulting mixture was extracted with ethyl acetate, exsiccated over Na₂SO₄ or K₂CO₃ and volatiles were evaporated under reduced pressure. The residue was purified by flash chromatography on NaHCO₃-treated silica gel or vacuum-distilled with the aid of a Kugelrhor apparatus to afford the required *N*-allenyl heteroarene.

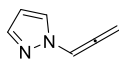


1-Propargyl-1*H*-pyrazole

To a solution of pyrazole (1.36 g, 20 mmol), Bu₄NHSO₄ (340 mg, 1.0 mmol) and propargyl *p*-toluenesulfonate (3.46 mL, 20 mmol) in CH₂Cl₂ (20 mL), a solution of NaOH (6.0 g, 150 mmol) in H₂O (6.0 mL) was added and the resulting biphasic mixture was vigorously stirred overnight at room temperature.

The amount of water necessary to dissolve the precipitated NaOTs was added and phases were separated. The aqueous layer was extracted with more CH₂Cl₂ (3 x 10 mL) and the combined organic phases were exsiccated over Na₂SO₄ and concentrated *in vacuo*. The residue was purified by Kugelrhor distillation at approx. 0.1 mbar to give the required compound, in a 1:1 mixture with the isomeric 1-allenyl-1*H*-pyrazole (**7a**), in the form of a pale yellow liquid (1.22 g, 58% combined yield).

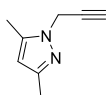
^1H NMR (300 MHz, CDCl_3): δ = 7.47-7.44 (m, 2H), 6.21 (t, J = 2.1 Hz, 1H), 4.79 (d, J = 2.5 Hz, 2H), 2.42 (t, J = 2.5 Hz, 1H) ppm. ^{13}C NMR (75 MHz, CDCl_3): δ = 140.1, 128.8, 106.3, 76.9, 74.7, 41.6 ppm. Spectral data are in agreement with the literature.^[32]



1-Allenyl-1H-pyrazole (7a)

The reaction of 1-propargyl-1H-pyrazole (in an approx. 50:50 mixture with the title product, as obtained by the PTC propargylation of pyrazole, 230 mg, 2.2 mmol) according to general procedure **I** (reaction time: 10 minutes, purification by Kugelrohr distillation at 0.1 mbar) gave the title compound in the form of a colorless oil (200 mg, 87%).

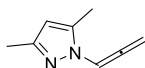
^1H NMR (300 MHz, CDCl_3): δ = 7.57 (d, J = 2.2 Hz, 1H), 7.53 (d, J = 2.2 Hz, 1H), 7.18 (t, J = 6.5 Hz, 1H), 6.32 (t, J = 2.2 Hz, 1H), 5.58 (d, J = 6.5 Hz, 2H). ^{13}C NMR (75 MHz, CDCl_3): δ = 202.0, 140.7, 127.6, 107.3, 101.6, 88.3 ppm. Spectral data are in agreement with the literature.^[27,33]



3,5-Dimethyl-1-propargyl-1H-pyrazole

The reaction of 3,5-dimethylpyrazole (481 mg, 5.0 mmol) according to general procedure **P** (reaction time: 16 h, no distillation or chromatographic purification needed) gave the title compound in the form of an off-white solid (537 mg, 80%).

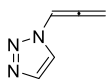
^1H NMR (300 MHz, CDCl_3): δ = 5.82 (s, 1H), 4.76 (d, J = 2.5 Hz, 2H), 2.35 (t, J = 2.5 Hz, 1H), 2.29 (s, 3H), 2.21 (s, 3H) ppm. ^{13}C NMR (75 MHz, CDCl_3): δ = 148.2, 139.2, 106.0, 77.7, 73.1, 38.7, 13.5, 11.0 ppm. Spectral data are in agreement with the literature.^[34]



3,5-Dimethyl-1-allenyl-1H-pyrazole (7b)

The reaction of 3,5-dimethyl-1-propargyl-1H-pyrazole (268 mg, 2.0 mmol) according to general procedure **I** (reaction time: 10 minutes, no chromatographic purification needed) gave the title compound in the form of a pale brown oil (260 mg, 97%).

^1H NMR (300 MHz, CDCl_3): δ = 6.99 (t, J = 6.5 Hz, 1H), 5.85 (s, 1H), 5.55 (d, J = 6.5 Hz, 2H), 2.28 (s, 3H), 2.23 (s, 3H) ppm. ^{13}C NMR (75 MHz, CDCl_3): δ = 203.2, 149.7, 139.7, 106.9, 98.8, 87.3, 13.7, 11.7 ppm. Spectral data are in agreement with those reported in the literature.^[35]



1-Allenyl-1H-1,2,3-triazole (7c)

To a suspension of 1,2,3-triazole (345 mg, 5.0 mmol) and K_2CO_3 (1.38 g, 10 mmol, 2.0 equiv) in MeOH (10 mL), propargyl bromide (80% solution in toluene, 815 μL , 7.5 mmol, 1.5 equiv) was added. The mixture was stirred overnight at room temperature.

Ethyl acetate (20 mL) was added and the suspension was filtered through a short plug of diatomaceous earth. Concentration *in vacuo* afforded a pale brown paste (411 mg). ¹H NMR analysis and comparison with literature data^[36] showed that this material was composed of 1-propargyl-1*H*-1,2,3-triazole (35%), 1-allenyl-1*H*-1,2,3-triazole (48%), 2-propargyl-2*H*-1,2,3-triazole (11%), 2-allenyl-2*H*-1,2,3-triazole (6%); overall yield of isomeric products: 77%. Signature ¹H NMR peaks (300 MHz, CDCl₃) are given below for each compound.

1-Propargyl-1*H*-1,2,3-triazole: $\delta = 5.22$ (d, $J = 2.5$ Hz, 2H), 2.57 (t, $J = 2.5$ Hz, 1H) ppm.

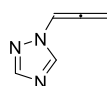
1-Allenyl-1*H*-1,2,3-triazole (7c): $\delta = 7.52$ (t, $J = 6.6$ Hz, 1H), 5.69 (d, $J = 6.6$ Hz, 2H) ppm.

2-Propargyl-2*H*-1,2,3-triazole: $\delta = 5.24$ (d, $J = 2.6$ Hz, 2H), 2.52 (t, $J = 2.6$ Hz, 1H) ppm.

2-Allenyl-2*H*-1,2,3-triazole: $\delta = 7.43$ (t, $J = 6.6$ Hz, 1H), 5.73 (d, $J = 6.6$ Hz, 2H) ppm.

An aliquot of this crude mixture of isomers (214 mg, 2.0 mmol) was dissolved in dry THF (10 mL) under Ar. ^tBuOK (1.0 M solution in THF, 0.4 mL, 0.40 mmol, 0.20 equiv) was added and the mixture was left for 10 minutes at room temperature. The reaction was quenched with a saturated aqueous NH₄Cl solution (1 mL) and most of the THF was evaporated *in vacuo*. The residue was extracted with ethyl acetate (3 x 10 mL). The pooled organic extracts were dried over Na₂SO₄ and concentrated under reduced pressure. The residue was purified by flash chromatography on NaHCO₃-washed silica gel (gradient elution: petroleum ether/ethyl acetate 70:30 to 60:40) to give the title product in the form of a pale yellow oil (104 mg, 49%); overall yield over two steps: 38%.

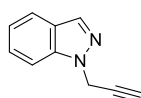
¹H NMR (300 MHz, CDCl₃): $\delta = 7.73$ (br s, 1H), 7.70 (br s, 1H), 7.52 (t, $J = 6.6$ Hz, 1H), 5.69 (d, $J = 6.5$ Hz, 2H) ppm. ¹³C NMR (75 MHz, CDCl₃): $\delta = 201.6, 134.4, 121.4, 98.5, 89.0$ ppm.



1-Allenyl-1*H*-1,2,4-triazole (7d)

The application of general procedure **P** to 1,2,4-triazole (691 mg, 10 mmol) did not give, after a reaction time of 4 h, the expected alkyne. The title compound was obtained instead in the form of a brown oil (232 mg, 22%), without chromatographic purification.

¹H NMR (300 MHz, CDCl₃): $\delta = 8.22$ (s, 1H), 7.99 (s, 1H), 7.16 (t, $J = 6.5$ Hz, 1H), 5.68 (d, $J = 6.5$ Hz, 2H) ppm. ¹³C NMR (75 MHz, CDCl₃): $\delta = 202.3, 152.5, 142.1, 98.0, 89.0$ ppm. Spectral data are in agreement with the literature.^[37]



1-Propargyl-1*H*-indazole and isomeric allenes

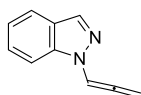
General procedure **P** was applied to 1*H*-indazole (354 mg, 3.0 mmol), reaction time: 16 h. ¹H NMR analysis showed that the crude was composed of 2-allenyl-2*H*-indazole (12%), 1-propargyl-1*H*-indazole (57%), and 1-allenyl-1*H*-indazole (**7e**, 31%). Careful separation by flash chromatography on NaHCO₃-washed silica gel (eluent: toluene/ethyl acetate 98.5:1.5) gave, in order of elution, 2-allenyl-2*H*-indazole (18 mg, 4%), 1-propargyl-1*H*-indazole (229 mg, 49%), 1-

allenyl-1*H*-indazole (**7e**, 135 mg, 29%); overall yield of isomers: 82%. The two allenes are quite unstable (they decompose almost completely in one night at 4 °C), while 1-propargyl-1*H*-indazole can be kept for at least one week without change.

1-Propargyl-1*H*-indazole - ¹H NMR (300 MHz, CDCl₃): δ = 8.03 (br s, 1H), 7.75 (d, *J* = 8.1 Hz, 1H), 7.55 (dd, *J* = 8.4 Hz, 1.0, 1H), 7.43 (ddd, *J* = 8.4, 6.8, 1.0 Hz, 1H), 7.19 (ddd, *J* = 8.1, 6.8, 1.0 Hz, 1H), 5.19 (d, *J* = 2.5 Hz, 2H), 2.40 (t, *J* = 2.5 Hz, 1H) ppm. ¹³C NMR (75 MHz, CDCl₃): δ = 139.3, 134.0, 126.8, 124.7, 121.4, 121.2, 109.4, 77.3, 73.7, 39.0 ppm. Spectral data are in agreement with those reported in the literature.^[30]

1-Allenyl-1*H*-indazole (7e) - ¹H NMR (300 MHz, CDCl₃): δ = 8.09 (br s, 1H), 7.80-7.71 (m, 2H), 7.52 (t, *J* = 6.6 Hz, 1H), 7.41 (ddd, *J* = 7.4, 6.9, 1.0 Hz, 1H), 7.21 (ddd, *J* = 7.9, 6.9, 0.9 Hz, 1H), 5.73 (d, *J* = 6.6 Hz, 2H) ppm. ¹³C NMR (75 MHz, CDCl₃): δ = 202.8, 138.9, 135.3, 127.1, 125.1, 121.8, 121.4, 110.7, 100.3, 88.3 ppm. Spectral data are in agreement with those reported in the literature.^[30]

2-Allenyl-2*H*-indazole - ¹H NMR (300 MHz, CDCl₃): δ = 8.10 (br s, 1H), 7.72 (br d, *J* = 8.8 Hz, 1H), 7.67-7.61 (m, 1H), 7.43 (t, *J* = 6.5 Hz, 1H), 7.33-7.26 (m, 1H), 7.14-7.07 (m, 1H), 5.76 (d, *J* = 6.5 Hz, 2H) ppm. This compound is not stable enough to record a well-resolved ¹³C spectrum. It has already been reported in the literature.^[38]



1-Allenyl-1*H*-indazole (**7e**)

The reaction of 1-propargyl-1*H*-indazole (147 mg, 0.94 mmol) according to general procedure **I** (reaction time: 1 minute) gave the title compound in the form of a pale greenish oil (130 mg, 88%). No chromatographic purification was needed.

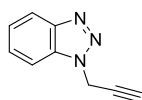
Spectral data agree with those reported above.

Isomeric *N*-propargyl and *N*-allenyl benzotriazoles

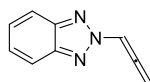
To a solution of 1*H*-benzotriazole (596 mg, 5.0 mmol) in methanol (10 mL), K₂CO₃ (1.38 g, 10 mmol) and propargyl bromide (80% solution in toluene, approx. 9.2 M, 652 μ L, 6.0 mmol) were added. The mixture was stirred overnight at room temperature. Toluene (40 mL) was added and the suspension was filtered through a short plug of diatomaceous earth.

Evaporation of the solvent gave a pale brown oil (785 mg). ¹H NMR analysis and comparison with literature data^[39-42] revealed that the material so obtained was a mixture of isomeric *N*-propargyl and *N*-allenyl benzotriazoles (signature ¹H NMR signals in CDCl₃ given): 1-propargyl-1*H*-benzotriazole [51%, δ = 5.47 (d, *J* = 2.6 Hz, 2H), 2.50 (t, *J* = 2.6 Hz, 1H) ppm], 2-allenyl-2*H*-benzotriazole [**7g**, 29%, δ = 7.66 (t, *J* = 6.5 Hz, 1H), 5.86 (d, *J* = 6.5 Hz, 2H) ppm], 1-allenyl-1*H*-benzotriazole [**7f**, 18%, δ = 5.82 (d, *J* = 6.6 Hz, 2H) ppm], 2-propargyl-2*H*-benzotriazole [2%, δ = 5.53 (d, *J* = 2.6 Hz, 2H), 2.62 (t, *J* = 2.6 Hz, 1H) ppm].

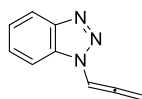
A part of this oil (200 mg) was separated by flash chromatography on NaHCO₃-washed silica gel (eluent: petroleum ether/ethyl acetate gradient from 95:5 to 85:15) and gave, in order of elution, 2-allenyl-2*H*-benzotriazole (**7g**, pale brown oil, 10.0 mg, 5%), 1-allenyl-1*H*-benzotriazole (**7f**, dark solid, 37.0 mg, 19%) and 1-propargyl-1*H*-benzotriazole (off white solid, 89.2 mg, 45%).



1-propargyl-1H-benzotriazole - ^1H NMR (300 MHz, CDCl_3): δ = 8.08 (dt, J = 8.4, 1.0 Hz, 1H), 7.72 (dt, J = 8.4, 1.0 Hz, 1H), 7.50-7.47 (m, 1H), 7.43-7.37 (m, 1H), 5.46 (d, J = 2.6 Hz, 2H), 2.50 (t, J = 2.6 Hz, 1H) ppm. ^{13}C NMR (75 MHz, CDCl_3): δ = 146.4, 132.6, 127.8, 124.3, 120.3, 109.9, 75.4, 75.2, 38.2 ppm. Spectral data are in agreement with the literature.^[39]



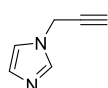
2-Allenyl-2H-benzotriazole (7g) - ^1H NMR (300 MHz, CDCl_3): δ = 7.91-7.82 (m, 2H), 7.66 (t, J = 6.5 Hz, 1H), 7.43-7.34 (m, 2H), 5.86 (d, J = 6.5 Hz, 2H) ppm. ^{13}C NMR (75 MHz, CDCl_3): δ = 204.3, 145.1, 127.2, 118.0, 103.5, 89.3 ppm. Spectral data are in agreement with the literature.^[37]



1-Allenyl-1H-benzotriazole (7f)

The reaction of crude 1-propargyl-1H-benzotriazole (in mixture with the isomeric allenes as obtained by alkylation of 1H-benzotriazole, 554 mg, 3.5 mmol) according to general procedure **C** (reaction time: 10 minutes, purification by flash chromatography on NaHCO_3 -washed silica gel, gradient elution petroleum ether/ethyl acetate 95:5 to 90:10) gave the title compound in the form of a dark solid (257 mg, 46%).

^1H NMR (300 MHz, CDCl_3): δ = 8.07 (dt, J = 8.2, 1.1 Hz, 1H), 7.89-7.82 (m, 2H), 7.49 (ddd, J = 8.2, 7.0, 1.1 Hz, 1H), 7.40 (ddd, J = 8.2, 7.0, 1.1 Hz, 1H), 5.82 (d, J = 6.6 Hz, 2H) ppm. ^{13}C NMR (75 MHz, CDCl_3): δ = 202.0, 146.7, 131.8, 128.0, 124.7, 120.3, 111.2, 98.2, 89.0 ppm. Spectral data are in agreement with the literature.^[40]



1-Propargyl-1H-imidazole

The reaction of imidazole (1.36 g, 20 mmol) according to general procedure **P**, after Kugelrohr distillation at reduced pressure (approx. 0.1 mbar, temperature: 150 °C) gave the title compound in mixture with the isomeric 1-allenyl-1H-imidazole in the form of a pale yellow oil, 2.05 g, 97% (79:21 molar ratio alkyne : allene). The mixture thus obtained was used for the subsequent isomerization without attempting any separation.

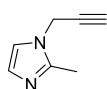
^1H NMR (300 MHz, CDCl_3): δ = 7.49 (br s, 1H), 6.99 (br s, 1H), 6.95 (br s, 1H), 4.64 (d, J = 2.6 Hz, 2H), 2.45 (t, J = 2.6 Hz, 1H) ppm. ^{13}C NMR (75 MHz, CDCl_3): δ = 136.6, 129.7, 118.7, 76.4, 74.7, 36.2 ppm. Spectral data are in agreement with those reported in the literature.^[43]



1-Allenyl-1*H*-imidazole (9a)

The reaction of 1-propargyl-1*H*-imidazole (in mixture with the isomeric allene, 318 mg, 3.0 mmol) according to general procedure **I** (reaction time: 10 minutes, purification by Kugelrohr distillation under reduced pressure (approx. 0.1 mbar, temperature: 150 °C) gave the title compound in the form of a colorless oil (306 mg, 96%).

¹H NMR (300 MHz, CDCl₃): δ = 7.49 (br s, 1H), 7.00 (br s, 1H), 6.94 (br s, 1H), 6.85 (t, J = 6.5 Hz, 1H), 5.47 (d, J = 6.5 Hz, 2H) ppm. ¹³C NMR (75 MHz, CDCl₃): δ = 202.1, 135.9, 130.0, 117.1, 96.4, 87.9 ppm. Spectral data are in agreement with the literature.^[44]



2-Methyl-1-propargyl-1*H*-imidazole

The reaction of 2-methyl-1*H*-imidazole (821 mg, 10 mmol) according to general procedure **I**, after Kugelrohr distillation under reduced pressure (approx. 0.1 mbar, temperature: 150 °C) gave the title compound in mixture with the isomeric 2-methyl-1-allenyl-1*H*-imidazole (pale yellow oil, 803 mg, 67%, 35:65 molar ratio alkyne : allene). The mixture thus obtained was used for the subsequent isomerization without attempting any separation.

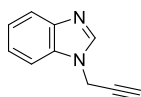
¹H NMR (300 MHz, CDCl₃): δ = 6.93-6.89 (m, 2H), 4.58 (d, J = 2.6 Hz, 2H), 2.41 (t, J = 2.6 Hz, 1H), 2.40 (s, 3H) ppm. ¹³C NMR (75 MHz, CDCl₃): δ = 144.5, 127.4, 119.2, 76.9, 74.1, 35.6, 13.0 ppm. This compound has already been described in the literature.^[45]



2-Methyl-1-allenyl-1*H*-imidazole (9b)

The reaction of 2-methyl-1-propargyl-1*H*-imidazole (in mixture with the isomeric allene, 360 mg, 3.0 mmol) according to general procedure **I** (reaction time: 10 minutes, purification by Kugelrohr distillation at 0.1 mbar, temperature: 150 °C) gave the title compound in the form of a pale yellow oil (353 mg, 98%).

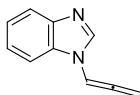
¹H NMR (300 MHz, CDCl₃): δ = 6.88-6.84 (m, 2H), 6.77 (t, J = 6.4 Hz, 1H), 5.44 (d, J = 6.4 Hz, 2H), 2.33 (s, 3H) ppm. ¹³C NMR (75 MHz, CDCl₃): δ = 202.7, 144.2, 128.0, 117.2, 95.8, 87.1, 13.2 ppm. Spectral data are in agreement with the literature.^[44]



1-Propargyl-1*H*-benzimidazole

The reaction of benzimidazole (1.18 g, 10 mmol) according to general procedure **P**, after Kugelrohr distillation under reduced pressure (approx. 0.1 mbar, temperature: 220 °C) gave the title compound in the form of a pale yellow oil (955 mg, 61%).

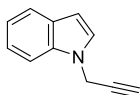
^1H NMR (300 MHz, CDCl_3): δ = 8.00 (s, 1H), 7.85-7.79 (m, 1H), 7.51-7.44 (m, 1H), 7.39-7.27 (m, 2H), 4.91 (dd, J = 2.6, 0.9 Hz, 2H), 2.49 (td, J = 2.6, 0.9 Hz, 1H) ppm. ^{13}C NMR (75 MHz, CDCl_3): δ = 144.0, 142.3, 133.4, 123.4, 122.6, 120.6, 109.7, 76.0, 75.0, 34.7 ppm. Spectral data are in agreement with the literature.^[46]



1-Allenyl-1*H*-benzimidazole (8)

The reaction of 1-propargyl-1*H*-benzimidazole (468 mg, 3.0 mmol) according to general procedure **I** (reaction time: 10 minutes, purification by flash chromatography on NaHCO_3 -washed silica gel, gradient elution - petroleum ether/ethyl acetate 60:40 to 50:50) gave the title compound in the form of a pale yellow oil (280 mg, 60%).

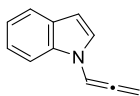
^1H NMR (300 MHz, CDCl_3): δ = 7.97 (s, 1H), 7.86-7.78 (m, 1H), 7.69-7.61 (m, 1H), 7.36-7.27 (m, 2H), 7.16 (t, J = 6.5 Hz, 1H), 5.70 (d, J = 6.5 Hz, 2H) ppm. ^{13}C NMR (75 MHz, CDCl_3): δ = 203.2, 144.4, 141.6, 132.9, 123.7, 123.0, 120.7, 110.8, 95.1, 88.3 ppm. Spectral data are in agreement with the literature.^[30]



1-Propargylindole

The reaction of indole (1.17 g, 10 mmol) according to general procedure **P**, after Kugelrohr distillation (oil pump vacuum, air bath temperature: 200 °C) gave the title compound in the form of a white solid (1.37 g, 88%).

^1H NMR (300 MHz, CDCl_3): δ = 7.70 (d, J = 7.8 Hz, 1H), 7.46 (d, J = 7.9 Hz, 1H), 7.38-7.15 (m, 3H), 6.59 (d, J = 3.1 Hz, 1H), 4.91 (d, J = 2.5 Hz, 2H), 2.44 (t, J = 2.5 Hz, 1H) ppm. ^{13}C NMR (75 MHz, CDCl_3): δ = 135.9, 129.0, 127.3, 122.0, 121.2, 120.0, 109.4, 102.2, 77.9, 73.6, 35.9 ppm. IR (ATR): ν = 3286, 3249, 3085, 3054, 2933, 2115, 1610, 1513, 1458, 1308, 1178, 744, 667 cm^{-1}

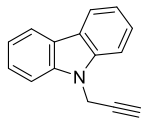


1-Allenyl-1*H*-indole (12b)

The reaction of 9-propargyl-9*H*-carbazole (310 mg, 1.0 mmol) according to general procedure **I** (reaction time: 1 minute) gave the title compound in an almost pure state and in after extraction and evaporation of the solvent with quantitative recovery. Any attempt to purify it further by column chromatography on NaHCO_3 -washed silica gel or distillation under reduced pressure (approx. 0.1 mbar) resulted in decomposition.

^1H NMR (300 MHz, CDCl_3): δ = 7.62 (d, J = 7.6 Hz, 1H), 7.56 (d, J = 7.6 Hz, 1H), 7.28-7.12 (m, 4H), 6.61 (t, J = 3.2 Hz, 1H), 5.63 (d, J = 6.4 Hz, 2H) ppm. ^{13}C NMR (75 MHz, CDCl_3): δ = 203.4, 135.5, 129.5, 125.8, 122.4, 121.3, 120.5, 110.1, 104.2, 97.6, 87.4 ppm. IR (ATR): ν =

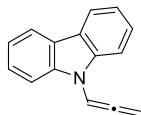
3052, 2921, 1961, 1664, 1611, 1464, 1478, 1317, 1321 cm^{-1} . NMR data are in agreement with the literature.^[47]



9-Propargyl-9H-carbazole

The reaction of carbazole (1.67 g, 10 mmol) according to general procedure **P** gave the title compound in the form of a pale brown solid (2.01 g, 98%) of satisfactory purity without the need of any further purification.

^1H NMR (300 MHz, CDCl_3): δ = 8.16 (d, J = 7.8 Hz, 2H), 7.59-7.48 (m, 4H), 7.33 (ddd, J = 7.9, 6.5, 1.6 Hz, 2H), 5.03 (d, J = 2.5 Hz, 2H), 2.29 (t, J = 2.5 Hz, 1H) ppm. ^{13}C NMR (75 MHz, CDCl_3): δ = 139.9, 126.0, 123.4, 120.5, 119.7, 108.8, 77.9, 72.3, 32.3 ppm. Spectral data are in agreement with literature.^[48]



9-Allenyl-9H-carbazole (12b)

The reaction of 9-propargyl-9H-carbazole (616 mg, 3.0 mmol) according to general procedure **I** (reaction time: 1 minute) gave the title compound in mixture with the isomeric ynamine 9-(prop-1-yn-1-yl)-9H-carbazole (75:25). No purification by chromatography on NaHCO_3 -washed silica gel, as the allene isomerized to the ynamine. The crude mixture was thus employed for the hydroamination reaction. Longer reaction times result in higher proportions of the undesired ynamine, thus reaction times should be kept as short as possible.

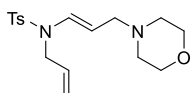
^1H NMR (300 MHz, CDCl_3): δ = 8.08 (br d, J = 7.8 Hz, 2H), 7.72 (br d, J = 8.3 Hz, 2H), 7.47 (td, J = 7.8, 1.0 Hz, 2H), 7.38 (t, J = 6.5 Hz, 1H), 7.29 (td, J = 7.8, 1.0 Hz, 2H), 5.70 (d, J = 6.5 Hz, 2H) ppm. This compound has already been described in the literature.^[30]

Here follow the NMR data of 9-(prop-1-yn-1-yl)-9H-carbazole, which can be obtained in low yield (approx. 15%) by purification of the crude by flash chromatography on NaHCO_3 -washed silica gel (eluent: petroleum ether).

^1H NMR (300 MHz, CDCl_3): δ = 8.02 (dt, J = 7.8, 0.9 Hz, 2H), 7.46 (dt, J = 8.2, 0.9 Hz, 2H), 7.50 (ddd, J = 8.2, 7.2, 0.9 Hz, 2H), 7.35-7.28 (m, 2H), 2.24 (s, 3H) ppm. ^{13}C NMR (75 MHz, CDCl_3): δ = 140.9, 126.6, 123.2, 121.6, 120.4, 111.1, 69.6, 69.0, 3.8 ppm.

3.10. Hydroamination of *N*-allenylsulfonamides

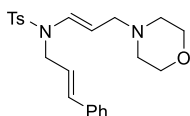
The general procedure described for the hydroamination of allenamides was applied without change to *N*-allenylsulfonamides. The characterization data of the products are given in the following.



(E)-N-Allyl-N-(3-morpholinoprop-1-en-1-yl)-p-toluenesulfonamide (16b)

The reaction of *N*-allyl-*N*-allenyl-*p*-toluenesulfonamide (**15b**, 125 mg, 0.50 mmol) with morpholine (52.5 μ L, 0.6 mmol) according to the general procedure (flash chromatography eluent: EtOAc) gave the title compound in the form of a pale brown oil (151 mg, 90%).

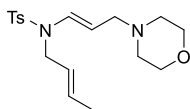
^1H NMR (300 MHz, CDCl_3): δ = 7.65 (d, J = 8.2 Hz, 2H), 7.28 (d, J = 8.2 Hz, 2H), 6.78 (d, J = 14.2 Hz, 1H), 5.61 (ddt, J = 17.3, 10.4, 5.3 Hz, 1H), 5.20-5.10 (m, 2H), 4.79 (dt, J = 14.2, 7.2 Hz, 1H), 3.99 (d, J = 5.3 Hz, 2H), 3.70-3.65 (m, 4H), 2.95 (d, J = 7.2 Hz, 2H), 2.41 (s, 3H), 2.40-2.34 (m, 4H) ppm. ^{13}C NMR (75 MHz, CDCl_3): δ = 144.0, 136.3, 131.6, 129.9, 129.2, 127.1, 118.0, 106.7, 67.0, 59.3, 53.3, 48.2, 21.7 ppm. IR (ATR): ν = 3084, 3048, 2965, 2946, 2916, 2858, 2812, 1658, 1348, 1158, 1113, 662 cm^{-1} . HRMS (EI) m/z : $[\text{M}]^+$ Calcd for $\text{C}_{17}\text{H}_{24}\text{N}_2\text{O}_3\text{S}$ 336.1508; Found 336.1521.



(E,E)-N-Cinnamyl-N-(3-morpholinoprop-1-en-1-yl)-p-toluenesulfonamide (16d)

The reaction of (*E*)-*N*-cinnamyl-*N*-allenyl-*p*-toluenesulfonamide (**15d**, 71.0 mg, 0.218 mmol) with morpholine (23.0 μ L, 0.262 mmol, 1.2 equiv) according to the general procedure (reaction time: 48 h, flash chromatography eluent: toluene / EtOAc 80:20) gave the title compound in the form of a yellow solid (50.0 mg, 56%).

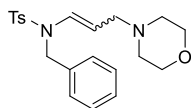
^1H NMR (300 MHz, CDCl_3): δ = 7.67 (d, J = 8.3 Hz, 2H), 7.32-7.17 (m, 7H), 6.80 (d, J = 14.3 Hz, 1H), 6.42 (d, J = 16.0 Hz, 1H), 5.90 (dt, J = 16.0, 6.8 Hz, 1H), 4.86 (dt, J = 14.3, 7.1 Hz, 1H), 4.17 (dd, J = 6.8, 1.7 Hz, 2H), 3.60 (t, J = 4.7 Hz, 4H), 2.95 (d, J = 7.1 Hz, 2H), 2.38 (s, 3H), 2.38-2.30 (m, 4H) ppm. ^{13}C NMR (75 MHz, CDCl_3): δ = 144.0, 136.4, 136.3, 133.3, 129.9, 128.6, 128.0, 127.2, 126.4, 122.8, 107.3, 66.9, 59.3, 53.4, 47.8, 21.6 ppm. HRMS (ESI) m/z : $[\text{M}+\text{H}]^+$ Calcd for $\text{C}_{23}\text{H}_{29}\text{N}_2\text{O}_3\text{S}$ 413.1899; Found 413.1899.



(E,E)-N-(But-2-en-1-yl)-N-(3-morpholinoprop-1-en-1-yl)-p-toluenesulfonamide (16e)

The reaction of (*E*)-*N*-(but-2-en-1-yl)-*N*-allenyl-*p*-toluenesulfonamide (**15e**, 163 mg, 0.62 mmol) with morpholine (65 μ L, 0.74 mmol, 1.2 equiv) according to the general procedure (reaction time: 72 h, flash chromatography eluent: toluene / EtOAc 80:20) gave the title compound in the form of a pale yellow oil (63.8 mg, 29%).

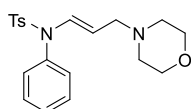
^1H NMR (300 MHz, CDCl_3): δ = 7.63 (d, J = 8.2 Hz, 2H), 7.27 (d, J = 8.2 Hz, 2H), 6.74 (d, J = 14.2 Hz, 1H), 5.70-5.45 (m, 1H), 5.34-5.15 (m, 1H), 4.80 (dt, J = 14.2, 7.1 Hz, 1H), 3.92 (dt, J = 5.8, 1.6 Hz, 2H), 3.68 (t, J = 4.7 Hz, 4H), 2.95 (d, J = 7.1 Hz, 2H), 2.46-2.32 (m, 4H), 2.40 (s, 3H), 1.58 (dd, J = 6.4, 1.6 Hz, 3H) ppm. ^{13}C NMR (75 MHz, CDCl_3): δ = 143.8, 136.4, 129.8, 129.6, 129.4, 127.0, 124.2, 106.5, 67.0, 59.3, 53.3, 47.6, 21.6, 17.6 ppm. HRMS (EI) m/z : $[\text{M}]^+$ Calcd for $\text{C}_{18}\text{H}_{26}\text{N}_2\text{O}_3\text{S}$ 350.1664; Found 350.1651.



(*E,Z*)-*N*-Benzyl-*N*-(3-morpholinoprop-1-en-1-yl)-*p*-toluenesulfonamide (16f)

The reaction of (*E*)-*N*-benzyl-*N*-allenyl-*p*-toluenesulfonamide (**15f**, 150 mg, 0.50 mmol) with morpholine (52.5 μ L, 0.60 mmol, 1.2 equiv) according to the general procedure (reaction time: 72 h, flash chromatography eluent: EtOAc) gave the title compound in the form of a pale brown solid (75.0 mg, 39%), *E/Z* ratio 83:17.

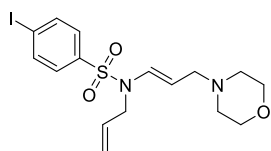
***E*-isomer**-¹H NMR (300 MHz, CDCl₃): δ = 7.71-7.64 (m, 2H), 7.38-7.15 (m, 7H), 6.77 (dd, *J* = 14.2, 1.2 Hz, 1H), 4.64 (dt, *J* = 14.3, 7.1 Hz, 1H), 4.51 (s, 2H), 3.60-3.51 (m, 4H), 2.84 (dd, *J* = 7.1, 1.2 Hz, 2H), 2.42 (s, 3H), 2.21-2.13 (m, 4H) ppm. ¹³C NMR (75 MHz, CDCl₃): δ = 144.1, 136.0, 135.3, 130.0, 129.0, 127.6, 127.1, 127.0, 108.5, 66.9, 59.1, 53.1, 49.5, 21.7 ppm. ***Z*-isomer**-¹H NMR (300 MHz, CDCl₃): δ = 7.71-7.64 (m, 2H), 7.38-7.15 (m, 7H), 5.58 (dt, *J* = 7.6, 6.4 Hz, 1H), 5.28 (dt, *J* = 7.6, 1.8 Hz, 1H), 4.14 (s, 2H), 3.09 (dd, *J* = 6.4, 1.8 Hz, 2H), 3.54-3.49 (m, 4H), 2.44 (s, 3H), 2.04-1.96 (m, 4H) ppm. ¹³C NMR (75 MHz, CDCl₃): δ = 143.9, 135.7, 135.0, 134.0, 129.9, 129.4, 128.6, 128.0, 127.7, 127.4, 67.0, 55.6, 54.9, 53.4, 21.7 ppm. HRMS (EI) *m/z*: [M]⁺ Calcd for C₂₁H₂₆N₂O₃S 386.1664; Found 386.1663.



(*E*)-*N*-(3-Morpholinoprop-1-en-1-yl)-*N*-phenyl-*p*-toluenesulfonamide (16g)

The reaction of *N*-phenyl-*N*-allenyl-*p*-toluenesulfonamide (**15g**, 100 mg, 0.35 mmol) with morpholine (36.8 μ L, 0.42 mmol, 1.2 equiv) according to the general procedure (flash chromatography eluent: EtOAc) gave the title compound in the form of a pale brown solid (90.0 mg, 69%).

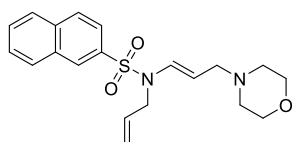
¹H NMR (300 MHz, CDCl₃) δ = 7.45 (d, *J* = 8.3 Hz, 2H), 7.28-7.21 (m, 3H), 7.18 (d, *J* = 8.3 Hz, 2H), 7.03 (dt, *J* = 13.9, 1.2 Hz, 1H), 6.90-6.83 (m, 2H), 4.30 (dt, *J* = 13.9, 7.3 Hz, 1H), 3.59-3.52 (m, 4H), 2.83 (dd, *J* = 7.3, 1.2 Hz, 1H), 2.34 (s, 3H), 2.29-2.22 (m, 4H) ppm. ¹³C NMR (75 MHz, CDCl₃): δ = 144.0, 136.4, 135.8, 132.2, 130.2, 129.6, 129.6, 129.1, 127.5, 106.9, 66.9, 58.7, 53.2, 21.6 ppm. IR (ATR): ν = 3066, 3039, 2957, 2894, 2855, 2808, 1654, 1595, 1354, 1166, 1113, 696, 662 cm⁻¹. HRMS (EI) *m/z*: [M]⁺ Calcd for C₂₀H₂₄N₂O₃S 372.1508; Found 372.1520.



(*E*)-*N*-Allyl-*N*-(3-morpholinoprop-1-en-1-yl)-*p*-iodobenzenesulfonamide (16h)

The reaction of *N*-allyl-*N*-propadienyl-*p*-iodobenzenesulfonamide (**15h**, 175 mg, 0.48 mmol) with morpholine (51 μ L, 0.58 mmol, 1.2 equiv) according to the general procedure (reaction time: 72 h, no chromatographic purification needed) gave the title compound in the form of a brown solid (194 mg, 89%).

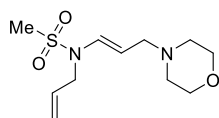
^1H NMR (300 MHz, CDCl_3): δ = 7.86 (d, J = 8.5 Hz, 2H), 7.48 (d, J = 8.5 Hz, 2H), 6.73 (d, J = 14.1 Hz, 1H), 5.61 (ddt, J = 17.2, 10.4, 5.3 Hz, 1H), 5.23-5.11 (m, 2H), 4.85 (dt, J = 14.1, 7.1 Hz, 1H), 4.01 (d, J = 5.3 Hz, 2H), 3.69 (t, J = 4.7 Hz, 4H), 2.96 (d, J = 7.1 Hz, 2H), 2.42-2.32 (m, 4H) ppm. ^{13}C NMR (75 MHz, CDCl_3): δ = 138.9, 138.6, 131.3, 128.7, 128.4, 118.4, 107.8, 100.6, 67.0, 59.2, 53.4, 48.4 ppm. HRMS (EI) m/z : $[\text{M}]^+$ Calcd for $\text{C}_{16}\text{H}_{21}\text{N}_2\text{O}_3\text{S}$ 448.0318; Found 448.0297.



(E)-N-Allyl-N-(3-morpholinoprop-1-en-1-yl)-2-naphthalenesulfonamide (16i)

The reaction of *N*-allyl-*N*-propadienyl-2-naphthalenesulfonamide (**15i**, 166 mg, 0.58 mmol) with morpholine (61 μL , 0.70 mmol, 1.2 equiv) according to the general procedure (reaction time: 72 h, no chromatographic purification needed) gave the title compound in the form of a pale brown oil (200 mg, 92%).

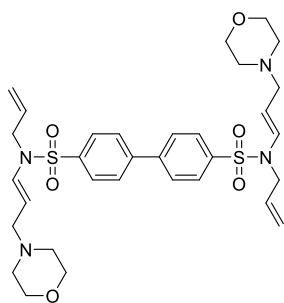
^1H NMR (300 MHz, CDCl_3): δ = 8.37 (d, J = 1.8 Hz, 1H), 7.99-7.88 (m, 3H), 7.72 (dd, J = 8.7, 1.9 Hz, 1H), 7.69-7.57 (m, 2H), 6.86 (d, J = 14.2 Hz, 1H), 5.63 (ddt, J = 17.2, 10.4, 5.4 Hz, 1H), 5.23-5.09 (m, 2H), 4.82 (dt, J = 14.2, 7.2 Hz, 1H), 4.06 (dt, J = 5.4, 1.7 Hz, 2H), 3.66-3.61 (m, 4H), 2.97 (d, J = 7.2 Hz, 2H), 2.39-2.30 (m, 4H) ppm. ^{13}C NMR (75 MHz, CDCl_3): δ = 136.1, 135.0, 132.3, 131.6, 129.7, 129.3, 129.3, 129.2, 128.6, 128.1, 127.9, 122.1, 118.2, 107.2, 67.0, 59.3, 53.4, 48.4 ppm.



(E)-N-Allyl-N-(3-morpholinoprop-1-en-1-yl)-methanesulfonamide (16j)

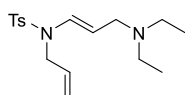
The reaction of *N*-allyl-*N*-propadienylmethanesulfonamide (**15j**, 60.5 mg, 0.35 mmol) with morpholine (36.6 μL , 0.42 mmol, 1.2 equiv) according to the general procedure (reaction time: 72 h, gradient elution: toluene / EtOAc 80:20 to 50:50) gave the title compound in the form of a pale yellow oil (53.5 mg, 59%).

^1H NMR (300 MHz, CDCl_3): δ = 6.66 (dt, J = 14.2, 1.2 Hz, 1H), 5.94-5.74 (m, 1H), 5.36-5.22 (m, 2H), 4.92 (dt, J = 14.3, 7.2 Hz, 1H), 4.16 (dt, J = 5.4, 1.6 Hz, 2H), 3.74-3.66 (m, 4H), 2.98 (dd, J = 7.2, 1.2 Hz, 2H), 2.91 (s, 3H), 2.46-2.39 (m, 4H) ppm. ^{13}C NMR (75 MHz, CDCl_3): δ = 131.4, 128.9, 118.7, 106.3, 67.1, 59.2, 53.4, 48.2, 40.2 ppm. HRMS (EI) m/z : $[\text{M}]^+$ Calcd for $\text{C}_{11}\text{H}_{20}\text{N}_2\text{O}_3\text{S}$ 260.1195; Found 260.1189.



***N,N'*-Diallyl-*N,N'*-bis((*E*)-3-morpholinoprop-1-en-1-yl)-[1,1'-biphenyl]-4,4'-disulfonamide (16k)**

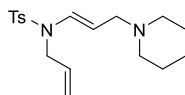
The reaction of *N,N'*-diallyl-*N,N'*-dipropadienylbiphenyl-4,4'-disulfonamide (**15k**, 79.3 mg, 0.17 mmol) with morpholine (35.5 μ L, 0.41 mmol, 1.2 equiv) according to the general procedure (reaction time: 72 h, no chromatographic purification needed) gave the title compound in the form of a pale brown solid (96.7 mg, 89%). ^1H NMR (300 MHz, CDCl_3): δ = 7.87 (d, J = 8.4 Hz, 4H), 7.70 (d, J = 8.4 Hz, 4H), 6.80 (d, J = 14.2 Hz, 2H), 5.71-5.57 (m, 2H), 5.24-5.11 (m, 4H), 4.86 (dt, J = 14.2, 7.1 Hz, 2H), 4.06 (d, J = 5.5 Hz, 4H), 3.67 (t, J = 4.7 Hz, 8H), 2.97 (d, J = 7.1 Hz, 4H), 2.38 (t, J = 4.7 Hz, 8H) ppm. ^{13}C NMR (75 MHz, CDCl_3): δ = 143.6, 139.1, 131.3, 128.8, 128.1, 127.7, 118.2, 107.4, 66.9, 59.1, 53.2, 48.2 ppm.



(*E*)-*N*-Allyl-*N*-(3-(diethylamino)prop-1-en-1-yl)-*p*-toluenesulfonamide

The reaction of *N*-allyl-*N*-propadienyl-*p*-toluenesulfonamide (74.8 mg, 0.30 mmol) with diethylamine (37.2 μ L, 0.36 mmol, 1.2 equiv) according to the general procedure (flash chromatography eluent: EtOAc) gave the title compound in the form of a pale brown oil (79.3 mg, 82%).

^1H NMR (300 MHz, CDCl_3): δ = 7.64 (d, J = 8.3 Hz, 2H), 7.28 (d, J = 8.3 Hz, 2H), 6.75 (dt, J = 14.2, 1.2 Hz, 1H), 5.62 (ddt, J = 17.3, 10.4, 5.4 Hz), 5.21-5.08 (m, 2H), 4.82 (dt, J = 14.2, 7.1 Hz, 1H), 3.98 (dt, J = 5.4, 1.7 Hz, 2H), 3.06 (dd, J = 7.1, 1.2 Hz, 2H), 2.45 (q, J = 7.2 Hz, 4H), 2.40 (s, 3H), 0.99 (t, J = 7.2 Hz, 6H) ppm. ^{13}C NMR (75 MHz, CDCl_3): δ = 143.9, 136.4, 131.7, 129.9, 128.6, 127.1, 118.0, 107.9, 53.2, 48.3, 46.3, 21.7, 11.6 ppm. IR (ATR): ν = 2969, 2929, 2809, 1656, 1613, 1354, 1164, 844, 813, 664 cm^{-1} . HRMS (EI) m/z : $[\text{M}]^+$ Calcd for $\text{C}_{17}\text{H}_{26}\text{N}_2\text{O}_2\text{S}$ 322.1715; Found 322.1708.

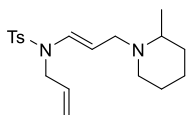


(*E*)-*N*-Allyl-*N*-(3-(piperidin-1-yl)prop-1-en-1-yl)-*p*-toluenesulfonamide

The reaction of *N*-allyl-*N*-propadienyl-*p*-toluenesulfonamide (74.8 mg, 0.30 mmol) with piperidine (35.6 μ L, 0.36 mmol, 1.2 equiv) according to the general procedure (flash chromatography eluent: EtOAc / petroleum ether 85:15) gave the title compound in the form of a pale brown oil (85.3 mg, 85%).

^1H NMR (300 MHz, CDCl_3): δ = 7.65 (d, J = 8.2 Hz, 2H), 7.29 (d, J = 8.2 Hz, 2H), 6.75 (dt, J = 14.2, 1.2 Hz, 1H), 5.63 (ddt, J = 17.2, 10.5, 5.3 Hz, 1H), 5.23-5.09 (m, 2H), 4.85 (dt, J = 14.2, 7.2

Hz, 1H), 3.99 (dt, $J = 5.4, 1.7$ Hz, 2H), 2.93 (dd, $J = 7.2, 1.2$ Hz, 2H), 2.42 (s, 3H), 2.32 (br t, $J = 5.5$ Hz, 4H), 1.62-1.35 (m, 6H) ppm. ^{13}C NMR (75 MHz, CDCl_3): $\delta = 143.9, 136.4, 131.7, 129.9, 128.8, 127.1, 118.0, 107.9, 59.7, 54.3, 48.3, 26.0, 24.5, 21.7$ ppm. IR (ATR): $\nu = 2932, 2853, 2800, 2759, 1656, 1357, 1306, 1164, 1090, 665$ cm^{-1} . HRMS (ESI) m/z : $[\text{M}+\text{H}]^+$ Calcd for $\text{C}_{18}\text{H}_{27}\text{N}_2\text{O}_2\text{S}$ 335.1793; Found 335.1793.



(*E*)-*N*-Allyl-*N*-(3-(2-methylpiperidin-1-yl)prop-1-en-1-yl)-*p*-toluenesulfonamide

The reaction of *N*-allyl-*N*-propadienyl-*p*-toluenesulfonamide (74.8 mg, 0.30 mmol) with 2-methylpiperidine (42.3 μL , 0.36 mmol, 1.2 equiv) according to the general procedure (flash chromatography eluent: EtOAc / petroleum ether 85:15) gave the title compound in the form of a pale brown oil (79.5 mg, 76%).

^1H NMR (300 MHz, CDCl_3): $\delta = 7.65$ (d, $J = 8.3$ Hz, 2H), 7.29 (d, $J = 8.3$ Hz, 2H), 6.74 (dt, $J = 14.0, 1.0$ Hz, 1H), 5.63 (ddt, $J = 17.3, 10.4, 5.3$ Hz, 1H), 5.23-5.10 (m, 2H), 4.85 (ddd, $J = 14.2, 8.2, 6.2$ Hz, 1H), 4.10-3.89 (m, 2H), 3.36 (ddd, $J = 14.0, 6.2, 1.0$ Hz, 1H), 2.96 (ddd, $J = 14.0, 8.2, 1.0$ Hz, 1H), 2.78 (ddd, $J = 11.3, 4.6, 3.3$ Hz, 1H), 2.42 (s, 3H), 2.26-2.11 (m, 1H), 2.03 (td, $J = 11.3, 3.3$ Hz, 1H), 1.73-1.44 (m, 4H), 1.36-1.16 (m, 2H), 1.07 (d, $J = 6.2$ Hz, 3H) ppm. ^{13}C NMR (75 MHz, CDCl_3): $\delta = 143.9, 136.4, 131.8, 129.9, 128.8, 127.1, 118.0, 107.0, 55.9, 54.4, 52.0, 48.3, 34.7, 26.1, 24.1, 21.7, 19.2$ ppm. IR (ATR): $\nu = 2928, 2856, 2791, 1654, 1598, 1355, 1306, 1163, 1090, 664$ cm^{-1} . HRMS (EI) m/z : $[\text{M}]^+$ Calcd for $\text{C}_{19}\text{H}_{28}\text{N}_2\text{O}_2\text{S}$ 348.1871; Found 348.1879.

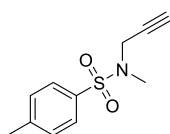
3.11. Synthesis of *N*-allenylsulfonamides

We will describe here the procedures for the preparation of the *N*-allenyl-*N*-allylsulfonamides used as substrates for the hydroamination reaction. In general, the general procedure **I** for the *t*BuOK-catalyzed isomerization of *N*-propargyl heterocycles has been applied without change to *N*-propargylsulfonamides, which were in turn obtained by the reaction of propargyl bromide with the corresponding secondary sulfonamides or by alkylation of *N*-propargylsulfonamides, or also by reaction of allyl propargylamine with the required sulfonyl chlorides.

General procedure **Q** for the *N*-propargylation of secondary sulfonamides

To a 1.7 M solution of the appropriate secondary sulfonamide in dry THF, exactly one equivalent of *t*BuOK (dispensed as a 1.0 M solution in THF) was added under an atmosphere of dry Ar. After stirring for the prescribed time (exothermic reaction), propargyl bromide (80% in toluene, approx. 9.2 M, 1.2 equiv) was added and the resulting solution was left overnight at room temperature.

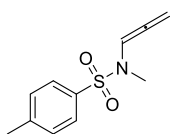
Volatiles are evaporated under reduced pressure and the residue was dissolved in toluene (5 mL for each mmol of product) and washed with a NaOH solution (1 M in water, 1 mL per mmol of product, repeat twice), then with brine and exsiccated over Na_2SO_4 . Removal of the solvent *in vacuo* gave the required *N*-propargylated tertiary sulfonamides in sufficient purity for the subsequent transformations.



N-Propargyl-N-methyl-*p*-toluenesulfonamide

The reaction of *N*-methyl-*p*-toluenesulfonamide (2.22 g, 12 mmol) according to general procedure **Q** gave the title compound in the form of an off-white solid (2.66 g, 99%).

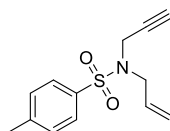
¹H NMR (300 MHz, CDCl₃): δ = 7.63 (d, *J* = 8.2 Hz, 2H), 7.24 (d, *J* = 8.2 Hz, 2H), 3.94 (d, *J* = 2.5 Hz, 2H), 2.75 (s, 3H), 2.36 (s, 3H), 2.01 (t, *J* = 2.5 Hz, 1H) ppm. ¹³C NMR (75 MHz, CDCl₃): δ = 143.8, 134.2, 129.6, 128.0, 76.4, 74.1, 39.9, 34.4, 21.6 ppm. Spectral data are in agreement with the literature.^[49]



N-Methyl-N-allenyl-*p*-toluenesulfonamide (15a)

The reaction of *N*-methyl-*N*-propargyl-*p*-toluenesulfonamide (1.34 mg, 6.0 mmol) according to general procedure **I** (reaction time: 18 h, no chromatographic purification needed) gave the title compound in the form of a pale brown solid (1.14 g, 85%).

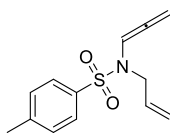
¹H NMR (300 MHz, CDCl₃): δ = 7.66 (d, *J* = 8.3 Hz, 2H), 7.31 (d, *J* = 8.3 Hz, 2H), 6.88 (t, *J* = 6.2 Hz, 1H), 5.29 (d, *J* = 6.2 Hz, 2H), 2.70 (s, 3H), 2.42 (s, 3H) ppm. ¹³C NMR (75 MHz, CDCl₃): δ = 201.5, 143.9, 133.7, 129.8, 127.5, 101.8, 87.8, 33.3, 21.7 ppm. Spectral data are in agreement with the literature.^[50]



N-Allyl-N-propargyl-*p*-toluenesulfonamide

The reaction of *N*-allyl-*p*-toluenesulfonamide (1.06 g, 5.0 mmol) according to general procedure **Q** gave the title compound in the form of an off-white solid (1.24 g, 99%).

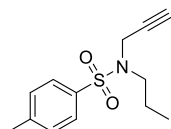
¹H NMR (300 MHz, CDCl₃): δ = 7.73 (d, *J* = 8.3 Hz, 2H), 7.29 (d, *J* = 8.3 Hz, 2H), 5.72 (ddt, *J* = 17.2, 10.0, 6.5 Hz, 1H), 5.33-5.20 (m, 2H), 4.08 (d, *J* = 2.5 Hz, 2H), 3.82 (dt, *J* = 6.5, 1.3 Hz, 2H), 2.42 (s, 3H), 2.00 (t, *J* = 2.5 Hz, 1H) ppm. ¹³C NMR (75 MHz, CDCl₃): δ = 143.7, 136.1, 132.0, 129.6, 127.8, 120.1, 76.6, 73.8, 49.1, 35.9, 21.7 ppm. IR (ATR): ν = 3269, 3089, 3074, 2979, 2923, 2908, 2860, 2119, 1644, 1600, 1324, 1157, 928, 752, 663 cm⁻¹. Spectral data are in agreement with the literature.^[51]



N-Allyl-N-allenyl-*p*-toluenesulfonamide (15b)

The reaction of *N*-allyl-*N*-propargyl-*p*-toluenesulfonamide (748 mg, 3.0 mmol) according to general procedure I (reaction time: 10 minutes, no purification needed) gave the title compound in the form of a pale yellow oil (701 mg, 94%).

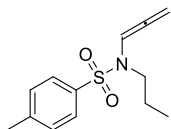
¹H NMR (300 MHz, CDCl₃): δ = 7.69 (d, *J* = 8.3 Hz, 2H), 7.31 (d, *J* = 8.3 Hz, 2H), 6.83 (t, *J* = 6.2 Hz, 1H), 5.76-5.60 (m, 1H), 5.27 (d, *J* = 6.2 Hz, 2H), 5.22-5.09 (m, 2H), 3.78 (d, *J* = 5.7 Hz, 2H), 2.43 (s, 3H) ppm. ¹³C NMR (75 MHz, CDCl₃): δ = 202.0, 143.9, 135.7, 132.5, 129.8, 127.4, 118.3, 100.1, 88.0, 49.0, 21.7 ppm. IR (ATR): ν = 3053, 2983, 2924, 1958, 1597, 1351, 1162, 662 cm⁻¹. HRMS (EI) *m/z*: [M]⁺ Calcd for C₁₃H₁₅NO₂S 249.0823; Found 249.0829.



***N*-Propargyl-*N*-propyl-*p*-toluenesulfonamide**

The reaction of *N*-propyl-*p*-toluenesulfonamide (1.07 g, 5.0 mmol) according to the general gave the title compound in the form of an off-white solid (1.25 g, 99%).

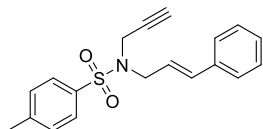
¹H NMR (300 MHz, CDCl₃): δ = 7.74-7.68 (m, 2H), 7.30-7.24 (m, 2H), 4.11 (d, *J* = 2.5 Hz, 2H), 3.17-3.10 (m, 2H), 2.40 (s, 3H), 2.00 (t, *J* = 2.5 Hz, 1H), 1.65-1.51 (m, 2H), 0.91 (t, *J* = 7.4 Hz, 3H) ppm. ¹³C NMR (75 MHz, CDCl₃): δ = 143.5, 136.1, 129.5, 127.8, 73.7, 48.1, 36.2, 21.6, 20.9, 11.2 ppm. IR (ATR): ν = 3274, 2968, 2934, 2876, 2120, 1598, 1334, 1330, 1156, 655 cm⁻¹. Spectral data are in agreement with the literature.^[51]



***N*-Allenyl-*N*-propyl-*p*-toluenesulfonamide (15c)**

The reaction of *N*-propargyl-*N*-propyl-*p*-toluenesulfonamide (656 mg, 2.6 mmol) according to general procedure I (reaction time: 10 minutes, flash chromatography eluent: petroleum ether/EtOAc 95:5) gave the title compound in the form of a pale yellow oil (468 mg, 71%).

¹H NMR (300 MHz, CDCl₃): δ = 7.68 (d, *J* = 8.2 Hz, 2H), 7.30 (d, *J* = 8.2 Hz, 2H), 6.82 (t, *J* = 6.2 Hz, 1H), 5.28 (d, *J* = 6.2 Hz, 2H), 3.05 (dd, *J* = 8.1, 6.4 Hz, 2H), 2.42 (s, 3H), 1.62-1.48 (m, 2H), 0.87 (t, *J* = 7.4 Hz, 3H) ppm. ¹³C NMR (75 MHz, CDCl₃): δ = 201.6, 143.7, 135.7, 129.8, 127.2, 100.3, 87.5, 48.3, 21.7, 21.3, 11.1 ppm.

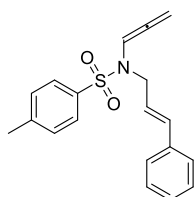


(*E*)-*N*-Cinnamyl-*N*-propargyl-*p*-toluenesulfonamide

N-Propargyl-*p*-toluenesulfonamide (627 mg, 3.0 mmol) and NaOH (120 mg, 3.0 mmol, 1.0 equiv) were dissolved in EtOH (6 mL). (*E*)-Cinnamyl chloride (418 μ L, 3.0 mmol, 1.0 equiv) was then added and the mixture was refluxed for 48 h.

The cooled reaction mixture was diluted with EtOAc (30 mL) and extracted sequentially with NaOH (1 M, 3 x 10 mL) and water (3 x 10 mL). The organic phase was evaporated and the residue purified by flash chromatography on silica gel (eluent: toluene / EtOAc 95:5) to give the title compound in the form of an off-white solid (766 mg, 78%).

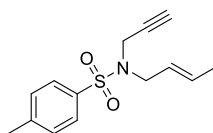
^1H NMR (300 MHz, CDCl_3): δ = 7.80-7.73 (m, 2H), 7.37-7.20 (m, 7H), 6.57 (dt, J = 15.8, 1.3 Hz, 1H), 6.08 (dt, J = 15.8, 6.8 Hz, 1H), 4.13 (d, J = 2.5 Hz, 2H), 4.00 (dd, J = 6.8, 1.3 Hz, 2H), 2.44 (s, 3H), 2.05 (t, J = 2.5 Hz, 1H) ppm. ^{13}C NMR (75 MHz, CDCl_3): δ = 143.7, 136.3, 135.1, 129.7, 128.5, 128.2, 127.9, 126.7, 123.1, 76.8, 73.9, 48.7, 36.0, 21.7 ppm.



(E)-N-Cinnamyl-N-allenyl-*p*-toluenesulfonamide (15d)

The reaction of (E)-N-cinnamyl-N-propargyl-*p*-toluenesulfonamide (325 mg, 1.0 mmol) according to general procedure (reaction time: 1 minute, flash chromatography eluent: toluene) gave the title compound in the form of a pale brown oil (119 mg, 37%).

^1H NMR (300 MHz, CDCl_3): δ = 7.72-7.67 (m, 2H), 7.32-7.18 (m, 7H), 6.86 (t, J = 6.2 Hz, 1H), 6.42 (d, J = 15.9 Hz, 1H), 5.95 (dt, J = 15.9, 6.2 Hz, 1H), 5.29 (d, J = 6.2 Hz, 2H), 3.97 (d, J = 6.2 Hz, 2H), 2.39 (s, 3H). ppm. ^{13}C NMR (75 MHz, CDCl_3): δ = 202.1, 143.9, 136.6, 135.9, 133.7, 129.9, 128.6, 127.9, 127.5, 126.5, 123.6, 100.2, 88.0, 48.7, 21.7 ppm.

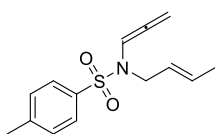


(E)-N-(Prop-2-en-1-yl)-N-propargyl-*p*-toluenesulfonamide

N-Propargyl-*p*-toluenesulfonamide (627 mg, 3.0 mmol) and NaOH (120 mg, 3.0 mmol, 1.0 equiv) were dissolved in EtOH (6 mL). (E)-Crotyl bromide (612, 4.5 mmol, 1.5 equiv) was then added and the mixture was refluxed for 48 h.

The cooled reaction mixture was diluted with EtOAc (30 mL) and extracted sequentially with NaOH (1 M, 3 x 10 mL) and water (3 x 10 mL). The organic phase was evaporated and the residue purified by flash chromatography on silica gel (eluent: toluene) to give the title compound in the form of a white solid (713 mg, 90%).

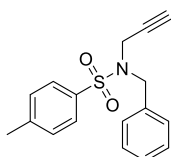
^1H NMR (300 MHz, CDCl_3): δ = 7.71 (d, J = 8.1 Hz, 2H), 7.28 (d, J = 8.1 Hz, 2H), 5.70 (dqt, J = 15.3, 6.5, 1.3 Hz, 1H), 5.35 (dtq, J = 15.3, 6.8, 1.3 Hz, 1H), 4.06 (d, J = 2.5 Hz, 2H), 3.74 (br d, J = 6.8 Hz, 2H), 2.41 (s, 3H), 1.98 (t, J = 2.5 Hz, 1H), 1.68 (br d, J = 6.5 Hz, 3H) ppm. ^{13}C NMR (75 MHz, CDCl_3): δ = 143.5, 136.3, 131.8, 129.5, 127.9, 124.6, 76.8, 73.6, 48.4, 35.6, 21.7, 17.8 ppm. Spectral data are in agreement with the literature.^[52]



(E)-N-Allenyl-N-(prop-2-en-1-yl)-p-toluenesulfonamide (15e)

The reaction of (E)-N-(prop-2-en-1-yl)-N-propargyl-p-toluenesulfonamide (342 mg, 1.3 mmol) according to general procedure **I** (reaction time: 10 minute, no chromatographic purification needed) gave the title compound in the form of a pale brown oil (310 mg, 90%).

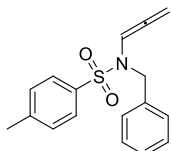
$^1\text{H NMR}$ (300 MHz, CDCl_3): $\delta = 7.68$ (d, $J = 8.3$ Hz, 2H), 7.30 (d, $J = 8.3$ Hz, 2H), 6.80 (t, $J = 6.2$ Hz, 1H), 5.58 (dq, $J = 15.5, 6.5, 1.3$ Hz, 1H), 5.36-5.24 (m, 1H), 5.27 (d, $J = 6.2$ Hz, 2H), 3.73 (br d, $J = 6.2$ Hz, 2H), 2.42 (s, 3H), 1.61 (br d, $J = 6.5$ Hz, 3H) ppm.



N-Benzyl-N-Propargyl-p-toluenesulfonamide

The reaction of N-benzyl-p-toluenesulfonamide (784 mg, 3.0 mmol) according to general procedure **Q** gave the title compound in the form of a pale brown solid (890 mg, 99%).

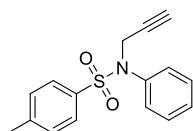
$^1\text{H NMR}$ (300 MHz, CDCl_3): $\delta = 7.80$ (d, $J = 8.3$ Hz, 2H), 7.38-7.29 (m, 7H), 4.36 (s, 2H), 3.95 (d, $J = 2.5$ Hz, 2H), 2.45 (s, 3H), 2.01 (t, $J = 2.5$ Hz, 1H) ppm. $^{13}\text{C NMR}$ (75 MHz, CDCl_3): $\delta = 143.8, 136.1, 135.0, 129.6, 128.9, 128.8, 128.2, 128.0, 76.4, 74.2, 49.9, 35.6, 21.7$ ppm. Spectral data are in agreement with the literature.^[53]



N-Benzyl-N-allenyl-p-toluenesulfonamide (15f)

The reaction of N-benzyl-N-propargyl-p-toluenesulfonamide (599 mg, 2.0 mmol) according to general procedure **I** (reaction time: 10 minutes, flash chromatography eluent: petroleum ether/EtOAc 95:5) gave the title compound in the form of a pale orange oil (260 mg, 43%).

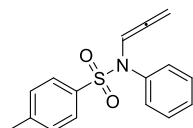
$^1\text{H NMR}$ (300 MHz, CDCl_3): $\delta = 7.79$ (d, $J = 8.3$ Hz, 2H), 7.44-7.30 (m, 7H), 6.89 (t, $J = 6.2$ Hz, 1H), 5.21 (d, $J = 6.2$ Hz, 2H), 4.36 (s, 2H), 2.52 (s, 3H) ppm. $^{13}\text{C NMR}$ (75 MHz, CDCl_3): $\delta = 202.3, 143.9, 136.3, 135.5, 129.9, 128.4, 128.0, 127.5, 127.4, 100.2, 88.2, 50.2, 21.7$ ppm.



N-Phenyl-N-Propargyl-p-toluenesulfonamide

The reaction of *N*-phenyl-*p*-toluenesulfonamide (1.24 g, 5.0 mmol) according to general procedure **Q** (25 mL of EtOH cosolvent added, refluxed overnight) gave the title compound in the form of an off-white solid (1.31 g, 90%).

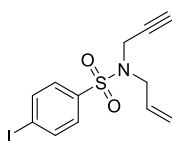
^1H NMR (300 MHz, CDCl_3): δ = 7.52 (d, J = 8.3 Hz, 2H), 7.32-7.17 (m, 7H), 4.42 (d, J = 2.5 Hz, 2H), 2.39 (s, 3H), 2.14 (t, J = 2.5 Hz, 1H) ppm. ^{13}C NMR (75 MHz, CDCl_3): δ = 143.8, 139.4, 135.6, 129.4, 129.1, 128.5, 128.3, 128.1, 78.2, 73.9, 41.1, 21.7 ppm. Spectral data are in agreement with the literature.^[54]



***N*-Phenyl-*N*-allenyl-*p*-toluenesulfonamide (15g)**

The reaction of *N*-phenyl-*N*-propargyl-*p*-toluenesulfonamide (142 mg, 0.50 mmol) according to general procedure **I** (reaction time: 10 minutes, no chromatographic purification needed) gave the title compound in the form of a pale brown oil (100 mg, 70%).

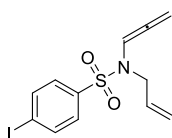
^1H NMR (300 MHz, CDCl_3) δ = 7.58-7.51 (m, 2H), 7.32-7.22 (m, 5H), 7.10 (t, J = 6.2 Hz, 1H), 7.02-6.96 (m, 2H), 5.01 (d, J = 6.2 Hz, 2H), 2.43 (s, 3H) ppm. ^{13}C NMR (75 MHz, CDCl_3) δ = 201.2, 144.0, 137.4, 135.4, 129.7, 129.7, 128.9, 128.8, 127.9, 102.4, 87.4, 21.6 ppm. IR (ATR): ν = 3052, 2977, 2923, 1959, 1595, 1489, 1357, 1164, 695, 663 cm^{-1} .



***N*-Allyl-*N*-propargyl-*p*-iodobenzenesulfonamide**

The title compound was prepared by a standard procedure^[55] from *p*-iodobenzenesulfonyl chloride and allyl propargyl amine in the presence of Et_3N .

^1H NMR (300 MHz, CDCl_3): δ = 7.86 (d, J = 8.5 Hz, 2H), 7.57 (d, J = 8.5 Hz, 2H), 5.74 (ddt, J = 16.6, 9.9, 6.5 Hz, 1H), 5.35-5.23 (m, 2H), 4.10 (d, J = 2.5 Hz, 2H), 3.82 (dt, J = 6.5, 1.3 Hz, 2H), 2.03 (t, J = 2.5 Hz, 1H) ppm. ^{13}C NMR (75 MHz, CDCl_3): δ = 138.9, 138.3, 131.6, 129.3, 120.5, 100.3, 76.3, 74.2, 49.2, 35.9 ppm.

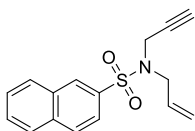


***N*-Allyl-*N*-allenyl-*p*-iodobenzenesulfonamide (15h)**

The reaction of *N*-allyl-*N*-propargyl-4-iodobenzenesulfonamide (300 mg, 0.83 mmol) according to the general procedure (reaction time: 1 minute, no chromatographic purification needed) gave the title compound in the form of a brown sticky oil (205 mg, 68%).

^1H NMR (300 MHz, CDCl_3): δ = 7.88 (d, J = 8.5 Hz, 2H), 7.52 (d, J = 8.5 Hz, 2H), 6.78 (t, J = 6.2 Hz, 1H), 5.67 (ddt, J = 17.2, 10.2, 5.8 Hz, 1H), 5.30 (d, J = 6.2 Hz, 2H), 5.22-5.11 (m, 2H),

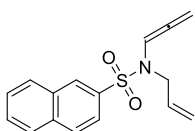
3.80 (d, $J = 5.8$ Hz, 2H) ppm. ^{13}C NMR (75 MHz, CDCl_3): $\delta = 202.1, 138.5, 138.4, 132.1, 128.7, 118.6, 100.5, 99.8, 88.3, 49.1$ ppm. IR (ATR): $\nu = 2987, 2971, 2922, 1646, 1355, 1165, 1084, 1004, 885, 730$ cm^{-1} .



***N*-Allyl-*N*-propargyl-2-naphthalenesulfonamide**

The title compound was prepared by a standard procedure^[55] from 2-naphthalenesulfonyl chloride and allyl propargyl amine in the presence of Et_3N .

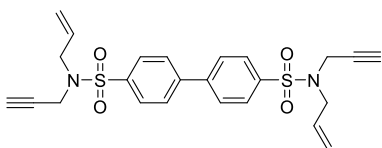
^1H NMR (300 MHz, CDCl_3): $\delta = 8.44$ (d, $J = 1.8$ Hz, 1H), 8.02-8.88 (m, 3H), 7.84 (dd, $J = 8.7, 1.9$ Hz, 1H), 7.70-7.57 (m, 2H), 5.76 (ddt, $J = 16.7, 10.0, 6.5$ Hz, 1H), 5.35-5.21 (m, 2H), 4.17 (d, $J = 2.5$ Hz, 2H), 3.90 (dt, $J = 6.5, 1.3$ Hz, 2H), 1.91 (t, $J = 2.5$ Hz, 1H) ppm. ^{13}C NMR (75 MHz, CDCl_3): $\delta = 136.1, 135.0, 132.3, 131.9, 129.4, 129.3, 129.2, 128.9, 128.0, 127.6, 123.1, 120.2, 76.6, 73.9, 49.2, 36.0$ ppm. Spectral data are in agreement with the literature.^[54]



***N*-Allyl-*N*-allenyl-2-naphthalenesulfonamide**

The reaction of *N*-allyl-*N*-propargyl-2-naphthalenesulfonamide (239 mg, 0.84 mmol) according to general procedure I (reaction time: 1 minute, no chromatographic purification needed) gave the title compound in the form of a pale brown viscous oil (195 mg, 82%).

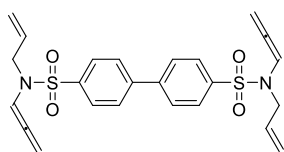
^1H NMR (300 MHz, CDCl_3): $\delta = 8.39$ (d, $J = 1.8$ Hz, 1H), 8.05-7.85 (m, 3H), 7.79 (dd, $J = 8.7, 1.9$ Hz, 1H), 7.74-7.54 (m, 2H), 6.92 (t, $J = 6.2$ Hz, 1H), 5.80-5.59 (m, 1H), 5.27 (d, $J = 6.2$ Hz, 2H), 5.19 (dq, $J = 17.2, 1.5$ Hz, 1H), 5.12 (dq, $J = 10.2, 1.5$ Hz, 1H), 3.85 (dd, $J = 5.8, 1.5$ Hz, 2H) ppm. ^{13}C NMR (75 MHz, CDCl_3): $\delta = 202.0, 135.7, 135.0, 132.5, 132.3, 129.5, 129.4, 129.0, 128.8, 128.1, 127.7, 122.6, 118.4, 100.1, 88.1, 49.1$ ppm.



***N,N'*-Diallyl-*N,N'*-dipropargylbiphenyl-4,4'-disulfonamide**

The title compound was prepared by a standard procedure^[55] from biphenyl-4,4'-disulfonyl chloride and allyl propargyl amine in the presence of Et_3N .

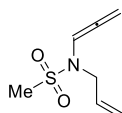
^1H NMR (300 MHz, CDCl_3): $\delta = 7.99$ -7.90 (m, 4H), 7.78-7.69 (m, 4H), 5.75 (ddt, $J = 16.6, 10.0, 6.5$ Hz, 2H), 5.39-5.20 (m, 4H), 4.14 (d, $J = 2.5$ Hz, 4H), 3.87 (d, $J = 6.5$ Hz, 4H), 2.03 (t, $J = 2.5$ Hz, 2H) ppm. ^{13}C NMR (75 MHz, CDCl_3): $\delta = 143.7, 139.0, 131.7, 128.6, 127.9, 120.4, 76.5, 74.1, 49.2, 35.9$ ppm.



***N,N'*-Diallyl-*N,N'*-diallenylbiphenyl-4,4'-disulfonamide (15k)**

The reaction of *N,N'*-Diallyl-*N,N'*-diallenylbiphenyl-4,4'-disulfonamide (111 mg, 0.31 mmol) according to the general procedure (reaction time: 1 minute, no chromatographic purification needed) gave the title compound in the form of a pale brown solid (88.1 mg, 80%).

^1H NMR (300 MHz, CDCl_3): δ = 7.96-7.89 (m, 4H), 7.82-7.68 (m, 4H), 6.86 (t, J = 6.3 Hz, 2H), 5.71 (ddt, J = 17.2, 10.2, 5.8 Hz, 2H), 5.31 (d, J = 6.3 Hz, 4H), 5.27-5.11 (m, 4H), 3.86 (d, J = 5.8 Hz, 4H) ppm. ^{13}C NMR (75 MHz, CDCl_3): δ = 202.1, 143.8, 138.6, 132.3, 128.1 (all the eight aromatic CH are isochronous), 118.6, 99.9, 88.3, 49.2 ppm.



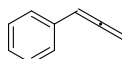
***N*-Allyl-*N*-propargylmethanesulfonamide (15j)**

The reaction of methanesulfonyl chloride with allyl propargyl amine according to the usual procedure (Et_3N 2.0 equiv, CH_2Cl_2 , r.t.) gave *N*-allyl-*N*-propargyl methanesulfonamide in mixture with the isomeric allene (30:70 ratio).

No purification was attempted and the crude mixture of isomers (111 mg, 0.64 mmol) was treated according to general procedure I (reaction time: 1 minute, no chromatographic purification needed) giving the title compound in the form of a pale brown oil (72.3 mg, 65%).

^1H NMR (300 MHz, CDCl_3): δ = 6.70 (t, J = 6.3 Hz, 1H), 5.92-5.73 (m, 1H), 5.40 (d, J = 6.3 Hz, 2H), 5.36-5.31 (m, 1H), 5.24 (dq, J = 10.2, 1.4 Hz, 1H), 3.98 (d, J = 5.9 Hz, 2H), 2.91 (s, 3H) ppm. ^{13}C NMR (75 MHz, CDCl_3): δ = 201.4, 132.2, 119.0, 99.8, 88.2, 49.1, 39.1 ppm.

3.12. Synthesis of miscellaneous allenes



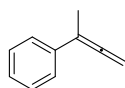
Phenylallene (1a)^[56]

A 250 mL two-necked flask equipped with a magnetic stirrer, a dropping funnel and an argon inlet tube was charged with LiBr (3.13 g, 36 mmol, 1.2 equiv) and evacuated. The inorganic solid was dried by strong heating in vacuo using a hot-air gun. After cooling, CuBr (5.16 g, 36 mmol, 1.2 equiv) was added under a flow of argon. Dry THF (75 mL) was introduced and the temperature was brought to -40 °C. Phenylmagnesium bromide (3.0 M solution in diethyl ether, 12 mL, 36 mmol, 1.2 equiv) was added dropwise from the dropping funnel. To the dark solution so obtained, propargyl *p*-toluenesulfonate (5.19 mL, 30 mmol) was added dropwise while keeping the temperature at -40 °C.

After stirring for 1 h at the same temperature, the mixture was brought to 0 °C and saturated NH_4Cl aqueous solution (100 mL) was added carefully. The mixture was diluted with diethyl ether (150 mL) and filtered to remove suspended solids. Concentrated ammonia solution (10 mL) was then added and phases separated. The organic extract was treated with a dilute KCN

solution (1 g in 50 mL of water) and then with brine. The organic extract was dried over MgSO_4 and evaporated under reduced pressure (bath temperature: 60 °C, pressure > 80 mbar). The residue was purified by short-path distillation with the aid of a Kugelrohr apparatus (pressure: 20 mbar) to give the title product in the form of a colorless liquid (2.10 g, 60%).

^1H NMR (300 MHz, CDCl_3): δ = 7.39-7.35 (m, 4H), 7.26 (ddt, J = 8.5, 5.4, 4.0 Hz, 1H), 6.23 (t, J = 6.8 Hz, 1H), 5.20 (d, J = 6.8 Hz, 2H) ppm. ^{13}C NMR (75 MHz, CDCl_3): δ = 209.9, 134.0, 128.7, 127.0, 126.8, 94.1, 78.9 ppm. IR (ATR): ν = 3061, 3029, 1942, 1598, 1494, 1457, 851 cm^{-1} . Spectral data are in agreement with the literature.^[57]



3-Phenyl-1,2-butadiene (1d)

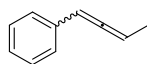
This compound was prepared by the EtMgBr -mediated Doering-Moore-Skattebøl rearrangement^[58] starting from 2,2-dibromo-1-methyl-1-phenylcyclopropane, which was in turn prepared by dibromocyclopropanation of *a*-methylstyrene.^[59]

To a mixture of *a*-methylstyrene (2.60 mL, 20 mmol) and CHBr_3 (5.25 mL, 60 mmol, 3.0 equiv) was added a solution of NaOH (3.2 g, 80 mmol, 4.0 equiv) and cetyltrimethylammonium bromide (146 mg, 0.4 mmol, 0.02 equiv) in water (3.2 mL). The biphasic mixture was vigorously stirred overnight at 60 °C. Extraction with diethyl ether (3 x 15 mL) and Kugelrohr distillation (0.1 mbar) gave 2,2-dibromo-1-methyl-1-phenylcyclopropane (**S3**) as a colorless liquid (5.12 g, 88%).

^1H NMR (300 MHz, CDCl_3): δ = 7.44-7.26 (m, 5H), 2.17 (d, J = 7.6 Hz, 1H), 1.78 (d, J = 7.6 Hz, 1H), 1.72 (s, 3H) ppm. ^{13}C NMR (75 MHz, CDCl_3): δ = 142.5, 128.6, 128.5, 127.4, 36.9, 35.9, 33.8, 27.9 ppm. IR (ATR): ν = 3058, 2981, 2959, 2924, 1600, 1496, 1444, 1055, 1010 cm^{-1} .

To a solution of 2,2-dibromo-1-methyl-1-phenylcyclopropane (**S3**, 4.79 g, 16.5 mmol) in dry THF (33 mL), EtMgBr (3.0 M solution in diethyl ether, 9.62 mL, 28.9 mmol, 1.75 equiv) was added dropwise at room temperature. After stirring for 1 h at room temperature, saturated NH_4Cl solution was slowly added and most THF was removed by distillation at atmospheric pressure. Extraction with diethyl ether (3 x 15 mL) and Kugelrohr distillation (0.1 mbar) gave the title compound in the form of a colorless liquid (1.62 g, 75%).

^1H NMR (300 MHz, CDCl_3): δ = 7.46-7.40 (m, 2H), 7.37-7.31 (m, 2H), 7.25-7.17 (m, 1H), 5.04 (q, J = 3.2 Hz, 2H), 2.11 (t, J = 3.2 Hz, 3 H) ppm. ^{13}C NMR (75 MHz, CDCl_3): δ = 209.1, 136.8, 128.4, 126.7, 125.8, 99.9, 77.1, 16.8 ppm. IR (ATR): ν = 3059, 2981, 1943, 1687, 1598, 1493, 1442, 1068 cm^{-1} . Spectral data are in agreement with the literature.^[60]



3-Phenyl-1,2-butadiene (1e)^[56]

A 50 mL two-necked flask equipped with an argon inlet tube and a magnetic stirrer was charged with CuBr (72 mg, 0.5 mmol, 0.05 equiv) and, after evacuation and back-filling with argon, 1-butyn-3-yl acetate (1.12 g, 10 mmol) and dry diethyl ether (10 mL) were introduced. The mixture was cooled to -18 °C with an ice-salt bath and PhMgBr (3.0 M solution in diethyl ether, 4.2 mL, 12.5 mmol, 1.25 equiv) was added dropwise.

After stirring for 1 h at -18 °C, saturated NH₄Cl solution was added and phases were separated. The aqueous phase was extracted with more ether (2 x 10 mL) and the combined extracts were treated with a dilute KCN solution (0.2 g in 10 mL of water) and then with brine. Evaporation of the solvent at atmospheric pressure, followed by short-path distillation in vacuum (0.1 mbar) and flash chromatography on silica gel (eluent: pentane) gave the title compound in the form of a pale yellow oil (494 mg, 38%).

¹H NMR (300 MHz, CDCl₃): δ = 7.36-7.19 (m, 4H), 7.21-7.11 (m, 1H), 6.07 (dq, J = 6.9, 3.2 Hz, 1H), 5.51 (pent, J = 6.9 Hz, 1H), 1.76 (dd, J = 6.9, 3.2 Hz, 3H) ppm. ¹³C NMR (75 MHz, CDCl₃): δ = 206.1, 135.2, 128.6, 126.8, 94.1, 89.7, 14.2 ppm. IR (ATR): ν = 3062, 3028, 2983, 1947, 1599, 1496, 1072, 872 cm⁻¹. Spectral data are in agreement with the literature.^[61]



1,2-Cyclononadiene (1c)

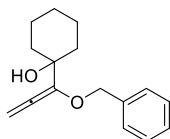
This compound was prepared from *cis*-cyclooctene using a sequence analogous to the one described for compound **1d**.^[58,59]

To a mixture of freshly distilled *cis*-cyclooctene (2.61 mL, 20 mmol) and CHBr₃ (5.25 mL, 60 mmol) was added a solution of NaOH (3.2 g, 80 mmol, 4.0 equiv) and cetyltrimethylammonium bromide (146 mg, 0.4 mmol, 0.02 equiv) in water (3.2 mL). The biphasic mixture was vigorously stirred overnight at 60 °C. Extraction with CH₂Cl₂ (3 x 15 mL) and Kugelrohr distillation in vacuum (0.1 mbar) gave 9,9-dibromobicyclo[6.1.0]nonane (**S4**) as a colorless liquid that congealed on standing (4.10 g, 73%).

¹H NMR (300 MHz, CDCl₃): δ = 2.04 (ddd, J = 10.8, 5.4, 2.4 Hz, 2H), 1.73-1.31 (m, 10H), 1.26-1.07 (m, 2H) ppm. ¹³C NMR (75 MHz, CDCl₃): δ = 37.3, 33.4, 28.0, 26.5, 25.6 ppm. IR (ATR): ν = 2921, 2853, 1465, 1446, 1163, 1059 cm⁻¹. Spectral data are in agreement with the literature.^[62]

To a solution of 9,9-dibromobicyclo[6.1.0]nonane (**S4**, 4.07 g, 14.4 mmol) in dry THF (30 mL), EtMgBr (3.0 M solution in diethyl ether, 8.40 mL, 25.3 mmol, 1.75 equiv) was added dropwise at room temperature. After stirring for 1 h at room temperature, saturated NH₄Cl solution was added cautiously and most THF was removed by distillation at atmospheric pressure. Extraction with diethyl ether (3 x 20 mL) and Kugelrohr distillation (pressure: 20 mbar) gave the title compound in the form of a colorless liquid (808 mg, 46%).

¹H NMR (300 MHz, CDCl₃): δ = 5.26 (pent, J = 4.4 Hz, 2H), 2.34-2.15 (m, 2H), 1.87-1.46 (m, 8H), 1.46-1.28 (m, 2H) ppm. ¹³C NMR (75 MHz, CDCl₃): δ = 205.7, 92.6, 28.1, 27.5, 25.5 ppm. IR (ATR): ν = 2923, 2855, 1958, 1452, 850 cm⁻¹. Spectral data are in agreement with the literature.^[62]



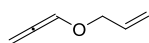
1-(1-(Benzyloxy)allenyl)cyclohexanol (1ag)

A Schlenk flask equipped with a magnetic stirrer and a rubber septum was charged with benzyloxyallene (**1af**, 292 mg, 2.0 mmol) and conditioned under argon. Dry THF (8 mL) was

introduced by syringe and the solution was cooled to $-78\text{ }^{\circ}\text{C}$. BuLi (1.6 M solution in hexanes, 1.25 mL, 2.0 mmol, 1.0 equiv) was slowly dropped in. The mixture was left at the aforementioned temperature for 1 h, then cyclohexanone (228 μL , 2.2 mmol, 1.1 equiv) was added by syringe. The clear solution was let to come to room temperature and left overnight.

Saturated NH_4Cl aqueous solution (2 mL) was added and the mixture was extracted with diethyl ether (3 x 10 mL). The combined organic extracts were dried over Na_2SO_4 and volatiles were evaporated under reduced pressure. The residue was purified by flash chromatography on NaHCO_3 -washed silica gel (eluent: petroleum ether / EtOAc 95:5) to give the title compound as a colorless oil (281 mg, 58%).

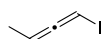
^1H NMR (300 MHz, CDCl_3): δ = 7.49-7.26 (m, 5H), 5.55 (s, 2H), 4.63 (s, 2H), 2.09 (s, 1H), 1.82-1.58 (m, 6H), 1.56-1.42 (m, 4H), 1.36-1.23 (m, 2H) ppm. ^{13}C NMR (75 MHz, CDCl_3): δ = 197.1, 138.0, 137.7, 128.5, 127.9, 127.7, 92.7, 71.9, 70.7, 35.6, 25.8, 22.2 ppm.



Allyloxyallene (1ah)

Allyl propargyl ether (**S3ah**, 961 mg, 10 mmol) was dropped slowly to a solution of *t*BuOK (224 mg, 2.0 mmol, 0.20 equiv) in dry DMSO (5.0 mL) under Ar. Cooling in a cold water bath is essential, since the reaction is highly exothermic. After stirring for 15 min at room temperature, saturated aqueous NH_4Cl solution was added (2 mL) and the mixture was extracted with diethyl ether (3 x 10 mL). The combined organic phases were washed thoroughly with water (5 x 10 mL) and dried over Na_2SO_4 . The solvent was removed by distillation at atmospheric pressure, then the residue was purified by Kugelrohr distillation (oil pump vacuum). The title product was thus obtained as a colorless liquid (184 mg, 17%).

^1H NMR (300 MHz, CDCl_3): δ = 6.76 (t, J = 5.9 Hz, 2H), 5.95 (ddt, J = 17.2, 10.4, 5.6 Hz, 1H), 5.45 (d, J = 5.9 Hz, 2H), 5.31 (dt, J = 17.2, 1.4 Hz, 1H), 5.22 (dt, J = 10.4, 1.4 Hz, 1H), 4.09 (dt, J = 5.6, 1.4 Hz, 2H) ppm. ^{13}C NMR (75 MHz, CDCl_3): δ = 201.5, 133.7, 121.5, 117.7, 91.0, 69.6 ppm.



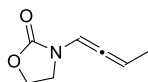
1-Iodo-1,2-butadiene^[63]

A solution 1-butyne-3-ol (1.18 mL, 15 mmol) in dry THF under argon was cooled to $-78\text{ }^{\circ}\text{C}$. A solution of BuLi (2.5 M in hexanes, 7.2 mL, 18 mmol, 1.2 equiv) was added dropwise by syringe, followed by methanesulfonyl chloride (1.28 mL, 16.5 mmol, 1.1 equiv). The mixture was stirred at $-78\text{ }^{\circ}\text{C}$ for 30 min. In the meantime, a 50 mL Schlenk flask was charged with LiI (2.41 g, 18 mmol, 1.5 equiv) and flame-dried under vacuum. After cooling, CuI (3.43 g, 18 mmol, 1.5 equiv) was introduced and the solids were dissolved in dry THF (20 mL) under argon. The CuI·LiI solution thus obtained was added to the reaction mixture at $-78\text{ }^{\circ}\text{C}$ and the cooling bath was removed.

After stirring for 2 h at room temperature, the flask was opened to the air and the reaction quenched by careful addition of a saturated aqueous solution of NH_4Cl (approx. 1 mL) and most THF was evaporated by distillation at atmospheric pressure. The residue was partitioned between pentane (25 mL) and saturated NH_4Cl solution (20 mL) containing a few drops of concentrated aqueous ammonia. The aqueous layer was extracted with more pentane (2 x 10 mL) and the combined organic phases dried over MgSO_4 . The solvent was evaporated by distillation at atmospheric pressure and the residue purified by Kugelrohr distillation under slightly

diminished pressure (approx. 200 mbar). The title compound was thus obtained in the form of a colorless oil (1.07 g, 40%), containing traces of THF and of the isomeric 3-iodo-1-butyne.

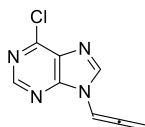
^1H NMR (300 MHz, CDCl_3): δ = 5.64 (dq, J = 5.7, 2.6 Hz, 1H), 5.06 (qd, J = 7.3, 5.7 Hz, 1H), 1.77 (dd, J = 7.3, 2.6 Hz, 3H) ppm. ^{13}C NMR (75 MHz, CDCl_3): δ = 206.2, 91.3, 68.1, 25.8 ppm.



3-(Buta-1,2-dien-1-yl)oxazolidin-2-one (1ai)^[64]

A 50 mL Schlenk flask was charged with 2-oxazolidinone (174 mg, 2.0 mmol, 1.25 equiv), CuCN (17.9 mg, 0.2 mmol, 0.125 equiv) and Cs_2CO_3 (1.30 g, 4.0 mmol, 2.5 equiv). After conditioning the apparatus under argon atmosphere, degassed toluene (10 mL), *N,N'*-dimethyl-1,2-ethylenediamine (43 μL , 0.4 mmol, 0.25 equiv) and 1-iodo-1,2-butadiene (containing THF and 3-iodo-1-butyne, 58% NMR purity, 497 mg, 1.6 mmol) were added sequentially. The mixture was stirred overnight under argon, then cooled, diluted with more toluene (20 mL) and filtered through a pad of diatomaceous earth. Volatiles were evaporated under reduced pressure and the residue was purified by flash chromatography on NaHCO_3 -washed silica gel (eluent: petroleum ether / EtOAc 70:30) to afford the title compound in the form of a pale yellow oil (86.9 mg, 39%).

^1H NMR (300 MHz, CDCl_3): δ = 6.76 (dq, J = 5.7, 2.8 Hz, 1H), 5.80 (qd, J = 6.9, 5.7 Hz, 1H), 4.40 (t, J = 8.0 Hz, 2H), 3.65-3.50 (ABX multiplet, 2H), 1.77 (dd, J = 6.9, 2.8 Hz, 3H) ppm. ^{13}C NMR (75 MHz, CDCl_3): δ = 195.6, 155.5, 99.1, 96.3, 62.3, 43.4, 16.5 ppm. Spectral data are in agreement with the literature.^[64]



6-Chloro-9-allenyl-9H-purine

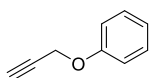
To a suspension of 6-chloropurine (773 mg, 5.0 mmol) in dry DMF (10 mL) under Ar, NaH (60% in mineral oil, 240 mg, 6.0 mmol, 1.2 equiv) was added slowly. When hydrogen evolution subsided, propargyl bromide (80% solution in toluene, 679 μL , 6.25 mmol, 1.25 equiv) was added and the mixture was stirred overnight at room temperature.

Saturated aqueous NH_4Cl solution (1 mL) was added and most of the DMF was evaporated under vacuum. The residue was dissolved in CH_2Cl_2 (50 mL) and the organic phase was washed with water (5 x 10 mL) and dried over Na_2SO_4 . Volatiles were evaporated under reduced pressure and the residue was purified by flash chromatography on NaHCO_3 -washed silica gel (eluent: CH_2Cl_2) to give the title compound in the form of a white solid (208 mg, 24%). The isomeric alkene elutes later (white solid, 181 mg, 19%).

^1H NMR (300 MHz, CDCl_3): δ = 8.78 (s, 1H), 8.25 (s, 1H), 7.38 (t, J = 6.6 Hz, 1H), 5.76 (d, J = 6.6 Hz, 2H) ppm. ^{13}C NMR (75 MHz, CDCl_3): δ = 202.6, 152.6, 142.9, 92.7, 89.7 ppm. Spectral data are in agreement with the literature.^[65]

6-Chloro-9-propargyl-9H-purine - ^1H NMR (300 MHz, CDCl_3): δ = 8.78 (s, 1H), 8.34 (s, 1H), 7.26 (s, 1H), 5.07 (d, J = 2.6 Hz, 2H), 2.59 (t, J = 2.6 Hz, 1H) ppm. Spectral data are in agreement with the literature.^[65]

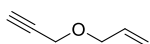
3.13. Synthesis of miscellaneous starting materials



Phenyl propargyl ether (S3ad)

Sodium phenoxide (3.51 g, 30 mmol, 1.2 equiv) was refluxed overnight with propargyl *p*-toluenesulfonate (4.33 mL, 25 mmol) in THF (20 mL). Then, most of the THF was evaporated under reduced pressure and the residue was dissolved in Et₂O (50 mL). The ethereal solution was extracted with aqueous NaOH solution (1 M, 3 x 20 mL) and evaporated *in vacuo*. Kugelrohr distillation of the residue (10 mbar) afforded the title compound in the form of a colorless liquid (2.67 g, 81%).

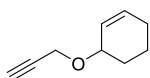
¹H NMR (300 MHz, CDCl₃): δ = 7.24-7.19 (m, 2H), 6.93-6.88 (m, 3H), 4.59 (d, *J* = 2.4 Hz, 2H), 2.42 (t, *J* = 2.4 Hz, 1H) ppm. ¹³C NMR (75 MHz, CDCl₃): δ = 157.6, 129.6, 121.7, 115.0, 78.7, 75.6, 55.8 ppm. Spectral data are in agreement with those reported in the literature.^[66]



Allyl propargyl ether (S3ah)

To a mixture of propargyl alcohol (2.91 mL, 50 mmol, 1.0 equiv), allyl bromide (4.39 mL, 50 mmol, 1.0 equiv) and ⁿBu₄NHSO₄ (849 g, 2.5 mmol, 0.05 equiv) in CH₂Cl₂ (30 mL), NaOH (8.0 g, 200 mmol, 4.0 equiv) in water (8 mL) was added. The biphasic mixture was stirred at reflux overnight. After cooling, it was transferred to a separatory funnel and phases were separated. The aqueous layer was extracted with a small amount of Et₂O and the combined organic extracts were dried over Na₂SO₄. Diethyl ether was distilled at atmospheric pressure and then the product under partial vacuum (150 mbar). The title product was thus obtained as a colorless, volatile liquid (4.10 g, contaminated with 4% Et₂O, 83%).

¹H NMR (300 MHz, CDCl₃): δ = 5.91 (ddt, *J* = 17.0, 10.1, 5.8 Hz, 1H), 5.32 (ddd, *J* = 17.0, 5.8, 1.4 Hz, 1H), 5.32 (dq, *J* = 10.1, 1.4 Hz, 1H), 4.16 (d, *J* = 2.4 Hz, 2H), 4.07 (dt, *J* = 5.8, 1.4 Hz, 2H), 2.43 (t, *J* = 2.4 Hz, 1H) ppm. ¹³C NMR (75 MHz, CDCl₃): δ = 133.8, 118.0, 79.6, 74.4, 70.6, 57.1 ppm.

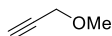


Cyclohexen-3-yl propargyl ether (S3ai)

A biphasic mixture of propargyl alcohol (699 μL, 12 mmol, 1.2 equiv), 3-bromocyclohexene (1.15 mL, 10 mmol), ⁿBu₄NHSO₄ (170 mg, 0.5 mmol, 0.05 equiv), Et₂O (10 mL) and NaOH (50% aqueous solution, 6.0 g, 75 mmol, 7.5 equiv) was stirred vigorously overnight.

It was then transferred to a separatory funnel, phases were separated and the organic layer was washed with water (3 x 3 mL). The organic extract was dried over Na₂SO₄ and diethyl ether was evaporated under slightly reduced pressure. The residue was distilled under high vacuum with the aid of a Kugelrohr apparatus to give the title product in the form of a colorless oil (819 mg, 60%).

¹H NMR (300 MHz, CDCl₃): δ = 5.88 (dtd, *J* = 10.1, 3.6, 1.2 Hz, 1H), 5.7 (ddt, *J* = 10.1, 3.4, 2.1 Hz, 1H), 4.20 (dd, *J* = 2.4, 1.5 Hz, 2H), 4.12 (m, 1H), 2.40 (t, *J* = 2.4 Hz, 1H), 2.13-1.36 (m, 6H) ppm. ¹³C NMR (75 MHz, CDCl₃): δ = 131.7, 127.2, 80.6, 74.0, 71.9, 55.4, 28.2, 25.3, 19.2 ppm.

**Methyl propargyl ether**^[56]

In a three-necked flask (50 mL) equipped with a reflux condenser, a magnetic stirrer and a dropping funnel, a solution of NaOH (7.2 g, 0.18 mol, 1.5 equiv) in water (12 mL) and propargyl alcohol (7.0 mL, 0.12 mol) was introduced. The dropping funnel was charged with dimethyl sulphate (CAUTION! Extremely toxic) (7.8 mL, 0.080 mmol, 0.67 equiv). The solution was cooled to 0-10 °C and the alkylating agent was slowly dropped in while stirring. After stirring overnight, the reflux condenser was substituted with a distillation head and the mixture distilled at atmospheric pressure. The title compound passed at 61-62 °C as a colorless liquid, together with a small amount of water. The distillate was dried over MgSO₄ and filtered. Yield: 6.65 g (79%).

¹H NMR (300 MHz, CDCl₃): δ = 4.10 (d, J = 2.4 Hz, 2H), 3.39 (s, 3H), 2.44 (t, J = 2.4, 2.4 Hz, 1H) ppm.

**1-(4-Methoxybut-2-yn-1-yl)piperidine**^[5]

A mixture of methyl propargyl ether (854 μ L, 10 mmol), piperidine (1.48 mL, 15 mmol, 1.5 equiv), paraformaldehyde (330 mg, 11 mmol, 1.1 equiv), and CuI (9.5 mg, 0.050 mmol, 0.5 mol%) in dioxane (5 mL) was heated at 100 °C in a sealed tube under argon for 2.5 h.

The cooled reaction mixture was diluted with Et₂O (20 mL) and extracted with a mixture of brine and concentrated aqueous ammonia (20 mL + 5 mL, subdivided into three portions). The organic phase was dried over MgSO₄, the solvents were removed *in vacuo* to afford a mixture of the title compound with excess piperidine. The latter amine was easily separated by adding TsCl (approx. 1 g), Et₂O (10 mL) and 1 M aqueous NaOH (10 mL). The biphasic mixture was stirred overnight, then phases were separated and the aqueous layer was extracted with more Et₂O (3 x 5 mL). The combined organic extracts were exsiccated over MgSO₄, concentrated *in vacuo* and the residue distilled under reduced pressure (25 mbar) with the aid of a Kugelrohr apparatus to give the title product in the form of a colorless liquid (1.13 g, 68%).

¹H NMR (300 MHz, CDCl₃): δ = 4.11 (t, J = 1.9 Hz 2H), 3.37 (s, 3H), 3.29 (t, J = 1.9 Hz, 2H), 2.48 (t, J = 5.5 Hz, 4H), 1.60 (d, J = 5.5 Hz, 4H), 1.49-1.35 (m, 2H) ppm. ¹³C NMR (75 MHz, CDCl₃): δ = 82.2, 80.6, 60.2, 57.7, 53.5, 48.0, 26.0, 24.0 ppm.

References

- [1] G. R. Fulmer, A. J. M. Miller, N. H. Sherden, H. E. Gottlieb, A. Nudelman, B. M. Stoltz, J. E. Bercaw, K. I. Goldberg, *Organometallics* **2010**, *29*, 2176–2179.
- [2] T. R. Hoye, B. M. Eklov, T. D. Ryba, M. Voloshin, L. J. Yao, *Org. Lett.* **2004**, *6*, 953–6.
- [3] M. R. Tracey, T. Grebe, J. A. Mulder, R. P. Hsung, *Org. Synth.* **2005**, *81*, 147–157.
- [4] R. Abonia, A. Albornoz, B. Insuasty, J. Quiroga, H. Meier, A. Hormaza, M. Noguerras, A. Sánchez, J. Cobo, J. N. Low, *Tetrahedron* **2001**, *57*, 4933–4938.
- [5] T. H. West, D. S. B. Daniels, A. M. Z. Slawin, A. D. Smith, *J. Am. Chem. Soc.* **2014**, *136*, 4476–4479.
- [6] A.-H. Khuthier, M. A. Sheat, *J. Prakt. Chem.* **1989**, *331*, 187–194.
- [7] M. S. Silva, R. S. Ferrarini, B. A. Sousa, F. T. Toledo, J. V. Comasseto, R. A. Gariani, *Tetrahedron Lett.* **2012**, *53*, 3556–3559.
- [8] A. R. Katritzky, K. Yannakopoulou, P. Lue, D. Rasala, L. Urogdi, *J. Chem. Soc. Perkin Trans. 1* **1989**, *2*, 225–233.
- [9] J. R. L. Smith, J. S. Sadd, *J. Chem. Soc. Perkin Trans. 1* **1975**, *12*, 1181–1184.
- [10] A. R. Katritzky, K. Yannakopoulou, W. Kuzmierkiewicz, J. M. Aurrecochea, G. J. Palenik, A. E. Koziol, M. Szczesniak, R. Skarjune, *J. Chem. Soc. Perkin Trans. 1* **1987**, 2673–2679.
- [11] A. R. Katritzky, S. K. Nair, G. Qiu, *Synthesis* **2002**, *2002*, 199–202.
- [12] W. B. Dickinson, P. C. Lang, *Tetrahedron Lett.* **1967**, *8*, 3035–3040.
- [13] Á. González-Gómez, L. Añorbe, A. Poblador, G. Domínguez, J. Pérez-Castells, *Eur. J. Org. Chem.* **2008**, *2008*, 1370–1377.
- [14] X. Yang, F. D. Toste, *Chem. Sci.* **2016**, *7*, 2653–2656.
- [15] B. M. Nilsson, H. M. Vargas, B. Ringdahl, U. Hacksell, *J. Med. Chem.* **1992**, *35*, 285–294.
- [16] L.-L. Wei, J. A. Mulder, H. Xiong, C. A. Zifcsak, C. J. Douglas, R. P. Hsung, *Tetrahedron* **2001**, *57*, 459–466.
- [17] R. Ocello, A. De Nisi, M. Jia, Q.-Q. Yang, M. Monari, P. Giacinto, A. Bottoni, G. Pietro Miscione, M. Bandini, *Chem. Eur. J.* **2015**, *21*, 18445–18453.
- [18] K. Inamoto, A. Yamamoto, K. Ohsawa, K. Hiroya, T. Sakamoto, *Chem. Pharm. Bull. (Tokyo)* **2005**, *53*, 1502–1507.
- [19] F. Barbot, B. Dauphin, P. Miginiac, *Synthesis* **1985**, *1985*, 768–770.
- [20] Y. Li, J. Chen, R. Qiu, X. Wang, J. Long, L. Zhu, C.-T. Au, X. Xu, *Tetrahedron Lett.* **2015**, *56*, 5504–5507.
- [21] Y. Liu, Z. Song, B. Yan, *Org. Lett.* **2007**, *9*, 409–412.
- [22] U. Anwar, A. Casaschi, R. Grigg, J. M. Sansano, *Tetrahedron* **2001**, *57*, 1361–1367.
- [23] J. Zhang, H.-N. Chen, F.-I. Chiang, J. Y. Takemoto, M. Bensaci, C.-W. T. Chang, *J. Comb. Chem.* **2007**, *9*, 17–19.
- [24] D. O. Kiesewetter, W. C. Eckelman, *J. Label. Compd. Radiopharm.* **2004**, *47*, 953–969.
- [25] L. A. Shastri, S. L. Shastri, C. D. Bathula, M. Basanagouda, M. V. Kulkarni, *Synth. Commun.* **2011**, *41*, 476–484.
- [26] K. Bao, W. Zhang, X. Bu, Z. Song, L. Zhang, M. Cheng, *Chem. Commun.* **2008**, *42*, 5429–5431.
- [27] A. J. Hubert, H. Reimlinger, *J. Chem. Soc. C Org.* **1968**, 606.
- [28] P. V. Tkachenko, I. I. Popov, A. M. Simonov, *Chem. Heterocycl. Compd.* **1974**, *10*, 1354–1356.
- [29] I. I. Popov, P. V. Tkachenko, A. M. Simonov, *Chem. Heterocycl. Compd.* **1975**, *11*, 347–351.
- [30] G. Broggin, L. Bruché, G. Zecchi, T. Pilati, *J. Chem. Soc., Perkin Trans. 1* **1990**, 533–539.
- [31] I. Akritopoulou-Zanze, *Curr. Opin. Chem. Biol.* **2008**, *12*, 324–31.
- [32] F. Mohr, A. Mendía, M. Laguna, *Eur. J. Inorg. Chem.* **2007**, *2007*, 3115–3123.
- [33] L. V. Baikalova, I. A. Zyryanova, O. A. Tarasova, N. N. Chipanina, E. Y. Shmidt, T. V. Kashik, A. V. Afonin, L. M. Sinegovskaya, A. V. Vashchenko, B. A. Trofimov, *Russ. J. Gen. Chem.* **2003**, *73*, 1634–1640.
- [34] G. B. Zakaryan, S. S. Hayotsyan, H. S. Attaryan, G. V. Hasratyan, *Russ. J. Gen. Chem.* **2015**, *85*, 1773–1774.
- [35] M. I. Rodríguez-Franco, I. Dorronsoro, A. Badía, J. E. Baños, *Arch. Pharm.* **2002**, *335*, 339–346.
- [36] G. J. Morriello, R. J. Devita, *Anti-hypercholesterolemic Biaryl Azetidinone Compounds*, **2008**, US Patent US 20080280836 A1.
- [37] E. Díez-Barra, A. de la Hoz, A. Loupy, A. Sánchez-Migallón, *Heterocycles* **1994**, *38*, 1367–1374.
- [38] P. V. Tkachenko, I. I. Popov, A. M. Simonov, Y. V. Medvedev, *Chem. Heterocycl. Compd.* **1975**, *11*, 1312–1314.

- [39] A. R. Katritzky, J. Li, N. Malhotra, *Liebigs Ann. der Chemie* **1992**, *1992*, 843–853.
- [40] A. R. Katritzky, S. V. Verin, *J. Heterocycl. Chem.* **1995**, *32*, 323–328.
- [41] A. R. Katritzky, J. R. Levell, J. Li, *Tetrahedron Lett.* **1996**, *37*, 5641–5644.
- [42] W. Yan, T. Liao, O. Tuguldur, C. Zhong, J. L. Petersen, X. Shi, *Chem. Asian J.* **2011**, *6*, 2720–2724.
- [43] K. Bouchmella, B. Boury, S. G. Dutremez, A. van der Lee, *Chem. Eur. J.* **2007**, *13*, 6130–6138.
- [44] L. V. Baikalo, O. A. Tarasova, I. A. Zyryanova, A. V. Afonin, L. M. Sinegovskaya, B. A. Trofimov, *Russ. J. Gen. Chem.* **2002**, *72*, 1294–1298.
- [45] H. Ehrhardt, H. Mildenerger, *Liebigs Ann. der Chemie* **1982**, *1982*, 989–993.
- [46] L. Meng, S. C. Wang, J. C. Fettinger, M. J. Kurth, D. J. Tantillo, *Eur. J. Org. Chem.* **2009**, *2009*, 1578–1584.
- [47] O. A. Tarasova, L. Brandsma, B. A. Trofimov, *Synthesis* **1993**, *1993*, 571–572.
- [48] I. Moggio, J. Le Moigne, H. Barrientos, L. Oswald, E. Arias, J. Romero, *Polym. Bull.* **2005**, *53*, 269–275.
- [49] Y. Zhou, J. A. Porco, J. K. Snyder, *Org. Lett.* **2007**, *9*, 393–396.
- [50] T. W. Bousfield, M. C. Kimber, *Tetrahedron Lett.* **2015**, *56*, 350–352.
- [51] S. E. Gibson, K. A. C. Kaufmann, P. R. Haycock, A. J. P. White, D. J. Hardick, M. J. Tozer, *Organometallics* **2007**, *26*, 1578–1580.
- [52] M. E. Krafft, L. V. R. Boñaga, J. A. Wright, C. Hirose, *J. Org. Chem.* **2002**, *67*, 1233–1246.
- [53] H.-J. Li, R. Guillot, V. Gandon, *J. Org. Chem.* **2010**, *75*, 8435–8449.
- [54] S. I. Lee, S. Y. Park, Y. K. Chung, *Adv. Synth. Catal.* **2006**, *348*, 2531–2539.
- [55] A. I. Vogel, B. S. Furniss, *Vogel's Textbook of Practical Organic Chemistry*, Longman, **1989**.
- [56] L. Brandsma, *Synthesis of Acetylenes, Allenes and Cumulenes: Methods and Techniques (Best Synthetic Methods)*, Elsevier Ltd., Oxford, **2003**.
- [57] H. Clavier, K. Le Jeune, I. de Raggi, A. Tenaglia, G. Buono, *Org. Lett.* **2011**, *13*, 308–311.
- [58] M. S. Baird, A. V. Nizovtsev, I. G. Bolesov, *Tetrahedron* **2002**, *58*, 1581–1593.
- [59] R.-J. De Lang, L. Brandsma, *Synth. Commun.* **1998**, *28*, 225–232.
- [60] A. M. Caporusso, L. Lardicci, *J. Chem. Soc., Perkin Trans. 1* **1983**, 949–953.
- [61] A. M. Caporusso, C. Polizzi, L. Lardicci, *J. Org. Chem.* **1987**, *52*, 3920–3923.
- [62] K. A. Campbell, H. O. House, B. W. Surber, W. S. Trahanovsky, *J. Org. Chem.* **1987**, *52*, 2474–2481.
- [63] J. B. Feltenberger, R. P. Hsung, *Org. Lett.* **2011**, *13*, 3114–3117.
- [64] L. Shen, R. P. Hsung, Y. Zhang, J. E. Antoline, X. Zhang, *Org. Lett.* **2005**, *7*, 3081–3084.
- [65] T. Wei, M.-S. Xie, G.-R. Qu, H.-Y. Niu, H.-M. Guo, *Org. Lett.* **2014**, *16*, 900–903.
- [66] A. Banerji, P. Saha (Née Sengupta), K. C. Majumdar, P. K. Choudhury, *Magn. Reson. Chem.* **1992**, *30*, 1145–1148.

Résumé

Le développement de nouvelles réactions d'intérêt synthétique est un enjeu important de la chimie organique. Les découvertes dans ce domaine peuvent donner accès à des nouvelles classes de molécules ou permettre d'effectuer des transformations connues d'une façon plus efficace. Malgré la richesse des informations disponibles sur d'innombrables réactions organiques, de nombreuses découvertes sont encore faites selon un processus d'essais et d'erreurs, ce qui nécessite beaucoup de temps et de ressources.

Le but de cette thèse est d'explorer les potentialités d'une approche différente, c'est-à-dire de réaliser en même temps l'étude mécanistique et le développement méthodologique d'une réaction organique. Ces deux processus ont été traditionnellement maintenus séparés, à la fois dans l'espace et dans le temps : le mécanisme d'une transformation est souvent étudié plusieurs années après la première publication et, dans la plupart des cas, par un groupe de recherche différent. Nous avons essayé de conduire ces deux activités dans le même laboratoire.

Nous avons également adopté une approche complémentaire utilisant à la fois des outils expérimentaux et théoriques pour les études mécanistiques. La modélisation théorique peut souvent répondre à des questions qui sont extrêmement difficiles à aborder expérimentalement et des expériences sont souvent nécessaires pour obtenir les informations clés nécessaires pour effectuer des calculs significatifs.

Après une introduction sur les fondements des principales méthodes expérimentales et théoriques utilisées dans cette thèse (chapitre I), le reste du matériel présenté ici peut être subdivisé en deux parties principales qui ont en commun le même *modus operandi*. La partie 1, comprenant les chapitres II et III, concerne deux transformations catalysées par le palladium, tandis que la partie 2, qui contient le chapitre IV et qui constitue le sujet principal de cette thèse, regarde l'hydroamination cupro-catalysée des allènes.

Chapitre II – Rôles multiples des isonitriles dans les couplages pallado-catalysés : une étude mécanistique

Les isonitriles sont des composés très utilisés dans le domaine des réactions multicomposants, comme les réactions de Passerini et de Ugi. Leur réactivité est très remarquable, car ils peuvent fonctionner d'abord comme nucléophiles et puis comme électrophiles (un exemple est montré dans le Schéma 1, haut). La raison de cette réactivité ambivalente est leur structure électronique, qui peut être considérée comme celle d'un carbène stable. En fait, ils sont isoélectroniques à la molécule de monoxyde de carbone. Comme cette dernière espèce chimique, ils peuvent s'insérer dans les liaisons carbone-métal (Schéma 1, bas).

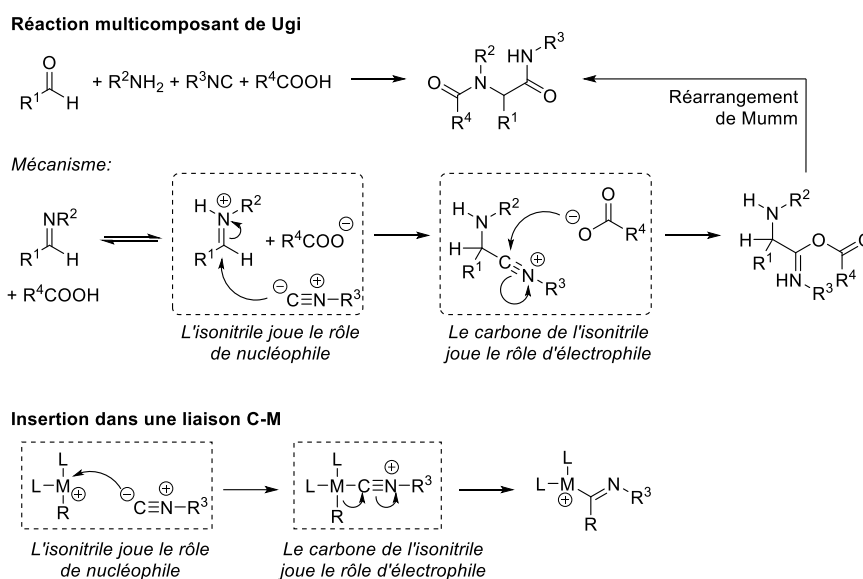


Schéma 1 – Deux réactions caractéristiques des isonitriles : réaction multicomposant de Ugi et insertion dans une liaison carbone-métal. Dans ces deux cas, le carbone terminal de l'isonitrile joue consécutivement le rôle de nucléophile et d'électrophile.

De nombreux couplages pallado-catalysés *carbonylants*, ayant une insertion migratoire de CO parmi les étapes de leur mécanisme, ont été développés à partir des années 80 du siècle dernier. Étonnamment, il a fallu attendre le début du XXI^{ème} siècle pour que des couplages analogues impliquant des isonitriles apparaissent dans la littérature. Une explication possible du développement tardif de cette chimie peut être la tendance des isonitriles à réaliser des insertions multiples consécutives dans la liaison C-Pd. De plus, en présence de catalyseurs à base de palladium, les isonitriles ont tendance à polymériser.

Compte tenu de la rareté des études concernant le mécanisme des couplages pallado-catalysés impliquant des isonitriles, contrastant avec la richesse des informations disponibles grâce à des études de chimie organométallique sur certaines étapes élémentaires du cycle catalytique, nous avons décidé de focaliser notre attention sur la synthèse d'amides par un couplage à trois composants entre un bromoarène, un isonitrile et une molécule d'eau développé par Jiang et collaborateurs (Schéma 2).^[1] C'est un exemple typique de couplage intramoléculaire qui pourrait être également représentatif d'autres transformations similaires. Ces auteurs ont établi que les meilleurs résultats étaient obtenus quand un mélange de PdCl₂ et PPh₃ dans un rapport molaire de 1: 2 était utilisé comme pré-catalyseur et un mélange DMSO / H₂O comme solvant (Schéma 2). Néanmoins, ils ont également vérifié que l'addition de phosphine n'est pas nécessaire. En fait, le protocole expérimental analogue « sans ligand » utilisant uniquement du PdCl₂ a donné le produit attendu avec un rendement satisfaisant (Schéma 2). Pour des raisons de simplicité, nous nous sommes donc intéressés à la réaction qui a lieu en absence de PPh₃.

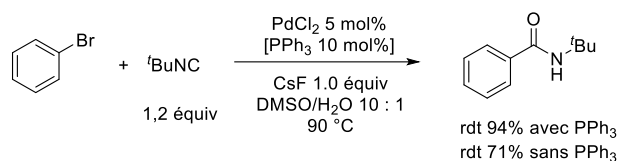


Schéma 2 – Amidification pallado-catalysée du bromobenzène, en présence de PPh_3 et en conditions « sans ligand ». [1]

Nous avons établi que l'isonitrile peut jouer le rôle de ligand dans tous les intermédiaires du cycle catalytique et moduler leur réactivité de plusieurs façons. Sur la base de nos résultats, nous pouvons proposer le mécanisme représenté dans la Figure 1, comportant des complexes ligandés par l'isonitrile à chaque étape du cycle catalytique. Les intermédiaires et les états stationnaires qui ont été isolés et caractérisés sont entourés par des rectangles tracés en pointillé.

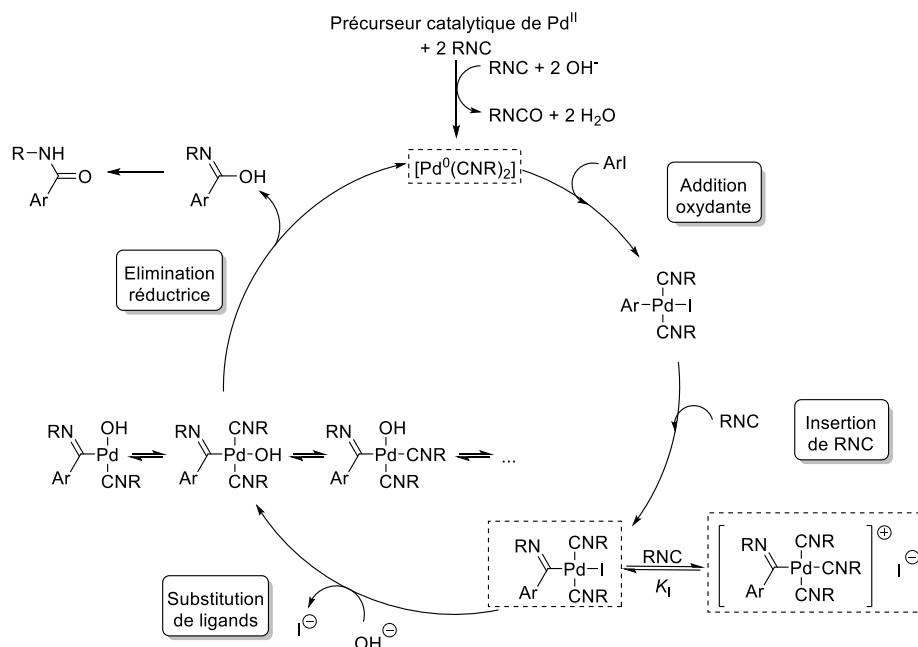


Figure 1 – Mécanisme proposé pour la réaction de synthèse d'amides à partir d'un iodoarène, un isonitrile et une molécule d'eau.

Les sels de palladium (II) sont presque universellement employés comme pré-catalyseurs dans les couplages impliquant des isonitriles. Nous avons tout d'abord vérifié qu'un isonitrile peut réduire le Pd(II) en Pd(0) en présence d'une source de OH^- (Schéma 3). En même temps, l'isonitrile est oxydé en l'isocyanate correspondant.

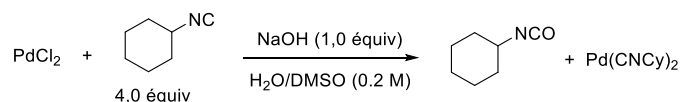


Schéma 3 – Réduction de Pd(II) par CyNC en présence d'une base.

L'addition oxydante, point d'entrée du cycle catalytique, peut avoir lieu sur des complexes de palladium(0) ligandés par l'isonitrile. La cinétique de cette étape a été étudiée et nous avons observé que l'excès d'isonitrile n'inhibe pas la réaction, comme cela se produit normalement avec d'autres ligands, tels que les phosphines. Ceux-ci, en effet, ont tendance à former des complexes tricordonnés à 16 électrons non réactifs à la place des espèces actives à 14 électrons (et donc dicoordonnées), mais ce n'est pas le cas pour les isonitriles. L'insertion de l'isonitrile dans la liaison C-Pd est plus rapide que l'addition oxydante, donc cette dernière réaction n'a pas pu être étudiée dans nos conditions opératoires, bien qu'elle ait été examinée en détail dans des études précédentes. Le complexe *trans*-[(ArC=N*t*Bu)Pd(CN*t*Bu)₂I] (Ar = 4-F-C₆H₄, **II.1**) a pu être préparé par la réaction de ArI avec Pd(dba)₂ comme source de Pd(0) en présence d'un excès de *t*BuNC.

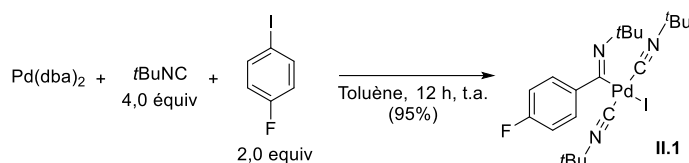


Schéma 4 – Synthèse de *trans*-[(ArC=N*t*Bu)Pd(CN*t*Bu)₂I] (**II.1**).

Dans les solvants polaires, tels que le DMSO, l'intermédiaire *trans*-[(ArC=N*t*Bu)Pd(CN*t*Bu)₂I] (**II.1**) a tendance à subir le déplacement de l'iodure coordonné par une molécule de *t*BuNC, donnant ainsi un complexe cationique [(ArC=N*t*Bu)Pd(CN*t*Bu)₂]⁺ (**II.2**, Schéma 5). Cette dernière espèce n'est pas directement impliquée dans l'élimination réductrice en présence de OH⁻, mais elle est fort probablement un état de repos responsable de la désactivation du catalyseur et des réactions secondaires, telles que les insertions multiples de l'isonitrile.

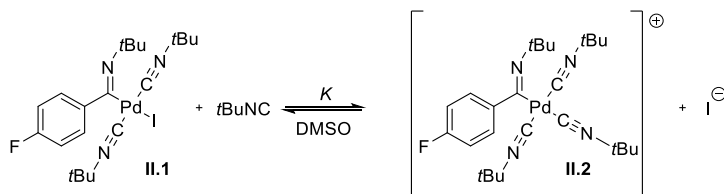
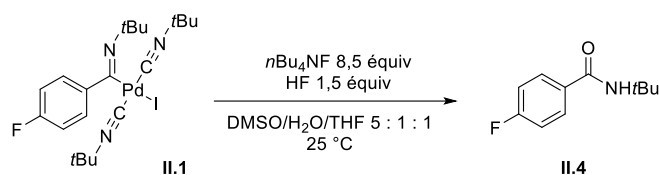


Schéma 5 – Substitution de I⁻ par *t*BuNC dans le complexe **II.1**.

Comme plusieurs réactions de couplages impliquant des isonitriles sont plus performants en présence de phosphines monodentées ou bidentées, l'interaction du complexe **II.1** avec deux ligands modèle (PPh₃ et 1,2-bis(diphénylphosphino)éthane – dppe) a été examinée. Dans ces deux cas, des complexes cationiques dérivant de l'expulsion d'I⁻ de la sphère de coordination se forment aisément dans des solvants polaires et modérément polaires. D'une manière générale, la formation de ces complexes cationiques n'est pas souhaitable, car ils ne sont pas intermédiaires du cycle catalytique, mais ils peuvent prendre part aux réactions secondaires.

Le complexe *trans*-[(ArC=N*t*Bu)Pd(CN*t*Bu)₂I] (**II.1**) isolé est capable de donner l'élimination réductrice en présence d'eau et d'un tampon F⁻ / HF à température ambiante (Schéma 6). Le produit final du couplage, c'est-à-dire l'amide secondaire **II.4**, est ainsi formée après tautomérisation céto-énolique.

Schéma 6 – Élimination réductrice de **II.1** en présence de F^-/HF .

Cette réaction est sévèrement ralentie par un excès d'isonitrile, probablement à cause de la formation des espèces cationiques susmentionnées et de la prévention de la formation de complexes insaturés. Ces derniers devraient être plus réactifs par rapport à l'élimination réductrice, comme l'attestent les calculs DFT. Plus en détail, plusieurs complexes comportant un arrangement *cis* du OH^- et du résidu imidoyle peuvent en principe être formés en solution et participer à ce processus, par éjection de l'un des ligands $tBuNC$ ou par substitution avec une autre espèce présente dans le milieu réactionnel. À l'aide de calculs DFT, nous avons évalué la stabilité relative de plusieurs de ces complexes et la barrière de l'élimination réductrice à partir de chacun d'eux (Schéma 7). La plus basse barrière associée à l'élimination réductrice est calculée à partir du complexe tricoordonné **II.I5b**, correspondant à l'état de transition **II.TS3b**. Ce fait peut être interprété par des raisonnements de type orbitalaire.

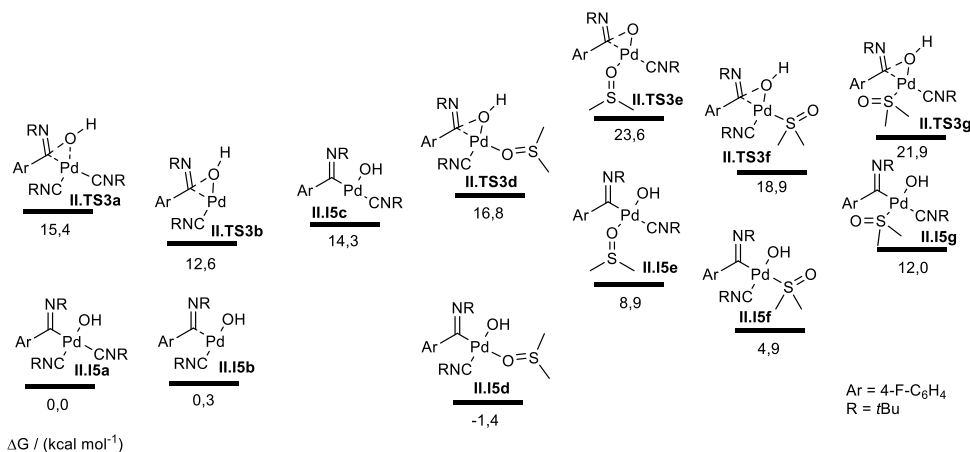


Schéma 7 – Stabilités relatives (ΔG calculées à 25 °C) de différents complexes comportant un arrangement *cis* du OH^- et du résidu imidoyle, et des états de transition respectifs pour l'élimination réductrice. Il n'a pas été possible de localiser un TS correspondant à **II.I5c**, car il se produit une isomérisation en **II.I5b** pendant l'optimisation de géométrie.

D'autres études sont en cours au laboratoire afin d'appliquer ces résultats au développement rationnel de nouvelles réactions pallado-catalysées impliquant l'insertion d'isonitriles.

Chapitre III – Synthèse d'indoles par ouverture réductrice du benzofurane catalysée au palladium *via* β -élimination d'un phénolate

Il y a quelques années, la réaction d'ouverture des furanes catalysée par le palladium conduisant à des composés carbonylés α,β -insaturés a été mise au point au laboratoire.^[2,3] La

fragmentation d'une série d'adduits de Ugi-Smiles dérivés de la furfurylamine en des indoles fonctionnalisés a été démontrée (Schéma 8). Les conditions réactionnelles optimales utilisent $\text{PdCl}_2(\text{PPh}_3)_2$ comme précurseur catalytique et de la diisopropyléthylamine (DIPEA) comme base dans l'acétonitrile à 130 °C (Schéma 8).^[2,3]

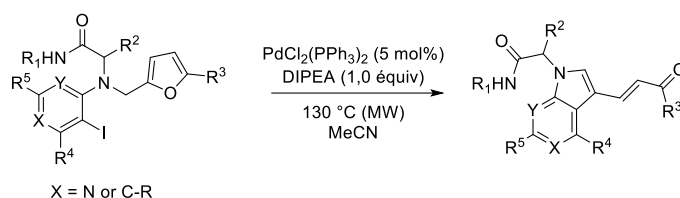


Schéma 8 – Ouverture pallado-catalysée de furanes.^[2,3]

Quand les mêmes conditions réactionnelles ont été appliquées aux dérivés correspondants du benzofurane comme **III.1a**, une réaction différente a été observée : un dérivé du 2-((1*H*-indol-3-yl)méthyl)phénol (**III.2a**) est obtenu dans ce cas (Schéma 9). Un simple décompte d'électrons atteste qu'il s'agit d'un processus de réduction, c'est-à-dire que le réactif **III.1a** est à un degré d'oxydation supérieur à celui du produit **III.2a**, alors que la fragmentation des furanes décrite précédemment (Schéma 8) est une transformation neutre du point de vue de l'oxydo-réduction.

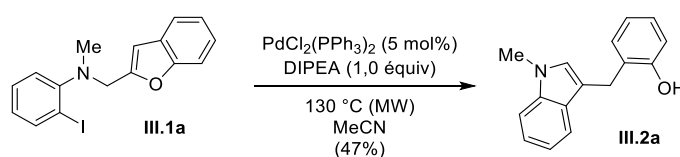


Schéma 9 – Premier essai d'ouverture pallado-catalysée d'un dérivé du benzofurane.

Il s'agit d'un résultat assez surprenant compte tenu de la synthèse de la (-)-Frondosine B proposée par Trauner (Schéma 10).^[4,5] Dans des conditions très proches de celles de notre réaction, une cyclisation d'un triflate vinylique avec activation C-H a lieu à la place de l'ouverture du cycle du benzofurane (Schéma 10).

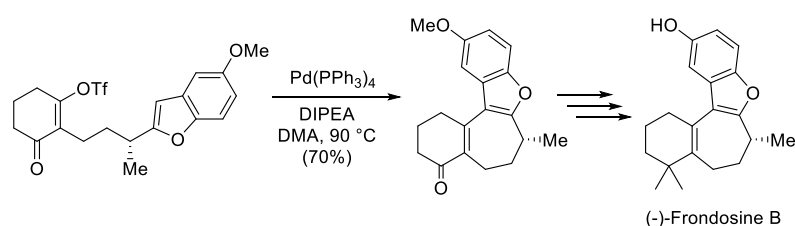


Schéma 10 – Vinylation intramoléculaire pallado-catalysée par activation C-H d'un dérivé du benzofurane au cours de la synthèse totale de la (-)-Frondosine B proposée par Trauner.^[4,5]

Nous avons tout d'abord optimisé les conditions opératoires pour effectuer cette réaction d'ouverture. Il s'est avéré que les premières conditions testées étaient déjà presque optimales, mais en substituant MeCN par EtCN le rendement a été amélioré. Nous nous sommes intéressés ensuite à l'étendue de cette réaction. Testés dans les conditions optimisées, plusieurs substrats ont permis d'isoler des indoles substitués avec des rendements satisfaisants (Schéma 11).

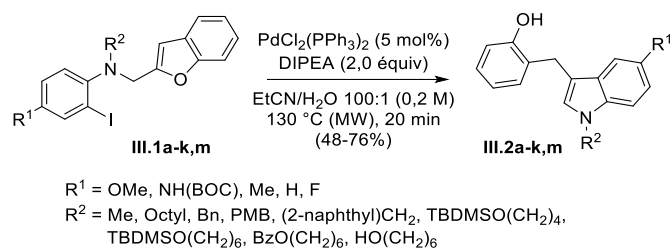
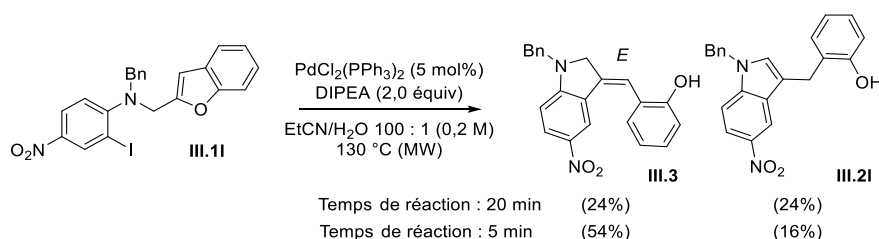


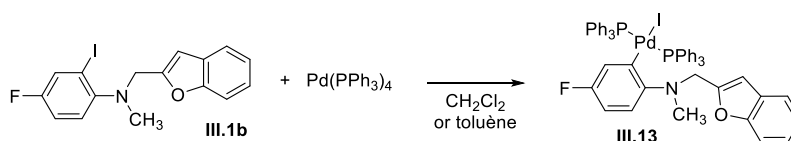
Schéma 11 – Etendue de la réaction d'ouverture pallado-catalysée des dérivés du benzofurane.

Le composé **III.11**, ayant un substituent NO_2 à la place de R^1 , a donné un rendement plus faible que les autres substrats. Nous avons donc analysé plus en détail le mélange réactionnel brut provenant de la réaction de **III.11**. En plus de **III.21**, le produit isomère **III.3** a été isolé (Schéma 12). Un temps de réaction diminué (5 minutes au lieu de 20) a permis d'isoler le composé **III.3** pur avec un rendement de 54% ainsi qu'une petite quantité de **III.21**. De façon intéressante, **III.3** a été obtenu sous la forme d'un stéréoisomère pur, la configuration *E* étant établie par RMN. Il est à noter que l'isomère *E* ne devrait pas être le plus stable du point de vue thermodynamique, comme le suggèrent des considérations élémentaires et des calculs théoriques. Aucune isomérisation de **III.3** à (*Z*)-**III.3** ne devrait donc être possible dans les conditions réactionnelles et, par conséquent, la formation de **III.3** serait sous contrôle cinétique.

Schéma 12 – Produits isomères obtenus par ouverture pallado-catalysée du substrat **III.11**.

Nous avons donc émis l'hypothèse que **III.3** est un intermédiaire réactionnel qui est transformé en **III.21** par migration de la double liaison. Un simple essai a démontré que cette isomérisation n'est pas catalysée par la DIPEA, mais un chauffage en présence du sel d'ammonium $\text{DIPEA} \cdot \text{HBr}$ a amené à une conversion de **III.3** en **III.21** avec un rendement de 80%. Considérant que HI est formellement produit au cours de la réaction catalytique, nous avons conclu que très probablement l'isomérisation se produit par catalyse acide.

Pour avoir des renseignements sur le mécanisme de la transformation étudiée, nous avons d'abord considéré l'addition oxydante du composé **III.2b** avec $\text{Pd(PPh}_3)_4$ comme source de Pd(0). Le composé marqué au fluor **III.2b** a été choisi pour suivre facilement la réaction par RMN ^{19}F . Un complexe de type *trans*- $[\text{ArPd(PPh}_3)_2\text{I}]$ a été identifié comme le seul produit formé à température ambiante (Schéma 13)

Schéma 13 – Formation du complexe **III.13** à partir du composé **III.1b**.

Le complexe **III.13** a été généré *in situ* à partir de Pd(PPh₃)₄ (40 mM dans CD₂Cl₂) et **III.1b** (1,5 équiv). Nous avons ensuite ajouté Et₃N·HI (2,5 équiv.) en tant que source de HI et le mélange résultant a été chauffé à 60 °C pendant 8 h. Après refroidissement, un précipité de *trans*-[Pd(PPh₃)₂I₂]·(CD₂Cl₂) sous la forme d'aiguilles rouge-orange est apparu. L'analyse du surnageant a révélé que 80% de **III.13** avait été converti en d'autres produits, dont le plus abondant que nous avons identifié comme le composé **III.14** (Schéma 14), qui a été obtenu avec env. rendement 70% (basé sur la quantité de **III.13** transformé). D'autres produits non identifiés se sont formés en petites quantités. Aucune trace d'indole **III.2b** n'a pu être identifiée par analyse RMN du mélange réactionnel brut. Une tentative d'isoler le composé **III.14** par CCM préparative sur gel de silice à écoué, car seul l'indole **III.2b** a été récupéré à la place. Nous supposons que dans les conditions réactionnelles, l'isomérisation de **III.14** en **III.2b** ne se fait pas facilement, alors que le gel de silice est capable de catalyser plus efficacement cette réaction.

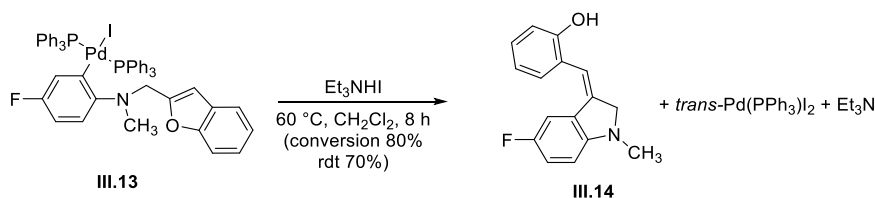


Schéma 14 – Décomposition thermique du complexe **III.13** en présence de Et₃N·HI.

Sur la base des données collectées, le cycle catalytique illustré dans la Figure 2 peut être mis en avant pour la transformation à l'étude. Les intermédiaires qui ont été isolés ou caractérisés spectroscopiquement sont encadrés en rectangles en pointillés.

La première étape est l'addition oxydante du substrat iodé avec le Pd(0). Le complexe d'arylpalladium(II) résultant effectue la carbopalladation de la double liaison C=C du benzofurane, donnant un intermédiaire organopalladié de type spiro. Cette réaction devrait se dérouler de manière synchrone avec une stéréochimie d'addition de type *syn*. Une étape d'*anti*-alcoxydépalladation pourrait fournir l'indoline ayant la double liaison exocyclique de la stéréochimie observée. Cet acte élémentaire peut être considéré comme l'inverse de l'étape clé du procédé Wacker-Hoechst, c'est-à-dire l'addition d'un nucléophile oxygéné à un complexe Pd(II)-alcène.

Ce dernier processus fournirait une espèce de Pd (II), qui doit être réduite en Pd(0) pour permettre au cycle catalytique de tourner. Nous proposons que le DIPEA puisse agir comme un agent réducteur, étant à son tour oxydée en l'imine ou en l'énamine correspondante. Il a déjà été démontré que la DIPEA peut remplir ce rôle.^[6] De plus, d'autres amines ayant des hydrogènes α peuvent remplacer la DIPEA (Et₃N, *i*Pr₂NH, *N*-méthylmorpholine), tandis que la 2,2,6,6-tétraméthylpipéridine – n'ayant pas d'hydrogène α – ne permet pas d'avoir une réaction catalytique. Enfin, l'isomérisation de la double liaison exocyclique rétablit l'aromaticité et forme l'indole qui est le produit final de la réaction.

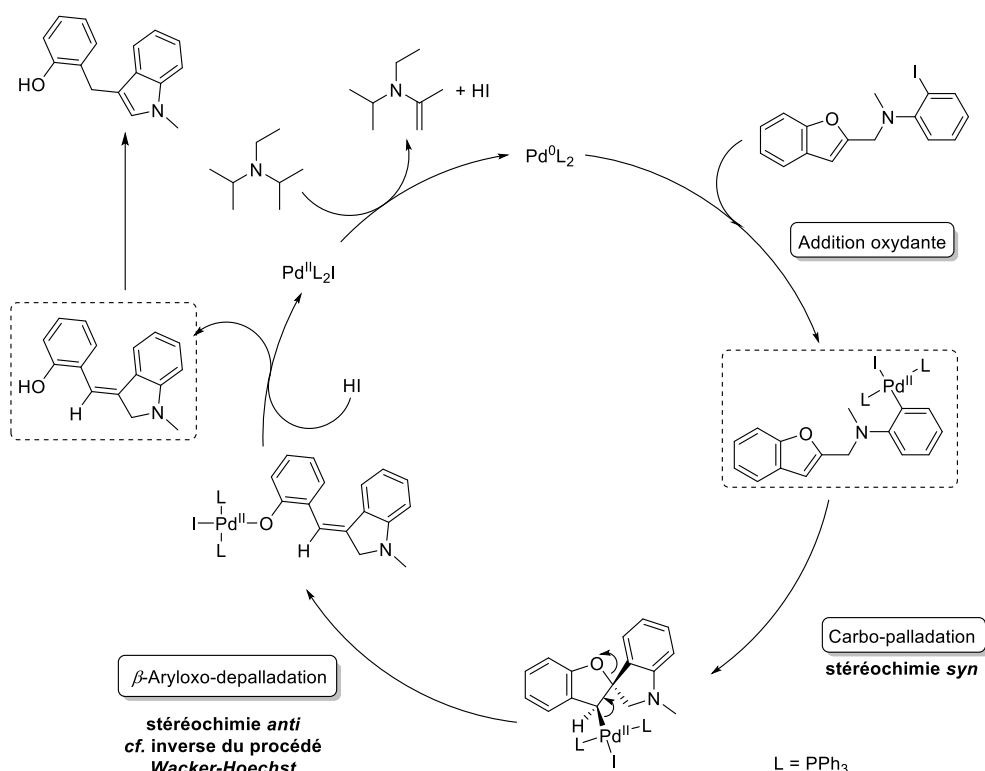


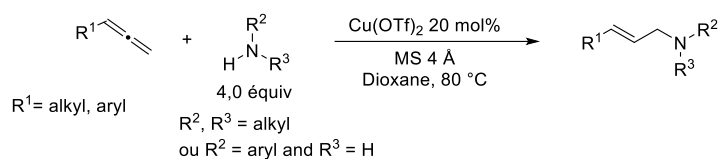
Figure 2 – Cycle catalytique proposé pour l'ouverture pallado-catalysée des benzofuranes. Les intermédiaires réactionnels qui ont été isolés ou caractérisés par voie spectroscopique sont mis en évidence dans des rectangles en pointillés.

Des calculs théoriques sont en cours pour éclaircir les détails de ce mécanisme et des applications synthétiques de cette réaction sont envisageables.

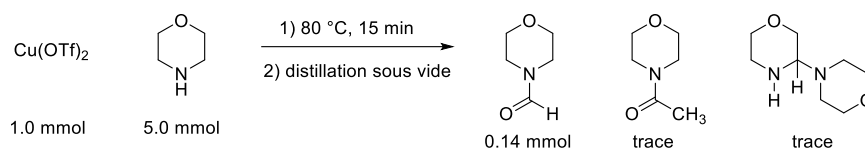
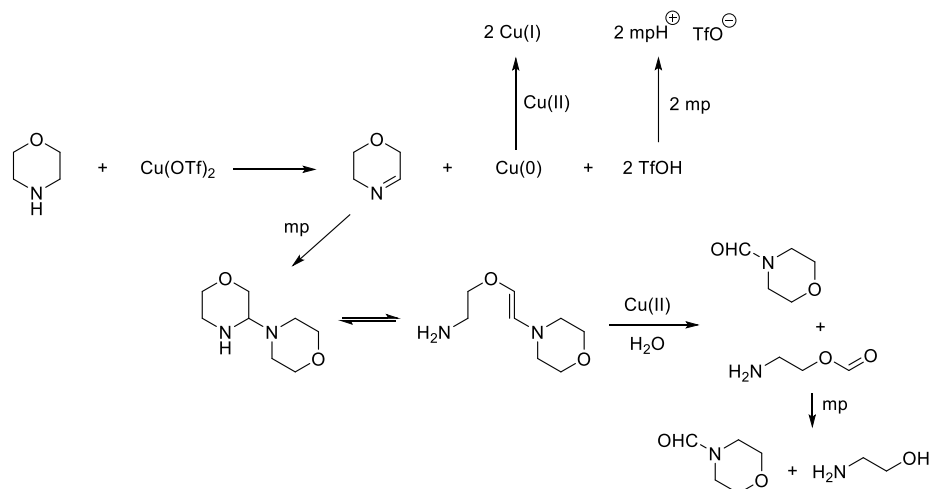
Chapitre IV – Hydroamination cupro-catalysée d'allènes : étude mécanistique et développements méthodologiques

L'addition directe d'une amine sur une liaison carbone-carbone double ou triple non-activée, que l'on appelle la réaction d'hydroamination, est une approche très prometteuse pour le développement d'une méthodologie de synthèse des amines plus complexes. La complète économie d'atomes rend cette réaction respectueuse d'un des principes fondamentaux de la chimie verte.

En collaboration avec Marc Taillefer et Florian Monnier (Ecole Nationale Supérieure de Chimie de Montpellier), nous avons étudié le système catalytique développé par leur groupe pour la réaction d'hydroamination d'allènes terminaux cupro-catalysée (Schéma 15). Nos collaborateurs ont démontré que par l'utilisation de $Cu(OTf)_2$ comme catalyseur, les allènes monosubstitués aromatiques et aliphatiques peuvent subir l'addition d'amines secondaires aliphatiques ou d'anilines primaires dans des conditions relativement douces (80 °C). L'amine allylique non ramifié ayant la stéréochimie *E* est obtenu sélectivement.

Schéma 15 – Hydroamination d'allènes cupro-catalysée.^[7]

Nous avons tout d'abord montré que le catalyseur est un complexe cationique de Cu(I). Cu(OTf)₂ est un précurseur catalytique qui est réduit *in situ* par l'amine. Afin de mieux caractériser la réaction qui a lieu avec la morpholine, nous avons identifié les produits organiques dérivants de la réaction d'un excès de cette amine avec Cu(OTf)₂. La *N*-formylmorpholine était le produit principal isolé. De petites quantités de *N*-acétylmorpholine (environ 4% par rapport à la *N*-formylmorpholine) et de 3,4'-bimorpholine (environ 2% par rapport à la *N*-formylmorpholine) ont aussi été identifiées (Schéma 16). Un mécanisme plausible pour la formation de ces produits est illustré dans le Schéma 17.

Schéma 16 – Réaction de la morpholine avec Cu(OTf)₂.Schéma 17 – Mécanisme envisageable pour la réduction du Cu(OTf)₂ à l'aide de la morpholine.

Il est connu que les sels de Cu(I) ayant des anions faiblement coordonnants, que l'on appellera sels de Cu(I) cationiques, ont une bonne affinité pour les composés insaturés, tels que les oléfines et les arènes. Par exemple, Cu(OTf) est commercialisé sous la forme d'adduit avec le benzène ou le toluène. Nous avons étudié l'interaction de trois allènes avec le composé modèle [Cu(NCMe)₄]PF₆ par spectroscopie RMN. Un traitement quantitatif des données spectroscopiques nous a permis d'obtenir les valeurs des constantes thermodynamiques associées aux équilibres de formation des complexes 1 : 1 entre les allènes et Cu(I). Les complexes cationiques de Cu(I) ont une bonne affinité pour les allènes, les constantes de

dissociation des complexes allène/Cu(I) étant de l'ordre de grandeur du mM. Cependant, dans les conditions de la réaction catalytique, un excès du substrat amine est présent, qui peut également servir de ligand et déplacer l'allène lui-même du centre métallique. Une estimation semi-quantitative de ce phénomène par spectroscopie RMN démontre que dans les conditions réactionnelles il y a une compétition entre les deux substrats pour se coordonner au centre métallique.

La réaction étudiée est à la fois régio- et stéréosélective : l'addition de l'amine a lieu principalement sur l'atome de carbone terminal de l'allène avec une sélectivité complète pour l'isomère *E* (**IV.2a**). L'isomère géométrique (*Z*)-**IV.2a** n'est pas formé en quantité détectable par RMN et le rapport des isomères **IV.2a** / **IV.3a** est de 92 : 8 (Schéma 18).

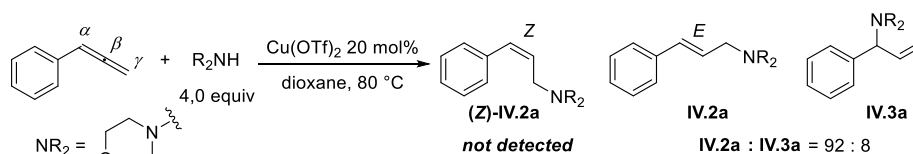


Schéma 18 – Régio- et stéréosélectivité de l'addition de la morpholine au phenylallène.

Nous avons vérifié que cette réaction est bien sous contrôle cinétique : le produit minoritaire **IV.3a** et l'isomère non observé (*Z*)-**IV.2a** ont été synthétisés par une voie indépendante et ils ont été mis dans les conditions de la réaction catalytique. Nous n'avons pas observé la transformation de ces deux composés en **IV.2a** (Schéma 19).

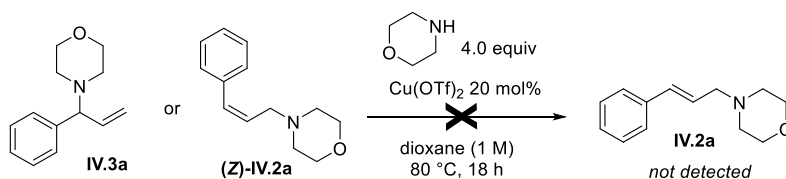


Schéma 19 – Essai d'isomérisation de **IV.3a** et (*Z*)-**IV.3a** en **IV.2a**.

Avec ces expériences, nous avons établi sans aucun doute que la réaction est sous contrôle cinétique, régiosélective et stéréosélective. Ayant également en main des informations expérimentales fiables sur la nature des espèces catalytiquement actives et sur son interaction avec les substrats, des calculs DFT ont pu être effectués pour expliquer les sélectivités observées. Nous avons émis l'hypothèse que la réaction d'hydroamination pourrait procéder par attaque nucléophile directe de l'amine secondaire sur un complexe cuivre-allène. Un intermédiaire alcényl-cuivre serait ainsi généré, ce qui pourrait donner le produit final après proto-démétallation. Les espèces organométalliques alcényl-cuivre sont normalement stéréochimiquement stables et ils subissent une proto-démétallation stéréospécifique en présence de sources de protons avec rétention de la configuration de la double liaison. Cela se produit, par exemple, pour les réactifs alcényl-cuivre stéréodéfinis dérivant de la carbocupration d'alcynes. En ce cas, la stéréosélectivité de l'attaque nucléophile déterminerait directement la sélectivité *E* / *Z* du processus global d'hydroamination. Les deux étapes sont illustrées dans le Schéma 20.

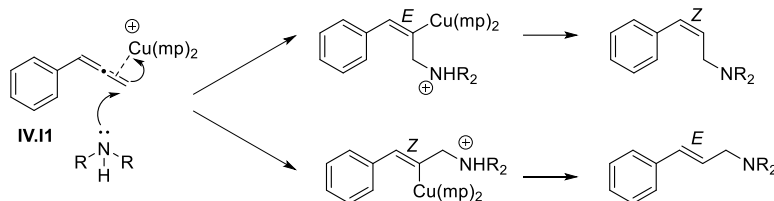


Schéma 20 – Attaque nucléophile d'une amine sur un complexe allène cuivre et proto-démétallation stéréospécifique de l'intermédiaire alcényl-cuivre.

Deux approches stéréochimiques idéalisées sont concevables pour l'attaque nucléophile de la morpholine sur le complexe $[\text{Cu}(\text{mp})_2]^+$ /allène (mp = morpholine). Par rapport au plan dans lequel se trouve la partie $\text{C}=\text{CH}_2$ de l'allène, l'approche des deux réactifs peut avoir lieu soit (1) du côté opposé à l'atome de Cu (c'est-à-dire d'une manière anti-périplanaire); (2) du même côté que Cu (c'est-à-dire avec une approche syn-périplanaire). Dans les deux cas, le substituent organique de l'allène peut se situer soit dans le même demi-espace que l'atome de Cu, ce qui donne l'intermédiaire alcénylcuivre Z, ou dans le demi-espace opposé, correspondant à la formation d'un alcénylcuivre E. Il est à noter que l'intermédiaire organométallique E produit l'allylamine Z après proto-démétallation avec rétention de configuration, tandis que l'organocuivreux Z donne l'allylamine E.

Tous les états de transition possibles correspondant aux approches stéréochimiques décrites ci-dessus sont représentés schématiquement dans la Figure 3 avec leurs énergies libres de formation (ΔG , par rapport à $[\text{Cu}(\text{mp})_2]^+$, mp, et **IV.1a** non interagissants). L'état de transition **IV.TS1**, qui correspond à l'attaque de la morpholine au C_α et à la formation du produit ramifié **IV.3a** est également représenté. Comme indiqué ci-dessus, après l'étape de proto-démétallation **IV.TS1a** conduit à **IV.2a**, **IV.TS1b** et **IV.TS1d** produisent (Z)-**IV.2a**, et **IV.TS1d** fournit **IV.3a**. Les énergies libres calculées sont en accord qualitatif avec le fait que **IV.2a** est le produit majeur, tandis que des quantités mineures de **IV.3a** sont observées et aucune quantité détectable de (Z)-**IV.2a** n'est produite, puisque $\Delta G(\text{IV.TS1a}) < \Delta G(\text{IV.TS1e}) < \Delta G(\text{IV.TS1b}) < \Delta G(\text{IV.TS1d})$ avec des valeurs respectives de 17,0, 18,7, 20,8 et 27,9 kcal mol⁻¹ (Figure 3). En effet, la différence d'énergie libre entre **IV.TS1a** et **IV.TS1e** correspond à un rapport de Boltzmann (94 : 6 à 80 °C) qui est du même ordre de grandeur que le rapport **IV.2a** : **IV.3a** expérimental (92 : 8).

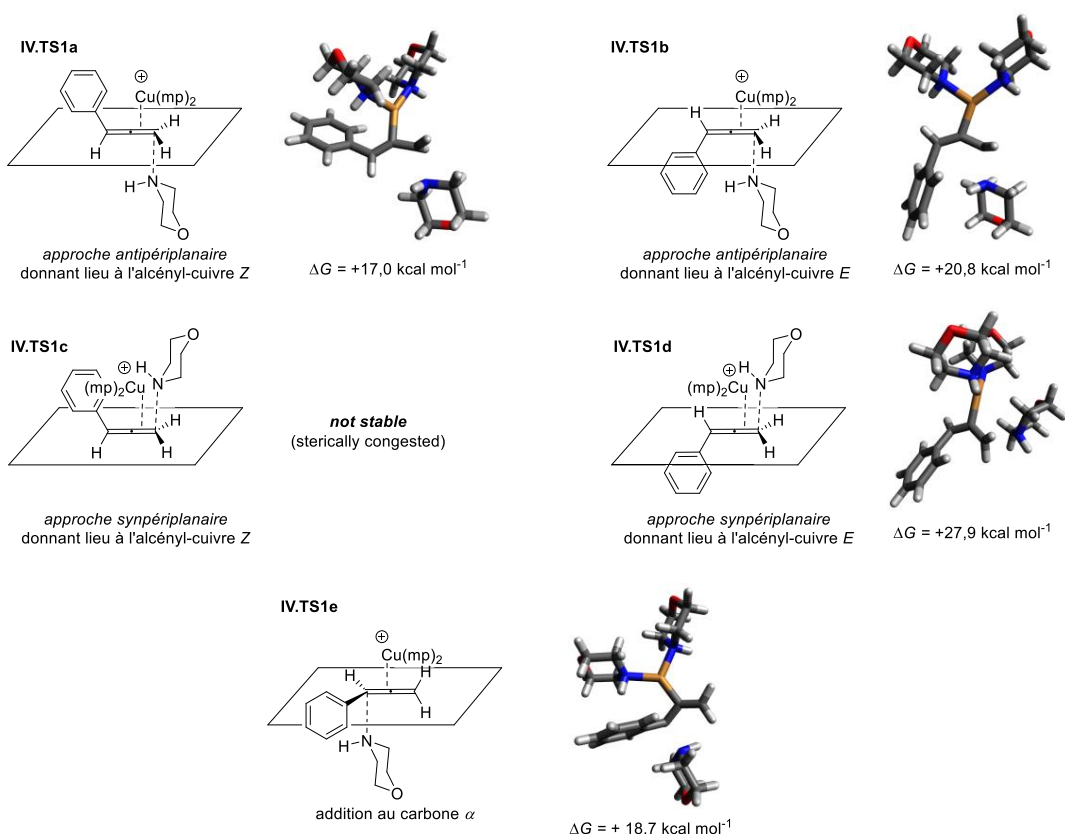


Figure 3 – Etats de transition pour l'attaque nucléophile de la morpholine sur les complexes **IV.1a**/Cu(I). Les valeurs montrées sont enthalpies libres de formation à 298 K (ΔG) calculées au niveau DFT par rapport à $\text{Cu}(\text{mp})_2]^+$, mp et **IV.1a** avant interaction, qui ont été choisis comme zéro de l'enthalpie libre.

Nous avons ensuite examiné la géométrie de l'état de transition **IV.TS1**. Une réorganisation structurale significative de l'allène coordonné a lieu avant la formation de la nouvelle liaison C-N : la distance C $_{\gamma}$ -N est longue (2,14 Å) et C $_{\beta}$ est essentiellement déjà un centre sp 2 ($\angle \text{C}_{\alpha}\text{C}_{\beta}\text{C}_{\gamma} = 138,8^\circ$, $\angle \text{CuC}_{\beta}\text{C}_{\gamma}\text{N} = 174,5^\circ$, $\angle \text{CuC}_{\beta}\text{C}_{\alpha}\text{H} = 170,0^\circ$). De cette manière, une charge partielle positive est accumulée au niveau du carbone allénique γ passant de l'intermédiaire **IV.I1** à **IV.TS1a**, comme l'analyse de charge NBO permet de l'établir (Figure 9).

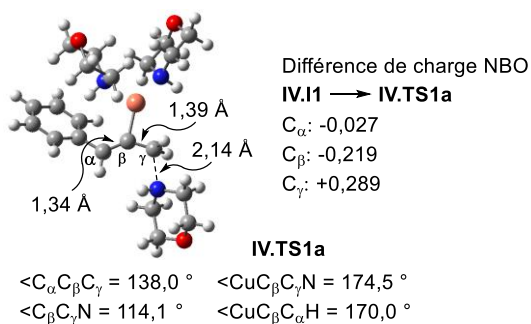


Figure 9 – Paramètres géométriques sélectionnés de **IV.TS1a**. La différence des charges atomiques partielles NBO entre de **IV.TS1a** et **IV.I1** est aussi montrée.

Dans le but d'étendre l'applicabilité de la réaction étudiée dans des conditions plus douces, nous avons raisonné qu'une substitution sur le carbone α avec un hétéroatome ayant un doublet libre pourrait stabiliser l'état de transition, en délocalisant efficacement la charge positive développée en C_γ . Nous n'avons pas utilisé les *N*-allénylamines, car elles sont des composés instables et très sujets à la polymérisation, mais les allénamides, qui sont facilement disponibles et qui sont souvent un compromis optimal entre réactivité et stabilité.

Nous avons testé la réaction de la *N*-allényl-2-pyrrolidinone (**IV.1b**) avec la morpholine catalysée par des complexes de cuivre(I). Nous avons trouvé, en accord avec nos attentes, que la transformation peut effectivement se dérouler à température ambiante pour cet allène et qu'un excès d'amine n'est pas nécessaire, contrairement au cas du phenylallène (**IV.1a**). En utilisant les nouvelles conditions opératoires optimisées, nous avons étudié le champ d'application de cette réaction (Schéma 21 et Schéma 22). Une variété d'allénamides, comportant des substituants aromatiques ou aliphatiques, sont des substrats viables (Schéma 21, **IV.2b,2f-2m**). En plus des allénamides, les *N*-allénylcarbamates peuvent être utilisés comme réactifs (**IV.2n,2o**). Les amines secondaires sont des substrats appropriés, y compris les amines aliphatiques à chaîne ouverte et les amines stériquement encombrées (Schéma 22). Ces conditions réactionnelles douces tolèrent plusieurs groupes fonctionnels, tels que les substituants bromés (**IV.2h**) et iodés (**IV.2u**), les groupes OH non protégés (**IV.2t**) et les esters boroniques (**IV.2v**), qui peuvent être utilisés dans des transformations ultérieures. Malheureusement, les amines primaires aliphatiques et aromatiques ne réagissent pas dans ces conditions opératoires.

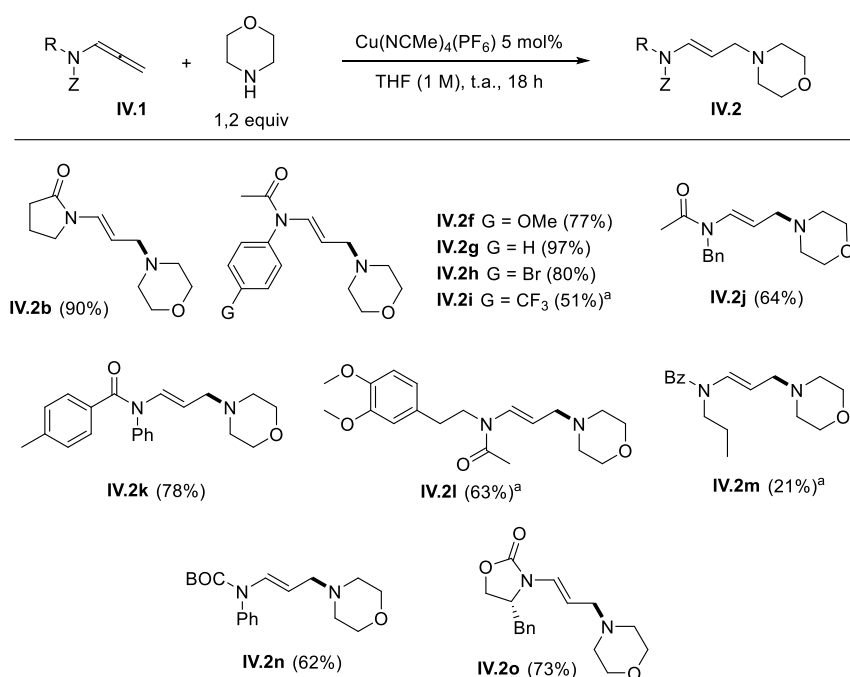


Schéma 21 - Hydroamination cupro-catalysée de différents allénamides et *N*-allénylcarbamates avec la morpholine.

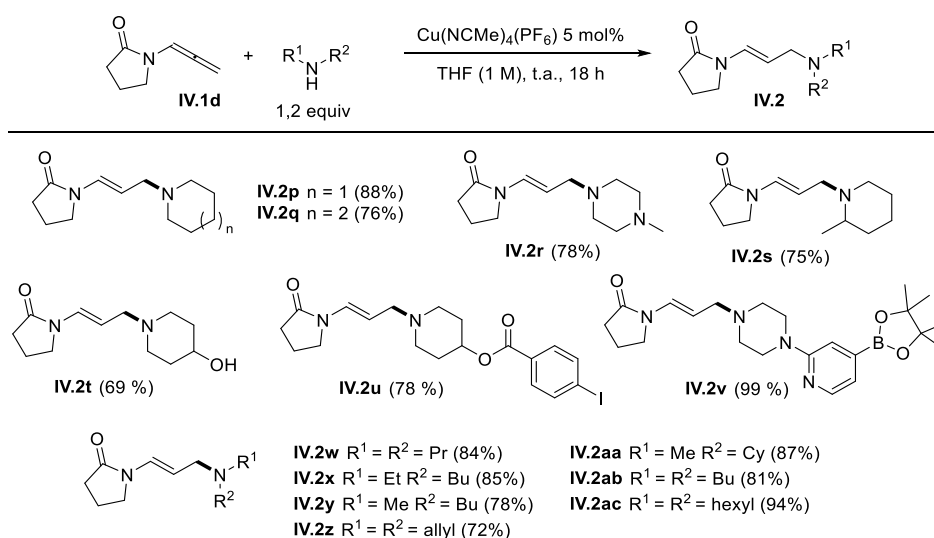


Schéma 22 - Hydroamination cupro-catalysée de la *N*-allénylpyrrolidinone (**IV.1d**) avec différentes amines secondaires.

Nous nous sommes intéressés ensuite au mécanisme détaillé de la réaction concernant les allénamides. Nous avons montré que la *N*-allényl-2-pyrrolidinone (**IV.1b**) a une plus grande affinité pour le cuivre(I) cationique que le phényllallène (**IV.1a**). En faisant l'hypothèse que le mécanisme d'hydroamination de ces substrats est similaire à celui que nous avons proposé pour le phényllallène (**IV.1a**), les états de transition correspondant à l'attaque nucléophile *anti*-périplanaire de l'amine au complexe allène / cuivre ont été identifiés par des calculs DFT. L'oxygène de la fonction amide joue un rôle important dans l'énergétique de ces états de transition. L'état de transition **IV.TS-3b**, dans lequel l'oxygène de l'amide coordonne le cuivre (distance O-Cu : 2,22 Å) en même temps que l'attaque nucléophile de la morpholine a lieu, est plus stable que les autres conformères d'au moins 3,9 kcal mol⁻¹.

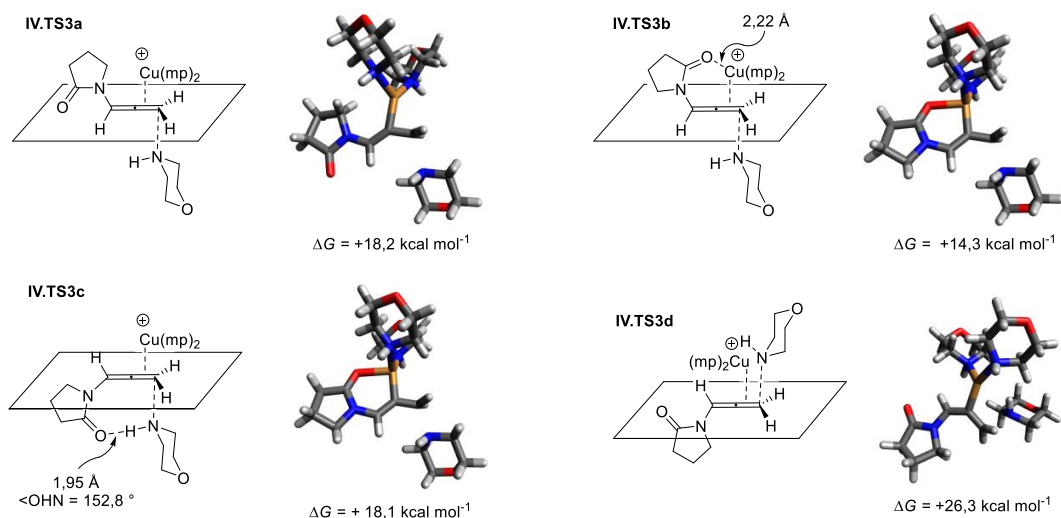


Figure 12 – États de transition pour l'attaque nucléophile de mp sur le complexe entre l'allénamide **IV.1b** et Cu(I). Les enthalpies libres de Gibbs calculées à 298 K sont indiquées par rapport à $[\text{Cu}(\text{mp})_2]^+$, mp et **IV.1b** avant interaction.

Nous avons donc conclu que l'atome d'oxygène de la fonction amide peut agir comme un groupement directeur *immé*, améliorant ainsi l'affinité du substrat pour le centre métallique et favorisant la réactivité. En gardant cette idée à l'esprit, nous avons essayé de concevoir une autre classe de dérivés d'allène pouvant également avoir un groupement fonctionnel qui serait capable de coordonner le métal et d'assurer aussi une réactivité accrue.

Les *N*-allényl-1,2-azoles sont des substances facilement accessibles qui remplissent ce profil (Schéma 23). Divers *N*-allényl-1,2-azoles réagissent efficacement avec la morpholine dans les conditions opératoires que nous avons établies précédemment (Schéma 24).

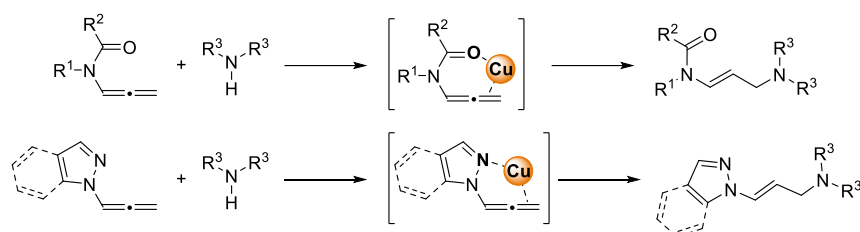


Schéma 23 – Allénamides et *N*-allényl-1,2-azoles comme substrats ayant des groupements directeurs innés dans la réaction d'hydroamination cupro-catalysée.

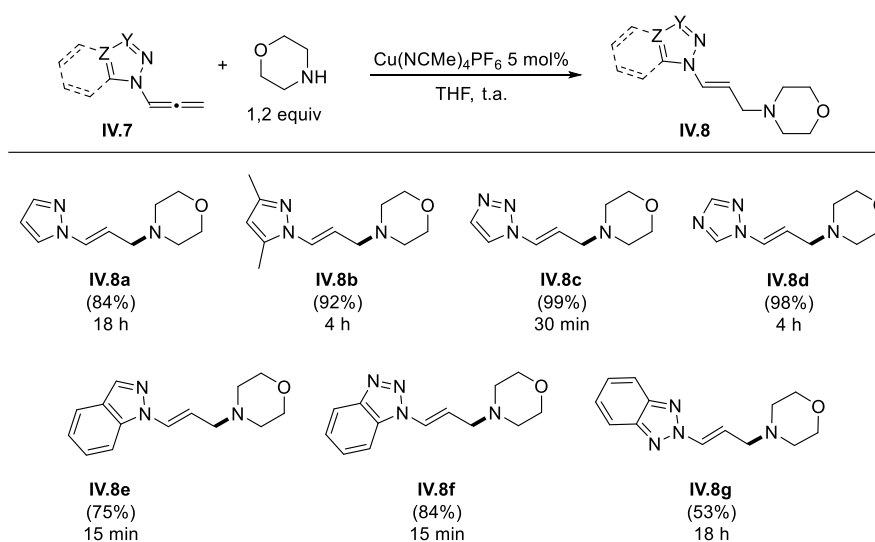
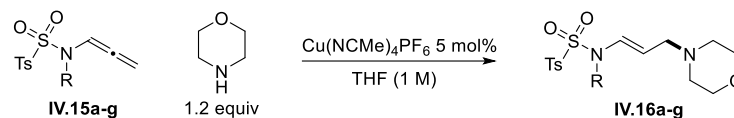


Schéma 24 – Hydroamination cupro-catalysée de *N*-allényl-1,2-azoles.

Dans notre quête d'autres allènes appropriés comme substrats pour la réaction d'hydroamination que nous avons développée, nous avons raisonné que les *N*-allénylsulfonamides étaient des candidats prometteurs. Compte tenu de la similitude structurale et électronique avec les allénamides, nous nous attendions à une réactivité comparable. De façon assez surprenante, lorsque le *N*-allényl-*N*-méthyl-*p*-toluènesulfonamide (**IV.15a**, Tableau 1, entrée 1) a été utilisé comme substrat dans nos conditions expérimentales, pratiquement aucune conversion n'a eu lieu à température ambiante (Tableau 1). L'introduction d'une double liaison stratégiquement placée augmente significativement la réactivité : le *N*-allényl-*N*-allényl-*p*-toluènesulfamide (**IV.15b**) est un excellent substrat pour notre réaction, car le produit d'addition de la morpholine a été obtenu avec un rendement de 90% à température ambiante (Tableau 1,

entrée 2). D'autres substrats ayant des chaînes insaturées sont aussi réactifs dans les mêmes conditions opératoires (Tableau 1, entrés 4-7).

Tableau 1 – Influence des substituants R sur la réactivité de TsNR(CH=C=CH₂) vis à vis de la réaction d'hydroamination cupro-catalysée.



	R	Réactif	Produit	Temps (h)	Temp. (°C)	Ratio E/Z	Rdt (%)
1	Me	IV.15a	IV.15a	72	40	>99:1	10 ^{a,b}
2	Allyl	IV.15b	IV.15b	18	r.t.	>99:1	90
3	Pr	IV.15c	IV.15c	48	r.t.	>99:1	20 ^a
4	(E)-PhCH=CHCH ₂ -	IV.15d	IV.15d	48	r.t.	>99:1	56
5	(E)-MeCH=CHCH ₂ -	IV.15e	IV.15e	48	r.t.	>99:1	29
6	Bn	IV.15f	IV.15f	72	r.t.	83:17	39
7	Ph	IV.15g	IV.15g	18	r.t.	>99:1	70

^a Rendement déterminé par RMN. ^b Pas de réaction à 25 °C.

Pour cette dernière famille de composés, la coordination de type η^2 impliquant la chaîne insaturée est fondamentale pour stabiliser l'état de transition. Des calculs DFT ont été effectués pour confirmer le mécanisme proposé, la structure de l'état de transition (**IV.TS6a**) comportant l'interaction la chaîne allylique de **IV.15b** avec le centre métallique est montrée dans la Figure 6.

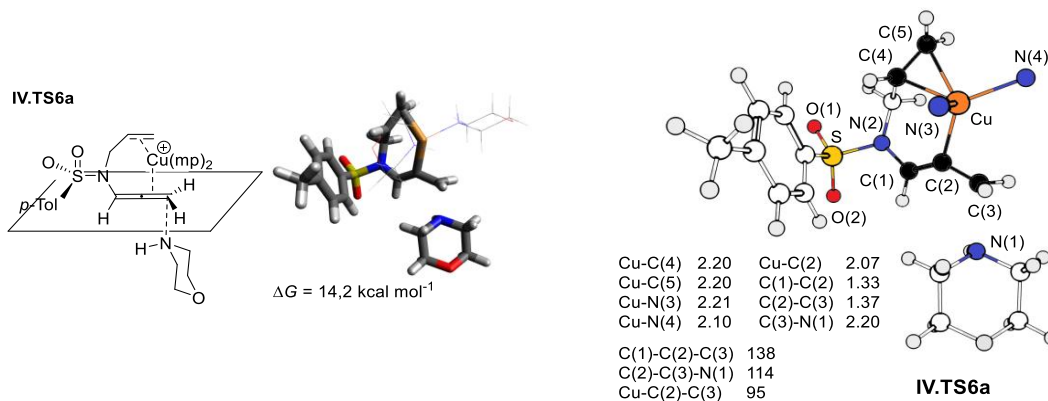


Figure 6 – Etat de transition à plus basse enthalpie libre pour l'hydroamination cupro-catalysée de **IV.15b**. Le rôle de la chaîne allyle comme groupement directeur est mis en évidence.

Références

- [1] H. Jiang, B. Liu, Y. Li, A. Wang, H. Huang, *Org. Lett.* **2011**, *13*, 1028–1031.
- [2] L. El Kaïm, L. Grimaud, S. Wagschal, *Chem. Commun.* **2011**, *47*, 1887–1889.
- [3] S. Wagschal, Synthèse d'hétérocycles et réactions pallado-catalysées, Thèse de doctorat, Ecole Polytechnique, **2010**.
- [4] C. C. Hughes, D. Trauner, *Angew. Chem. Int. Ed.* **2002**, *114*, 1639–1642.
- [5] C. C. Hughes, D. Trauner, *Tetrahedron* **2004**, *60*, 9675–9686.
- [6] S. Mannathan, S. Raoufmoghaddam, J. N. H. Reek, J. G. de Vries, A. J. Minnaard, *ChemCatChem* **2016**, *8*, 2572–2572.
- [7] R. Blicek, J. Bahri, M. Taillefer, F. Monnier, *Org. Lett.* **2016**, *18*, 1482–1485.

Résumé

Dans cette thèse les mécanismes de trois réactions catalysées par des complexes de palladium et de cuivre ont été étudiés en utilisant des méthodes expérimentales et théoriques.

La première réaction est la synthèse d'amides à partir d'halogénoarènes, d'isonitriles et d'eau, qui est un exemple de couplage catalysé par le palladium impliquant l'insertion d'un isonitrile. Cette dernière molécule sert à la fois de ligand et de substrat, et son influence sur chaque étape du cycle catalytique a été mise en évidence.

La deuxième réaction est l'ouverture des benzofuranes conduisant à des dérivés indoliques catalysée par des sels de palladium. Les conditions opératoires ont été optimisées et les étapes clés du mécanisme ont été élucidées.

La dernière réaction étudiée, qui est le sujet principal de cette thèse, est l'addition d'amines sur des allènes catalysée par des sels de cuivre (hydroamination). La caractérisation des espèces catalytiques de cuivre(I) et l'étude théorique du mécanisme ont permis d'étendre cette réaction à différents substrats (allénamides, *N*-allénylazoles, *N*-allénylsulfamides) dans des conditions particulièrement douces et efficaces.

Mots Clés

catalyse, études mécanistiques, chimie organique, synthèse organique, chimie organométallique, DFT

Abstract

In this thesis, the mechanism of three organic reactions catalyzed by palladium and copper complexes has been elucidated by the use of both experimental and theoretical methods.

The first reaction is the synthesis of amides from haloarenes, isocyanides and water as an example of the broad family of palladium-catalyzed imidoylative couplings. Multiple roles of the isocyanide as both a ligand and a substrate in the different steps of the catalytic cycle have been disclosed.

The second transformation is the palladium-catalyzed ring opening of benzofurans leading to indoles. Optimal conditions for this transformation have been found and the key aspects of its mechanism clarified.

The last reaction, which is the main topic of this thesis, is the addition of amines to allenes catalyzed by copper salts (hydroamination). A characterization of the catalytically active copper(I) species and insight from theoretical calculations suggested how to extend this reaction to other substrates (allenamides, *N*-allenylazoles, *N*-allenylsulfonamides) under mild and efficient conditions.

Keywords

catalysis, mechanistic studies, organic chemistry, organic synthesis, organometallic chemistry, DFT